Biochemische Untersuchungen zu mono-, di- und oligomeren mikrobiellen Naturstoffen aus Aminosäuren

Dissertation
zur Erlangung des akademischen Grades
„doctor rerum naturalium“ (Dr. rer. nat.)

vorgelegt dem Rat der Fakultät für Biowissenschaften
der Friedrich-Schiller-Universität Jena

von Dipl.-Pharm. Florian Ewald Baldeweg

geboren am 23. August 1990 **in** Naila

Die Arbeit wurde von November 2015 bis Dezember 2018 am Lehrstuhl Pharmazeutische Mikrobiologie der Friedrich-Schiller-Universität Jena, assoziiert mit dem Leibniz-Institut für Naturstoff-Forschung und Infektionsbiologie - Hans-Knöll-Institut Jena, unter Leitung von Prof. Dr. Dirk Hoffmeister in Kooperation mit Prof. Dr. Markus Nett von der Technischen Universität Dortmund angefertigt.

Gutachter 1: Prof. Dr. Dirk Hoffmeister
Friedrich-Schiller-Universität Jena

Gutachter 2: Dr. Pierre Stallforth
Leibniz-Institut für Naturstoff-Forschung und Infektionsbiologie Jena

Externer Gutachter: Prof. Dr Harald Groß
Eberhard Karls Universität Tübingen

Tag der Verteidigung: 20. Juni 2019

Für meine Frau

Inhaltsverzeichnis

Abkürzungsverzeichnis

4'-PP	4'-Phosphopantetheinyl
A.	*Aspergillus*
A-Domäne	Adenylierungsdomäne
AA	Arachidonsäure
ACP	Acyl-Carrier-Protein
B.	*Burkholderia*
C-Domäne	Kondensationsdomäne
Cy-Domäne	Zyklisierungsdomäne
E-Domäne	Epimerisierungsdomäne
FAAL	Fettsäure-Acyl-AMP Ligase
HIV	Humanes Immundefizienz-Virus
LSD	Lysergsäurediethylamid
M.	*Mortierella*
MALDI	Matrix–Assistierte Laser–Desorption–Ionisierung
MS	Massenspektrometrie
MT-Domäne	Methylierungsdomäne
NIS	NRPS-unabhängige Siderophor-Synthetasen
NMR	Nuclear Magnetic Resonance/Kernspinresonanz
NRP	Nonribosomale peptide/Nichtribosomales Peptid
NRPS	Nonribosomal peptide synthetase/Nichtribosomale Peptidsynthetase
OSMAC	One-Strain-Many-Compounds
Ox-Domäne	Oxidationsdomäne
P.	*Psilocybe*
PK	Polyketid
PKS	Polyketidsynthase
PUFA	Polyunsaturated fatty acid/Mehrfach ungesättigte Fettsäure
R.	*Ralstonia*
RiPPs	Ribosomally synthesized and post-translationally modified peptides/ Ribosomal synthetisierte und posttranslational modifizierte Peptide
T-Domäne	Thiolierungsdomäne
TE-Domäne	Thioesterasedomäne

Abbildungsverzeichnis

Tabellenverzeichnis

1 Einleitung

1.1 Mikrobielle Sekundärmetabolite als Wirkstoffe aus der Natur

„Denn die Natur ist aller Meister Meister!“ Dieses Zitat von Johann Wolfgang von Goethe lässt sich auch auf die Wirkstoffforschung und -entwicklung anwenden. Bei den von 1981 bis 2014 zugelassenen Wirkstoffen sind 6,7 % den Naturstoffen zuzuordnen. Dazu kommen noch einmal 33 % an synthetischen Wirkstoffen, welche von Naturstoffen abgeleitet sind.[1] Ein bemerkenswerter Teil der pharmazeutisch verwendeten Naturstoffe kommt aus dem Reich der Bakterien und Pilze. Deren Sekundärmetabolom beinhaltet Substanzen mit sehr heterogenen Grundstrukturen, Wirkmechanismen und Anwendungsgebieten. Eine der wichtigsten Arzneistoffgruppen sind Antibiotika. Zu diesen gehören Stoffe wie Cephalosporin C (**1**) aus *Acremonium chrysogenum*, Erythromycin (**2**) aus *Saccharopolyspora erythraea* oder Pleuromutilin (**3**) aus *Clitopilus passeckerianus*.[2,3,4] Weitere wichtige Naturstoffe sind Antihypercholesterinämie-Mittel wie Lovastatin (**4**) aus *Aspergillus (A.) terreus*, Immunsuppressiva wie Cyclosporin A (**5**) aus *Tolypocladium inflatum*, Anthelmintica wie die Avermectine (**6**) aus *Streptomyces avermitilis* oder Zytostatika wie Doxorubicin (**7**) aus *Streptomyces peucetius* (siehe Abbildung 1).[5,6,7,8] Anhand dieser wenigen Beispiele lässt sich bereits die Bedeutung der Isolation bakterieller und pilzlicher Naturstoffe erkennen.

Während im vergangenen Jahrhundert bioaktive Naturstoffe aus Mikroorganismen hauptsächlich durch aktivitätsgeleitete Isolierung oder über chemische Eigenschaften (z.B. Anwesenheit eines Chromophors) von vorwiegend terrestrisch vorkommenden Actinomyceten und Pilzen isoliert wurden, führt dieses Vorgehen nun zu einer erhöhten Quote an Reisolierungen bereits bekannter Strukturen.[9,10] Daher rücken nun auch ungewöhnliche Produzenten wie etwa pflanzenpathogene oder marine Mikroorganismen in den Fokus wissenschaftlicher Untersuchungen.[11,12] Zudem tragen die Etablierung der Genom-Sequenzierung und die Aufklärung von Biosynthese-Mechanismen heute maßgeblich zur Entdeckung neuer Naturstoffe bei. Da in Bakterien und Pilzen die Gene der Biosynthese-Enzyme im Regelfall als Cluster vorliegen, können nun anhand der im Genom enthaltenen Biosynthesecluster verborgene Biosynthesekapazitäten vorhergesagt werden.[13,14] Die dort codierten Biosynthese-Enzyme des Sekundärmetabolismus katalysieren die Bildung von Naturstoffen aus einfachen Bausteinen wie beispielsweise Acetyl-CoA,

Isopentenyl-Pyrophosphat oder Aminosäuren.[15] Damit lassen sich diese Naturstoffe entsprechend ihrer Biosynthese oder der Anzahl der Bausteine kategorisieren.

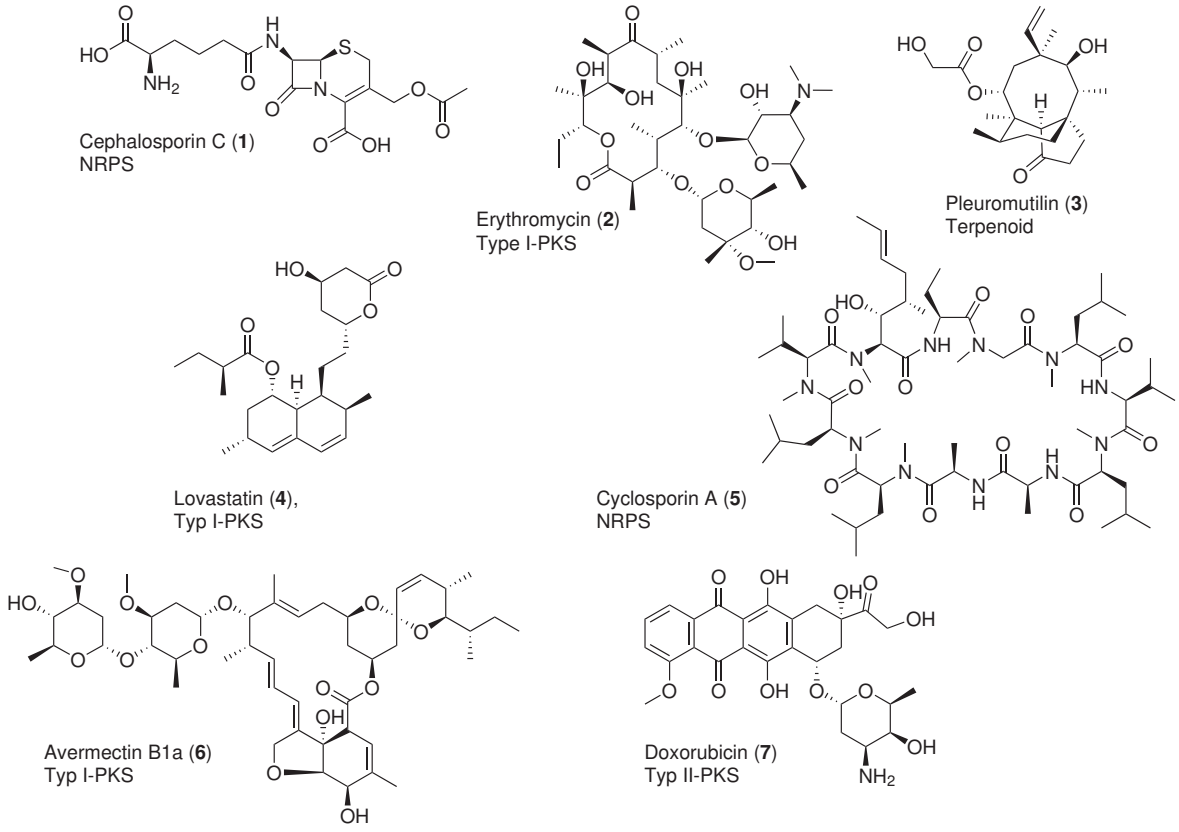

Abbildung 1: Strukturen therapeutisch genutzter bakterieller und pilzlicher Sekundärmetabolite mit Kategorisierung anhand der Biosynthesewege nach Kapitel 1.2.

1.2 Kategorisierung von mikrobiellen Sekundärmetaboliten

Zur besseren Übersicht sind im Folgenden nur die vier größten Biosynthese-Gruppen erläutert. Terpenoide und Terpene stellen die größte Gruppe mit über 60000 bekannten Verbindungen dar. Darunter befinden sich unter anderem Steroide, Carotinoide oder Pflanzenfarbstoffe.[16] Sie werden alle aus Isopentenyl-Pyrophosphat und dessen Isomer Dimethylallyl-Pyrophosphat zusammengesetzt. Ein therapeutisch genutztes Beispiel ist das Diterpen **3** (Abbildung 1).
Eine weitere sehr vielfältige Naturstoffgruppe sind die Polyketide. Sie leiten sich formal aus Acetateinheiten ab und werden durch Polyketidsynthasen (PKSs) durch decarboxylierende Claisen-Thioester-Kondensationen gebildet. Man unterscheidet drei Arten von Polyketidsynthasen nach ihrem Aufbau. Während bakterielle Typ I-PKSs multimodulare Megaenzyme sind und

beispielsweise Makrozyklen (z.B. **2**) synthetisieren, sind pilzliche Typ I-PKSs monomodular, iterativ-arbeitend und katalysieren beispielsweise die Bildung reduzierter Polyketide (z.B. **4**). Bei Typ II-PKSs liegen die Module als eigenständige, monofunktionelle Enzyme in einem Komplex vor. Sie synthetisieren aromatische polyzyklische Polyketide (z.B. **7**). Typ III-PKSs sind iterativ-arbeitende, multifunktionelle, homodimere Enzyme, welche oft aromatische Mono- oder Bizyklen synthetisieren. Bei Typ III-PKSs fehlt zudem das Acyl-Carrier-Protein (ACP).[17,18,19,20]
Ähnlich den bakteriellen Typ I-PKSs sind auch nichtribosomale Peptidsynthetasen (NRPS) modular aufgebaute Megaenzyme. Im Gegensatz zu diesen katalysieren sie jedoch die Ausbildung von Peptidbindungen und nutzten in der Regel Aminosäuren als Substrate. Nichtribosomale Peptide (NRPs) sind eine unverzichtbare Quelle für Antibiotika (z.B. **1**) und Immunsuppressiva (z.B. **5**). Allein β-Lactam-Antibiotika generieren einen Umsatz von 20 Milliarden US-Dollar jährlich.[21]
Anders als NRPs werden ribosomal synthetisierte und posttranslational modifizierte Peptide (RiPPs), wie der Name aussagt, ribosomal aus proteinogenen Aminosäuren synthetisiert und im Anschluss modifiziert. Eine generelle Nomenklatur ist noch nicht etabliert, jedoch können sie nach ihren Strukturelementen (z.B. Lanthipeptide), ihrer Wirkung (z.B. Bacteriocine) oder ihrer Herkunft (z.B. Microcine) gruppiert werden.[22]
Naturstoffe lassen sich auch nach ihren chemischen Eigenschaften oder Grundstrukturen einteilen. Alkaloide etwa sind Sekundärmetabolite mit einem zyklisch gebundenen, basischen Stickstoff. Sie leiten sich formal von Aminosäuren ab. Eines der wohl bekanntesten Beispiele aus der Welt der Mikroorganismen ist das Indolalkaloid Psilocybin (**8**), welches vor allem in Pilzen der Gattung *Psilocybe* zu finden ist.[15]
Betrachtet man nur Verbindungen, die sich strukturell von Aminosäuren ableiten, lassen sich diese nach der Anzahl der Aminosäureeinheiten in Mono-, Di- und Oligomere einteilen.

1.3 Biosynthese von mikrobiellen Sekundärmetaboliten

1.3.1 Biosynthese von Oligomeren durch nichtribosomale Peptidsynthetase

Der Mechanismus zur Biosynthese von Oligomeren durch NRPSs wurde 1971 anhand der von *Bacillus* sp. produzierten NRPs Gramicidin S und Tyrocidin beschrieben.[23] Es handelt sich um modular aufgebaute Megaenzyme, welche den Fettsäure-Synthasen ähnlich sind. Die bisher

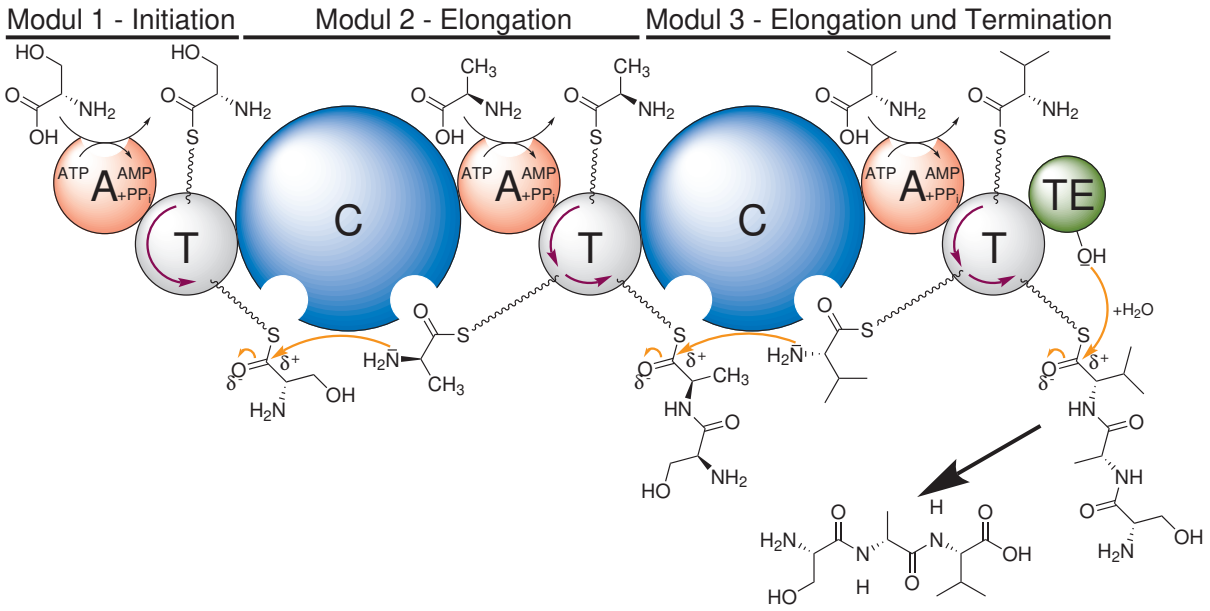

Abbildung 2: Ablauf der Synthese eines Tripeptids aus L-Serin, D-Alanin und L-Valin durch eine NRPS. Modul 1 initiiert die Synthese, während Modul 2 und 3 das Rückgrat verlängern. Abschließend wird die Peptidkette durch die Thioesterase abgeladen. Die nukleophilen Angriffe werden durch orange Pfeile dargestellt, das Wandern des 4'-PP-Arms durch violette Pfeile.

größte gefundene bakterielle NRPS mit 15 Modulen und einer Größe von 1.8 MDa ist die Kol-NRPS aus *Photorhabdus luminescens*.[24] In der Regel führt jedes Modul einer NRPS die Aktivierung und Kondensation einer einzelnen Aminosäure aus (Kollinearitätsregel). Die Module bestehen aus unterschiedlichen Proteindomänen, welche die für die Peptidsynthese notwendigen katalytischen Zentren beinhalten.[25] Die drei grundlegenden Domänen sind die Adenylierungsdomäne (A-Domäne), die Thiolierungsdomäne (T-Domäne) und die Kondensationsdomäne (C-Domäne), siehe Abbildung 2.[26]

Die A-Domäne (ca. 550 Aminosäuren) selektiert die richtige Aminosäure und aktiviert diese als Aminoacyladenylat unter ATP-Verbrauch. Die Selektion des Substrats findet über die umgebenden Aminosäuren in der Bindetasche der A-Domäne statt, welche mittels des nichtribosomalen Codes angegeben werden.[27] Über einen Sequenzabgleich einer unbekannten A-Domäne mit bereits charakterisierten A-Domänen kann über diese Codes eine Vorhersage der Substratspezifität getroffen werden. Jedoch lassen sich längst nicht alle Substratspezifitäten alleine mit dem Code erklären, weswegen z.B. physisch-chemische Fingerabdrücke oder auf *Hidden Markov Models* basierende Profile in Datensammlungen gespeist werden, um *in silico* Analysen mit höherer Genauigkeit zu ermöglichen. Während die Datenlage bereits zufriedenstellende

Ergebnisse bei bakteriellen NRPSs liefert, besteht bei pilzlichen NRPSs noch Verbesserungspotential.[28,29] Als Substrate dienen nicht nur, wie bei ribosomalen Peptiden üblich, proteinogene Aminosäuren, sondern auch ungewöhnliche Bausteine wie hydroxylierte (z.B. β-Hydroxytyrosin) und halogenierte (z.B. 6,7-Dichlortryptophan) Aminosäuren, β-Aminosäuren (z.B. β-Alanin), Aminobenzoesäuren (z.B. 4-Aminobenzoesäure) oder D-konfigurierte Aminosäuren. Im Ausnahmefall werden sogar α-Hydroxysäuren selektiert.[30,31]

Im nächsten Schritt wird das aktivierte Substrat kovalent als Thioester an den 4'-Phosphopantetheinyl (4'-PP)-Rest der T-Domäne (ca. 80-100 Aminosäuren) gebunden.[26] Der 4'-PP-Rest wurde zuvor über eine 4'-Phosphopantetheinyl-Transferase von Coenzym A beim sogenannten Priming auf ein konserviertes Serin der T-Domäne übertragen.[32,33] Der Rest fungiert als eine Art Transportarm und erlaubt die Wanderung der Substrate zwischen den verschiedenen katalytischen Zentren wie etwa die der C-Domänen (ca. 450 Aminosäuren). Diese kondensieren das Aminoacyl- und Peptidylsubstrat der T-Domänen über die Bildung einer Amidbindung aneinander. Hierbei katalysiert das aktive Zentrum den nucleophilen Angriff des Stickstoffes der aktivierten Aminosäure, welche an die nachfolgende T-Domäne gekoppelt ist (Donorseite) an das positiv polarisierte Kohlenstoffatom der Carbonyl-Funktion des vorhergehenden Substrates (Akzeptorseite). Das so erzeugte Peptid kann wiederum als elektrophiler Donor für die nächste C-Domäne dienen.[26] Zusätzlich können C-Domänen auch eine Substratspezifität an der Akzeptorseite besitzen, während an der Donorseite kaum differenziert wird.[34]

Wenn die verknüpfte Peptidkette alle Module durchlaufen hat, findet im Regelfall an einer Thioesterasedomäne (TE-Domäne, ca. 250 Aminosäuren) die Freisetzung statt. Die TE-Domäne katalysiert dabei den nukleophilen Angriff von Wasser oder Nukleophilen innerhalb des Moleküls, um beispielweise ein Makrolakton zu bilden.[35] In den Modulen können auch weitere Domänen zur Modellierung des Peptids vorhanden sein, wie beispielsweise eine Zyklisierungsdomäne (Cy-Domäne) zur Heterozyklisierung von Serin, Threonin oder Cystein, eine Epimerisierungsdomäne (E-Domäne) zur Epimerisierung, eine Oxidationsdomäne (Ox-Domäne) zur Oxidation oder eine Methylierungsdomäne (MT-Domäne) zur Methylierung.[36]

1.3.2 Biosynthese von Dimeren durch NRPS-ähnliche Enzyme

Neben den NRPSs gibt es auch NRPS-ähnliche Enzyme. Diese bestehen in der Regel aus einer A-, einer T- und einer C-terminalen TE-Domäne, besitzen keine C-Domäne und bilden daher

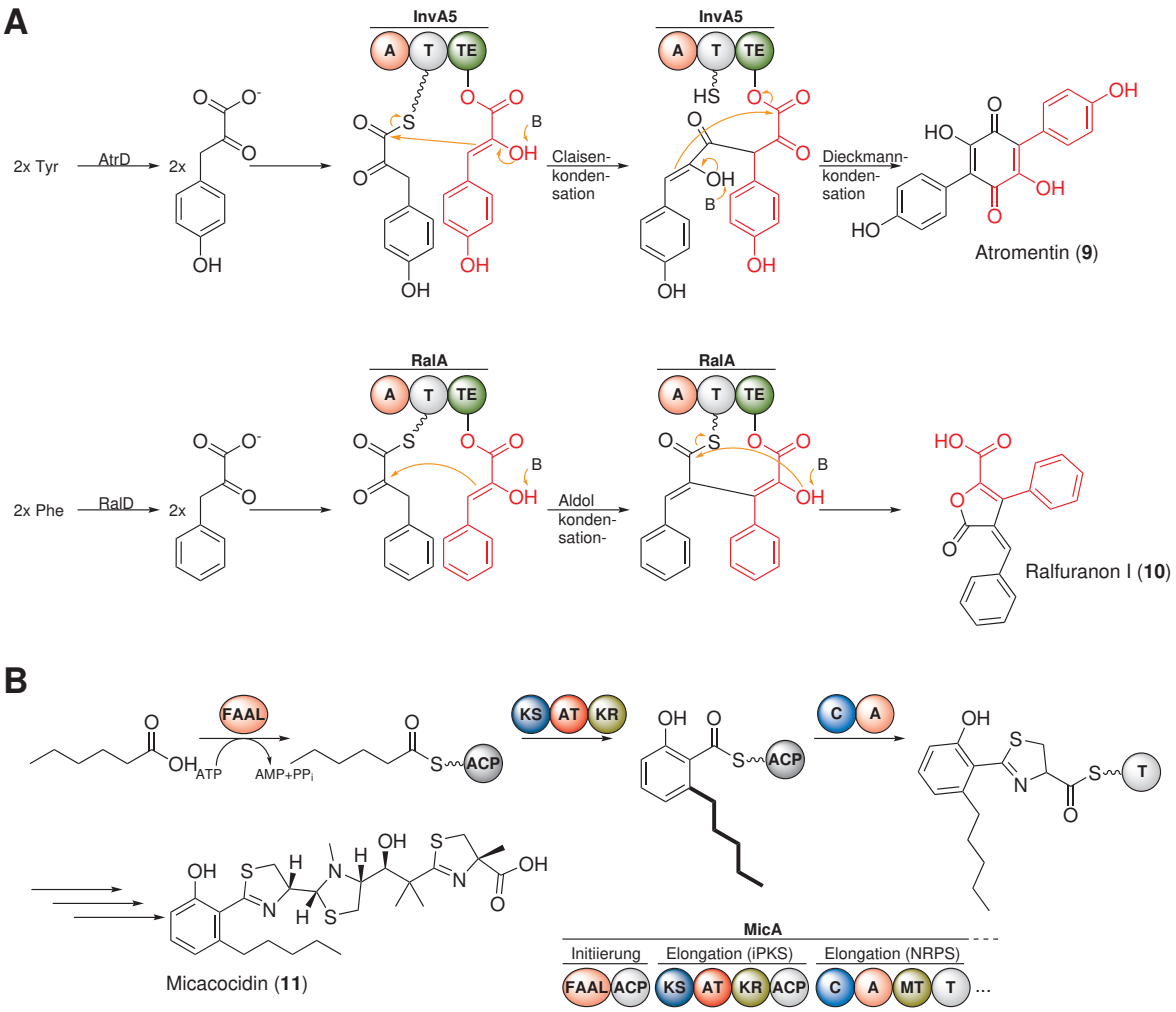

C

Typ	Domänenstruktur	Produkt
NRPS-ähnliche Enzyme	A T TE	Chinon, Furanon, Dioxolon ...
NRPS-ähnliche Enzyme	A T R	Piperazin
NRPS	A T [...] C A T TE	Peptid, Cyclopeptid
PKS/NRPS-Hybrid	FAAL ACP KS AT ACP [...] C A T TE	Lipopeptid
PKS	AT ACP KS AT ACP [...] TE	Polyketid

Abbildung 3: A: Ablauf der Synthese von **9** und **10** durch NRPS-ähnliche Enzyme. Anstelle einer C-Domäne knüpft eine TE-Domäne kovalente Bindungen zwischen den zuvor getrennten Monomeren. **B**: Darstellung eines Teiles der Biosynthese von **11**. Fettsäureaufladung durch FAAL, Elongation um drei Malony-CoA durch ein iterativ-arbeitendes PKS-Modul und Elongation und Zyklisierung von Cystein durch ein NRPS-Modul. **C**: Vergleich der Domänenarchitektur von NRPS, PKS, NRPS-ähnlichen Enzymen und PKS/NRPS-Hybriden.

keine Peptidbindung aus. Stattdessen katalysieren sie in den meisten Fällen die nicht-oxidative Homodimerisierung zweier α-Keto-Säuren, welche beispielweise aus Phenylalanin, Tyrosin und Tryptophan abgeleitet sind, zu Ringsystemen.[37]

So knüpft die Atromentin-Synthetase InvA5 aus *Paxillus involutus* zwei C-C-Bindungen (Claisenkondensation) zur Bildung des Chinonringes in Atromentin (**9**), siehe Abbildung 3.[38] Im Gegensatz dazu katalysiert die Furanonsynthetase RalA aus *Ralstonia (R.) solanacearum* die Bildung des Furanringes in Ralfuranon I (**10**) durch die Knüpfung einer C-C (Aldolkondensation) und einer C-O Bindung (nukleophile Addition).[39] Auch die ungewöhnliche Knüpfung zweier C-O Bindungen zu einem Dioxolanon oder von nicht-peptischen C-N Bindungen zu Piperazinen (durch eine Reduktionsdomäne anstelle einer TE-Domäne) wurden bereits beschrieben.[40,41]

1.3.3 Biosynthese von Oligomeren durch PKS/NRPS-Hybriden

Eine Mischform aus NRPS und PKS stellen PKS/NRPS-Hybride dar. Bei Micacocidin (**11**) aus *R. solanacearum* wird beispielsweise der Hexansäure-Startbaustein über eine iterativ-arbeitende bakterielle Typ I-PKS zu 6-Pentylsalicylat aufgebaut, um anschließend durch weitere NRPS und PKS-Module verlängert zu werden.[42,43] Die Aufladung von Fettsäuren wird durch Fettsäure-Acyl-AMP Ligasen (FAAL), die ähnlich wie A-Domänen arbeiten, katalysiert.[44,45] Die Fettsäure kann, wie es bei einigen Lipopeptiden der Fall ist, zusätzlich durch eine PKS verlängert und durch weitere Enzyme wie Aminotransferasen oder Oxygenasen modifiziert werden. Das Endprodukt, eine α-Hydroxy-β-aminofettsäure dient dann wiederum als Starter-Einheit für die Verlängerung durch eine NRPS.[46]

1.3.4 Biosynthese von Monomeren am Beispiel von Psilocybin

Auch Biosynthesewege, bei denen die Enzyme einzeln in der Zelle vorliegen und dort die Modifikation von Aminosäure-Monomeren katalysieren, tragen zur Naturstoffvielfalt bei. Aus den Aminosäure-Monomeren können niedermolekulare, pharmakologisch aktive Stoffe, wie etwa Psilocybin (**8**) entstehen. Während die Struktur von **8** bereits seit Albert Hofmann bekannt ist, blieben die Details der Biosynthese lange Zeit unklar.[47] Zwar wurden bereits einige Biosynthesewege vorgeschlagen, deren Richtigstellung erfolgte aber erst im Jahre 2017 (Abbildung 4).[48,49,50] PsiD katalysiert die Decarboxylierung von L-Tryptophan zu Tryptamin und gehört zur

Familie der PLP-unabhängigen-Phosphatidylserin-Decarboxylasen. Nach der Hydroxylierung von Tryptamin zu 4-Hydroxytryptamin durch die Monooxygenase PsiH wird durch die Kinase PsiK das Substrat phosphoryliert. Abschließend katalysiert die S-Adenosyl-L-Methionin-abhängige Methyltransferase PsiM die iterative N-Methylierung. Psilocin (**12**) entsteht nicht-enzymatisch aus **8**, kann aber durch PsiK wieder in **8** umgewandelt werden. Interessanterweise akzeptiert PsiD auch 4-Hydroxy-L-tryptophan als Substrat, was eine effizientere Möglichkeit zur biotechnologischen Produktion von Psilocybin eröffnete.[51]

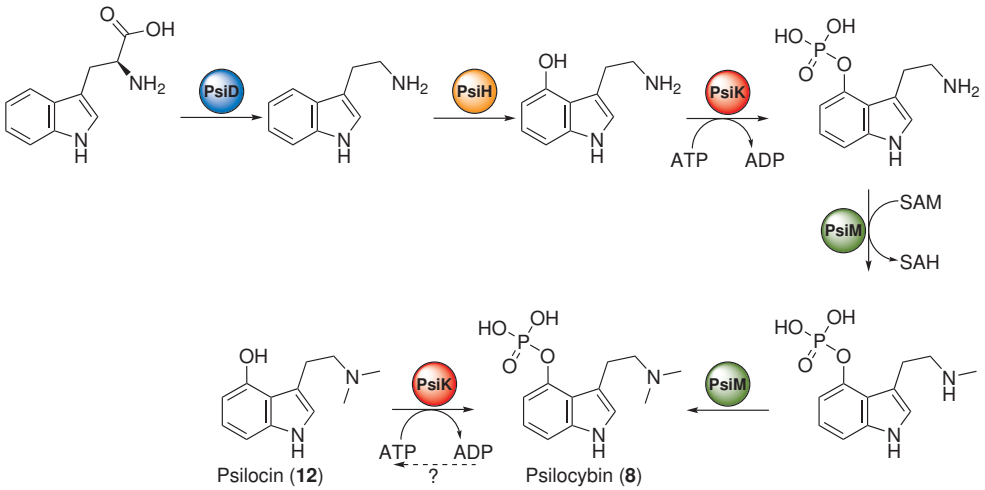

Abbildung 4: Natürliche Biosynthese von **8** und **12** aus Tryptophan in *Psilocybe*. Der gestrichelte Pfeil steht für eine hypothetische, intrazelluläre Dephosphorylierung.

1.4 Bekannte Naturstoffe aus den untersuchten Mikroorganismen

1.4.1 Monomere, dimere und oligomere Naturstoffe aus *Ralstonia solanacearum*

Das Betaproteobacterium *R. solanacearum* ist ein weltweit verbreitetes Pflanzenpathogen aus der Familie der Burkholderiaceae. Dabei ist es nicht, wie der Name vermuten lässt, auf Nachtschattengewächse als Wirt begrenzt, sondern verursacht eine tödliche Welke bei über 200 mono- und dicotylen Pflanzenspezies. Aufgrund der genetischen Vielfalt wird unter dem Begriff weniger eine Art gesehen als vielmehr ein Artenkomplex, welcher sich in vier Phylotypen unterteilen lässt.[52] Der Stamm GMI1000, welcher Gegenstand dieser Arbeit ist, lässt sich Phylotyp I zuordnen. Dessen Erbgut ist auf ein zirkuläres Chromosom (3.7 Mbp) und ein zirkuläres Megaplasmid (2.1 Mbp) aufgeteilt, deren Sequenzierung im Jahre 2002 das unerwartete

Biosynthesepotential von GMI1000 offenbarte.[53] Auf Grundlage der Genomsequenzierung erfolgte die Isolierung von Micacocidin (**11**),[42] Staphyloferrin B (**13**),[54] Hrp-dependent-factor (**14**)[55] und der Ralfuranone (**15**).[39,56]

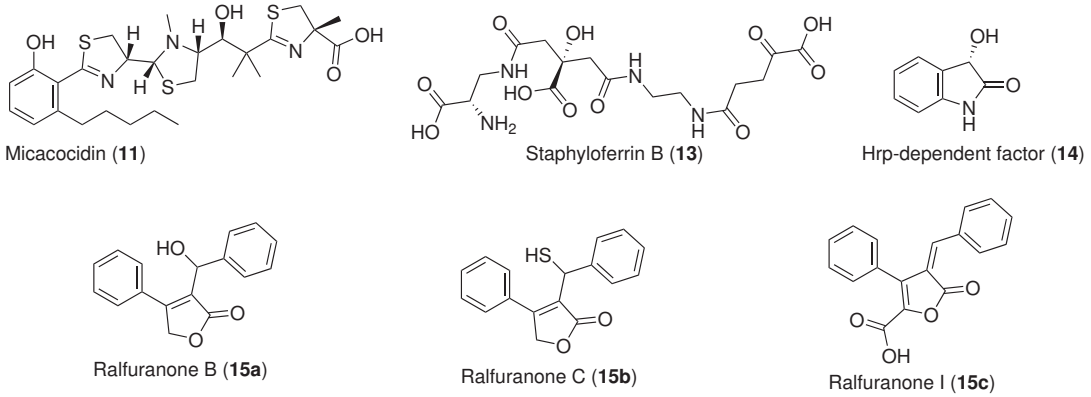

Abbildung 5: Bekannte Naturstoffe aus *R. solanacearum* GMI1000. **11** wird über einen PKS/NRPS-Hybriden, die Ralfuranone werden über NRPS-ähnliche Enzyme, **13** wird über NRPS-unabhängige Siderophor-Synthetasen (NIS) und **14** wird über einzelne Biosynthese-Enzyme, beispielweise eine Tryptophan-2,3-dioxygenase, hergestellt.

1.4.2 Oligomere Naturstoffe aus *Mortierella alpina*

Der weltweit vorkommende, bodenbesiedelnde Pilz *Mortierella (M.) alpina* ist den Mucoromycota (bzw. den umgangssprachlichen „Zygomyceten“) zuzuordnen. Die von Mortierellen produzierten Lipide können ungefähr 50 % des Trockengewichts ausmachen und bestehen zu einem hohen Anteil aus mehrfach ungesättigten Fettsäuren (PUFA).[57,58] Biotechnologisch wird daher der Pilz für die Gewinnung von Arachidonsäure (AA) für Kleinkinder- und Säuglingsnahrung eingesetzt. Die Extraktion aus Kulturen von *M. alpina* stellt eine der zur Zeit effizientesten Methoden zur Gewinnung von AA dar und wird generell als sicher betrachtet, wie es in der „Entscheidung 2008/968/EG der Kommission vom 12. Dezember 2008 zur Genehmigung des Inverkehrbringens von arachidonsäurereichem Öl aus *Mortierella alpina* als neuartige Lebensmittelzutat im Sinne der Verordnung (EG) Nr. 258/97 des Europäischen Parlaments und des Rates“ für den Stamm 1S-4 bekannt gegeben wurde.[59,60] Im Laufe der letzten Jahre rückte die Gattung *Mortierella* auch bei Naturstoffforschern vermehrt in den Fokus. In *M. verticillata* wurden Lacton-Verbindungen wie „CJ-12,950“ (**16**) und in einer noch nicht benannten *Mortierella* sp. die Mortiamide A-D (**17**) gefunden.[61,62] Aus *M. alpina* wurden

die Peptide „MBJ-0173“ (**18**), „MBJ-0174“ (**19**), Calpinactam (**20**) und „Ro 09-1679“ (**21**) isoliert (Abbildung 6).[63,64,65] Eine AntiSMASH-Analyse des publizierten Genoms von *M. alpina* ATCC 32222 offenbart eine große Anzahl an NRPS-Genclustern, deren Produkte noch nicht isoliert wurden.

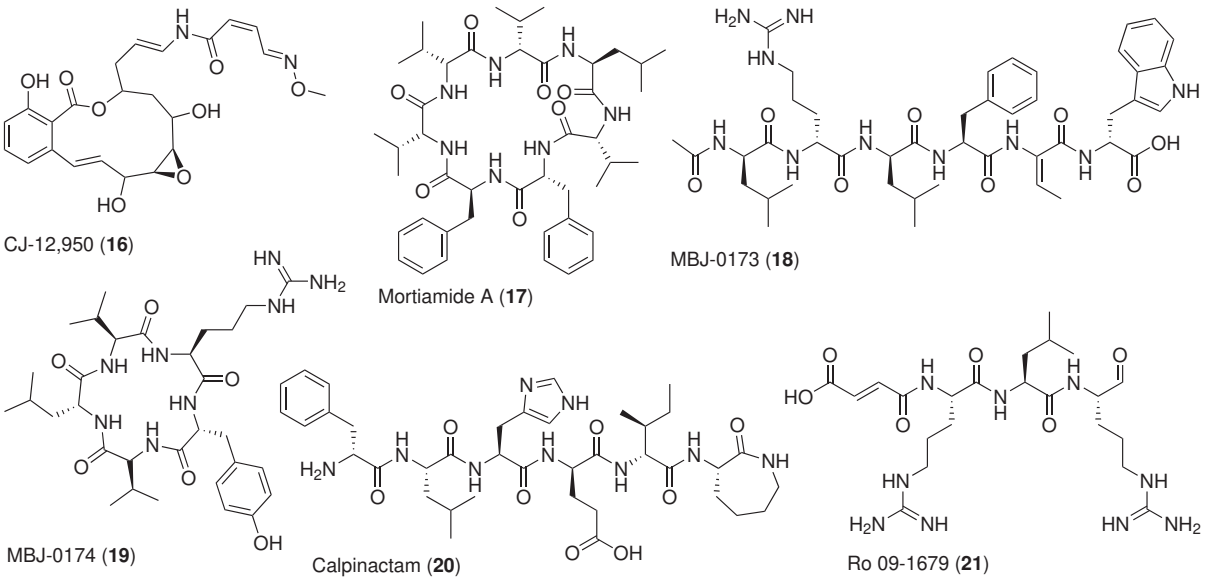

Abbildung 6: Bekannte oligomere Naturstoffe des Genus *Mortierella*. Bis auf **16** werden alle Verbindungen über NRPSs synthetisiert.

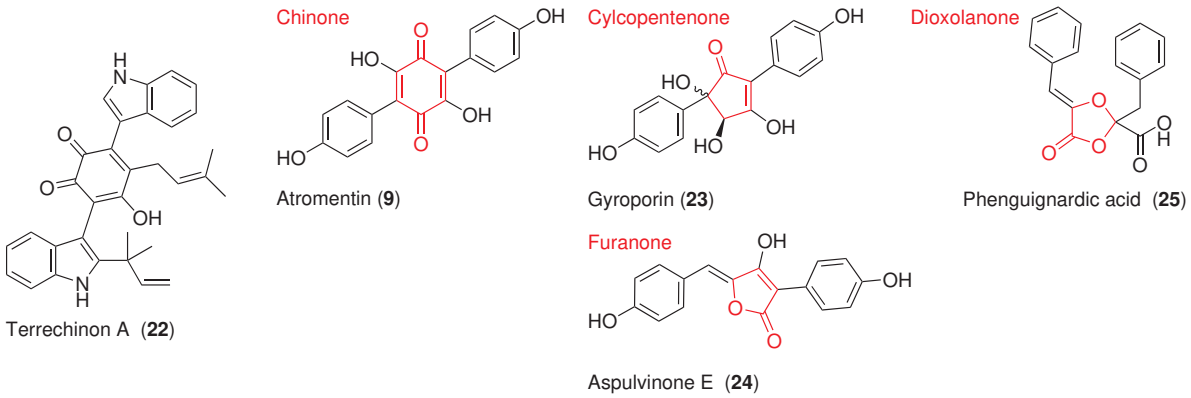

Abbildung 7: Ausgewählte dimere Naturstoffe der Genera *Aspergillus* und *Paxillus*. Die Verknüpfung der Monomere zu den rot-eingezeichneten Grundstrukturen werden über NRPS-ähnliche Enzyme katalysiert.

1.4.3 Dimere Naturstoffe aus den Gattungen *Aspergillus* und *Paxillus*

Im Reich der Pilze gibt es eine große Zahl an NRPS-ähnlichen Enzymen, welche Dimere ausgehend von aromatischen Aminosäuren bilden. Terrechinon A (**22**) aus *A. nidulans* war

das erste Produkt, welches nachweislich von einem solchem Enzym synthetisiert wird.[66,67] In den Jahrzehnten vorher waren bereits eine Vielzahl dieser Dimeren isoliert und chemisch charakterisiert worden. Darunter fallen zum Beispiel die in *Paxillus involutus* vorkommenden Chinone wie das Atromentin (**9**) oder Cyclopentenone wie Gyroporin (**23**).[38,68] *A. terreus* bildet unter anderem Furanone wie Aspulvinon E (**24**) oder Dioxolanone wie Phenguignardic acid (**25**) (Abbildung 7).[40,69] Während die Familie *Paxillus* zu den Basidiomycota gehört, gehört *Aspergillus* zu den Ascomycota. Dies zeigt wie weit verbreitet die Biosynthese von aromatischen Dimeren auch zwischen den einzelnen *Divisio* ist.

1.4.4 Tryptophan-abgeleitete Monomere aus *Psilocybe cubensis*

Das Genus *Psilocybe* (*P.*) gehört zu den Basidiomycota und lebt hauptsächlich saprobiotisch. Einige Arten wie *P. cubensis* und *P. cyanescens* werden aufgrund ihrer halluzinogenen Wirkung umgangssprachlich auch als *magic mushrooms* bezeichnet. Sie beinhalten als Hauptalkaloid Psilocybin (**8**), ein von Tryptophan abgeleitetes Monomer, welches zuerst von Albert Hofmann isoliert und dessen Struktur aufgeklärt wurde.[47,70] Das Psilocybin wird im Körper als Prodrug durch Dephosphorylierung zum aktiven Psilocin (**12**) umgewandelt. Dieses löst als modifiziertes Tryptamin vorwiegend über Partialagonismus am 5-HT_{2A}-Rezeptor seine pharmakologische Wirkung aus.[71,72] Zur Zeit erlebt Psilocybin eine Renaissance und wird als mögliches Medikament zur Behandlung von Depressionen,[73] Angstzuständen[74] und Nicotinabhängigkeit[75] in Erwägung gezogen. Zusätzlich konnten die demethylierten Derivate Baeocystin (**26**), Norbaeocystin (**27**) und Norpsilocin (**28**) isoliert werden (Abbildung 8).[76,77]

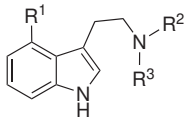

Psilocybin (**8**):	R^1=O-PO_3H_2	R^2=R^3=CH_3	Psilocin (**12**):	R^1=OH	R^2=R^3=CH_3
Baeocystin (**26**):	R^1=O-PO_3H_2	R^2=H, R^3=CH_3	Norpsilocin (**28**):	R^1=OH	R^2=H, R^2=CH_3
Norbaeocystin (**27**):	R^1=O-PO_3H_2	R^2=R^3=H			

Abbildung 8: Bekannte monomere Naturstoffe des Genus *Psilocybe*. Die Biosynthese erfolgt über einzelne Enzyme.

1.5 *Genome Mining*

Mit dem Eintreten in das post-genomische Zeitalter zeigte sich, dass das mikrobielle Biosynthesepotential weit unterschätzt wurde. Eine nicht unerhebliche Zahl an Biosynthesegenen in den

Genomen lassen sich nicht mit bekannten Sekundärmetaboliten verknüpfen.[78] Zwei mögliche Ursachen hierfür sind, dass für funktionell nicht charakterisierte (engl. *orphan*) Gencluster die Produkte noch nicht entdeckt wurden, weil sie beispielsweise nur in sehr geringen Mengen produziert werden oder dass „stille“ (engl. *silent*) Gencluster unter Laborbedingungen nicht exprimiert werden, also erst gar kein Produkt entsteht.[79] Ein sich schnell entwickelnder Ansatz beim Aufspüren dieser Metabolite ist das *Genome Mining*. Dieses bezeichnet den Prozess vom Auffinden der Biosynthesegene aus der Genomsequenz bis zum Vorliegen der aufgereinigten Moleküle durch das Durchführen bioinformatischer Analysen sowie das Anwenden genetischer und biochemischer Methoden.[80,81,14]

Zum ersten Mal kam das *Genome Mining* bei *Streptomyces coelicolor* A3(2) zur Anwendung. In dessen Genomsequenz wurden die Gene für eine nicht charakterisierte NRPS gefunden und die Substratspezifität der A-Domänen vorhergesagt. Über eine vergleichende metabolische Analyse einer Knockout-Mutante und dem Wildtyp wurde schließlich das zugehörige Peptidsiderophor namens Coelichelin gefunden.[82] Während die Genomanalysen damals weitestgehend manuell durchgeführt wurden, gibt es heute unzählige Anwendungen zur bioinformatischen Analyse, wie etwa AntiSMASH 4.0.[83] AntiSMASH vereint verschiedene Einzelprogramme unter einer Benutzeroberfläche und bietet, soweit möglich, damit einen umfassenden Einblick in das Biosynthesepotential von sequenzierten Mikroorganismen. Allerdings werden Biosynthesegene abseits der in Abschnitt 1.2 vorgestellten Kategorien häufig nicht erkannt. Beispiele hierfür sind die Biosynthesegene von Psilocybin oder von volatilen Stoffen wie modifizierten mittelkettigen Fettsäuren. Bioinformatische Analysen sind häufig eine Voraussetzung für das *Genome Mining*, wie etwa beim peptidogenomischen Ansatz. Hier wird über das Fragmentierungsmuster eines NRPs oder RiPPs bei der Tandem-Massenspektroskopie ein Teil der Aminosäuresequenz bestimmt und der Naturstoff mittels Bioinformatik dann mit den Biosynthesegenen verknüpft, die wiederum Auskunft über weitere Teile der Struktur geben können.[84]

Alternativ oder ergänzend zur Knockout-Methode werden die Zielgene häufig überexprimiert. Stille oder schwach aktivierte Gencluster werden unter die Kontrolle eines induzierbaren Promotors gebracht und durch dessen Induktion überexprimiert.[85] Eine oftmals stark erhöhte Produktion der Zielsubstanz ist ein klarer Vorteil dieses Ansatzes. Lässt sich der Organismus nur schwierig genetisch verändern bietet es sich an, den Gencluster in einem anderen Mikroorganismus heterolog zu exprimieren, was beispielsweise entscheidend zur Aufklärung der Struktur

und Biosynthese des neuartigen Gyraseinhibitors Albicidin (aus *Xanthomonas albilineans* in *Xanthomonas axonopodis* pv. *vesicatoria*) beigetragen hat.[86] Ohne genetische Manipulation können stille Gencluster auch mit der **O**ne **S**train-**MA**ny **C**ompounds (OSMAC)-Methode aktiviert werden. Hierbei werden Veränderungen im Metabolom durch eine Veränderung der Kultivierungsbedingungen (pH, Temperatur, Sauerstoffgehalt, Lichtexposition, etc.) erreicht.[87,88] Das Standardrepertoire kann beliebig erweitert werden, etwa um die Kokultivierung mit anderen Organismen oder Einsatz epigenetischer Modulatoren.[89,90] Ein erfolgreiches Beispiele ist die Entdeckung des Jagaricin aus dem Champignonpathogen *Janthinobacterium agaricidamnosum* durch MALDI-MS-Analysen der bakteriell induzierten Läsionen auf Champignons nach Kokultivierung.[91]

Eine weitere Methode im Werkzeugkasten des GM ist der genomisotopische Ansatz.[9] Die Substrate der Biosynthese-Enzyme werden bioinformatisch vorhergesagt, um anschließend das Medium mit einem markierten Substrat (z.B. ^{15}N-markierte Aminosäuren) zu supplementieren. Auf Grundlage des Isotopenmusters im MS-Spektrum oder der Signalintensitäten in NMR-Spektren werden die Extrakte fraktioniert und die markierten Metabolite isoliert. Dieser Ansatz führte zur Entdeckung der Orfamide (aus *Pseudomonas fluorescens* Pf-5) und deren Zuordnung zu einem bis dahin funktionell nicht charakterisierten Genclusters.[92]

2 Zielsetzung dieser Arbeit

Einen ersten Schritt zur Gewinnung neuer Wirkstoffe aus Mikroorganismen stellt die Isolation und Strukturaufklärung neuer Sekundärmetabolite, die Aufklärung deren Biosynthese und gegebenenfalls deren biotechnologische Herstellung dar.

Isolierung und Strukturaufklärung von aminosäurehaltigen Oligomeren

Ein NRP von *R. solanacearum* GMI1000, dessen NRPS von den Genen *rmyA* und *rmyB* codiert wird, könnte eine Beteiligung an dessen Virulenz besitzen. In den Rohextrakten von *M. alpina* ATCC 32222 befinden sich einige Verbindungen mit Massen und UV-Absorptionen, die auf NRPs, welche aromatische Aminosäuren enthalten, schließen lassen. Im Zuge dieser Arbeit sollen diese unbekannten aminosäurehaltigen Naturstoffe isoliert und aufgereinigt werden. Anschließend soll die Struktur über NMR-Spektroskopie, chemische Derivatisierung und Synthesen aufgeklärt werden. Abschließend sollen die Biosynthese dargelegt sowie die Bioaktivität untersucht werden (insbesondere der Beitrag zur Virulenz von *R. solanacearum*).
Eine Übersichtsarbeit soll die Vielfalt der Naturstoffbiosynthese von pflanzenpathogenen Bakterien aus genomischer Perspektive zeigen und somit den gefundenen Naturstoff von *R. solanacearum* in den Kontext zu anderen Sekundärmetaboliten aus Pflanzenpathogenen setzen.

Strukturaufklärung von aminosäure-abgeleiteten Monomeren und Dimeren zur Charakterisierung von Biosynthese-Enzymen und -Routen

NRPS-ähnliche Enzyme sind noch nicht zufriedenstellend charakterisiert. Im Rahmen dieser Arbeit sollen die Strukturen neuer Sekundärmetabolite, welche von Atromentin-Synthetase in *Aspergillus* heterolog produziert werden, aufgeklärt werden. Die Ergebnisse sollen dazu beitragen die wirtsabhängige Produktion von strukturell verschiedenen Sekundärmetaboliten durch Atromentin-Synthetasen über *cross-chemistry* zu erklären und damit die Ringbildung durch Thioesterase-Domänen näher beleuchten.
Durch Vorläufer-gesteuerte Biosynthese können, aufgrund niedriger Substratspezifitäten von Enzymen, neue Produkte generiert werden. Im Rahmen der Etablierung einer effizienteren Route zur biotechnologischen Herstellung von Psilocybin unter Verwendung der Tryptophansynthase TrpB, sollen in dieser Arbeit die Strukturen von nicht natürlichen Produkten strukturell

aufgeklärt werden. Die Ergebnisse sollen die Substratflexibilität von TrpB und damit dessen Wert zur biotechnologischen Herstellung neuer Psilocybin-Derivate unterstreichen.

3 Publikationen

3.1 Publikation 1

Structure of Ralsolamycin, the Interkingdom Morphogen from the Crop Plant Pathogen *Ralstonia solanacearum*

Baldeweg, F.; Kage, H.; Schieferdecker, S.; Allen, C.; Hoffmeister, D.; Nett, M. *Org. Lett.* **2017**, *19*, 4868–4871.

Zusammenfassung:
R. solanacearum gehört zu den weltweit wichtigsten Pflanzenpathogenen. Eine vorhergehende Publikation berichtete über die Entdeckung eines neuen, Chlamydosporen induzierenden Lipopeptids aus dem Modellstamm GMI1000. Die strukturelle Charakterisierung über Tandem-Massenspektrometrie des Metaboloms war jedoch unzureichend. Die volle Strukturaufklärung des Lipopeptids Ralsolamycin mittels NMR-Spektroskopie und Tandem-MS nach Isolation des Reinstoffes wird nun in dieser Studie präsentiert. Die Stereochemie wurde mittels chemischer Derivatisierung und bioinformatischer Vorhersagen zugeordnet. Auf Grundlage der Struktur konnte die Genomsequenz des Biosynthesegenclusters als fehlerhaft erkannt und ausgebessert werden. Die Resultate dieser Arbeit unterstreichen den Wert von chemischen und molekularbiologischen Methoden bei der Komplementierung von bioinformatischen Vorhersagen.

Angaben zum Eigenanteil von Florian Baldeweg (50%):
Kultivierung der Bakterien und Isolation von Ralsolamycin. NMR-basierte Strukturaufklärung sowie Bestimmung der absoluten Konfiguration der Aminosäuren. Charakterisierung des Beitrags zur Virulenz. Klonierung der A-Domäne aus Modul 5 und Bestimmung der Substratspezifität. Phylogenetische Analysen der C-Domänen. Mitarbeit am Manuskript.

Jena, den

Prof. Dirk Hoffmeister

Organic LETTERS

Letter

pubs.acs.org/OrgLett

Structure of Ralsolamycin, the Interkingdom Morphogen from the Crop Plant Pathogen *Ralstonia solanacearum*

Florian Baldeweg,[†] Hirokazu Kage,[‡] Sebastian Schieferdecker,[§] Caitilyn Allen,[∥] Dirk Hoffmeister,[†] and Markus Nett*[,‡]

[†]Department of Pharmaceutical Microbiology at the Hans-Knöll-Institute, Friedrich-Schiller-University Jena, Winzerlaer Strasse 2, 07745 Jena, Germany

[‡]Department of Biochemical and Chemical Engineering, Technical University Dortmund, Emil-Figge-Strasse 66, 44227 Dortmund, Germany

[§]Leibniz Institute for Natural Product Research and Infection Biology, Hans-Knöll-Institute, Beutenbergstrasse 11a, 07745 Jena, Germany

[∥]Department of Plant Pathology, University of Wisconsin—Madison, 1630 Linden Drive, Madison, Wisconsin 53706, United States

Supporting Information

ABSTRACT: Ralsolamycin, an inducer of chlamydospore formation in fungi, was recently reported from the plant pathogenic bacterium *Ralstonia solanacearum*. Although interpretation of tandem mass data and bioinformatics enabled a preliminary chemical characterization, the full structure of ralsolamycin was not resolved. We now report the recovery of this secondary metabolite from an engineered *R. solanacearum* strain. The structure of ralsolamycin was elucidated by extensive spectroscopic analyses. Chemical derivatization as well as bioinformatics were used to assign the absolute stereochemistry. Our results identified an erroneous genome sequence, thereby emphasizing the value of chemical methods to complement bioinformatics-based procedures in natural product research.

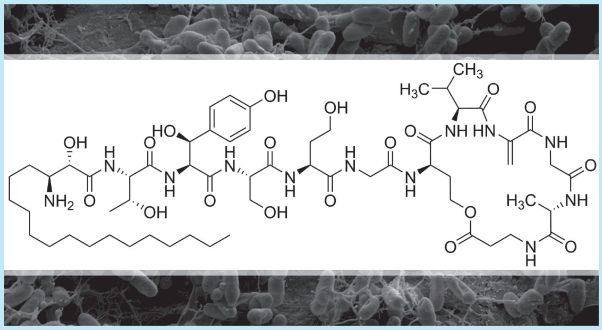

Ralstonia solanacearum is a globally distributed bacterial plant pathogen that causes a lethal wilting disease in economically important crops, among them potato, tomato, tobacco, and banana.[1] Over the years, *R. solanacearum* has been identified as a producer of structurally diverse secondary metabolites,[2−5] and several studies focused on the biosyntheses[6] and biological activities[7] of the isolated compounds. While the ralfuranone family of natural products might have a role in virulence,[7b,c] other secondary metabolites from *R. solanacearum* appear to contribute to the competitiveness of the phytopathogen outside its host plants.[2,3] Recently, a novel diffusible lipopeptide was reported from the *R. solanacearum* model strain GMI1000.[8] This compound, ralsolamycin, was found to induce chlamydospore formation in fungi. Moreover, it was observed that the natural product-mediated process initiates an invasion of fungal hyphae. These findings indicate that *R. solanacearum* is capable of an endofungal lifestyle, which has important implications for the persistence of this agriculturally relevant phytopathogen.[8] Although ralsolamycin was subject to a preliminary characterization by MS−MS and bioinformatic analyses, only a partial structure was deduced in the original study,[8] and no stereochemical information was provided. We thus set out to clarify the structure of this ecologically important natural product.

The biosynthesis locus of ralsolamycin includes the two nonribosomal peptide synthetase (NRPS) genes *rmyA* and *rmyB* (Figure 1A). Their protein products were reported to constitute a lipopeptide assembly line featuring nine NRPS modules along with a fatty acid loading and extension module.[8] To facilitate the identification of ralsolamycin from culture extracts of *R. solanacearum* GMI1000, we used insertional mutagenesis to disrupt the *rmyA* gene from the ralsolamycin biosynthetic locus. Comparative metabolic profiling of the wild type and mutant strain revealed a distinctive peak, which was exclusively present in wild type extracts (Figure 1B). Its mass (m/z 1291.7 $[M + H]^+$) was consistent with the value previously reported for ralsolamycin.[8] Initial attempts to further characterize this compound were unsuccessful because only trace amounts could be recovered from GMI1000 cultures grown in standard laboratory media. To secure sufficient quantities of ralsolamycin for structure elucidation, the native regulation of ralsolamycin biosynthesis was overridden by placing the expression of *rmyA* and *rmyB* under the control of an arabinose-inducible promoter (Figure 1B). This approach allowed the production of ∼200 mg of ralsolamycin from 30 L of culture broth, which was purified by

Received: July 28, 2017
Published: August 28, 2017

DOI: 10.1021/acs.orglett.7b02329
Org. Lett. 2017, 19, 4868−4871

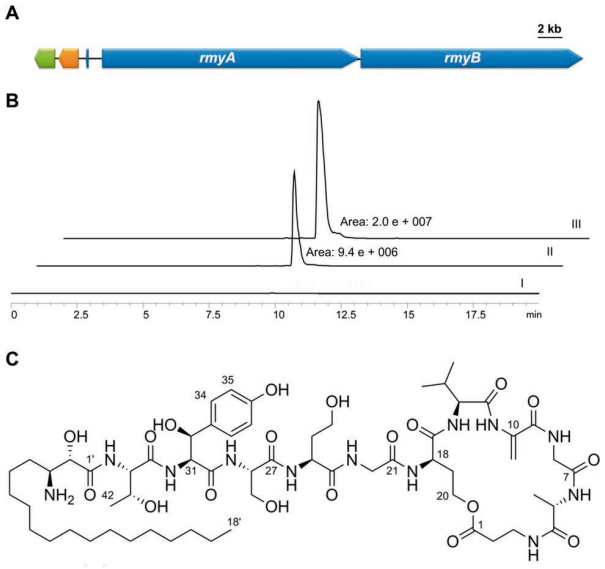

Figure 1. (A) Organization of the ralsolamycin gene locus; NRPS and accessory genes (blue), transporter gene (green), hypothetical gene (orange). (B) Extracted ion chromatograms of m/z 1291.7 $[M + H]^+$ from the *rmyA* disruption mutant (profile I), the wildtype (profile II), and the overproduction strain upon arabinose induction (profile III). (C) Structure of ralsolamycin.

flash column chromatography and RP-HPLC. Furthermore, we identified a ralsolamycin derivative (m/z 1305.7 $[M + H]^+$) as a minor component in the culture of the overexpression strain (Figure S1). The isolation and structure elucidation of this compound are described in the Supporting Information.

High-resolution ESIMS of ralsolamycin yielded m/z 1291.7142 for the $[M + H]^+$ ion, which is consistent with a molecular formula of $C_{60}H_{98}N_{12}O_{19}$ and accounts for 18 degrees of unsaturation. Analysis of the ^{13}C NMR spectrum revealed 12 carbonyl signals (Table S1). Six signals, of which two showed exceptionally high intensities, possessed chemical shifts in the aromatic range of the spectrum. Following an inspection of HSQC, ^1H NMR, and HMBC spectra, it was evident that each of the signals at 127.5 and 114.5 ppm represented two magnetically equivalent carbon atoms (C-34/C-38 and C-35/C-37, respectively). In conclusion, ralsolamycin must contain four C−C double bonds. Together with the carbonyl groups, this left two degrees of unsaturation, which were hence ascribed to ring structures. Extensive 1D and 2D NMR measurements (Figure S2) allowed the successive identification of 11 amino acid residues. Among them were alanine, two glycines, serine, threonine, valine, as well as β-alanine (Ala-b), β-hydroxytyrosine (Bht), dehydroalanine (Dha), and two homoserines (Hse). Dipolar and scalar interactions of the amide protons with adjacent groups were used to determine the amino acid sequence in ralsolamycin. A long-range correlation from the γ-methylene protons of the Hse-2 residue to the carbonyl group of Ala-b established the lactone linkage in the peptide chain. The remaining carbons and heteroatoms not accounted for by amino acids constituted a 3-amino-2-hydroxyoctadecanoyl moiety, which could be connected to the N-terminal Thr residue on the basis of HMBC data. The planar structure of ralsolamycin was subsequently confirmed by MALDI-TOF/TOF fragmentation (Figures S3 and S4).

Surprisingly, the Hse-Gly-Hse motif in ralsolamycin was not consistent with the number of NRPS modules in the predicted RmyA sequence.[8] The apparent lack of two modules and the ensuing violation of the colinearity rule, which is valid for most NRPSs,[9] could not be explained by an iterative usage of the C-terminal module in RmyA, considering the extension of the peptide chain with structurally different amino acids (i.e., Gly and Hse). Instead, we hypothesized that the reported sequence of RmyA might be incomplete. To test this possibility, we manually sequenced the *rmyA* gene and its surrounding genomic region. This approach confirmed that the nucleotide sequence of the *rmyA* gene is actually about 6.3 kb larger than previously reported,[10] and it encodes for two additional NRPS modules. Subsequent bioinformatic[11] and biochemical analyses revealed the amino acid substrates of RmyA and RmyB (Table S2). The deduced sequence was fully consistent with the results from the spectroscopic analysis.

In order to determine the configuration of the amino acid monomers, the lipopeptide was hydrolyzed with HCl and derivatized with Nα-(2,4-dinitro-5-fluorophenyl)-L-leucinamide (L-FDLA) and D/L-FDLA, respectively. The advanced Marfey's analysis[12] indicated the exclusive presence of L-Ala, L-Ser, L-Thr, and L-Val in the acid hydrolysate (Figure S5). In the case of Hse, both the D- and the L-forms were identified. The occurrence of the D-amino acid suggested that at least one condensation (C) domain of RmyA or RmyB acts as a ^DC_L catalyst with epimerase activity. A distinctive feature of dual epimerization/condensation (E/C) domains is the presence of two conserved His motifs.[13] A sequence based analysis uncovered that two C domains of RmyB fulfilled this criterion. While the E/C domain of the third module in RmyB remains without consequences due to a dehydration event, the E/C domain of the first module can be expected to invert the configuration of the preceding Hse moiety. A phylogenetic tree built from a large number of C domains confirmed this finding (Figure S6). Therefore, we concluded that the lactone-forming Hse residue in ralsolamycin must be D-configured. The configurational assignment of the Bht residue was challenging because no derivatives of this amino acid were detected after FDLA treatment of the ralsolamycin hydrolysate. It is well-known that Bht and the related β-methoxytyrosine are prone to acid-catalyzed decomposition,[14,15] thereby limiting the use of the standard Marfey method. However, the coupling constant between the α and β protons in Bht was reported to enable a differentiation of its *syn*- and *anti*-conformers.[14] In the case of ralsolamycin, the observed coupling constant of 2.9 Hz indicated an *anti*-configuration of the respective protons (31*R**,32*R**). Because the experimentally determined configuration of the Ala, Ser, Thr, Val, and Hse residues was fully consistent with the arrangement of C and E/C domains in the biosynthetic assembly line (Figure 2), it was concluded that the L-Tyr building block is not epimerized after its loading onto RmyA. Since the following hydroxylation of the β carbon in the Tyr moiety[16] does also not change the configuration at the α carbon, we assigned the absolute configuration of the two chiral centers in the Bht moiety as (31*S*,32*S*). The configuration at C-3′ of the fatty acid moiety was determined as *S* by the advanced Marfey's method.[17] To resolve the configuration at C-2′, 3-amino-2-hydroxystearate was purified from the acid hydrolysate and converted into the corresponding 2-oxazolidinone derivative. The coupling constant between the oxazolidinone ring protons (J = 8.5 Hz) indicated a *cis* stereochemistry,[18] and this meant that the absolute configuration at C-2′ was *S* in ralsolamycin (Figure 1C).

DOI: 10.1021/acs.orglett.7b02329
Org. Lett. 2017, 19, 4868−4871

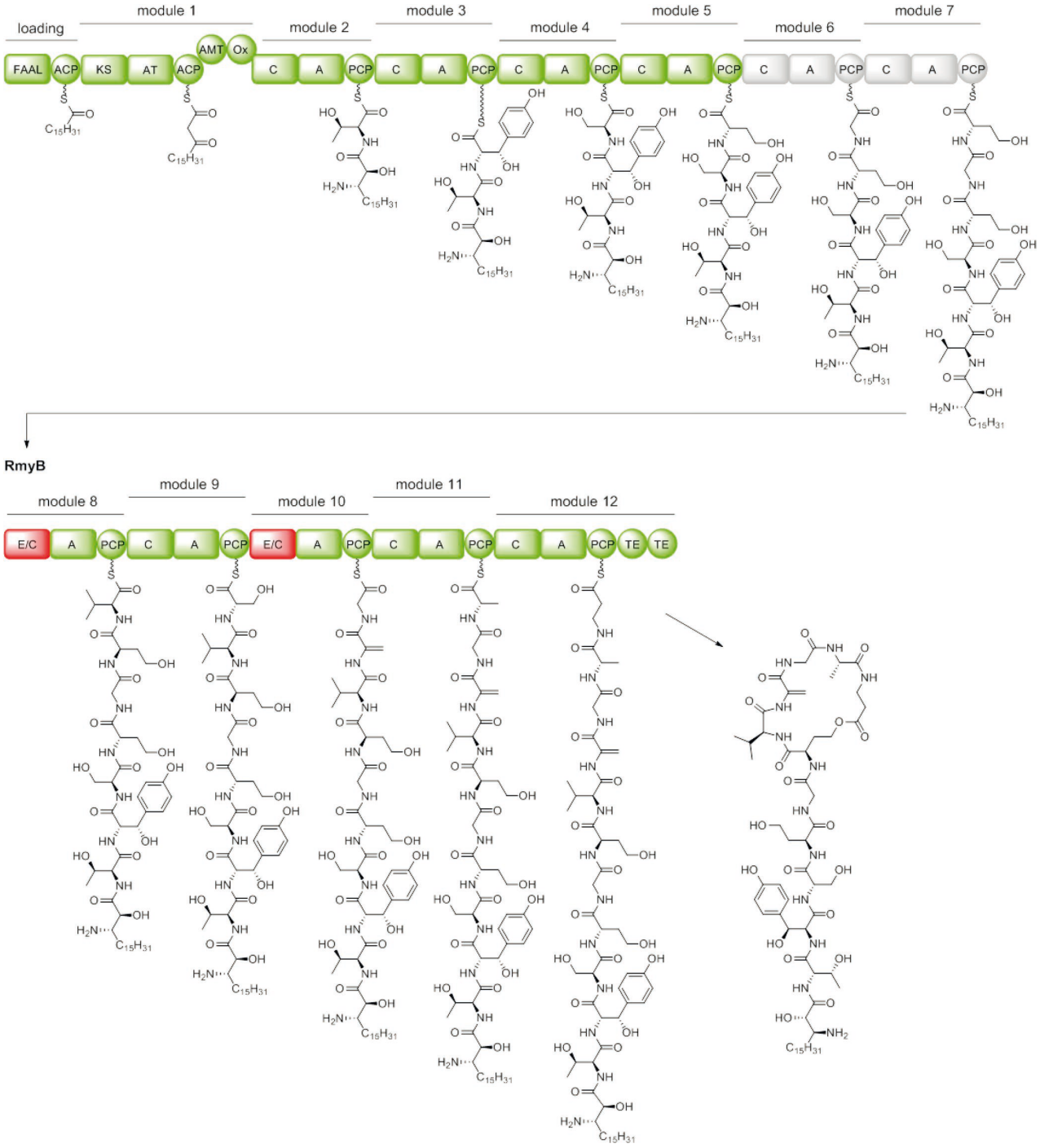

Figure 2. Proposed biosynthesis of ralsolamycin. Domains that are highlighted in white were missing in the original annotation of RmyA. Domain notation: FAAL, fatty acyl-AMP ligase; ACP, acyl carrier protein; KS, ketoacyl synthase; AT, acyl transferase; AMT, aminotransferase; Ox, oxidase; C, condensation; A, adenylation; PCP, peptidyl carrier protein; E/C, epimerization/condensation; TE, thioesterase.

Based on the domain organization of RmyA and RmyB, a plausible biosynthetic model can be proposed for ralsolamycin (Figure 2). The assembly would hence start with palmitic acid, which is tethered to the N-terminal ACP domain of RmyA upon ATP-dependent activation. A decarboxylative thio-Claisen condensation with malonate yields a β-ketostearyl acyl unit, which is transaminated in the β position and hydroxylated at the α carbon atom. Afterward, the 11 amino acid residues of ralsolamycin are sequentially incorporated by condensation reactions before the mature lipopeptide is released from the assembly line by intramolecular lactonization. A phylogenetic analysis confirmed that both TE domains of RmyB are type I thioesterases (Figure S7). Precedence for the presence of two consecutive C-terminal thioesterase (TE) domains comes from the biosynthesis of cyclic lipopeptides in *Pseudomonas* spp., where the tandem TE domains were shown to improve the

DOI: 10.1021/acs.orglett.7b02329
Org. Lett. 2017, 19, 4868−4871

macrocyclization efficiency.[19] The only structural features of ralsolamycin that cannot be deduced from the domain architecture of RmyA and RmyB include the β-hydroxylation of the Tyr residue and the dehydration that gives rise to the Dha moiety in the lactone ring. Evidence from other natural product pathways suggests that the former reaction could be catalyzed by a discrete P450 monooxygenase, which requires a carrier protein-bound substrate for oxidation.[16] Considering the predicted substrate specificity of module 3 (Table S2), this scenario is also likely for ralsolamycin biosynthesis. A candidate enzyme for this transformation is encoded in the *R. solanacearum* genome, even though the corresponding gene (RSp0709) is located about 77 kb downstream of the *rmy* locus. Unlike the situation in ribosomally made peptides, the enzymatic basis for the dehydration of serine and threonine residues in NRPS-derived natural products is not known.[20]

The virulence of the ralsolamycin-deficient mutant was compared with the GMI1000 wild-type strain by direct petiole inoculation of tomato plants. However, no significant differences became evident. We also evaluated the phytotoxicity of HPLC-purified ralsolamycin in a necrosis assay using tomato leaves. Again, no effects were observed, suggesting that ralsolamycin has a negligible role in the pathogenesis of wilting disease.

In summary, we resolved the full structure of ralsolamycin including its absolute configuration by combining spectroscopic methods, chemical derivatization, and bioinformatics. A prerequisite was the isolation of sufficient material, which became possible with an engineered strain and optimized production conditions. As opposed to current trends in natural product research, which favor purely bioinformatic methods for structure determination, the largely NMR-based analysis of ralsolamycin turned out to be instrumental for the curation of genomic data. The present study unveiled the limits of in silico structure predictions and highlights, once more, the indispensable role of analytical chemistry in structure elucidation.

■ ASSOCIATED CONTENT

Supporting Information

The Supporting Information is available free of charge on the ACS Publications website at DOI: 10.1021/acs.orglett.7b02329.

Details of isolation, derivatization and chemical characterization of ralsolamycins, cloning strategy and phylogenetic analysis (PDF)

■ AUTHOR INFORMATION

Corresponding Author

*E-mail: markus.nett@bci.tu-dortmund.de.

ORCID

Markus Nett: 0000-0003-0847-086X

Notes

The authors declare no competing financial interest.

■ ACKNOWLEDGMENTS

F.B. thanks the graduate school Jena School for Microbial Communication (JSMC) for a doctoral fellowship. We thank J. Pauly (Department of Pharmaceutical Microbiology, Hans-Knöll-Institute Jena) and M. F. Kreutzer (Hans-Knöll-Institute Jena) for preliminary analyses as well as A. Perner and H. Heinecke (Hans-Knöll-Institute Jena) for recording mass and NMR spectra, respectively.

■ REFERENCES

(1) (a) Ephinstone, J. G. The current bacterial wilt situation: A global overview. In *Bacterial wilt disease and the Ralstonia solanacearum species complex*; Allen, C., Prior, P., Hayward, A. C., Eds.; American Phytopathological Society: St. Paul, MN, 2005; pp 9−28. (b) Genin, S.; Denny, T. P. *Annu. Rev. Phytopathol.* **2012**, *50*, 67.

(2) Bhatt, G.; Denny, T. P. *J. Bacteriol.* **2004**, *186*, 7896.

(3) Delaspre, F.; Nieto Penalver, C. G.; Saurel, O.; Kiefer, P.; Gras, E.; Milon, A.; Boucher, C.; Genin, S.; Vorholt, J. A. *Proc. Natl. Acad. Sci. U. S. A.* **2007**, *104*, 15870.

(4) Schneider, P.; Jacobs, J. M.; Neres, J.; Aldrich, C. C.; Allen, C.; Nett, M.; Hoffmeister, D. *ChemBioChem* **2009**, *10*, 2730.

(5) Kreutzer, M. F.; Kage, H.; Gebhardt, P.; Wackler, B.; Saluz, H. P.; Hoffmeister, D.; Nett, M. *Appl. Environ. Microbiol.* **2011**, *77*, 6117.

(6) (a) Wackler, B.; Schneider, P.; Jacobs, J. M.; Pauly, J.; Allen, C.; Nett, M.; Hoffmeister, D. *Chem. Biol.* **2011**, *18*, 354. (b) Pauly, J.; Nett, M.; Hoffmeister, D. *J. Nat. Prod.* **2014**, *77*, 1967. (c) Kai, K.; Ohnishi, H.; Kiba, A.; Ohnishi, K.; Hikichi, Y. *Biosci., Biotechnol., Biochem.* **2016**, *80*, 440. (d) Kage, H.; Kreutzer, M. F.; Wackler, B.; Hoffmeister, D.; Nett, M. *Chem. Biol.* **2013**, *20*, 764. (e) Kage, H.; Riva, E.; Parascandolo, J. S.; Kreutzer, M. F.; Tosin, M.; Nett, M. *Org. Biomol. Chem.* **2015**, *13*, 11414.

(7) (a) Pauly, J.; Spiteller, D.; Linz, J.; Jacobs, J.; Allen, C.; Nett, M.; Hoffmeister, D. *ChemBioChem* **2013**, *14*, 2169. (b) Kai, K.; Ohnishi, H.; Mori, Y.; Kiba, A.; Ohnishi, K.; Hikichi, Y. *ChemBioChem* **2014**, *15*, 2590. (c) Mori, Y.; Ishikawa, S.; Ohnishi, H.; Shimatani, M.; Morikawa, Y.; Hayashi, K.; Ohnishi, K.; Kiba, A.; Kai, K.; Hikichi, Y. *Mol. Plant Pathol.* **2017**, DOI: 10.1111/mpp.12537. (d) Kreutzer, M. F.; Kage, H.; Herrmann, J.; Pauly, J.; Hermenau, R.; Müller, R.; Hoffmeister, D.; Nett, M. *Org. Biomol. Chem.* **2014**, *12*, 113.

(8) Spraker, J. E.; Sanchez, L. M.; Lowe, T. M.; Dorrestein, P. C.; Keller, N. P. *ISME J.* **2016**, *10*, 2317.

(9) Strieker, M.; Tanović, A.; Marahiel, M. A. *Curr. Opin. Struct. Biol.* **2010**, *20*, 234.

(10) Salanoubat, M.; Genin, S.; Artiguenave, F.; Gouzy, J.; Mangenot, S.; Arlat, M.; Billault, A.; Brottier, P.; Camus, J. C.; Cattolico, L.; Chandler, M.; Choisne, N.; Claudel-Renard, C.; Cunnac, S.; Demange, N.; Gaspin, C.; Lavie, M.; Moisan, A.; Robert, C.; Saurin, W.; Schiex, T.; Siguier, P.; Thebault, P.; Whalen, M.; Wincker, P.; Levy, M.; Weissenbach, J.; Boucher, C. A. *Nature* **2002**, *415*, 497.

(11) Röttig, M.; Medema, M. H.; Blin, K.; Weber, T.; Rausch, C.; Kohlbacher, O. *Nucleic Acids Res.* **2011**, *39*, W362.

(12) (a) Marfey, P. *Carlsberg Res. Commun.* **1984**, *49*, 591. (b) Fujii, K.; Ikai, Y.; Oka, H.; Suzuki, M.; Harada, K.-i. *Anal. Chem.* **1997**, *69*, 5146.

(13) Rausch, C.; Hoof, I.; Weber, T.; Wohlleben, W.; Huson, D. H. *BMC Evol. Biol.* **2007**, *7*, 78.

(14) Lin, Z.; Falkinham, J. O.; Tawfik, K. A.; Jeffs, P.; Bray, B.; Dubay, G.; Cox, J. E.; Schmidt, E. W. *J. Nat. Prod.* **2012**, *75*, 1518.

(15) Oku, N.; Krishnamoorthy, R.; Benson, A. G.; Ferguson, R. L.; Lipton, M. A.; Phillips, L. R.; Gustafson, K. R.; McMahon, J. B. *J. Org. Chem.* **2005**, *70*, 6842.

(16) (a) Chen, H.; Walsh, C. T. *Chem. Biol.* **2001**, *8*, 301. (b) Cryle, M. J.; Meinhart, A.; Schlichting, I. *J. Biol. Chem.* **2010**, *285*, 24562. (c) Uhlmann, S.; Süssmuth, R. D.; Cryle, M. J. *ACS Chem. Biol.* **2013**, *8*, 2586.

(17) Fujii, K.; Shimoya, T.; Ikai, Y.; Oka, H.; Harada, K.-i. *Tetrahedron Lett.* **1998**, *39*, 2579.

(18) Futagawa, S.; Inui, T.; Shiba, T. *Bull. Chem. Soc. Jpn.* **1973**, *46*, 3308.

(19) (a) Gross, H.; Loper, J. E. *Nat. Prod. Rep.* **2009**, *26*, 1408. (b) Roongsawang, N.; Washio, K.; Morikawa, M. *ChemBioChem* **2007**, *8*, 501.

(20) (a) Pearson, L. A.; Barrow, K. D.; Neilan, B. A. *J. Biol. Chem.* **2007**, *282*, 4681. (b) Graupner, K.; Scherlach, K.; Bretschneider, T.; Lackner, G.; Roth, M.; Gross, H.; Hertweck, C. *Angew. Chem., Int. Ed.* **2012**, *51*, 13173.

Structure of Ralsolamycin, the Inter-Kingdom Morphogen from the Crop Plant Pathogen *Ralstonia solanacearum*

Florian Baldeweg,[†] Hirokazu Kage,[‡] Sebastian Schieferdecker,[§] Caitilyn Allen,[⊥] Dirk Hoffmeister,[†] and Markus Nett*[,‡]

[†]Department of Pharmaceutical Microbiology at the Hans-Knöll-Institute, Friedrich-Schiller-University Jena, Winzerlaer Str. 2, 07745 Jena, Germany

[‡]Department of Biochemical and Chemical Engineering, Technical University Dortmund, Emil-Figge-Str. 66, 44227 Dortmund, Germany

[§]Leibniz Institute for Natural Product Research and Infection Biology, Hans-Knöll-Institute, Beutenbergstr. 11a, 07745 Jena, Germany

[⊥]Department of Plant Pathology, University of Wisconsin-Madison, 1630 Linden Drive, Madison, WI 53706, United States

Table of contents

General experimental procedures. LC-MS experiments were performed on an Agilent 1260 HPLC system equipped with a Zorbax Eclipse XDB C_{18} column (150 × 4.6 mm, 5 µm) coupled to a 6130 Single Quad MS detector. For metabolic profiling, a gradient of acetonitrile (CH_3CN) in water + 0.1% trifluoroacetic acid (TFA) and a flow rate of 1 mL min^{-1} were used. The CH_3CN concentration was increased from 30% to 90% over 11 min, kept for 4 min at 90%, and subsequently decreased to 30% within 2 min. MS/MS measurements were conducted using a Q Exactive Plus mass spectrometer (Thermo Scientific). NMR spectra were recorded at 300 K on a Bruker Avance III 600 MHz spectrometer with DMSO-d_6 as solvent and internal standard. The solvent signals were referenced to δ_H 2.49 ppm and δ_C 39.5 ppm.

Strains and growth conditions. *Ralstonia solanacearum* GMI1000 as well as the mutant strains RS13 and RS15 were grown at 30 °C on BG agar (15 g L^{-1} Bacto-Agar, 5 g L^{-1} D-glucose) or in ¼ M63 minimal medium[1] supplemented with 0.2% glucose and 0.02% sodium acetate, if not stated otherwise. The mutant strain RS15 was kept under antibiotic selection pressure (kanamycin, 20 µg mL^{-1}). *Escherichia coli* strains were routinely grown in Luria broth (LB) medium. When required, antibiotics were added at the following concentrations: ampicillin (100 µg mL^{-1}), chloramphenicol (25 µg mL^{-1}), and kanamycin (50 µg mL^{-1}).

Construction of the *rmyA* disruption mutant strain RS13. A 3.1-kb gene fragment of *rmyA* was PCR amplified from *R. solanacearum* GMI1000 genomic DNA using the primers P22 (5'-GCAGCGATCGGTATCAGCAGG-3') and P23 (5'-CCGACCGA TAGGCCTCGTACAG-3'). The PCR product was blunt-end cloned into pJET1.2 (Thermo Fisher Scientific) to give pHiK015a. This plasmid was subsequently introduced into *E. coli* BW25113 harboring pIJ790.[2] A kanamycin resistance cassette was amplified by PCR from pAphA-3[3] with the primers P24 (5'-GCCGATCCGGCCTGTTCGATCGGCAGGCTGGCGTTGCTGTGACT AACTAGGAGGAATAA-3') and P25 (5'-TGCCAGCGTCTGCTCCACCTCGCCTTGCGGCGCTTCGTATATTCCTTCCAGT ACTAAAC-3'). This cassette was inserted into the *rmyA* fragment of pHiK015a exploiting the lambda red recombination functions provided by pIJ790.[2] For this, we followed a previously described protocol.[4] Afterwards the counter selection marker *sacB* was ligated into the XhoI site of pHiK015b yielding the vector pHiK015. Competent cells of *R. solanacearum* GMI1000 were electro-transformed with pHiK015 using a Bio-Rad GenePulser II set to 200 Ω, 25 µF, and 2.5 kV. After regeneration in SOC medium for 3 hours, the culture was spread onto BG agar containing 25 µg/mL of kanamycin. The obtained transformants were transferred to BG agar supplemented with 10% (w/v) sucrose to select for double crossing-over events. The successful double crossing-over in the *rmyA* gene of strain RS13 was confirmed by PCR using primers P30 (5'-TGGAGCGCCATCAAGCCTAC-3') and P31 (5'-CGCGTACTGGATCGGCAAAG-3') and subsequent sequencing.

Construction of the *rmyA* promoter mutant strain RS15. The non-coding upstream region of *rmyA* was amplified by PCR from *R. solanacearum* GMI1000 genomic DNA using the primers P26 (5'-GAGCTCGTTTGCATTTATAAAGATTTGGAAA C-3') and P27 (5'-GCTAGCTGCAGACGGCCTTGGTTTTAGTG-3'). The PCR product (830 bp) was blunt-end cloned into pJET1.2 to give pHiK016a. The arabinose-inducible promoter P_{BAD} was amplified from pIJ790 by PCR using the primers P28 (5'-CGAAAGCTTTATGACAACTTGACGGCTA-3') and P29 (5'-CGACTCGAGGTTCTTATGGCTCTTGTAT-3'). The 3.2-kb amplicon was blunt-end cloned into pJET1.2, yielding pHiK016b. Subsequently, the upstream region of *rmyA* was excised from pHiK016a by restriction digest with SacI and NheI and ligated into the corresponding site of pHiK16b. The resulting plasmid pHiK016c was digested with HindIII and the fragment containing the P_{BAD} promoter together with the upstream region of *rmyA* was blunted. Blunt-end ligation with the kanamycin resistance gene from pAphA-3[3] yielded pHiK016. The cloning strategy for the generation of this vector is depicted in Figure S16. After transformation of *R. solanacearum* GMI1000, pHiK016 became integrated into the megaplasmid by homologous recombination to give the *rmyA* promoter mutant strain RS15. The identity of the latter was confirmed by PCR using two primer pairs. The first primer pair consisted of P32 (5'-TTAACAACAACGCAAAA ATCCGA-3') and P33 (5'-CTTACTGGGGATCAAGCCTGATTG-3'). The second primer pair included P34 (5'-TCAATTCCG GTGATATTCTCATTTTAGC-3') and P35 (5'-GTTTGATCGTTCTTGGACAT-3').

Production, isolation and purification of ralsolamycin. For ralsolamycin production, the *rmyA* promoter mutant strain RS15 was grown in FB1 medium (0.1% casamino acids, 0.1% yeast extract, 0.1% fructose, 5.30 mM $(NH_4)_2SO_4$, 4.04 mM KH_2PO_4, 4.19 mM K_2HPO_4, 24.34 µM $MgSO_4 \times 7H_2O$, 0.21 µM $ZnSO_4 \times 7H_2O$, 0.42 µM $Ca(NO_3)_2 \times 4H_2O$, 0.24 µM $MnSO_4 \times H_2O$, 0.37 µM $FeCl_3$). To facilitate the recovery of secreted metabolites, the medium was supplemented with 4% Amberlite XAD-7 HP. The production cultures were inoculated with a seed culture (1% of final volume) and grown on a rotary shaker at 30 °C. When the production cultures reached an OD_{600} of 0.4, they were induced with 0.2% L-arabinose and the fermentation temperature was lowered to 25 °C. Following a 24-h incubation period, the induction was repeated. Afterwards, the cultivation was continued for 2 days. At the end of cultivation, the adsorber resin was harvested by filtration on Miracloth (Calbiochem) and rinsed with water. The adsorbed metabolites were eluted from the resin with methanol (MeOH). After removal of the solvent, the extract was initially fractionated by flash column chromatography over Polygoprep 60-50 C_{18} (Macherey-Nagel) using increasing concentrations of MeOH in H_2O. Ralsolamycin-containing fractions were identified by LC-MS, pooled and further purified on an Agilent Infinity 1260 preparative HPLC system equipped with a Luna C_{18} column (250 × 21.2 mm, 10 µm; Phenomenex) using a gradi-

ent of CH_3CN in H_2O. Final purification was accomplished by two consecutive HPLC steps on an Agilent Infinity 1200 HPLC system. The first separation was carried out with a Zorbax Eclipse XDB-C_8 column (250 × 9.4 mm, 5 µm) using a flow rate of 2.0 mL min^{-1} and the following gradient of CH_3CN in H_2O + 0.1% TFA: from 30 to 50% CH_3CN in 3 min, from 50 to 65% CH_3CN in 2 min, from 65 to 100% CH_3CN in 4 min. The second separation was conducted on a Zorbax Eclipse XDB-C_{18} column (150 × 4.6 mm, 5 µm) using a linear gradient of CH_3CN in H_2O + 0.1% TFA: from 30 to 90% CH_3CN in 11 min. The elution of ralsolamycin was detected by wavelength monitoring at 272 nm. Ralsolamycin was obtained as a colorless solid.

Isolation and structure elucidation of ralsolamycin B. The production and purification of ralsolamycin B was according to the protocol described for ralsolamycin. Ralsolamycin B was obtained as a colorless solid (9.8 mg from 50 L culture broth). The empirical formula of the molecule was assigned to be $C_{61}H_{100}N_{12}O_{19}$ by high-resolution ESIMS (*m/z* 1305.7303 $[M+H]^+$. An inspection of the NMR spectra (Figures S21 – S26) immediately revealed the structural relatedness to ralsolamycin. However, two methyl resonances in the ^{13}C NMR spectrum are shifted upfield, while a methine signal is shifted downfield. Furthermore, ralsolamycin B features an additional methylene group (Table S3). The observed chemical shifts were consistent with an isoleucine residue replacing the valine moiety in ralsolamycin. Since ralsolamycin B originates from the same biosynthetic pathway as ralsolamycin, the stereochemistry was assigned as depicted in Figure S21.

Cloning, expression and purification of RmyA-A (module 5). The nucleotide sequence encoding the adenylation domain of module 5 in RmyA was amplified by PCR from *R. solanacearum* GMI1000 genomic DNA using the primers oBW17 (5'-ATTATACCATGG ATGCATCGACGATCCACGG-3') and oBW19 (5'-AATTATCTCGAGCAAGGCACGGCGGTC-3'). The product was ligated into pET28a(+) to give pBW12. *E. coli* BL21(DE3) served as host for heterologous production of the recombinant protein. The strain was grown at 37 °C in 900 mL LB medium supplemented with 50 µg/mL kanamycin. After reaching an OD_{600} of 0.75, gene expression was induced by adding 0.75 mM isopropyl 1-thio-β-D-galactopyranoside (IPTG). The cultivation was continued at 16 °C for 20 hours. Cells were harvested by centrifugation (3,200*g*, 40 min, 4 °C) and suspended in lysis buffer (20 mM imidazole, 50 mM sodium phosphate, 300 mM sodium chloride, pH 8.0). Cells were disrupted with a Sonopuls ultrasonic sonifier (Bandelin). The lysate was centrifuged (17,000*g*, 30 min, 4 °C) to remove cellular debris. The protein was purified by metal affinity chromatography using an Äkta FPLC (GE Healthcare) equipped with a HisTrap FF crude HP column (GE Healthcare), subjecting the sample to a stepwise imidazole gradient (20–500 mM) in lysis buffer. Proteins were desalted on a Amicon Ultra-15 Centrifugal Filter Unit (50.000 Da) by centrifugation (6,000 *g*, 10 min, 4 °C) and eluted with reaction buffer (80 mM Tris x HCl, pH 7.5, 10 mM MgCl2). Purification was confirmed by SDS-PAGE (Figure S7).

ATP-[^{32}P]-pyrophosphate exchange assay. The purified protein featuring the adenylation domain of module 5 in RmyA (166 nM) was added to a 100 µL reaction mixture containing 80 mM Tris-HCl (pH 7.5), 10 mM $MgCl_2$, 5 mM ATP, 0.1 mM [^{32}P]-pyrophosphate, and 2 mM amino acid. Afterwards the mixture was incubated at 30 °C for 30 min. The reaction was stopped by quenching with 500 µL of charcoal suspension (1% charcoal and 4.5% $Na_4P_2O_7$ in 3.5% perchloric acid). Precipitate was collected with paper filter discs under vacuum. Following three consecutive washing steps with 40 mM $Na_4P_2O_7$ in 1.4% perchloric acid (200 mL) and water (200 mL), the filter papers were added to 2.5 mL of scintillation fluid. Eventually the radioactivity was measured in a Beckman Coulter LS6500 multipurpose scintillation counter. All reactions were run in triplicate.

Marfey's method. Ralsolamycin was hydrolyzed in 6 N HCl (500 µL) at 100 °C for 18 h. After the solution was brought to room temperature and evaporated to dryness, the residue was redissolved in 50 µL H_2O and 20 µL sodium bicarbonate (1 M). For derivatization, 100 µL of a 1% (w/v) solution of Marfey's reagent (1-fluoro-2,4-dinitrophenyl-5-L-leucine amide, L-FDLA)[6] in acetone were added. The mixture was incubated at 37 °C for 60 min, after which 20 µL 1 N HCl was added to stop the reaction. The derivatized sample was analyzed by LC-MS together with chiral amino acid standards, which had been prepared the same way. LC-MS analyses was performed with a Zorbax Eclipse XDB-C_{18} column (150 × 4.6 mm, 5 µm) using a linear gradient of CH_3CN in water + 0.1% TFA from 30% CH_3CN to 100% CH_3CN over 22 min. A separation of L-homoserine and L-threonine was accomplished on a Zorbax Eclipse XDB-C_{18} column (250 × 4.6 mm, 5 µm) with the following gradient of CH_3CN in H_2O + 0.1% TFA: from 50 to 22% CH_3CN in 1 min, from 22 to 35% CH_3CN over 16 min, and from 35 to 100% CH_3CN in 4 min, held at 100% CH_3CN for 6 min.

Isolation and purification of 3-amino-2-hydroxystearic acid. Ralsolamycin (150 mg) was solved in 10 mL 6 N HCl and heated under reflux for 3 h. Subsequently, the hydrolysate was neutralized with 6 N NaOH. After pre-purification on a NUCLEODUR C18 ec column (Macherey-Nagel), the 3-amino-2-hydroxystearic acid-containing fraction was subjected to RP-HPLC using a Zorbax Eclipse XDB-C_{18} column (150 × 4.6 mm, 5 µm) and a linear gradient of CH_3CN in H_2O + 0.1% TFA: from 30 to 80% CH_3CN in 9 min, from 80% to 100% in 1 min, holding 100% CH_3CN for 3.5 minutes. The purification yielded 28 mg of 3-amino-2-hydroxystearic acid as a colorless solid.

Preparation of methyl 2-oxo-4-pentadecyloxazolidine-5-carboxylate. TMS-diazomethane (2 M in hexane) was added to a stirred methanolic solution of 3-amino-2-hydroxystearic acid (3 mg) until the yellow color persisted. After additional stirring for one hour at room temperature the reaction was quenched by addition of acetic acid and the solvent was removed under reduced pressure. The residue was dissolved in dichloromethane. Two equivalents of triphosgene and DIPEA and a catalytic amount of DMAP were added and the resulting solution was stirred over night at room temperature. Brine was added and the crude product was extracted three times with dichloromethane. The organic phases were combined, residual water was removed by addition of Na_2SO_4 and the solvent was removed under reduced pressure. Methyl 2-oxo-4-pentadecyloxazolidine-5-carboxylate was obtained as a colorless oil (2.6 mg; yield: 78%) after purification by silica gel column chromatography using a gradient from dichloromethane to ethyl acetate.

Phylogenetic analysis. Amino acid sequences of NRPS condensation (C) domains were retrieved from GenBank. Thioesterase (TE) sequences were taken from Buntin et al.[7] Sequences were aligned with MUSCLE.[8,9] The evolutionary history was inferred by using the Maximum Likelihood method based on the JTT matrix-based model.[10] MEGA7 was used for the tree construction.[11] To estimate the confidence of the tree topologies, bootstrap-resampling analysis with 100 replicates was performed.

Petiole inoculation assay. The virulence of mutant and wild-type *R. solanacearum* strains was tested by direct petiole inoculation of 30-days old tomato plants (*Lycopersicon esculentum* Mill., cultivar Moneymaker).[12] The latter were grown from surface-sterilized seed. For the petiole inoculation, the first true leaf above the cotyledons was cut horizontally 5 mm from its base. The resulting stump was immediately treated with 20,000 CFU in a total volume of 2 µL. For the testing of purified ralsolamycin, the stump was treated with 2.5 µL of a 50 mM solution (in methanol). Plants were monitored daily for disease progress. Each experiment contained a minimum of 12 plants per strain.

Leaf necrosis assay. Leaves were detached from a 3-week old tomato plant and individually spotted with 2.5 µL of a ralsolamycin solution (50 mM in MeOH) or pure MeOH. The petioles of the leaves were dipped in sterile water and covered in a petri dish. The response was evaluated after an incubation of 24 h at room temperature.

Table S1. NMR data of ralsolamycin in DMSO-d_6

pos.	δC, type	δH, M (*J* in Hz)	HMBC (^{1}H→^{13}C)	pos.	δC, type	δH, M (*J* in Hz)	HMBC (^{1}H→^{13}C)
1	171.4, C			34	127.5, CH	7.15, d (8.5)	32, 36, 38
2	35.8, CH2	a: 2.37, m	1	35	114.5, CH	6.63, d (8.5)	33, 36, 37
		b: 2.31, m	1	36	156.4, C		
3	35.3, CH2	a: 3.46, m	1, 4	37	114.5, CH	6.63, d (8.5)	33, 35, 36
		b: 3.28, m	1, 4	38	127.5, CH	7.15, d (8.5)	32, 34, 36
4	173.1, C			39	169.2, C		
5	47.5, CH	4.37, dq (8.4, 7.1)	4, 6	40	56.9, CH	4.29, dd (7.9, 3.9)	1', 39, 42
6	18.3, CH3	1.21, d (7.1)	4, 5	41	66.3, CH	4.04, dq (6.3, 3.9)	39, 42
7	168.3, C			42	18.6, CH3	0.96, d (6.3)	40, 41
8	42.4, CH2	a: 3.98, dd (16.9, 7.3)	7, 9	1'	170.3, C		
		b: 3.44, m	7, 9	2'	71.0, CH	4.22, n.r.	1', 3', 4', 40
9	164.2, C			3'	52.9, CH	3.39, m	2', 4', 5'
10	137.7, C			4'	26.9, CH2	a: 1.48, m	2', 3', 5', 6'
11	108.6, CH2	a: 5.33, s	9, 10			b: 1.36, m	2', 3', 5', 6'
		b: 5.21, s	9, 10	5'	24.8, CH2	a: 1.34, m	4', 6'
12	170.9, C					b: 1.20, m	4', 6'
13	57.9, CH	4.24, n.r.	12, 15, 16	6'	28.8, CH2	1.22, m	4', 5'
14	29.8, CH	2.03, m	15, 16	7'	29.0, CH2	1.22, m	n.r.
15	18.8, CH3	0.83, d (7.1)	13, 16	8'	29.0, CH2	1.22, m	n.r.
16	18.4, CH3	0.87, d (6.8)	13, 15	9'	29.0, CH2	1.22, m	n.r.
17	171.8, C			10'	29.0, CH2	1.22, m	n.r.
18	50.0, CH	4.46, n.r.	17, 19, 20	11'	29.0, CH2	1.22, m	n.r.
19	31.3, CH2	a: 2.08, m	17, 20	12'	28.9, CH2	1.22, m	n.r.
		b: 1.82, m	17, 20	13'	28.7, CH2	1.22, m	n.r.
20	60.1, CH2	a: 4.24, m	1, 17, 18, 19	14'	28.7, CH2	1.22, m	n.r.
		b: 3.91, m	1, 17, 18, 19	15'	28.6, CH2	1.22, m	16'
21	169.1, C			16'	31.0, CH2	1.23, m	17', 18'
22	41.8, CH2	a: 3.77, dd (16.8, 6.1)	21, 23	17'	22.1, CH2	a: 1.32, m	16', 18'
		b: 3.69, dd (16.8, 5.5)	21, 23			b: 1.22, m	16', 18'
23	171.9, C			18'	13.9, CH3	0.84, t (6.1)	16', 17'
24	50.6, CH	4.32, n.r.	23, 25	N-1		8.36, t (5.5)	2, 3, 4
25	34.6, CH2	a: 1.86, m	23, 24, 26	N-2		7.93, d (8.4)	5, 6, 7
		b: 1.69, m	23, 24, 26	N-3		8.19, t (7.3)	8, 9
26	57.5, CH2	3.44, m	25	N-4		10.34, s	7, 9, 10, 11, 12
27	170.3, C			N-5		8.20, n.r.	13, 17
28	54.9, CH	4.34, ddd (6.8, 6.3, 5.7)	27, 29	N-6		8.03, d (6.8)	18, 19, 21
29	61.7, CH2	a: 3.63, dd (10.6, 5.7)	27	N-7		8.10, t (6.1, 5.5)	21, 22
		b: 3.56, dd (10.6, 6.3)	27	N-8		8.17, d (8.1)	24, 25, 26, 27
30	169.4, C			N-9		8.00, n.r.	28, 30
31	58.7, CH	4.47, dd (8.4, 2.9)	30, 32	N-10		7.91, d (8.4)	30, 31, 32, 39
32	71.5, CH	5.02, d (2.9)	30, 33, 34, 38	N-11		7.70, d (7.9)	1', 40, 41
33	131.9, C			N-12		8.00, n.r.	1', 4'

n.r., not resolved

Table S2. Substrate specificities for the adenylation domains of the NRPSs encoded in the *rmy* gene cluster

Protein	Adenylation (A) domain	Signature sequence	Substrate according to prediction
RmyA	module 2	DFWNIGMVHK	threonine
	module 3	DASTIAAVCK	tyrosine
	module 4	DVWHLSLIDK	serine
	module 5	DLKNVGSDVK	homoserine[b]
	module 6[a]	DILQLGVIWK	glycine
	module 7[a]	DLKNVGSDVK	homoserine[b]
RmyB	module 8	DALWMGGTFK	valine
	module 9	DVWHLSLIDK	serine
	module 10	DILQLGVIWK	glycine
	module 11	DLFNNALTYK	alanine
	module 12	VDTVVSFGDK	β-alanine

[a] Modules 6 and 7 were missing in the originally reported sequence.

[b] A bioinformatic prediction[13] suggested β-lysine as a substrate, albeit with a low score. Biochemical characterization of the recombinantly produced adenylation domain from module 5 revealed L-homoserine as the true substrate (see Figure S8).

Table S3. NMR data of ralsolamycin B in DMSO-d_6

pos.	δC, type	δH, M (*J* in Hz)	HMBC (^{1}H→^{13}C)	pos.	δC, type	δH, M (*J* in Hz)	HMBC (^{1}H→^{13}C)
1	171.4, C			33	132.0, C		
2	35.8, CH2	a: 2.37, m	1, 3	34	127.5, CH	7.15, d (8.5)	36, 38
		b: 2.32, m	1, 3	35	114.4, CH	6.63, d (8.5)	33, 36, 37
3	35.3, CH2	a: 3.44, m	1, 2	36	156.3, C		
		b: 3.30, m	1, 2	37	114.4, CH	6.63, d (8.5)	33, 35, 36
4	173.1, C			38	127.5, CH	7.15, d (8.5)	34, 36
5	47.4, CH	4.38, dq (8.4, 7.2)	4	39	169.2, C		
6	18.4, CH3	1.22, d (7.2)	4, 5	40	56.8, CH	4.30, dd (8.1, 3.9)	39
7	168.3, C			41	66.3, CH	4.04, dq (6.3, 3.9)	
8	42.3, CH2	a: 3.99, m	7	42	18.7, CH3	0.96, d (6.3)	40, 41
		b: 3.43, m	7, 9	1’	170.3, C		
9	164.2, C			2’	70.9, CH	4.20, n.r.	1’, 3’
10	137.6, C			3’	52.9, CH	3.38, m	2’
11	108.3, CH2	a: 5.32, s	9, 10	4’	26.8, CH2	a: 1.47, m	5’, 6’
		b: 5.22, s	9, 10			b: 1.36, m	5’, 6’
12	171.1, C			5’	24.7, CH2	a: 1.33, m	n.r.
13	56.5, CH	4.34, n.r.	n.r.			b: 1.18, m	n.r.
14	36.2, CH	1.81, m	n.r.	6’	28.8, CH2	1.22, m	n.r.
15	25.3, CH2	a: 1.33, m	n.r.	7’	29.0, CH2	1.22, m	n.r.
		b: 1.05, m		8’	29.0, CH2	1.22, m	n.r.
16	14.7, CH3	0.83, d (7.1)	13, 14, 15	9’	29.0, CH2	1.22, m	n.r.
16”	11.4, CH3	0.83, t (7.1)	14, 15	10’	29.0, CH2	1.22, m	n.r.
17	171.7, C			11’	29.0, CH2	1.22, m	n.r.
18	50.2, CH	4.41, n.r.	17	12’	28.9, CH2	1.22, m	n.r.
19	31.3, CH2	a: 2.07, m	17, 20	13’	28.7, CH2	1.22, m	n.r.
		b: 1.83, m	17, 20	14’	28.7, CH2	1.22, m	n.r.
20	60.1, CH2	a: 4.23, m	18	15’	28.6, CH2	1.22, m	n.r.
		b: 3.91, m	18	16’	30.8, CH2	1.23, m	n.r.
21	169.1, C			17’	22.1, CH2	1.25, m	16’, 18’
22	41.8, CH2	a: 3.77, dd (16.8, 6.2)	21, 23	18’	13.9, CH3	0.84, t (6.9)	16’, 17’
		b: 3.69, dd (16.8, 5.5)	21, 23	N-1		8.35, t (5.9)	
23	171.9, C			N-2		7.89, d (8.4)	5, 7
24	50.6, CH	4.31, n.r.	23, 25	N-3		8.15, t (7.8)	9
25	34.6, CH2	a: 1.86, m	26	N-4		10.32, s	9, 12
		b: 1.68, m	24, 26	N-5		8.12, d (8.3)	13
26	57.5, CH2	3.43, m	n.r.	N-6		8.04, d (7.1)	18, 21
27	170.3, C			N-7		8.09, t (6.2, 5.5)	22
28	54.8, CH	4.35, m	27, 29	N-8		8.16, n.r.	
29	61.7, CH2	a: 3.59, n.r.	27	N-9		7.96, d (7.3)	28, 30
		b: 3.54, n.r.	27, 28	N-10		7.90, d (7.8)	31, 39
30	169.4, C			N-11		7.70, d (8.1)	1’, 40
31	58.7, CH	4.47, dd (8.5, 3.1)	30, 33	N-12		7.90, n.r.	
32	71.4, CH	5.01, d (3.1)	30, 33				

n.r., not resolved

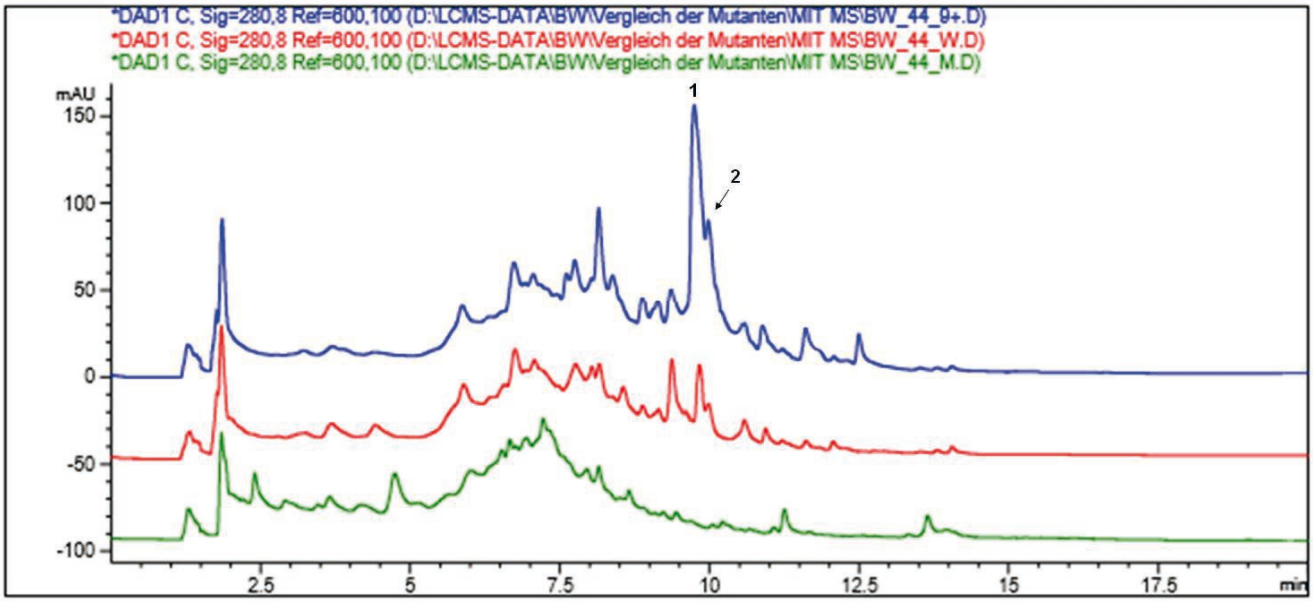

Figure S1. Metabolic profiles of the *R. solanacearum* rmyA promoter mutant strain RS15 (blue), the wild type strain GMI1000 (red) and the *rmyA* disruption mutant strain RS13 (green). All chromatograms were recorded at 280 nm. Peak 1 corresponds to ralsolamycin, peak 2 corresponds to ralsolamycin B.

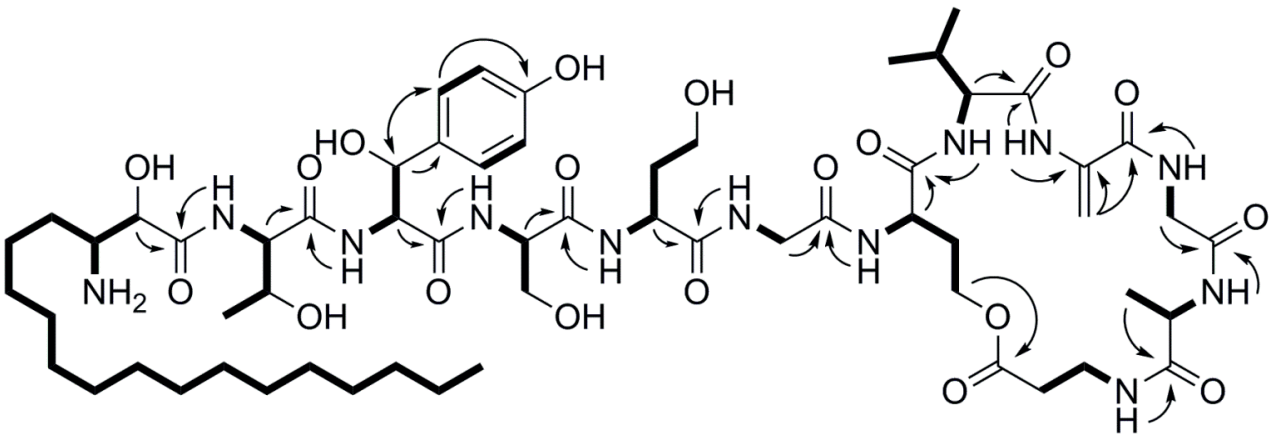

Figure S2. COSY (bold lines) and selected HMBC (arrows) correlations in ralsolamycin.

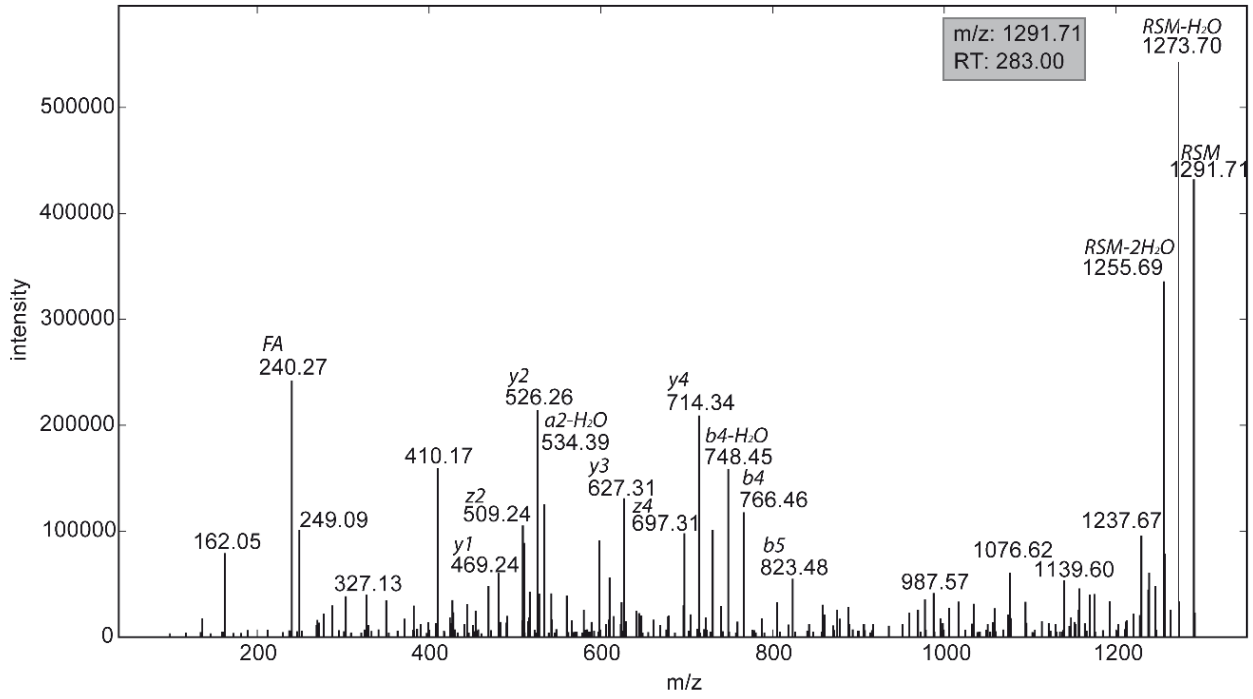

Figure S3. MS/MS spectrum of ralsolamycin.

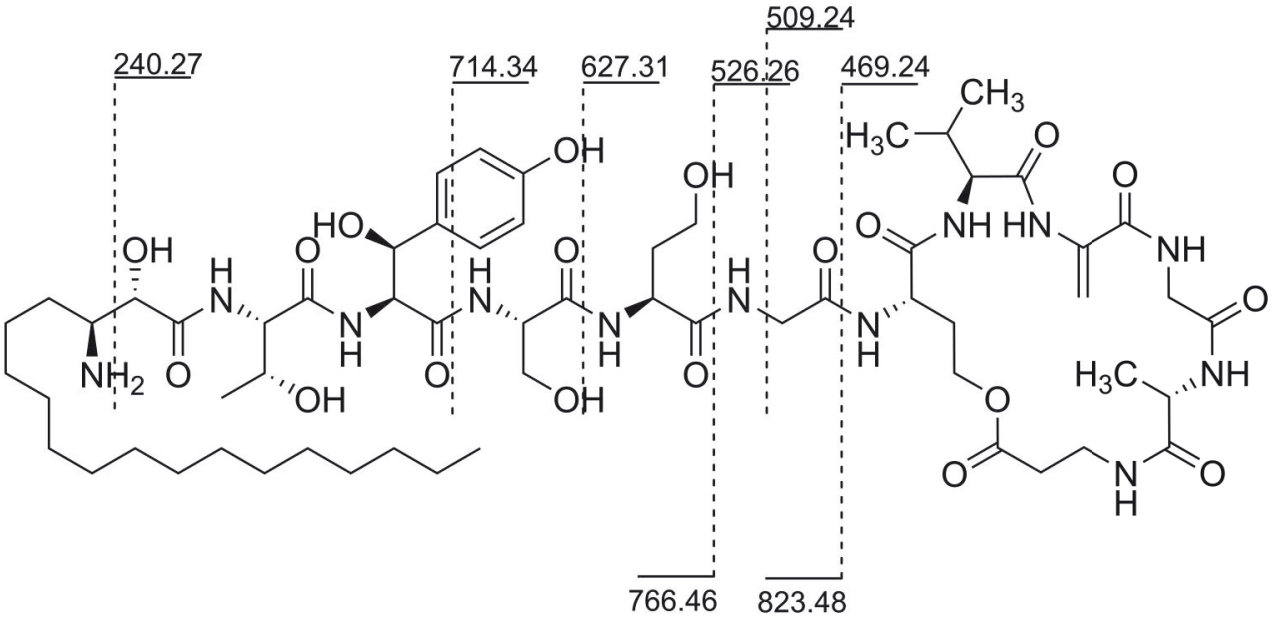

Figure S4. Fragmentation of ralsolamycin. The dashed lines show the "y" and "b" fragments that were detected in the tandem MS experiment. The depicted numbers refer to the corresponding *m/z* values.

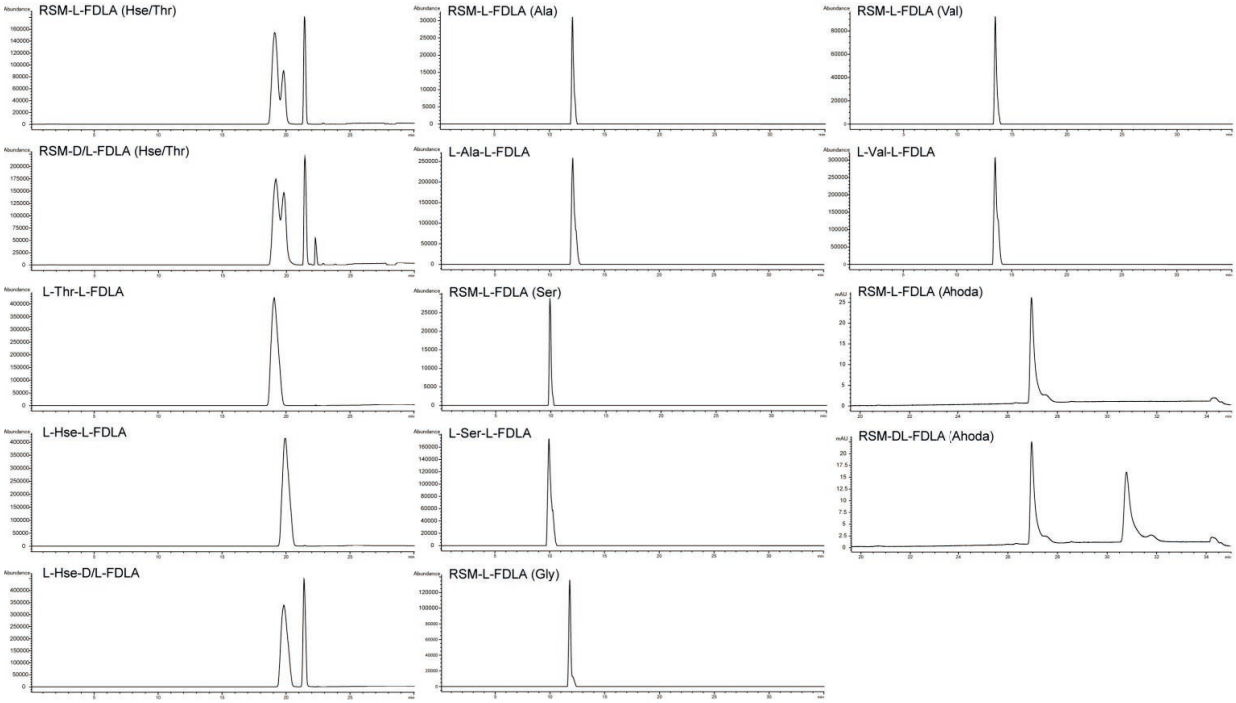

Figure S5. Marfey's analysis of the amino acid constituents of ralsolamycin. The FDLA derivatization was also used to determine the absolute configuration of the carbon bearing the primary amino group in the 3-amino-2-hydroxystearate (Ahoda) residue of ralsolamycin. In this particular case, no derivatization of an authentic standard is required. Instead the elution order of the DL- and L-FDLA derivatives can be predicted from the hydrophobicity of the two substituents at the asymmetric carbon with the primary amino group.[14]

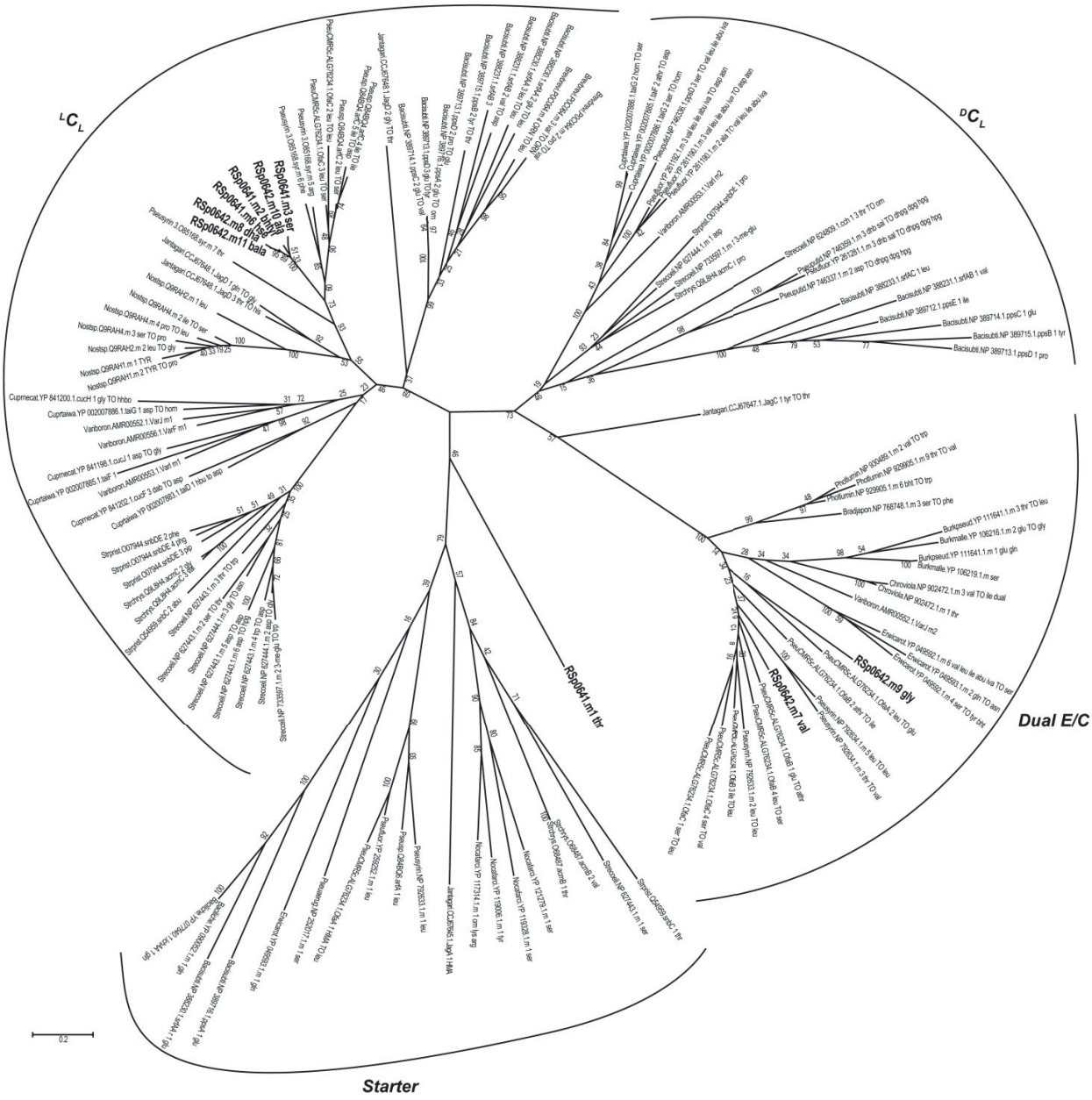

Figure S6. Phylogenetic tree of condensation (C) domains. The phylogeny of the different C subtypes ($^{L}C_{L}$, $^{D}C_{L}$, Starter and Dual E/C) was reconstructed using MEGA7 with the Maximum Likelihood method based on the JTT matrix-based model. To estimate the confidence of the tree topologies, bootstrap-resampling analysis with 100 replicates was performed.. The numbers on the branches indicate the bootstrap values (%) from 100 resamplings. Bar, 0.2 substitutions per site. Condensation domains from the ralsolamycin assembly line are highlighted in bold.

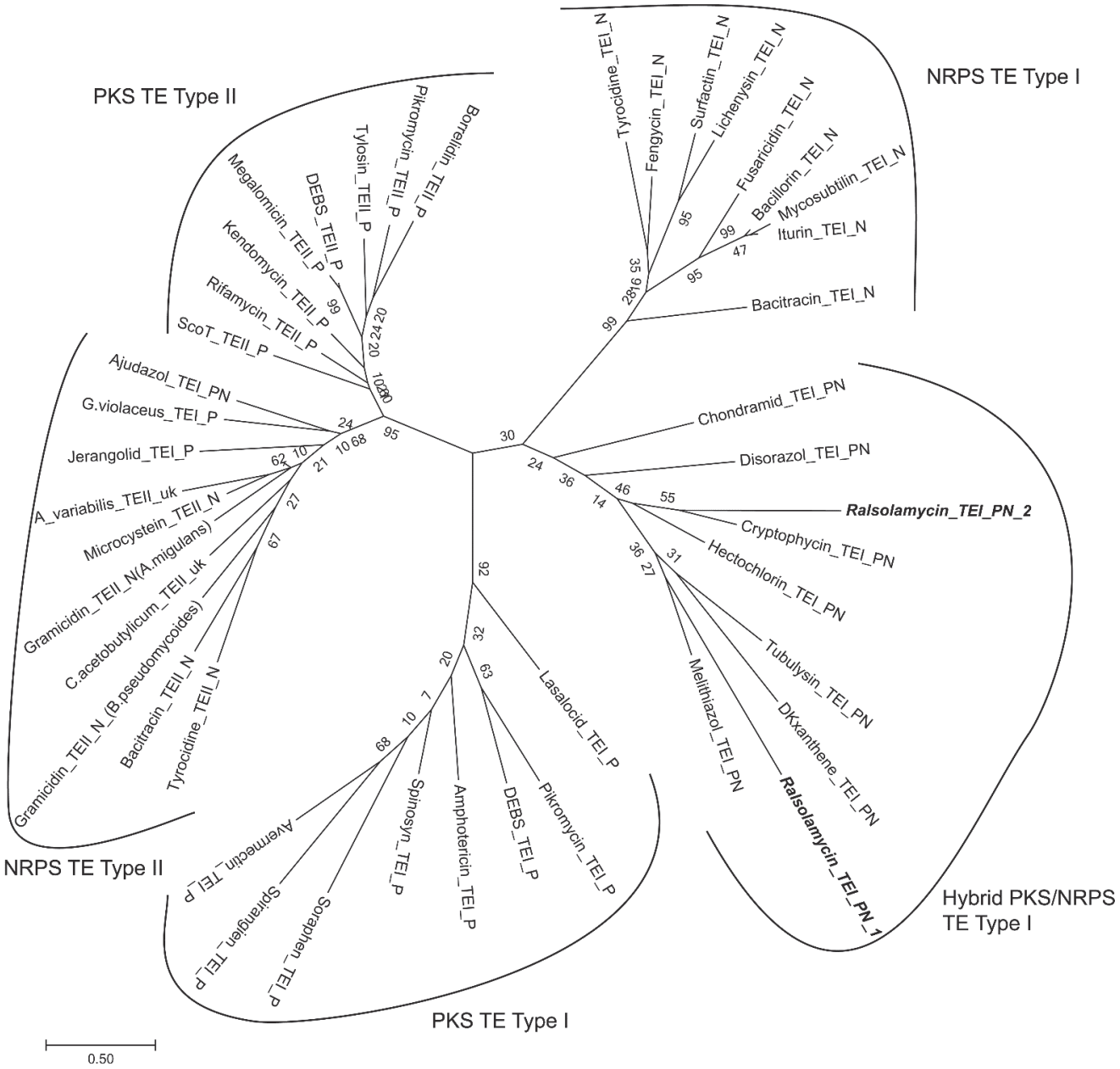

Figure S7. Phylogenetic tree of thioesterase (TE) domains. The phylogeny of the different TE subtypes (PKS Type I, PKS Type II, Hybrid PKS/NRPS Type I, NRPS Type I, NRPS-Type II) was reconstructed using MEGA7 with the Maximum Likelihood method based on the JTT matrix-based model. To estimate the confidence of the tree topologies, bootstrap-resampling analysis with 100 replicates was performed.. The numbers on the branches indicate the bootstrap values (%) from 100 resamplings. Bar, 0.2 substitutions per site. TE-domains from the ralsolamycin assembly line are highlighted in bold.

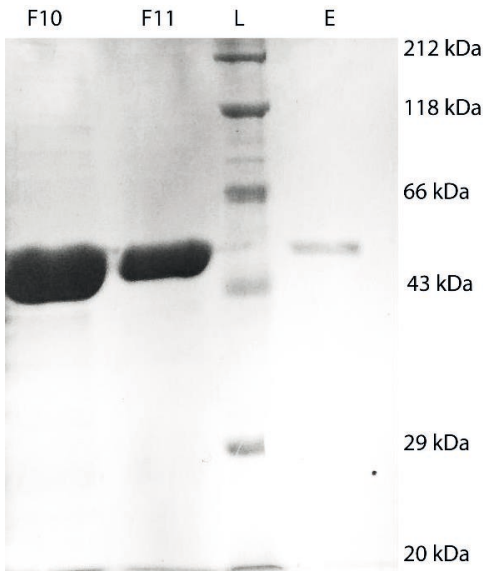

Figure S8. SDS-PAGE of the purified recombinant protein featuring the adenylation domain of module 5 in RmyA. The predicted molecular weight is 54.5 kDa. Lanes F10 & F11, protein-containing fractions from the FPLC purification; L, ladder; E, diluted and desalted protein.

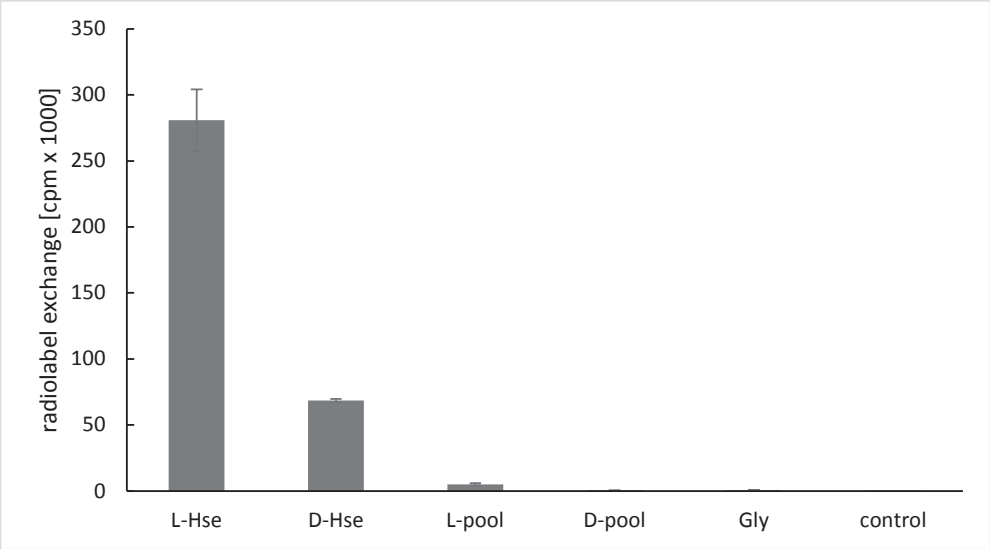

Figure S9. Substrate specificity of recombinant RmyA-A (module 5). Pool of L-amino acids: L-Ala, L-Val, L-Leu, L-Ile, L-Cys, L-Met, L-Ser, L-Thr, L-Pro, L-His, L-Phe, L-Tyr, L-Trp, L-Asp, L-Asn, L-Glu, L-Gln, L-Lys, L-Arg, L-Orn; pool of D-amino acids: D-Ala, D-Val, D-Leu, D-Cys, D-Met, D-Ser, D-Thr, D-His, D-Phe, D-Tyr, D-Trp, D-Asp, D-Glu, D-Gln, D-Lys, D-Arg; control, water.

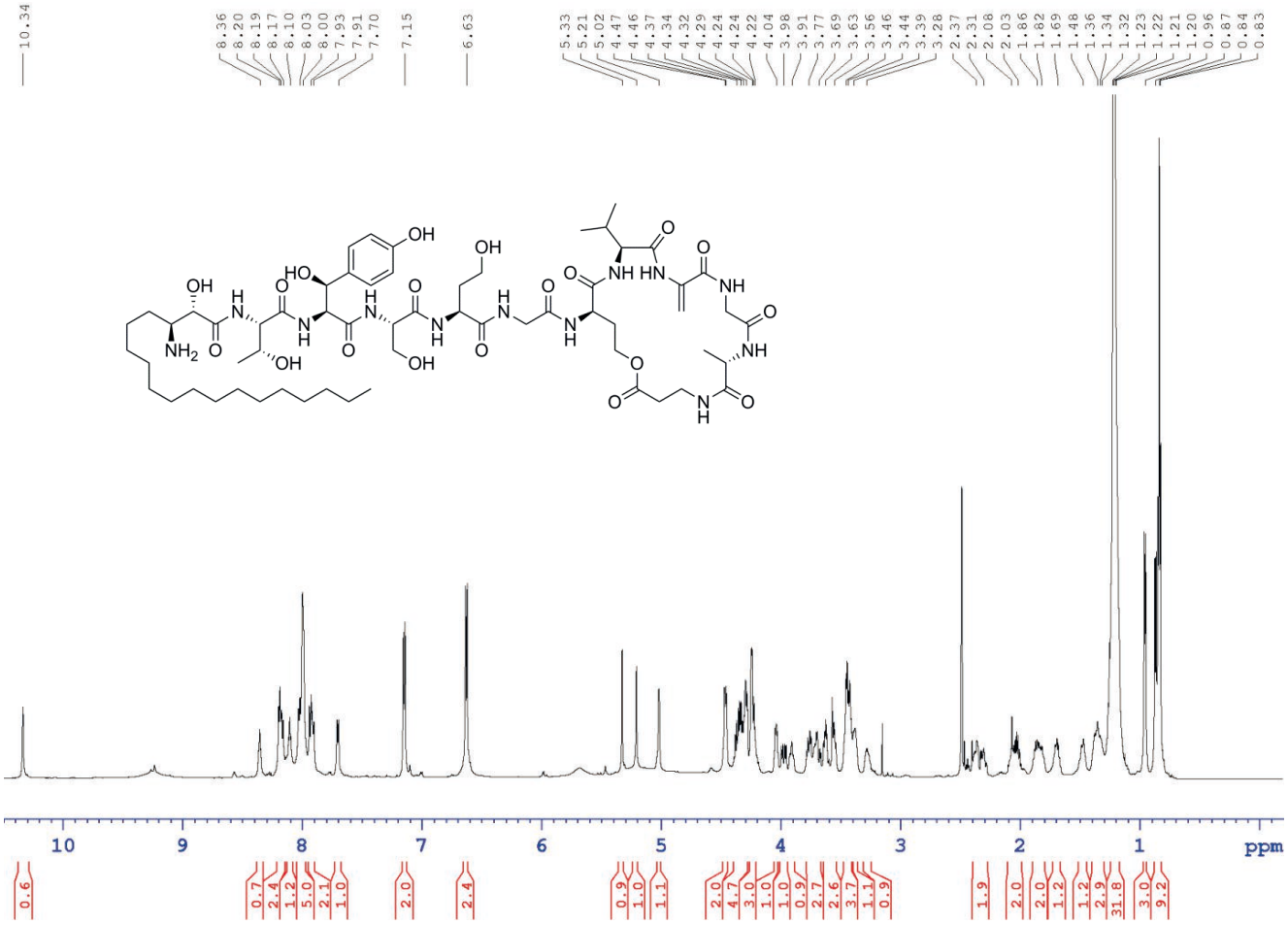

Figure S10. ^{1}H NMR spectrum of ralsolamycin in DMSO-d_6

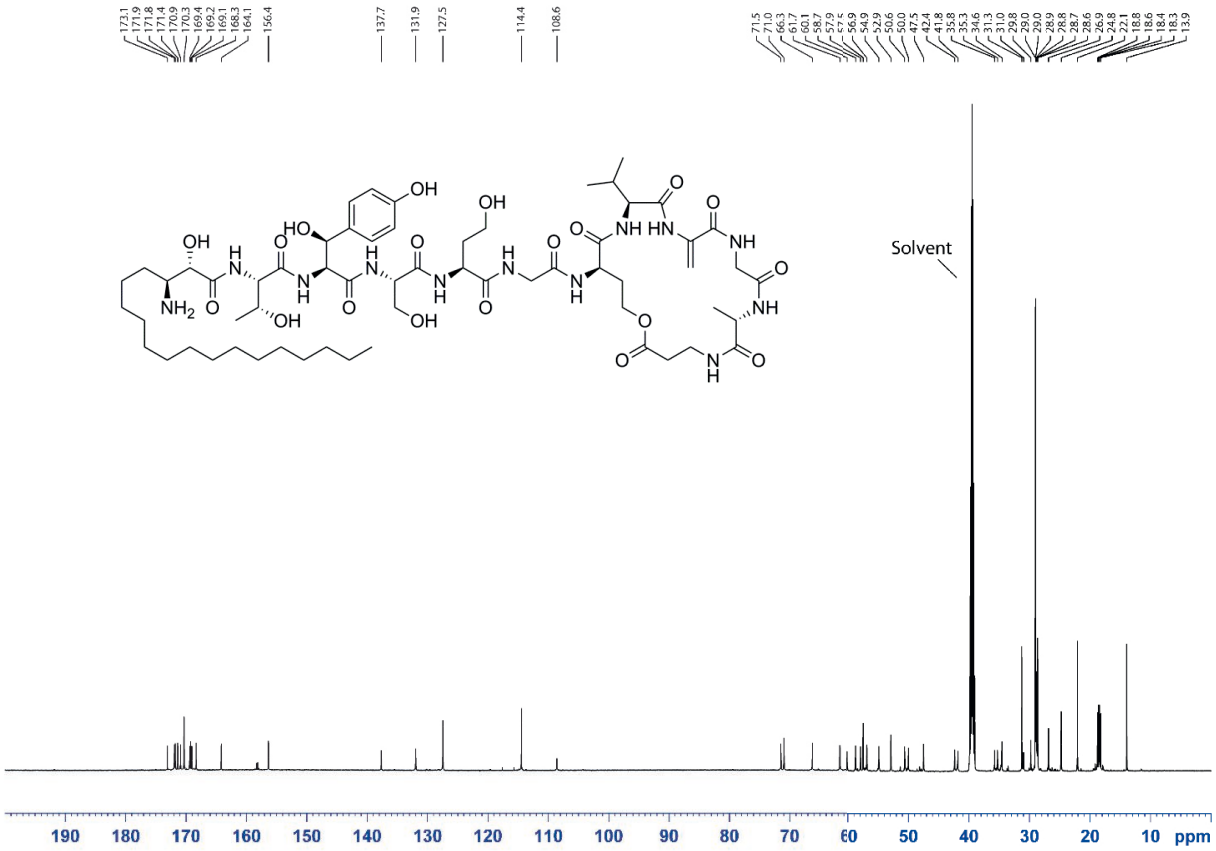

Figure S11. ^{1}H decoupled ^{13}C NMR spectrum of ralsolamycin in DMSO-d_6

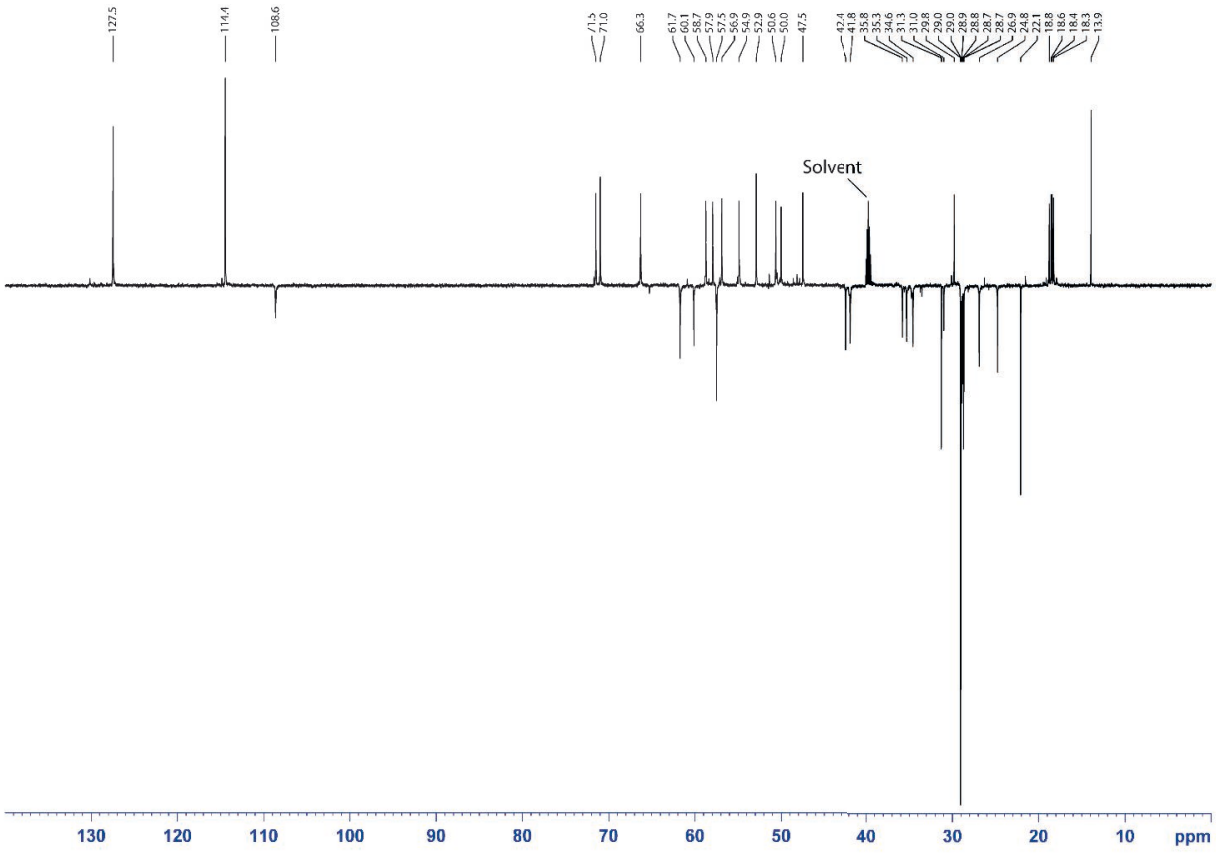

Figure S12. DEPT135 spectrum of ralsolamycin in DMSO-d_6

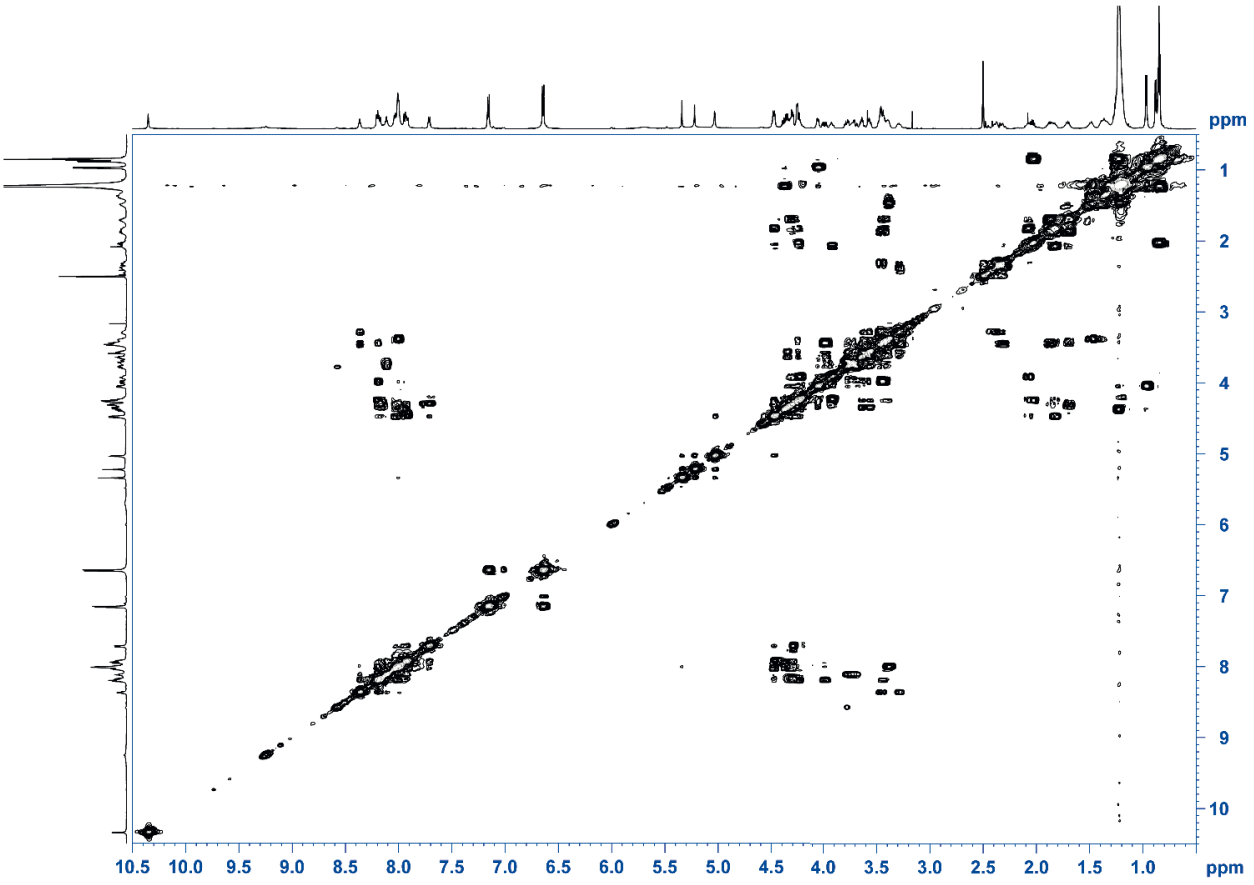

Figure S13. ^{1}H, ^{1}H COSY spectrum of ralsolamycin in DMSO-d_6

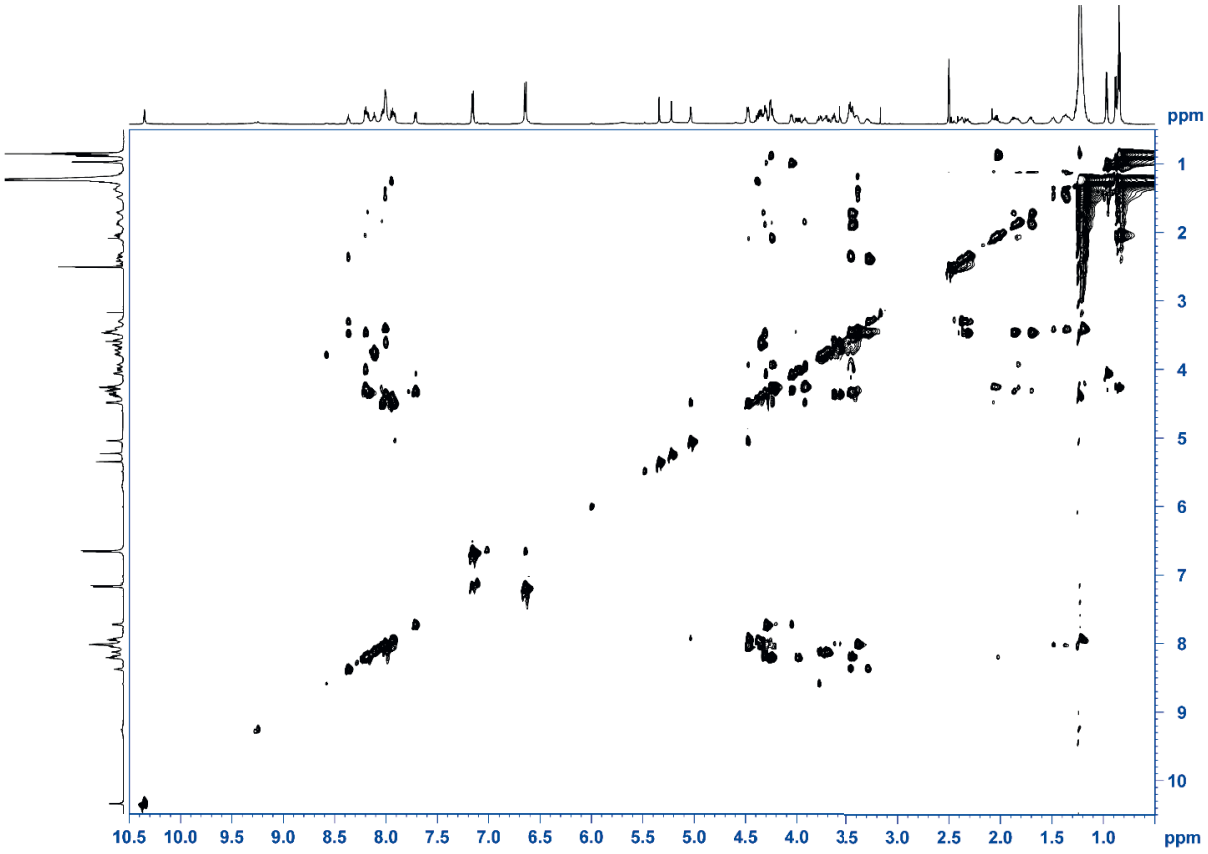

Figure S14. TOCSY spectrum of ralsolamycin in DMSO-d_6

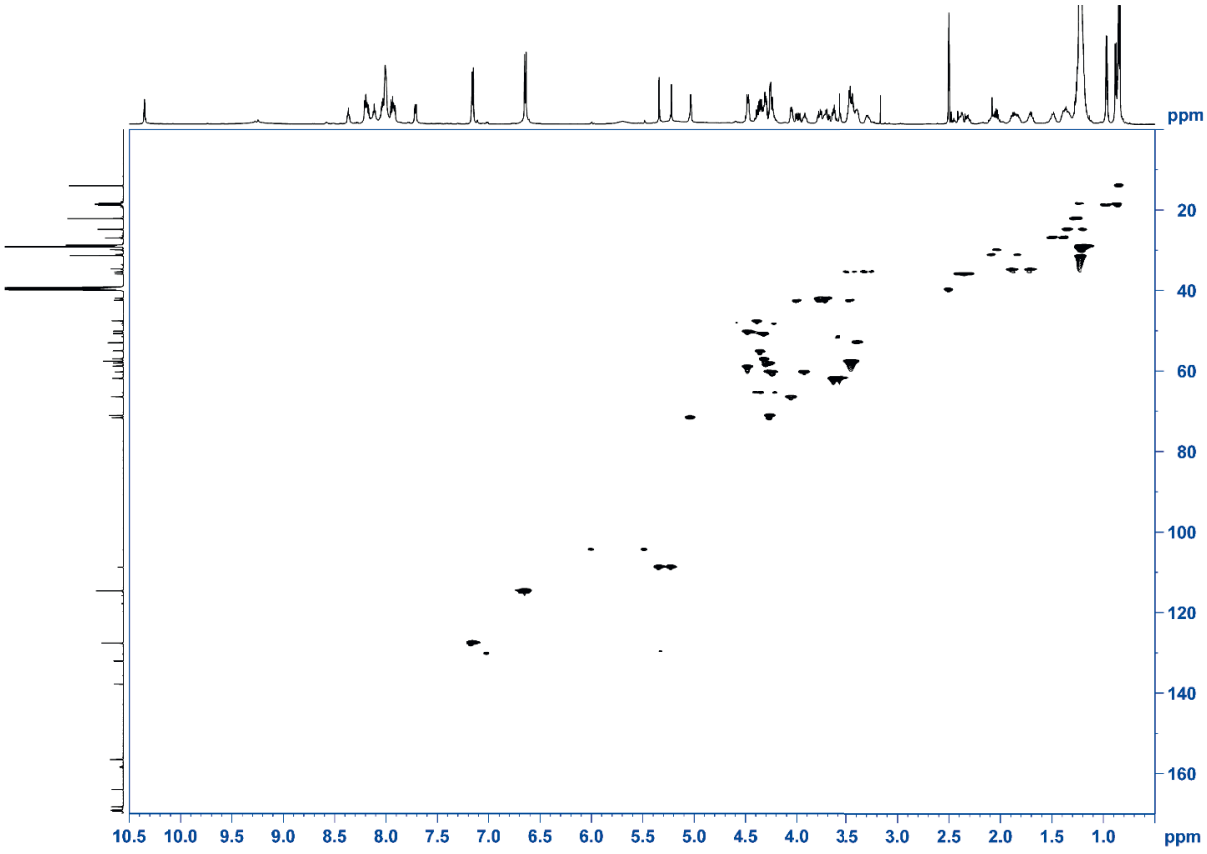

Figure S15. ^{1}H, ^{13}C HSQC spectrum of ralsolamycin in DMSO-d_6

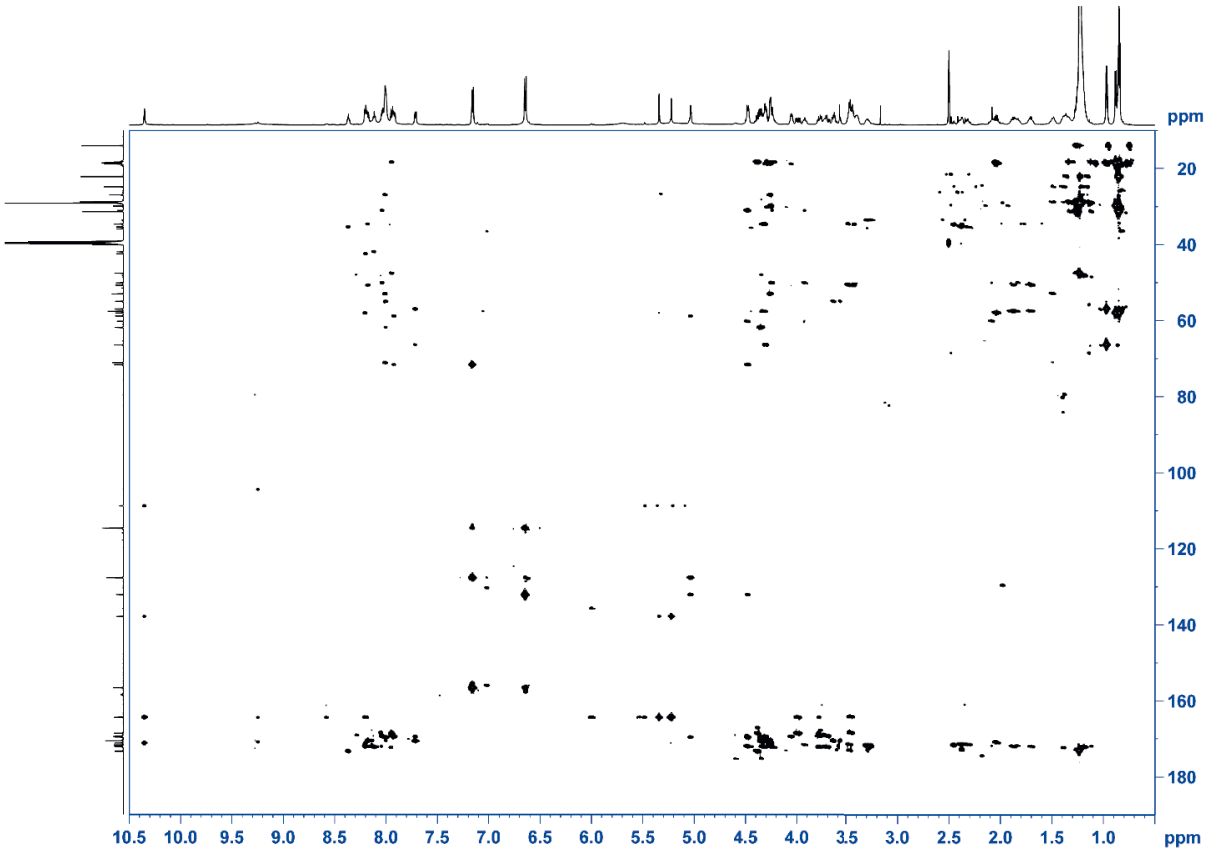

Figure S16. ^{1}H, ^{13}C HMBC spectrum of ralsolamycin in DMSO-d_6

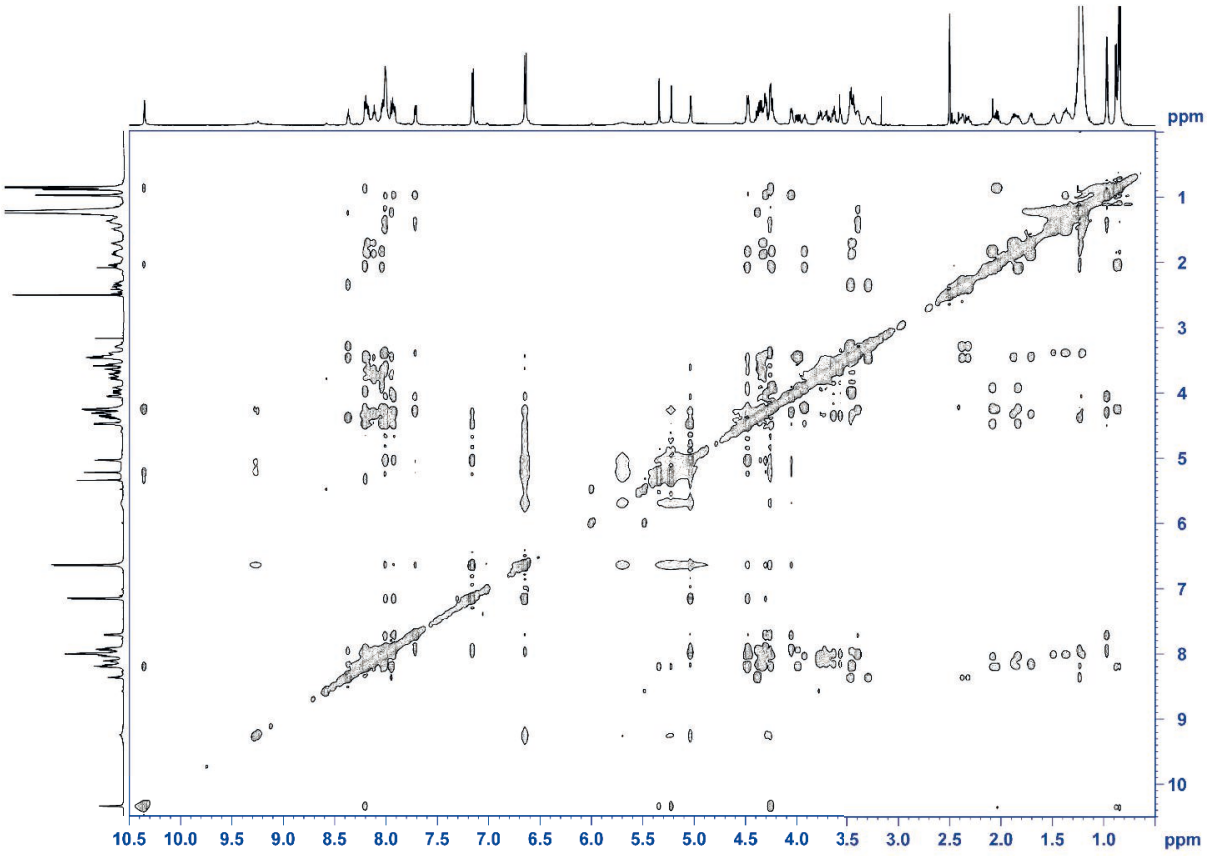

Figure S17. NOESY spectrum of ralsolamycin in DMSO-d_6

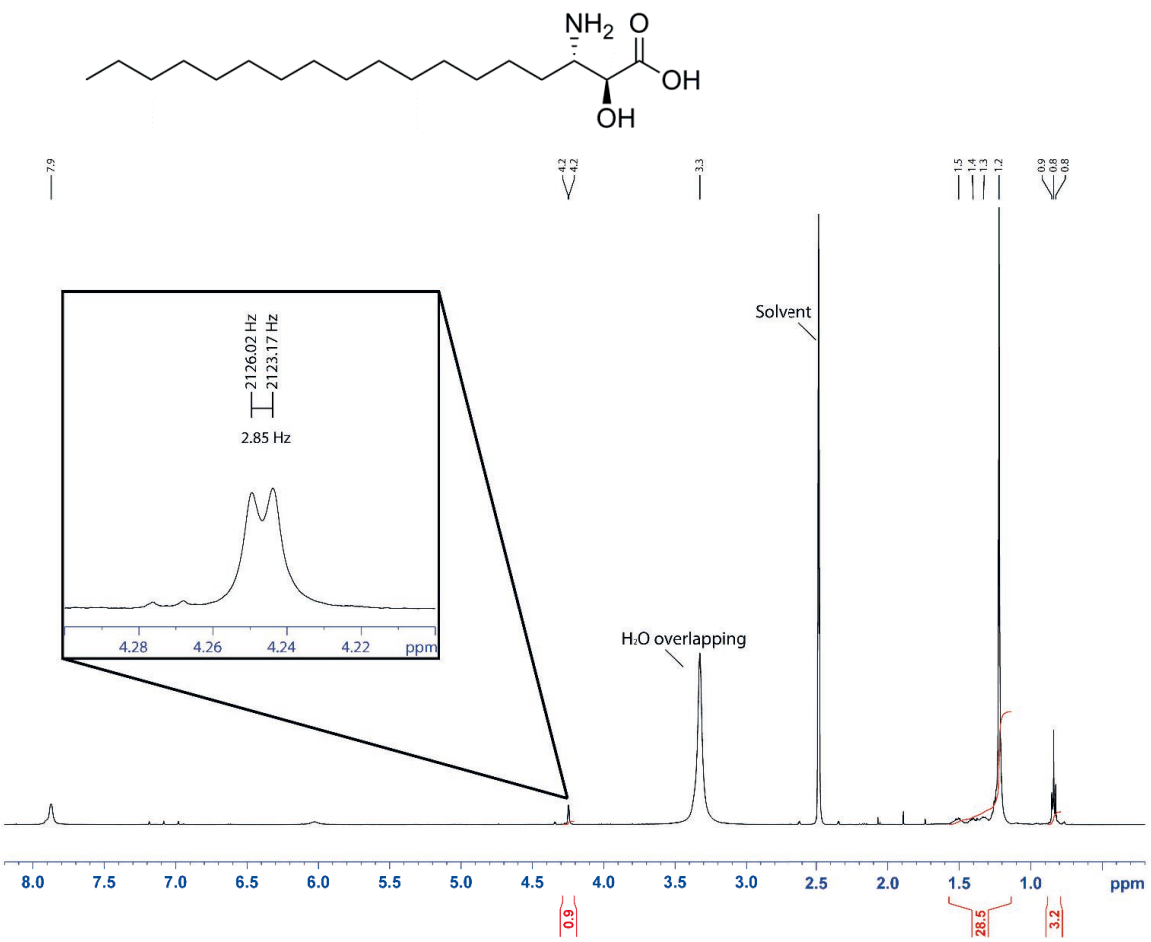

Figure S18. ^{1}H NMR spectrum of 3-amino-2-hydroxystearic acid in DMSO-d_6

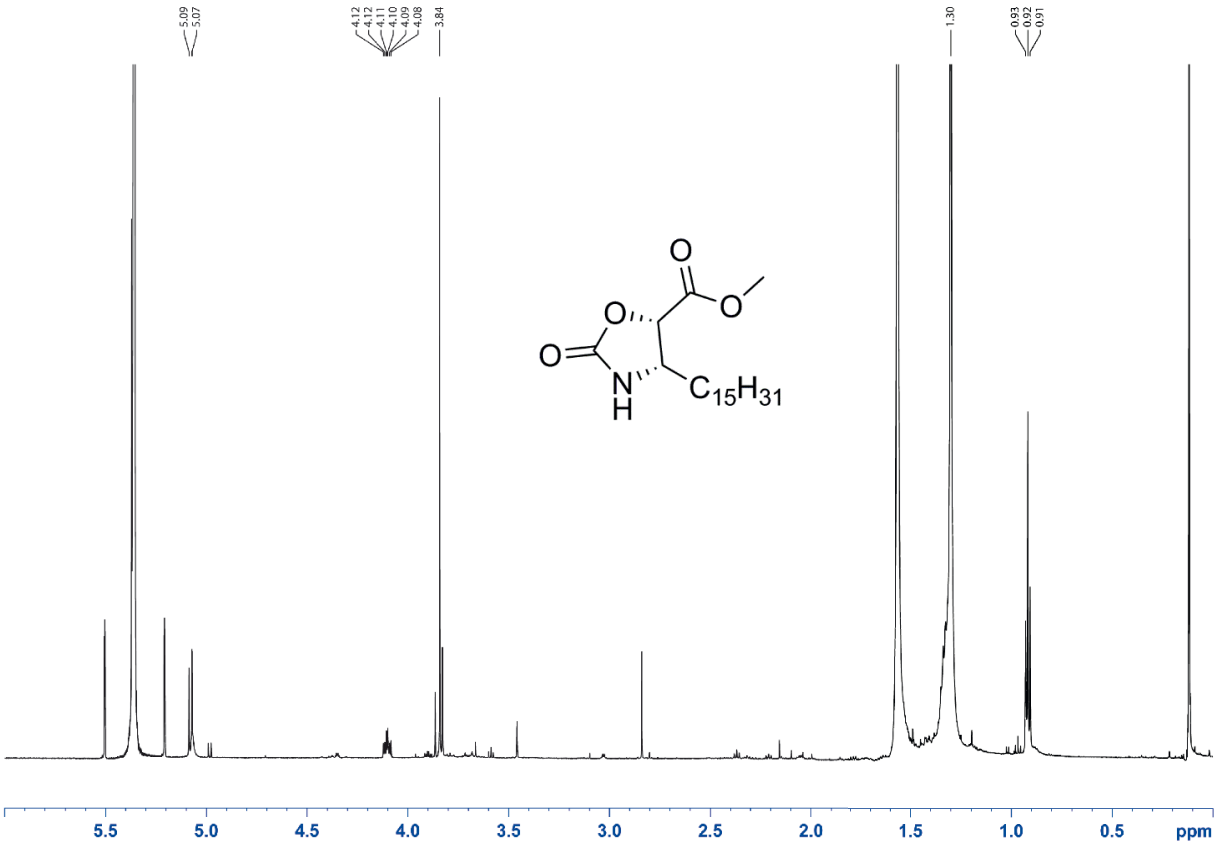

Figure S19. ^{1}H NMR spectrum of methyl 2-oxo-4-pentadecyloxazolidine-5-carboxylate in dichloromethane-d_2

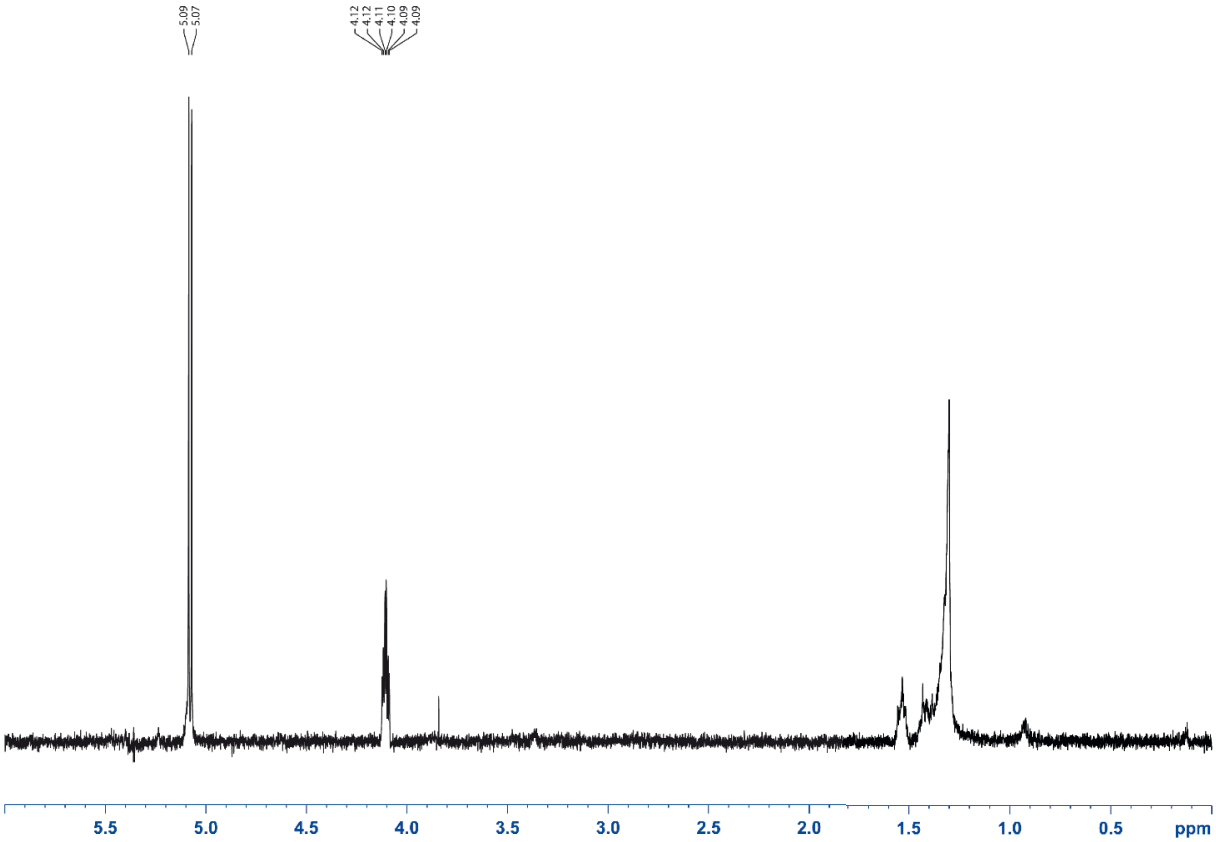

Figure S20. Selective TOCSY spectrum of methyl 2-oxo-4-pentadecyloxazolidine-5-carboxylate in dichloromethane-d_2

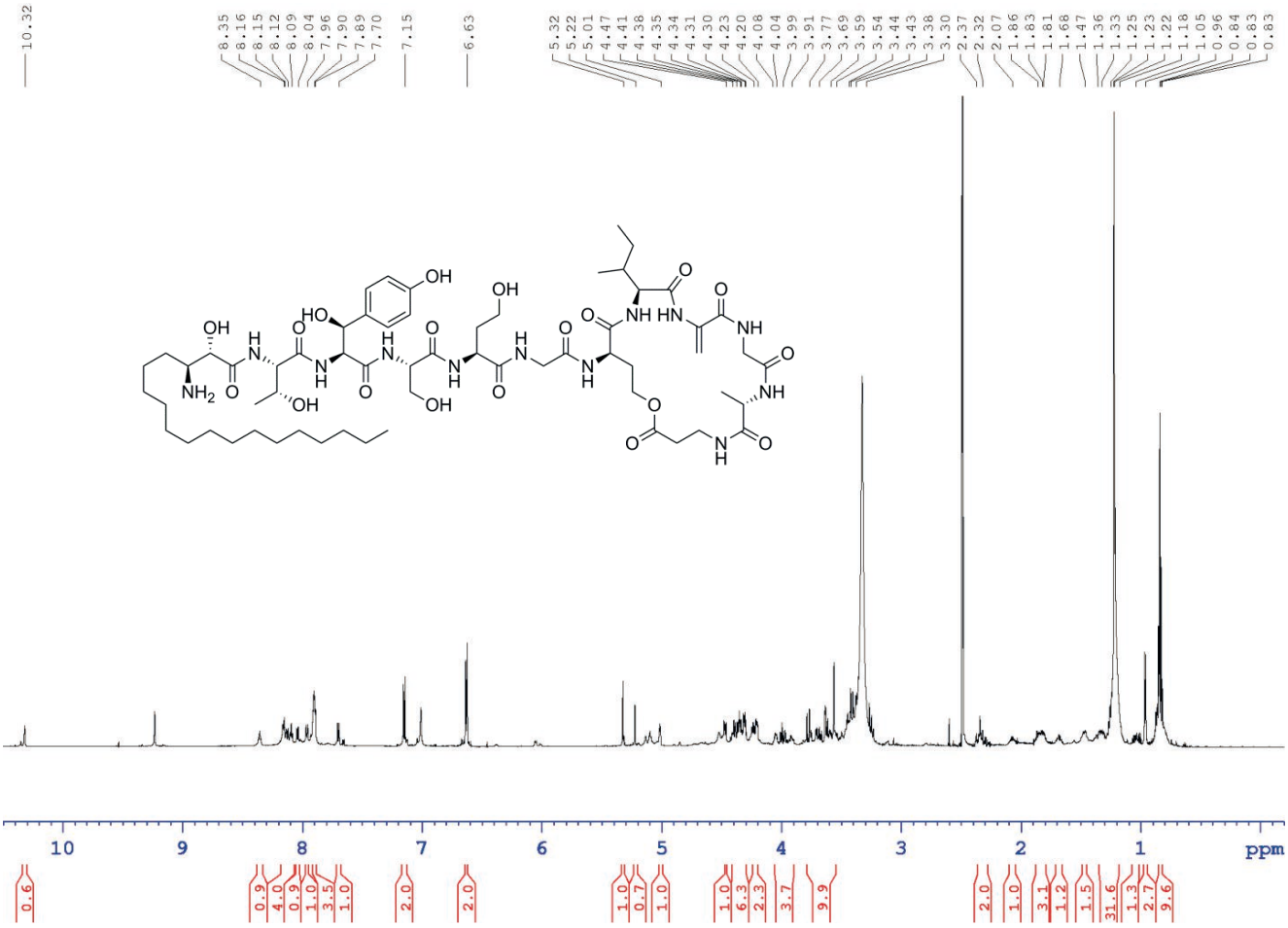

Figure S21. ^{1}H NMR spectrum of ralsolamycin B in DMSO-d_6

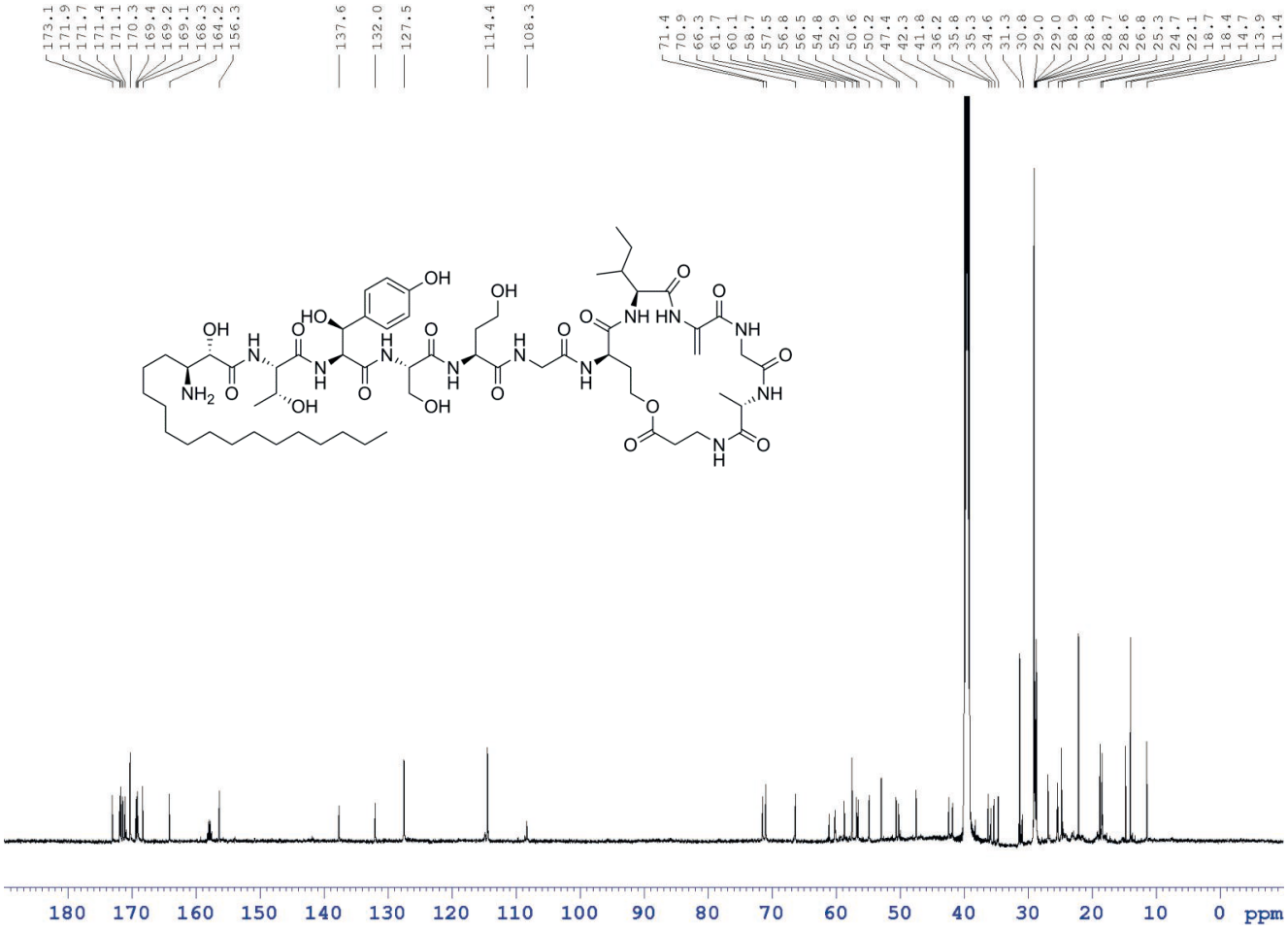

Figure S22. ^{1}H decoupled ^{13}C NMR spectrum of ralsolamycin B in DMSO-d_6

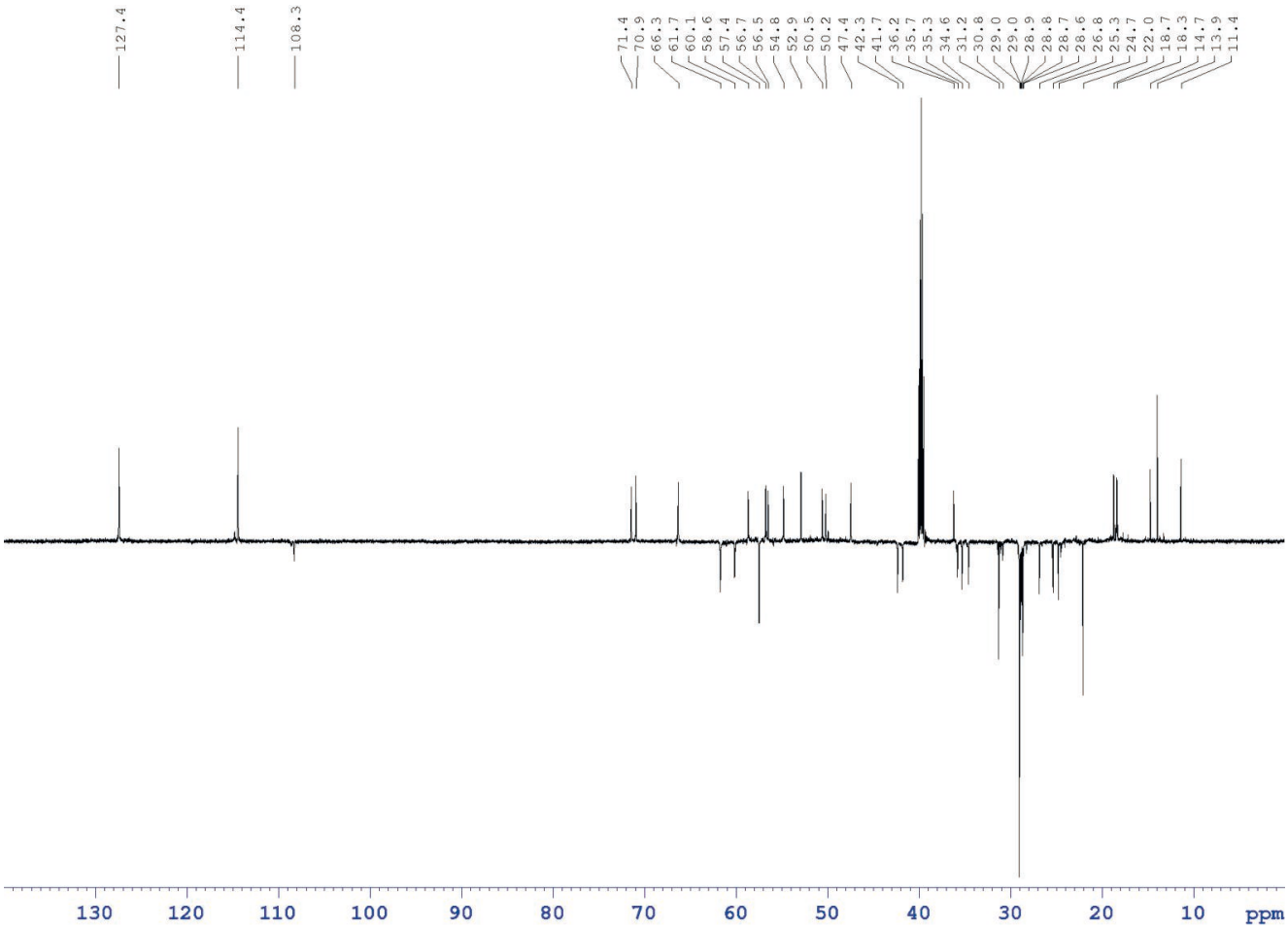

Figure S23. DEPT135 spectrum of ralsolamycin B in DMSO-d_6

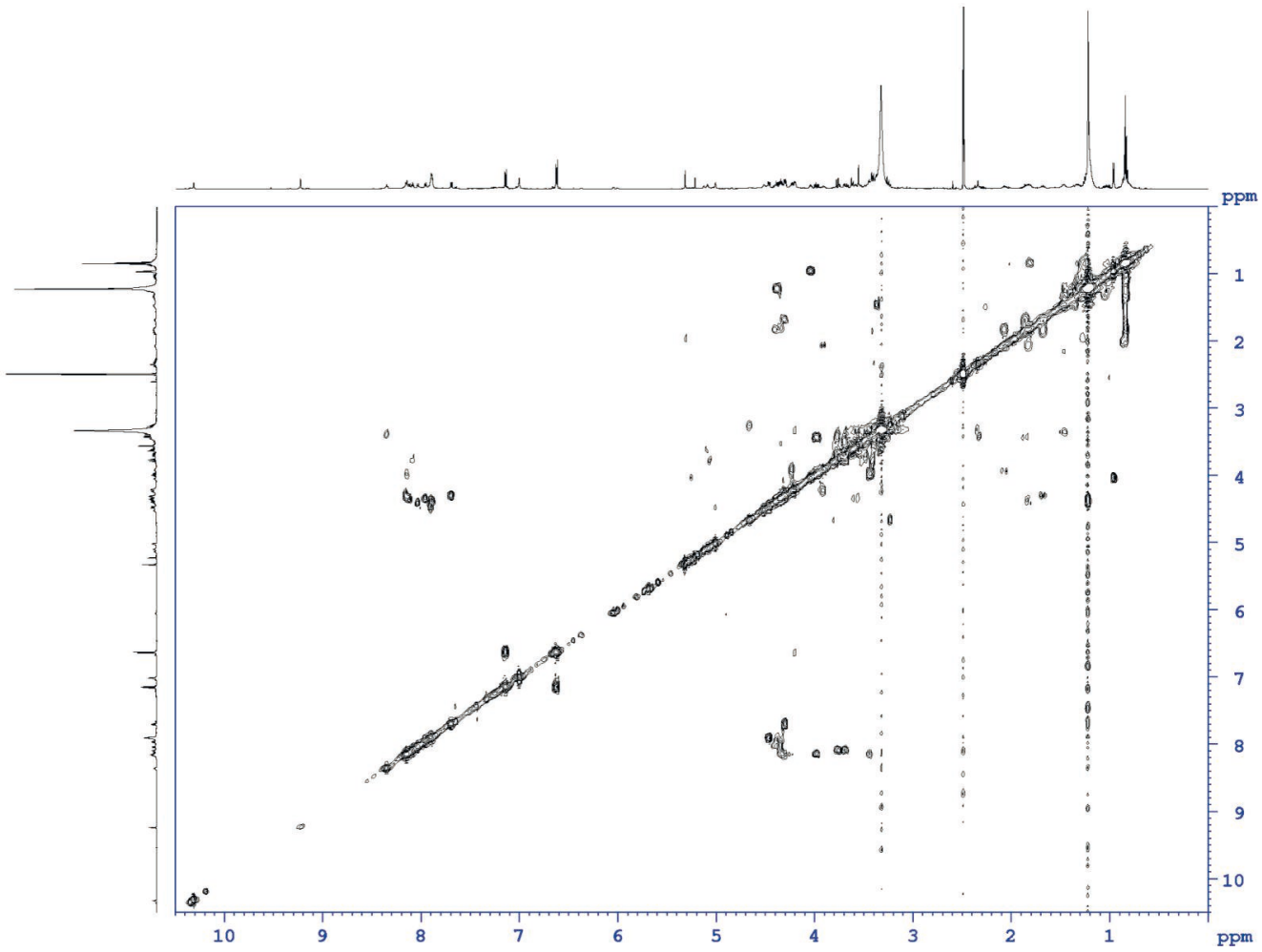

Figure S24. ^{1}H, ^{1}H COSY spectrum of ralsolamycin B in DMSO-d_6

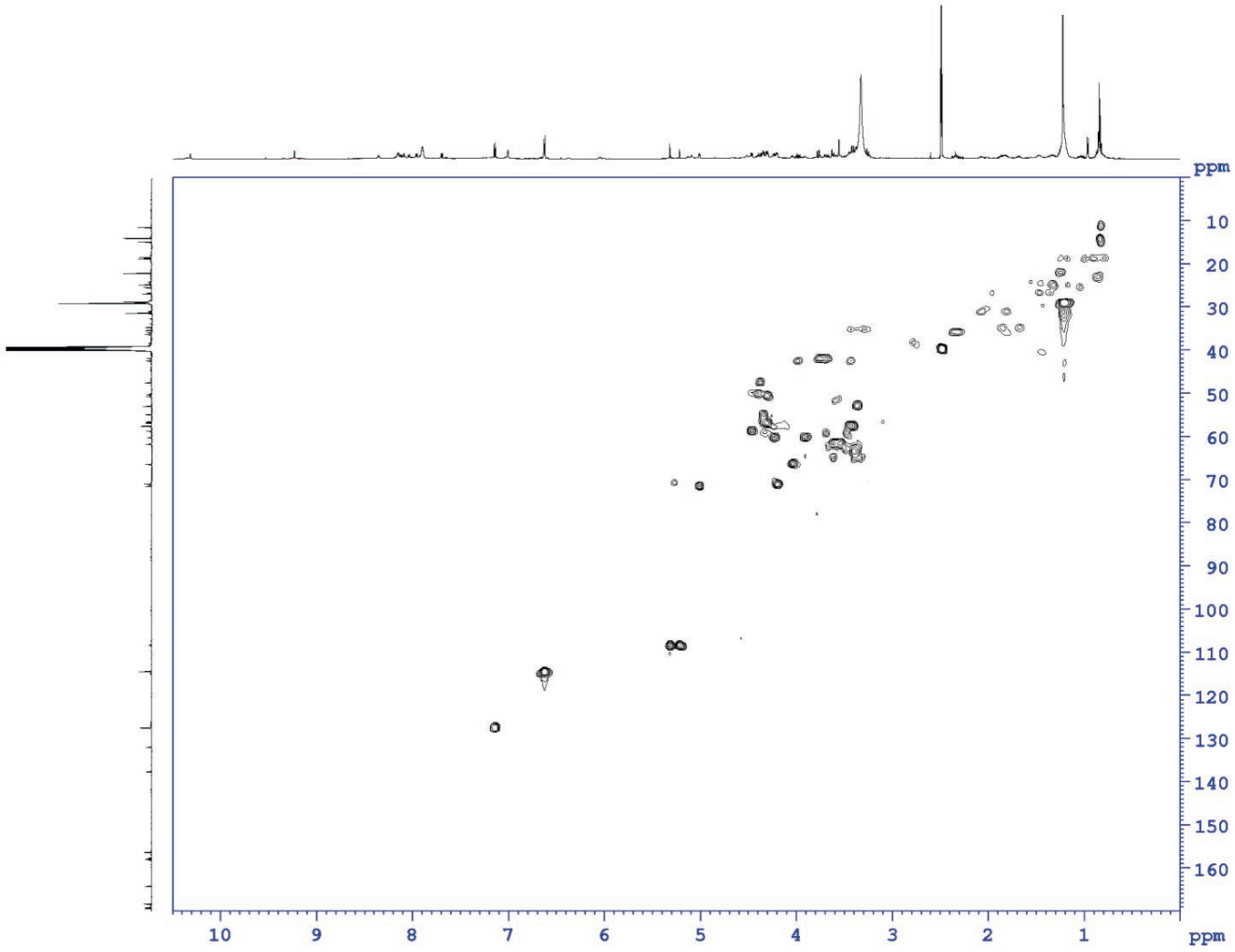

Figure S25. ^{1}H, ^{13}C HSQC spectrum of ralsolamycin B in DMSO-d_6

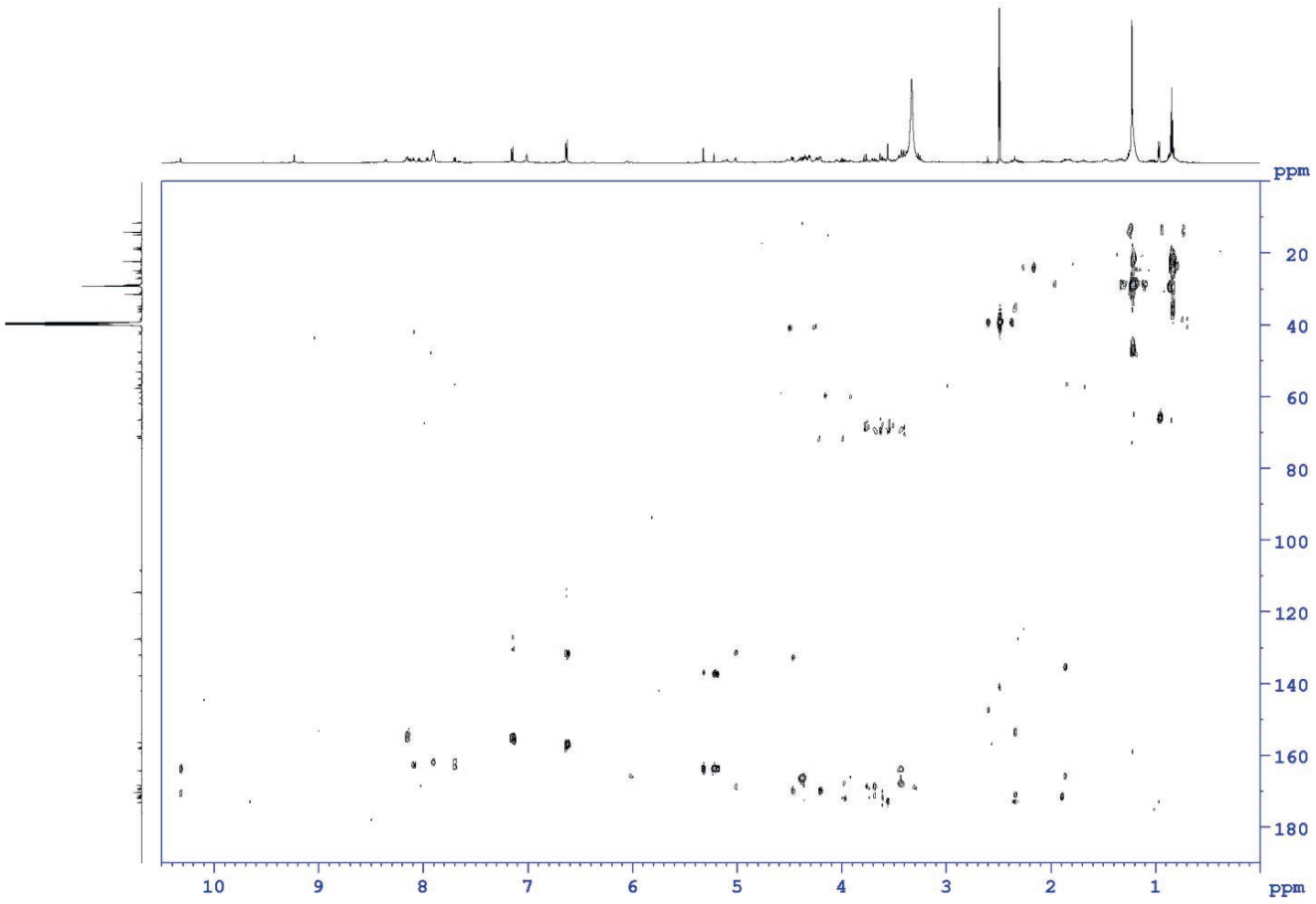

Figure S26. ^{1}H, ^{13}C HMBC spectrum of ralsolamycin B in DMSO-d_6

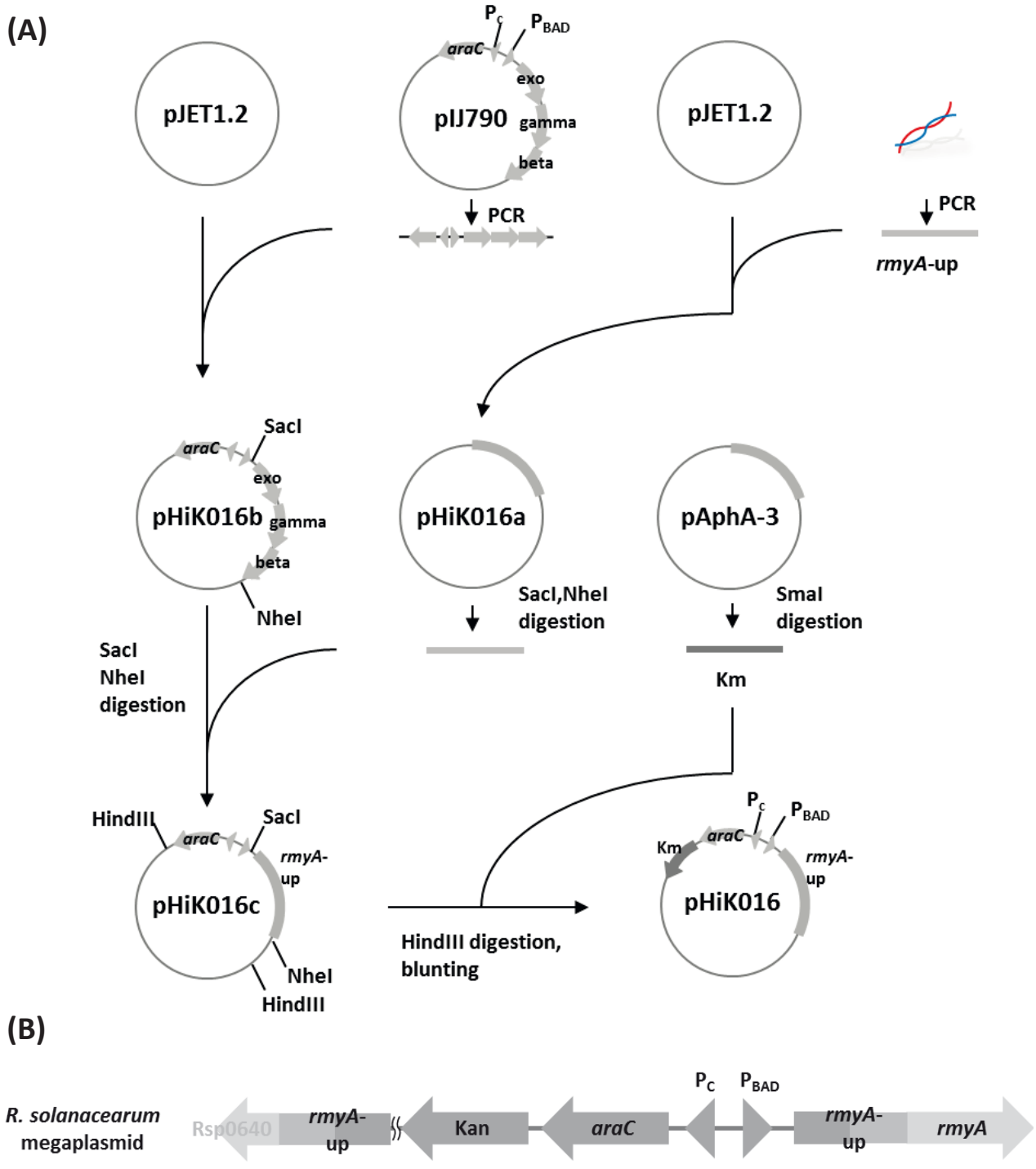

Figure S27. Cloning strategy to generate pHiK016. (A) The plasmid was constructed to integrate the arabinose-inducible promoter system into the chromosome of *R. solanacearum* GMI1000 at the non-coding upstream region of *rmyA* (*rmyA*-up). The PCR-amplified non-coding region of *rmyA* is tandemly cloned directly after the arabinose inducible promoter (P_{BAD}). Moreover the kanamycin resistance cassette (Km) was subcloned into the final plasmid construct to provide a positive selection marker during chromosomal integration in *R. solanacearum* GMI1000. (B) Ralsolamycin biosynthesis locus in strain RS15. For further details of pHiK016 construction, see the experimental procedures on page 2 in this supporting information.

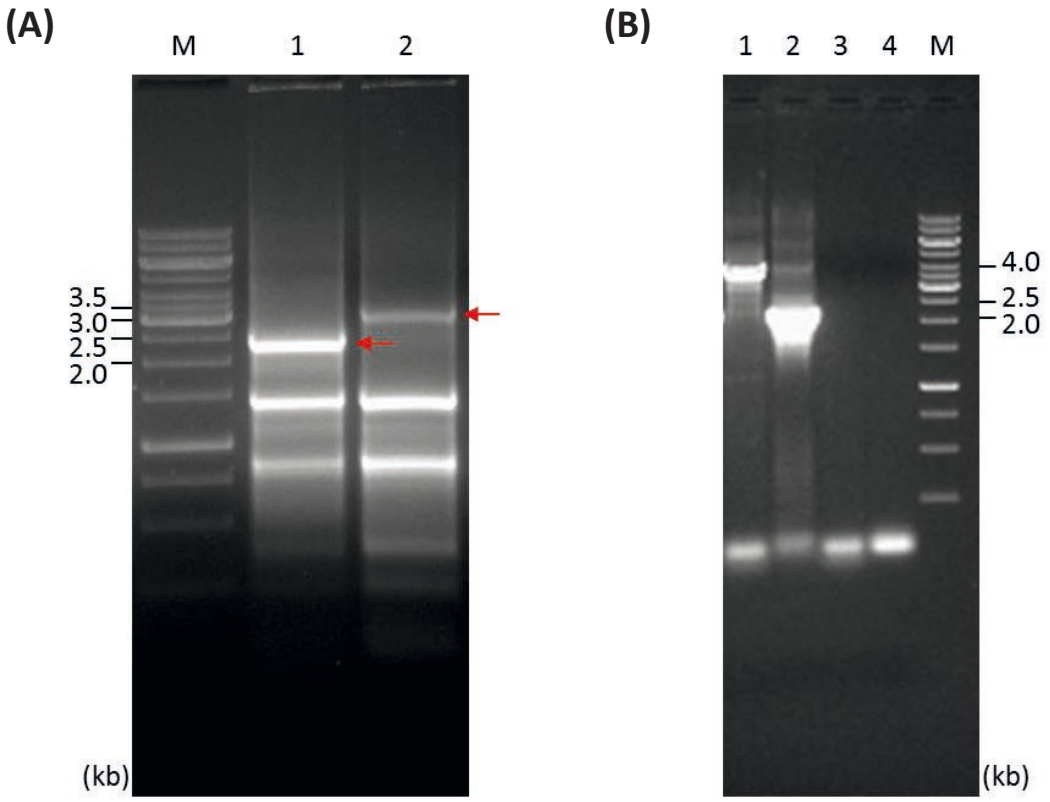

Figure S28. PCR-based confirmation of *R. solanacearum* mutants. Genomic DNA from the mutant or GMI1000 wild type strains served as template. (A) Analysis of the *rmyA* disruption mutant strain RS13. The expected size of the amplicons were 2.4 kb for RS13 (lane 1) and 3.1 kb for wild type (lane 2), indicated by red arrows in the figure. M, DNA ladder; lane 1, RS13; lane 2 GMI1000. (B) Analysis of the *rmyA* promoter mutant strain RS15. The chromosomal integration of pHiK16 in the stain RS15 was analyzed using two primer pairs. These primer pairs were designed to amplify the 4.0 kb (lane 1) and 2.1 kb (lane 2) DNA fragments in the strain RS15, consisting of the regions between the kanamycin cassette and the outside of the homologous recombination sites located in the genome of *R. solanacearum*. Since the kanamycin cassette is unique to RS15, no PCR products were obtained after using genomic DNA from the wild type GMI1000 strain (lane 3 and 4). M, DNA ladder; lane 1 and 2, RS15; lane 3 and 4, GMI1000.

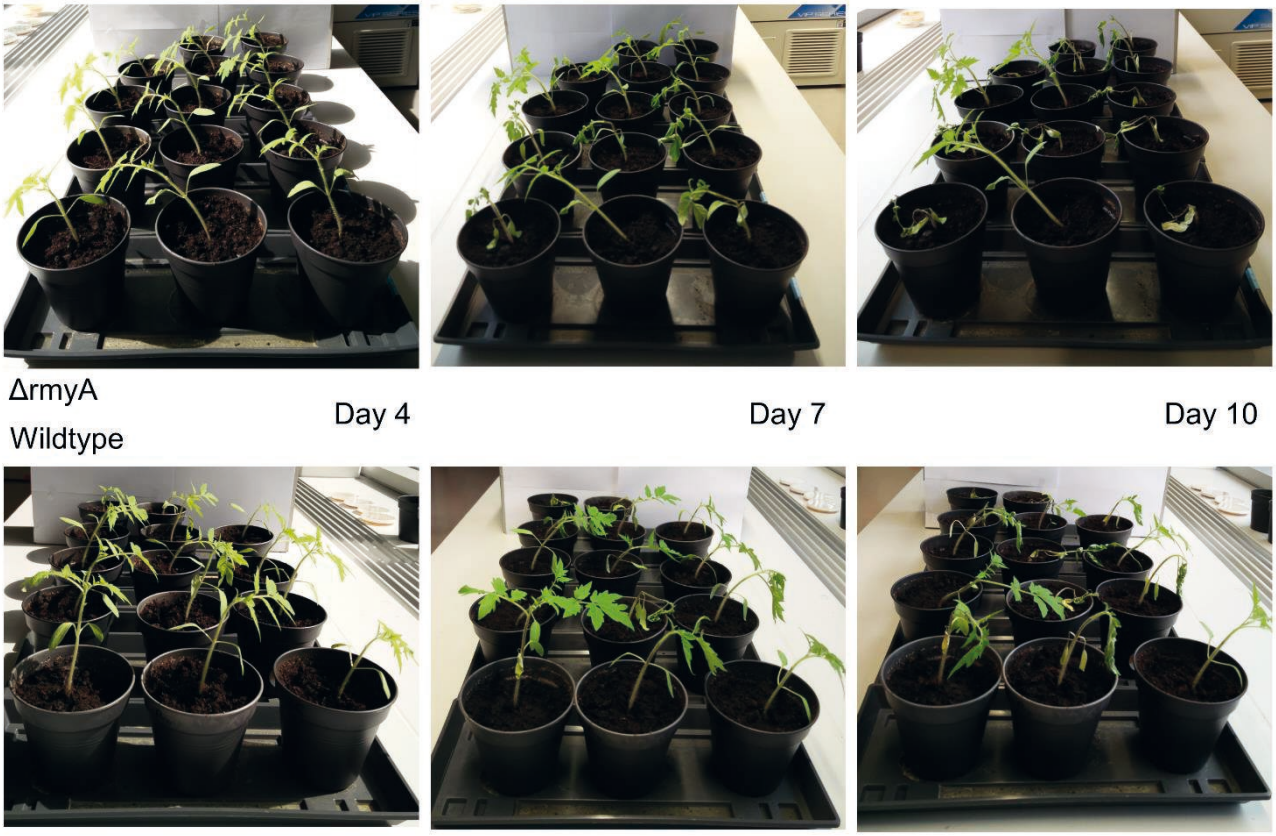

Figure S29. Petiole infection study with *R. solanacearum* strains. Photos of tomato plants following a petiole infection with *R. solanacearum* GMI1000 or the ralsolamycin-deficient mutant strain RS13.

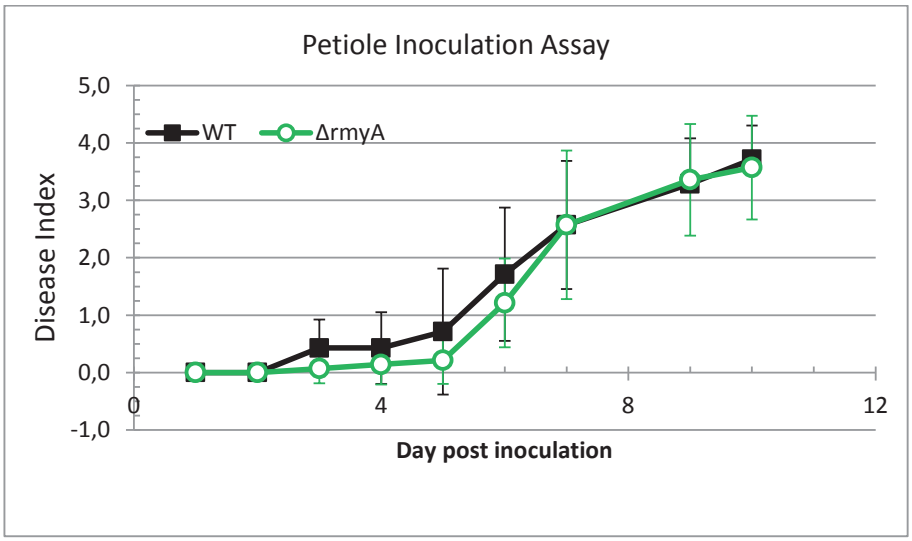

Figure S30. Monitoring of wilting disease in tomato plants following a petiole infection with *R. solanacearum* GMI1000 or the ralsolamycin-deficient mutant strain RS13. Disease index: 1, browning or discoloration; 2, dicotyle or one true leaf wilting; 3, dicotyle and/or two true leaf wilting; 4, collapsed.

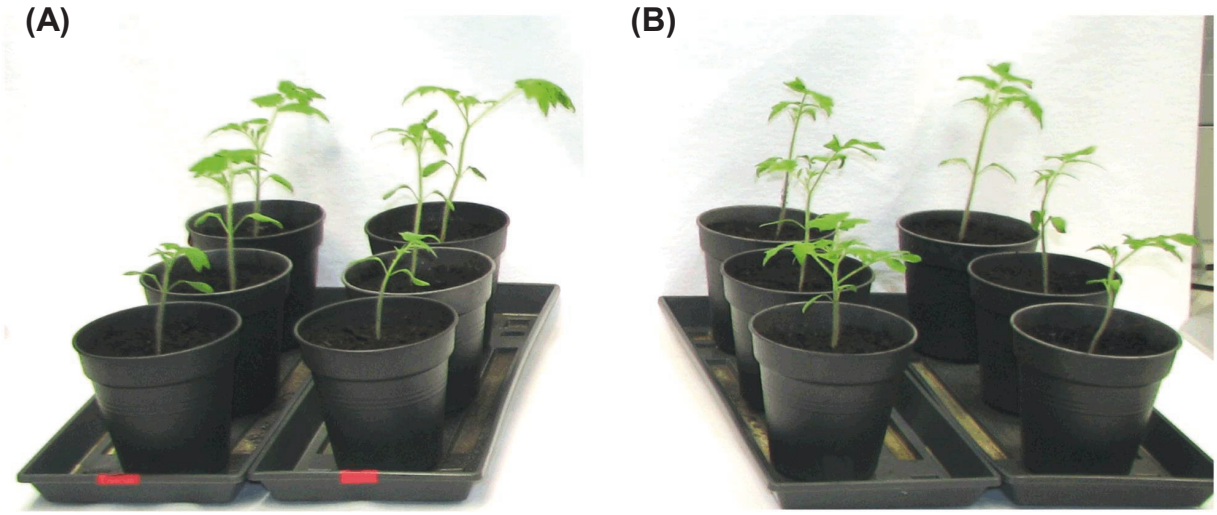

Figure S31. Photos of tomato plants, which were taken 7 days following a petiole inoculation with (A) methanol or (B) ralsolamycin. Necrosis, chlorosis or wilting were not observed in any plant.

References

(1) Cohen, G. N.; Rickenberg, H. V. *Ann. Inst. Pasteur* **1956**, *91*, 693–720.
(2) Gust, B.; Challis, G. L.; Fowler, K.; Kieser, T.; Chater, K. F. *Proc. Natl. Acad. Sci. U. S. A.* **2003**, *100*, 1541–1546.
(3) Menard, R.; Sansonetti, P. J.; Parsot, C. *J. Bacteriol.* **1993**, *175*, 5899–5906.
(4) Kage, H.; Kreutzer, M. F.; Wackler, B.; Hoffmeister, D.; Nett, M. *Chem. Biol.* **2013**, *20*, 764–771.
(5) Meng, F.; Yao, J.; Allen, C. *J. Bacteriol.* **2011**, *193*, 2477–2486.
(6) Marfey, P. *Carlsberg Res. Commun.* **1984**, *49*, 591–596.
(7) Buntin, K.; Weissman, K. J.; Müller, R. *ChemBioChem* **2010**, *11*, 1137–1146.
(8) Edgar, R. C. *BMC Bioinformatics* **2004**, *5*, 113.
(9) Edgar, R. C. *Nucleic Acids Res.* **2004**, *32*, 1792–1797.
(10) Jones, D. T.; Taylor, W. R.; Thornton, J. M. *Comput. Appl. Biosci.* **1992**, *8*, 275–282.
(11) Kumar, S.; Stecher, G.; Tamura, K. *Mol. Biol. Evol.* **2016**, *33*, 1870–1874.
(12) Meng, F.; Yao, J.; Allen, C. *J. Bacteriol.* **2011**, *193*, 2477-2486.
(13) Röttig, M.; Medema, M. H.; Blin, K.; Weber, T.; Rausch, C.; Kohlbacher, O. *Nucleic Acids Res.* **2011**, *39*, W362–W367.
(14) Fujii, K.; Shimoya, T.; Ikai, Y.; Oka, H.; Harada, K.-i. *Tetrahedron Lett.* **1998**, *39*, 2579–2582.

3.2 Publikation 2

A genomics perspective on natural product biosynthesis in plant pathogenic bacteria

Baldeweg, F.; Hoffmeister, D.; Nett, M. *Nat. Prod. Rep.* **2019**, *36*, 307–325.

Zusammenfassung:
Das Potential von pflanzenpathogenen Bakterien zur Biosynthese von Naturstoffen blieb lange Zeit unterschätzt. Mit dem Einzug der Genomsequenzierung und damit der Bioinformatik konnten verborgene Biosynthesekapazitäten aufgedeckt werden. Kombiniert mit modernen analytischen Methoden wurden unentdeckte Naturstoffe, die zur Virulenz der Pathogene beitragen, identifiziert und deren Struktur aufgeklärt. Daneben wurden auch weitere Moleküle isoliert, die nicht krankheits-assoziiert sind und zum Beispiel zur Persistenz von Bakterien außerhalb der Wirtspflanzen beitragen. Unter den gefunden Naturstoffen waren auch bioaktive Verbindungen mit pharmazeutischem Potential. In dieser Übersichtsarbeit werden die herausragendsten Forschungsergebnisse aus diesem Gebiet zusammengefasst. Ein besonderer Fokus liegt dabei auf einzigartigen Merkmalen von Biosynthesewegen sowie der biologischen Aktivität der Verbindungen.

Angaben zum Eigenanteil von Florian Baldeweg (40%):
Erstellung von Abbildungen, Bioinformatische Analyse von Genclustern, Berechnung phylogenetischer Abstammung und Literaturrecherche. Mitarbeit am Manuskript.

Jena, den

Prof. Dirk Hoffmeister

Natural Product Reports

REVIEW

Cite this: *Nat. Prod. Rep.*, 2019, **36**, 307

A genomics perspective on natural product biosynthesis in plant pathogenic bacteria

Florian Baldeweg,[a] Dirk Hoffmeister[a] and Markus Nett *[b]

Received 27th March 2018

DOI: 10.1039/c8np00025e

rsc.li/npr

Covering: up to February 2018

In recent years, genome sequencing revealed the full biosynthetic potential of bacteria causing plant diseases. Bioinformatics and advanced analytical techniques paved the way to clarify the structures of long-sought natural products with a role in virulence. Furthermore, several compounds without disease-associated function were discovered. The exploration of these molecules disclosed persistence strategies of plant pathogenic bacteria outside their hosts and provided access to new bioactive compounds with therapeutic potential. In this review, we will summarize some of the striking findings in the field, paying particular attention to unique natural product pathways and their unprecedented biosynthetic features as well as the biological activities of the retrieved compounds.

1. Introduction

The blueprints for the biosynthesis of natural products are genetically fixed. It is therefore no surprise that genome sequences provide comprehensive maps of secondary metabolism. This is particularly evident in bacteria and fungi, where associated genes are locally concentrated in compact clusters.[1] Advances in the mechanistic and molecular understanding of natural product biosynthesis set the foundation for decoding genetic into chemical information and, by means of bioinformatic analyses, it has become possible to predict the natural products encoded in a microbial genome.[2] In the case of well-studied producer strains, this approach typically reveals many more metabolites than previously observed in culture-based investigations[3] and, by now, there are numerous examples in the literature, in which genomic information was successfully exploited for the discovery of so-called "cryptic" or "orphan" metabolites.[4,5]

Recent years have seen a number of detailed reviews on the genomic potential of selected microorganisms for natural product biosynthesis. Most of these articles cover established producer organisms, such as actinomycetes,[6] myxobacteria,[7] cyanobacteria,[8] pseudomonads,[9] and ascomycetes.[10] However, there are also reports on microbes, such as clostridia, which have only recently been identified as producers of bioactive secondary metabolites.[11] Unlike many reviews in this field, the present work does not focus on a single taxonomic lineage. Instead, we will provide genomic snapshots of natural product biosynthesis in a very heterogeneous group of bacteria, of which the commonality is the capability to provoke plant diseases.

2. Genome sequencing projects of plant pathogenic bacteria

Soon after the sequencing of bacterial genomes became a reality in 1995,[12] researchers initiated sequencing projects of pathogens, including those that pose a threat to agricultural crops. The motivation behind these efforts was to identify molecular determinants of virulence, to achieve a better understanding of pathogen evolution and, eventually, to find possible targets for disease control.[13] In case of plant pathogenic bacteria, the first genome to be fully sequenced was that of *Xylella fastidiosa* 9a5c in 2000.[14] In rapid succession, other prominent pathogens were

[a]*Department of Pharmaceutical Microbiology at the Hans Knöll Institute, Friedrich-Schiller-University Jena, Winzerlaer Strasse 2, 07745 Jena, Germany*

[b]*Department of Biochemical and Chemical Engineering, TU Dortmund University, Emil-Figge-Strasse 66, 44227 Dortmund, Germany. E-mail: markus.nett@tu-dortmund.de*

sequenced. Among them were representatives of species causing substantial economic damage, such as *Pseudomonas syringae* and *Ralstonia solanacearum*, as well as bacteria of scientific interest beyond the field of plant pathology, *e.g.*, the transformation vehicle *Agrobacterium tumefaciens* or the xanthan gum producer *Xanthomonas campestris*.[15–24]

A comparison of their genomic features shows that plant pathogens in the phylum Proteobacteria typically possess genome sizes between 4 and 6.5 Mb (Table 1). However, there are also noticeable exceptions, such as the orange pathogen *X. fastidiosa* 9a5c. Although this bacterium belongs to the same family as *Xanthomonas axonopodis* and *X. campestris*, its genome is only about half the size of the latter. Comparative genomics indicated that the ancestral genome of *X. fastidiosa* had been shaped by extensive gene losses, and it was speculated that this erosion had been accompanied by niche specialization.[25] While most xanthomonads are capable to colonize different plant tissues, *X. fastidiosa* is confined to live in dead xylem cells and tracheary elements exclusively. The enterobacterium *Erwinia amylovora* also features a rather small genome relative to other plant pathogens of the Proteobacteria and to the Enterobacteriaceae, in particular. For *E. amylovora*, the reduced genome size was attributed to deletion and pseudogenization of genes involved in anaerobic respiration and nitrate assimilation.[26] Again, host adaptation was proposed to account for the gene loss.[26] At the other extreme, *Burkholderia* spp. feature large multireplicon genomes consisting of multiple chromosomes and plasmids. The largest chromosome usually harbors essential, housekeeping genes, while the other replicons endow the bacterium with the information necessary to survive under different environmental conditions. The genomes of the actinobacterial pathogens differ considerably in size, ranging from 2.6 Mb of the xylem-inhabiting *Leifsonia xyli* ssp. *xyli* to 10.1 Mb of the soil-borne *Streptomyces scabiei*. The giant size of the *Streptomyces* genome as well as its linear architecture are typical for members of this genus,[6] and no characteristic hallmarks of pathogenicity.

To assess the biosynthetic potential of the bacteria listed in Table 1, their genomes were analyzed with the bioinformatic platform antiSMASH 4.0, which rapidly identifies loci involved in secondary metabolite biosynthesis and predicts their gene boundaries.[27] This testing revealed that almost all plant pathogens possess the genetic prerequisites for synthesizing natural products. The only organism lacking biosynthetic capabilities is the obligate intracellular parasite Cand. *Phytoplasma asteris*. Concerning the other bacteria, it became evident that the biosynthetic proficiency is not evenly distributed. Only few strains have the capacity to produce more than 10 secondary metabolites (Table 1). Most noteworthy among these talented bacteria are the *Streptomyces* and *Burkholderia* species, although the common assumption that larger genomes harbor also more biosynthetic gene clusters (BGCs)[3] was only partially confirmed. This is obvious for the two *Clavibacter michiganensis* subspecies,[28,29] which have almost identical genome sizes, but show significant discrepancy in the number of BGCs and the respective genome portion dedicated to natural product biosynthesis. The *Pseudomonas syringae* strain DC3000 has a genome that is about 0.4 Mb larger than that of strain B728a. Still, antiSMASH indicated a lower number of BGCs for the DC3000 strain (8 *vs.* 11). Among the missing loci are two gene clusters directing the biosynthesis of the phytotoxins syringomycin and syringopeptin.[24] A surprising finding of the bioinformatic analysis was the comparatively large number of

Florian Baldeweg studied pharmacy at the Friedrich-Schiller-University Jena. Following his diploma project at Excella GmbH, he joined the research group of Professor Markus Nett as fellow of the graduate school Jena School for Microbial Communication. Actually, Florian is an associate researcher in the Department of Pharmaceutical Microbiology at the Hans Knöll Institute in Jena. His PhD project is about the isolation and structure elucidation of secondary metabolites from plant pathogenic bacteria.

Dirk Hoffmeister is Professor for Pharmaceutical Microbiology at the Friedrich-Schiller-University Jena (Germany). He is also affiliated with the Leibniz Institute for Natural Product Research and Infection Biology – Hans Knöll Institute. Before having moved to Jena, he worked as Assistant Professor in the Department of Plant Pathology at the University of Minnesota – Saint Paul. Research in his group is focused on the biochemical and genetic basis underlying the biosyntheses of microbial natural products.

Markus Nett obtained his PhD degree from the University of Bonn, followed by postdoctoral research at the Scripps Institution of Oceanography in La Jolla. In 2009, he established his independent research group at the Leibniz Institute for Natural Product Research and Infection Biology in Jena, where he was working on the secondary metabolism of predatory bacteria. Since 2016 he is Professor for Technical Biology at TU Dortmund University. His research interests are in the field of genomics-guided drug discovery as well as in the engineering of biosynthetic pathways.

Table 1 Genomic features of representative plant pathogenic bacteria

	Genome architecture[a]	Total genome size (Mbp)	NP genome portion[b] (%)	Total number of BGCs[c,d]	Classification of BGCs PKS-PKS/NRPS-NRPS-RiPP-terpene-NIS-other[c,d]
Actinobacteria					
Clavibacter michiganensis ssp. *michiganensis* NCPPB382	c: 1C, p: 2C	3.40	8.0	8	1-0-1-2-1-1-2
Clavibacter michiganensis ssp. *sepedonicus* ATCC 33113	c: 1C, p: 1C 1L	3.40	4.2	5	1-0-0-1-1-1-1
Leifsonia xyli ssp. *xyli* CTCB07	c: 1C	2.58	7.1	5	2-0-1-1-1-0-0
Streptomyces scabiei str. 87.22	c: 1L	10.15	12.1	32	5-1-4-5-8-4-5
Proteobacteria					
Agrobacterium tumefaciens C58	c: 1C 1L, p: 2C	5.67	2.9	4	0-1-0-0-1-0-2
Burkholderia gladioli BSR3	c: 2C, p: 4C	9.05	11.2	23	2-3-7-4-4-0-3
Burkholderia glumae BGR1	c: 2C, p: 4C	7.28	10.5	15	2-4-2-1-4-0-2
Burkholderia plantarii ATCC 43733	c: 2C, p: 1C	8.08	11.8	24	2-2-6-3-4-1-6
Dickeya dadantii DSM 18020	c: 1C	5.00	8.2	8	0-2-1-3-0-1-1
Dickeya solani str. 3337	c: 1C	4.92	10.2	10	1-2-1-3-0-1-2
Dickeya zeae Ech586	c: 1C	4.81	8.3	9	0-1-2-3-0-1-2
Erwinia amylovora CFBP 1430	c: 1C, p: 1C	3.83	3.4	3	0-1-1-0-0-1-0
Erwinia pyrifoliae Ep1/96	c: 1C, p: 4C	4.07	1.8	2	0-0-1-0-0-1-0
Pectobacterium atrosepticum SCRI1043*b*	c: 1C	5.06	6.3	7	1-0-2-0-0-1-3
Pseudomonas syringae pv. *syringae* B728a	c: 1C	6.09	11.4	11	1-1-4-0-0-0-5
Pseudomonas syringae pv. *tomato* DC3000	c: 1C, p: 2C	6.54	7.2	8	1-1-2-0-0-1-3
Ralstonia solanacearum GMI1000	c: 1C, p: 1C	5.81	7.6	11	0-2-2-1-1-1-4
Ralstonia solanacearum Po82	c: 1C, p: 1C	5.43	7.3	10	1-1-1-2-1-1-3
Ralstonia solanacearum PSI07	c: 1C, p: 1C	5.61	6.7	8	1-1-1-1-1-0-3
Xanthomonas albilineans GPE PC73	c: 1C, p: 3C	3.85	11.4	8	0-2-3-1-0-1-1
Xanthomonas axonopodis pv. *citri* str. 306	c: 1C, p: 2C	5.27	3.5	5	0-0-2-1-0-1-1
Xanthomonas campestris pv. *campestris* ATCC 33913	c: 1C	5.08	2.0	3	0-0-1-0-0-1-1
Xanthomonas oryzae pv. *oryzae* MAFF 311018	c: 1C	4.94	1.3	2	0-0-0-0-0-1-1
Xylella fastidiosa str. 9a5c	c: 1C, p: 2C	2.73	1.5	1	0-0-0-0-0-0-1
Tenericutes					
Candidatus *Phytoplasma asteris* str. OY-M	c: 1C, p: 2C	0.86	0.0	0	0-0-0-0-0-0-0

[a] Numbers of chromosomes (c) and plasmids (p) as well as their topology: C, circular replicon; L, linear replicon. [b] Genome portion involved in natural product (NP) biosynthesis according to the cluster boundary prediction by antiSMASH.[27] [c] Assignment of the NP loci to certain biosynthetic classes according to antiSMASH.[27] [d] Abbreviations: BGCs, biosynthetic gene clusters; PKS, polyketide synthase; NRPS, nonribosomal peptide synthetase; RiPP, ribosomally synthesized and post-translationally modified peptide; NIS, NRPS-independent siderophore synthetase.

BGCs encoded in the genomes of *Ralstonia solanacearum* and *Dickeya* spp. Unlike *Streptomyces*, *Burkholderia* and *Pseudomonas*, the genera *Ralstonia* and *Dickeya* are not well-known sources of secondary metabolites. In the following chapters, we will focus our attention on genomics-inspired natural product research in plant pathogenic bacteria and provide snapshots of the genomic potential of some selected strains.

3. *Ralstonia solanacearum*

R. solanacearum is the causative agent of a lethal wilt disease. It has an unusually wide host range, including more than 200 mono- and dicotyledonous plant species.[30] The soil-borne pathogen typically invades plants through the roots and then disseminates *via* the vascular system. Infected plants wilt and die, probably because water transport is impeded by the sheer mass of bacteria and associated extracellular polymeric substances. *R. solanacearum* causes severe losses in agriculture due to the global occurrence of the pathogen, the susceptibility of many crop plants, and the limited means of control currently available.[31]

Natural product research in *R. solanacearum* did not start before 2004. At this time, the genome sequence of the model strain GMI1000 was already available,[18] which had a strong

impact on the following investigations. The first compound reported from *R. solanacearum* was the siderophore staphyloferrin B (**1**). Bhatt and Denny had observed that mutants, which were defective in the virulence regulator PhcA, exhibited stronger iron-scavenging activity compared to the wild type.[32] To clarify the genetic basis of this observation, they subjected *phcA* mutants to transposon mutagenesis and screened for transformants, in which the aforementioned effect was reversed. This approach led to the identification of a siderophore biosynthesis operon (RSp0415-0424; see Fig. 1 and Table 2) and its product **1**.[32] Soon after this discovery, evidence emerged that *R. solanacearum* GMI1000 produces another small molecule. Using a pan-genomic microarray, Stéphane Genin's and Christian Boucher's group identified a BGC (RSp0693-0698) under the transcriptional control of HrpB.[33] This finding was interesting for three reasons: first, the activator HrpB is known to govern the production of a type III secretion system, which is indispensable for the injection of effector proteins into plant cells. Therefore, it appeared possible that other HrpB-dependent genes might also have a role in virulence. Secondly, the RSp0693-0698 operon is fully conserved in the genome of the plant pathogen *Xanthomonas campestris* pv. *campestris*, where it resides within the *hrp* pathogenicity island.[17] Thirdly, the identified locus could not be associated with the production of a known secondary metabolite and the annotation of the individual biosynthesis genes gave hardly any clue regarding the structure of this molecule. Following the optimization of production and isolation conditions, the structure of the so-called Hrp-dependent factor (HDF, **2**) could be eventually determined as 3-hydroxy-indolin-2-one.[34] Although HDF-deficient mutants remained fully pathogenic, it was shown that **2** is actually produced *in planta* and that the absence of this metabolite affects the growth of the bacterium in its host.[35]

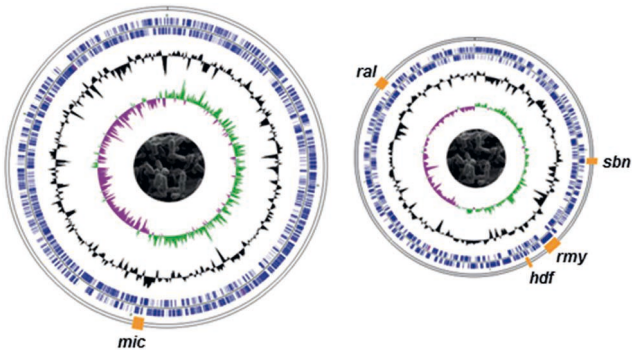

Fig. 1 Genome of *R. solanacearum* GMI1000, consisting of a chromosome (left) and a megaplasmid (right). The inner circles show a normalized plot of GC skew, while the center circles show a normalized plot of GC content. Orange boxes on the outer circles indicate the position of biosynthesis gene clusters: Hrp-dependent factor (*hdf*), micacocidin (*mic*), ralfuranone (*ral*), ralsolamycin (*rmy*), staphyloferrin B (*sbn*).

Table 2 Biosynthetic loci in *Ralstonia solanacearum* GMI1000

No.	Cluster location	Actual or predicted product[a]	References
1	RSc0424-0436	Arylpolyene	
2	RSc1652	Terpene	
3	RSc1804-1813	**Micacocidin** (**5**)	43
4	RSc3286-3287	*N*-Acylhomoserine lactone	
5	RSp0163-0165	—[b]	
6	RSp0354-0372	Arylpolyene	
7	RSp0415-0424	**Staphyloferrin B** (**1**)	32
8	RSp0638-0642	**Ralsolamycin** (**6**)	52 and 53
9	RSp0693-0698	**Hrp-dependent factor** (**2**)[c]	34
10	RSp0778-0779	*N*-Acylhomoserine lactone	
11	RSp1070-1078	Microcin	
12	RSp1417-1425	**Ralfuranone** (**3**)	36 and 37

[a] Observed products are highlighted in bold. [b] The gene cluster features an NRPS pseudogene and is hence not functional. [c] The HDF locus was not identified by antiSMASH[27] but assigned on the basis of literature data.

Subsequent research into the secondary metabolism of strain GMI1000 originated from phenotypic characterization of mutants that were defective in regulatory genes. Metabolites that were lost upon inactivation of global virulence regulators included the compound ralfuranone (**3a**),[36] which represented the first member of a natural product family specific for *R. solanacearum* strains. Initially, the biosynthetic basis of ralfuranone formation was elusive. Yet, a genome-wide search for potential biosynthesis genes led to two candidates, RSp1419 and RSp1424. While the former encodes a tri-domain NRPS-like enzyme named RalA, the latter was annotated as transaminase, RalD. Biochemical analysis showed that RalD deaminates L-phenylalanine to phenylpyruvate and, thus, was expected to provide RalA with substrate.[37] RalA-like enzymes are composed of an adenylation domain selective for α-keto acids, a thiolation and a thioesterase domain. Consistent with the absent α-amino group in the substrate, RalA-type enzymes do not include a condensation domain. Rather, the thioesterase catalyzes furanone formation by introducing a C–C bond between the α- and β-carbon atoms of two phenylpyruvate building blocks and subsequent intramolecular lactonization (Fig. 2). This biosynthetic model was supported by the discovery of ralfuranone B (**3b**), a phenyl, benzyl substituted furane-2-one, which reflects the biosynthetic origin from two phenylpropanoid units. Final evidence came from stable-isotope feeding experiments which proved that ralfuranone biosynthesis is taking a previously unknown route for aryl-substituted γ-lactone formation.[38] In-depth chemical analyses revealed ralfuranones C through E featuring thiol-, methyl thioether, and methyl sulfoxide groups, respectively.[39] *In vivo* stable-isotope labeling and GC/MS-based headspace analysis established a non-enzymatic transfer of an intact methylthio moiety from L-methionine or, alternatively, from α-keto-γ-methylthiobutyric acid onto ralfuranone I (**3c**), a highly reactive Michael acceptor intermediate.[39] It represents the precursor to **3b**, **3a**, and other ralfuranones.[40,41] The biological function of the ralfuranones has not been fully elucidated yet. The reactivity of **3c** with thiols, including glutathione, may point to a role in interfering with glutathione-mediated host cell signaling during colonization by the pathogen.[39] A Δ*ralA* mutant showed a trend for delayed onset of symptoms with

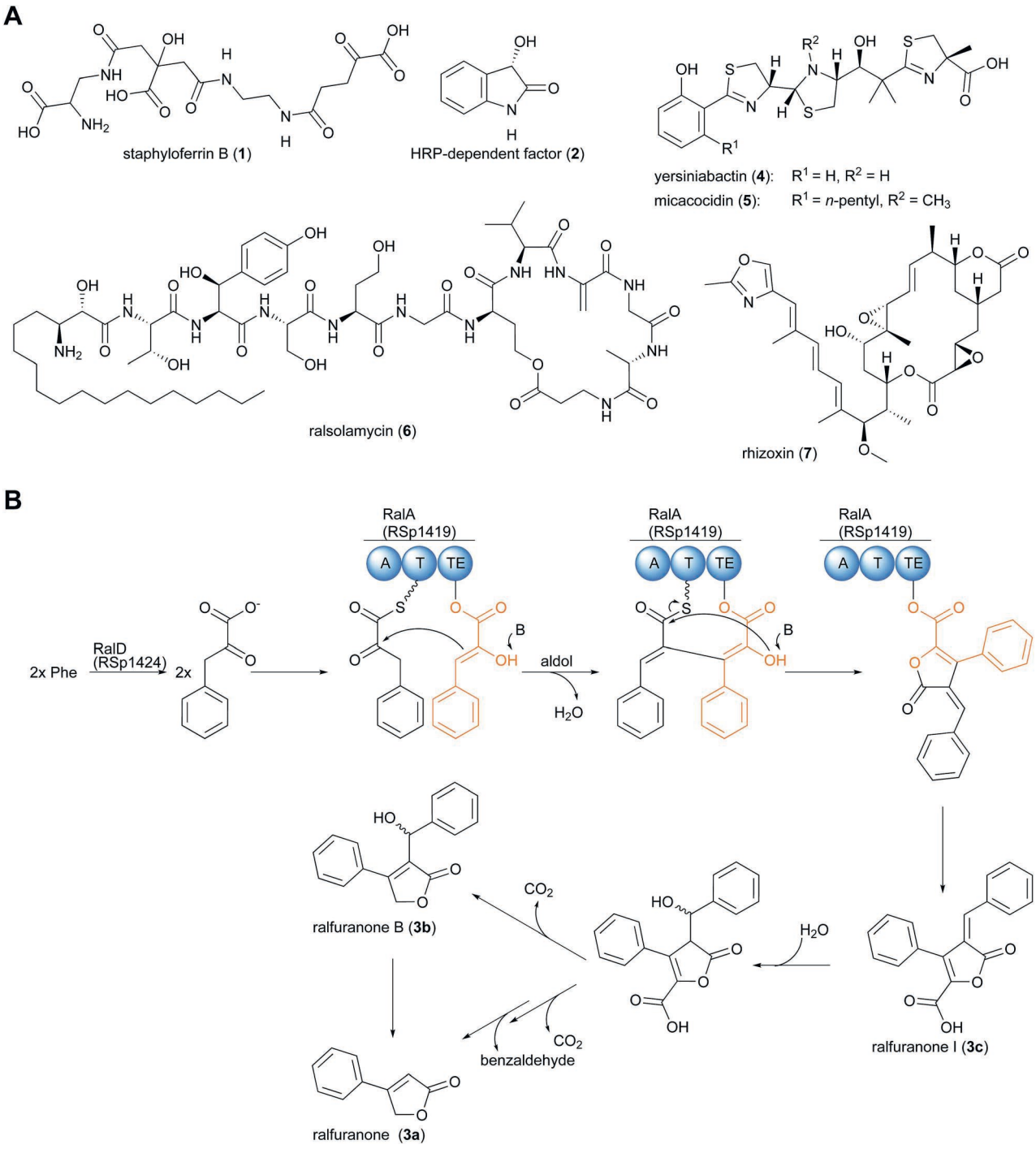

Fig. 2 (A) Structures of secondary metabolites produces by *R. solanacearum*. (B) Model for ralfuranone biosynthesis.

infected tomato plant, but no apparent toxicity in tobacco.[41] Further, a role of ralfuranones to interfere with quorum sensing was suggested.[42]

While the analysis of virulence regulatory proteins provoked initial investigations on the secondary metabolism in *R. solanacearum*, later studies targeted selected BGCs by reverse genetics. The first such example involved the *mic* gene cluster (RSc1804-1813), which resides in the GMI1000 chromosome (Fig. 1). Comparative genomics had revealed that the *mic* locus is conserved in different phylotypes of the *R. solanacearum* species complex, as well as in the plant pathogenic bacterium *Burkholderia gladioli* BSR3.[43] The gene annotation suggested further that the *mic* cluster encodes a novel pathway to a yersiniabactin-like natural product. Since yersiniabactin (**4**) serves as a siderophore for its producers,[44] this finding suggested that *R. solanacearum* GMI1000 might produce another iron-chelating agent in addition to the previously described **1**. Combined chemical and genetic analyses eventually connected the *mic*

locus with the production of micacocidin (**5**).[43] Subsequently, the biosynthesis of the unusual 6-pentylsalicylate (6-PSA) moiety in **5** attracted some attention. The PSA motif, which is missing in the closely related **4**, contributes to the potent activity of **5** against *Mycoplasma* bacteria and could not be explained on the basis of biosynthetic precedence.[45,46] Using a combination of stable isotope feeding experiments, mutational analysis as well as heterologous reconstitution, it was demonstrated that the assembly of 6-PSA is catalyzed by a partially reducing iterative type I polyketide synthase (prPKS), which is integrated into a multimodular assembly line.[47] The programming of this enzyme was solved by intercepting the individual biosynthetic steps with synthetic chain terminators.[48] Furthermore, the substrate tolerance of the prPKS was successfully exploited for introducing alternative starter units into **5** biosynthesis, thereby providing access to new antimycoplasma agents.[49]

More recently, the *rmy* locus (RSp0638-0642) became subject of intense research. The corresponding cluster includes the two largest ORFs in the genome of strain GMI1000 (RSp0641 and RSp0642), coding for NRPSs. Together, these two enzymes constitute a giant assembly line for the biosynthesis of a lipopeptide. First evidence for the predicted natural product was obtained by imaging mass spectrometry, when *R. solanacearum* GMI1000 was cocultured with different fungi on agar plates.[50] Under these conditions the bacterium induced the formation of chlamydospore-like structures in nearby growing fungi and this effect was accompanied by the secretion of a metabolite with a distinctive mass of 1290 Da. Tandem mass spectrometry in conjunction with an automated peptidogenomics analysis[51] traced the secreted metabolite back to the *rmy* locus. The assumed relationship between the biosynthesis genes and the chlamydospore-inducing molecule, which was subsequently referred to as ralsolamycin (**6**), was ultimately confirmed in a gene disruption experiment.[50] The originally reported partial structure for **6**, deduced from MS-MS and bioinformatic analyses, was later independently revised by two groups.[52,53] To secure sufficient material for structure elucidation, the researchers had to address the low production level of **6** in *R. solanacearum*. This was done by large-scale fermentation in one case,[52] and by engineering of an overproduction strain in another.[53] Surprisingly, the structure of **6** was not consistent with bioinformatic predictions, suggesting an erroneous genome sequence. Targeted resequencing of the genomic region harboring the *rmy* locus confirmed this suspicion and, hence, enabled the curation of the GMI1000 genome sequence.[53] Further studies revealed that the production of **6** depends on the population density of *R. solanacearum* and that the expression of the *rmy* gene cluster is controlled by the PhcBSR quorum sensing system.[54]

From the previous description, it is evident that the existing knowledge on the chemistry of *R. solanacearum* stems mainly from investigations of the model strain GMI1000. However, the species *R. solanacearum* has long been known to incorporate phenotypically diverse organisms with relatively high genetic distances. Due to this variation, four phylotypes of *R. solanacearum* are distinguished, which correlate with their geographic origin from Asia (phylotype I), America (phylotypes IIA and IIB), Africa (phylotype III) and Indonesia (phylotype IV).[55] Recently, the phylotypes I, III and IV were even reclassified into distinct species (Fig. 3).[56] This raises the question whether all strains originally designated as *R. solanacearum* actually share the biosynthetic potential of GMI1000. The answer to this question has also important ecological implications. Secondary metabolism is increasingly recognized as an adaptive trait, which contributes to the colonization of specific habitats.[57,58] In case of the *R. solanacearum* species complex, the genetic diversification could hence involve a location-dependent acquisition of selected biosynthetic pathways. Bioinformatic analyses of available genome sequences reveal the distribution of the BGCs for the production of HDF, ralfuranones and other GMI1000 metabolites (Table 3). Loci directing the biosynthesis of yersiniabactin (**4**)[44] and the antimitotic toxin rhizoxin (**7**)[59] were also included in this computational screening. Although there is no report describing the isolation of **4** or **7** from *R. solanacearum* to date, fully conserved BGCs for the two compounds were already found in some strains.[43,60]

An inspection of Table 3 shows that, with a single exception, all *R. solanacearum* strains possess the genetic prerequisites for the production of **1**. Only the genome of the *R. solanacearum* type strain K60 is devoid of staphyloferrin B biosynthesis genes.[61] Another common BGC is responsible for the production of **2**, even though the corresponding locus is consistently missing in phylotype IV strains. Of particular note is the

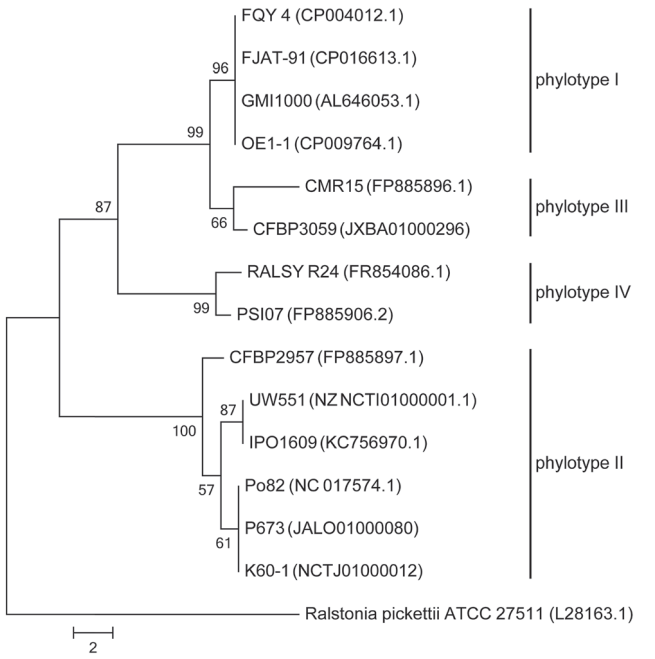

Fig. 3 Neighbour-joining tree of 16S–23S rRNA ITS region sequences of *R. solanacearum* strains. The phylogeny was reconstructed using MEGA7 with the Neighbor-Joining method.[157,158] The evolutionary distances were computed using the number of differences method.[159] The numbers on the branches indicate the bootstrap values (%) from 1000 resamplings.

Table 3 Distribution of biosynthetic loci in *R. solanacearum* strains and related bacteria: BDB, blood disease bacterium; RALSY, *R. syzygii*; abbreviations for biosynthetic loci: *sbn*, staphyloferrin B; *hdf*, HRP-dependent factor; *ral*, ralfuranone; *ybt*, yersiniabactin; *mic*, micacocidin; *rmy*, ralsolamycin; *rhi*, rhizoxin

Strain	Phylotype	*sbn* (1)	*hdf* (2)	*ral* (3)	*ybt* (4)	*mic* (5)	*rmy* (6)	*rhi* (7)
GMI1000	I	+	+	+	–	+	+	–
OE1-1	I	+	+	+	–	+	+	–
FJAT-91	I	+	+	+	–	+	+	–
FQY_4	I	+	+	+	–	+	+	–
K60	IIA	–	+	–	–	–	–	–
CFBP2957	IIA	+	+	–	+	–	–	+
Po82	IIB	+	+	+	+	–	–	–
UW551	IIB	+	+	–	+	–	+	–
IPO1609	IIB	+	+	–	+	–	–	–
P673	IIB	+	+	+	+	–	–	–
CMR15	III	+	+	–	–	+	+	–
CFBP3059	III	+	+	+	–	+	–	+
PSI07	IV	+	–	–	–	+	–	+
BDB R229	IV	+	–	–	–	+	–	+
RALSY R24	IV	+	–	–	–	–	–	–

significant conformity in the secondary metabolomes of phylotype I and III strains, which is in accordance with their phylogenetic relatedness.[56,62] These bacteria are typically capable to synthesize **3**, **5** and **6**, which clearly distinguishes them from phylotype II strains. There are only few representatives of the latter, which can make **3** or **6**, and no producers of **5**. Except for K60, all phylotype II strains harbor the **4** locus, which is absent in other phylotypes. Considering the structural relatedness of **4** and **5**, it seems reasonable to assume that the different strains utilize either molecule for the same biological function. In stark contrast to the secondary metabolites **2–6**, the production of **7** appears not to be linked to certain phylotypes. Few *R. solanacearum* strains possess the genes for the biosynthesis of **7** and these bacteria belong to different phylotypes, which might indicate independent acquisitions of this BGC by horizontal gene transfer (HGT). Up to now, it is unclear whether **7** promotes the virulence of these bacteria, as might be expected from its role in rice seedling blight (see Chapter 4).

Despite the limited number of strains covered in Table 3, some conclusions can be drawn. First, the distribution of BGCs in *R. solanacearum* strains seems largely consistent with the phylotype affiliation of these organisms. Secondly, it is likely possible to date the acquisition of specific BGCs in relation to the divergence of the entire species complex. Thirdly, the strong conservation of certain biosynthetic pathways suggests that the associated secondary metabolites confer, at least to some degree, a competitive advantage that is useful to many *R. solanacearum* strains.

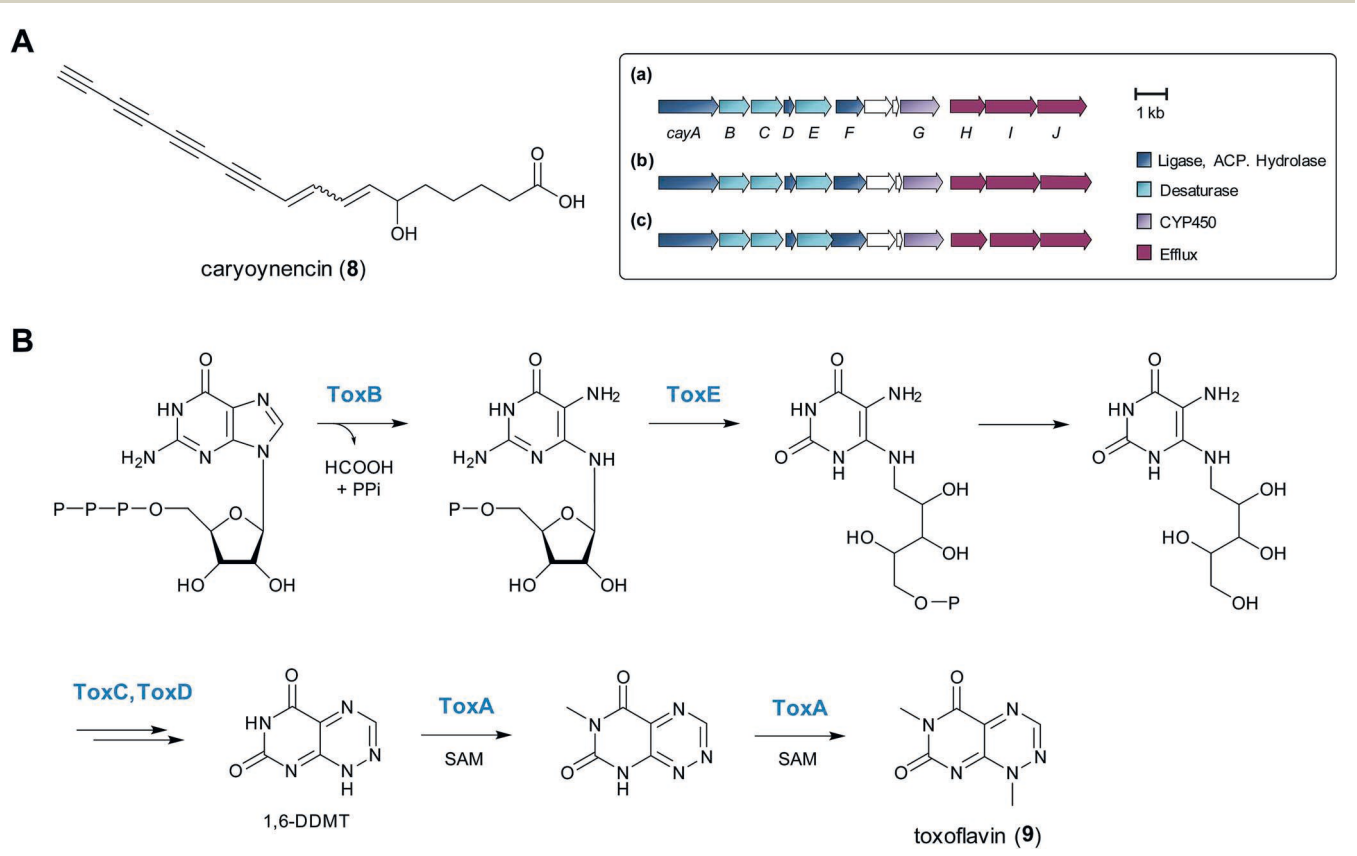

Fig. 4 (A) Structure of caryoynencin (**8**) and syntenic caryoynencin (*cay*) BGCs in *B. caryophylli* (a), *B. gladioli* BSR3 ((b); bgla_1g20240-20130), and *B. plantarii* ATCC 43733 (c); bpln_2g06190-06080. (B) Proposed biosynthetic pathway to toxoflavin (**9**).

4. *Burkholderia* spp.

Members of the genus *Burkholderia* can be isolated from a variety of natural and managed ecosystems. Phylogenetic studies indicate that these highly versatile bacteria constitute two distinct lineages. The larger clade includes mainly plant growth-promoting bacteria, whereas the other cluster is dominated by human, animal and plant pathogens.[63,64] Among the phytopathogens are species causing wilts, rots, blights, or cankers. An example is *B. gladioli*, which is responsible for bacterial soft rot in onions, leaf-sheath browning and grain rot in rice, as well as leaf and corm diseases in gladioli and irises.[65] Of note are also *Burkholderia* species which live as endosymbionts of plant pathogenic fungi. Although these bacteria cannot cause plant diseases in the absence of their fungal hosts, they were occasionally reported to produce phytotoxins, such as *B. rhizoxinica*, which is associated with the zygomycete *Rhizopus microsporous*. The latter is known as the causative agent of rice seedling blight, albeit the characteristic symptom of the disease is actually due to the endosymbiont-derived antimitotic natural product rhizoxin (**7**).[66]

The genomes of *Burkholderia* spp. feature up to three chromosomes and several large (>100 kb) plasmids. Genome sizes of *Burkholderia* spp. range from 3.7 to 9.1 Mb, which is likely due to their varying lifestyles as endosymbionts or free-living bacteria.[67] Genomics has undoubtedly contributed to the recognition of *Burkholderia* species as competent producers of secondary metabolites.[68,69] Up to now, however, chemical investigations have primarily focused on bacteria of the *Burkholderia cepacia* complex (Bcc), which represent opportunistic human pathogens. A noteworthy exception is the carnation pathogen *B. caryophylli*, which produces the polyacetylene caryoynencin (**8**).[70] To clarify the genetic basis for the biosynthesis of this potent antibiotic, the Hertweck group abolished its production in the native producer by transposon mutagenesis.[71] The disruption site was subsequently traced back to a Δ9 desaturase-like gene, orthologs of which were identified in the genomes of the plant pathogens *B. gladioli* BSR3 and *B. gladioli* pv. *cocovenenans*. A comparative genomics analysis then revealed a highly conserved BGC in the three strains, and subsequent chemical analyses confirmed that the BSR3 strain is also capable of polyacetylene production.[71] The caryoynencin (*cay*) locus, is in fact conserved in several plant pathogenic *Burkholderia* strains (see Fig. 4A). Its discovery was of particular note, because it disclosed for the first time a bacterial polyacetylene pathway.

While the assembly of the *B. caryophylli* genome is in scaffold stage, the fully assembled genome of *B. gladioli* BSR3 already permits a global view on the secondary metabolism of this rice pathogen. Bioinformatics reveal an impressive number of 24 BGCs (Table 4). Except for caryoynencin, however, only the product of one further locus (1g04520-04610) has been experimentally confirmed in the BSR3 strain.[72] The corresponding metabolite, toxoflavin (**9**), is the key virulence factor in rice grain rot, causing chlorotic damage and suppressing the growth of both leaves and roots.[73] According to the current hypothesis, the toxin interferes with electron transport processes. Its NADH-dependent reduction gives rise to the production of reactive oxygen species, which then lead to the known disease symptoms.[74] Genomics indicate that the toxoflavin biosynthesis gene cluster, the so-called *tox* operon,[75] is widely distributed in the plant pathogens *B. gladioli* and *B. glumae*. Interestingly, toxoflavin-like gene clusters have also been reported from *Burkholderia* strains that are not associated with plant diseases, but due to differences in gene architectures of *tox* and *tox*-like BGCs, it was speculated that the latter direct the production of different compounds.[76]

The first biosynthetic studies on **9** date back to the 1960s when feeding experiments involving labeled precursors were conducted.[77] The outcome of these experiments as well as recent gene inactivation studies[78] indicate that the formation of **9** parallels riboflavin biosynthesis in its early steps and hence starts with GTP (Fig. 4B). The opening of the imidazole ring in this nucleoside triphosphate and the concomitant release of formate and pyrophosphate were proposed to be catalyzed by ToxB, an enzyme homologous to the GTP cyclohydrolase II in the riboflavin pathway. The product of this cleavage reaction would then be processed by ToxE, an enzyme predicted to possess both deaminase and reductase activity similar to RibD, which is the second enzyme in the riboflavin pathway.[79] At the

Table 4 Biosynthetic loci in *Burkholderia gladioli BSR3*

No.	Cluster location	Actual or predicted product[a]	References
1	1g04520-04610	**Toxoflavin (9)**[b]	75, 78 and 80
2	1g07050-07110	Polyketide	
3	1g16280-16580	NRPS-derived peptide	
4	1g16280-16580	Bongkrekic acid	
5	1g20130-20240	**Caryoynencin (8)**[b]	70 and 71
6	1g24060	Terpene	
7	1g30450-30470	Lassopeptide	
8	2g01630-01650	NRPS-derived compound	
9	2g02160-02330	PKS/NRPS-derived compound	
10	2g03020	Bacteriocin	
11	2g03260	Terpene	
12	2g10690	NRPS-derived peptide	
13	2g11020-11070	Homoserine lactone	
14	2g13340-13400	Phosphonate	
15	2g15500-15520	Bacteriocin	
16	2g16330-16410	NRPS-derived peptide	
17	2g16840-16960	NRPS-derived lipopeptide	
18	2g17770-17830	Indigoidine	
19	2g19620-19790	NRPS-derived peptide	
20	2g28490-28550	Terpene	
21	2g29860-29890	Terpene	
22	1p0770-0860	PKS/NRPS-derived compound	
23	1p1580-1760	PKS/NRPS-derived compound	
24	4p2050-2140	Micacocidin	

[a] Observed products are highlighted in bold. [b] The loci for toxoflavin and caryoynencin biosynthesis were not identified by antiSMASH[27] and, hence, assigned on the basis of literature data. The presence of another bacteriocin locus predicted by antiSMASH[27] could not be confirmed.

stage of 5-amino-6-D-ribityl-aminouracil, toxoflavin biosynthesis diverts from the known riboflavin route. The following steps are mechanistically not understood. In-frame deletions of the genes coding for ToxC and ToxD suggest that the two enzymes play a crucial role in the synthesis of 1,6-didesmethyl-toxoflavin (1,6-DDMT), which is the immediate precursor of **9**.[78] The concluding methylation reactions were recently demonstrated to be catalyzed by a single enzyme, ToxA, in a defined sequence with the initial methylation occurring at N6 of 1,6-DDMT.[80]

While few natural products have actually been isolated from *B. gladioli* BSR3, we still expected to find several BGCs in its genome that are shared with strains belonging to the Bcc. To our surprise, however, this was not the case. Only three predicted loci from the BSR3 genome could be connected with secondary metabolites known from other bacteria (see predictions for gene clusters no. 4, 18 and 24 in Table 4).

The presence of a gene cluster for the biosynthesis of **5** was already mentioned in chapter 3. The corresponding locus resides on a plasmid and appears to be restricted to strain BSR3 in the entire genus *Burkholderia*. It is thus likely that the *mic* gene cluster was acquired by HGT. BGCs for the production of indigoidine were reported from several diverse bacteria,[81,82] including the plant pathogen *Dickeya dadantii* (formerly *Erwinia chrysanthemi*), where this blue pigment was proposed to contribute to the virulence.[83] To our knowledge, the production of indigoidine has not been associated with *Burkholderia* spp. before in contrast to bongkrekic acid, which is produced by pathovars involved in food poisoning.[84]

The large number of BGCs in the *B. gladioli* BSR3 genome, of which only a small portion can be linked to known natural products, in conjunction with many unique pathways that are not found in the Bcc reflect the situation of many plant pathogenic *Burkholderia* strains and could make these bacteria worthwhile targets for future natural product discovery programmes.

5. *Pseudomonas syringae*

The γ-proteobacterium *Pseudomonas syringae* represents a globally distributed plant pathogen that is capable to infect numerous crop plants and trees. About 50 pathovars can be distinguished within the species *P. syringae* based on pathogenicity and host range. This diversity is also reflected in the genomes of these bacteria, which feature a large number of variable regions.[24] Among the virulence determinants characteristic of certain pathovars are several phytotoxins (*e.g.*, syringomycin, coronatine, phaseolotoxin, tabtoxin).[85] In contrast to other plant pathogenic bacteria, *P. syringae*'s biosynthetic potential was already comprehensively reviewed from a genomics perspective and readers are therefore referred to the corresponding article by Gross and Loper.[9]

6. *Erwinia amylovora*

Erwinia amylovora causes fire blight, a destructive disease of species of the Rosaceae, specifically of members of the subfamily, traditionally defined as Maloideae. Pome fruit production, such as pear, apple, and quince, is affected most, along with ornamental trees. Consequently, this pathogen represents a severe economic burden. The 3.83 Mbp-sized genome of *E. amylovora* CFBP 1430 was published in 2010.[86] A manual bioinformatic analysis reveals the presence of four BGCs (Table 5). This number slightly differs from the three loci predicted by antiSMASH (see Table 1), which is due to the gene cluster for 6-thioguanine (**10**) production. The genetic basis for the biosynthesis of **10**, which is known as a cytotoxic apotosis-inducing antimetabolite, was only recently elucidated in *E. amylovora*.[87] Because the assembly does not require prevalent biosynthetic enzymes, such as PKS, NRPS, or terpene cyclases, which are typically used to anchor searches for clusters of secondary metabolism genes, automatic sequence-analyzing algorithms easily miss the **10** locus in the *E. amylovora* genome.

Table 5 Biosynthetic loci in *Erwinia amylovora* CFBP1430

No.	Cluster location	Actual or predicted product[a]	References
1	EAMY_0439-0451	PKS/NRPS-derived compound	
2	EAMY_1020-1024	**Thioguanine (10)**[b]	87 and 88
3	EAMY_2516-2517	NRPS-derived hexapeptide	
4	EAMY_3238-3241	**Desferrioxamine**	89

[a] Observed products are highlighted in bold. [b] The locus for thioguanine biosynthesis was not identified by antiSMASH[27] but assigned on the basis of literature data.

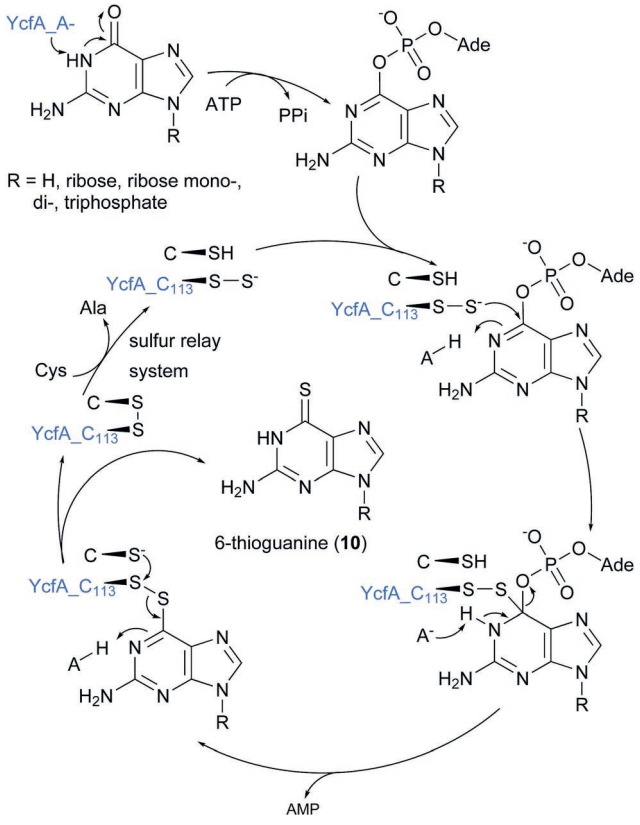

Fig. 5 Biosynthesis of 6-thioguanine (**10**).

A reaction sequence analogous to 4-thiouridine formation was postulated to give rise to **10**.[87] According to the proposal, a guanine precursor is initially adenylated and then nucleophilically attacked by an intermediary cysteine-derived persulfide group of YcfA (EAMY_1021), displacing adenosine monophosphate and generating a disulfide bond (Fig. 5). The latter is then cleaved upon attack of a second active site-cysteine residue in YcfA, yielding **10** as well as an enzymic disulfide bridge. Reduction of the enzyme would eventually restore the catalytic function of YcfA. Evidence supporting the biochemical role of YcfA came from site-directed mutagenesis experiments.[87]

Of particular interest was the observation that the inactivation of *ycfA* not only abolished **10** formation, but also affected the virulence of *E. amylovora*. Neither did the Δ*ycfA* mutant of *E. amylovora* cause necrosis or other symptoms, nor was phytoalexine formation detectable.[87] It now seems established that **10** represents a long neglected virulence factor in fire blight disease.

In comparison to other plant pathogenic bacteria, *Erwinia* spp. possess only few BGCs, which is likely due to their small genome sizes. Despite the presence of some orphan NRPS loci, it appears unlikely that these pathogens will attract significant attention in natural product research.

7. *Dickeya* spp.

The enterobacterial genus *Dickeya* was introduced in 2005, assimilating the plant pathogens previously known as *Pectobacterium chrysanthemi* and *Brenneria paradisiaca*.[90] *Dickeya* spp. are pectinolytic bacteria, which cause soft rot and blackleg diseases in angiosperms, among them numerous crop and ornamental plants.[91] Recently, the rapid spread of an aggressive *Dickeya* species, *i.e.*, *Dickeya solani*, has raised great concern due to its potential impact on potato production.[92]

At the time of writing, complete genomes sequences are available for several members of the genus, including *D. dadantii*,[93] *D. solani*,[94] and *D. zeae*.[95] These data resources along with many draft genome sequences offer valuable insights into the secondary metabolism of the entire genus. An in-depth analysis of the *D. solani* 3337 genome unearthed ten BGCs (Table 6), of which one encodes a *trans*-AT PKS that is also found in *D. paradisiaca* 703 and *D. dadantii* Ech703.[96] In the latter pathogen, the BGC was shown to be responsible for the production of oocydin A (**11**),[97] which is known for its potent antifungal effects.[98] Another BGC from *D. solani* 3337 is conserved in the rice pathogen *D. zeae*, where it directs the biosynthesis of the zeamines.[95] The polyamine zeamine (**12**), being the first representative of this natural product family, was originally discovered in *D. zeae* DZ1 due to its antimicrobial effects.[99] ^{13}C labeling experiments revealed acetate and valine as its biosynthetic building blocks.[99] The PKS ZmsA, which is involved in zeamine assembly, was subsequently identified by the Zhang group in *D. zeae* EC1 by means of transposon mutagenesis. During this study, a biosynthetic precursor of **12** was isolated and given the name zeamine II (**13**).[100] Further analyses suggested the condensing enzyme ZmsK as the missing biosynthetic link between **12** and **13**.[101] At the same time, the Lavigne group reported the full zeamine (*zms*) gene cluster as well as the previously unknown derivative zeamine I (**14**).[102] The observation that the *zms* locus encoded a multimodular NRPS (ZmsG and ZmsI) and a carbon–nitrogen hydrolase (ZmsN) led to a biosynthetic model, in which **12** and **14** derive from precursor molecules, the prezeamines **15** and **16**, upon proteolytic cleavage (Fig. 6).[102]

Initial evidence for this proposal came from the Bode group who proved the involvement of a similarly organized BGC from *Xenorhabdus* strains in the production of zeamine-like molecules by targeted gene inactivation experiments.[103] *In vitro* biochemical assays and feeding studies eventually confirmed the pathway depicted in Fig. 6.[104] Aside from their unusual biosynthesis, the zeamines have received considerable attention due to their potent activity against bacteria, fungi and nematodes.[21,104–106] Of particular note in the context of this review is the report of the Zhang group that *D. zeae* mutants, which are deficient in the production of zeamines, also show decreased virulence on rice, potato, and Chinese cabbage.[101] The mechanism underlying this effect seems not to be clear yet.

Further *Dickeya* natural products, which have an important role in pathogenicity, are the NRPS-derived siderophores chrysobactin (**17**) and achromobactin (**18**).[107] Expert and coworkers showed in a series of experiments that the virulence of *D. dadantii* 3937 (formerly *Erwinia chrysanthemi* 3937) depends to a large extent on these two iron chelators, which are produced during different stages of the plant infection to secure the iron supply of the pathogen.[108–110] The isolation and structural characterization of **17** from *D. dadantii* dates back to 1989,[111] but only recently evidence was obtained that *Dickeya* species produce dimers and trimers of this natural product.[112] A bioinformatic analysis revealed that the BGCs for **17**[113] and **18**[108] are also present in the genome of *D. solani* 3337 (Table 6). Another conserved BGC in many *Dickeya* genomes is that of indigoidine (**19**).[83] The production of this blue pigment by enterobacterial plant pathogens is long known.[114] In the case of *D. dadantii* 3937, **19** was shown to be crucial for the systemic invasion of *Saintpaulia ionantha*.[83] Apparently, members of the genus *Dickeya* maintain a number of secondary metabolite pathways, which increase the virulence of these bacteria.

Table 6 Biosynthetic loci in *Dickeya solani* str. 3337

No.	Cluster location	Actual or predicted product[a]	References
1	D083_0058-0075	Thiopeptide	
2	D083_0938-0952	PKS/NRPS-derived compound	
3	D083_1093-1108	**Chrysobactin** (**17**)	113
4	D083_1985-2008	**Oocydin A** (**11**)	97
5	D083_2115-2130	Cyanobactin	
6	D083_2512-2529	Arylpolyene	
7	D083_2658-2661	**Indigoidine** (**19**)	83
8	D083_3631-3638	Bacteriocin	
9	D083_4037-4055	**Zeamine** (**12**)	101 and 102
10	D083_4195-4208	**Achromobactin** (**18**)	108

[a] Observed products are highlighted in bold.

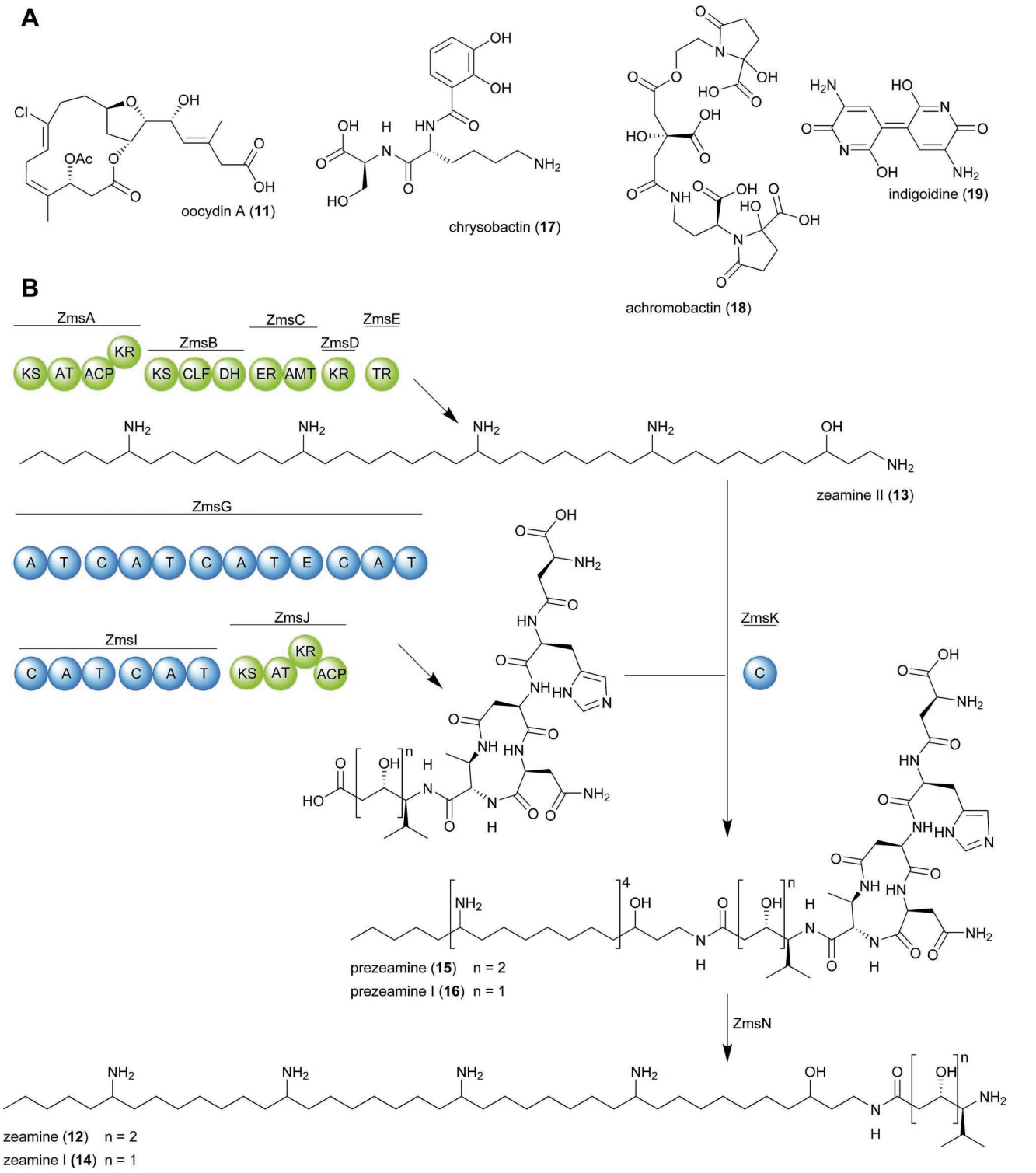

Fig. 6 (A) Structures of secondary metabolites produced by *Dickeya* spp. (B) Biosynthesis of the zeamines. Domain notation: KS, ketosynthase; AT, acyltransferase; KR, ketoreductase; ACP, acyl carrier protein; CLF, chain length factor; DH, dehydratase; ER, enoyl reductase; AMT, aminotransferase; TR, thioester reductase; A, adenylation; T, thiolation; C, condensation.

8. *Xanthomonas* spp.

The yellow-pigmented bacteria of the genus *Xanthomonas* are the causal agents of plant diseases, which affect economically important crops, including rice, citrus, cotton, and sugarcane. Although the collective host range of the xanthomonads comprises about 400 plant species, individual strains typically exhibit a high degree of host and even tissue specificity.[115,116]

In the pregenomic era, chemical analyses of these bacteria led to the discovery of arylpolyenes, such as xanthomonadin I,[117] some coronatine analogs,[118] and the potent DNA gyrase inhibitor albicidin (**20**).[119] While the chemical constitution of **20** remained unclear for many years owing to its low production level, it was soon realized that this secondary metabolite is responsible for the characteristic white foliar stripe symptoms in sugarcane leaf scald disease.[119–121] Advances in genomics and molecular biology eventually delivered the tools to elucidate the structure of **20**. Firstly, the **20** biosynthesis genes were identified after mutagenesis and complementation studies in the native producer *X. albilineans*.[122] Subsequently, the complete BGC was transferred into the faster growing bacterium *X. axonopodis* pv. *vesicatoria* and heterologously expressed, which led to a sixfold increase in production yield.[123] Following the optimization of purification protocols, the structural analysis disclosed an extremely rare structural scaffold consisting of a chain of *para*-aminobenzoates, which is suspended by a 3-cyanoalanine moiety.[124]

At first glance, the biosynthesis of **20** appears to follow a textbook-like thiotemplate-based assembly mechanism (Fig. 7). A more thorough inspection, however, unveils some

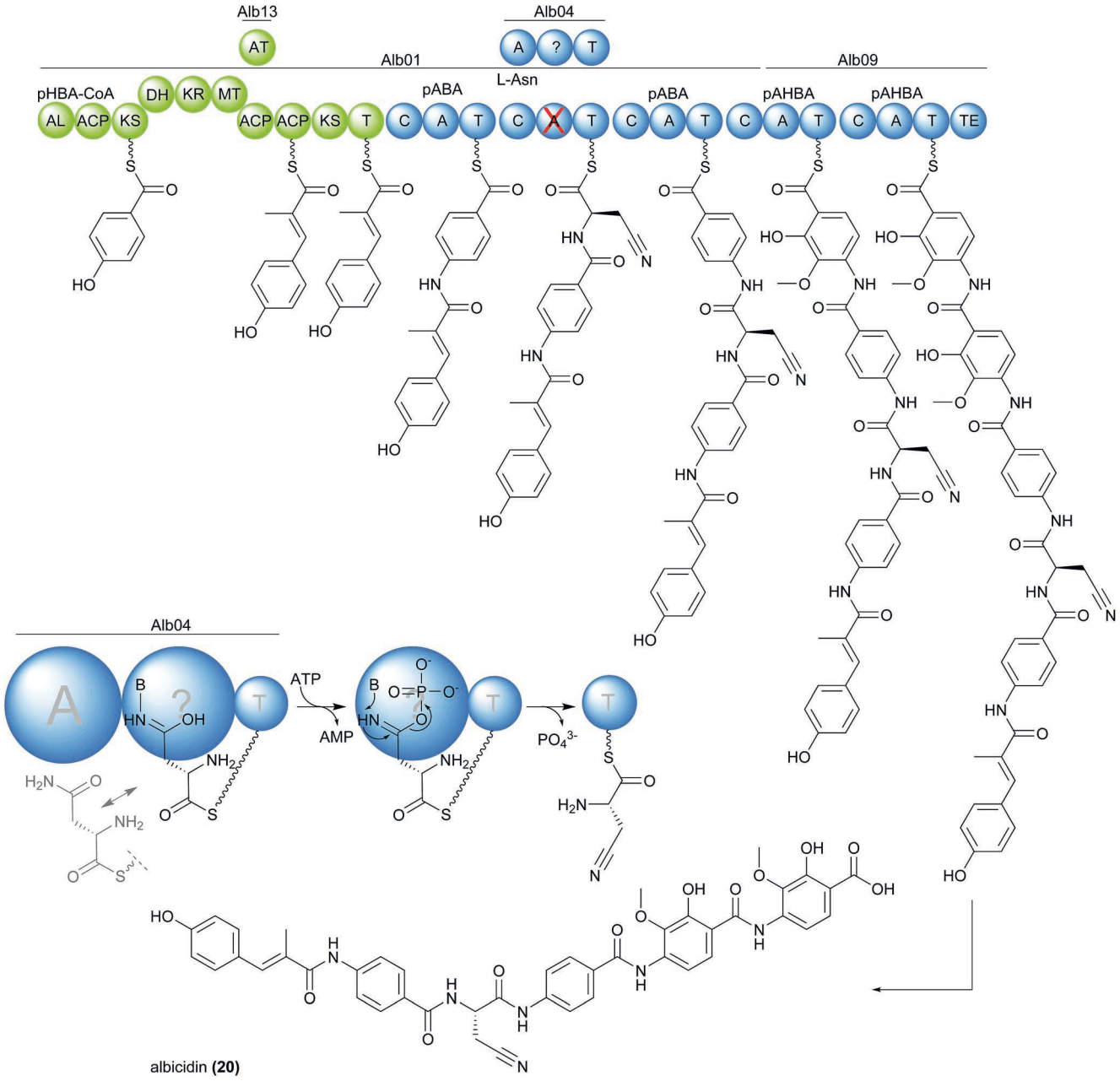

Fig. 7 Biosynthesis of albicidin (**20**) in *Xanthomonas albilineans* GPE PC73. Domain notation: AL, acyl-coA ligase; ACP, acyl carrier protein; KS, ketosynthase; DH, dehydratase; KR, ketoreductase; MT, methyltransferase; AT, *trans*-acting acyltransferase; A, adenylation; T, thiolation; C, condensation, TR, thioesterase.

Table 7 Biosynthetic loci in *Xanthomonas albilineans* GPE PC73

No.	Cluster location	Actual or predicted product[a]	References
1	XALC_0122-0137	**Xanthomonadin**	127
2	XALC_0358-0368	NRPS-derived peptide	
3	XALC_0718-0724	**Xanthoferrin**[b]	128
4	XALC_0772-0792	NRPS-derived peptide	
5	XALC_1054-1068	NRPS-derived peptide	
6	XALC_1143-1145	NRPS-derived peptide	
7	XALC_1514-1535	**Albicidin (20)**[c]	122 and 124
8	XALC_1550-1551	NRPS-derived peptide[c]	
9	XALC_1995-1998	Bacteriocin	

[a] Observed products are highlighted in bold. [b] The structure of xanthoferrin has not been elucidated up to now. [c] The two loci were recognized as a single BGC by antiSMASH.[27]

peculiarities. The most obvious is the usage of aromatic δ-type amino acid substrates by several NRPS biosynthesis enzymes, which was referred to an unusual binding pocket motive in the respective adenylation domains. The rare 3-cyanoalanine building block was proposed to derive from L-asparagine *via* an enzyme-bound phosphorylated intermediate and is incorporated *in trans* from a discrete NRPS, thereby compensating for the deficiency of an inactive module in the albicidin assembly line. More recent studies suggest that **20** is not the true end product of the *X. albilineans* pathway, and subject to an enzymatic carbamoylation, which gives rise to a more active gyrase inhibitor.[125]

Despite its comparatively small size,[25] the genome of *X. albilineans* GPE PC73 was found to harbor significant biosynthetic capabilities beyond the production of **20** (Table 7). Amongst others, five additional gene clusters encoding NRPS assembly lines were annotated, of which (at least) three are shared with other xanthomonads.[126] It must be stated, however, that in comparison to closely related bacteria, *X. albilineans* GPE PC73 is particularly gifted regarding its secondary metabolism. Most xanthomonads were found to have a rather low potential for natural product biosynthesis (see Table 1).

9. *Streptomyces scabiei*

The Gram-positive streptomycetes are famous for their potential to produce a variety of secondary metabolites, which help to compete with other microorganisms and communicate with their environment. These bacteria are commonly found in the soil, but only few members of the genus *Streptomyces* are associated with plant diseases.[129] A noteworthy exception is *S. scabiei*, which causes the economically important scab disease in potatoes. The genome sequence of the *S. scabiei* strain 87.22 contains an enormous number of 36 BGCs according to a manual inspection (Table 8). Three of these loci can be associated with the production of known phytotoxins, namely thaxtomins, coronatines, and concanamycins.[130] Of these compounds, the thaxtomins were probably most intensively studied and their importance as virulence factors is indisputable. Thaxtomin A (**21**), which is the predominant thaxtomin derivative in *S. scabiei*, causes plant cell necrosis through an

Table 8 Biosynthetic loci in *Streptomyces scabiei* 87.22

No.	Cluster location	Actual or predicted product[a]	References
1	SCAB_1371-1481	**Pyochelin (27)**	153 and 154
2	SCAB_3201-3361	NRPS-derived peptide	
3	SCAB_3621-3651	Lantipeptide	
4	SCAB_5031-5051	2-Methylisoborneol	
5	SCAB_5431-5521	Isorenieratene	
6	SCAB_8591-8711	Lantipeptide	
7	SCAB_12081-12121	γ-Butyrolactone	
8	SCAB_12881-13001	Hopene	
9	SCAB_18371-18451	NIS-derived siderophore	
10	SCAB_19681-19731	NRPS-derived compound	
11	SCAB_20121	Geosmin	
12	SCAB_23181-23221	Terpene	
13	SCAB_24251-24271	Bacteriocin	
14	SCAB_24671-24691	NIS-derived siderophore	
15	SCAB_31761-31841	**Thaxtomin (21)**[b]	136 and 146
16	SCAB_32011-32171	lantipeptide[b]	
17	SCAB_43271-43351	Polyketide	
18	SCAB_43941-43991	PKS/NRPS-derived	
19	SCAB_47531-47671	Lantipeptide	
20	SCAB_56591-56711	**Bottromycin (26)**	149 and 151
21	SCAB_57921-57971	Desferrioxamine	
22	SCAB_59191-59281	Melanin	
23	SCAB_62831-62991	Polyketide[b]	
24	SCAB_63011-63031	γ-Butyrolactone[b]	
25	SCAB_63071-63191	LAP[b,c]	
26	SCAB_70711-70741	Ectoine	
27	SCAB_72961-72991	Other	
28	SCAB_73681-73741	Terpene	
29	SCAB_78881-78991	Polyketide	
30	SCAB_79601-79731	**CFA conjugates (23, 24)**	141 and 142
31	SCAB_82161-82171	Terpene	
32	SCAB_83841-84141	**Concanamycin (25)**[b]	145 and 147
33	SCAB_84131-84241	Linaridin[b]	
34	SCAB_84491-84521	NIS-derived siderophore	
35	SCAB_85431-85521	**Scabichelin (28)**	155
36	SCAB_86121-86211	Terpene	

[a] Observed products are highlighted in bold. [b] The respective loci were annotated as single BGCs by antiSMASH. [c] LAP = linear azole containing peptide.

inhibition of cellulose synthesis.[131] Its mode of action makes **21** an interesting candidate for weed control and, thus, the thaxtomins have also attracted considerable interest from the synthetic community.[132–136] Chemically, the thaxtomins are 2,5-diketopiperazines. Their most striking structural feature, which is also essential for the phytotoxic activity, is the nitro substituent on the tryptophan residue.[136] The site-specific nitration of the amino acid is carried out by a dedicated cytochrome P450.[137] Nitric oxide (NO), which serves as a co-substrate, is generated from arginine by a NO synthase.[138] In the *S. scabiei* genome, the genes for both enzymes are clustered together with further biosynthesis genes, which are involved in the assembly of the diketopiperazine scaffold and in the subsequent hydroxylation of the phenylalanine moiety.[139] Homologs of the thaxtomin (*txt*) locus from *S. scabiei* were also detected in the genomes of other plant pathogenic streptomycetes.[129]

While *S. scabiei* has been known as a producer of thaxtomins since 1989,[140] its potential for the synthesis of coronatine-type compounds was only recently realized after the discovery of

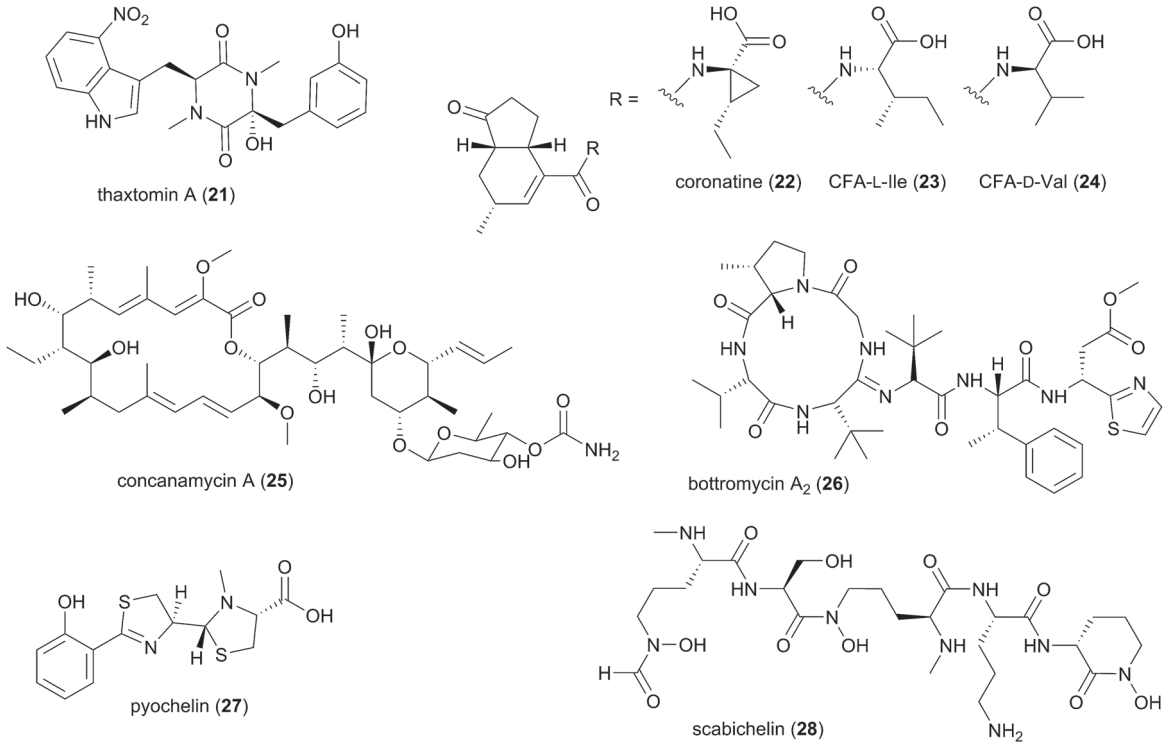

a coronafacic acid (CFA)-like gene cluster in the chromosome of strain 87.22.[141] CFA is a polyketide, which upon linkage with the L-*allo*-isoleucine derived amino acid coronamic acid (CMA) gives coronatine (COR, **22**). The latter is a well-known phytotoxin from *P. syringae*[9] and *Pectobacterium atrosepticum*,[19] and was long thought to be restricted to these taxa. From a bioinformatic analysis, it was evident that *S. scabiei* cannot produce **22** itself, as the biosynthesis genes for CMA are not present on its genome.[141] The metabolic products of the *cfa* locus in *S. scabiei* were later identified as L-isoleucine and D-valine conjugates of CFA (**23**, **24**).[142] Although *S. scabiei* mutants, which were impaired in the biosynthesis of **23** and **24**, showed a reduced virulence phenotype on tobacco seedlings,[141] it is still unclear whether these compounds contribute to scab disease development.[130]

In addition to the *txt* and *cfa* loci, the genome of *S. scabiei* 87.22 harbors a gene cluster for concanamycin biosynthesis.[130] Originally reported from other *Streptomyces* strains,[143–146] the production of concanamycin A (**25**) was recently verified in culture extracts of strain 87.22.[147] An involvement of **25** in lesion development during scab disease was proposed.[148] Genome mining also led to the discovery of a genetic locus that is involved in the production of bottromycins, after the ribosomal biosynthesis of these antibiotics had been recognized.[149–151] The actual production of bottromycin A_2 (**26**) and further derivatives was experimentally confirmed.[149,150] By means of mass spectral networking analysis, the Truman group further determined the reaction sequence in bottromycin biosynthesis.[152] Eventually, multiple loci were predicted to be involved in the production of siderophores. An example is the *scab_1371-scab_1481* locus, which is homologous to the pyochelin gene cluster from the opportunistic human pathogen *Pseudomonas aeruginosa*.[153] The production of pyochelin (**27**) by *S. scabiei* was demonstrated following the deletion of a cluster-associated repressor gene.[154] Another BGC was reported to encode the biosynthesis of a novel tris-hydroxamate siderophore named scabichelin (**28**).[155]

Aside from *R. solanacearum* GMI1000, *S. scabiei* 87.22 is likely the plant pathogenic bacterium, where genome sequencing delivered the most new insights into its secondary metabolism. It is now apparent that *S. scabiei* possesses pathways for the production of structurally diverse phytotoxins. The corresponding loci can also be found in the genomes of other plant-pathogenic bacteria, but they are generally missing in non-pathogenic relatives,[130] which suggests a selection-driven acquisition. Some studies have already been initiated to clarify the ancestry and dissemination of the *txt* and *cfa* BGCs.[129,156]

10. Concluding remarks

In this review, we have compiled recent findings on secondary metabolites from selected plant pathogenic bacteria. What is certain is that genome sequence analyses have strongly influenced our understanding of the chemistry of these microbes. It has become apparent that natural product biosynthesis is rule rather than exception in plant pathogenic bacteria, even though their biosynthetic capabilities usually fall behind established producer organisms. Nonetheless, compounds like the antibiotic albicidin or the herbicide thaxtomin illustrate the long overlooked potential of plant pathogenic bacteria for the discovery of new therapeutic drugs and agrochemicals. The increasing knowledge on their secondary metabolites also

transforms the way in which we think about the ecological versatility and persistence strategies of these bacteria. Natural products, such as ralsolamycin, indicate the necessity of pathogens to interact with organisms other than their host. In bacteria, such as *S. scabiei* 87.22, the genomic preservation of diverse phytotoxin loci could provide an advantage in the infection and colonization of different plant hosts. One of the great future challenges in the field will be to achieve a better understanding of the biological roles that natural products have for plant pathogenic bacteria under different conditions. For strains, such as *P. syringae* pv. *syringae* B728a, *R. solanacearum* GMI1000 or *S. scabiei* 87.22, of which the secondary metabolomes are already quite well characterized, the basic premises for such research are given. For other bacteria, above all the plant pathogenic *Burkholderia* species, additional chemical analyses would be desirable to further unlock their hidden chemistry. The authors would be glad, if this review gave some incentive for such studies.

11. Conflicts of interest

There are no conflicts to declare.

12. Acknowledgements

F. B. thanks the graduate school Jena School for Microbial Communication (JSMC) for a doctoral fellowship.

13. References

1 A. E. Osbourn and B. Field, *Cell. Mol. Life Sci.*, 2009, **66**, 3755–3775.
2 N. Ziemert, M. Alanjary and T. Weber, *Nat. Prod. Rep.*, 2016, **33**, 988–1005.
3 R. H. Baltz, *J. Ind. Microbiol. Biotechnol.*, 2017, **44**, 573–588.
4 P. J. Rutledge and G. L. Challis, *Nat. Rev. Microbiol.*, 2015, **13**, 509–523.
5 E. J. Helfrich, S. Reiter and J. Piel, *Curr. Opin. Biotechnol.*, 2014, **29**, 107–115.
6 M. Nett, H. Ikeda and B. S. Moore, *Nat. Prod. Rep.*, 2009, **26**, 1362–1384.
7 S. C. Wenzel and R. Müller, *Nat. Prod. Rep.*, 2009, **26**, 1385–1407.
8 J. A. Kalaitzis, F. M. Lauro and B. A. Neilan, *Nat. Prod. Rep.*, 2009, **26**, 1447–1465.
9 H. Gross and J. E. Loper, *Nat. Prod. Rep.*, 2009, **26**, 1408–1446.
10 A. A. Brakhage and V. Schroeckh, *Fungal Genet. Biol.*, 2011, **48**, 15–22.
11 A. C. Letzel, S. J. Pidot and C. Hertweck, *Nat. Prod. Rep.*, 2013, **30**, 392–428.
12 R. D. Fleischmann, M. D. Adams, O. White, R. A. Clayton, E. F. Kirkness, A. R. Kerlavage, C. J. Bult, J. Tomb, B. A. Dougherty, J. M. Merrick, K. Mckenney, G. Sutton, W. Fitzhugh, C. Fields, J. D. Gocayne, J. Scott, R. Shirley, L. Liu, A. Glodek, J. M. Kelley, J. F. Weidman, C. A. Phillips, T. Spriggs, E. Hedblom, M. D. Cotton, T. R. Utterback, M. C. Hanna, D. T. Nguyen, D. M. Saudek, R. C. Brandon, L. D. Fine, J. L. Fritchman, J. L. Fuhrmann, N. S. M. Geoghagen, C. L. Gnehm, L. A. Mcdonald, K. V. Small, C. M. Fraser, H. O. Smith and J. C. Venter, *Science*, 1995, **269**, 496–512.
13 M. Lindeberg, *Annu. Rev. Phytopathol.*, 2012, **50**, 111–132.
14 A. J. Simpson, F. C. Reinach, P. Arruda, F. A. Abreu, M. Acencio, R. Alvarenga, L. M. Alves, J. E. Araya, G. S. Baia, C. S. Baptista, M. H. Barros, E. D. Bonaccorsi, S. Bordin, J. M. Bove, M. R. Briones, M. R. Bueno, A. A. Camargo, L. E. Camargo, D. M. Carraro, H. Carrer, N. B. Colauto, C. Colombo, F. F. Costa, M. C. Costa, C. M. Costa-Neto, L. L. Coutinho, M. Cristofani, E. Dias-Neto, C. Docena, H. El-Dorry, A. P. Facincani, A. J. Ferreira, V. C. Ferreira, J. A. Ferro, J. S. Fraga, S. C. Franca, M. C. Franco, M. Frohme, L. R. Furlan, M. Garnier, G. H. Goldman, M. H. Goldman, S. L. Gomes, A. Gruber, P. L. Ho, J. D. Hoheisel, M. L. Junqueira, E. L. Kemper, J. P. Kitajima, J. E. Krieger, E. E. Kuramae, F. Laigret, M. R. Lambais, L. C. Leite, E. G. Lemos, M. V. Lemos, S. A. Lopes, C. R. Lopes, J. A. Machado, M. A. Machado, A. M. Madeira, H. M. Madeira, C. L. Marino, M. V. Marques, E. A. Martins, E. M. Martins, A. Y. Matsukuma, C. F. Menck, E. C. Miracca, C. Y. Miyaki, C. B. Monteriro-Vitorello, D. H. Moon, M. A. Nagai, A. L. Nascimento, L. E. Netto, A. Nhani Jr, F. G. Nobrega, L. R. Nunes, M. A. Oliveira, M. C. de Oliveira, R. C. de Oliveira, D. A. Palmieri, A. Paris, B. R. Peixoto, G. A. Pereira, H. A. Pereira Jr, J. B. Pesquero, R. B. Quaggio, P. G. Roberto, V. Rodrigues, M. R. A. J. De, V. E. de Rosa Jr, R. G. de Sa, R. V. Santelli, H. E. Sawasaki, A. C. da Silva, A. M. da Silva, F. R. da Silva, W. A. da Silva Jr, J. F. da Silveira, M. L. Silvestri, W. J. Siqueira, A. A. de Souza, A. P. de Souza, M. F. Terenzi, D. Truffi, S. M. Tsai, M. H. Tsuhako, H. Vallada, M. A. Van Sluys, S. Verjovski-Almeida, A. L. Vettore, M. A. Zago, M. Zatz, J. Meidanis and J. C. Setubal, *Nature*, 2000, **406**, 151–159.
15 D. W. Wood, J. C. Setubal, R. Kaul, D. E. Monks, J. P. Kitajima, V. K. Okura, Y. Zhou, L. Chen, G. E. Wood, J. Almeida, L. Woo, Y. Chen, I. T. Paulsen, J. A. Eisen, P. D. Karp, S. Bovee, D. P. Chapman, J. Clendenning, G. Deatherage, W. Gillet, C. Grant, T. Kutyavin, R. Levy, M. J. Li, E. McClelland, A. Palmieri, C. Raymond, G. Rouse, C. Saenphimmachak, Z. Wu, P. Romero, D. Gordon, S. Zhang, H. Yoo, Y. Tao, P. Biddle, M. Jung, W. Krespan, M. Perry, B. Gordon-Kamm, L. Liao, S. Kim, C. Hendrick, Z. Y. Zhao, M. Dolan, F. Chumley, S. V. Tingey, J. F. Tomb, M. P. Gordon, M. V. Olson and E. W. Nester, *Science*, 2001, **294**, 2317–2323.
16 B. Goodner, G. Hinkle, S. Gattung, N. Miller, M. Blanchard, B. Qurollo, B. S. Goldman, Y. Cao, M. Askenazi, C. Halling, L. Mullin, K. Houmiel, J. Gordon, M. Vaudin, O. Iartchouk, A. Epp, F. Liu, C. Wollam, M. Allinger, D. Doughty, C. Scott, C. Lappas, B. Markelz, C. Flanagan, C. Crowell, J. Gurson, C. Lomo, C. Sear, G. Strub, C. Cielo and S. Slater, *Science*, 2001, **294**, 2323–2328.

17 A. C. R. Da Silva, J. A. Ferro, F. C. Reinach, C. S. Farah, L. R. Furlan, R. B. Quaggio, C. B. Monteiro-Vitorello, M. A. Van Sluys, N. F. Almeida, L. M. C. Alves, A. M. Do Amaral, M. C. Bertolini, L. E. A. Camargo, G. Camarotte, F. Cannavan, J. Cardozo, F. Chambergo, L. P. Ciapina, R. M. B. Cicarelli, L. L. Coutinho, J. R. Cursino-Santos, H. El-Dorry, J. B. Faria, A. J. S. Ferreira, R. C. C. Ferreira, M. I. T. Ferro, E. F. Formighieri, M. C. Franco, C. C. Greggio, A. Gruber, A. M. Katsuyama, L. T. Kishi, R. P. Leite, E. G. M. Lemos, M. V. F. Lemos, E. C. Locali, M. A. Machado, A. M. B. N. Madeira, N. M. Martinez-Rossi, E. C. Martins, J. Meidanis, C. F. M. Menck, C. Y. Miyaki, D. H. Moon, L. M. Moreira, M. T. M. Novo, V. K. Okura, M. C. Oliveira, V. R. Oliveira, H. A. Pereira, A. Rossi, J. A. D. Sena, C. Silva, R. F. De Souza, L. A. F. Spinola, M. A. Takita, R. E. Tamura, E. C. Teixeira, R. I. D. Tezza, M. Trindade dos Santos, D. Truffi, S. M. Tsai, F. F. White, J. C. Setubal and J. P. Kitajima, *Nature*, 2002, **417**, 459–463.

18 M. Salanoubat, S. Genin, F. Artiguenave, J. Gouzy, S. Mangenot, M. Arlat, A. Billault, P. Brottiert, J. C. Camus, L. Cattolico, M. Chandler, N. Choisne, C. Claudel-Renard, S. Cunnac, N. Demange, C. Gaspin, M. Lavie, A. Moisan, C. Robert, W. Saurin, T. Schiex, P. Siguler, P. Thébault, M. Whalen, P. Wincker, M. Levy, J. Weissenbach and C. A. Boucher, *Nature*, 2002, **415**, 497–502.

19 C. R. Buell, V. Joardar, M. Lindeberg, J. Selengut, I. T. Paulsen, M. L. Gwinn, R. J. Dodson, R. T. Deboy, A. S. Durkin, J. F. Kolonay, R. Madupu, S. Daugherty, L. Brinkac, M. J. Beanan, D. H. Haft, W. C. Nelson, T. Davidsen, N. Zafar, L. Zhou, J. Liu, Q. Yuan, H. Khouri, N. Fedorova, B. Tran, D. Russell, K. Berry, T. Utterback, S. E. Van Aken, T. V. Feldblyum, M. D'Ascenzo, W. L. Deng, A. R. Ramos, J. R. Alfano, S. Cartinhour, A. K. Chatterjee, T. P. Delaney, S. G. Lazarowitz, G. B. Martin, D. J. Schneider, X. Tang, C. L. Bender, O. White, C. M. Fraser and A. Collmer, *Proc. Natl. Acad. Sci. U.S.A.*, 2003, **100**, 10181–10186.

20 K. Oshima, S. Kakizawa, H. Nishigawa, H. Y. Jung, W. Wei, S. Suzuki, R. Arashida, D. Nakata, S. I. Miyata, M. Ugaki and S. Namba, *Nat. Genet.*, 2004, **36**, 27–29.

21 C. B. Monteiro-Vitorello, L. E. A. Camargo, M. A. Van Sluys, J. P. Kitajima, D. Truffi, A. M. do Amaral, R. Harakava, J. C. F. de Oliveira, D. Wood, M. C. de Oliveira, C. Miyaki, M. A. Takita, A. C. R. da Silva, L. R. Furlan, D. M. Carraro, G. Camarotte, N. F. Almeida, H. Carrer, L. L. Coutinho, H. A. El-Dorry, M. I. T. Ferro, P. R. Gagliardi, E. Giglioti, M. H. S. Goldman, G. H. Goldman, E. T. Kimura, E. S. Ferro, E. E. Kuramae, E. G. M. Lemos, M. V. F. Lemos, S. M. Z. Mauro, M. A. Machado, C. L. Marino, C. F. Menck, L. R. Nunes, R. C. Oliveira, G. G. Pereira, W. Siqueira, A. A. de Souza, S. M. Tsai, A. S. Zanca, A. J. G. Simpson, S. M. Brumbley and J. C. Setúbal, *Mol. Plant-Microbe Interact.*, 2004, **17**, 827–836.

22 K. S. Bell, M. Sebaihia, L. Pritchard, M. T. G. Holden, L. J. Hyman, M. C. Holeva, N. R. Thomson, S. D. Bentley, L. J. C. Churcher, K. Mungall, R. Atkin, N. Bason, K. Brooks, T. Chillingworth, K. Clark, J. Doggett, A. Fraser, Z. Hance, H. Hauser, K. Jagels, S. Moule, H. Norbertczak, D. Ormond, C. Price, M. A. Quail, M. Sanders, D. Walker, S. Whitehead, G. P. C. Salmond, P. R. J. Birch, J. Parkhill and I. K. Toth, *Proc. Natl. Acad. Sci. U.S.A.*, 2004, **101**, 11105–11110.

23 B. M. Lee, Y. J. Park, D. S. Park, H. W. Kang, J. G. Kim, E. S. Song, I. C. Park, U. H. Yoon, J. H. Hahn, B. S. Koo, G. B. Lee, H. Kim, H. S. Park, K. O. Yoon, J. H. Kim, C. H. Jung, N. H. Koh, J. S. Seo and S. J. Go, *Nucleic Acids Res.*, 2005, **33**, 577–586.

24 H. Feil, W. S. Feil, P. Chain, F. Larimer, G. DiBartolo, A. Copeland, A. Lykidis, S. Trong, M. Nolan, E. Goltsman, J. Thiel, S. Malfatti, J. E. Loper, A. Lapidus, J. C. Detter, M. Land, P. M. Richardson, N. C. Kyrpides, N. Ivanova and S. E. Lindow, *Proc. Natl. Acad. Sci. U.S.A.*, 2005, **102**, 11064–11069.

25 I. Pieretti, M. Royer, V. Barbe, S. Carrere, R. Koebnik, S. Cociancich, A. Couloux, A. Darrasse, J. Gouzy, M. A. Jacques, E. Lauber, C. Manceau, S. Mangenot, S. Poussier, B. Segurens, B. Szurek, V. Verdier, M. Arlat and P. Rott, *BMC Genom.*, 2009, **10**, 616.

26 M. Sebaihia, A. M. Bocsanczy, B. S. Biehl, M. A. Quail, N. T. Perna, J. D. Glasner, G. A. DeClerck, S. Cartinhour, D. J. Schneider, S. D. Bentley, J. Parkhill and S. V. Beer, *J. Bacteriol.*, 2010, **192**, 2020–2021.

27 K. Blin, T. Wolf, M. G. Chevrette, X. Lu, C. J. Schwalen, S. A. Kautsar, H. G. Suarez Duran, E. L. C. De Los Santos, H. U. Kim, M. Nave, J. S. Dickschat, D. A. Mitchell, E. Shelest, R. Breitling, E. Takano, S. Y. Lee, T. Weber and M. H. Medema, *Nucleic Acids Res.*, 2017, **45**, W36–W41.

28 K. H. Gartemann, B. Abt, T. Bekel, A. Burger, J. Engemann, M. Flügel, L. Gaigalat, A. Goesmann, I. Gräfen, J. Kalinowski, O. Kaup, O. Kirchner, L. Krause, B. Linke, A. McHardy, F. Meyer, S. Pohle, C. Rückert, S. Sehneiker, E. M. Zeilermann, A. Pühler, R. Eichenlaub, O. Kaiser and D. Bartels, *J. Bacteriol.*, 2008, **190**, 2138–2149.

29 S. D. Bentley, C. Corton, S. E. Brown, A. Barron, L. Clark, J. Doggett, B. Harris, D. Ormond, M. A. Quail, G. May, D. Francis, D. Knudson, J. Parkhill and C. A. Ishimaru, *J. Bacteriol.*, 2008, **190**, 2150–2160.

30 S. Genin and T. P. Denny, *Annu. Rev. Phytopathol.*, 2012, **50**, 67–89.

31 J. Mansfield, S. Genin, S. Magori, V. Citovsky, M. Sriariyanum, P. Ronald, M. Dow, V. Verdier, S. V. Beer, M. A. Machado, I. Toth, G. Salmond and G. D. Foster, *Mol. Plant Pathol.*, 2012, **13**, 614–629.

32 G. Bhatt and T. P. Denny, *J. Bacteriol.*, 2004, **186**, 7896–7904.

33 A. Occhialini, S. Cunnac, N. Reymond, S. Genin and C. Boucher, *Mol. Plant Microbe Interact.*, 2005, **18**, 938–949.

34 F. Delaspre, C. G. Nieto Peñalver, O. Saurel, P. Kiefer, E. Gras, A. Milon, C. Boucher, S. Genin and J. A. Vorholt, *Proc. Natl. Acad. Sci. U.S.A.*, 2007, **104**, 15870–15875.

35 A. P. Macho, A. Guidot, P. Barberis, C. R. Beuzón and S. Genin, *Mol. Plant-Microbe Interact.*, 2010, **23**, 1197–1205.

36 P. Schneider, J. M. Jacobs, J. Neres, C. C. Aldrich, C. Allen, M. Nett and D. Hoffmeister, *ChemBioChem*, 2009, **10**, 2730–2732.
37 B. Wackler, P. Schneider, J. M. Jacobs, J. Pauly, C. Allen, M. Nett and D. Hoffmeister, *Chem. Biol.*, 2011, **18**, 354–360.
38 J. Pauly, M. Nett and D. Hoffmeister, *J. Nat. Prod.*, 2014, **77**, 1967–1971.
39 J. Pauly, D. Spiteller, J. Linz, J. Jacobs, C. Allen, M. Nett and D. Hoffmeister, *ChemBioChem*, 2013, **14**, 2169–2178.
40 K. Kai, H. Ohnishi, A. Kiba, K. Ohnishi and Y. Hikichi, *Biosci. Biotechnol. Biochem.*, 2016, **80**, 440–444.
41 K. Kai, H. Ohnishi, Y. Mori, A. Kiba, K. Ohnishi and Y. Hikichi, *ChemBioChem*, 2014, **15**, 2590–2597.
42 Y. Mori, S. Ishikawa, H. Ohnishi, M. Shimatani, Y. Morikawa, K. Hayashi, K. Ohnishi, A. Kiba, K. Kai and Y. Hikichi, *Mol. Plant Pathol.*, 2018, **19**, 454–463.
43 M. F. Kreutzer, H. Kage, P. Gebhardt, B. Wackler, H. P. Saluz, D. Hoffmeister and M. Nett, *Appl. Environ. Microbiol.*, 2011, **77**, 6117–6124.
44 R. D. Perry, P. B. Balbo, H. A. Jones, J. D. Fetherston and E. Demoll, *Microbiology*, 1999, **145**, 1181–1190.
45 S. Kobayashi, S. Hidaka, Y. Kawamura, M. Ozaki and Y. Hayase, *J. Antibiot.*, 1998, **51**, 323–327.
46 S. Kobayashi, Y. Ikenishi, Y. Takinami, M. Takema, W. Y. Sun, A. Ino and Y. Hayase, *J. Antibiot.*, 2000, **53**, 532–539.
47 H. Kage, M. F. Kreutzer, B. Wackler, D. Hoffmeister and M. Nett, *Chem. Biol.*, 2013, **20**, 764–771.
48 H. Kage, E. Riva, J. S. Parascandolo, M. F. Kreutzer, M. Tosin and M. Nett, *Org. Biomol. Chem.*, 2015, **13**, 11414–11417.
49 M. F. Kreutzer, H. Kage, J. Herrmann, J. Pauly, R. Hermenau, R. Müller, D. Hoffmeister and M. Nett, *Org. Biomol. Chem.*, 2014, **12**, 113–118.
50 J. E. Spraker, L. M. Sanchez, T. M. Lowe, P. C. Dorrestein and N. P. Keller, *ISME J.*, 2016, **10**, 2317–2330.
51 R. D. Kersten, Y.-L. Yang, Y. Xu, P. Cimermancic, S.-J. Nam, W. Fenical, M. A. Fischbach, B. S. Moore and P. C. Dorrestein, *Nat. Chem. Biol.*, 2011, **7**, 794–802.
52 F. Baldeweg, H. Kage, S. Schieferdecker, C. Allen, D. Hoffmeister and M. Nett, *Org. Lett.*, 2017, **19**, 4868–4871.
53 Y. Murai, S. Mori, H. Konno, Y. Hikichi and K. Kai, *Org. Lett.*, 2017, **19**, 4175–4178.
54 P. Li, W. Yin, J. Yan, Y. Chen, S. Fu, S. Song, J. Zhou, M. Lyu, Y. Deng and L. H. Zhang, *Front. Microbiol.*, 2017, **8**, 1172.
55 P. Prior and M. Fegan, *Acta Hortic.*, 2005, **695**, 127–136.
56 I. Safni, I. Cleenwerck, P. De Vos, M. Fegan, L. Sly and U. Kappler, *Int. J. Syst. Evol. Microbiol.*, 2014, **64**, 3087–3103.
57 K. Penn, C. Jenkins, M. Nett, D. W. Udwary, E. A. Gontang, R. P. McGlinchey, B. Foster, A. Lapidus, S. Podell, E. E. Allen, B. S. Moore and P. R. Jensen, *ISME J.*, 2009, **3**, 1193–1203.
58 N. Ziemert, A. Lechner, M. Wietz, N. Millan-Aguinaga, K. L. Chavarria and P. R. Jensen, *Proc. Natl. Acad. Sci. U.S.A.*, 2014, **111**, E1130–E1139.
59 L. P. Partida-Martinez and C. Hertweck, *ChemBioChem*, 2007, **8**, 41–45.
60 B. Remenant, B. Coupat-Goutaland, A. Guidot, G. Cellier, E. Wicker, C. Allen, M. Fegan, O. Pruvost, M. Elbaz, A. Calteau, G. Salvignol, D. Mornico, S. Mangenot, V. Barbe, C. Médigue and P. Prior, *BMC Genom.*, 2010, **11**, 379.
61 M. M. Hayes, A. M. MacIntyre and C. Allen, *Genome Announc.*, 2017, **5**, e01088–17.
62 P. Prior, F. Ailloud, B. L. Dalsing, B. Remenant, B. Sanchez and C. Allen, *BMC Genom.*, 2016, **17**, 90.
63 P. Estrada-de los Santos, F. U. Rojas-Rojas, E. Y. Tapia-García, M. S. Vásquez-Murrieta and A. M. Hirsch, *Ann. Microbiol.*, 2016, **66**, 1303–1314.
64 L. Eberl and P. Vandamme, *F1000Research*, 2016, **5**, 1007.
65 S. Compant, J. Nowak, T. Coenye, C. Clément and E. Ait Barka, *FEMS Microbiol. Rev.*, 2008, **32**, 607–626.
66 L. P. Partida-Martinez and C. Hertweck, *Nature*, 2005, **437**, 884–888.
67 G. Lackner, N. Moebius, L. P. Partida-Martinez, S. Boland and C. Hertweck, *BMC Genom.*, 2011, **12**, 210.
68 J. M. Winter, S. Behnken and C. Hertweck, *Curr. Opin. Chem. Biol.*, 2011, **15**, 22–31.
69 J. Masschelein, M. Jenner and G. L. Challis, *Nat. Prod. Rep.*, 2017, **34**, 712–783.
70 T. Kusumi, I. Ohtani, K. Nishiyama and H. Kakisawa, *Tetrahedron Lett.*, 1987, **28**, 3981–3984.
71 C. Ross, K. Scherlach, F. Kloss and C. Hertweck, *Angew. Chem., Int. Ed.*, 2014, **53**, 7794–7798.
72 J. Lee, J. Park, S. Kim, I. Park and Y. S. Seo, *Mol. Plant Pathol.*, 2016, **17**, 65–76.
73 L. M. Naughton, S. Q. An, I. Hwang, S. H. Chou, Y. Q. He, J. L. Tang, R. P. Ryan and J. M. Dow, *Environ. Microbiol.*, 2016, **18**, 780–790.
74 H. E. Latuasan and W. Berends, *Biochim. Biophys. Acta*, 1961, **52**, 502–508.
75 J. Kim, J. G. Kim, Y. Kang, J. Y. Jang, G. J. Jog, J. Y. Lim, S. Kim, H. Suga, T. Nagamatsu and I. Hwang, *Mol. Microbiol.*, 2004, **54**, 921–934.
76 M. K. Fenwick, K. H. Almabruk, S. E. Ealick, T. P. Begley and B. Philmus, *Biochemistry*, 2017, **56**, 3934–3944.
77 B. Levenberg and S. N. Linton, *J. Biol. Chem.*, 1966, **241**, 846–852.
78 B. Philmus, B. T. Shaffer, T. A. Kidarsa, Q. Yan, J. M. Raaijmakers, T. P. Begley and J. E. Loper, *ChemBioChem*, 2015, **16**, 1782–1790.
79 A. Bacher, S. Eberhardt, M. Fischer, K. Kis and G. Richter, *Annu. Rev. Nutr.*, 2000, **20**, 153–167.
80 M. K. Fenwick, B. Philmus, T. P. Begley and S. E. Ealick, *Biochemistry*, 2016, **55**, 2748–2759.
81 A. O. Brachmann, F. Kirchner, C. Kegler, S. C. Kinski, I. Schmitt and H. B. Bode, *J. Biotechnol.*, 2012, **157**, 96–99.
82 H. Takahashi, T. Kumagai, K. Kitani, M. Mori, Y. Matoba and M. Sugiyama, *J. Biol. Chem.*, 2007, **282**, 9073–9081.
83 S. Reverchon, C. Rouanet, D. Expert and W. Nasser, *J. Bacteriol.*, 2002, **184**, 654–665.
84 N. Moebius, C. Ross, K. Scherlach, B. Rohm, M. Roth and C. Hertweck, *Chem. Biol.*, 2012, **19**, 1164–1174.
85 R. N. Strange, *Nat. Prod. Rep.*, 2007, **24**, 127–144.

86 T. H. M. Smits, F. Rezzonico, T. Kamber, J. Blom, A. Goesmann, J. E. Frey and B. Duffy, *Mol. Plant-Microbe Interact.*, 2010, **23**, 384–393.

87 S. Coyne, C. Chizzali, M. N. A. Khalil, A. Litomska, K. Richter, L. Beerhues and C. Hertweck, *Angew. Chem., Int. Ed.*, 2013, **52**, 10564–10568.

88 S. Coyne, A. Litomska, C. Chizzali, M. N. A. Khalil, K. Richter, L. Beerhues and C. Hertweck, *ChemBioChem*, 2014, **15**, 373–376.

89 T. H. M. Smits and B. Duffy, *Arch. Microbiol.*, 2011, **193**, 693–699.

90 R. Samson, J. B. Legendre, R. Christen, M. Fischer-Le Saux, W. Achouak and L. Gardan, *Int. J. Syst. Evol. Microbiol.*, 2005, **55**, 1415–1427.

91 S. Leonard, F. Hommais, W. Nasser and S. Reverchon, *Environ. Microbiol.*, 2017, **19**, 1689–1716.

92 I. K. Toth, J. M. van der Wolf, G. Saddler, E. Lojkowska, V. Hélias, M. Pirhonen, L. Tsror Lahkim and J. G. Elphinstone, *Plant Pathol.*, 2011, **60**, 385–399.

93 J. D. Glasner, C. H. Yang, S. Reverchon, N. Hugouvieux-Cotte-Pattat, G. Condemine, J. P. Bohin, F. van Gijsegem, S. Yang, T. Franza, D. Expert, G. Plunkett, M. J. S. Francisco, A. O. Charkowski, B. Py, K. Bell, L. Rauscher, P. Rodriguez-Palenzuela, A. Toussaint, M. C. Holeva, S. Y. He, V. Douet, M. Boccara, C. Blanco, I. Toth, B. D. Anderson, B. S. Biehl, B. Mau, S. M. Flynn, F. Barras, M. Lindeberg, P. R. J. Birch, S. Tsuyumu, X. Shi, M. Hibbing, M. N. Yap, M. Carpentier, E. Dassa, M. Umehara, J. F. Kim, M. Rusch, P. Soni, G. F. Mayhew, D. E. Fouts, S. R. Gill, F. R. Blattner, N. T. Keen and N. T. Perna, *J. Bacteriol.*, 2011, **193**, 2076–2077.

94 S. Khayi, P. Blin, T. M. Chong, K. G. Chan and D. Faure, *Stand. Genomic Sci.*, 2016, **11**, 87.

95 J. Zhou, Y. Cheng, M. Lv, L. Liao, Y. Chen, Y. Gu, S. Liu, Z. Jiang, Y. Xiong and L. Zhang, *BMC Genom.*, 2015, **16**, 571.

96 J. Pédron, S. Mondy, Y. Raoul des Essarts, F. Van Gijsegem and D. Faure, *BMC Genom.*, 2014, **15**, 283.

97 M. A. Matilla, H. Stöckmann, F. J. Leeper and G. P. C. Salmond, *J. Biol. Chem.*, 2012, **287**, 39125–39138.

98 G. Strobel, J. Y. Li, F. Sugawara, H. Koshino, J. Harper and W. M. Hess, *Microbiology*, 1999, **145**, 3557–3564.

99 J. Wu, H. B. Zhang, J. L. Xu, R. J. Cox, T. J. Simpson and L. H. Zhang, *Chem. Commun.*, 2010, **46**, 333–335.

100 J. Zhou, H. Zhang, J. Wu, Q. Liu, P. Xi, J. Lee, J. Liao, Z. Jiang and L.-H. Zhang, *Mol. Plant-Microbe Interact.*, 2011, **24**, 1156–1164.

101 Y. Cheng, X. Liu, S. An, C. Chang, Y. Zou, L. Huang, J. Zhong, Q. Liu, Z. Jiang, J. Zhou and L.-H. Zhang, *Mol. Plant-Microbe Interact.*, 2013, **26**, 1294–1301.

102 J. Masschelein, W. Mattheus, L. J. Gao, P. Moons, R. van Houdt, B. Uytterhoeven, C. Lamberigts, E. Lescrinier, J. Rozenski, P. Herdewijn, A. Aertsen, C. Michiels and R. Lavigne, *PLoS One*, 2013, **8**, e54143.

103 S. W. Fuchs, F. Grundmann, M. Kurz, M. Kaiser and H. B. Bode, *ChemBioChem*, 2014, **15**, 512–516.

104 J. Masschelein, C. Clauwers, U. R. Awodi, K. Stalmans, W. Vermaelen, E. Lescrinier, A. Aertsen, C. Michiels, G. L. Challis and R. Lavigne, *Chem. Sci.*, 2015, **6**, 923–929.

105 L. Liao, J. Zhou, H. Wang, F. He, S. Liu, Z. Jiang, S. Chen and L. H. Zhang, *Sci. Rep.*, 2015, **5**, 15719.

106 J. E. E. U. Hellberg, M. A. Matilla and G. P. C. Salmond, *Front. Microbiol.*, 2015, **6**, 137.

107 H. Fones and G. M. Preston, *FEMS Microbiol. Rev.*, 2013, **37**, 495–519.

108 C. Enard, A. Diolez and D. Expert, *J. Bacteriol.*, 1988, **170**, 2419–2426.

109 C. Neema, J. P. Laulhere and D. Expert, *Plant Physiol.*, 1993, **102**, 967–973.

110 T. Franza, B. Mahé and D. Expert, *Mol. Microbiol.*, 2005, **55**, 261–275.

111 M. Persmark, D. Expert and J. B. Neilands, *J. Biol. Chem.*, 1989, **264**, 3187–3193.

112 M. Sandy and A. Butler, *J. Nat. Prod.*, 2011, **74**, 1207–1212.

113 T. Franza and D. Expert, *J. Bacteriol.*, 1991, **173**, 6874–6881.

114 M. P. Starr, G. Cosens and H. J. Knackmuss, *Appl. Microbiol.*, 1966, **14**, 870–872.

115 R. P. Ryan, F. J. Vorhölter, N. Potnis, J. B. Jones, M. A. Van Sluys, A. J. Bogdanove and J. M. Dow, *Nat. Rev. Microbiol.*, 2011, **9**, 344–355.

116 M.-A. Jacques, M. Arlat, A. Boulanger, T. Boureau, S. Carrère, S. Cesbron, N. W. G. Chen, S. Cociancich, A. Darrasse, N. Denancé, M. Fischer-Le Saux, L. Gagnevin, R. Koebnik, E. Lauber, L. D. Noël, I. Pieretti, P. Portier, O. Pruvost, A. Rieux, I. Robène, M. Royer, B. Szurek, V. Verdier and C. Vernière, *Annu. Rev. Phytopathol.*, 2016, **54**, 163–187.

117 A. G. Andrewes, C. L. Jenkins, M. Starr, J. Shepherd and H. Hope, *Tetrahedron Lett.*, 1976, **17**, 4023–4024.

118 R. E. Mitchell, *Phytochemistry*, 1991, **30**, 3917–3920.

119 R. G. Birch and S. S. Patil, *Physiol. Mol. Plant Pathol.*, 1987, **30**, 199–206.

120 R. G. Birch and S. S. Patil, *Physiol. Mol. Plant Pathol.*, 1987, **30**, 207–214.

121 S. M. Hashimi, M. K. Wall, A. B. Smith, A. Maxwell and R. G. Birch, *Antimicrob. Agents Chemother.*, 2007, **51**, 181–187.

122 M. Royer, L. Costet, E. Vivien, M. Bes, A. Cousin, A. Damais, I. Pieretti, A. Savin, S. Megessier, M. Viard, R. Frutos, D. W. Gabriel and P. C. Rott, *Mol. Plant-Microbe Interact.*, 2004, **17**, 414–427.

123 E. Vivien, D. Pitorre, S. Cociancich, I. Pieretti, D. W. Gabriel, P. C. Rott and M. Royer, *Antimicrob. Agents Chemother.*, 2007, **51**, 1549–1552.

124 S. Cociancich, A. Pesic, D. Petras, S. Uhlmann, J. Kretz, V. Schubert, L. Vieweg, S. Duplan, M. Marguerettaz, J. Noëll, I. Pieretti, M. Hügelland, S. Kemper, A. Mainz, P. Rott, M. Royer and R. D. Süssmuth, *Nat. Chem. Biol.*, 2015, **11**, 195–197.

125 D. Petras, D. Kerwat, A. Pesic, B.-F. Hempel, L. von Eckardstein, S. Semsary, J. Arasté, M. Marguerettaz, M. Royer, S. Cociancich and R. D. Süssmuth, *ACS Chem. Biol.*, 2016, **11**, 1198–1204.

126 A. Etchegaray, M. E. Silva-Stenico, D. H. Moon and S. M. Tsai, *Microbiol. Res.*, 2004, **159**, 425–437.
127 A. R. Poplawsky, M. D. Kawalek and N. W. Schaad, *Mol. Plant-Microbe Interact.*, 1993, **6**, 545–552.
128 S. S. Pandey, P. K. Patnana, R. Rai and S. Chatterjee, *Mol. Plant Pathol.*, 2017, **18**, 949–962.
129 J. C. Huguet-Tapia, T. Lefebure, J. H. Badger, D. Guan, G. S. Pettis, M. J. Stanhope and R. Loria, *Appl. Environ. Microbiol.*, 2016, **82**, 2146–2155.
130 D. R. D. Bignell, J. K. Fyans and Z. Cheng, *J. Appl. Microbiol.*, 2014, **116**, 223–235.
131 R. Loria, J. Kers and M. Joshi, *Annu. Rev. Phytopathol.*, 2006, **44**, 469–487.
132 H. Zhang, Q. Wang, X. Ning, H. Hang, J. Ma, X. Yang, X. Lu, J. Zhang, Y. Li, C. Niu, H. Song, X. Wang and P. G. Wang, *J. Agric. Food Chem.*, 2015, **63**, 3734–3741.
133 J. P. Bourgault, A. R. Maddirala and P. R. Andreana, *Org. Biomol. Chem.*, 2014, **12**, 8125–8127.
134 H. Zhang, X. Ning, H. Hang, X. Ru, H. Li, Y. Li, L. Wang, X. Zhang, S. Yu, Y. Qiao, X. Wang and P. G. Wang, *Org. Lett.*, 2013, **15**, 5670–5673.
135 P. P. Molesworth, M. G. Gardiner, R. C. Jones, J. A. Smith, R. S. Tegg and C. Wilson, *Aust. J. Chem.*, 2010, **63**, 813.
136 R. R. King and L. A. Calhoun, *Phytochemistry*, 2009, **70**, 833–841.
137 J. A. Kers, M. J. Wach, S. B. Krasnoff, J. Widom, K. D. Cameron, R. A. Bukhalid, D. M. Gibson, B. R. Crane and R. Loria, *Nature*, 2004, **429**, 79–82.
138 S. M. Barry, J. A. Kers, E. G. Johnson, L. Song, P. R. Aston, B. Patel, S. B. Krasnoff, B. R. Crane, D. M. Gibson, R. Loria and G. L. Challis, *Nat. Chem. Biol.*, 2012, **8**, 814–816.
139 R. Loria, D. R. D. Bignell, S. Moll, J. C. Huguet-Tapia, M. V. Joshi, E. G. Johnson, R. F. Seipke and D. M. Gibson, *Antonie van Leeuwenhoek*, 2008, **94**, 3–10.
140 R. R. King, C. H. Lawrence, M. C. Clark and L. A. Calhoun, *J. Chem. Soc., Chem. Commun.*, 1989, **13**, 849–850.
141 D. R. D. Bignell, R. F. Seipke, J. C. Huguet-Tapia, A. H. Chambers, R. J. Parry and R. Loria, *Mol. Plant-Microbe Interact.*, 2010, **23**, 161–175.
142 J. K. Fyans, M. S. Altowairish, Y. Li and D. R. D. Bignell, *Mol. Plant-Microbe Interact.*, 2015, **28**, 443–454.
143 J. W. Westley, C.-M. Liu, L. H. Sello, R. H. Evans, N. Troupe, J. F. Blount, A. M. Chiu, L. J. Todaro and P. A. Miller, *J. Antibiot.*, 1984, **37**, 1738–1740.
144 K. U. Bindseil and A. Zeeck, *Helv. Chim. Acta*, 1993, **76**, 150–157.
145 M. Natsume, R. Ryu and H. Abe, *Ann. Phytopathol. Soc. Jpn.*, 1996, **62**, 411–413.
146 M. Natsume, A. Yamada, N. Tashiro and H. Abe, *Ann. Phytopathol. Soc. Jpn.*, 1998, **64**, 202–204.
147 J. K. Fyans, L. Bown and D. R. D. Bignell, *Phytopathology*, 2016, **106**, 123–131.
148 M. Natsume, N. Tashiro, A. Doi, Y. Nishi and H. Kawaide, *J. Gen. Plant Pathol.*, 2017, **83**, 78–82.
149 W. J. K. Crone, F. J. Leeper and A. W. Truman, *Chem. Sci.*, 2012, **3**, 3516–3521.
150 J. P. Gomez-Escribano, L. Song, M. J. Bibb and G. L. Challis, *Chem. Sci.*, 2012, **3**, 3522–3525.
151 Y. Hou, M. D. B. Tianero, J. C. Kwan, T. P. Wyche, C. R. Michel, G. A. Ellis, E. Vazquez-Rivera, D. R. Braun, W. E. Rose, E. W. Schmidt and T. S. Bugni, *Org. Lett.*, 2012, **14**, 5050–5053.
152 W. J. K. Crone, N. M. Vior, J. Santos-Aberturas, L. G. Schmitz, F. J. Leeper and A. W. Truman, *Angew. Chem., Int. Ed.*, 2016, **55**, 9639–9643.
153 L. Serino, C. Reimmann, P. Visca, M. Beyeler, V. Della Chiesa and D. Haas, *J. Bacteriol.*, 1997, **179**, 248–257.
154 R. F. Seipke, L. Song, J. Bicz, P. Laskaris, A. M. Yaxley, G. L. Challis and R. Loria, *Microbiology*, 2011, **157**, 2681–2693.
155 S. Kodani, J. Bicz, L. Song, R. J. Deeth, M. Ohnishi-Kameyama, M. Yoshida, K. Ochi and G. L. Challis, *Org. Biomol. Chem.*, 2013, **11**, 4686–4694.
156 L. Bown, Y. Li, F. Berrué, J. T. P. Verhoeven, S. C. Dufour and D. R. D. Bignell, *Appl. Environ. Microbiol.*, 2017, **83**, e01169–17.
157 S. Kumar, G. Stecher and K. Tamura, *Mol. Biol. Evol.*, 2016, **33**, 1870–1874.
158 N. Saitou and M. Nei, *Mol. Biol. Evol.*, 1987, **4**, 406–425.
159 M. Nei and S. Kumar, *Molecular evolution and phylogenetics*, Oxford University Press, New York, 2000.

3.3 Publikation 3

Fungal bio-surfactants from *Mortierella alpina*

Baldeweg, F.; Warnke, P.; Fischer D.; Markus, G. *Org. Lett.* **2019**, *21*, 1444–1448.

Zusammenfassung:
Mortierella alpina wird biotechnologisch zur Synthese von mehrfach ungesättigten Fettsäuren eingesetzt, wogegen die Biosynthese von Naturstoffen noch relativ unerforscht ist. Der Stamm ATCC 32222 besitzt mehrere Gencluster zur Biosynthese von NRPS-abgeleiteten Naturstoffen, welche aromatische Aminosäuren beinhalten. In dieser Studie wird die Isolation und Strukturaufklärung der Acylpeptide Malpinin A-E, deren Abbauprodukte Malpikynin A-E und der Zyklopeptide Malpinin A-C mittels spektroskopischer Methoden, chemischer Derivatisierung und Vollsynthese gezeigt. Aufgrund des Nachweises von grenzflächenaktiven Eigenschaften der Malpinine und dem Vorkommen in den Öltröpfchen auf den Kulturen von *M. alpina* konnte eine Funktion im Lipidtransport oder der Lipidspeicherung postuliert werden. Die Vielfalt der gefundenen Metabolite beweist, dass niedere Pilze ein übersehenes Reservoir für neue Naturstoffe sind.

Angaben zum Eigenanteil von Florian Baldeweg (40%):
Kultivierung der Pilze, Isolierung der Naturstoffe, Aufklärung der planaren Struktur sowie der absoluten Konfiguration der Aminosäuren. Chemische Synthese. Charakterisierung der Bioaktivität. Mitarbeit am Manuskript.

Jena, den

Prof. Dirk Hoffmeister

OL | Organic Letters

Letter

Cite This: *Org. Lett.* 2019, 21, 1444−1448

pubs.acs.org/OrgLett

Fungal Biosurfactants from *Mortierella alpina*

Florian Baldeweg,[†] Paul Warncke,[‡] Dagmar Fischer,[‡] and Markus Gressler*[,†]

[†]Pharmaceutical Microbiology, Leibniz Institute for Natural Product Research and Infection Biology - Hans-Knöll-Institute, Friedrich-Schiller-University Jena, Winzerlaer Strasse 2, 07745 Jena, Germany

[‡]Pharmaceutical Technology and Biopharmacy, Friedrich-Schiller-University Jena, Lessingstrasse 8, 07743 Jena, Germany

Supporting Information

ABSTRACT: The zygomycete *Mortierella alpina* is a well-known producer of polyunsaturated fatty acids in the food industry. Two series of its secondary metabolites are reported: Malpinins, a family of amphiphilic acetylated hexapeptides, were chemically characterized and serve as natural emulsifiers during lipid secretion. Additionally, hydrophobic cyclopentapeptides, malpibaldins, were structurally elucidated by NMR experiments, and their absolute stereochemistry was elucidated through chemical derivatization and synthesis. This work highlights lower fungi as a novel reservoir for natural products.

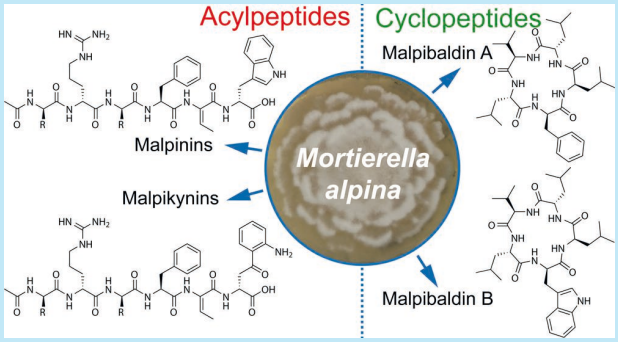

Over the past century, ascomycetes, such as *Aspergillus* and *Penicillium* sp., have been used as a prolific resource of pharmacologically important secondary metabolites (SM). Hence, the biosynthetic basic principles of SM biosynthesis, its regulation, and its potential in food industry and medicine have been investigated in detail.[1] In contrast, lower fungi, formerly combined in the kingdom of zygomycetes, are yet underestimated regarding their biosynthetic capacities. Apart from β-carotene-derived trisporoids, signal compounds found in *Blakeslea trispora* and *Phycomyces blakesleeanus* during mating processes,[2] little is known about the production and the pharmaceutical impact of SM produced by Mortierellaceae.

Various genomes of *Mortierella* sp. have been sequenced that revealed an unexpected high number of SM genes coding for nonribosomal peptide synthetases (NRPS).[3] For instance, the genome of *Mortierella alpina* encodes 22 potential NRPS and NRPS-like genes.[3] Anecdotal evidence exists that the fungus produces small peptides of pharmaceutical interest such as the antimycobacterial agent calpinactam[4,5] or the thrombin inhibitor Ro 09-1679.[6] Both metabolites represent linear or cyclic oligopeptides composed of a mixture of D- and L-amino acids and are therefore most likely NRPS products.

The filamentous fungus *M. alpina* is used as a producer of polyunsaturated fatty acids (PUFAs) such as α-linolenic acid or arachidonic acid for nutritional supplements in the food industry.[7] Lipids from *M. alpina* are stored in intracellular droplets.[8] During culture aging, the oily lipids are secreted to the hyphal surface and are visible by the naked eye as brownish droplets on the mycelium.[9] PUFA levels are elevated at low cultivation temperatures and are hence discussed as essential membrane compounds to increase the membrane fluidity and enable normal cellular processes during growth in subpolar regions.[10,11] The mechanism how *Mortierella* sp. tolerates high levels of lipids is poorly understood. However, oil-rich plants such as soybean emulsify lipids by production of amphiphilic lecithins which are widely used as transdermal drug carriers in biomedicine.[12,13]

Butanolic extracts from *M. alpina* ATCC32222 mycelium were characterized by the abundance of a series of masses according to UHPLC−MS (Figure 1 and Table S1), of which

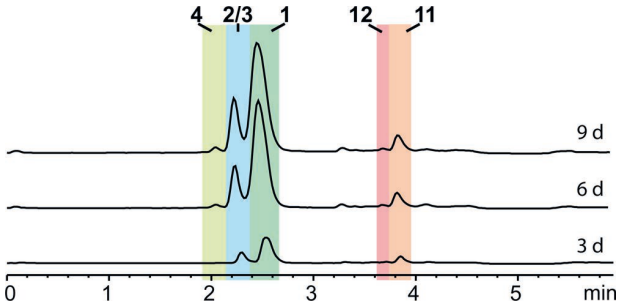

Figure 1. UHPLC−MS profiles of butanolic crude extracts from *M. alpina* ATCC32222 showing production of malpinins (blue/green) and malpibaldins (pink/orange) during growth for 3, 6, and 9 d.

one has been reported previously.[14] This compound, preliminarily designated as MBJ-0173, is a linear *N*-terminally acetylated hexapeptide (Ac-D-Leu-D-Arg-D-Leu-L-Phe-Dba-D-Trp) and was found to represent one compound of an entire series of metabolites and was hence named as malpinin A (**1**, t_R = 2.5 min) (Figure 2). Besides **1**, three novel compounds were

Received: January 16, 2019
Published: February 21, 2019

DOI: 10.1021/acs.orglett.9b00193
Org. Lett. 2019, 21, 1444−1448

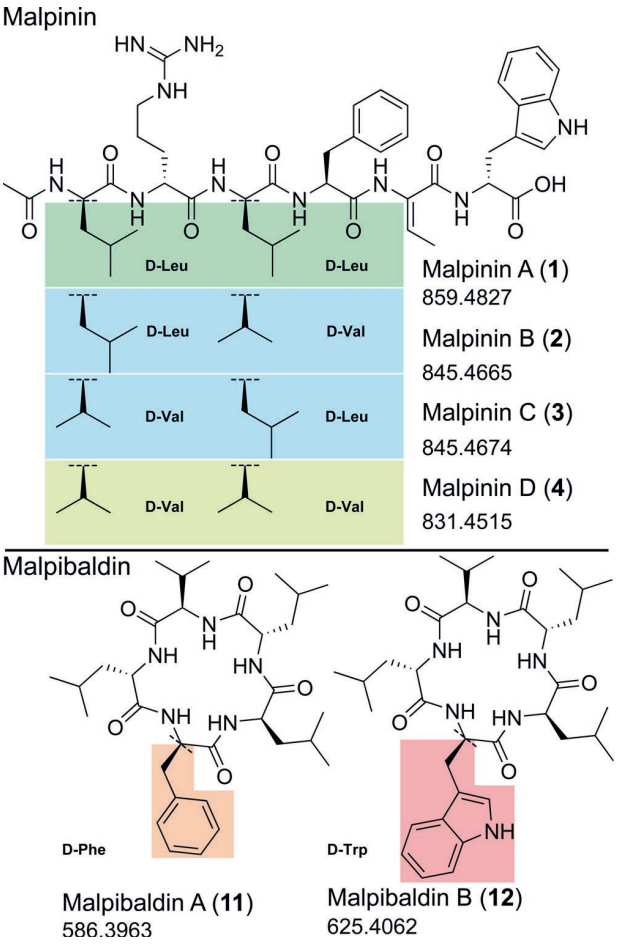

Figure 2. Structures of malpinin series **1**–**4** and malpibaldin series **11** and **12**. HR-MS data are given as m/z $[M + H]^+$. For detailed carbon atom numbering, see Figure S1. Physical properties of the compounds are listed in Table S1 and the Supporting Information.

detected: malpinins B and C (**2** and **3**) coeluting as at t_R = 2.3 min and malpinin D (**4**, t_R = 2.1 min) (Figure 1). All three compounds are most likely derivatives of **1** that differ in one or two methyl groups according to UHPLC–MS analysis (Table S1). The significant abundance of malpinins in mycelial extracts of the tested cultivations conditions suggested that malpinins are the predominant SMs of *M. alpina*. Besides the malpinins, two additional water-insoluble, highly hydrophobic compounds were identified, here referred to as malpibaldins A and B (**11** and **12**, t_R = 3.7 and 3.9 min) (Figure 1, Table S1).

Under standard cultivation conditions, sufficient quantities for subsequent structure elucidation were obtained for **1**, **11**, and **12**. However, trace amounts of the novel malpinin derivatives (**2**–**4**) required an optimization of the cultivation conditions (Supporting Information). Compared to **1**, the mass shift and MS–MS fragmentation pattern indicated the incorporation of one (in **2** and **3**) or two valine residues (in **4**) in place of leucine(s). Hence, the production of **2**–**4** in the absence and presence of D-valine or L-valine as an alternative nitrogen source was tested. The supplementation with L-valine as sole organic nitrogen source doubled the titers of **2** and **3** and increased the titers of **4** by the factor 4.5, while supplementation with D-valine had no effect (Table S2). In contrast, when L-leucine was provided as preferred nitrogen source, production of **2**–**4** was suppressed (data not shown). Instead, besides an intensified signal for **1**, an additional signal, malpinin E (**5**), was observed as minor compound by UHPLC–MS. Malpinins were accompanied by traces of shunt products with a mass shift of 4 (**6**–**10**) (Table S1 and Figures S1 and S2).

Analysis of the ^{13}C NMR spectra of **1**–**4** revealed seven carbonyl signals in each derivative. Fourteen signals possessed chemical shifts in the aromatic range of the spectrum, of which two showed exceptionally high intensities (δ_C = 126.3, 128.0). An inspection of HSQC, ^1H NMR, and HMBC spectra revealed that each of the signals of C-20/C-24 and C-21/C-23 represented two magnetically equivalent carbon atoms. In conclusion, **1**–**4** must contain eight C–C double bonds. Together with the seven degrees of unsaturation (DOU) of the carbonyl groups, this left four DOU, which were hence ascribed to three ring systems. Fourteen aromatic carbon atoms were assigned to tryptophan and phenylalanine, while the two remaining (δ_C = 130.2 and 128.1 ppm) could be assigned to dehydrobutyric acid (Dba) by 1D and 2D NMR (Tables S3 and S4 and Figures S3–S24). The sole quaternary signal at δ_C = 156.7 ppm was assigned to a guanidinium group of an arginine moiety. This assumption was additionally confirmed by ^{15}N stable isotope labeling experiments (Figure S25). While signals of these four amino acids were identical in **1**–**4**, a variable incorporation pattern of valine and leucine was found. Dipolar and scalar interactions of the amide protons with adjacent groups were used to determine the amino acid sequence, which showed the replacement of one or two leucines by valines on position 1 and 3 in **2**–**4** (Figure 2). The remaining carbons, not accounted for amino acids, constituted an acetyl moiety allocated to the *N*-terminal amino acid (Figure 2). Compounds **1**–**4** partially degraded over time. These compounds, named malpikynins (**6**–**9**), possessed a mass shift of 4 and only 18 DOU when compared to their parental malpinins (Figure 2, Table S1 and Figure S1). Chemical shifts above δ_C = 198.3 ppm suggested an additional carbonyl moiety. 2D NMR spectra (Tables S3 and S5 and Figures S2 and S26–S37) revealed that the C-terminal tryptophan was oxidatively converted to the nonproteinogenic amino acid kynurenine. This was proven by oxidation of **1** to **6** by hydrogen peroxide (Figure S38).

By analyzing the ^{13}C NMR spectra of **11** and **12**, five carbonyl signals were identified. In addition, five amide protons were identified by the inspection of the HSQC spectrum. Since each amide proton correlated with one of the above-mentioned carbonyl signal in the HMBC spectrum, a cyclic structure was proposed. Eight methyl moieties were identified in the aliphatic region of each ^1H NMR spectrum. Consistently, an inspection of 2D NMR spectra revealed the presence of one valine and three leucine moieties in each compound (Table S6 and Figures S39–S48). Correlations of aromatic protons disclosed a phenylalanine residue in **11** and a tryptophan residue in **12**, respectively. Dipolar and scalar interactions of the amide protons with adjacent groups were used to determine the amino acid sequence as cyclo(-Val-Leu-Phe/Trp-Leu-Leu-) (Figure 2 and Figures S1 and S2). The structures of all compounds were subsequently confirmed by LC-ESI-MS/MS fragmentation (Figure S49). The absolute configuration was established by acid hydrolysis and subsequent derivatization of the obtained amino acids as described by Marfey (Table S7).[15] However, L- and D-leucine were detected in both **11** and **12** in a molar ratio of 2:1 and

DOI: 10.1021/acs.orglett.9b00193
Org. Lett. 2019, 21, 1444–1448

Scheme 1. Principle of Liquid-Phase Peptide Synthesis of Stereoisomers of 12[a]

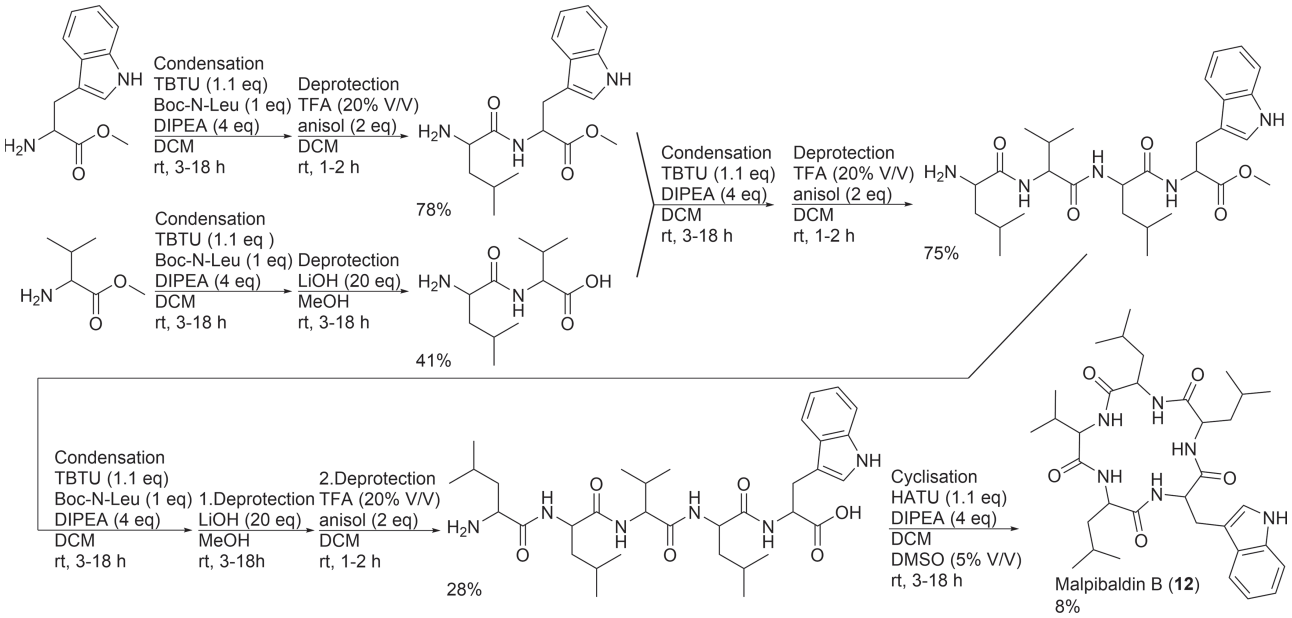

[a]Yields are representatively indicated for the synthesis of **12**. The synthetic standard of **11** was prepared analogously using Me-O-D-Phe as the priming amino acid.

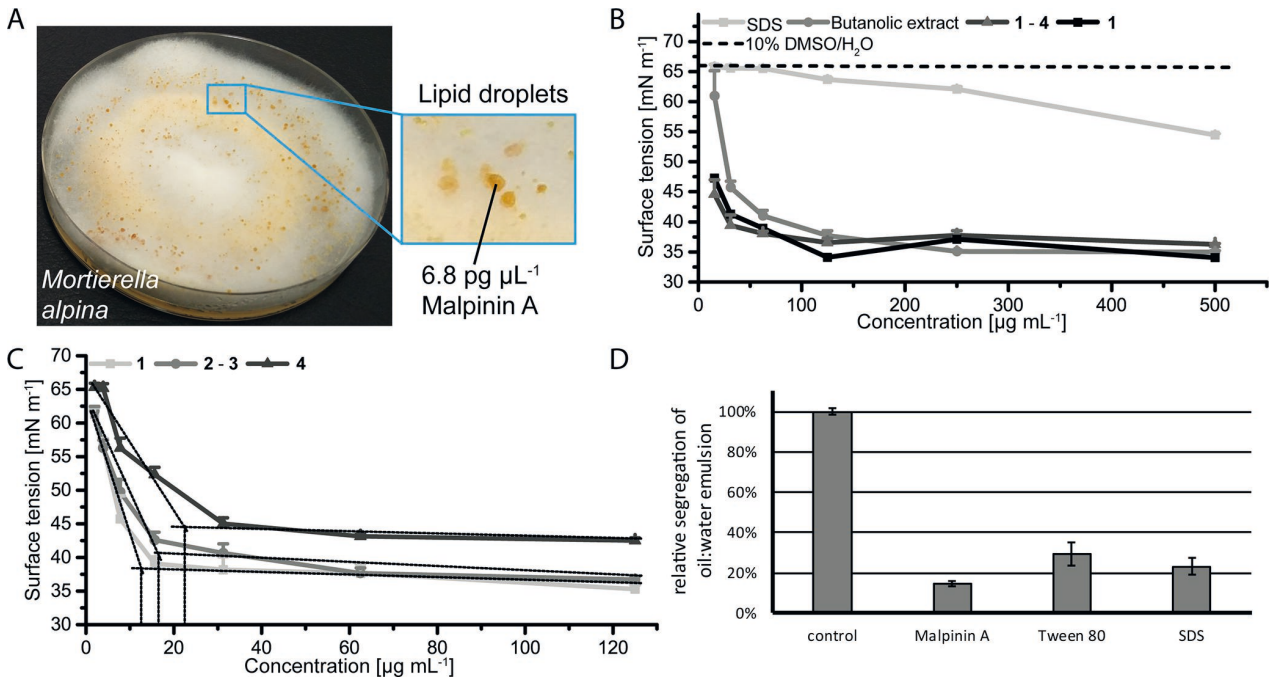

Figure 3. Physicochemical properties of malpinins. (A) Malpinins were isolated from lipid droplets from *M. alpina* ATCC32222. (B) Surface tension-reducing activity of butanolic extracts of *M. alpina*, malpinin mixtures (**1**–**4**) and pure **1**. SDS served as control. (C) Determination of the critical micelle concentration of **1**, **2** + **3**, and **4**. (D) Relative phase segregation of oil-in-water emulsions analyzed by light scattering at 650 nm. Emulsions without detergents served as reference control, while Tween 80 and SDS were positive controls.

hence could not be assigned to precise positions in the cyclopeptides. Therefore, all isomers of **12** were synthesized in which L- and D-leucine were permutated (Scheme 1). By comparison of the ^{1}H NMR spectra, cyclo(-D-Val-L-Leu-D-Trp-D-Leu-L-Leu-) was identified to be the sole naturally occurring isomer of **12** (Figure S50). To verify our assumption, its Phe-derivative **11** was additionally synthesized. The identical ^{1}H NMR spectra of natural and synthesized **11** confirmed the proposed structure: cyclo(-D-Val-L-Leu-D-Phe-D-Leu-L-Leu-). Trace amounts of malpinin E (**5**), malpikynin E (**10**), and malpibaldin C (**13**) were identified as side products by UHPLC–MS. LC–ESI–MS/MS fragmentation data sup-

DOI: 10.1021/acs.orglett.9b00193
Org. Lett. 2019, 21, 1444–1448

ported the exchange of phenylalanine to leucine at position 4 in **5** and **10** when compared to **1** (Figure 2 and Figure S51). Analogously, phenylalanine in **11** was replaced by tyrosine in **13** (Figure 2 and Figure S52).

Production of malpinins and malpibaldins appears to be a general feature of the *M. alpina* clade. All tested *M. alpina* strains (ATCC32222, DH187, DH189, DH192) produced malpinins and malpibaldins with quantitative and qualitative differences (Figure S53). In contrast, the related strain *Mortierella cystojenkinii* DH191 produced none of the compounds. The high abundance of these oligopeptides in *M. alpina* prompted us to investigate their possible functional role. Malpinins and malpibaldins show only moderate antimicrobial activities or antiproliferative effects against cancer cell lines (Figure S54 and Table S8). Recent studies on the cyclo-*all*-L-pentadepsipeptide sansalvamide A from a marine *Fusarium* sp. suggested cytotoxic properties of malpibaldins against mammalian cells.[16] However, subsequent synthesis of second generation derivatives of sansalvamide A revealed that the activity is negligible when L-amino acids were replaced by their D-configured counterparts at positions 1−3.[17] Thus, the stereochemistry of cyclopentapeptides seems to play a critical role in cell cytotoxicity.

Linear *N*-terminally acetylated oligopeptides have been isolated from various species and often comprise compounds of ecological importance.[18−20] During the purification procedure, foam formation in aqueous solutions of malpinins was observed. Hence, an emulsifying function of malpinins during lipid secretion was investigated. Indeed, **1** was detectable in lipid droplets of *M. alpina* cultures (6.88 ± 4.61 pg μL^{-1}) by UHPLC−MS (Figure 3A), supporting our hypothesis. Furthermore, butanolic mycelial extracts, malpinin mixtures (**1**−**4**) and pure **1** reduced the surface tension of aqueous solutions at concentrations from 1−500 $\mu g\ mL^{-1}$ as determined by the ring tear-off method (Figure 3B). The calculated critical micelle concentration (CMC) for **1** (14 μM), **2** + **3** (16 μM), and **4** (27 μM) is consistent with the decreasing hydrophobicity of the molecules (HLB values: 10.1, 10.3 and 10.4, respectively) (Figure 3C). The obtained CMC values are 600- to 300-fold lower than that of SDS (8.2 mM) but are in a similar range as bile salts (5 μM), indicating that malpinins are fungal lipid emulsifiers.[21] Indeed, oil-in-water emulsions show a retarded phase segregation, when **1** was added, similar to observations with detergents, such as SDS or Tween 80, known to stabilize emulsions (Figure 3D). In contrast to other amphiphilic molecules such as SDS no hemolytic activity in erythrocytes was observed up to 500 $\mu g\ mL^{-1}$, exceeding by far the CMC (Figure S55).

Combining NMR spectroscopy, chemical derivatization, and synthesis, the full structure and absolute configuration of four members of the malpinin family was resolved, including their oxidative shunt products as well as two members of the novel malpibaldin family. Malpinins may have an enormous potential for various applications in pharmacy, health care, food, cosmetics, or textiles since they offer a highly biocompatible and biodegradable alternative for synthetic surfactants in formulations. Biosurfactants can act as detergents, emulsifiers, foam-forming, and dispersing agents. The use of biosurfactants in the field of nanomedicine, e.g., the development of self-assembling drug delivery systems or as stabilizer for nanoparticle dispersions, are promising applications to overcome many therapeutic limitations, especially for the formulation of highly lipophilic drugs.[22] In particular, the low hemolytic and cytotoxic effects compared to synthetic tensides makes the malpinines promising candidates. This study establishes *Mortierellaceae* as relevant producers of natural products with new physicochemical properties.

■ ASSOCIATED CONTENT

Supporting Information

The Supporting Information is available free of charge on the ACS Publications website at DOI: 10.1021/acs.orglett.9b00193.

Details of strain identification, cultivation, metabolite isolation, derivatization, and chemical characterization (PDF)

■ AUTHOR INFORMATION

Corresponding Author

*E-mail: markus.gressler@leibniz-hki.de.

ORCID

Markus Gressler: 0000-0001-5669-7618

Notes

All procedures were approved by the Department for Animal Welfare of the Thuringian State Authority in compliance with the National Animal Protection Act (registration number: UKJ-18-101).

The authors declare no competing financial interest.

■ ACKNOWLEDGMENTS

F.B. acknowledges the Jena School for Microbial Communication (JSMC) for a doctoral fellowship. We thank S. Ziethe and S. Scheide (Friedrich-Schiller-University Jena) for preliminary experiments as well as A. Perner and H. Heinecke (Hans-Knöll-Institute Jena) for recording mass and NMR spectra, respectively. F.B. and M.G. acknowledge K. Voigt and H.-M. Dahse (Hans-Knöll-Institute Jena) for antimicrobial and antiproliferative tests. P.W. and D.F. thank K. Werz (Friedrich-Schiller-University Jena) for excellent technical assistance with the surface tension measurements and the Institute of Experimental Animal Science and Animal Welfare Jena for providing sheep blood samples.

■ REFERENCES

(1) Shwab, E. K.; Keller, N. P. *Mycol. Res.* **2008**, *112*, 225−230.

(2) Schimek, C.; Wöstemeyer, J. *Phytochemistry* **2009**, *70*, 1867−1875.

(3) Voigt, K.; Wolf, T.; Ochsenreiter, K.; Nagy, G.; Kaerger, K.; Shelest, E.; Papp, T. In *The Mycota: Biochemistry and Molecular Biology*, 3rd ed.; Springer International Publishing: Cham, 2016; pp 361−385.

(4) Koyama, N.; Kojima, S.; Nonaka, K.; Masuma, R.; Matsumoto, M.; Omura, S.; Tomoda, H. *J. Antibiot.* **2010**, *63*, 183−186.

(5) Koyama, N.; Kojima, S.; Fukuda, T.; Nagamitsu, T.; Yasuhara, T.; Omura, S.; Tomoda, H. *Org. Lett.* **2010**, *12*, 432−435.

(6) Kamiyama, T.; Umino, T.; Nakayama, N.; Itezono, Y.; Satoh, T.; Yamashita, Y.; Yamaguchi, A.; Yokose, K. J. *J. Antibiot.* **1992**, *45*, 424−427.

(7) Kikukawa, H.; Sakuradani, E.; Ando, A.; Shimizu, S.; Ogawa, J. *J. Adv. Res.* **2018**, *11*, 15−22.

(8) Yu, Y.; Li, T.; Wu, N.; Jiang, L.; Ji, X.; Huang, H. *Sci. Rep.* **2017**, *7*, 43896.

(9) Wang, L.; Chen, W.; Feng, Y.; Ren, Y.; Gu, Z.; Chen, H.; Wang, H.; Thomas, M. J.; Zhang, B.; Berquin, I. M.; Li, Y.; Wu, J.; Zhang, H.; Song, Y.; Liu, X.; Norris, J. S.; Wang, S.; Du, P.; Shen, J.; Wang,

N.; Yang, Y.; Wang, W.; Feng, L.; Ratledge, C.; Zhang, H.; Chen, Y. Q. *PLoS One* **2011**, *6*, No. e28319.
(10) Shinmen, Y.; Shimizu, S.; Akimoto, K.; Kawashima, H.; Yamada, H. *Appl. Microbiol. Biotechnol.* **1989**, *31*, 11−16.
(11) Melo, I. S.; Santos, S. N.; Rosa, L. H.; Parma, M. M.; Silva, L. J.; Queiroz, S. C.; Pellizari, V. H. *Extremophiles* **2014**, *18*, 15−23.
(12) Willimann, H.; Walde, P.; Luisi, P. L.; Gazzaniga, A.; Stroppolo, F. *J. Pharm. Sci.* **1992**, *81*, 871−874.
(13) Kateh Shamshiri, M.; Momtazi-Borojeni, A. A.; Khodabandeh Shahraky, M.; Rahimi, F. *J. Cell. Biochem.* **2018**, 1−11.
(14) Kawahara, T.; Itoh, M.; Izumikawa, M.; Sakata, N.; Tsuchida, T.; Shin-Ya, K. *J. Antibiot.* **2017**, *70*, 226−229.
(15) Marfey, P. *Carlsberg Res. Commun.* **1984**, *49*, 591−596.
(16) Otrubova, K.; Styers, T. J.; Pan, P. S.; Rodriguez, R.; McGuire, K. L.; McAlpine, S. R. *Chem. Commun. (Cambridge, U. K.)* **2006**, No. 9, 1033−1034.
(17) Rodriguez, R. A.; Pan, P. S.; Pan, C. M.; Ravula, S.; Lapera, S.; Singh, E. K.; Styers, T. J.; Brown, J. D.; Cajica, J.; Parry, E.; Otrubova, K.; McAlpine, S. R. *J. Org. Chem.* **2007**, *72*, 1980−2002.
(18) Kodani, S.; Komaki, H.; Suzuki, M.; Hemmi, H.; Ohnishi-Kameyama, M. *BioMetals* **2015**, *28*, 381−389.
(19) Lukat, P.; Katsuyama, Y.; Wenzel, S.; Binz, T.; Konig, C.; Blankenfeldt, W.; Bronstrup, M.; Muller, R. *Chem. Sci.* **2017**, *8*, 7521−7527.
(20) Robbel, L.; Knappe, T. A.; Linne, U.; Xie, X.; Marahiel, M. A. *FEBS J.* **2010**, *277*, 663−676.
(21) Reis, S.; Moutinho, C. G.; Matos, C.; de Castro, B.; Gameiro, P.; Lima, J. L. *Anal. Biochem.* **2004**, *334*, 117−126.
(22) Verma, G.; Hassan, P. A. *Phys. Chem. Chem. Phys.* **2013**, *15*, 17016−17028.

DOI: 10.1021/acs.orglett.9b00193
Org. Lett. 2019, 21, 1444−1448

Fungal bio-surfactants from *Mortierella alpina*

Florian Baldeweg,[†] Paul Warncke,[‡] Dagmar Fischer[‡] and Markus Gressler*[,†]

[†]Pharmaceutical Microbiology, Leibniz Institute for Natural Product Research and Infection Biology - Hans-Knöll-Institute, Friedrich-Schiller-University Jena, Winzerlaer Strasse 2, 07745 Jena, Germany

[‡]Pharmaceutical Technology and Biopharmacy, Friedrich-Schiller-University Jena, Lessingstrasse 8, 07743 Jena, Germany

Table of contents

Experimental procedures

Cultivation, extraction and metabolite purification

Organisms and strain identification. *M. alpina* strain ATCC32222 was obtained from the American Type Culture Collection (ATCC). All other *M. alpina* strains DH187 (= SF:6524), DH189 (= SF:9789), and DH192(= SF:2698) as well as the *M. cystojenkinii* strain DH191 (= SF:11396) were provided by the Jena Microbial Resource Collection (JMRC) and were maintained on MEP agar plates (30 g malt extract, 3 g soya peptone, 20 g agar per L) for 7 d at 25 °C prior to inoculation. Genomic DNA from all strains was isolated from 2 d old cultures grown in LB medium (180 RPM, 25 °C) as described previously.[1] Using oligonucleotides oITS1_f (5´-TCCGTAGGTGAACCTGCGG-3´) and oITS4_r (5´-TCCTCCGCTTATTGATATGC-3´) the internal transcribed spacer (ITS) spanning regions were amplified with Phusion DNA polymerase (Thermo) according to the manufacturer´s protocol. The gel-purified DNA fragments were ligated into the pJET1.2/blunt vector, sequenced and compared to the fungal genomes using NCBI BLASTn. The ITS sequence alignment and phylogenetic analysis were conducted with the MEGA 7 software.[2]

Medium optimization for malpinin production. 100 mL *Aspergillus* minimal medium[3] (AMM) containing 150 mM glucose and 35 mM NH_4NO_3 was supplemented with either L-leucine (25 mM), L-valine (25 mM), D-valine (25 mM) or was used without valine. Three replicates of the cultures were incubated at 25 °C, 120 RPM for one week. The mycelium was filtered through miracloth (Merck Millipore), resuspended in 40 mL butanol and homogenized for 5 minutes by a homogenizer (Ultra turrax, Ika). The suspension was then centrifuged (10 min, 4 °C, 3200 × g) and the resulting supernatant was evaporated to dryness. The residue was solved in 2 mL methanol and analyzed by UHPLC-MS equipped with a Zorbax Eclipse XDB-C_{18} column (50 × 2.1 mm, 1.8 µm) using a gradient of CH_3CN (eluent A) in H_2O with 0.1% FA (eluent B) with the following settings: flow:1 mL min^{-1}; temperature: 30 °C; gradient: 0-5 min: 5-100% A, 5-7 min 100% A. Chromatograms of *m/z* 859, 845 and 831 $[M + H]^+$ were extracted and the area under the curve (AUC) was calculated. AUC_{845} and AUC_{831} of the amino acid samples were normalized to the ratio of $AUC_{859, control}$ to $AUC_{859, sample}$. The factor of enhancement was calculated as $AUC_{normalized}$ to $AUC_{control}$ (Tab S1). For ^{15}N stable isotope labeling studies of **1,** 100 mL AMM containing 150 mM glucose was supplemented with 35 mM $(^{15}NH_4)_2SO_4$ or 35 mM $(^{14}NH_4)_2SO_4$. *M. alpina* ATCC 32222 was cultivated for 12 days at 25 °C prior to extraction as described above.

Cultivation, extraction and purification of 1 - 4. 15 flasks with 100 mL of optimized AMM were inoculated with *M. alpina* ATCC32222 and incubated at 25 °C, 120 RPM for one week. The mycelium was collected, resuspended in 300 mL butanol, homogenized by a homogenizer (Uultra turrax, Ika) and stirred for 2h. The suspension was then centrifuged (10 min, 4 °C, 3200 g) and the resulting supernatant was evaporated to dryness. The residue was resuspended in 2 mL of methanol/DMSO mixture (50:50). The crude extract was purified on an Agilent Infinity 1260 preparative HPLC system equipped with a Luna C_{18} column (250 × 21.2 mm, 10 µm; Phenomenex) using a gradient of CH_3CN in (eluent A) H_2O with 0.1% TFA (eluent B): flow: 20 mL min^{-1}; temperature: 20 °C; gradient: 0-1 min: 20% A, 1-21 min 20-100% A, 21-26 min 100% A. Final purification was accomplished by separation on an Agilent Infinity 1200 HPLC system equipped with a Zorbax Eclipse XDB-C_{18} column (250 × 9.4 mm, 5 µm; Agilent) using a gradient of CH_3CN (eluent A) in H_2O with 0.1% TFA (eluent B): flow: 2 mL min^{-1}; temperature: 12 °C; gradient: 0-0.5 min: 30% A, 0.5-12.5 min 30-60% A, 12.5-13 min 60-100% A, 13-15 min 100% A. The detection of malpinins was at λ = 225 nm.

Cultivation and extraction of 11 and 12. 25 flasks with 100 mL of LB medium (yeast extract 5 g, tryptone 10 g, NaCl 10 g per liter) were inoculated with *M. alpina* ATCC 32222. After two weeks of incubation at 25 °C and 120 RPM, the mycelium was collected and resuspended in a mixture of methanol, butanol and DMSO (500 mL, 12:12:1), homogenized by homogenizer (Uultra turrax, Ika) and stirred for 2 h. The suspension was then centrifuged (10 min, 20 °C, 3,200 × g) and the resulting supernatant was evaporated to dryness. The crude extract was purified on a preparative HPLC as described above with a modified gradient: 0-1 min: 5% A, 1-12.5 min 5-90% A, 12.5-13 min 90-100% A, 13-15 min 100% A. The elution of the malpibaldins was detected at λ = 205 nm.

Chemical analysis

General. LC-MS experiments were performed on an Agilent 1290 Infinity II UHPLC coupled to a 6130 Single Quadrupol mass spectrometer. MS/MS measurements were conducted using a Q Exactive Plus mass spectrometer (Thermo Scientific). NMR spectra were recorded on a Bruker Avance III 600 MHz spectrometer at 300 K. DMSO-d_6 served as solvent and internal standard (δ_H 2.49 ppm and δ_C 39.5 ppm, respectively).

Marfey's method. Marfey's method was carried out as described previously.[4] In brief, 0.25 mg of **1** - **4** were hydrolyzed in 6 N HCl (400 µL) at 150 °C for 1 h and 0.25mg of **11** and **12** were hydrolyzed in HCl (300 µL), H_2O (100 µL) and acetic acid (200 µL) at 110 °C for 18 h. After chilling the solution to ambient temperature, the hydrolysate was neutralized by adding KOH, evaporated to dryness and the residue was dissolved in 100 µL H_2O. For the derivatization reaction, 25 µL of the hydrolysate, 10 µL sodium bicarbonate (1 M) and 50 µL of a 1% (w/v) solution of Marfey's reagent (1-fluoro-2,4-dinitrophenyl-5- L-leucine amide, L-FDLA) in acetone were mixed. and incubated at 40 °C for 60 min. To stop the reaction, 10 µL 1 N HCl was added. The derivatized sample was analyzed by LC-MS using chiral FDLA amino acid standards as reference. LC-MS analyses were performed with a Luna Omega Polar C_{18} column (50×2.1 mm, 1.6 µm; Phenomenex) using a gradient of CH_3CN (eluent A) in H_2O with 0.1% FA (eluent B) with the following settings: flow: 1 mL min^{-1}; temperature: 30 °C; gradient: 0-4 min: 5-100% A, 5-6 min 100% A). The amino acid derivatives were detected by their mass ($[M + H]^+ = M_{amino\ acid} + M_{FDLA} - M_{Fluorine}$).

Detection of 1 from oil droplets. From the surface of MEP agar plates with *M. alpina*, 0.2 µL of oily droplets were diluted in 20 µl methanol and subjected to UHPLC-MS analysis. The separation was carried out on a Zorbax RRHD Eclipse Plus C_{18} column (50 × 2.1 mm, 1.8 µm; Agilent) using a gradient of CH_3CN with 0.1% FA (eluent A) in H_2O with 0.1% FA (eluent B) according to the following settings: flow: 1 mL min^{-1}; temperature: 30 °C; gradient: 0-1 min: 80-95% A, 1-1.5 min 95% A. The compounds were detected by ESI-MS in positive and negative ionization mode.

Peptide synthesis

General. Protected amino acids (Trp-O-Me, D-Phe-O-Me, D-Val-O-Me, L-Leu-N-Boc, D-Leu-N-Boc) were purchased from Carl Roth, all other reagents were purchased from Sigma-Aldrich. Water was removed by lyophilization. All reactions were performed with water-free solvent and under nitrogen atmosphere. The progress of conversion during the reaction was followed by UHPLC-MS. Intermediates were used without further purification for subsequent synthesis.

Amine deprotection. The peptide (0.125 M) and two equivalents of anisole (0.25 M) were dissolved in methylene chloride (CH_2Cl_2). Subsequently, TFA was added dropwise to make a 20% solution. The reaction was stopped after 1 to 2 hours by neutralization with KOH, extraction with H_2O and extraction with a saturated NH_4Cl solution. The organic layer was concentrated under reduced pressure.

Acid deprotection. The peptide (0.1 M) was dissolved in methanol and at least 20 equivalents of lithium hydroxide (2 M) were added (pH >11). The reaction was stopped after 3 to 18 hours by doubling the volume with H_2O and acidification with HCl to pH 4. Subsequently, methanol was removed under reduced pressure and the remaining aqueous solution was extracted three times with CH_2Cl_2. The organic extracts were pooled and concentrated.

Linear peptide coupling. To extend the linear peptide, the deprotected acid was dissolved in $CH_2Cl_2$to give a solution of 0.2 M. 4 equivalents of DIPEA (*N,N*-diisopropyl ethylamine) and 1.1 equivalents of TBTU (2-(1*H*-benzotriazole-1-yl)-1,1,3,3-tetramethylaminium tetrafluoroborate) were added and incubated 5 minutes. The peptide coupling solution was added immediately to the deprotected amines (0.2 M) in CH_2Cl_2 to give a final concentration of 0.1 M. The reaction was stopped after 3 to 18 hours by extraction with a saturated NH_4Cl solution and aqueous extraction. The organic phase was concentrate.

Macrocyclization procedure. The linear pentapeptide was deprotected as described above, starting with the acid deprotection procedure. The resulting deprotected linear peptide was either purified by HPLC (see below) or recrystallized in methanol. In a mixture of 5% DMSO in CH_2Cl_2, the linear pentapeptide and 4 equivalents of DIPEA were added (final concentration of 0.01 M). To initiate the reaction 1.1 equivalents HATU (1-[Bis(dimethylamino)methylene]-1*H*-1,2,3-triazolo[4,5-*b*] pyridinium 3-oxid hexafluorophosphate) were added. Additional amounts of HATU were added, if educts were evident by HPLC-MS. The reaction proceeded for 3 to 18 hours. Without stopping the reaction, CH_2Cl_2 was removed under reduced pressure and additional DMSO was added to a maximal volume of 9 mL.

Purification by preparative HPLC. The cyclopeptide solution (in DMSO) was immediately subjected to an Agilent Infinity 1260 preparative HPLC system equipped with a Luna C_{18} column (250 × 21.2 mm, 10 µm; Phenomenex) using a gradient of CH_3CN (eluent A) in H_2O with 0.1% TFA (eluent B) with the following protocol: flow: 20 mL min^{-1}; temperature: 20 °C; gradient: 0-1 min: 20% A, 1-21 min 20-100% A, 21-26 min 100% A. The elution of the peptides was detected at 225 nm. The fractions containing the peptide were concentrated under reduced pressure.

Purification by semi-preparative HPLC. Purification of the linear intermediates and cyclized synthetic peptides were accomplished by separation on an Agilent Infinity 1200 HPLC system equipped with a Synergi Polar-RP column (150 × 4.6 mm, 4 µm) using a gradient of CH_3CN (eluent A) in H_2O with 0.1% TFA (eluent B) according to the following protocol: flow: 1.5 mL min^{-1}; temperature: 10 °C; gradient: 0-0.5 min: 30% A, 0.5-12.0 min 30-66.8% A, 12.0-12.5 min 66.8-100% A, 12.5-14 min 100% A). The elution of the peptides was monitored at 205 nm.

Detection by UHPLC-MS. Each reaction was followed by UHPLC-MS. The separation was carried out on a Zorbax RRHD Eclipse Plus C_{18} column (50 × 2.1 mm, 1.8 µm; Agilent) using the following gradient of CH_3CN (eluent A) in H_2O with 0.1% TFA (eluent B): flow: 1.0 mL min^{-1}; temperature: 20 °C; gradient: 0-0.5 min: 5-95% A, 0.5-1 min 95% A. Compounds of higher hydrophobicity was separated using a second protocol: flow: 1.0 mL min^{-1}; temperature: 20° C; gradient: 0-4 min: 5-72% A, 4-4.5 min 72-95% A, 4.5-5 min 95% A. Signals were detected by ESI-MS in positive and negative ionization mode.

Determination of biological activities

Bacterial growth inhibition assay. The following organisms were tested for their susceptibility to the compounds as described previously[5]: *Bacillus subtilis JMRC:STI:10880*, *Staphylococcus aureus JMRC:STI:10760*, *Escherichia coli JMRC:ST:33699* , *Pseudomonas aeruginosa* JMRC:ST:33772, *Pseudomonas aeruginosa JMRC:ST:337721*, *Staphylococcus aureus* JMRC :ST :33793 (multi-resistent), *Enterococcus faecalis* JMRC:ST:33700 (vancomycin-resistent), *Mycobacterium vaccae* JMRC :STI:10670, *Sporobolomyces salmonincolor*, JMRC:ST:35974, *Candida albicans* JMRC: STI:25000, *Penicillium notatum* JMRC:STI:50164.

Cytotoxicity assay. Cells were grown in RPMI 1640 (CAMBREX 12-167F) medium supplemented with 2 mM ultraglutamine 1 (CAMBREX 17-605E/U1), 550 µL L^{-1} gentamicin sulfate (CAMBREX 17-518Z), and 10% heat inactivated fetal bovine serum (GIBCO Life Technologies 10270-106) at 37 °C in 5% CO_2 in high density polyethylene flasks (NUNC 156340). For the cytotoxicity assay approximately 10,000 HeLa cells were seeded in 0.1 mL culture medium in microplates and incubated for 48 hours without the test substances. To test the cytotoxic effect of natural products on HeLa, the dilutions of the compounds were carried out carefully on the subconfluent monolayers of HeLa cells after the preincubation time. The cells were incubated for 72 hours at 37 °C in a humidified atmosphere and 5% CO_2. The adherent HeLa cells were fixed by glutaraldehyde (MERCK 1.04239.0250) and stained with a 0.05% solution of methylene blue (SERVA 29198) for 15 min. After gently washing, the stain was eluted by 0.2 mL of 0.33 N HCl in the wells. The optical densities were measured at 660 nm (methylene blue) in a SUNRISE microplate reader (TECAN). Under the experimental conditions, the signal from the methylene blue is proportional to the number of viable cells. The cytolytic effect of compounds were analyzed in compare to negative control. The 50% cytotoxicity concentration (CC_{50}) was defined as the test compound concentration required for destruction in 50% of the cell monolayer compared to untreated control. Four replicates were assayed.

Determination of physicochemical properties

Surface tension measurements. The surface tension of sample solutions was determined by the ring tear-off method using a De Nouy ring tensiometer (Krüss Processor Tensiometer K12, Krüss) equipped with a platinum ring (radius 9.545 mm). Stock solutions of the samples were prepared in dimethyl sulfoxide (DMSO, RotiSolv®, Carl Roth) and serially diluted in concentrations ranging from 1.95 µg mL^{-1} – 500 µg mL^{-1} in 10% (v/v) DMSO/water mixture. 10 mL of each sample was filled in a tempered 43 mL glass vessel (SV10) for measurements at 25 °C. The density of the solvent mixture was set to 1.011 g cm^{-3}.[6] Additionally, the detergent sodium dodecyl sulfate (SDS, Carl Roth) was used as control in the same concentration range and measured analogous. Each sample and concentration were measured in triplicates. Data were reported as mean ± standard deviation. The surface tension vs. concentration plots were extrapolated to estimate the critical micelle concentration (CMC).[7]

Phase segregation in O/W emulsions. 25 µL of olive oil was suspended in 9.975 mL of water by ultra-sonication for 5 min. This emulsion was added to the substances und ultraonicated again for 2 minutes to prepare the following solutions: 1 (0.1 mg mL^{-1}), Tween 80 (1 mg mL^{-1}), SDS (2 mg mL^{-1}) and water (served as reference). The slope of the phase segregation was monitored at λ = 650 nm with a UV/VIS photometer for up to 4 hours. Relative phase segregation was determined:

$$\textbf{\textit{relative phase segregation}}\ [\%] = \frac{\textbf{\textit{slope}}\ (\textbf{\textit{detergent}})}{\textbf{\textit{slope}}\ (\textbf{\textit{water}})}\ \textbf{\textit{x}}\ \mathbf{100\%}$$

Calculation of HLB values: Hydrophilic-lipophilic balance (HLB) values have been calculated according to Griffin´s method.[8]

Quantities and physical properties of isolated metabolites and synthesized compounds

Isolated metabolites

Malpinin A (**1**), 37.7 mg, white greyish amorphous powder, UV (CH_3CN) λ_{max} 224 nm, 280 nm; HR-ESI-MS data, see Table S1; ^1H and ^{13}C NMR spectroscopic data, see Table S4.

Malpinin B (**2**), 15.6 mg, white greyish amorphous powder, UV (CH_3CN) λ_{max} 224 nm, 280 nm; HR-ESI-MS data, see Table S1; ^1H and ^{13}C NMR spectroscopic data, see Table S4.

Malpinin C (**3**), 3.0 mg, white greyish amorphous powder, UV (CH_3CN) λ_{max} 224 nm, 280 nm; HR-ESI-MS data, see Table S1; ^1H and ^{13}C NMR spectroscopic data, see Table S4.

Malpinin D (**4**), 6.0 mg, white greyish amorphous powder, UV (CH_3CN) λ_{max} 224 nm, 280 nm; HR-ESI-MS data, see Table S1; ^1H and ^{13}C NMR spectroscopic data, see Table S4.

Malpibaldin A (**11**), 7.5 mg, white yellowish amorphous powder, UV (CH_3CN) λ_{max} 202 nm; HR-ESI-MS data, see Table S1; ^1H and ^{13}C NMR spectroscopic data, see Table S6.

Malpibaldin B (**12**), 3.6 mg, white yellowish amorphous powder, UV (CH_3CN) λ_{max} 218 nm, 282 nm; HR-ESI-MS data, see Table S1; ^1H and ^{13}C NMR spectroscopic data, see Table S6.

Malpikynin A-E (**6-10**) and *malpibaldin C* (**13**) were detected as accompanying compounds by UPLC-MS (Fig. S2), HR-ESI-MS (Table S1, Fig. S51-S52) and ^1H NMR spectroscopy (Table S5) and could not be isolated in quantifiable amounts.

Synthesized compounds

Malpibaldin A (**11**), cyclo-(D-Val-L-Leu-D-Phe-D-Leu-L-Leu), 1.7 mg, white yellowish amorphous powder, UV (CH_3CN) λ_{max} 202 nm; HR-ESI-MS data, see Table S1; ^1H NMR spectroscopic data, see Fig. S50.

Malpibaldin B (**12**), cyclo-(D-Val-L-Leu-D-Trp-D-Leu-L-Leu), 1.0 mg, white yellowish amorphous powder, UV (CH_3CN) λ_{max} 218 nm, 282 nm; HR-ESI-MS data, see Table S1; ^1H NMR spectroscopic data, see Fig. S50.

Malpibaldin B stereoisomer a (**12a**), cyclo-(D-Val-L-Leu-D-Trp-L-Leu-D-Leu), 1.1 mg, white yellowish amorphous powder, UV (CH_3CN) λ_{max} 218 nm, 282 nm; ^1H NMR spectroscopic data, see Fig. S50.

Malpibaldin B stereoisomer b (**12b**), cyclo-(D-Val-D-Leu-D-Trp-L-Leu-L-Leu), 1.6 mg, white yellowish amorphous powder, UV (CH_3CN) λ_{max} 218 nm, 282 nm; ^1H NMR spectroscopic data, see Fig. S50.

Table S1. HR-ESI-MS-data of derivatives of malpinins, malpikynins and malpibaldins. DOU = Degree of unsaturation.

compound	no.	$[M + H]^+$	chem. formula of M	DOU
Malpinin A	**1**	859.4827	$C_{44}H_{62}N_{10}O_8$	19
Malpinin B	**2**	845.4665	$C_{43}H_{60}N_{10}O_8$	19
Malpinin C	**3**	845.4674	$C_{43}H_{60}N_{10}O_8$	19
Malpinin D	**4**	831.4515	$C_{42}H_{58}N_{10}O_8$	19
Malpinin E	**5**	825.4971	$C_{41}H_{65}N_{10}O_8$	14.5
Malpikynin A	**6**	863.4777	$C_{43}H_{62}N_{10}O_9$	18
Malpikynin B	**7**	849.4641	$C_{42}H_{60}N_{10}O_9$	18
Malpikynin C	**8**	849.4635	$C_{42}H_{60}N_{10}O_9$	18
Malpikynin D	**9**	835.4475	$C_{41}H_{58}N_{10}O_9$	18
Malpikynin E	**10**	829.4950	$C_{40}H_{65}N_{10}O_9$	13.5
Malpibaldin A	**11**	586.3963	$C_{32}H_{51}N_5O_5$	9.5
Malpibaldin B	**12**	625.4062	$C_{34}H_{52}N_6O_5$	11.5
Malpibaldin C	**13**	602.3912	$C_{32}H_{51}N_5O_6$	9.5

Table S2. Optimization of AMM by supplementation with 25 mM valine.

	control	L-valine			D-valine		
$[M + H]^+$	AUC [mAu min]	AUC [mAu min]	$AUC_{normalized}$ [mAu min]	Factor	AUC [mAu min]	$AUC_{normalized}$ [mAu min]	Factor
859	6.99 E + 07	4.89 E + 07	6.99 E + 07	1.00	3.23 E + 07	6.99 E + 07	1.00
845	1.94 E + 07	2.79 E + 07	3.99 E + 07	2.06	9.59 E + 06	2.08 E + 07	1.07
831	3.32 E + 06	1.05 E + 07	1.50 E + 07	4.52	1.34 E + 06	2.90 E + 06	0.87

Table S3. ESI-MS-MS data of **1** – **4** and **6** – **9**.

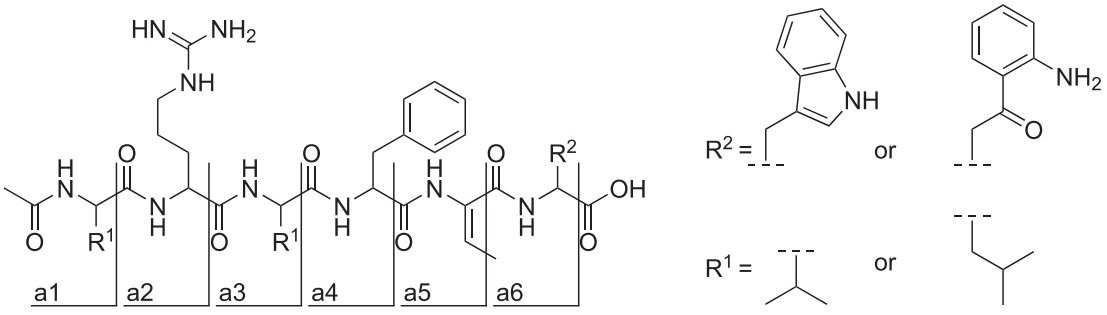

	fragments *m/z* $[M + H]^+$					
compound	a1	a2	a3	a4	[a5+2H]	a6
malpinin A (**1**)	128.11	284.21	397.29	544.36	629.41	813.47
malpinin B (**2**)	128.11	284.21	383.28	530.35	615.40	799.46
malpinin C (**3**)	114.09	270.19	383.28	530.35	615.40	799.46
malpinin D (**4**)	114.09	270.19	369.26	516.33	599.37	785.45
malpikynin A (**6**)	128.11	284.21	397.29	544.36	629.41	813.47
malpikynin B (**7**)	128.11	284.21	383.28	530.35	615.40	799.46
malpikynin C (**8**)	114.09	270.19	383.28	530.35	615.40	803.47
malpikynin D (**9**)	114.09	270.19	369.26	516.33	603.38	789.43

Table S4. NMR data of **1** – **4** in DMSO-d_6. *signals overlapping.

pos.	**malpinin A (1)** δ_C [ppm]	δ_H [ppm], M (J [Hz])	**malpinin B (2)** δ_C [ppm]	δ_H [ppm], M (J [Hz])	**malpinin C (3)** δ_C [ppm]	δ_H [ppm], M (J [Hz])	**malpinin D (4)** δ_C [ppm]	δ_H [ppm], M (J [Hz])
	D-tryptophan							
1	173.3		173.3		173.3		173.3	
2-NH		7.81, d (7.6)		7.84, d (7.5)		7.83, d (7.6)		7.84, d (7.6)
2	53.5	4.46, dt (5.3, 12.1)	53.4	4.46, dt (5.3, 12.0)	53.4	4.45, m (5.5)	53.4	4.46, m
3	26.9	a: 3.11, m*	26.9	a: 3.11, m*	26.8	a: 3.12, m*	26.8	a: 3.11, m*
		b: 3.21, dd (5.2, 14.8)		b: 3.21, dd (5.0, 14.6)		b: 3.21, dd (5.1, 14.6)		b: 3.21, dd (5.0, 14.6)
4	109.9		109.9		109.9		109.9	
5	123.8	7.19, d (2.6)	123.7	7.18, d (3.7)	123.8	7.18, m*	123.8	7.18, m*
5-NH		10.84, d (1.8)		10.84, d (1.4)		10.83, d (1.4)		10.82, d (1.5)
6	127.1		127.1		127.1		127.1	
7	118.1	7.52, d (8.0)	118.1	7.52, d (7.9)	118.1	7.52, d (7.8)	118.1	7.52, d (8.0)
8	118.4	6.97, t (7.0)	118.3	6.97, t (7.4)	118.4	6.97, t (7.4)	118.4	6.97, t (7.5)
9	120.9	7.05, t (7.1)	120.9	7.05, t (7.5)	120.9	7.05, t*	120.9	7.05, t (8.1)
10	111.4	7.32, d (8.0)	111.4	7.32, d (8.1)	111.4	7.32, d (8.1)	111.4	7.32, d (8.1)
11	136.1		136.1		136.1		136.1	
	dehydrobutyric acid							
12	164.3		164.3		164.3		164.3	
13-NH		9.11, s		9.16, s		9.11, s		9.16, s
13	130.2		130.2		130.2		130.2	
14	128.2	6.32, q (7.0)	128.0	6.31, q (7.0)	128.0	6.31, q (7.1)	128.1	6.31, q (7.1)
15	13.1	1.52, d (7.1)	13.1	1.51, d (7.0)	13.1	1.52, d (7.1)	13.1	1.51, d (7.1)
	L-phenylalanine							
16	170.2		170.2		170.2		170.2	
17-NH		8.35, d (8.0)		8.35, d (8.0)		8.36, d (8.0)		8.35, d (7.9)
17	54.3	4.58, m (8.0, 10.7)	54.2	4.65, m (4.6, 10.9)	54.2	4.58, m	54.2	4.64, m
18	37.2	a:2.77, dd (10.8, 13.6)	37.4	a:2.74, dd* (11.0,	37.3	a:2.75, dd (11.0, 13.5)	37.3	a:2.74, dd (11.0, 13.4)
		b:3.11, m*		13.5)		b:3.09, m*		b:3.09, m*
				b:3.08, m*				
19	137.8		137.8		137.8		137.7	
20-24	129.3	7.26, d (7.5)	129.2	7.27, d (7.3)	129.2	7.26, d* (7.3)	129.2	7.27, d* (7.5)
21-23	128.0	7.23, t (7.5)	128.0	7.22, t (7.5)	128.0	7.23, t* (7.5)	128.0	7.23, t* (7.6)
22	126.3	7.17, t (7.2)	126.3	7.16, t (7.2)	126.2	7.17, t* (7.2)	126.3	7.16, t* (7.5)
	D-leucine		D-valine		D-leucine		D-valine	
25	172.0		170.8		172.0		170.8	
26-NH		7.73, d (7.8)		7.50, d (8.8)		7.77, d (7.7)		7.57, d (9.1)
26	51.1	4.22, m*	57.2	4.16, dd (8.6,6.0)	51.1	4.23, m*	57.4	4.15, m
27	41.0	1.16, m	30.8	1.75, m	41.1	1.14, m	30.7	1.73, m
28	23.8	1.23, m*	18.9	0.56, d (6.7)	23.8	1.22, m*	18.9	0.54, d (6.7)
29	22.9	0.72, d (6.7)	17.3	0.50, d (6.7)	22.8	0.71, d* (6.5)	17.4	0.51, d (6.8)
29'	21.7	0.70, d (6.4)			21.7	0.69, d* (6.5)		
	D-arginine							
30	171.0		171.0		171.0		171.1	
31-NH		8.04, d (7.7)		8.09, d (7.9)		8.01, d (7.8)		8.06, d (8.2)
31	51.9	4.21, m*	51.9	4.26, m*	51.9	4.22, m*	52.1	4.27, m
32	28.5	a:1.48, m*	28.4	a:1.47, m*	28.7	a:1.45, m*	28.7	a:1.47, m*
		b:1.63, m*		b:1.63, m		b:1.60, m		b:1.61, m
33	25.0	a:1.39, m*	25.0	a:1.39, m*	25.0	a:1.38, m	25.0	a:1.39, m
		b:1.45, m*		b:1.44, m*		b:1.43, m*		b:1.45, m*
34	40.4	3.03, dt (5.9, 11.8)	40.4	3.03, m*	40.4	3.03, m	40.1	3.04, m
34-NH		7.54, t (5.7)		7.41, m		7.44, m		7.45, m
35	156.7		156.6		156.6		156.6	
	D-leucine		D-leucine		D-valine		D-valine	
36	172.5		172.5		171.3		171.3	
37-NH		8.02, d (7.6)		8.00, d (7.8)		7.89, d (8.3)		7.88, d (8.5)
37	51.2	4.23, m*	51.0	4.24, m*	57.9	4.09, m	57.8	4.11, m
38	40.6	a: 1.37, m*	40.8	a: 1.38, m*	30.3	1.88, m	30.3	1.88, m
		b: 1.41, m*		b: 1.41, m*				
39	24.1	1.57, m	24.1	1.56, m	19.1	0.81, d* (3.5)	19.2	0.81, d (6.3)
40	23.0	0.84, d (6.7)	23.0	0.84, d (6.6)	18.2	0.80, d* (3.5)	18.2	0.79, d (6.3)
40'	21.6	0.80, d (6.6)	21.6	0.80, d (6.5)				
	acetic acid							
41	169.4		169.3		169.5		169.4	
42	22.4	1.81, s	22.4	1.80, s	22.5	1.84, s	22.4	1.83, s

Table S5. NMR data of kynurenine moieties of **6** - **9** in DMSO-d_6. *signals overlapping.

	malpikynin A (6)				**malpikynin B (7)**			
pos.	δ_C [ppm]	δ_H [ppm], M (*J* [Hz])	COSY ($^1H \rightarrow ^1H$)	HMBC ($^1H \rightarrow ^{13}C$)	δ_C [ppm]	δ_H [ppm], M (*J* [Hz])	COSY ($^1H \rightarrow ^{13}C$)	HMBC ($^1H \rightarrow ^1H$)
	D-kynurenine				D-kynurenine			
1	173.2				n.d.			
2-NH		7.83, d*	2			7.82, d*	2	
2	48.4	4.79, m	2-NH, 3	3, 4	48.1	4.79, m	2-NH	
3	40.2	a:3.40, m*	2	1, 2, 4	39.7	a:3.39, m*		4
		b:3.44, m*				b:3.44, m*		
4	198.5				198.3			
5	116.3				116.1			
6	151.4				151.3			
6-NH2		n.d.				n.d.		
7	116.6	6.75, d (8.4)	8	5, 9	116.4	6.74, d (8.3)	8	5, 9
8	134.3	7.25, m*	7, 9	6, 10	134.3	7.25, m*	7, 9	6, 10
9	114.5	6.53, t (7.5)	8, 10	5, 7	114.5	6.53, t (7.5)	8, 10	5, 7
10	130.9	7.71, d*	9	4, 6, 8	131.1	7.72, d*	9	4, 6, 8
	malpikynin C (8)				**malpikynin D (9)**			
pos.	δ_C [ppm]	δ_H [ppm], M (*J* [Hz])	COSY ($^1H \rightarrow ^1H$)	HMBC ($^1H \rightarrow ^{13}C$)	δ_C [ppm]	δ_H [ppm], M (*J* [Hz])	COSY ($^1H \rightarrow ^{13}C$)	HMBC ($^1H \rightarrow ^1H$)
	D-kynurenine				D-kynurenine			
1	173.0				172.9			
2-NH		7.84, d*	2			7.82, d*	2	
2	48.2	4.79, m	2-NH, 3	1, 4	48.2	4.79, m	2-NH, 3	1
3	40.2	a:3.40, m*	2	1, 2, 4	40.2	a:3.38, m*	2	1, 2, 4
		b:3.46, m*				b:3.47, m*		
4	198.4				198.4			
5	115.8				115.9			
6	151.2				151.1			
6-NH2		n.d.				n.d.		
7	116.6	6.74, d (8.2)	8	5, 9	116.4	6.74, d (8.5)	8	5, 9
8	134.3	7.25, m*	7, 9	6, 10	134.3	7.25, m*	7, 9	6
9	114.5	6.53, t (7.4)	8, 10	5, 7	114.5	6.53, t (7.8)	8, 10	5, 7
10	131.2	7.72, d (8.7)	9	4, 6, 8	131.0	7.72, d (8.9)	9	4, 6, 8

Table S6. NMR data of **11** and **12** in DMSO-d_6. *overlapping.

	malpibaldin A (11)			**malpibaldin B (12)**	
pos.	δ_C [ppm]	δ_H [ppm], M (*J* [Hz])	pos.	δ_C [ppm]	δ_H [ppm], M (*J* [Hz])
	L-leucine			L-leucine	
1	171.5	8.84, d (7.6)	1	171.4	
2-NH		4.34, m	2-NH		7.84, d (7.5)
2	50.1	8.84, d (7.6)	2	50.1	4.46, dt (5.3, 12.0)
3	36.5	a:1.44, m*	3	36.6	a: 3.11, m*
		b:1.50, m*			b: 3.21, dd (5.0, 14.6)
4	24.1	1.54, m*	4	24.1	1.55, m*
5	22.9	0.86, d (6.5)	5	22.8	0.86, d (6.5)
6	21.5	0.77, d (6.4)	6	21.5	0.78, d (6.4)
	D-leucine			D-leucine	
7	170.8		7	170.9	
8-NH		4.29, m	8-NH		7.21, d (7.1)
8	52.0	7.26, d (7.0)	8	51.9	4.30, m
9	40.3	a: 1.39, m*	9	40.4	a: 1.39, m*
		b: 1.64, m			b: 1.62, m*
10	25.0	1.38, m*	10	24.9	1.38, m*
11	23.2	0.84, d (6.0)	11	23.2	0.84, d (6.1)
12	22.8	0.88, d (6.3)	12	22.3	0.88, d (6.1)
	D-phenylalanine			D-tryptophan	
13	170.8		13	171.2	
14-NH		8.82, d (8.0)	14-NH		8.71, d (8.2)
14	55.9	4.21, ddd (3.3, 8.6, 11.9)	14	55.3	4.23, m
15	36.7	a:2.74, dd (12.1, 13.6)	15	27.1	a: 2.90, dd (3.1, 14.4)
		b:3.09, dd (3.4, 13.8)			b: 3.19, dd (11.3, 14.5)
16	138.4		16	110.5	
17/21	128.9	7.22, m*	17	123.7	7.12, d (1.9)
18/20	128.1	7.22, m*	17-NH		10.79, d (1.4)
19	126.2	7.16, m	18	126.9	
			19	118.1	7.51, d(7.9)
			20	118.3	6.95, t (7.5)
			21	120.8	7.03, t (7.2)
			22	111.3	7.30, d (8.0)
			23	136.2	
	L-leucine			L-leucine	
22	171.7		24	171.8	
23-NH		8.49, d (6.6)	25-NH		8.45, d (6.9)
23	52.1	4.07, dt (6.5, 9.5)	25	51.9	4.12, m*
24	38.9	a: 1.13, m	26	38.8	a: 1.18, m
		b: 1.30, m			b: 1.20, m
25	23.8	0.87, m*	27	23.9	0.99, m (6.7)
26	22.8	0.62, d (6.6)	28	22.4	0.62, d (6.6)
27	21.9	0.70, d (6.5)	29	22.0	0.72, d (6.5)
	D-valine			D-valine	
28	171.6		30	171.5	
29-NH		7.57, d (9.2)	31-NH		7.59, d (9.2)
29	57.1	4.12, dd (6.8, 9.1)	31	57.2	4.11, m*
30	30.7	1.80, m (6.7)	32	30.7	1.79, m (6.7)
31	19.2	0.79, d (6.6)	33	19.1	0.81, d (6.7)
32	17.9	0.81, d (6.7)	34	18.0	0.79, d (6.7)

Table S7. Determination of the absolute configuration of amino acids by Marfey's method. A. Results for 1 - 4 compared to authentic standards. B. Results for 11 and 12 compared to authentic standards. Retention times of D- and L-amino acids are highlighted in blue and red, respectively.

A

	retention time of derivatized amino acids [min]				
sample	Leu	Val	Arg	Phe	Kyn
malpinin A (**1**)	2.66	-	1.62	2.39	2.50
malpinin B (**2**)	2.67	2.52	1.63	2.40	2.52
malpinin C (**3**)	2.66	2.51	1.63	2.39	2.51
malpinin D (**4**)	-	2.51	1.63	2.39	2.51
L-Standard	2.31	2.19	1.68	2.37	2.29
D-Standard	2.65	2.50	1.60	2.55	2.49

B

	retention time of derivatized amino acids [min]			
sample	Leu (ratio)	Val	Phe	Kyn
malpibaldin A (**11**)	2.31 + 2.61 (2:1)	2.47	2.55	-
malpibaldin B (**12**)	2.32 + 2.62 (2:1)	2.48	-	2.47
L-Standard	2.31	2.19	2.35	2.29
D-Standard	2.61	2.45	2.55	2.46

Table S8. Antiproliferative and cytotoxic activity of **1 - 4** and **11** and **12**. Compounds have been tested in a range of 1.5-50 µg mL^{-1}.

compound	antiproliferative effect		cytotoxicity	solubility
	HUVEC	K-562	HeLa	
	GI50 [µg mL^{-1}]	GI50 [µg mL^{-1}]	CC50 [µg mL^{-1}]	
malpinin A (**1**)	>50	>50	>50	DMSO
malpinin B (**2**)	>50	>50	>50	DMSO
malpinin C (**3**)	>50	>50	42.8 (± 0.7)	DMSO
malpinin D (**4**)	>50	>50	>50	DMSO
malpibaldin A (**11**)	>50	>50	>50	DMSO
malpibaldin B (**12**)	>50	>50	>50	DMSO

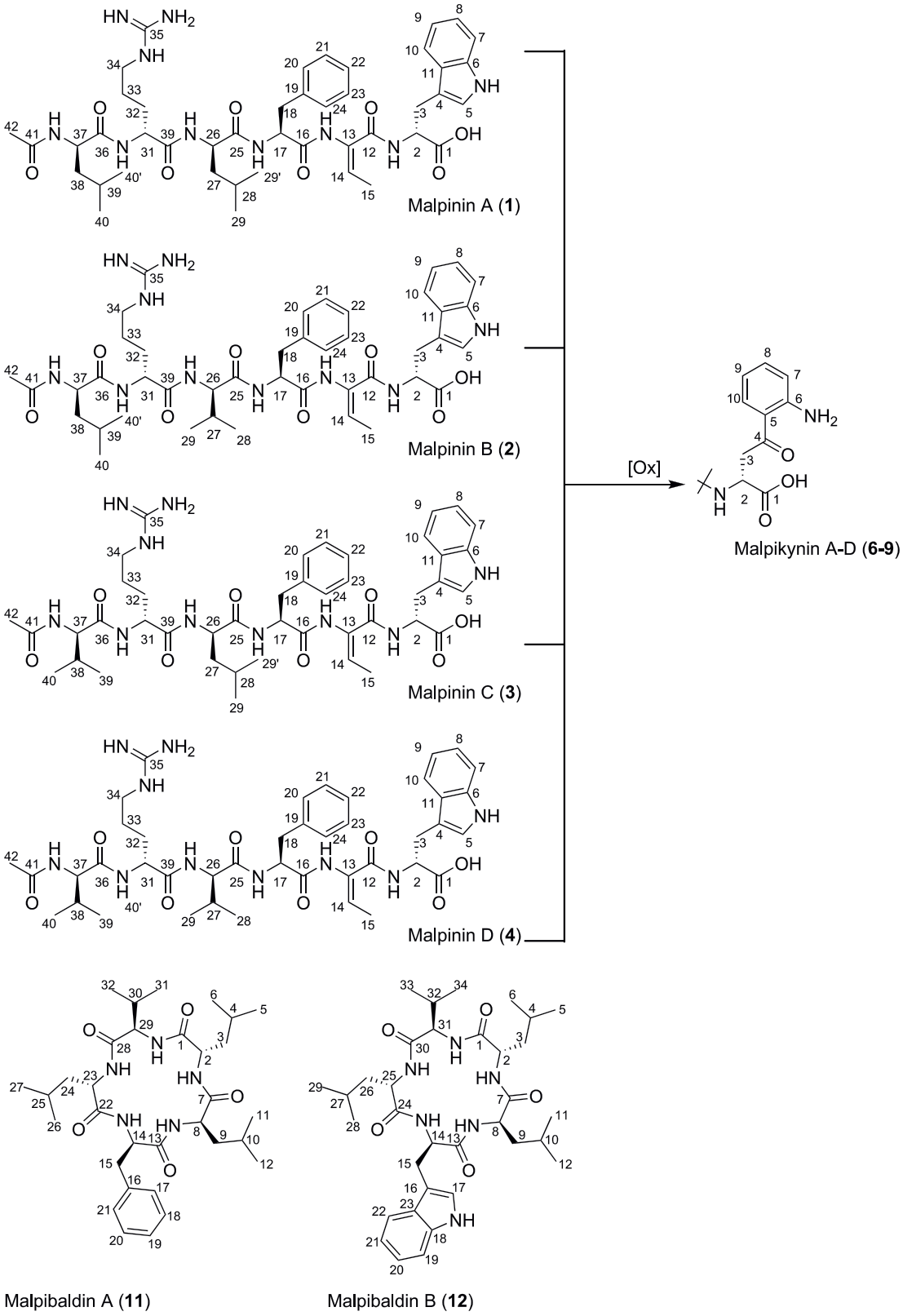

Figure S1. Numbering of carbon atoms in compounds **1 - 4, 6 - 9** and **11 - 12**.

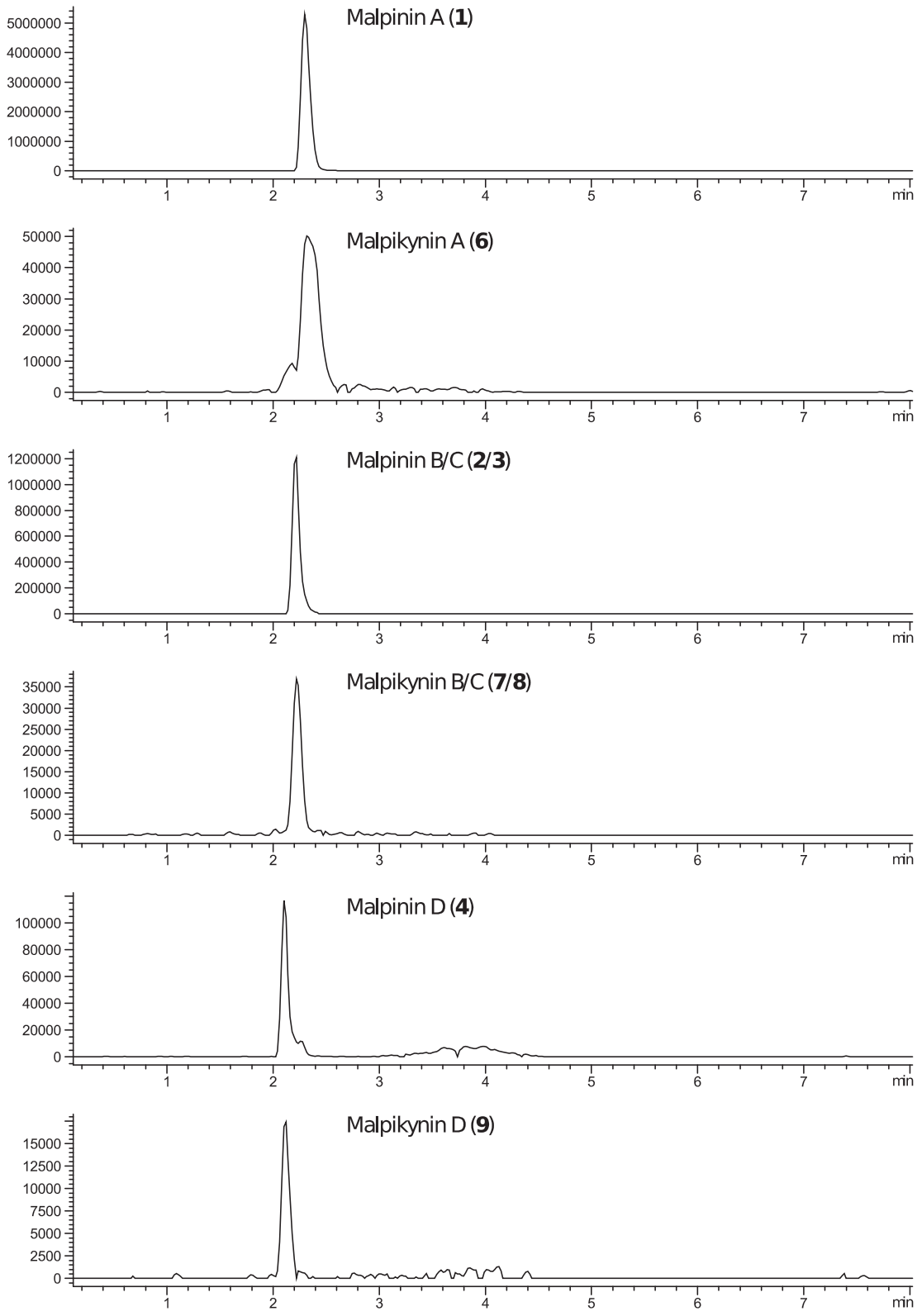

Figure S2. Abundance of malpinins **(1 – 4)** and malpikynins **(6 - 9)** in the butanolic crude extracts of *M. alpina*. EIC detected in positive mode are shown for **1** (m/z 859[M + H]$^+$), **2/3** (m/z 845[M + H]$^+$), **4** (m/z 831 [M + H]$^+$), **6** (m/z 863 [M + H]$^+$), **7/8** (m/z 849 [M + H]$^+$) and **9** (m/z 835 [M + H]$^+$). Note, that malpikynins are detectable in trace amounts (1-2%) when compared to malpibaldins.

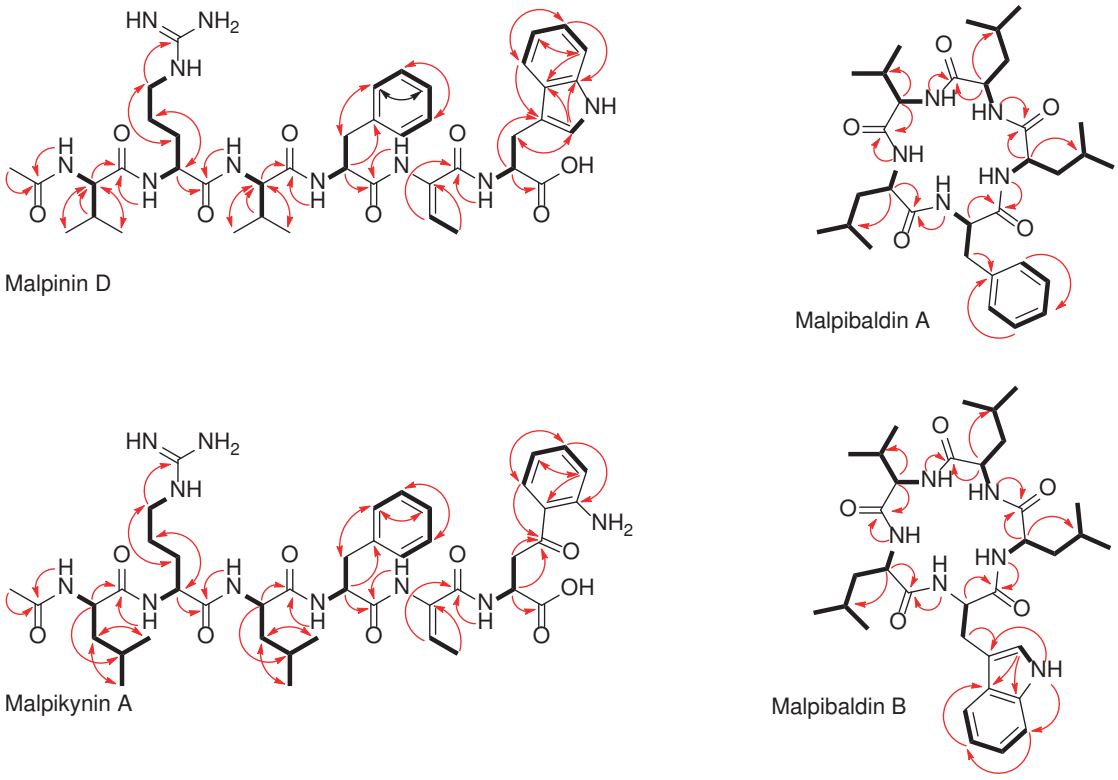

Figure S3. COSY (bold lines) and selected HMBC (red arrows) key correlations in **4** (two valine-residues), ***6*** (two leucine-residues), **11** and **12**.

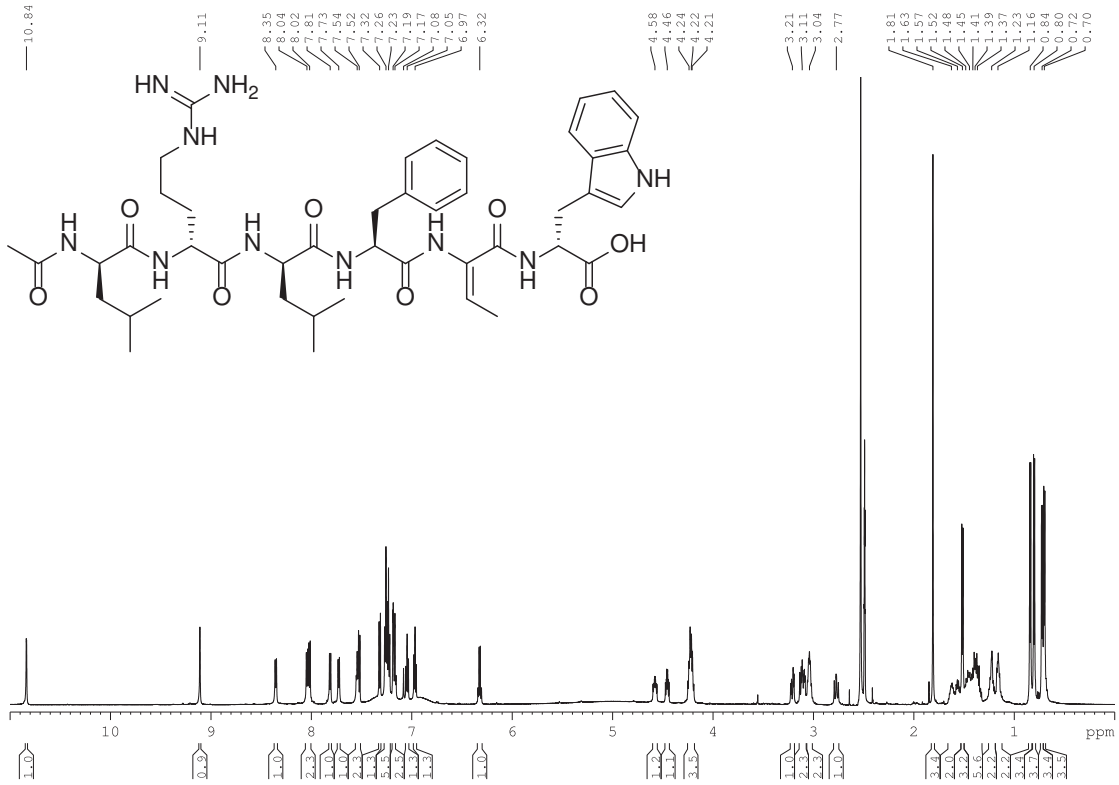

Figure S4. ^{1}H NMR spectrum of **1** in DMSO-d_6

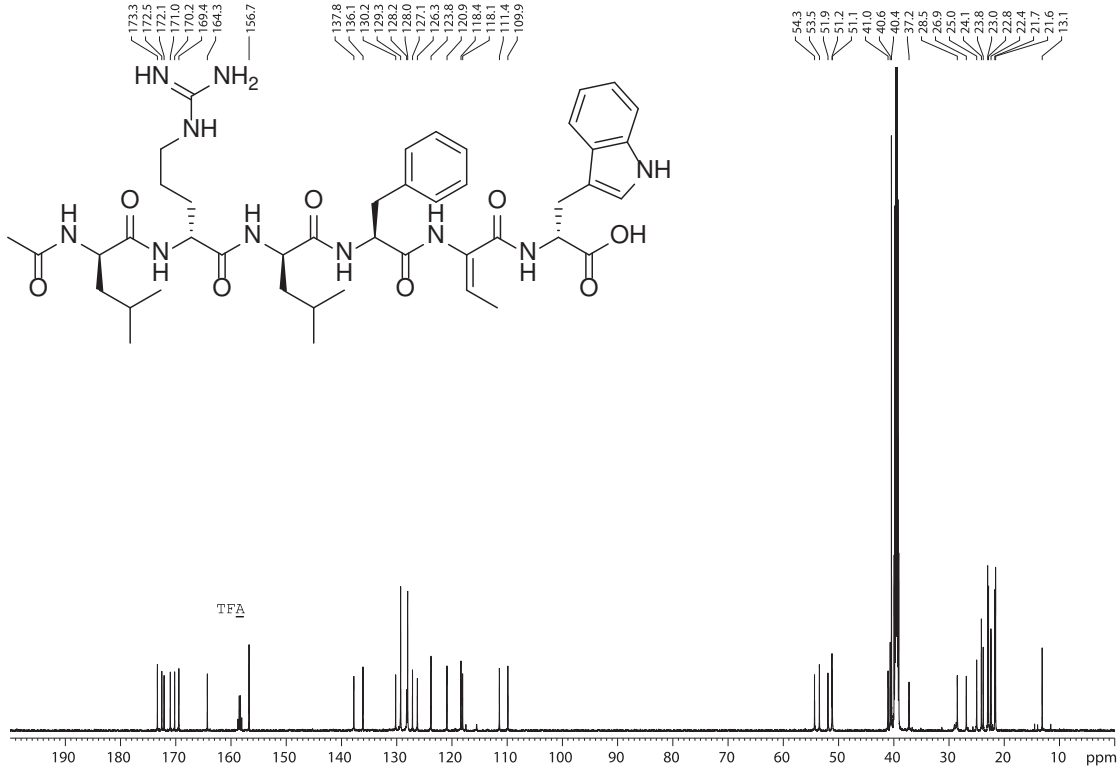

Figure S5. ^{1}H decoupled ^{13}C NMR spectrum of **1** in DMSO-d_6

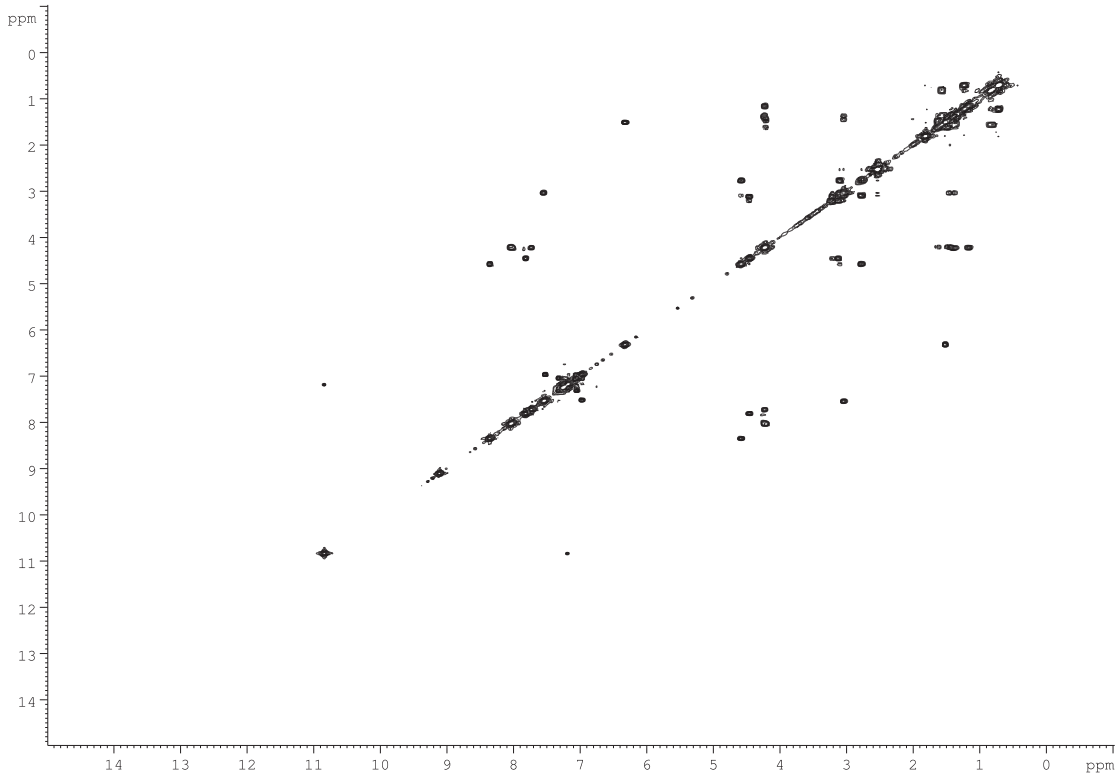

Figure S6. ^{1}H, ^{1}H COSY spectrum of **1** in DMSO-d_6

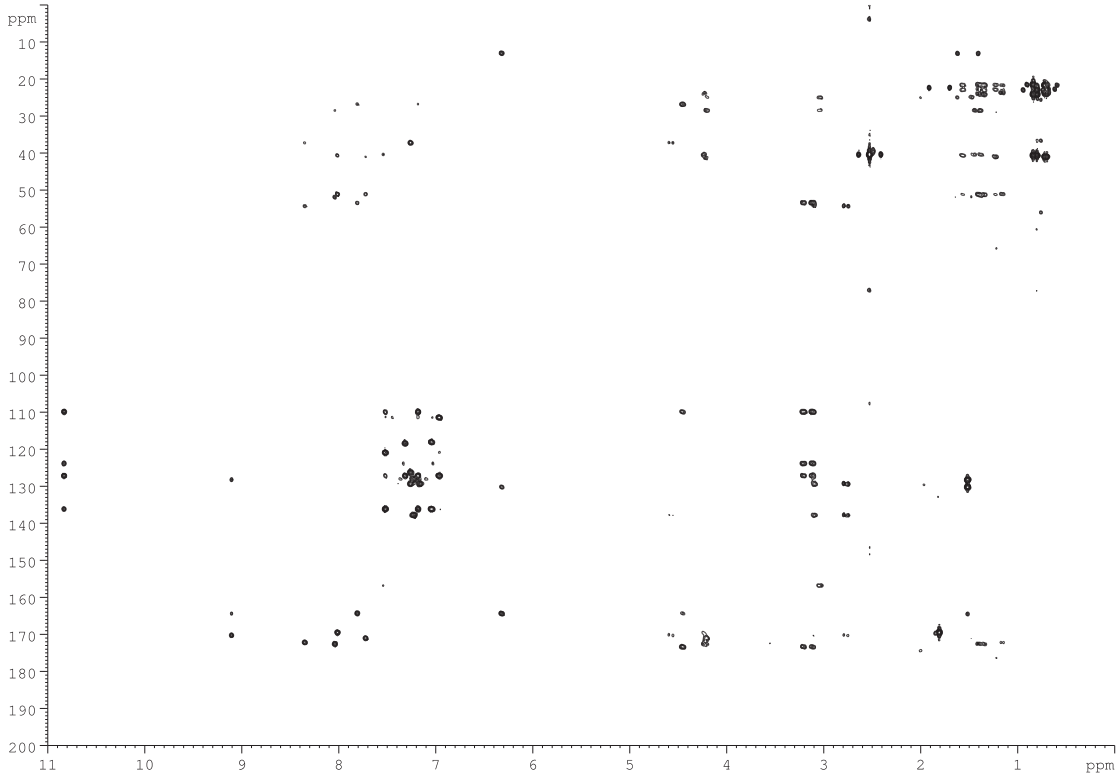

Figure S7. ^{1}H, ^{13}C HMBC spectrum of **1** in DMSO-d_6

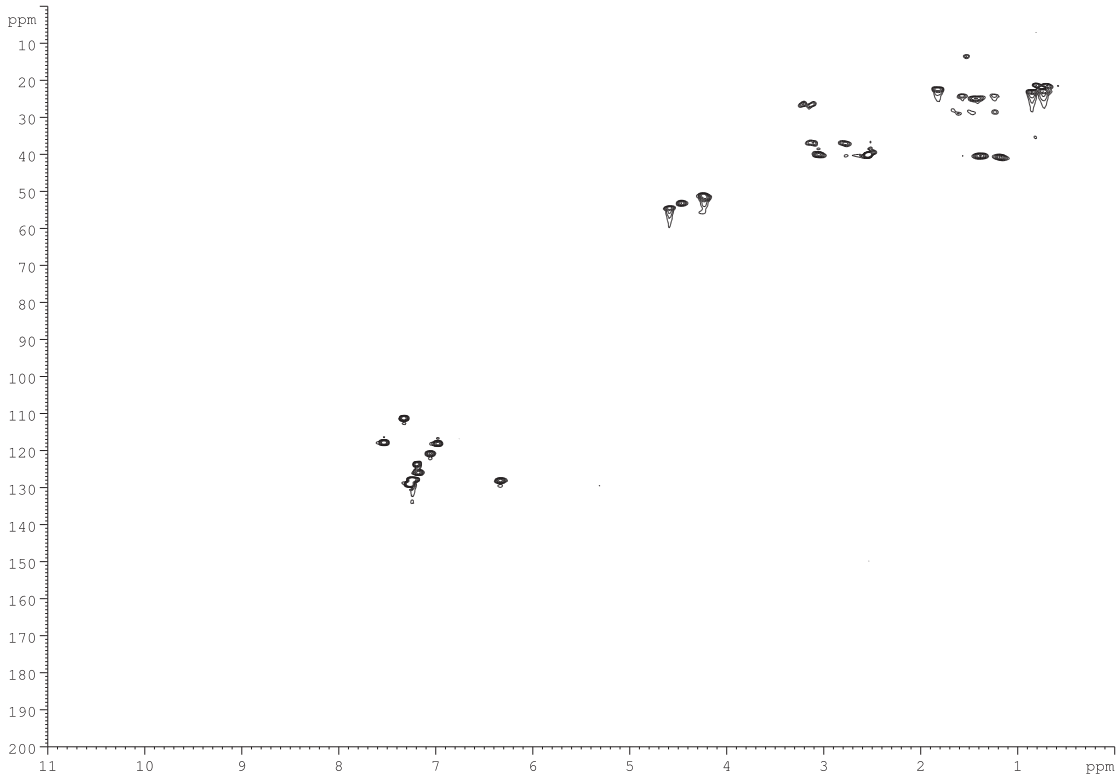

Figure S8. ^{1}H, ^{13}C HSQC spectrum of **1** in DMSO-d_6

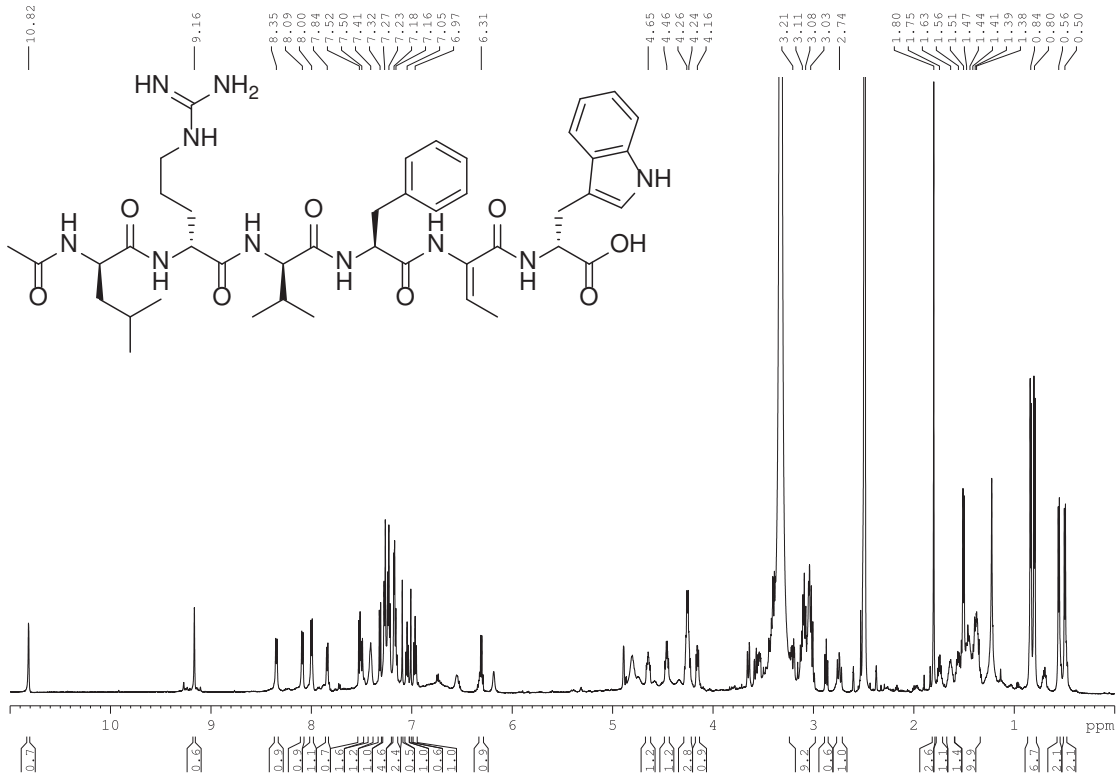

Figure S9. ^{1}H NMR spectrum of **2** in DMSO-d_6

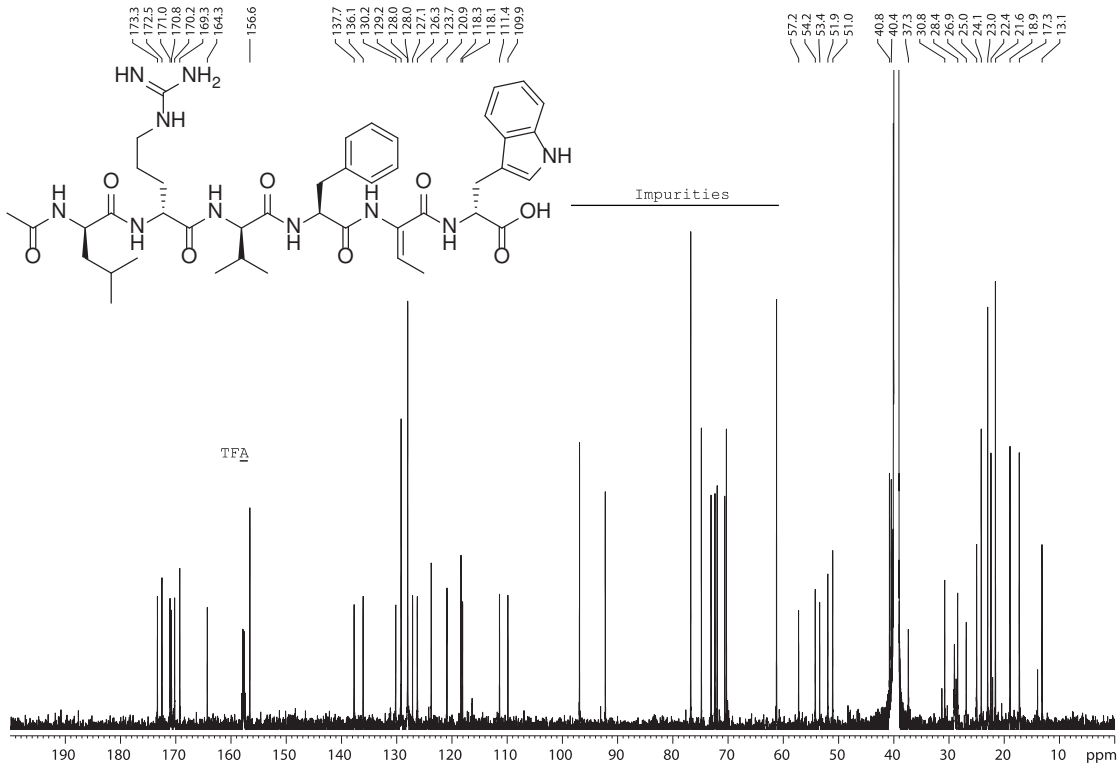

Figure S10. ^{1}H decoupled ^{13}C NMR spectrum of **2** in DMSO-d_6

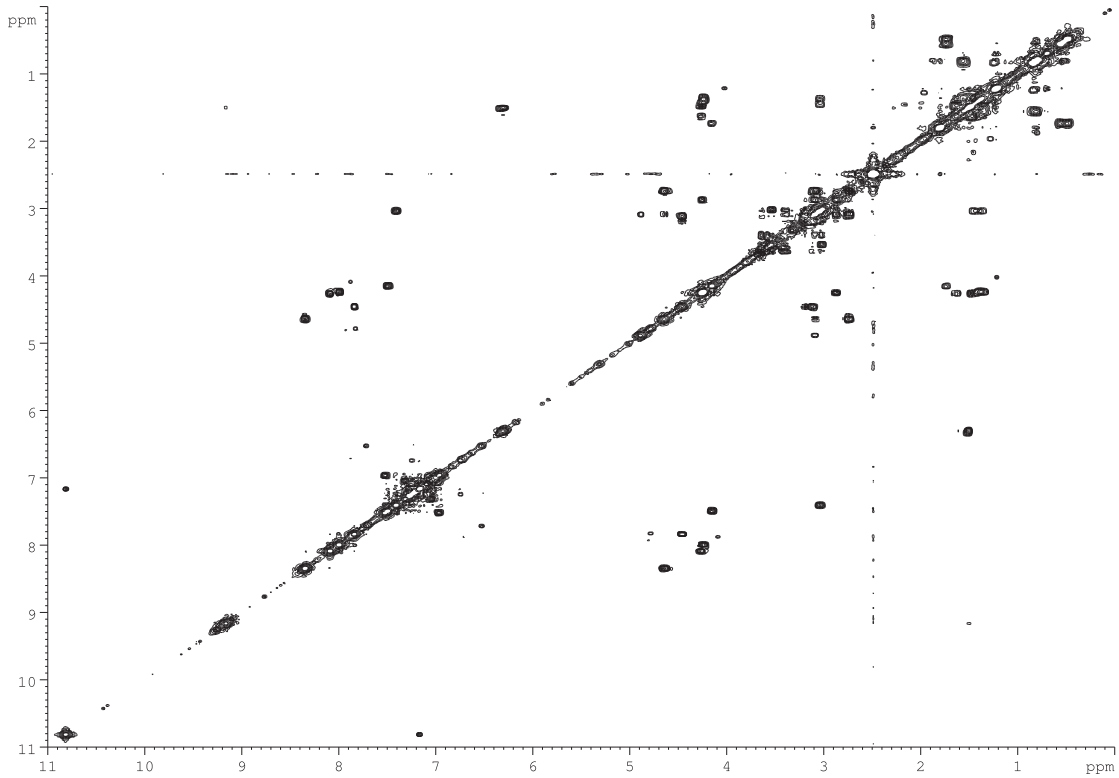

Figure S11. ^{1}H, ^{1}H COSY spectrum of **2** in DMSO-d_6

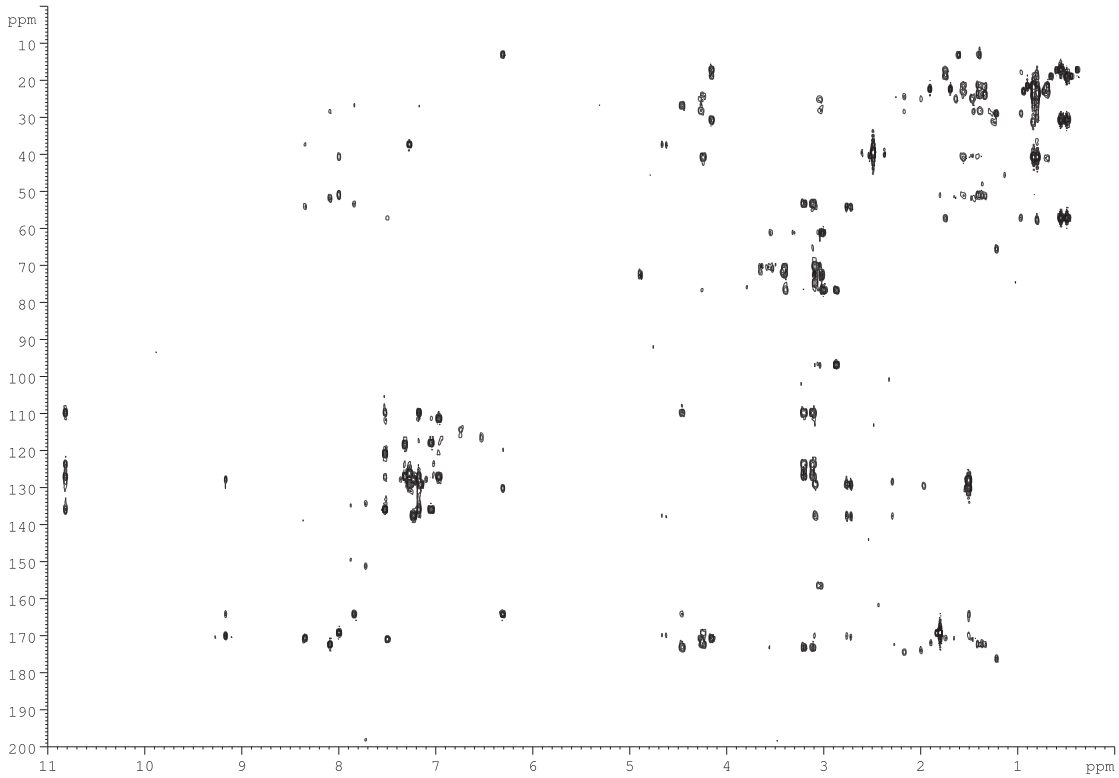

Figure S12. ^{1}H, ^{13}C HMBC spectrum of **2** in DMSO-d_6

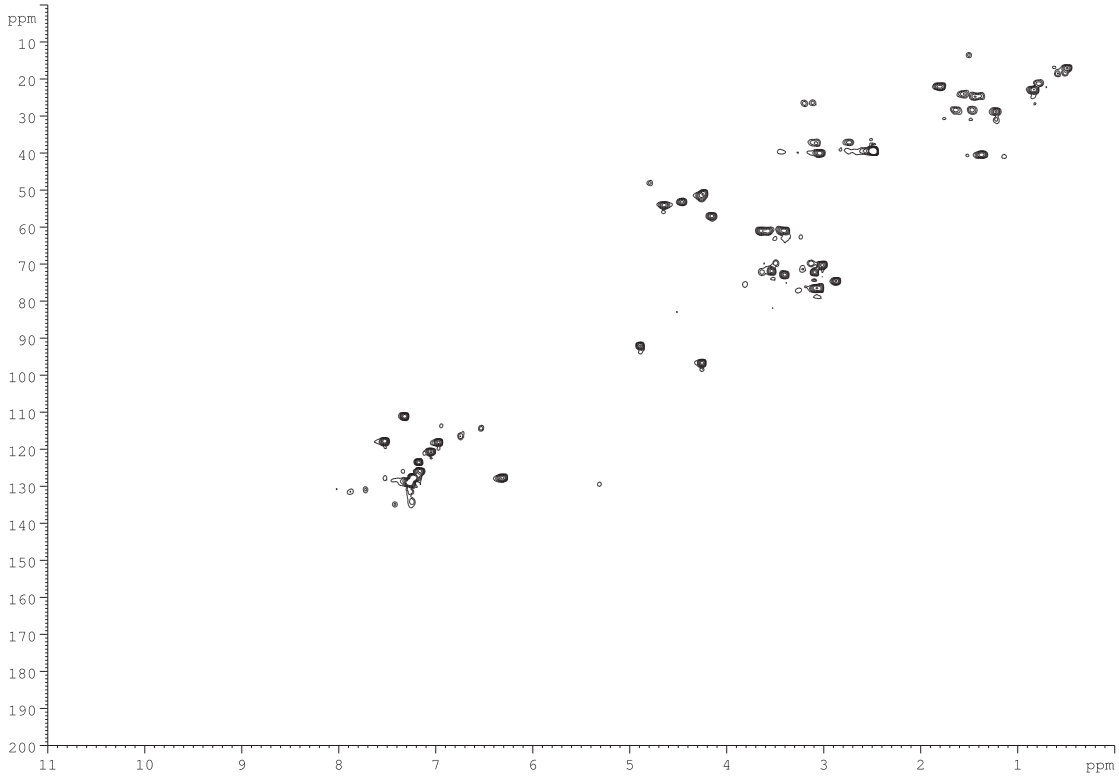

Figure S13. ^{1}H, ^{13}C HSQC spectrum of **2** in DMSO-d_6

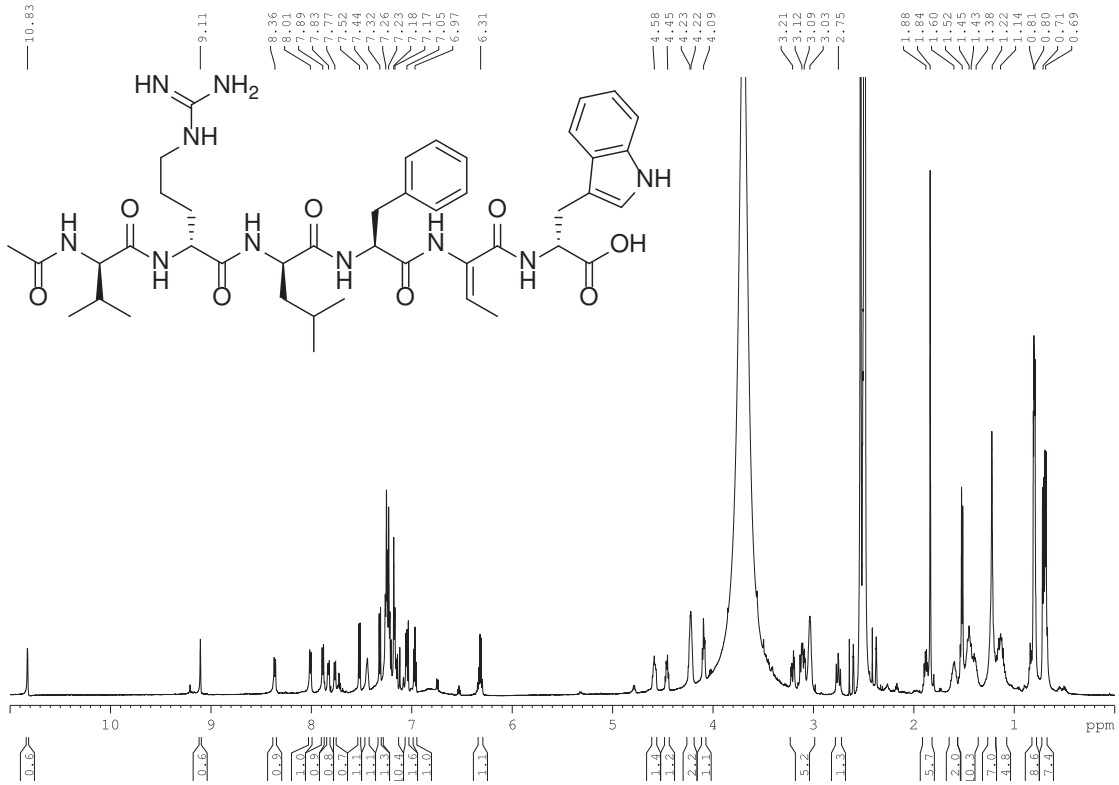

Figure S14. ^{1}H NMR spectrum of **3** in DMSO-d_6

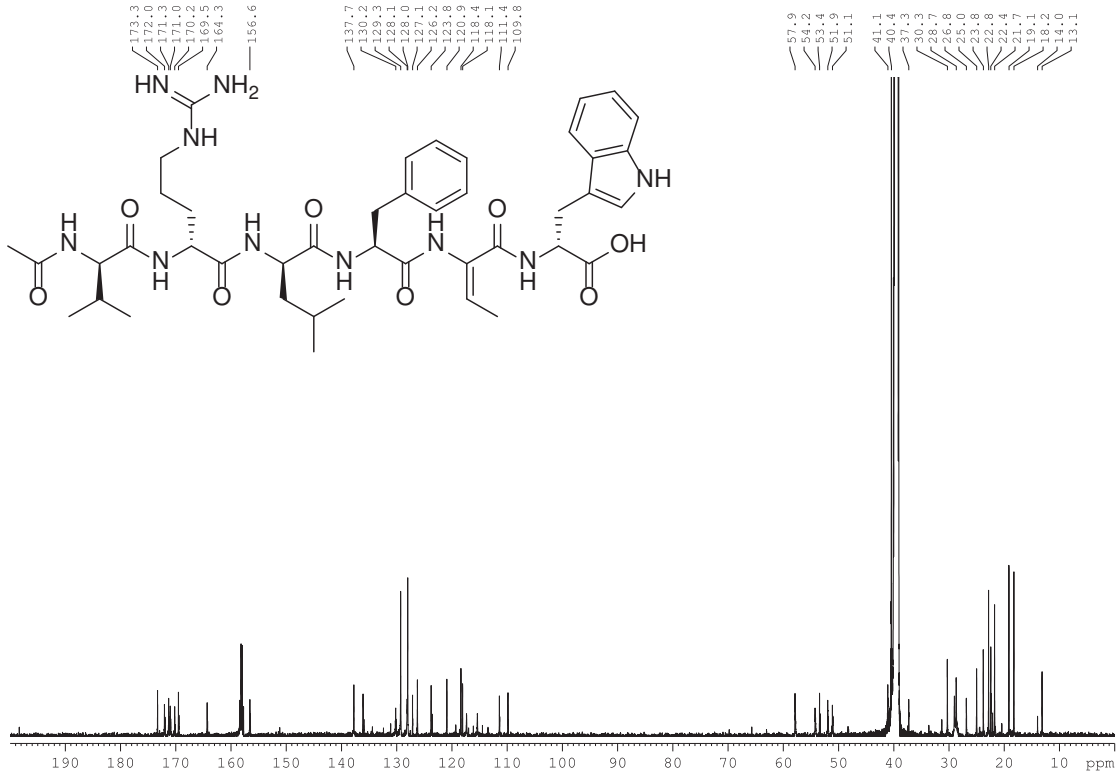

Figure S15. ^{1}H decoupled ^{13}C NMR spectrum of **3** in DMSO-d_6

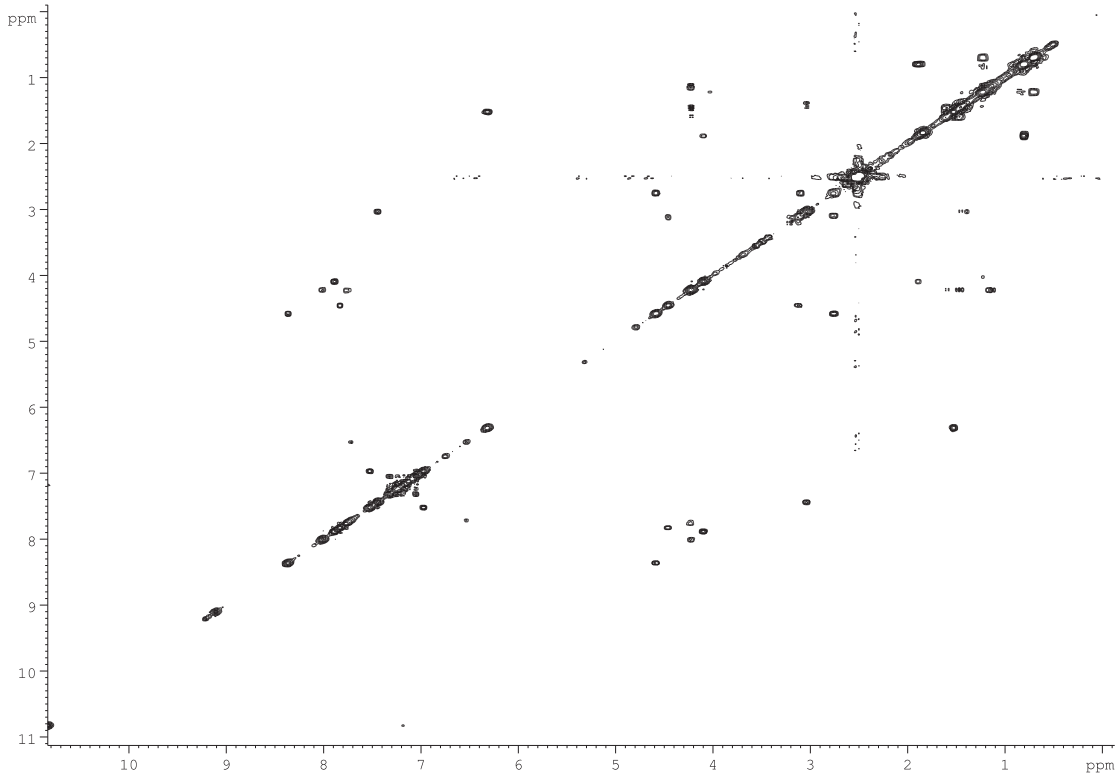

Figure S16. ^{1}H, ^{1}H COSY spectrum of **3** in DMSO-d_6

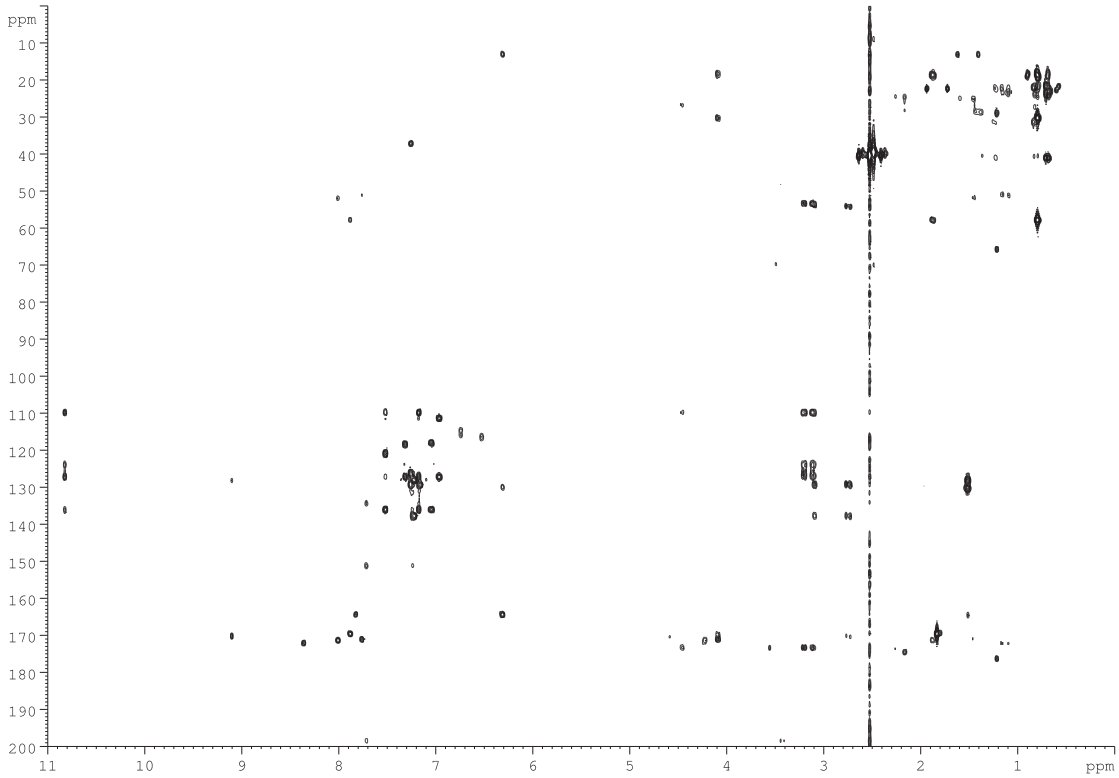

Figure S17. ^{1}H, ^{13}C HMBC spectrum of **3** in DMSO-d_6

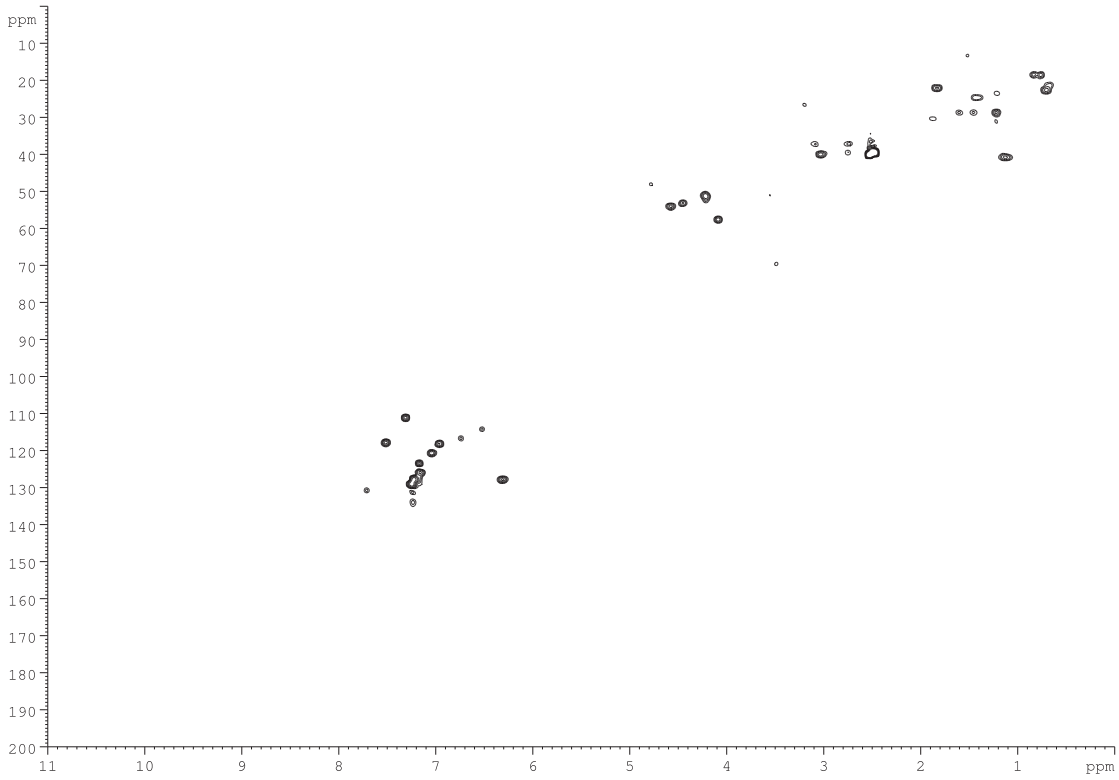

Figure S18. ^{1}H, ^{13}C HSQC spectrum of **3** in DMSO-d_6

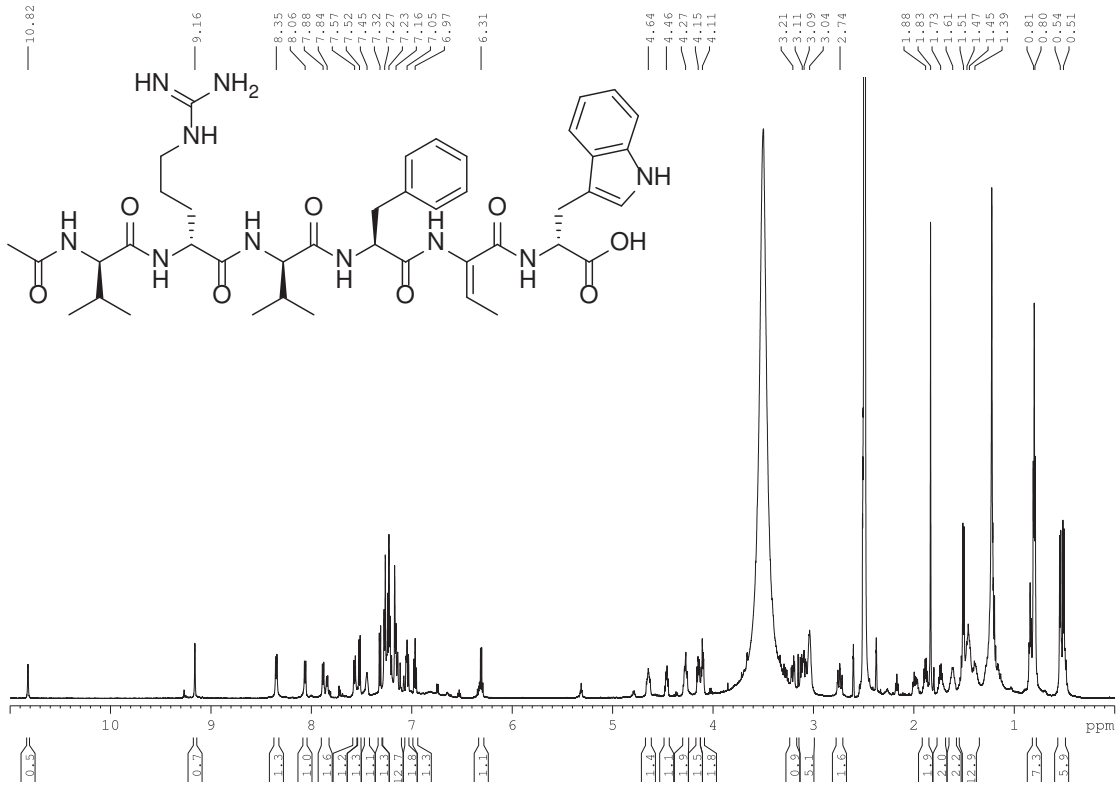

Figure S19. ^{1}H NMR spectrum of **4** in DMSO-d_6

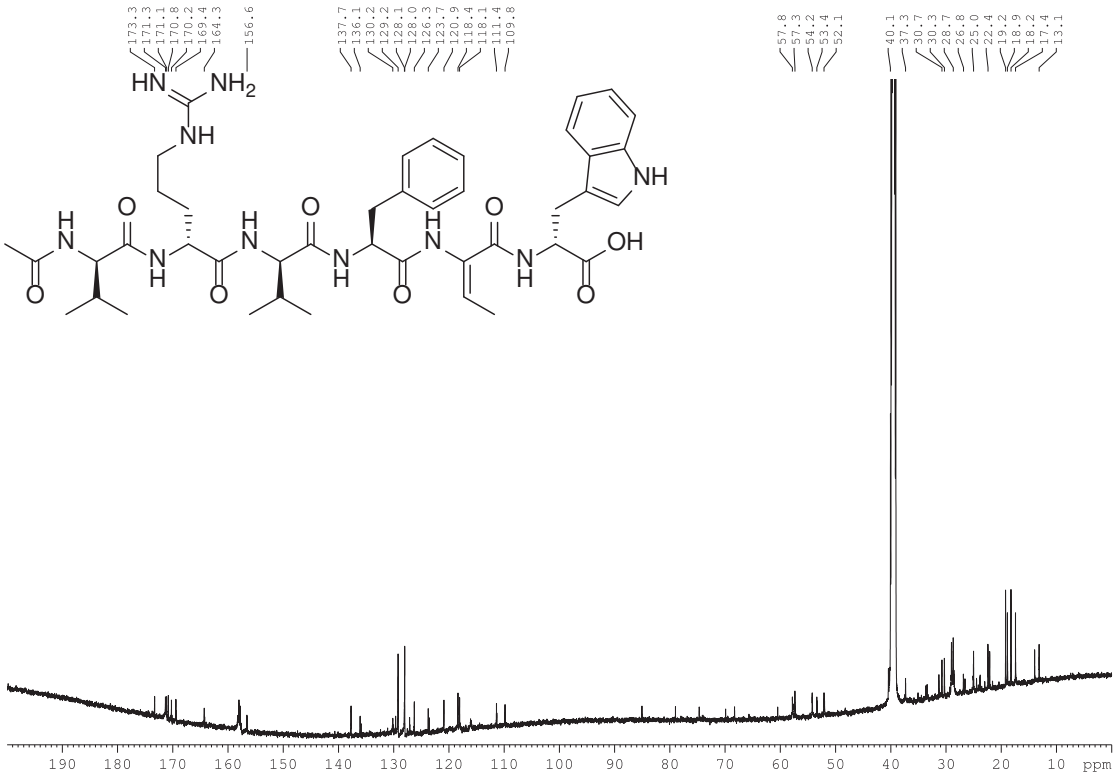

Figure S20. ^{1}H decoupled ^{13}C NMR spectrum of **4** in DMSO-d_6

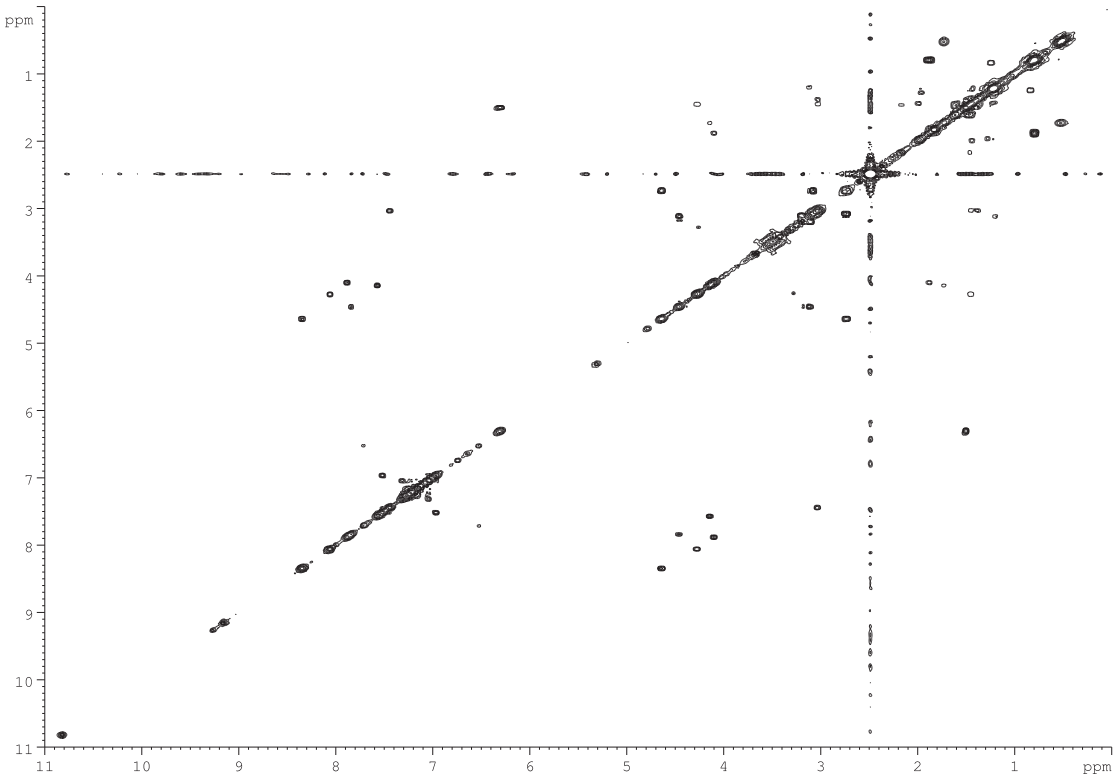

Figure S21. ^{1}H, ^{1}H COSY spectrum of **4** in DMSO-d_6

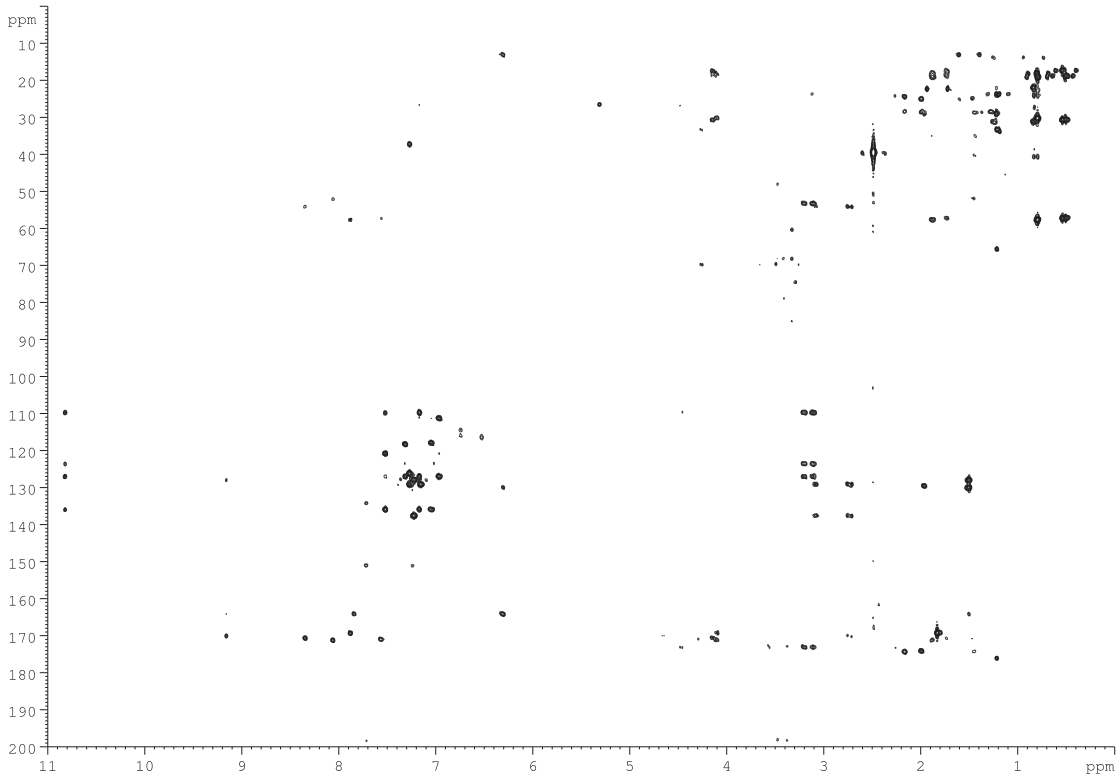

Figure S22. ^{1}H, ^{13}C HMBC spectrum of **4** in DMSO-d_6

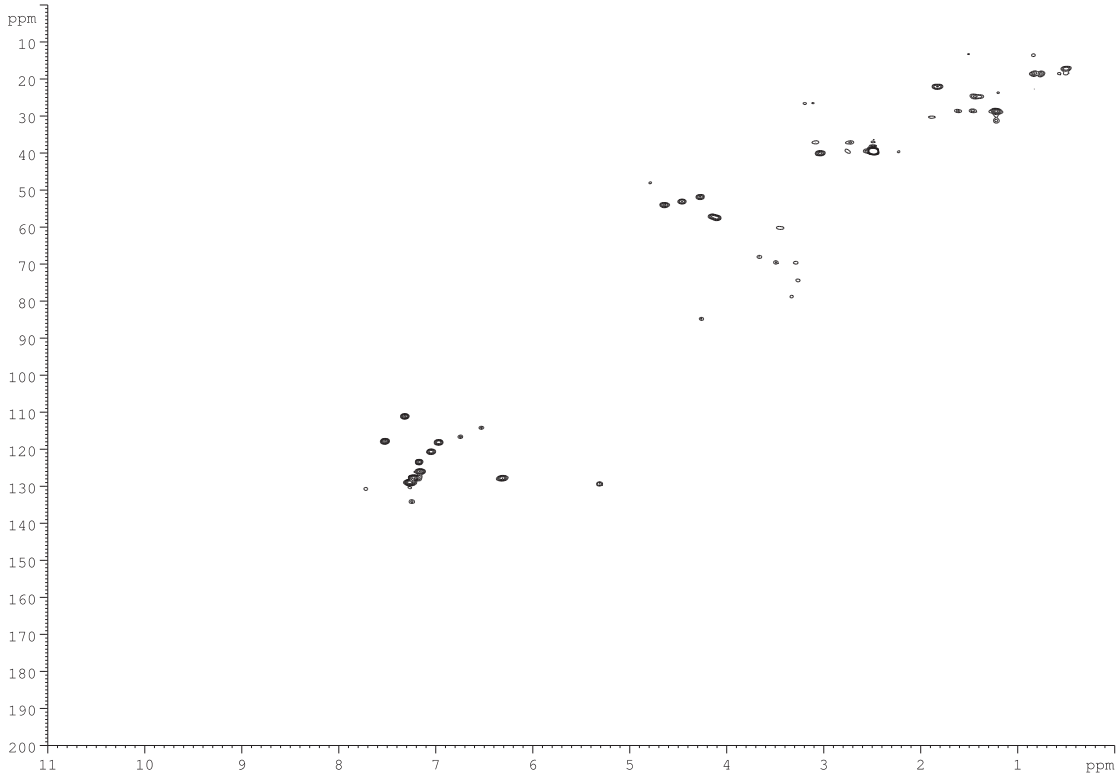

Figure S23. ^{1}H, ^{13}C HSQC spectrum of **4** in DMSO-d_6

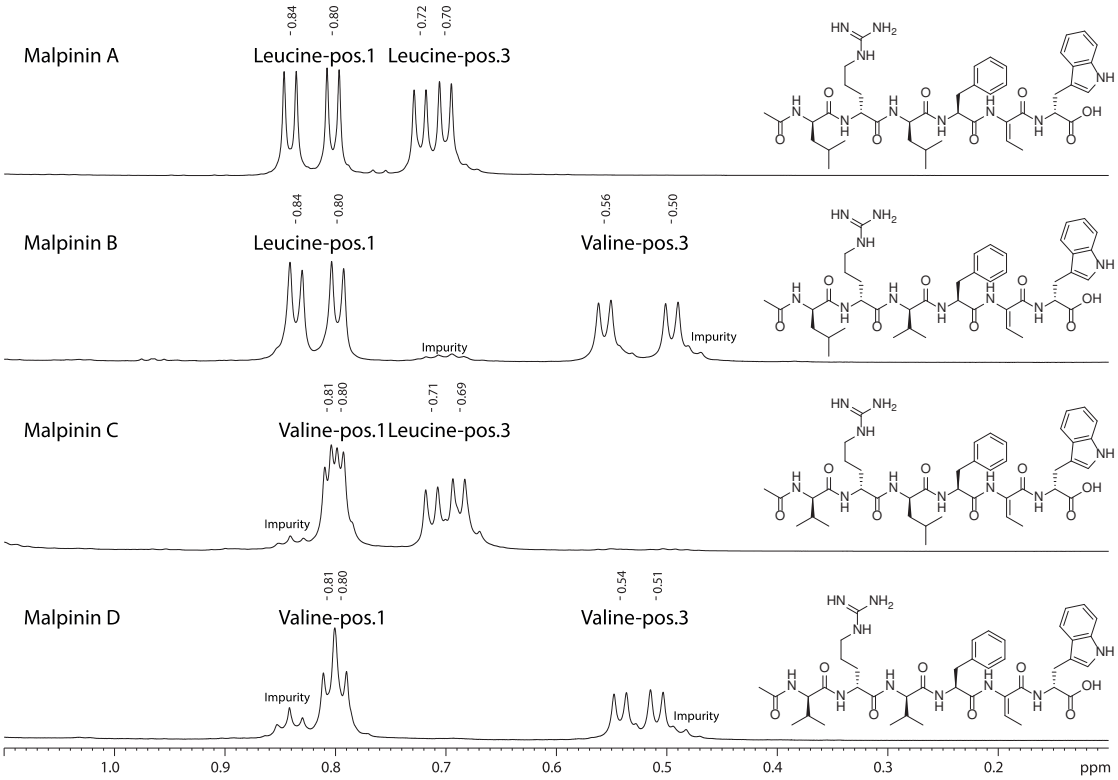

Figure S24. Upfield region of the ^{1}H NMR spectra of **1** - **4**. The chemical shift signals of the methyl moieties of valine and leucine clearly demonstrate the amino acid exchange on position 1 (δ_H(leu/val) = 0.85 - 0.75 ppm), and 3 (δ_H(leu) = 0.72 - 0.67 ppm or δ_H(val) = 0.55 - 0.49 ppm).

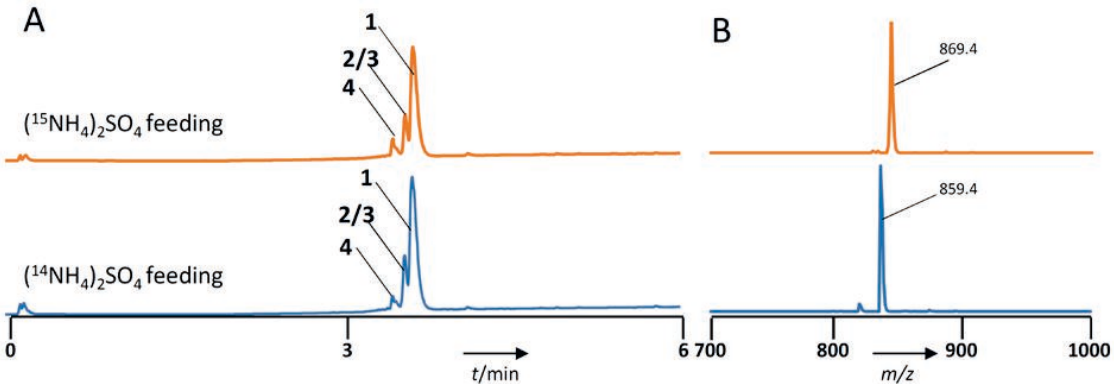

Figure S25. ^{15}N stable isotope labeling experiment. AMM cultures of *M. alpina* ATCC32222 were supplemented with 35 mM $(^{15}NH_4)_2SO_4$ (upper lane) or 35 mM $(^{14}NH_4)_2SO_4$ (lower lane, control) and incubated for 12 days at 25°C,180 RPM. Mycelium was extracted and subjected to UHPLC-MS analysis. ESI-MS was carried out in positive ionization mode $[M + H]^+$. (**A**) UHPLC profile of butanolic extracts. (**B**) Mass spectrum $[M + H]^+$ of **1** at t_R = 3.8 min. The mass shift of 10 compared to the control indicates the incorporation of 10 nitrogen atoms in **1**, supporting the presence of a guanidine group in **1.**

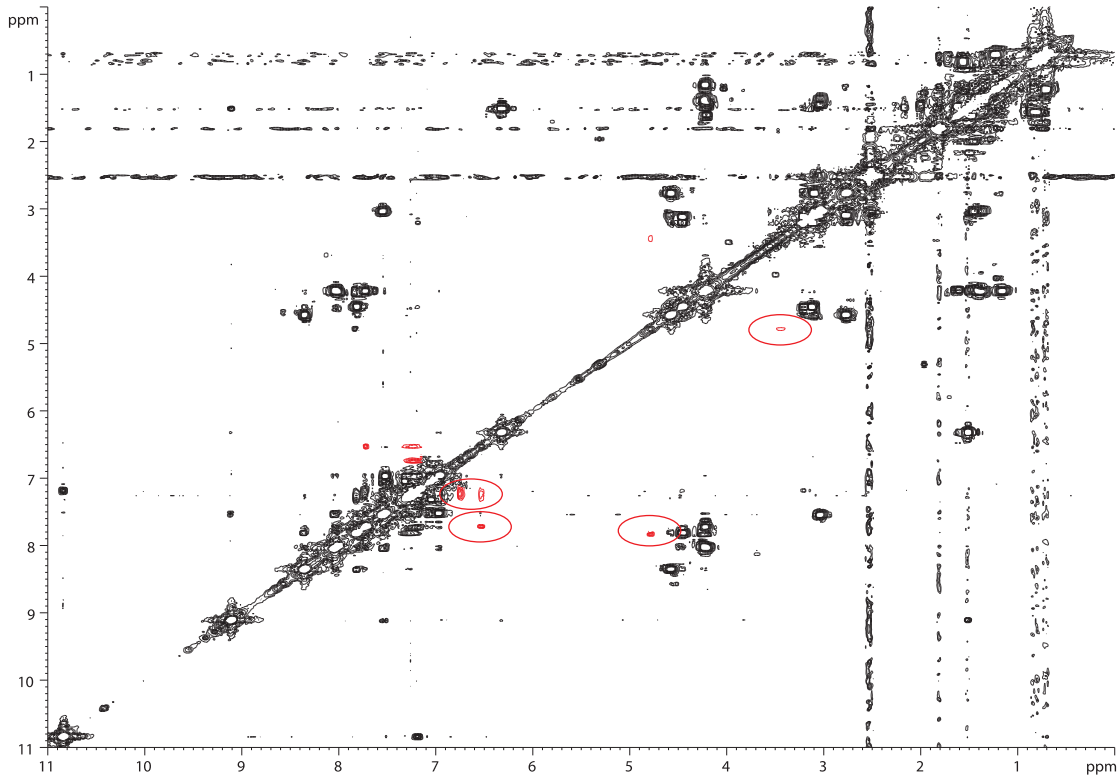

Figure S26. ^{1}H, ^{1}H COSY spectrum of **6** in DMSO-d_6

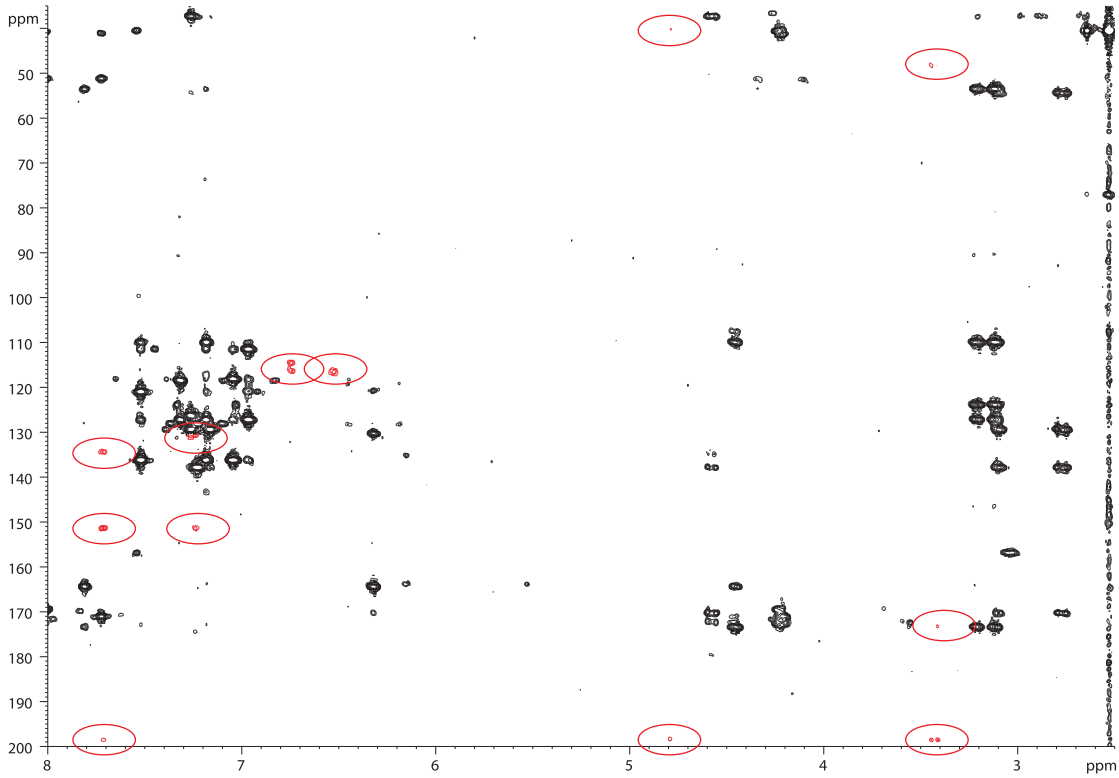

Figure S27. ^{1}H, ^{13}C HMBC spectrum of **6** in DMSO-d_6

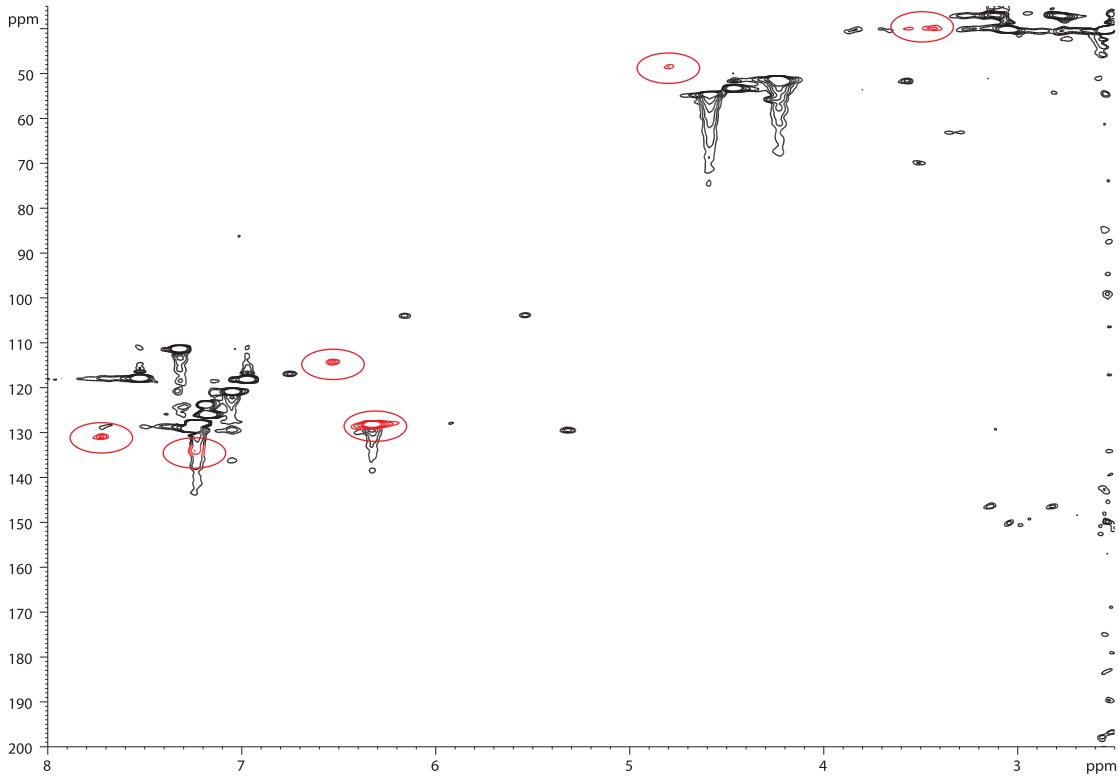

Figure S28. ^{1}H, ^{13}C HSQC spectrum of **6** in DMSO-d_6

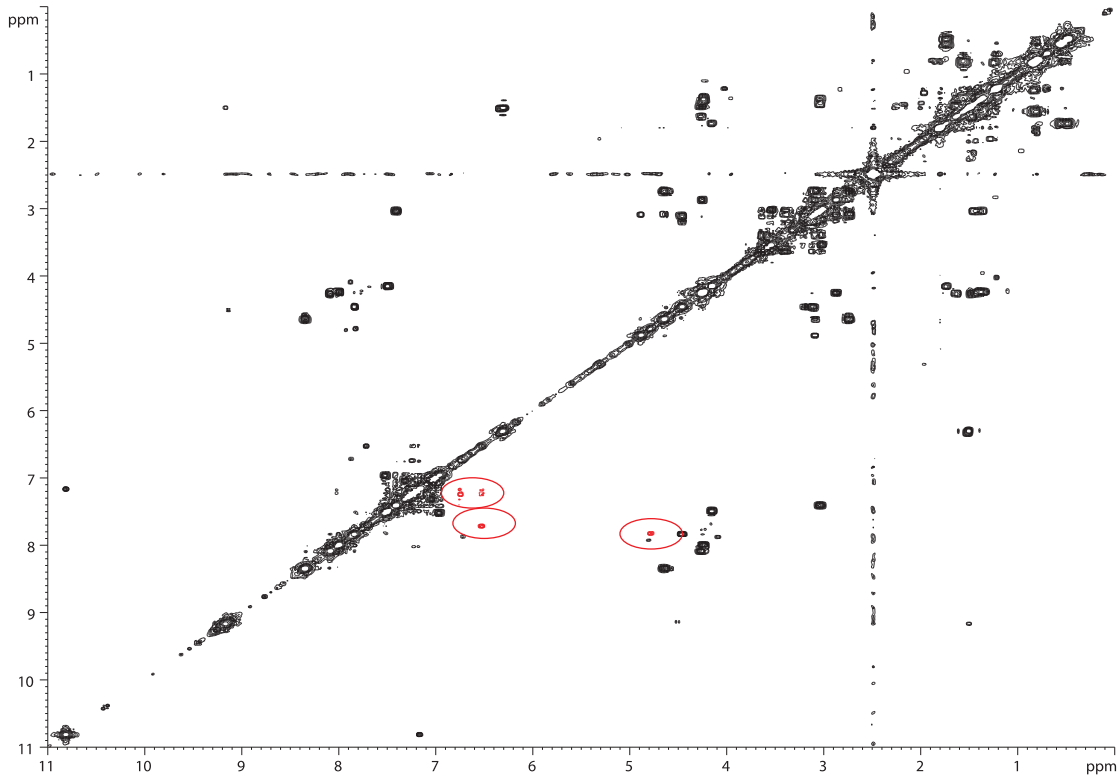

Figure S29. ^{1}H, ^{1}H COSY spectrum of **7** in DMSO-d_6

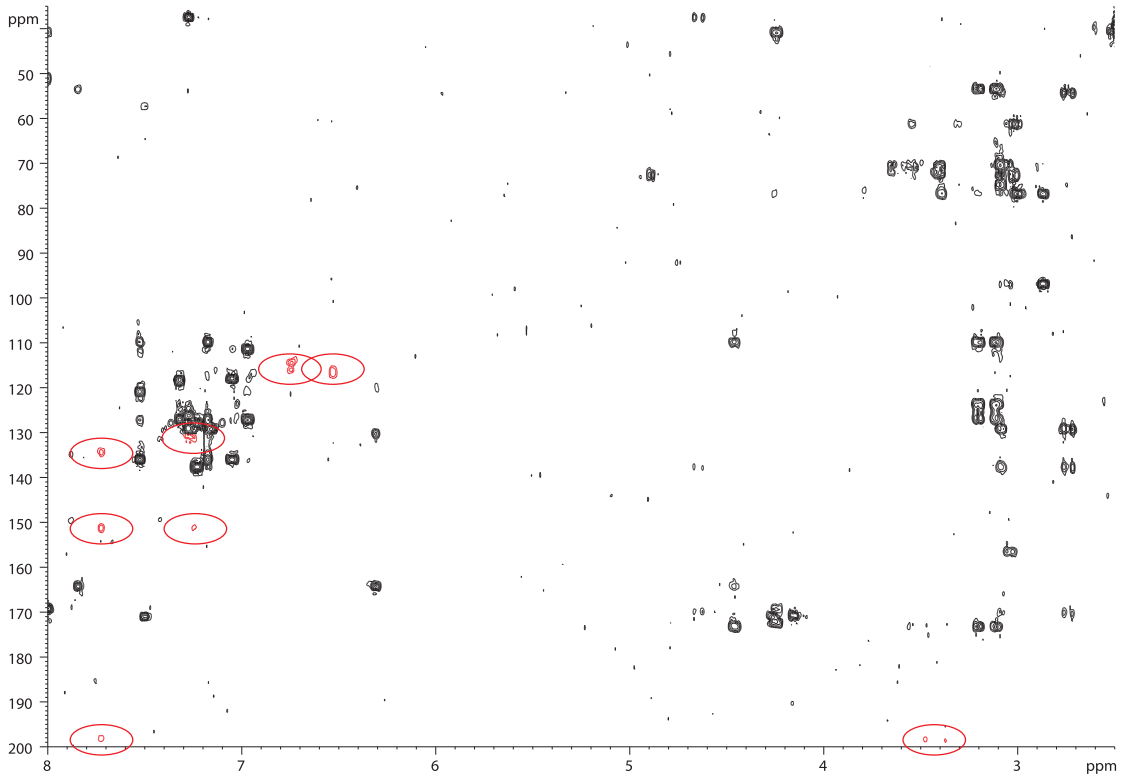

Figure S30. ^{1}H, ^{13}C HMBC spectrum of **7** in DMSO-d_6

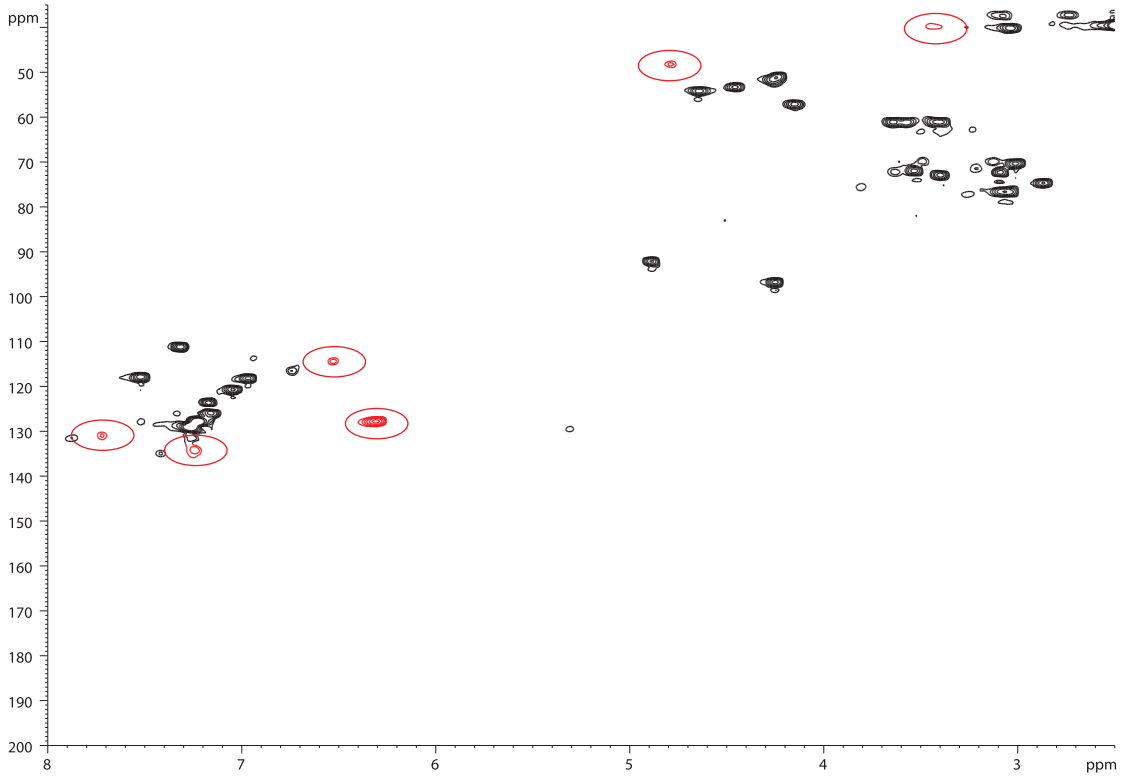

Figure S31. ^{1}H, ^{13}C HSQC spectrum of **7** in DMSO-d_6

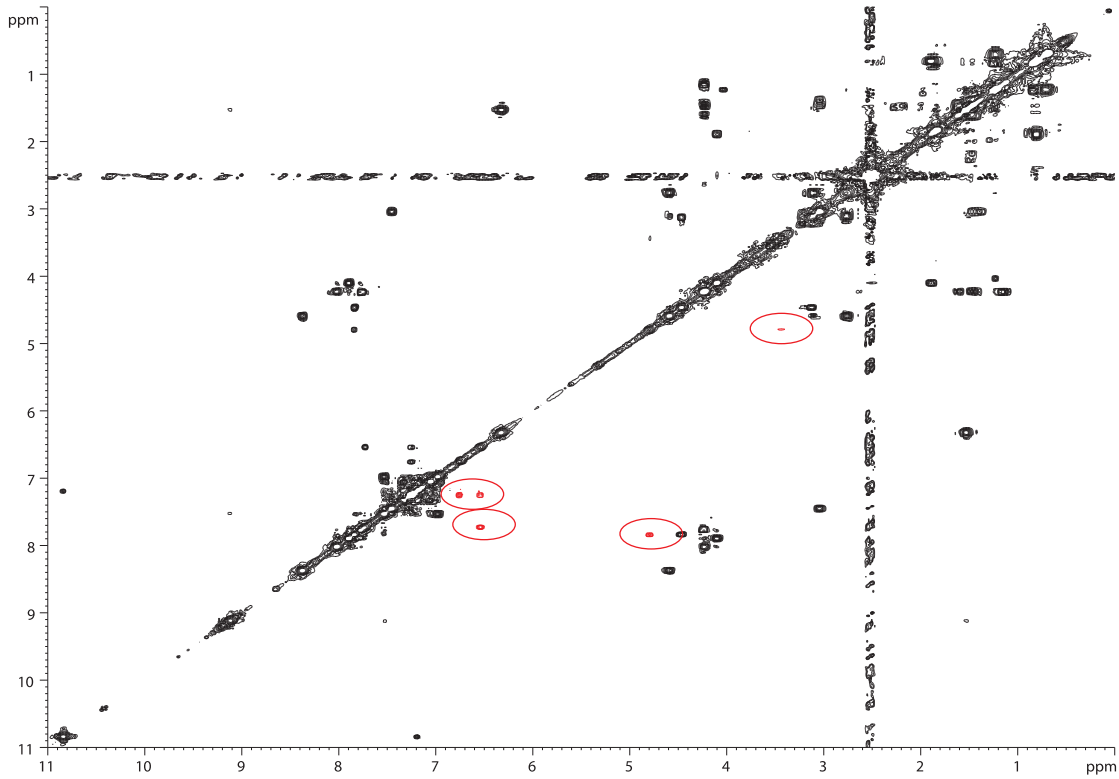

Figure S32. ^{1}H, ^{1}H COSY spectrum of **8** in DMSO-*d*6

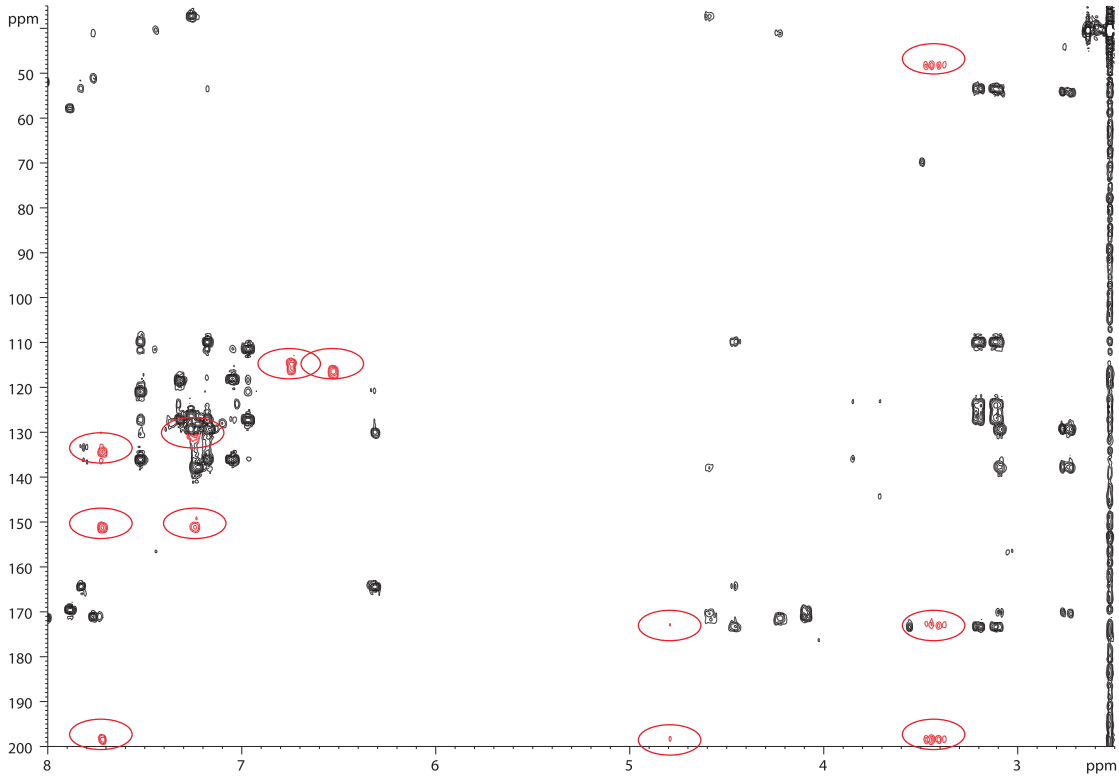

Figure S33. ^{1}H, ^{13}C HMBC spectrum of **8** in DMSO-*d*6

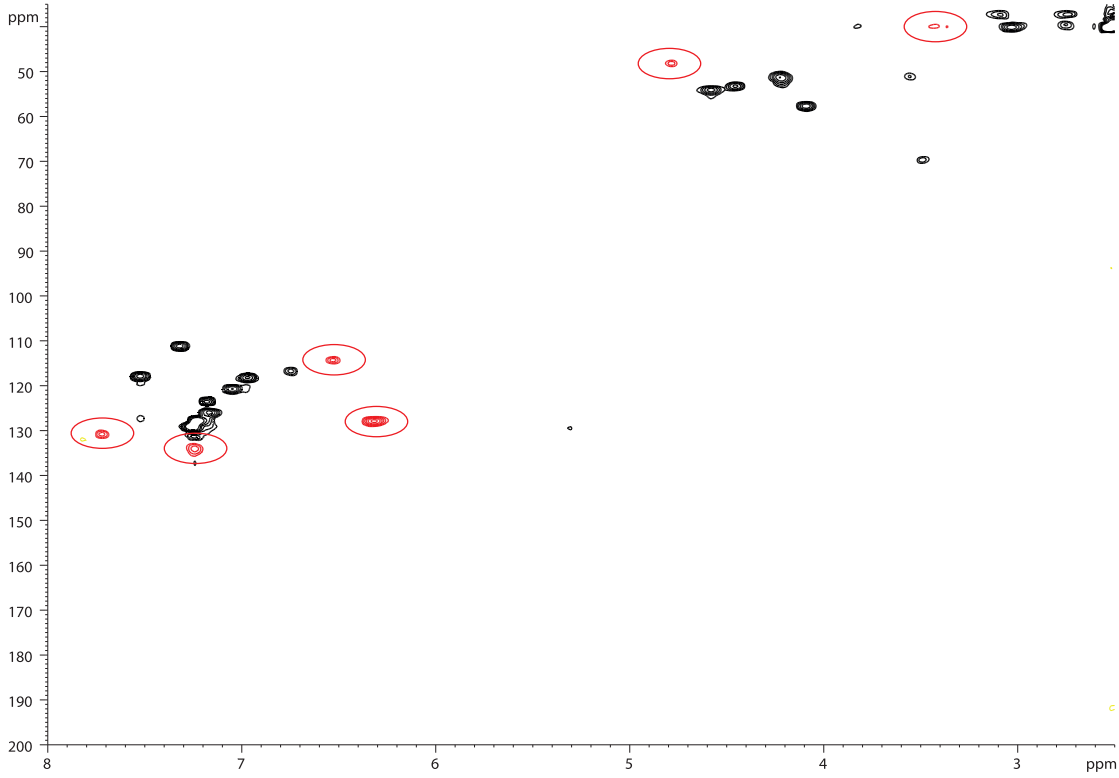

Figure S34. ^{1}H, ^{13}C HSQC spectrum of **8** in DMSO-d_6

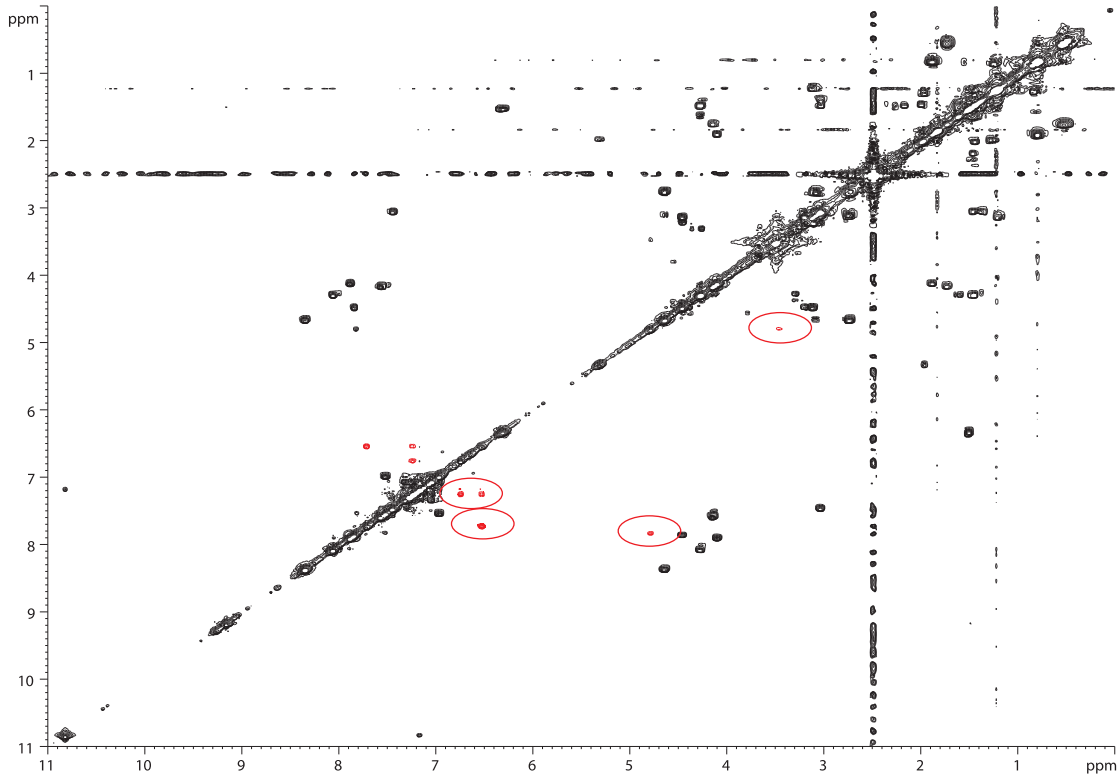

Figure S35. ^{1}H, ^{1}H COSY spectrum of **9** in DMSO-d_6

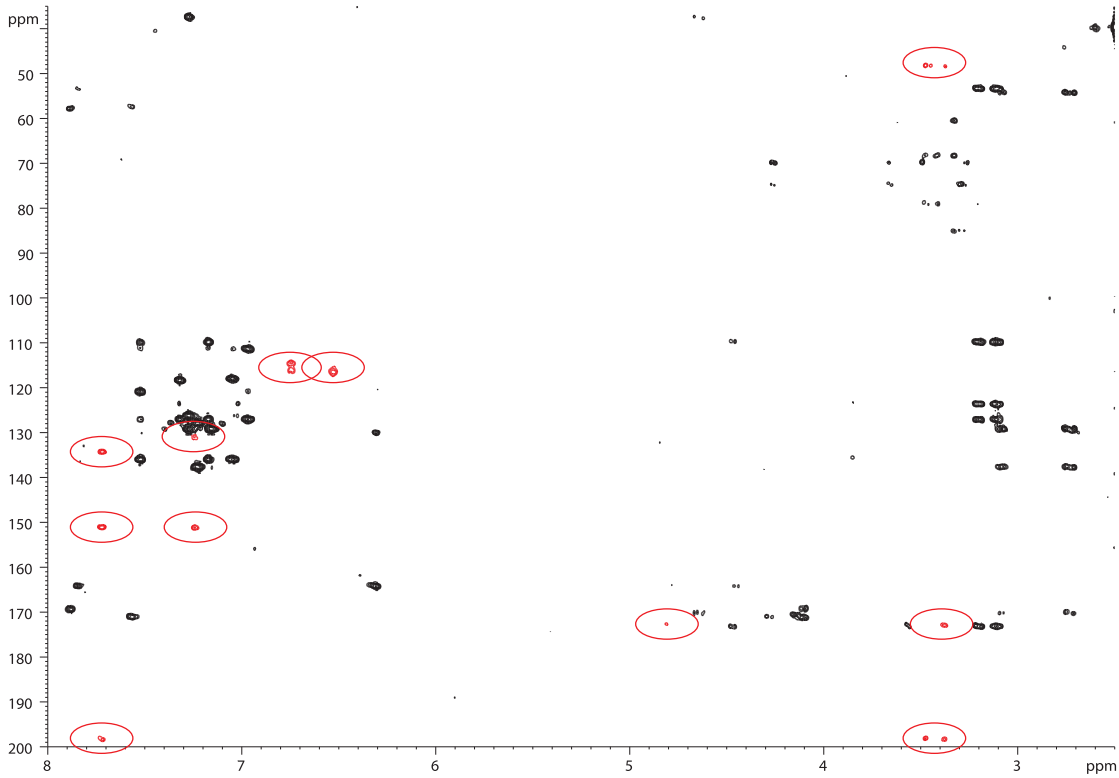

Figure S36. ^{1}H, ^{13}C HMBC spectrum of **9** in DMSO-d_6

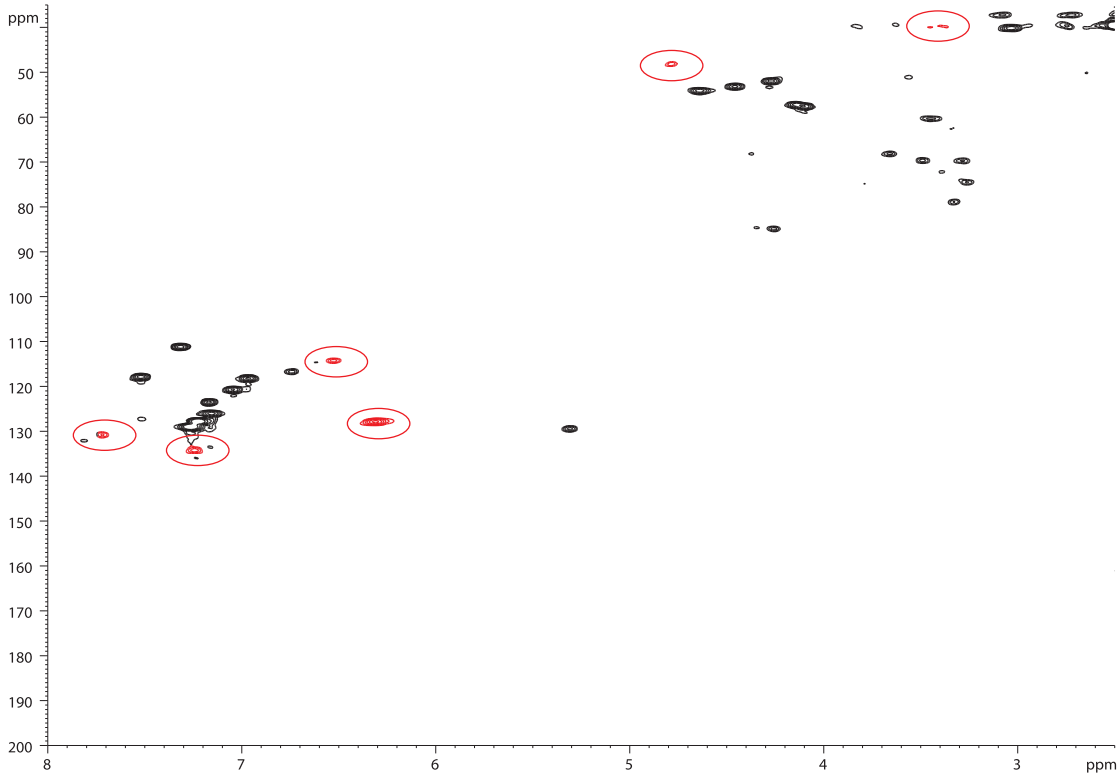

Figure S37. ^{1}H, ^{13}C HSQC spectrum of **9** in DMSO-d_6

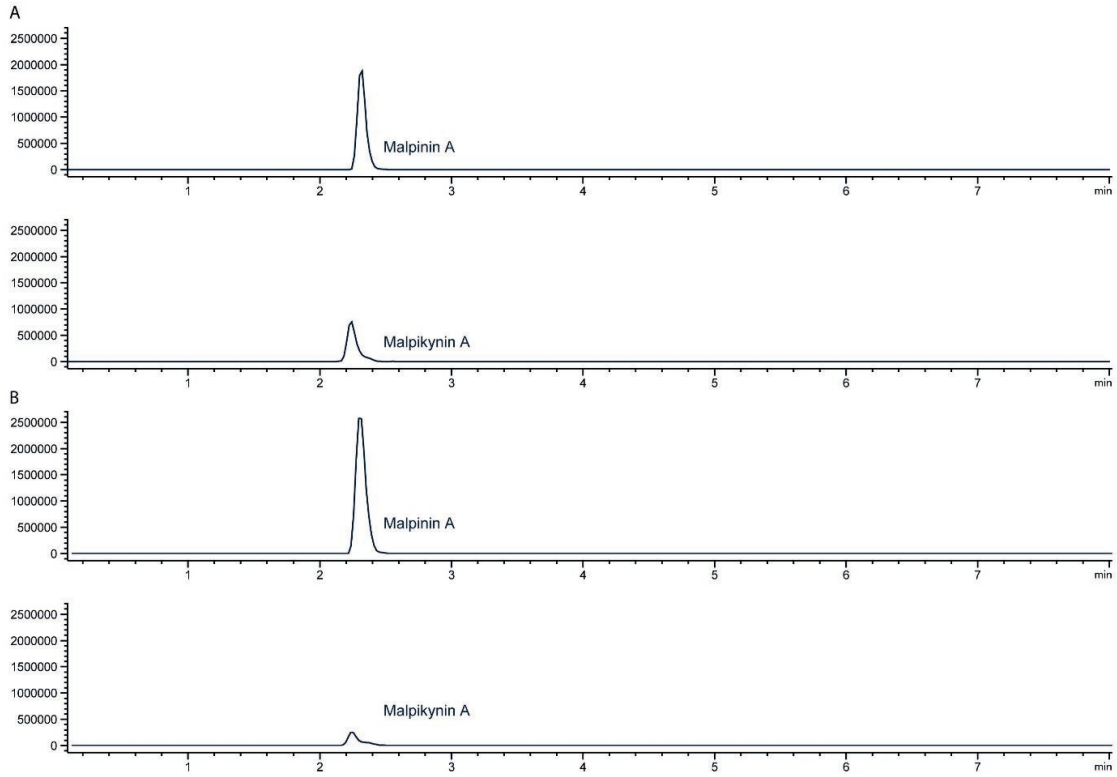

Figure S38. Oxidative conversion of malpinin A (**1**) to malpikynin (**6**). 10 µL of H_2O_2 or H_2O (control) was added to 90 µL of **1** in methanol and analyzed after 7 days of incubation at room temperature via UHPLC-MS. **A.** Relative abundance of **1** and **6** after treatment with H_2O_2. **B.** Relative abundance of **1** and **6** after treatment with H_2O (control). While the quantity of **6** increased, the amount of **1** decreased under H_2O_2-treatment.

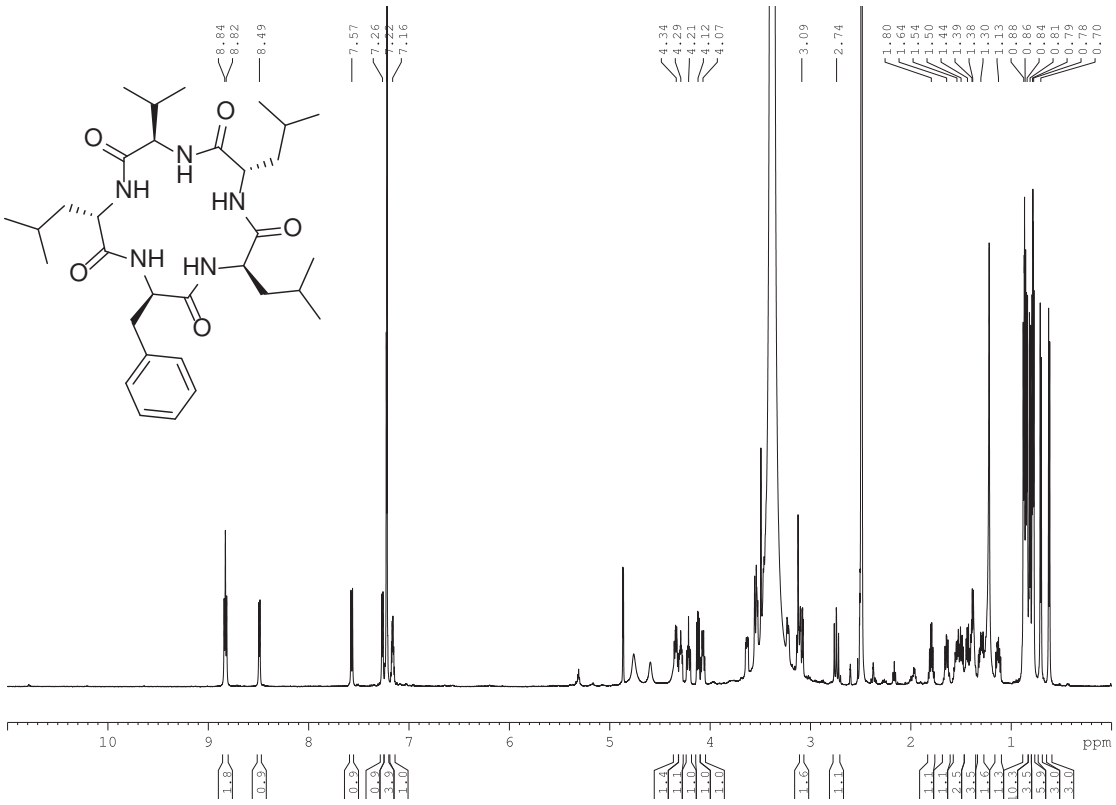

Figure S39. ^{1}H NMR- spectrum of **11** in DMSO-d_6

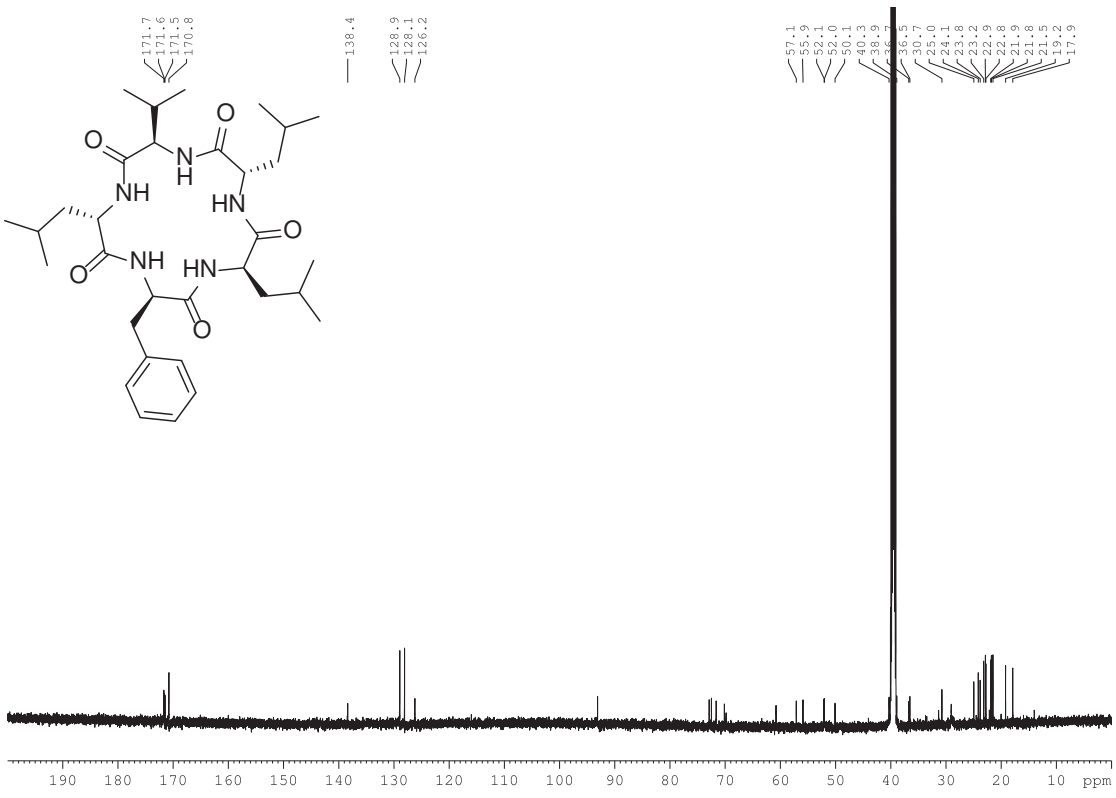

Figure S40. ^{1}H decoupled ^{13}C NMR spectrum of **11** in DMSO-d_6

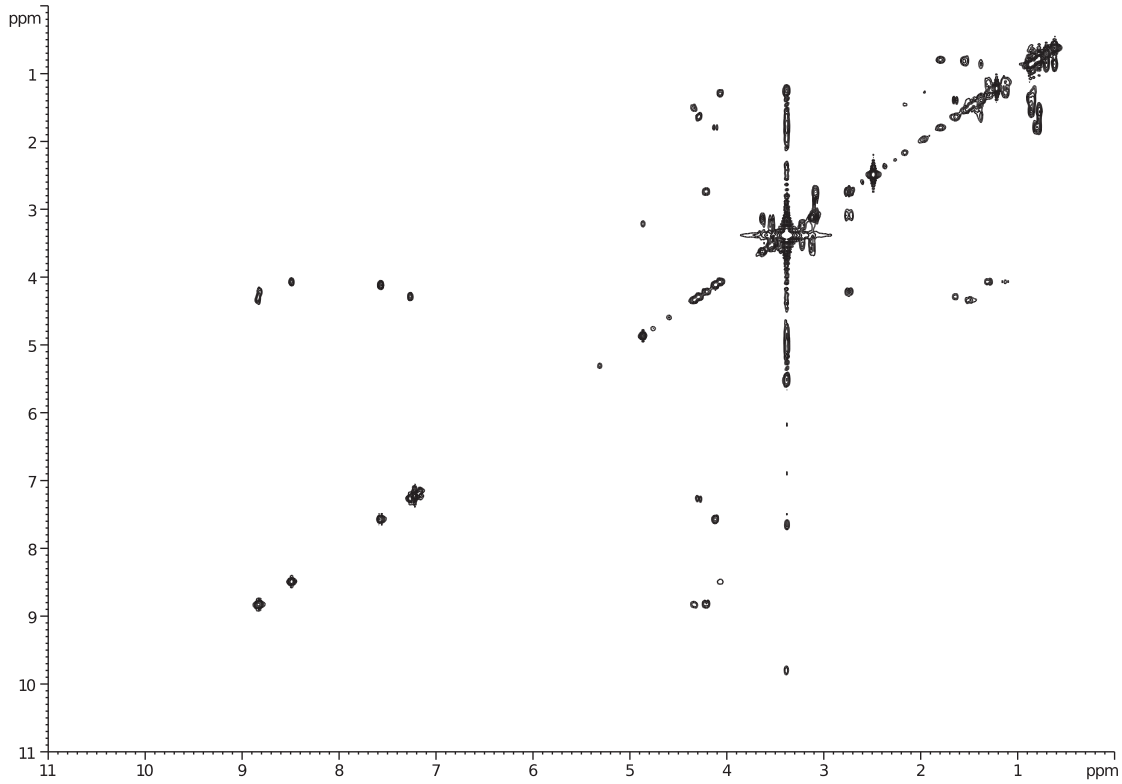

Figure S41. ^{1}H, ^{1}H COSY spectrum of **11** in DMSO-d_6

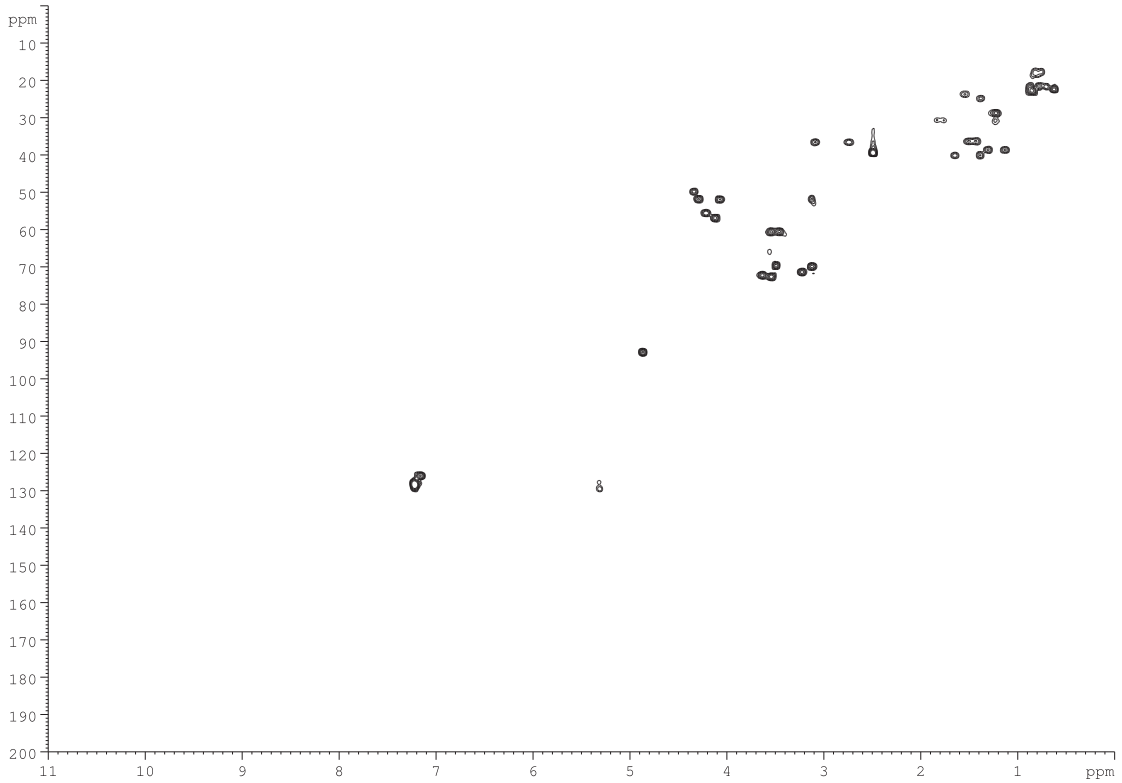

Figure S42. ^{1}H, ^{13}C HSQC spectrum of **11** in DMSO-d_6

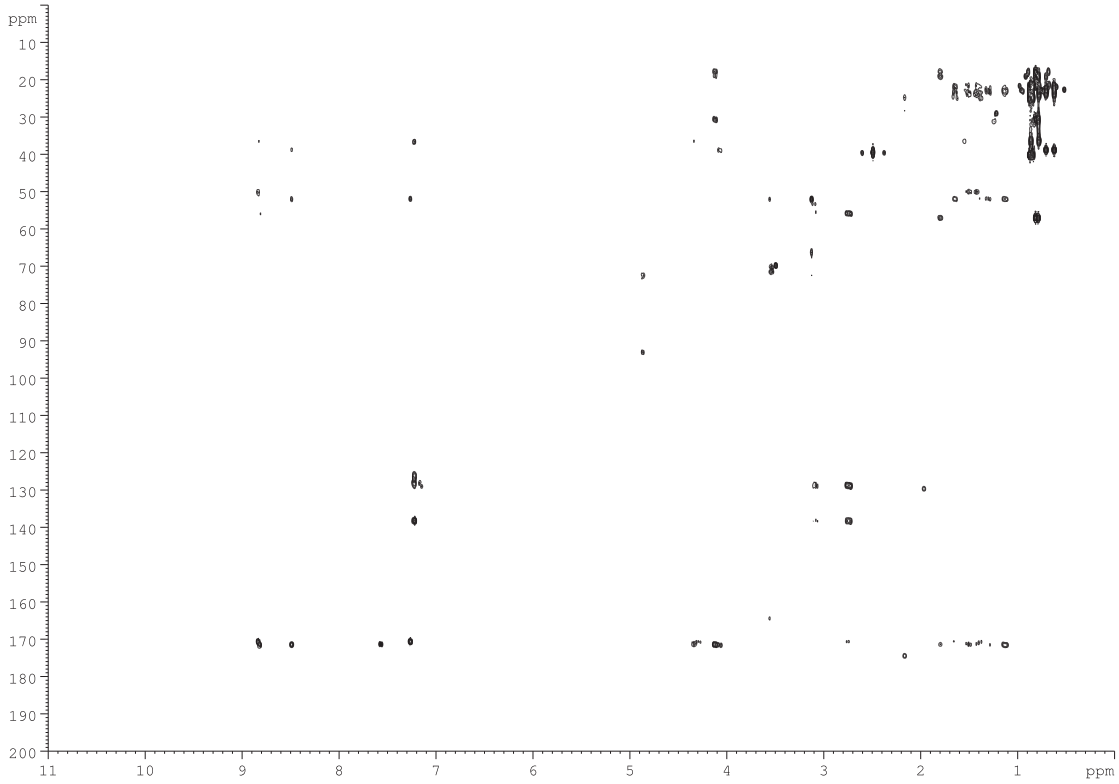

Figure S43. ^{1}H, ^{13}C HMBC spectrum of **11** in DMSO-d_6

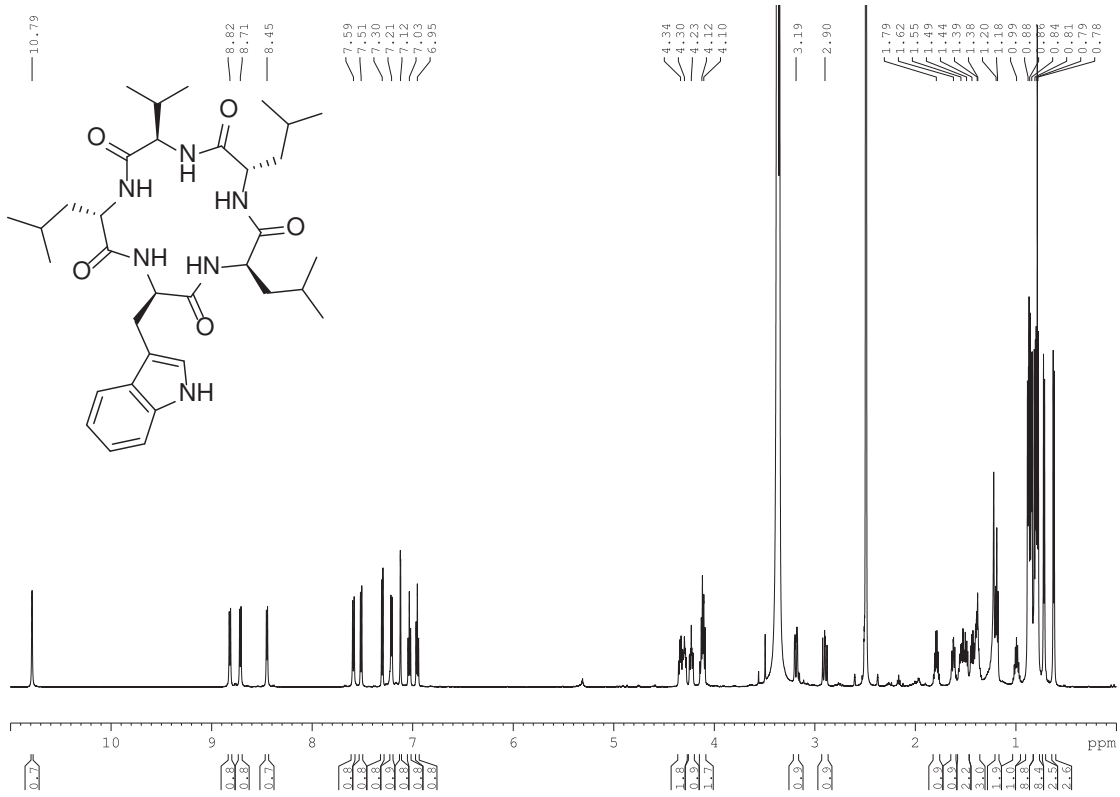

Figure S44. ^{1}H NMR- spectrum of **12** in DMSO-d_6

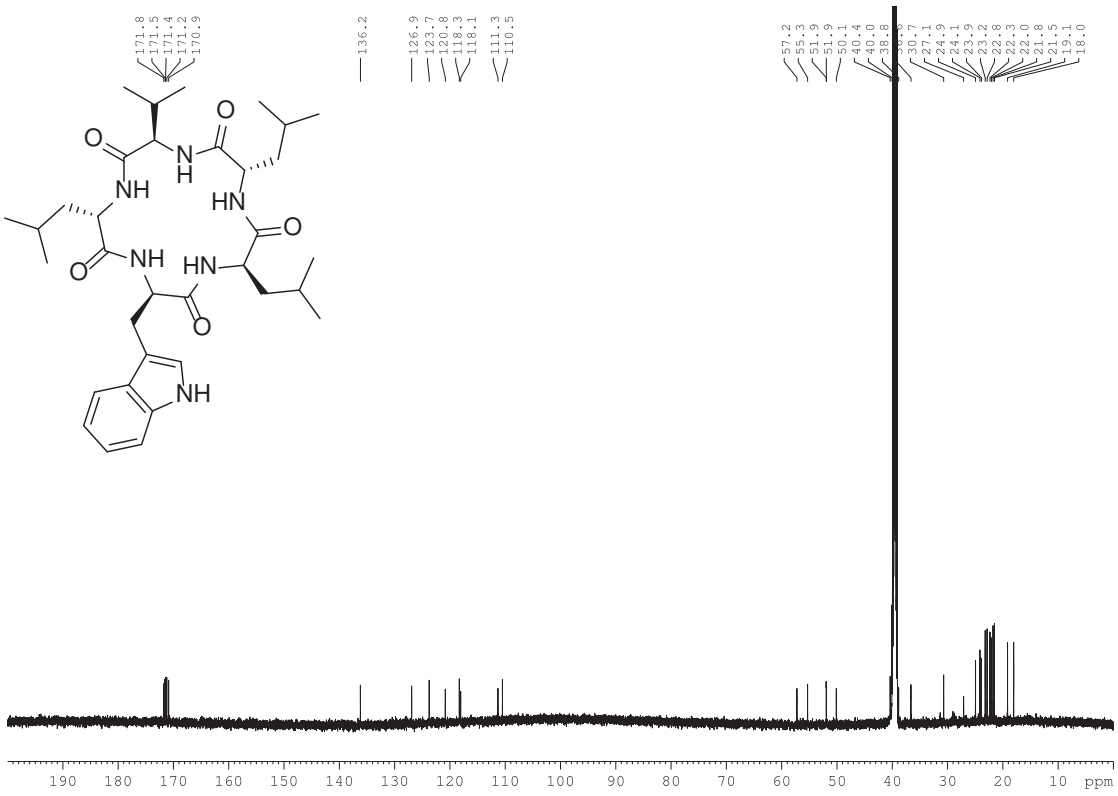

Figure S45. ^{1}H decoupled ^{13}C NMR spectrum of **12** in DMSO-d_6

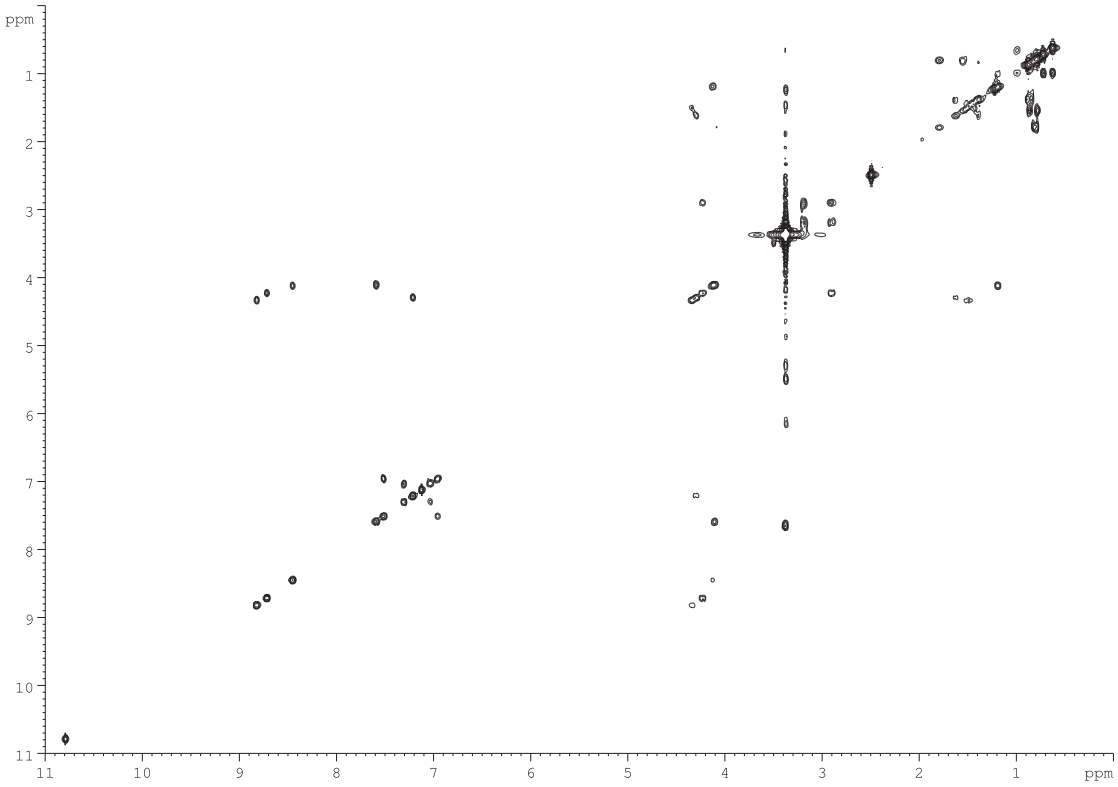

Figure S46. ^{1}H, ^{1}H COSY spectrum of **12** in DMSO-d_6

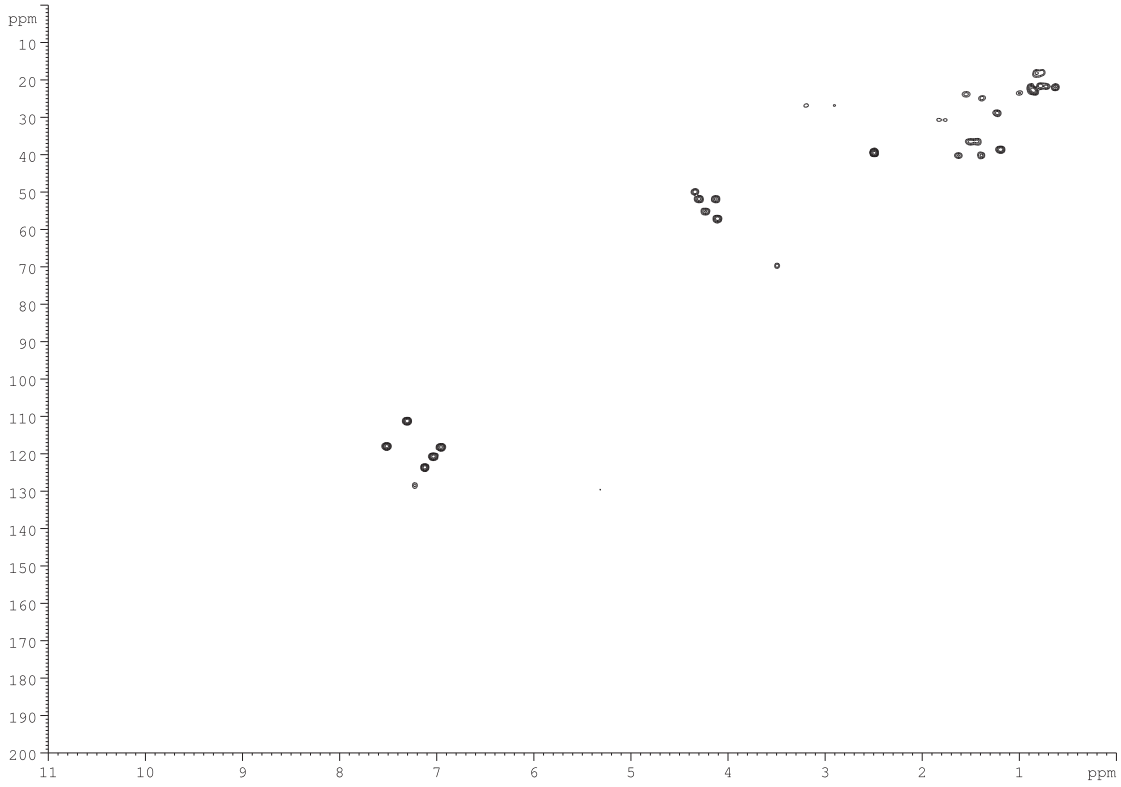

Figure S47. ^{1}H, ^{13}C HSQC spectrum of **12** in DMSO-d_6

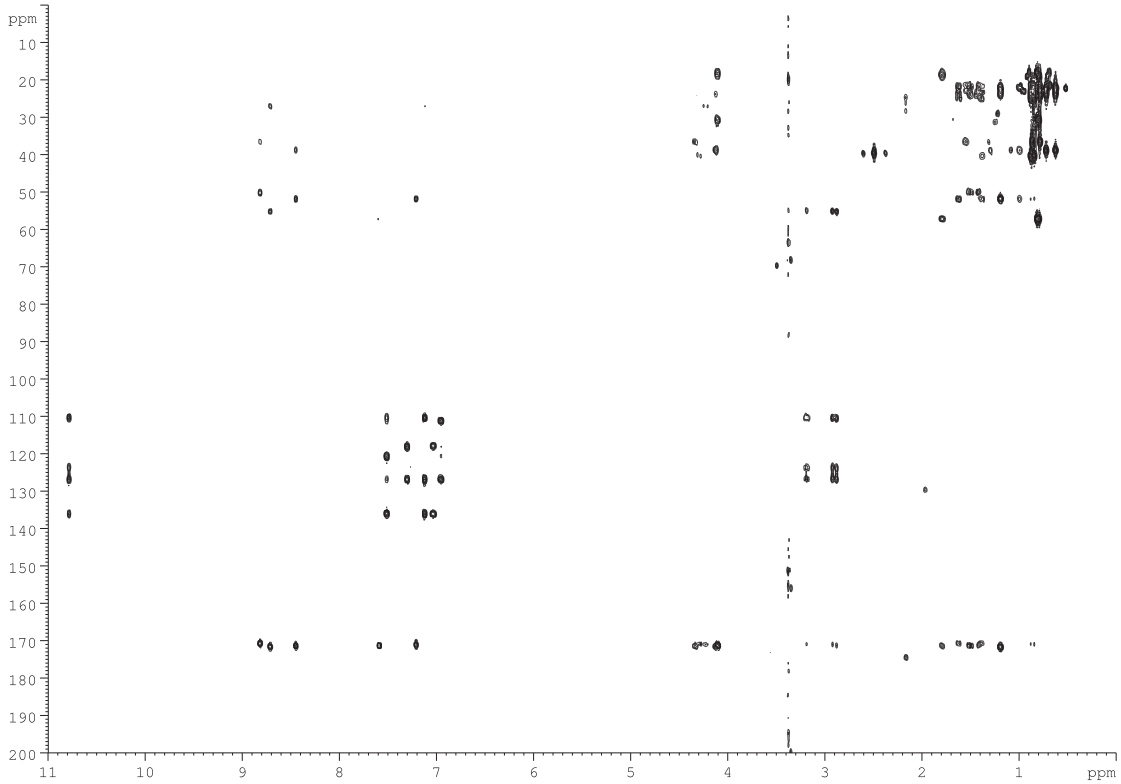

Figure S48. ^{1}H, ^{13}C HMBC spectrum of **12** in DMSO-d_6

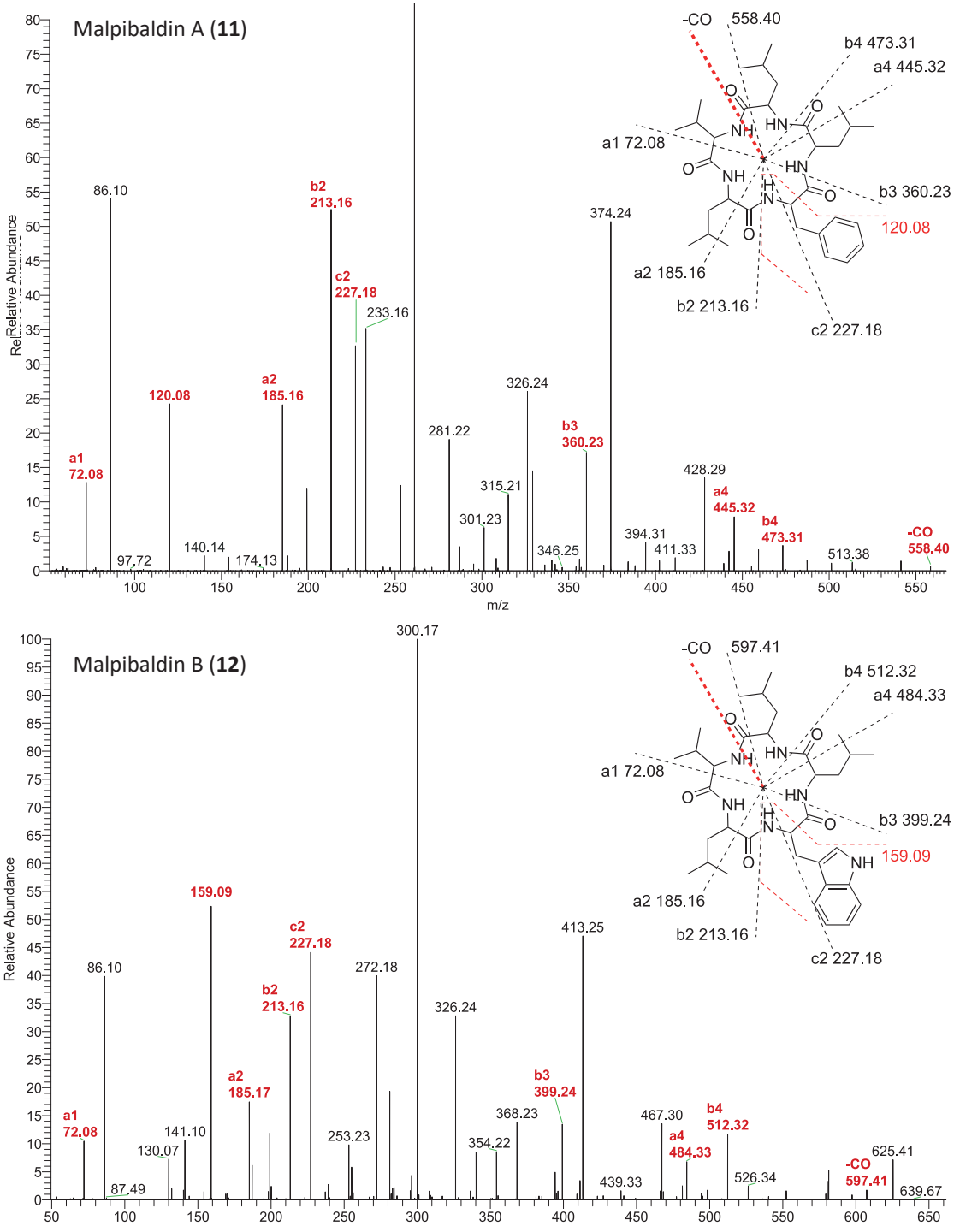

Figure S49. ESI-MS-MS-data of **11** and **12** with most likely ion fragments of the proposed structures.

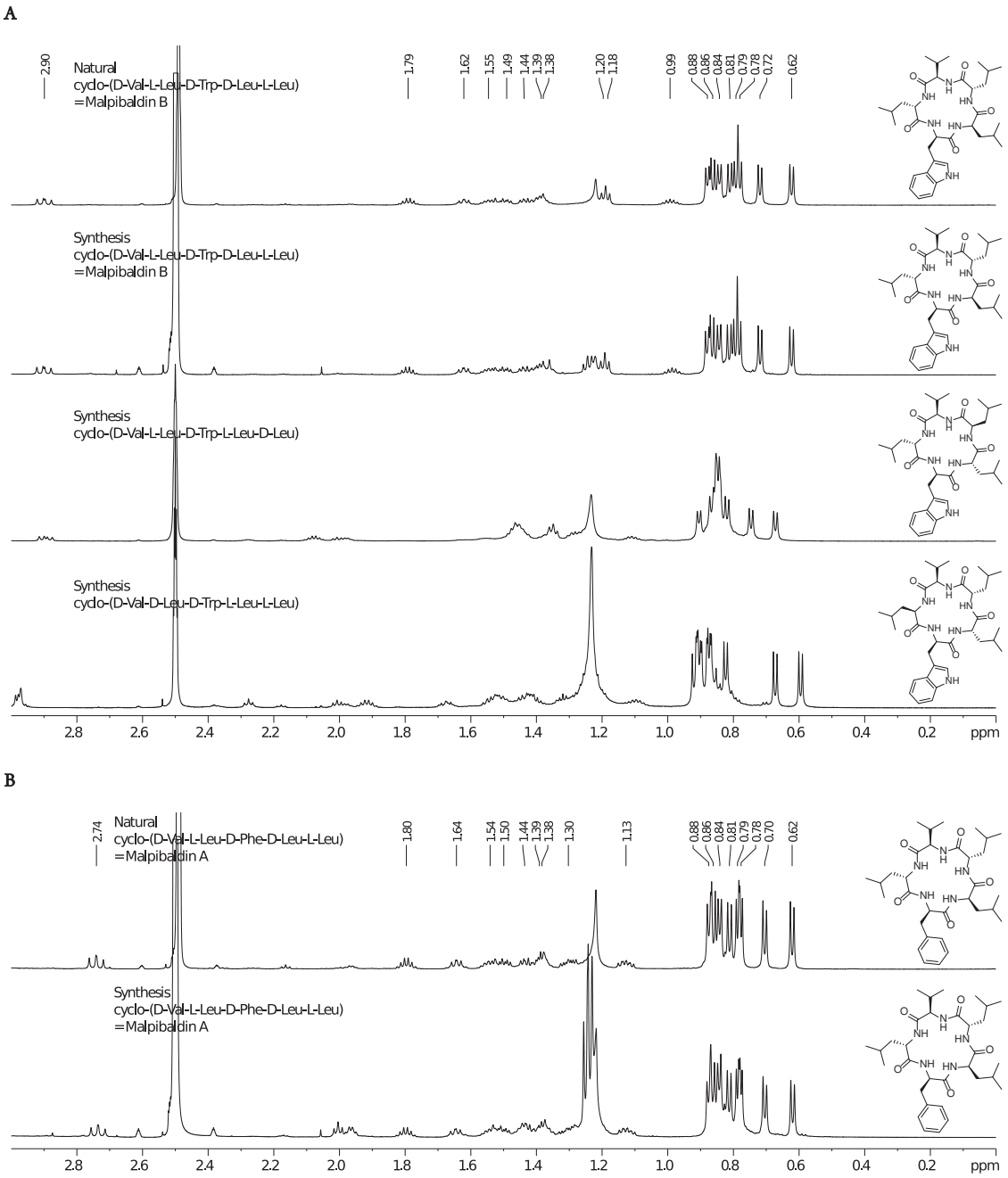

Figure S50. Comparison of ^{1}H NMR spectra of synthetic stereoisomers of **11** and **12**. (**A**) Comparison of three synthetic stereoisomers of **12** with permutated L- and D-configured leucine moieties. (**B**) Comparison of the natural and synthetic **11**. The configuration determines the chemical shifts and coupling constants of the methyl groups of the leucine moieties (Tab. S5).

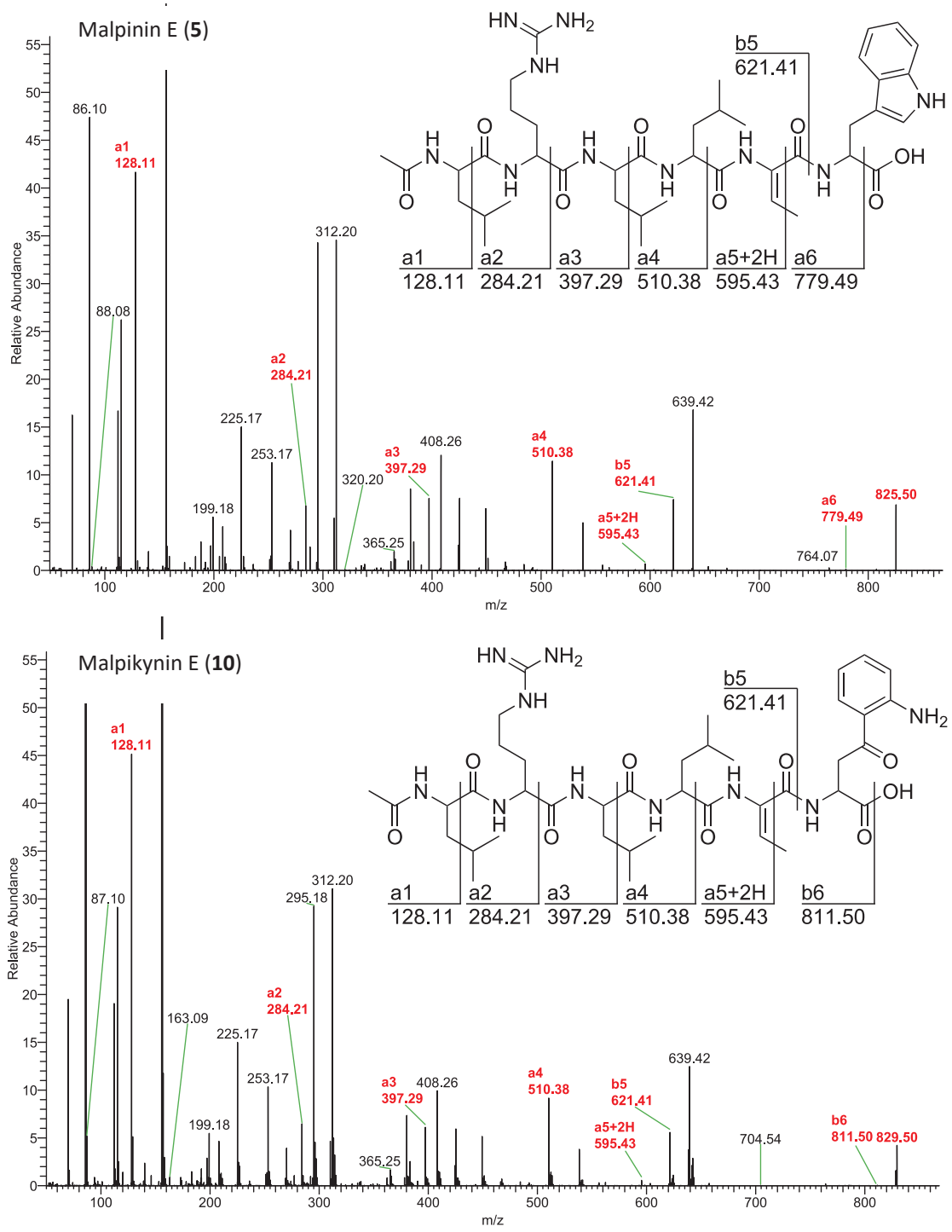

Figure S51. ESI-MS-MS-data of **5** and **10** with most likely ion fragments of the proposed structures.

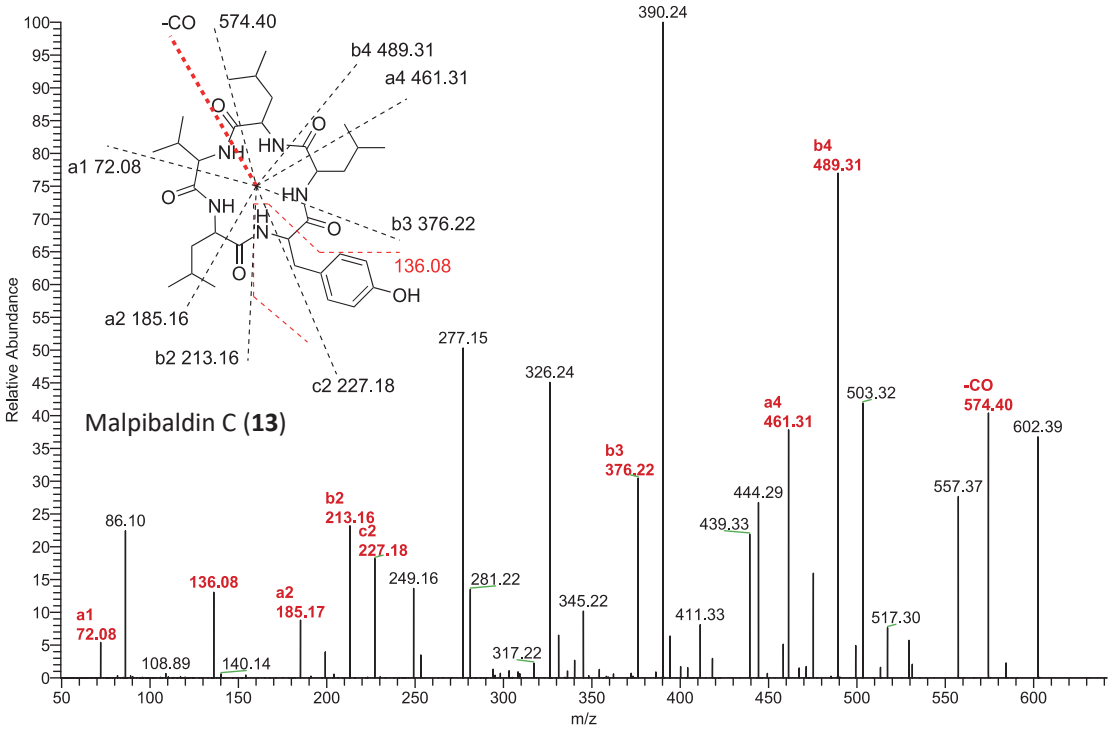

Figure S52. ESI-MS-MS-data of **13** with most likely ion fragments of the proposed structures.

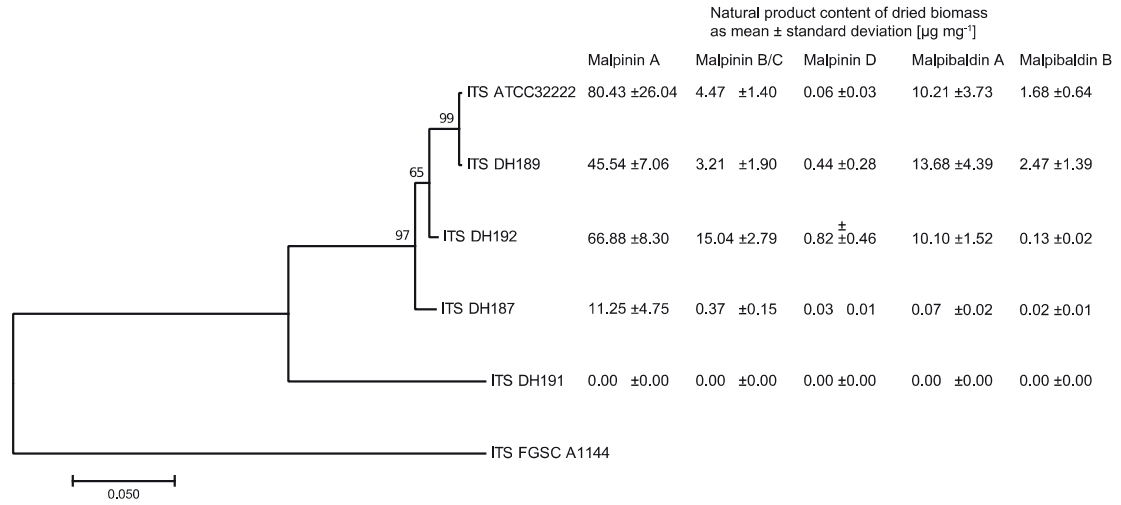

Figure S53. Phylogenetic analysis and metabolite production in *M. alpina* strains ATCC32222, DH187, DH189, DH192 and *M. cystojenkinii* strain DH191. (**A**) The phylogenetic analysis based on the internal transcribed spacer (ITS) sequence was inferred by using the Maximum Likelihood method based on the Tamura-Nei model.[9] The percentage of trees in which the associated taxa clustered together is shown next to the branches (bootstrap values). Initial tree(s) for the heuristic search were obtained automatically by applying Neighbor-Join and BioNJ algorithms to a matrix of pairwise distances estimated using the Maximum Composite Likelihood (MCL) approach, and then selecting the topology with superior log likelihood value. The tree is drawn to scale, with branch lengths measured in the number of substitutions per site. Evolutionary analyses were conducted in MEGA7.[2] The ITS sequence of the ascomycete *Aspergillus niger* FGSC A1144 served as outgroup. (**B**) Production of malpinins and malpibaldins in *Mortierella alpina* strains were calculated as µg metabolite per mg fungal dry weight according to a metabolite calibration standard.

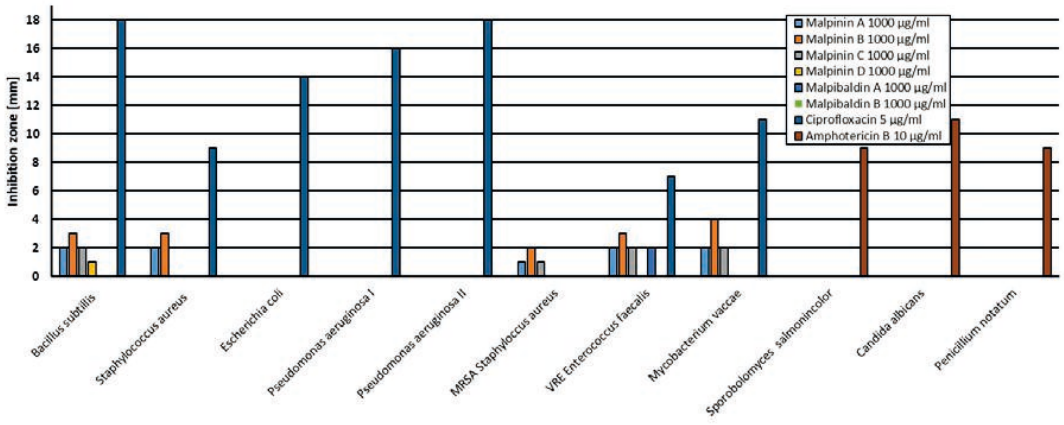

Figure S54. Antimicrobial activity of **1 - 4** and **11** – **12.** Apart from a slight inhibition of Gram-positive bacteria in the case of malpinins, none of the metabolites show severe antimicrobial activity. Ciprofloxacin and amphotericin B served as antibacterial and antifungal positive controls, respectively.

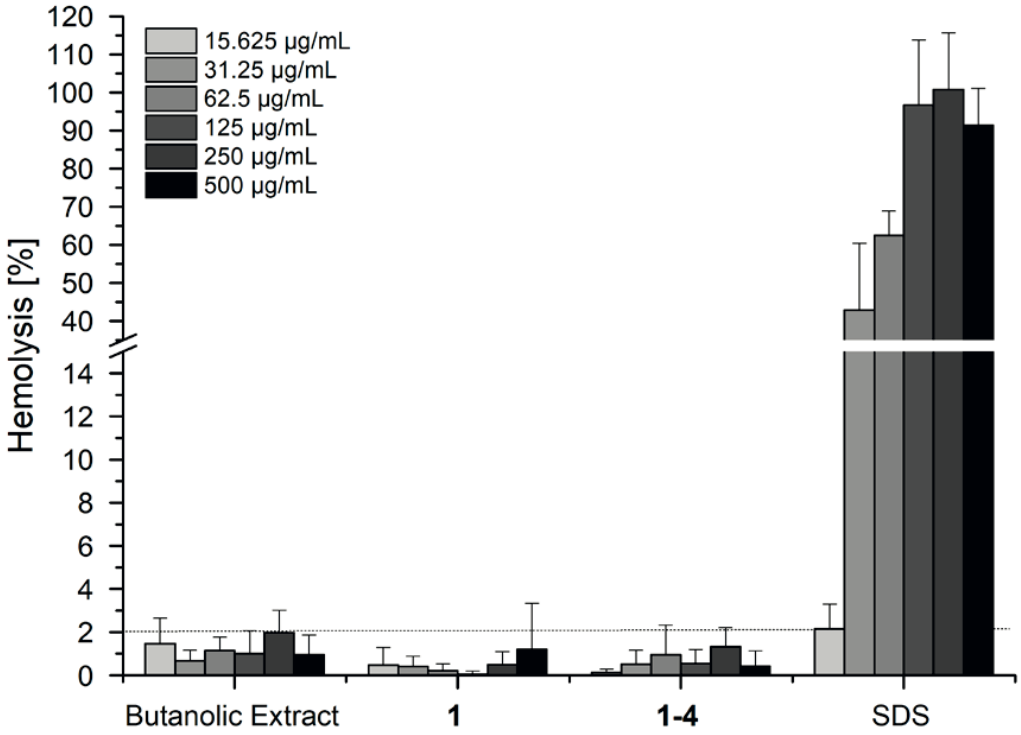

Figure S55. Hemolytic activity of butanolic extracts, **1** – **4** and **1** compared to SDS.

References

(1) Brandenburger, E.; Gressler, M.; Leonhardt, R.; Lackner, G.; Habel, A.; Hertweck, C.; Brock, M.; Hoffmeister, D. *Appl. Environ. Microbiol.* **2017**, *83(21)*, e01478-17.

(2) Kumar, S.; Stecher, G.; Tamura, K. *Mol. Biol. Evol.* **2016**, 33, 1870-1874.

(3) Pontecorvo, G.; Roper, J. A.; Hemmons, L. M.; Macdonald, K. D.; Bufton, A.W.J. The Genetics of *Aspergillus nidulans*. In *Advances in Genetics*; Demerec, M., Ed.; 5; Academic Press: New York, N.Y., **1953**, pp 141–238.

(4) Harada, K.; Fujii, K.; Mayumi, T.; Y., H.; Suzuki, M. *Tetrahedron Lett.* **1995,** *36*, 1515-1518.

(5) Krieg, R.; Jortzik, E.; Goetz, A.-A.; Blandin, S.; Wittlin, S.; Elhabiri, M.; Rahbari, M.; Nuryyeva, S.; Voigt, K.; Dahse, H.-M.; Brakhage, A.; Beckmann, S.; Quack, T.; Grevelding, C. G.; Pinkerton, A. B.; Schönecker, B.; Burrows, J.; Davioud-Charvet, E.; Rahlfs, S.; Becker, K. *Nat. Commun.* **2017**, *8*, 14478.

(6) LeBel, R.; Goring, D. *J. Chem. Eng. Data* **1962,** *7*, 100-101.

(7) Patist, A.; Bhagwat, S. S.; Penfield, K. W.; Aikens, P.; Shah, D. O. *J. Surfactants Deterg.* **2000**, *3*, 53-58.

(8) Li, Y.; Song, J.; Tian, N.; Cai, J.; Huang, M.; Xing, Q.; Wang, Y.; Wu, C.; Hu, H. *Int. J. Pharm.* **2014,** *473*, 316-325.

(9) Tamura, K.; Nei, M. *Mol. Biol. Evol.* **1993,** *10*, 512-526.

3.4 Publikation 4

Cross-chemistry leads to product diversity from atromentin synthetases in Aspergilli from section *Nigri*

Geib, E.; Baldeweg, F.; Doerfer M.; Nett M.; Brock M. *Cell Chem. Biol.* **2019**, *26*, 223-234.e6.

Zusammenfassung:
Obwohl bereits gezeigt wurde, dass nichtribosomale Peptidsynthetasen-ähnliche Enzyme die nichtoxidative Homodimerisierung von α-Ketosäuren katalysieren, ist wenig über den exakten Mechanismus bekannt. Daher gestaltet sich die Vorhersage zwischen Furanring-bildenden und Chinonring-bildenden Thioesterasedomänen als schwierig. Der Austausch der TE-Domäne mit denen von Atromentin-Synthetasen aus *Paxillus involutus* oder *A. terreus* zeigt zum einen, dass die phylogenetische Nachbarschaft bei der Funktionserhaltung eine Rolle spielt, zum anderen, dass durch Domänenaustausch eine Umwandlung erreicht werden kann. Die heterologe Expression von Atromentin-Synthetasen in *A. niger* und *A. oryzae* offenbart zudem eine wirtsabhängige Biosynthese von entweder Atromentin oder eines bisher noch unbekannten Produktes namens Atrofuransäure, deren Struktur im Zuge dieser Arbeit aufgeklärt wurde. Ein zusätzliches Screening von Aspergillen der Sektion *Nigri* bestätigt außerdem die Produktion von Atrofuransäure durch Atromentin-Synthetasen in einem homologen Wirt.

Angaben zum Eigenanteil von Florian Baldeweg (15%):
Aufreinigung von Rohextrakten und Aufklärung der Struktur von Atrofuransäure mittels Derivatisierung, Isotopenmarkierung und NMR-Spektroskopie. Mitarbeit am Manuskript.

Jena, den

Prof. Dirk Hoffmeister

Article

Cell Chemical Biology

Cross-Chemistry Leads to Product Diversity from Atromentin Synthetases in Aspergilli from Section *Nigri*

Graphical Abstract

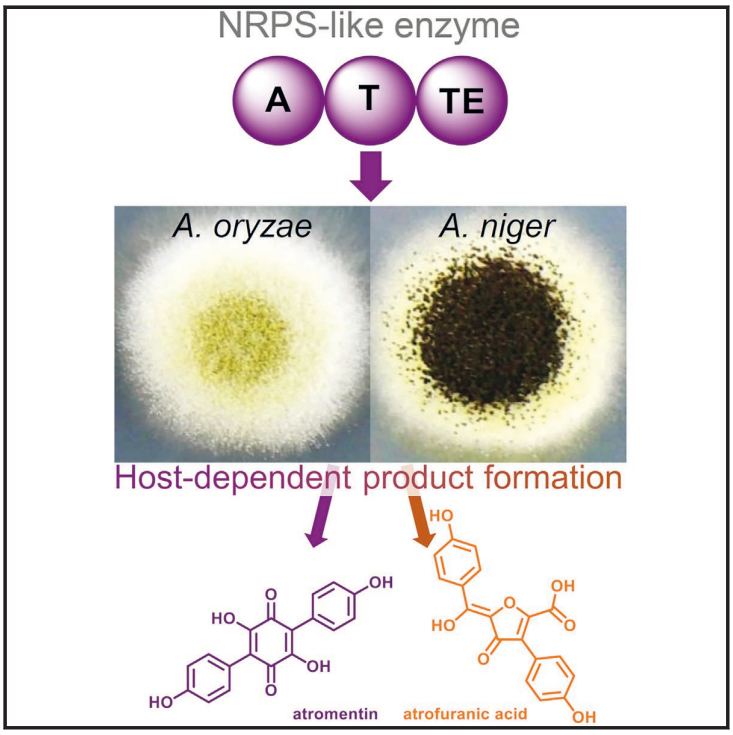

Highlights

- The product spectrum of NRPS-like enzymes depends on the expression platform
- Cross-chemistry occurs on quinone core structures in aspergilli from section *Nigri*
- Cross-chemistry produces novel metabolites such as atrofuranic acid
- Identification of an atromentin synthetase from *Aspergillus brasiliensis*

Authors

Elena Geib, Florian Baldeweg, Maximilian Doerfer, Markus Nett, Matthias Brock

Correspondence

matthias.brock@nottingham.ac.uk

In Brief

Geib et al. investigated core structure formation by thioesterase domains of fungal NRPS-like enzymes. Exchange of thioesterase domains alters product formation, but requires close phylogenetic relationship of donor and acceptor. Product formation further depends on expression hosts with furanic acid rather than quinone core formation in aspergilli from section *Nigri*.

Geib et al., 2019, Cell Chemical Biology *26*, 1–12
February 21, 2019
https://doi.org/10.1016/j.chembiol.2018.10.021

CellPress

Please cite this article in press as: Geib et al., Cross-Chemistry Leads to Product Diversity from Atromentin Synthetases in Aspergilli from Section *Nigri*, Cell Chemical Biology (2018), https://doi.org/10.1016/j.chembiol.2018.10.021

Cell Chemical Biology
Article

CellPress

Cross-Chemistry Leads to Product Diversity from Atromentin Synthetases in Aspergilli from Section *Nigri*

Elena Geib,[1] Florian Baldeweg,[2] Maximilian Doerfer,[2] Markus Nett,[3] and Matthias Brock[1,4,*]
[1]Fungal Genetics and Biology, School of Life Sciences, University of Nottingham, University Park, Nottingham NG7 2RD, UK
[2]Department of Pharmaceutical Microbiology at the Leibniz Institute for Natural Product Research and Infection Biology – Hans Knoell Institute, Friedrich-Schiller-University Jena, Adolf-Reichwein Straße 23a, 07745 Jena, Germany
[3]Department of Biochemical and Chemical Engineering, TU Dortmund University, Emil-Figge-Straße 66, 44227 Dortmund, Germany
[4]Lead Contact
*Correspondence: matthias.brock@nottingham.ac.uk
https://doi.org/10.1016/j.chembiol.2018.10.021

SUMMARY

Non-ribosomal peptide synthetase (NRPS)-like enzymes catalyze the non-oxidative homodimerization of aromatic α-keto acids, but the exact reaction mechanism is unknown. The furanone-forming thioesterase domain of the *Aspergillus terreus* aspulvinone E synthetase MelA displays a predicted quinone-forming motif, whereby its catalytic triad contains an essential cysteine indicating an unusual thioester intermediate. To convert MelA into a quinone-forming atromentin synthetase its thioesterase domain was replaced with that from a *Paxillus involutus* or *A. terreus* atromentin synthetase. Phylogenetic proximity of donor and acceptor seems important, as only replacement with the *A. terreus* thioesterase was functional. Heterologous expression of atromentin synthetases in *Aspergillus niger* and *Aspergillus oryzae* revealed host-dependent product formation whereby cross-chemistry directed atromentin biosynthesis in *A. niger* toward atrofuranic acid. Screening of aspergilli from section *Nigri* identified an atromentin synthetase in *Aspergillus brasiliensis* that produced atrofuranic acid in the homologous host. Therefore, cross-chemistry on quinone cores appears common to section *Nigri*.

INTRODUCTION

Non-ribosomal peptide synthetase (NRPS)-like enzymes are widespread in the fungal kingdom, and even closely related species seem to contain a large number of non-homologous enzymes. For instance, *Aspergillus terreus* contains 15 NRPS-like genes (van Dijk et al., 2016) and 14 NRPS-like genes are found in *Aspergillus nidulans* (Yeh et al., 2012). Corresponding to other NRPSs, NRPS-like enzymes are composed of several catalytic domains. They feature an adenylation (A), thiolation (T), and thioesterase (TE) or, alternatively, a reductase (R) domain, but lack the condensation domain (C) of prototypical NRPSs (van Dijk et al., 2016). Therefore, rather than forming peptide bonds from individual amino acids, NRPS-like enzymes generally catalyze the condensation of two identical α-keto acids. For a long time, the importance of NRPS-like enzymes in the production of secondary metabolites had been neglected and biochemical information on their catalytic properties was rare (Schneider et al., 2007). However, in recent years it has been shown that NRPS-like enzymes, either alone or embedded in gene clusters, produce metabolites important for fungal development and environmental competition. The first fungal product confirmed to derive from a gene cluster containing an NRPS-like enzyme was terrequinone A (**1**) (for metabolite structures refer to Figure 1) from *A. nidulans* (Bok et al., 2006; Balibar et al., 2007). While the direct contribution of terrequinone A to environmental competition has not yet been described, terrequinone A exhibits cytotoxic activity (He et al., 2004). The γ-butyrolactones from *A. terreus* are also formed by NRPS-like enzymes (Guo et al., 2013), and have been shown to stimulate sporulation in submerged cultures and increase the production of secondary metabolites such as lovastatin (Schimmel et al., 1998). In addition, butyrolactone I (**2**) can scavenge reactive oxygen species and acts as inhibitor of α-glucosidase, which is an important feature for the treatment of type 2 diabetes (Dewi et al., 2012). Aspulvinone E (**3**) is the precursor of the Asp-melanin pigment in *A. terreus* conidia that is significantly different from the dihydroxynaphthalene melanin found in other *Aspergillus* species (Geib et al., 2016). Another NRPS-like enzyme from *A. terreus* was shown to direct the biosynthesis of phenguignardic acid (**4**) (Sun et al., 2016), which had previously been reported from the grape black rot fungus, *Guignardia bidwellii*, together with the structurally related guignardic acid (**5**) (Molitor et al., 2012; Rodrigues-Heerklotz et al., 2001). These two dioxolanone natural products were demonstrated to cause plant leaf necrosis and might thus act as virulence factors of *G. bidwellii* (Molitor et al., 2012). Furthermore, the ectomycorrhizae-forming basidiomycete *Paxillus involutus* produces atromentin (**6**) that is subsequently converted into involutin (Braesel et al., 2015) and is assumed to contribute to the oxidative degradation of lignocellulose via Fenton chemistry by reducing Fe^{3+} to Fe^{2+} (Shah et al., 2015). Atromentin also possesses estrogenic activity and may act as potent inhibitor of 17β-hydroxysteroid dehydrogenase (Dellafiora et al., 2019). Very recently, an atromentin synthetase

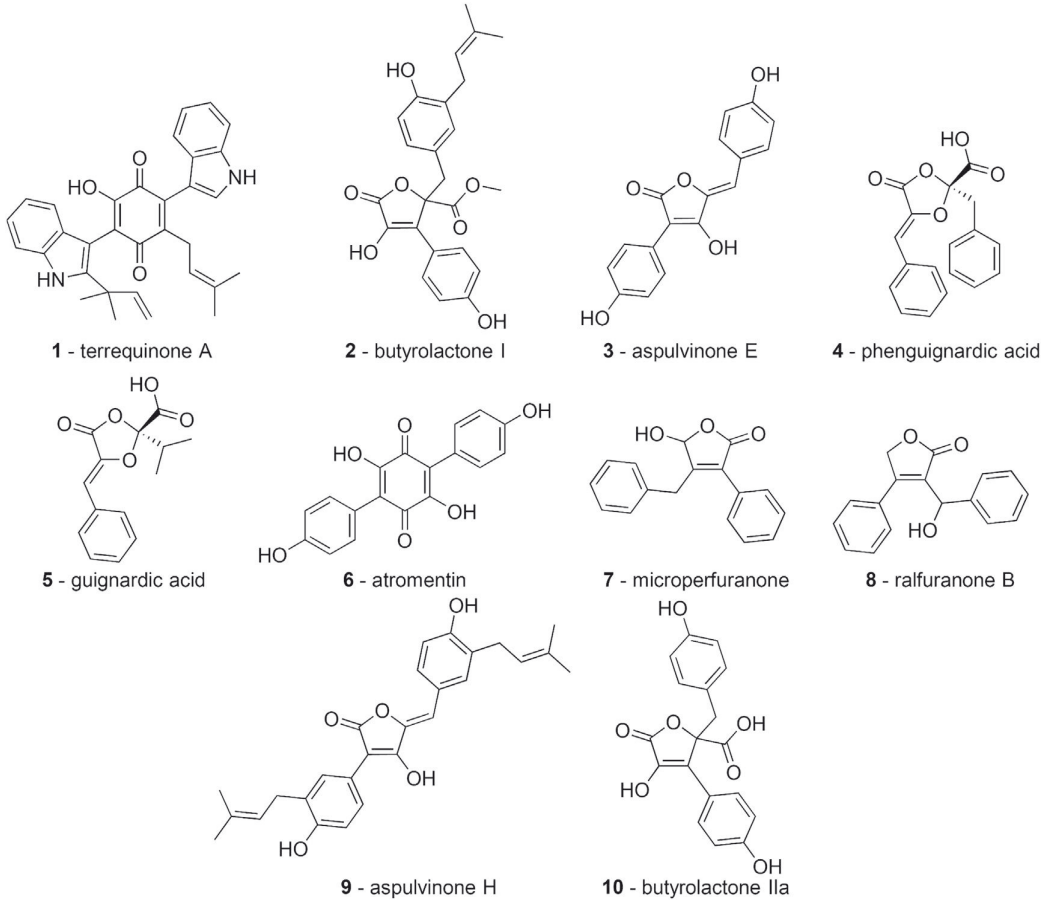

Figure 1. Metabolites Produced by NRPS-like Enzymes

has also been identified from *A. terreus* by recombinant expression of the $atrA_{At}$ gene in yeast, but the naturally inducing conditions in *A. terreus* have not yet been identified (Hühner et al., 2018). These and other examples show that NRPS-like enzymes are widespread in the fungal kingdom. They direct fungal development and support virulence and nutrition. Furthermore, due to described antitumor and antidiabetic properties, this class of compounds has several interesting pharmaceutical properties.

The α-keto acids of the aromatic amino acids phenylalanine, tyrosine, and tryptophan provide the major substrates of fungal NRPS-like enzymes (Hühner et al., 2018). This is at least true for all examples mentioned above except for guignardic acid (**5**), for which the molecular basis of its biosynthesis is still unknown. The condensation of aromatic α-keto acids results in a variety of interconnecting core ring structures, which in non-reducing NRPS-like enzymes were proposed to be performed by the thioesterase domain of these enzymes (Balibar et al., 2007; Braesel et al., 2015). While the exact mechanism of product formation by the thioesterase domain has not yet been solved, Braesel et al. (2015) suggested that certain sequence motifs could specify the formation of the core ring structures. A motif with a catalytic triad made from serine, asparagine, and histidine in combination with a branched-chain aliphatic amino acid and two proline residues was described to be consistent with the formation of a core quinone ring structure as found in atromentin (**6**). In contrast, furanone structures were assumed to be formed by a triad made from serine, aspartate, and histidine (Braesel et al., 2015) as found in microperfuranone (**7**) biosynthesis by MicA from *A. nidulans* (Yeh et al., 2012) or ralfuranone B (**8**) biosynthesis by RalA from the bacterium *Ralstonia solanacearum* (Wackler et al., 2011). In contrast to this prediction, the NRPS-like proteins MelA and ApvA from *A. terreus* form a furanone in aspulvinone E (**3**) and aspulvinone H (**9**) but show a sequence motif similar to that of quinone-forming TE domains except that the serine residue in the catalytic triad is replaced by a cysteine (Geib et al., 2016). As the InvA atromentin synthetases from *P. involutus* and the aspulvinone E synthetase from *A. terreus* both use the substrate *p*-hydroxyphenylpyruvate, our intention was to perform mutation analyses on the *melA* gene to identify the contribution of specific amino acids in product formation. Accordingly, by using expression systems that are based on the transcriptional activator TerR from terrein biosynthesis in combination with its *terA* target promoter (Gressler et al., 2015; Geib and Brock, 2017), we expressed different versions of the *melA* and the *invA5* gene and characterized the

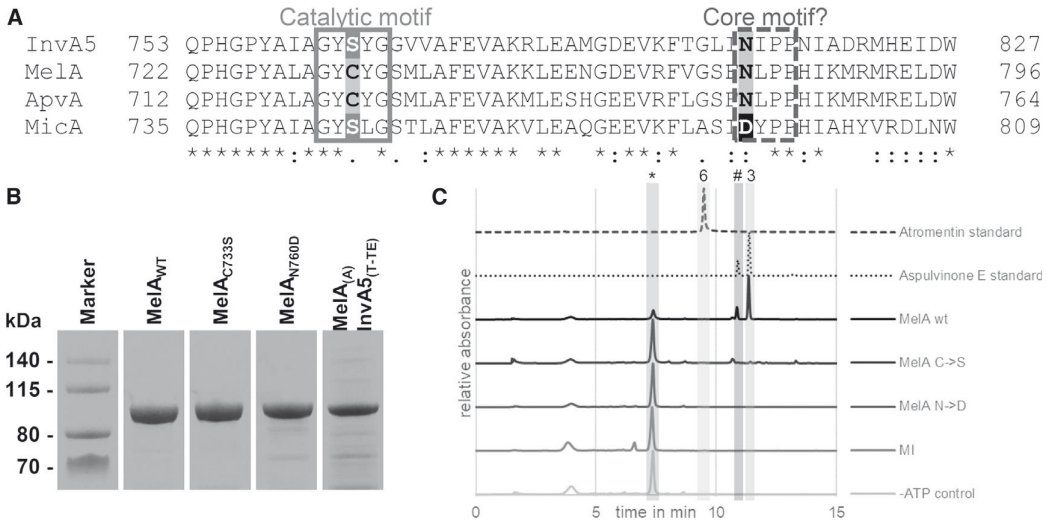

Figure 2. Characterization and Mutation of the Aspulvinone E Synthetase MelA

(A) Partial sequence alignment from thioesterase domains of four NRPS-like enzymes. InvA5, atromentin synthetase from *P. involutus*; MelA, aspulvinone E synthetase for Asp-melanin biosynthesis from *A. terreus*; ApvA, aspulvinone E synthetase for aspulvinone H biosynthesis from *A. terreus*; MicA, microperfuranone synthetase from *A. nidulans*. The catalytic motif and the proposed fingerprint region directing the core structure formation are highlighted.

(B) SDS-PAGE analysis of wild-type and mutated MelA proteins.

(C) HPLC chromatograms from *in vitro* assays from purified MelA proteins shown in (B) in comparison with authentic standards of aspulvinone E (**3**), the UV-interconvertible isoaspulvinone E (**#**), and atromentin (**6**). The asterisk denotes the peak derived from the substrate *p*-hydroxyphenylpyruvate. MI, chimeric $MelA_{(A)}$:$InvA5_{(T\text{-}TE)}$. HPLC runs were recorded at 254 nm.

corresponding products. Additionally, we studied the products formed from the *A. terreus* atromentin synthetase $AtrA_{At}$ in different expression platform strains (Hühner et al., 2018) and determined the products of a yet uncharacterized NRPS-like enzyme from *Aspergillus brasiliensis* with similarity to aspulvinone E and atromentin synthetases.

RESULTS

Mutation of C733S and N760D in the Aspulvinone E Synthetase MelA from *A. terreus*

A sequence alignment of thioesterase domains of the aspulvinone E and H synthetases MelA and ApvA from *A. terreus* revealed sequence motifs matching with the predicted sequence motif of quinone core formation as found in the atromentin synthetase InvA5 from *P. involutus* rather than the predicted furanone motif as found in the microperfuranone synthetase MicA (Figure 2A). However, MelA and ApvA that were identified as furanone synthetases both possess a cysteine instead of a serine in the postulated catalytic triad. This suggests that during furanone core structure formation in aspulvinone E (**3**) biosynthesis, the intermediate is bound by a thioester rather than an oxoester. As MelA activity was found to depend on a reducing environment (Geib et al., 2016), the thiol group was assumed to be essential. To confirm this assumption and to test whether a change of the catalytic triad from a cysteine into a serine alters product formation, we introduced a C733S mutation. The mutated gene was cloned with an *N*-terminal His tag into the SM-Xpress vector (Gressler et al., 2015) and used for transformation of the *A. niger* expression platform strain P2. No change in the metabolite profile compared with the parental strain was observed with the C733S mutant, although enzyme purification confirmed the production of a full-length protein (Figure 2B). In addition, an *in vitro* assay with native and mutated MelA only revealed product formation with the wild-type but not with the C733S mutant (Figure 2C). This indicates that the cysteine in the thioesterase domain is essential in the formation of aspulvinone E (**3**). We next analyzed the importance of asparagine 760 in MelA, which also matches the pattern in quinone, but not furanone, core-forming enzymes (Figure 2A). Like the C733S mutant, an N760D mutant was generated and expressed in *A. niger*. Again, no metabolite was produced and the purified enzyme (Figure 2B) did not show product formation (Figure 2C). These results indicate that both amino acids, C733 and N760, essentially contribute to the catalytic mechanism and/or the correct folding of the thioesterase domain of the aspulvinone E synthetase, but the core motifs predicted to discriminate between quinone and furanone core formation seem to be more complex.

Generation of a Chimeric $MelA_{(A)}$:$InvA5_{(T\text{-}TE)}$ Protein

As the mutation of C733 and N760 in MelA inactivated the enzyme, we were interested in whether replacement of the MelA thiolation and thioesterase domains with those from *P. involutus* InvA5 converts the aspulvinone E synthetase into an atromentin synthetase. Previous studies on the aspulvinone H synthetase ApvA from *A. terreus* showed that an exchange of the thiolation and thioesterase domain with that from the butyrolactone IIa (**10**) synthetase BtyA from *A. terreus* successfully converted the enzyme into a butyrolactone synthetase (van Dijk et al., 2016). To produce a chimeric MelA:InvA5 protein,

we selected highly conserved residues in the stretch between adenylation and thiolation domain to generate the $MelA_{(A)}$:$InvA5_{(T\text{-}TE)}$ fusion protein. While a full-length protein was successfully reisolated from *A. niger* (Figure 2B), neither under *in vivo* nor *in vitro* conditions (Figure 2C) was atromentin (**6**) or any other metabolite detected. This observation led to the following hypotheses: (1) as InvA5 is derived from a basidiomycete, it might not properly fold when produced in the ascomycete *A. niger*; (2) the reaction mechanism discriminating furanone and quinone core formation is also directed by the A domain; or (3) the gene fusion was placed at an incompatible position.

Heterologous Expression of the Atromentin Synthetase Gene *invA5* in *A. niger*

To test the first hypothesis that InvA5 cannot be produced as a functional protein in *A. niger*, we cloned the full-length *invA5* gene including an *N*-terminal His tag into the SM-Xpress expression vector and transformed several *A. niger* expression platform strains. These included the sugar-inducible P2 strain (Gressler et al., 2015) and the doxycycline-inducible ATNT16 strain (Geib and Brock, 2017), both derived from the parental *A. niger* wild-type A1144. Furthermore, the sugar-inducible expression system was transferred into *A. niger* N402 and the resulting expression platform strain NP4 was also used for *invA5* expression. Transformants produced a bright-yellow culture broth under inducing conditions, which was extracted for metabolite analysis. While a single major metabolite peak for atromentin (**6**) was expected, only a very minor peak identical to the retention time and UV-visible (UV-vis) profile of atromentin was observed (Figures 3A and S1). By contrast, several other major metabolite peaks (**11**, **12**, **13**, **X**) were detected with strikingly different retention times compared with atromentin (**6**). However, when InvA5 was purified and subjected to an *in vitro* assay, atromentin (**6**) was the exclusive metabolite produced from the substrate *p*-hydroxyphenylpyruvate (Figure 3D). Furthermore, when a crude cell-free extract of an *invA5* expressing *A. niger* strain was used in an enzymatic assay with *p*-hydroxyphenylpyruvate as substrate, traces of **13** were detected as a carry-over from the cell-free extract and atromentin (**6**) was the major metabolite produced (Figure S1C). This confirms that InvA5 is functionally produced in *A. niger*, but under *in vivo* conditions atromentin biosynthesis seems to undergo unexpected modifications that are not observed in cell-free extracts.

Time-Dependent Metabolite Production from *invA5* Expression in *A. niger*

While InvA5 was confirmed to act as atromentin synthetase under *in vitro* conditions, several different metabolites were produced in the heterologous host *A. niger* regardless of the expression platform strain used. However, peak intensities of individual metabolites strongly varied among the different strains in this screening. Therefore, we selected individual transformants and extracted culture supernatant and mycelium at different time points (Figures 3A, 3B, and S1). A metabolite at a retention time of 14.99 min (**13**) and with a molecular mass of 340.29 g/mol was dominant at early time points, but its intensity in the culture broth decreased during prolonged cultivation. However, at 72 hr the metabolite again accumulated in the culture supernatant. In agreement, this metabolite was nearly exclusively isolated from the mycelium at 36 and 48 hr. Furthermore, at least three other dominant metabolites with molecular masses of 342.30 g/mol (**X**), 312.28 g/mol (**11**), and 138.12 g/mol (**12**) (retention times 3.74 min, 4.88 min, and 5.09 min, respectively) accumulated during cultivation.

Identification of Metabolites from Heterologous *invA5* Expression in *A. niger*

Metabolite **X** showed an exact molecular mass of 341.0669 $[M\text{-}H]^-$ resulting in a sum formula of $C_{18}H_{14}O_7$. Stability issues prevented the structural elucidation of this compound. In contrast, structures of metabolites with exact masses of *m/z* 339.0514 $[M\text{-}H]^-$ (**13**) and *m/z* 311.0566 $[M\text{-}H]^-$ (**11**) as well as that of metabolite (**12**) with an exact mass of *m/z* 137.0232 $[M\text{-}H]^-$ were elucidated by nuclear magnetic resonance (NMR) spectroscopy. Metabolite (**11**) was identified as gyroporin, a known atromentin-derived metabolite in *P. involutus* (Besl et al., 1973). Metabolite (**12**) was identified as *p*-hydroxybenzoic acid (Table S1).

The molecular formula of the previously undescribed atrofuranic acid (**13**) was determined as $C_{18}H_{12}O_7$ by high-resolution electrospray ionization mass spectrometry (ESI-MS) measurement (*m/z* 340.0583), which is consistent with 13 degrees of unsaturation. The ^1H NMR spectrum showed only four signals in the aromatic range. These signals were ascribed to two *p*-substituted benzene residues based on their chemical shifts, splitting, and 2D NMR correlations (Figures S2–S4 and Table S2). The deduced number of eight aromatic protons together with the molecular formula indicated that **13** must contain four hydroxyl groups with exchangeable protons. Because the treatment of **13** with acetic anhydride in pyridine yielded exclusively a triacetylated product (**14**) (Figures S2–S4 and Table S3), it became evident that one hydroxyl group in **13** is part of a carboxylic acid moiety (Chattaway, 1931). The remaining two oxygen atoms are due to a ketone, which shows a resonance at 180.6 ppm in the ^{13}C NMR spectrum, and an ether function, respectively. The four as yet unassigned signals in the ^{13}C NMR spectrum possess chemical shifts characteristic of sp^2-hybridized carbons and were thus attributed to two carbon-carbon double bonds. The presence of two benzene rings, two carbonyl groups, and two C-C double bonds in **13** left a single degree of unsaturation unassigned, which must be due to another ring structure. Consolidating the above information with the chemical shifts of the respective nuclei as well as data from a heteronuclear multiple bond correlation experiment, the structure of **13** was finally elucidated. As evidenced by the signal doubling in the ^{13}C NMR spectrum, **13** is subject to keto-enol tautomerism and, therefore, exists as a mixture of *E* and *Z* isomers. After feeding *A. niger* cultures with 2-^{13}C-labeled tyrosine, spectroscopic analysis of isolated **13** revealed four intensified ^{13}C NMR signals (Figure S3) that were in agreement with the proposed structure of atrofuranic acid and its tautomerism.

Metabolite Production from Atrofuranic Acid

To elucidate the interconnection of products formed by heterologous expression of the atromentin synthetase InvA5 in *A. niger*, we performed feeding studies. When atromentin (**6**) was fed to *A. niger* cultures, subsequent product analysis did not provide any

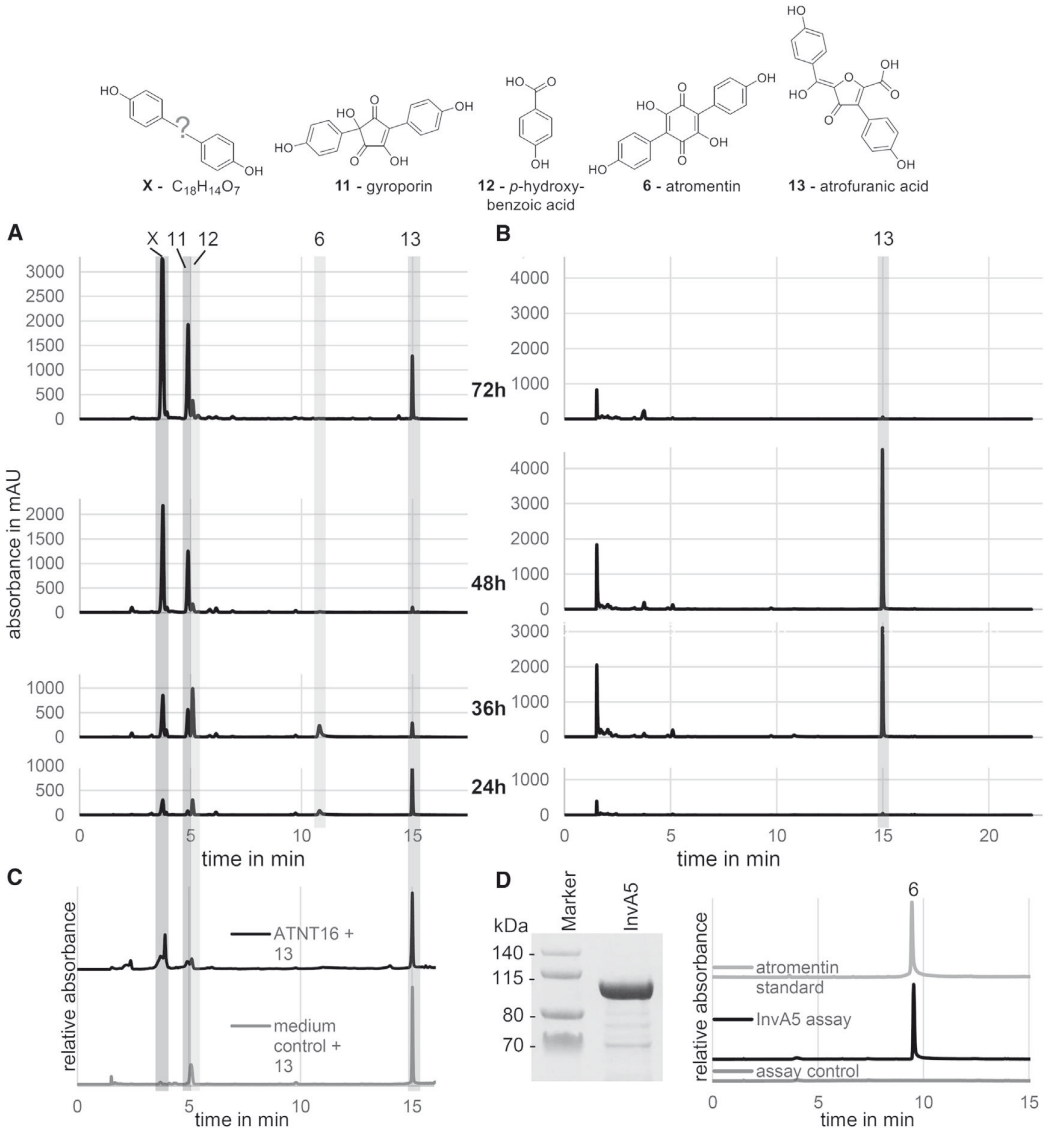

Figure 3. Analysis of Products Formed from *invA5* Expression in *A. niger* and from Purified InvA5

(A and B) Time-dependent extraction of (A) culture filtrates and (B) mycelium from heterologous *invA5* expression in the *A. niger* P2 strain.

(C) Analysis of metabolite formation from atrofuranic acid (**13**). When **13** is incubated for 24 hr in sterile culture medium *p*-hydroxybenzoic acid (**12**) is formed. In the presence of *A. niger* **13** is additionally transformed into gyroporin (**11**) and metabolite X.

(D) InvA5 purification and HPLC analysis of products formed from an *in vitro* assay.

In (A) to (C) a modified HPLC method (COR_ESIA_25–50) was used to achieve higher peak resolution, whereas method COR_ESIA was used in (D). All HPLC runs were recorded at 254 nm. For heterologous expression of atromentin synthetases in *A. niger* strains NP4 and ATNT16 and *in vitro* assay with an i*nvA5* expressing *A. niger* cell extract, refer to Figure S1. NMR data for structure elucidation of compounds are provided in Tables S1–S3 and Figures S2 and S3.

evidence for the presence of atrofuranic acid (**13**), metabolite X (**X**), gyroporin (**11**), or *p*-hydroxybenzoic acid (**12**). This indicates that either externally added atromentin (**6**) does not enter *A. niger* or that atromentin (**6**) does not act as precursor for any of these metabolites. Therefore, atrofuranic acid (**13**) was added to *A. niger* ATNT16 cultures and to a control medium (Figure 3C). Analysis of the control revealed the presence of *p*-hydroxybenzoic acid (**12**), indicating that **13** can spontaneously decompose into **12** in the culture broth. However, when *A. niger* cultures supplemented with **13** were extracted, **12** was detected along with metabolite X (**X**) and gyroporin (**11**). This implies that atrofuranic acid (**13**) is the prime metabolite formed by heterologous expression of the *invA5* gene in *A. niger* with all other metabolites deriving from this compound. Furthermore, metabolite X and gyroporin (**11**) production seems dependent on the presence of *A. niger* cells.

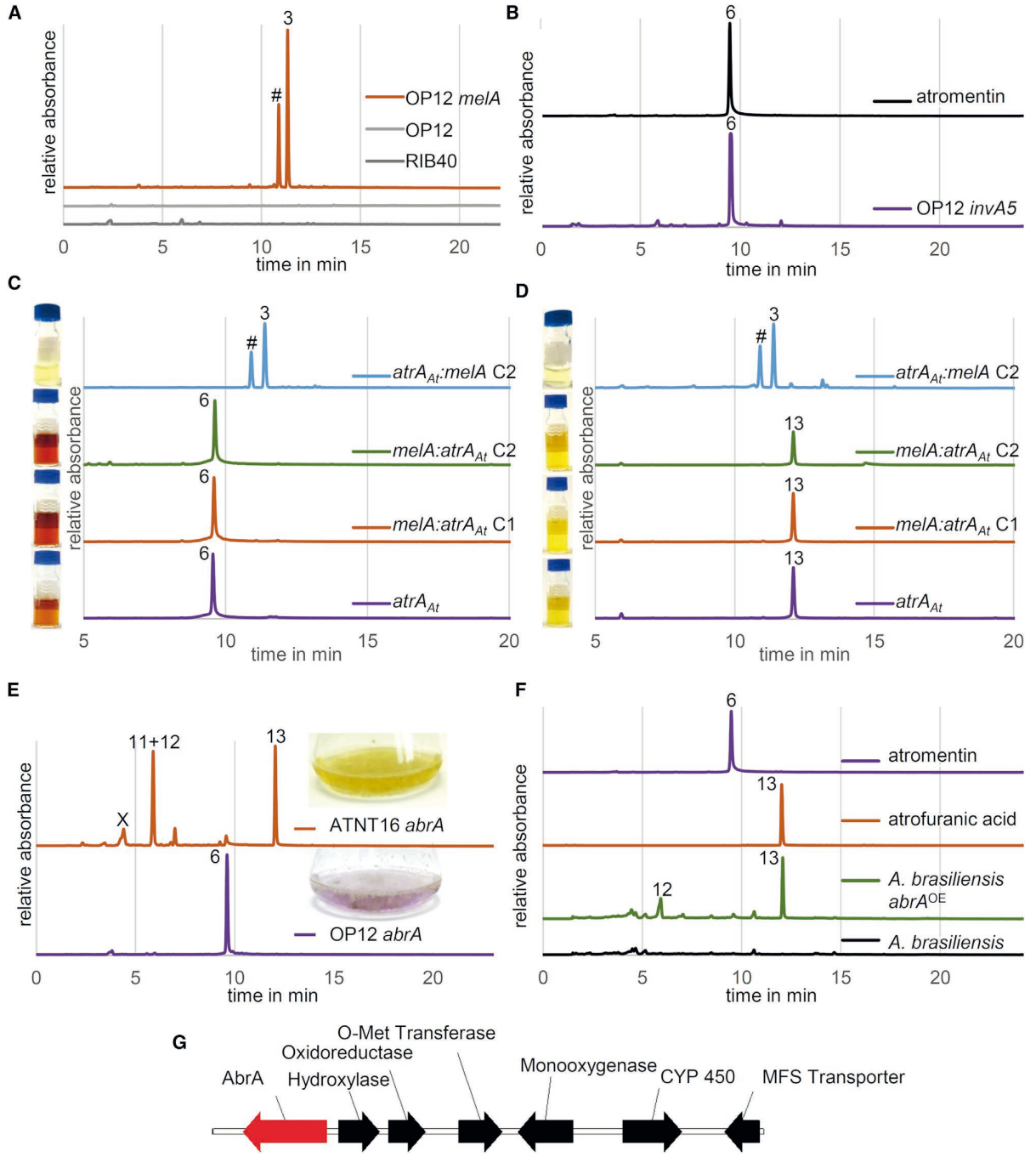

Figure 4. Expression of Different NRPS-like Enzymes in *A. niger* and *A. oryzae* and Product Analysis by HPLC

(A) Background metabolite production in the *A. oryzae* wild-type strain RIB40, the expression platform strain *A. oryzae* OP12, and identification of aspulvinone E (**3**) and its *cis* isomer isoaspulvinone E (**#**) from an OP12 strain expressing the *melA* gene from *A. terreus*.

(B) Analysis of a culture extract of an OP12 strain expressing the atromentin synthetase *invA5*. Authentic atromentin (**6**) was run as a reference standard and confirms the production of atromentin (**6**) in *A. oryzae*.

(C and D) Analysis of metabolites formed from recombinant production of the atromentin synthetase AtrA$_{At}$ and the chimeric proteins MelA$_{(A)}$:AtrA$_{At(T-TE)}$ (C1), MelA$_{(A-T)}$:AtrA$_{At(TE)}$ (C2), and AtrA$_{At(A-T)}$:MelA$_{(TE)}$ (C2) in *A. oryzae* OP12 and *A. niger* ATNT16. (C) Culture extracts from *A. oryzae* OP12 with accumulation of atromentin (**6**). (D) Mycelium extractions from *A. niger* ATNT 16 with accumulation of atrofuranic acid (**13**). The construct AtrA$_{At(A-T)}$:MelA$_{(TE)}$ (C2) produces aspulvinone E (**3**) and isoaspulvinone E (**#**).

(legend continued on next page)

Heterologous *invA5* and *melA* Expression in *A. oryzae*

Our data showed that InvA5 was produced as a functional protein in *A. niger*, whereby under *in vivo* conditions a cross-chemistry during product formation resulted in the production of a furanic acid core structure. To investigate whether atromentin (**6**) production is generally directed toward other metabolites in *Aspergillus* species, we introduced the *A. terreus* transcriptional regulator gene *terR* under control of the P*amyB* promoter (Gressler et al., 2015) into the genome of *Aspergillus oryzae* RIB40. The single copy transformant OP12 was selected as *A. oryzae* expression platform strain. Cultivation of OP12 and its parental RIB40 strain in glucose or starch containing minimal medium revealed no significant background production of secondary metabolites in either strain (Figure 4A).

To test the general suitability of OP12 to produce metabolites from an NRPS-like enzyme, we first introduced the *A. terreus melA* gene under control of the *terA* promoter. As with *melA* expression in the *A. niger* P2 strain (Geib et al., 2016), production of aspulvinone E (**3**) and its UV-interconvertible isomer isoaspulvinone E (**#**) was confirmed by high-performance liquid chromatography (HPLC) analysis from culture extracts of the OP12 *melA* strain (Figure 4A). Next, we transformed the OP12 strain with the *invA5* expression construct. Transformants secreted a purple metabolite into the solid and liquid growth medium. Analytical HPLC from culture extracts revealed a single metabolite peak matching the retention time and UV spectrum of authentic atromentin (**6**) (Figure 4B). This experiment confirmed that cross-chemistry on the benzoquinone core of atromentin (**6**) does not occur in *A. oryzae*, and no other metabolites were detected in this expression host. This indicates further that the physiology of *Aspergillus* species used for heterologous gene expression differs and is important for identification of metabolites from a specific yet uncharacterized gene of interest.

Generation of Chimeric Proteins by Domain Fusions from MelA and $AtrA_{At}$

Analyses showed that InvA5 is functionally expressed in *A. niger* and *A. oryzae*, which indicates that the failure to retrieve a functional chimeric protein from the fusion of MelA with InvA5 was due to either selection of an incorrect protein fusion site or an incompatibility between an *A. terreus* (ascomycete) and *P. involutus* (basidiomycete) enzyme. To test these assumptions further, we fused the MelA protein with the atromentin synthetase $AtrA_{At}$ from *A. terreus* (Hühner et al., 2018) and selected two different fusion sites. The first construct (C1) used the identical fusion site as selected for the fusion of MelA and InvA5, resulting in $MelA_{(A)}$:$AtrA_{At(T\text{-}TE)}$. In the second construct (C2) we only replaced the thioesterase domain of MelA, resulting in the chimeric protein $MelA_{(A\text{-}T)}$:$AtrA_{At(TE)}$. Both gene fusions as well as the full-length $atrA_{At}$ gene were cloned into the tag-SM-Xpress expression plasmid (Geib et al., 2016) for transformation of the *A. oryzae* OP12 and *A. niger* ATNT16 expression platform strains. *A. oryzae* transformants secreted a purple metabolite, and HPLC analyses of extracts confirmed the production of atromentin (**6**) from all three constructs (Figure 4C). In contrast, all *A. niger* transformants regardless of the integrated construct produced a yellow culture broth and mycelium under inducing conditions. In agreement, HPLC analyses of mycelium extractions confirmed the production of atrofuranic acid (**13**) (Figure 4D). As functional proteins were produced from both gene fusion strategies, the fusion site selected for generation of the $MelA_{(A)}$:$InvA5_{(T\text{-}TE)}$ chimeric protein was suitable and unlikely to cause the production of an inactive enzyme. More importantly, this experiment indicated that the thioesterase domain directs the chemistry of an NRPS-like enzyme and that a furanone-forming enzyme can be successfully converted into a quinone-forming enzyme by exchange of the TE domain. To confirm this assumption, we also produced a fusion protein that contained the A and T domains of the atromentin synthetase $AtrA_{At}$ and the TE domain of MelA. The gene fusion was cloned into the tag-SM-Xpress vector and used for transformation of the *A. oryzae* OP12 and *A. niger* ATNT16 expression platform strains. Culture supernatants turned in a fluorescent yellow, indicating the production of aspulvinone E (**3**) and its UV-interconvertible isomer isoaspulvinone E (**#**) (Geib et al., 2016), which was confirmed by HPLC analysis of culture extracts (Figures 4C and 4D; construct $atrA_{At}$:*melA* C2). Therefore, we conclude that a successful replacement of the thioesterase domain of an NRPS-like enzyme depends on the phylogenetic relationship of the fusion partners. Furthermore, while the furanone core-containing product aspulvinone E (**3**) is produced in both *A. niger* and *A. oryzae*, the product formed from atromentin synthetases differs among the two species. While *A. oryzae* produces atromentin (**6**), the major primary metabolite produced in *A. niger* is atrofuranic acid (**13**).

Identification of an Atromentin Synthetase from *A. brasiliensis*

As *A. niger* mainly produced atrofuranic acid (**13**) from the expression of atromentin synthetase genes, we were interested in metabolites produced from NRPS-like enzymes in aspergilli from section *Nigri*. For this purpose, we used the MelA protein sequence from *A. terreus* as a template and screened the genome of *A. brasiliensis* strain CBS101740. A protein with accession number GenBank: OJJ76880 was identified which, when used as a template in BLAST searches against *A. terreus*, revealed the best hits with the atromentin synthetase $AtrA_{At}$ (57% identity, 72% similarity; GenBank: AUO29225), the aspulvinone H synthetase ApvA (54% identity, 72% similarity, GenBank: AUO29222), and the aspulvinone E synthetase MelA (55% identity, 72% similarity; GenBank: AND66115). This shows that a simple BLAST analysis of NRPS-like enzymes does not necessarily allow the prediction of the metabolite produced. However, it appeared likely that the *A. brasiliensis* enzyme, subsequently called AbrA, produces an atromentin-like metabolite, as no cysteine was detected in the active site of the thioesterase domain. To confirm this assumption, we amplified the *abrA* gene from genomic DNA of *A. brasiliensis* CBS101740 and cloned it into the tag-SM-Xpress expression vector, then used it for

(E) Cultures and HPLC profiles of extracts from heterologous expression of *abrA* from *A. brasiliensis* in ATNT16 and OP12.
(F) Homologous overexpression of *abrA* in *A. brasiliensis* and authentic standards of atrofuranic acid (**13**) and atromentin (**6**). For a metabolite screening on *A. brasiliensis* culture extracts, refer to Figure S5. All HPLC runs were recorded at 254 nm.
(G) Putative *abrA* containing biosynthesis gene cluster in *A. brasiliensis*.

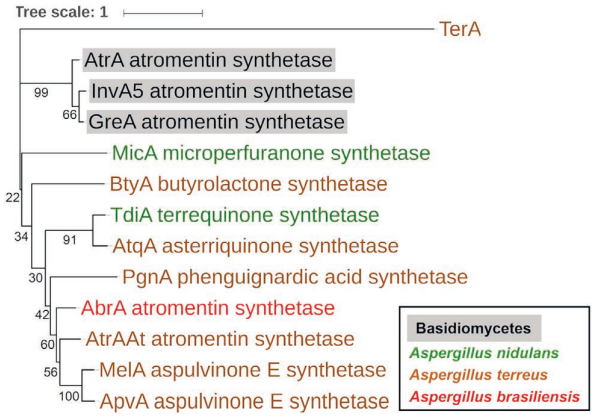

Figure 5. Phylogenetic Tree of Thioesterase Domains of NRPS-like Enzymes from Basidiomycetes and *Aspergillus* Species

Bootstrap support is shown at the nodes of the tree, and enzyme names and enzymatic activity are provided. The originating organism can be extracted from the color coding. Black letters with gray background denote atromentin synthetases from the basidiomycetes *Tapinella panuoides* (AtrA), *P. involutus* (InvA5), and *Suillus grevillei* (GreA). Enzymes in green derive from *A. nidulans*, in brown from *A. terreus*, and in red from *A. brasiliensis*. The thioesterase domain of the polyketide synthase TerA from *A. terreus* served as outgroup. For protein accession numbers, refer to STAR Methods.

transformation of *A. niger* ATNT16 and *A. oryzae* OP12. In *A. niger*, the culture supernatant and mycelium turned bright yellow, whereas *A. oryzae* produced a purple compound (Figure 4E), indicating that the *A. brasiliensis abrA* gene encodes an atromentin synthetase. When extracts were analyzed by HPLC, this assumption was confirmed as metabolite X, gyroporin (**11**), *p*-hydroxybenzoic acid (**12**), and atrofuranic acid (**13**) were identified from *A. niger* extracts, whereas a single metabolite peak of atromentin (**6**) was detected from the OP12 strain. Furthermore, atromentin (**6**) was the sole product produced under *in vitro* conditions from purified AbrA (Figure S1D). This shows that atromentin synthetases are common to ascomycetes and more specifically shows that *A. brasiliensis* belonging to the section *Nigri* possesses such an enzyme.

Cross-Chemistry on Benzoquinones in Section *Nigri*

Preliminary trials to identify atromentin from *A. brasiliensis* under some selected cultivation conditions failed (Figure S5). We were, therefore, interested in the fate of atromentin (**6**) biosynthesis when induced in *A. brasiliensis*. Therefore, the atromentin synthetase gene *abrA* was cloned under control of the constitutively expressed *A. nidulans gpdA* promoter, and *A. brasiliensis* was transformed using pyrithiamine as selection marker. Positive transformants were cultivated in glucose-containing minimal medium, and the culture broth and mycelium were extracted and analyzed for the metabolite profile. The parental *A. brasiliensis* wild-type strain served as negative control. Unexpectedly, no atromentin (**6**) was identified from transformants, whereas peaks with retention times and UV-vis spectra of atrofuranic acid (**13**) and *p*-hydroxybenzoic acid (**12**) were detected (Figure 4F). Further inspection of the genomic region surrounding the *abrA* gene identified a putative biosynthesis gene cluster including a predicted hydroxylase, an oxidoreductase, an O-methyltransferase, a monooxygenase, a CYP450 protein, and an MFS transporter (Figure 4G). This leads to the speculation that if atromentin is produced under certain growth conditions, it might get instantly converted into a yet unknown metabolite. However, it appears even more likely that atrofuranic acid (**13**) is the precursor molecule for further modification in *A. brasiliensis*. Furthermore, since atrofuranic acid (**13**) was identified from both *A. niger* and *A. brasiliensis*, cross-chemistry on a benzoquinone core seems not limited to *A. niger* but appears common to *Aspergillus* species from section *Nigri*.

Phylogeny of Fungal Atromentin Synthetases

The identification of AbrA from *A. brasiliensis* acting as atromentin synthetase under *in vitro* conditions tempted us to study the phylogenetic relationship of fungal NRPS-like enzymes. The failure to produce a functional chimeric protein from the gene fusion of MelA and InvA5, but successful fusions between MelA and $AtrA_{At}$, led to the speculation of a separated phylogeny of atromentin synthetases in ascomycetes and basidiomycetes. Therefore, we extracted the thioesterase domains of all fungal NRPS-like enzymes characterized so far by using InterPro (Finn et al., 2017). Sequences were aligned by Clustal Omega (Sievers and Higgins, 2018) and used to calculate a phylogenetic tree with IQ-Tree (Kalyaanamoorthy et al., 2017) that was plotted with iTOL (Letunic and Bork, 2016). The thioesterase domain from the polyketide synthase TerA (Gressler et al., 2015) served as outgroup (Figure 5). More details are provided in STAR Methods. Indeed, atromentin synthetases originating from basidiomycetes (AtrA from *Tapinella panuoides*, InvA5 from *P. involutus*, and GreA from *Suillus grevillei*) formed a cluster that was distinct from all thioesterase domains from *Aspergillus* species. While the number of NRPS-like enzymes with known products is limited, a tendency for clustering of enzymes producing the same product also became visible among the *Aspergillus*-derived enzymes. Thereby, aspulvinone E and atromentin synthetases in particular showed a close phylogenetic relationship. This supports the idea that this close phylogenetic relationship enabled the successful generation of functional chimeric proteins. These results additionally imply that atromentin synthetases from basidiomycetes and ascomycetes evolved independently. However, additional enzymes from both families need to be characterized to confirm this assumption.

DISCUSSION

Although non-reducing NRPS-like enzymes generally only use aromatic α-keto acids as substrates, they are responsible for the formation of a large variety of different natural products. The main interconnecting core structures identified so far are furanones, benzoquinones, and dioxolanones, which arise from the action of the C-terminal thioesterase domain. However, due to the limited number of non-reducing NRPS-like enzymes characterized so far, prediction of the thioesterase chemistry by sequence pattern analysis remains difficult. Previous work suggested a catalytic triad made from serine, asparagine, and histidine in combination with a branched-chain aliphatic amino acid and two proline residues as indicative for benzoquinone core formation (Braesel et al., 2015). While this may still hold true, more discriminating amino acids seem to be required for core

structure prediction. The aspulvinone E synthetases MelA and ApvA also resemble this benzoquinone-forming amino acid pattern, but contain an essential cysteine instead of a serine in the catalytic triad. An oxidative environment (Geib et al., 2016) or the exchange of the cysteine by a serine inactivates the aspulvinone E synthetase MelA. This indicates that formation of a substrate thioester is essential for the furanone-forming chemistry of this specific thioesterase. However, other furanone core-forming enzymes with a substitution pattern different to that from aspulvinone E (**3**), such as the microperfuranone (**7**) synthetase MicA from *A. nidulans* (Yeh et al., 2012), also contain a serine rather than a cysteine and, thus, form a substrate oxoester in the active site. Therefore, the substrate thioester formation in aspulvinone E synthetases proceeds differently and depicts an exception in furanone core production rather than the rule. This shows that understanding of the precise chemistry of thioesterase domains from non-reducing NRPS-like enzymes remains limited, and more reliable predictions on the core structure formation will require the analysis of a protein crystal structure and the characterization of additional enzymes for identification of prognostic sequence patterns.

For conversion of the furanone-forming MelA protein into a benzoquinone-forming enzyme, domain swapping currently appears as the method of choice, although a close phylogenetic proximity may be a prerequisite for the success of such experiments. Previous studies have shown that the exchange of the thioesterase domain of an *A. terreus* aspulvinone E synthetase with that from an *A. terreus* butyrolactone synthetase successfully converted the enzyme into a butyrolactone IIa synthetase (van Dijk et al., 2016). Our first approach on MelA from *A. terreus* (Geib et al., 2016) in combination with InvA5 from the basidiomycete *P. involutus* (Braesel et al., 2015) failed, whereas a combination with the atromentin synthetase $AtrA_{At}$ from *A. terreus* (Hühner et al., 2018) was successful. This clearly demonstrates that a conversion is possible but may be limited to domain exchanges within species rather than across fungal divisions. In agreement, our phylogenetic analysis indicates a significant distance between NRPS-like enzymes from ascomycetes and basidiomycetes (Figure 5). The identification of an additional atromentin synthetase from *A. brasiliensis* will allow further domain exchange studies to analyze the possibility of successful combinations of NRPS-like enzymes from aspergilli deriving from different sections.

Interestingly, despite functional expression of atromentin synthetases in both *A. niger* and *A. oryzae*, we were surprised to detect only marginal amounts of atromentin in *A. niger*. The fact that we discovered the yet undescribed metabolite atrofuranic acid (**13**) as well as the metabolites gyroporin (**11**) and *p*-hydroxybenzoic acid (**12**) implies that the physiology of *A. niger* initiates a cross-specificity and cross-chemistry event on the NRPS-like enzyme.

The host-physiology-dependent cross-chemistry described here differs from that described for the biosynthesis of the meroterpenoids austinol and dehydroaustinol in *A. nidulans*, in which one biosynthesis gene cluster contains a polyketide synthase producing an orsellinic acid core structure, whereas a second biosynthesis gene cluster is responsible for the prenylation of the polyketide moiety (Lo et al., 2012). In contrast, the production of atrofuranic acid (**13**) and other products observed in *A. niger* is independent from a specific cross-acting biosynthesis gene cluster, as *A. niger* does not seem to contain its own intrinsic atromentin synthetase. It also appears unlikely that atromentin (**6**) acts as a precursor molecule for any of the metabolites in *A. niger*, as feeding with atromentin (**6**) did not result in the production of atrofuranic acid (**13**). Therefore, atrofuranic acid (**13**) may not derive from an oxidative ring-opening of atromentin (**6**). In contrast, feeding of atrofuranic acid (**13**) resulted in the production of gyroporin (**11**) and metabolite X. Based on the analysis of atrofuranic acid generated from 2-^{13}C-labeled L-tyrosine in combination with previous labeling studies performed on atromentin (Gill and Steglich, 1987), we hypothesize the biosynthesis pathway for metabolites produced in *A. niger* as proposed in Figure 6. A redirection of the chemistry of the thioesterase domain under physiologic conditions in *A. niger* gives rise to a dihydrofuroic acid, even though it is unclear whether the proposed reaction occurs with the substrate being tethered to the thioesterase domain as depicted in Figure 6. It would also be conceivable that the redirection of the thioesterase chemistry promotes the release of a linear intermediate, which is subsequently converted into a dihydrofuroic acid. In any case, dehydration and oxidation would then lead to the formation of atrofuranic acid (**13**). As we did not detect an intermediate without the final hydroxylation, this modification occurs either prior to the final release from the enzyme or instantly and quantitatively after product release. The speculation on a quantitative hydroxylation in *A. niger* without detection of an intermediate lacking the hydroxylation is also in agreement with previous studies on *A. terreus* terrein biosynthesis. Expression of the terrein synthase gene *terA* in *A. niger* should lead to the production of the polyketide 2,3-dehydro-6-hydroxymellein. However, the modified terrein precursor 6,7-dihydroxymellein was isolated from *A. niger* extracts even without traces of 2,3-dehydro-6-hydroxymellein being detected (Zaehle et al., 2014).

While *p*-hydroxybenzoate seems to spontaneously derive from incubation of atrofuranic acid in the culture broth, the biosynthesis of gyroporin (**11**) might proceed via metabolite X. Thereby, the structure of metabolite X could derive from a Piancatelli-type rearrangement (Piutti and Quartieri, 2013; Verrier et al., 2018), which is subsequently decarboxylated and oxidized to form gyroporin (**11**). Interestingly, if this biosynthetic pathway holds true, it differs from gyroporin (**11**) production as described for *P. involutus* during biosynthesis of involutin (Braesel et al., 2015). In *P. involutus*, atromentin (**6**) acts as precursor for gyroporin (**11**) biosynthesis, in which an oxidative ring contraction of atromentin (**6**) first results in the production of gyrocyanin. Gyrocyanin can then either become converted into involutin or, by a further oxidation event, into gyroporin (**6**) (Figure 6). Since atrofuranic acid (**13**) has not been detected in *P. involutus* and, in turn, gyrocyanin was not found in *A. niger*, the biosynthesis of gyroporin (**11**) may indeed differ among these organisms. However, the elucidation of the structure of the unstable metabolite X will be a prerequisite to confirm the biosynthesis route of gyroporin (**11**) in *A. niger*.

Despite the cross-chemistry events observed in *A. niger* during the expression of atromentin synthetases, this study confirmed that atromentin synthetases are not limited to basidiomycetes but seem to be widely distributed also among ascomycetes. Nevertheless, it needs to be confirmed that atromentin (**6**)

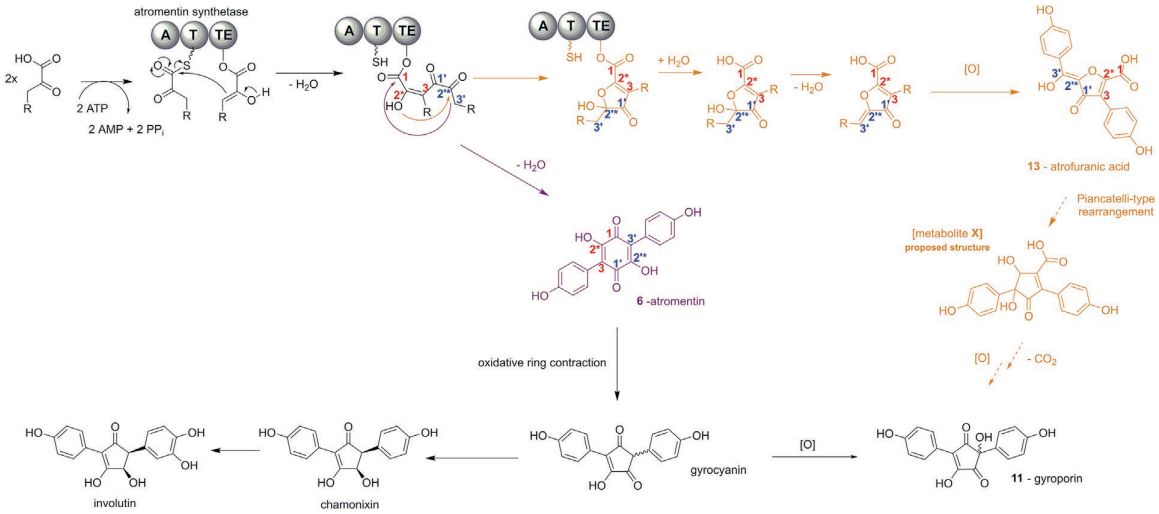

Figure 6. Proposed Scheme for Metabolite Biosynthesis

The predicted biosynthetic pathway of atrofuranic acid (**13**) is supported by molecule labeling derived from feeding 2-^{13}C-labeled L-tyrosine. The three C atoms from the two tyrosine side chains are numbered in red and blue and the ^{13}C-labeled C-atoms are indicated by an additional asterisk. The purple arrow indicates the formation of atromentin (**6**) at the thioesterase domain of atromentin synthetases, which acts as precursor for gyrocyanin that can be further converted into gyroporin (**11**) and involutin as suggested for *P. involutus*. Orange arrows indicate the formation of atrofuranic acid in *Aspergillus* species from section *Nigri*. A subsequent Piancatelli-type rearrangement and decarboxylation results in the formation of gyroporin (**11**). For NMR data of atrofuranic acid (**13**), refer to Figures S2–S4 and Table S2.

is indeed an intermediate or final metabolite produced in the original ascomycete hosts. A recent study showed that the NRPS-like enzyme AtrA$_{At}$ from *A. terreus* produces atromentin (**6**) when heterologously expressed in yeast (Hühner et al., 2018), but it needs to be confirmed that atromentin is also produced in *A. terreus*. Similarly, we discovered the atromentin synthetase AbrA from *A. brasiliensis*. When *abrA* was expressed in the *A. oryzae* expression platform, atromentin (**6**) was produced in significant amounts and no other by-products were observed. Not unexpectedly, expression in *A. niger* resulted in the production of *p*-hydroxybenzoic acid (**12**), gyroporin (**11**), and, mainly, atrofuranic acid (**13**). However, most interestingly, when *abrA* was homologously expressed in *A. brasiliensis*, atrofuranic acid (**13**) rather than atromentin (**6**) was the major metabolite produced. This suggests that: (1) atromentin (**6**) also undergoes cross-chemistry in *A. brasiliensis*, indicating that modifications of benzoquinone core structures are common to *Aspergillus* species of the section *Nigri*; and (2) atromentin (**6**) is unlikely to be a product that can be identified from *A. brasiliensis*. Finally, as *A. brasiliensis* produces atrofuranic acid (**13**), it appears unlikely that the genes forming a putative biosynthesis gene cluster with *abrA* (Figure 4G) act on atromentin (**6**). Additional analyses will be required to identify the respective metabolite(s) produced in *A. brasiliensis*, but the existence of these possibly modifying enzymes also supports the function of non-reducing NRPS-like enzymes to act as producers of core intermediates in secondary metabolite biosynthesis. Further examples for such biosynthesis gene clusters are the formation of Asp-melanin (Geib et al., 2016) and aspulvinone H (**9**) (Guo et al., 2013) from aspulvinone E (**3**), involutin from atromentin (**6**), (Braesel et al., 2015) or terrequinone A (**1**) from didemethylasterriquinone (Schneider et al., 2007; Balibar et al., 2007). Given the fact that NRPS-like enzymes are widespread in fungal genomes and their metabolites have hardly been characterized as yet, these enzymes and their accompanying biosynthesis gene clusters provide a treasure chest for metabolites of pharmacological interest. Nevertheless, characterization of products from NRPS-like enzymes may be hampered by cross-chemistry occurring on metabolite core structures during heterologous expression. Therefore, it is recommended to use different heterologous expression platforms in parallel to elucidate the true nature of products formed from uncharacterized NRPS-like enzymes.

SIGNIFICANCE

While terpenes, polyketides, and products from non-ribosomal peptide synthetases (NRPS) are known for a great variety of biological activities, products from NRPS-like enzymes are less well studied. However, metabolites analyzed so far show phytotoxic, antiviral, antiproliferative, and antidiabetic activities, making them interesting candidates for further exploitation. NRPS-like enzymes with a C-terminal thioesterase domain catalyze the condensation of two aromatic α-keto acids by forming connecting indolylquinone, benzoquinone, dioxolanone, or furanone core structures, but the exact reaction mechanisms are hardly understood. Current knowledge on sequence patterns in thioesterase domains is too limited for core structure prediction, as the *A. terreus* furanone-forming aspulvinone E synthetase MelA was not converted into a quinone-forming atromentin synthetase by site-directed mutagenesis. However, mutagenesis experiments confirmed that MelA forms a substrate thioester, which is unprecedented in NRPS-like enzymes. Despite the inability of MelA conversion into an atromentin

synthetase by site-directed mutagenesis, this was successfully achieved by domain swapping. Conversion required use of a thioesterase domain from an atromentin synthetase of the same species. This successful reassembly from closely related enzymes may also explain the expansion in the number of NRPS-like enzymes in individual fungal species. Furthermore, this study demonstrated that host physiology in heterologous expression has a significant impact on product formation. While atromentin synthetases produce atromentin *in vitro* and in *A. oryzae*, cross-chemistry directs the formation of atrofuranic acid and eventually gyroporin in *A. niger*. This cross-chemistry was not limited to *A. niger* but also occurred in *A. brasiliensis*, which contains an intrinsic atromentin synthetase. Therefore, a single enzyme can form different products depending on the physiology of the producer. While this cross-chemistry widens the product portfolio from NRPS-like enzymes, a single expression platform might be insufficient when analyzing product formation from yet uncharacterized secondary metabolite biosynthesis genes.

STAR★METHODS

Detailed methods are provided in the online version of this paper and include the following:

- KEY RESOURCES TABLE
- CONTACT FOR REAGENT AND RESOURCE SHARING
- EXPERIMENTAL MODEL AND SUBJECT DETAILS
- METHOD DETAILS
  - Preparation of Conidia Suspensions and Selection of Fungal Transformants
  - Generation of Expression Platform Strains *A. niger* NP4, *A. oryzae* OP12 and *pyrG*$^{-}$ Strains
  - Generation of a URA-Blaster Cassette for Transformation of *pyrG*- Expression Platform Strains
  - Generation of Expression Constructs for Production of NRPS-like and Chimeric Proteins
  - Fungal Transformation and Transformant Analysis
  - Southern Blot Analysis
  - Heterologous Expression and Purification of Proteins
  - *In Vitro* Assays
  - Secondary Metabolite Analysis
  - Isolation and Structure Elucidation of Natural Products
  - Phylogenetic Tree Construction
- QUANTIFICATION AND STATISTICAL ANALYSIS
- DATA AND SOFTWARE AVAILABILITY
- ADDITIONAL RESOURCES

SUPPLEMENTAL INFORMATION

Supplemental Information includes five figures and five tables and can be found with this article online at https://doi.org/10.1016/j.chembiol.2018.10.021.

ACKNOWLEDGMENTS

We thank Andrea Perner for HR-ESI-MS analysis and Heike Heinecke for recording NMR spectra. We are grateful to the School of Life Sciences of the University of Nottingham (UK) for financial support and a scholarship to E.G. F.B. thanks the graduate school Jena School for Microbial Communication for a PhD fellowship.

AUTHOR CONTRIBUTIONS

E.G. and M.B. conceived and designed experiments. E.G., M.B., F.B., and M.D. performed experiments. M.N., F.B., and M.D. analyzed NMR data. All authors contributed to writing of the manuscript and approved the final version.

DECLARATION OF INTERESTS

All authors declare no conflicts of interest.

Received: May 18, 2018
Revised: September 7, 2018
Accepted: October 22, 2018
Published: December 6, 2018

REFERENCES

Balibar, C.J., Howard-Jones, A.R., and Walsh, C.T. (2007). Terrequinone A biosynthesis through L-tryptophan oxidation, dimerization and bisprenylation. Nat. Chem. Biol. *3*, 584–592.

Besl, H., Bresinsky, A., Steglich, W., and Zipfel, K. (1973). Pilzpigmente, {XVII}. Über Gyrocyanin, das blauende Prinzip des Kornblumenröhrlings (*Gyroporus cyanescens*), und eine oxidative Ringverengung des Atromentins. Chem. Ber. *106*, 3223–3229.

Bok, J.W., Hoffmeister, D., Maggio-Hall, L.A., Murillo, R., Glasner, J.D., and Keller, N.P. (2006). Genomic mining for *Aspergillus* natural products. Chem. Biol. *13*, 31–37.

Braesel, J., Götze, S., Shah, F., Heine, D., Tauber, J., Hertweck, C., Tunlid, A., Stallforth, P., and Hoffmeister, D. (2015). Three redundant synthetases secure redox-active pigment production in the basidiomycete *Paxillus involutus*. Chem. Biol. *22*, 1325–1334.

Brock, M., Darley, D., Textor, S., and Buckel, W. (2001). 2-Methylisocitrate lyases from the bacterium *Escherichia coli* and the filamentous fungus *Aspergillus nidulans*: characterization and comparison of both enzymes. Eur. J. Biochem. *268*, 3577–3586.

Chattaway, F.D. (1931). CCCXLII.—Acetylation in aqueous alkaline solutions. J. Chem. Soc. 2495–2496.

Dellafiora, L., Aichinger, G., Geib, E., Sánchez, L., Brock, M., Cánovas, D., Dall'Asta, C., and Marko, D. (2019). Hybrid *in silico/in vitro* target fishing to assign function to "orphan" compounds of food origin - the case of the fungal metabolite atromentin. Food Chem. *270*, 61–69.

Dewi, R.T., Tachibana, S., and Darmawan, A. (2012). Antidiabetic and antioxidative activities of butyrolactone I from *Aspergillus terreus* MC751. World Acad. Sci. Eng. Technol. Int. J. Biotechnol. Bioeng. *6*, 929–934.

van Dijk, J.W.A., Guo, C., and Wang, C.C.C. (2016). Engineering fungal nonribosomal peptide synthetase-like enzymes by heterologous expression and domain swapping. Org. Lett. *18*, 6236–6239.

Finn, R.D., Attwood, T.K., Babbitt, P.C., Bateman, A., Bork, P., Bridge, A.J., Chang, H., Dosztányi, Z., El-Gebali, S., Fraser, M., et al. (2017). InterPro in 2017-beyond protein family and domain annotations. Nucleic Acids Res. *45*, D190–D199.

Fleck, C.B., and Brock, M. (2010). *Aspergillus fumigatus* catalytic glucokinase and hexokinase: expression analysis and importance for germination, growth, and conidiation. Eukaryot. Cell *9*, 1120–1135.

Geib, E., and Brock, M. (2017). ATNT: an enhanced system for expression of polycistronic secondary metabolite gene clusters in *Aspergillus niger*. Fungal Biol. Biotechnol. *4*, 13.

Geib, E., Gressler, M., Viediernikova, I., Hillmann, F., Jacobsen, I.D., Nietzsche, S., Hertweck, C., and Brock, M. (2016). A non-canonical melanin biosynthesis pathway protects *Aspergillus terreus* conidia from environmental stress. Cell Chem. Biol. *23*, 587–597.

Gill, M., and Steglich, W. (1987). Pigments of fungi (macromycetes). In Fortschritte der Chemie organischer Naturstoffe/Progress in the Chemistry

of Organic Natural Products, *vol. 51*, W. Herz, H. Grisebach, G.W. Kirby, and C.H. Tamm, eds. (Springer), pp. 1–297.

Gressler, M., Hortschansky, P., Geib, E., and Brock, M. (2015). A new high-performance heterologous fungal expression system based on regulatory elements from the *Aspergillus terreus* terrein gene cluster. Front. Microbiol. *6*, 184.

Guo, C., Knox, B.P., Sanchez, J.F., Chiang, Y., Bruno, K.S., and Wang, C.C.C. (2013). Application of an efficient gene targeting system linking secondary metabolites to their biosynthetic genes in *Aspergillus terreus*. Org. Lett. *15*, 3562–3565.

He, J., Wijeratne, E.M.K., Bashyal, B.P., Zhan, J., Seliga, C.J., Liu, M.X., Pierson, E.E., Pierson, L.S., VanEtten, H.D., and Gunatilaka, A.A.L. (2004). Cytotoxic and other metabolites of *Aspergillus* inhabiting the rhizosphere of Sonoran desert plants. J. Nat. Prod. *67*, 1985–1991.

Hoang, D.T., Chernomor, O., von Haeseler, A., Minh, B.Q., and Vinh, L.S. (2018). UFBoot2: improving the ultrafast bootstrap approximation. Mol. Biol. Evol. *35*, 518–522.

Hühner, E., Backhaus, K., Kraut, R., and Li, S. (2018). Production of α-keto carboxylic acid dimers in yeast by overexpression of NRPS-like genes from *Aspergillus terreus*. Appl. Microbiol. Biotechnol. *102*, 1663–1672.

Kalyaanamoorthy, S., Minh, B.Q., Wong, T.K.F., von Haeseler, A., and Jermiin, L.S. (2017). ModelFinder: fast model selection for accurate phylogenetic estimates. Nat. Methods *14*, 587–589.

Letunic, I., and Bork, P. (2016). Interactive tree of life (iTOL) v3: an online tool for the display and annotation of phylogenetic and other trees. Nucleic Acids Res. *44*, W242–W245.

Lo, H., Entwistle, R., Guo, C., Ahuja, M., Szewczyk, E., Hung, J., Chiang, Y., Oakley, B.R., and Wang, C.C.C. (2012). Two separate gene clusters encode the biosynthetic pathway for the meroterpenoids austinol and dehydroaustinol in *Aspergillus nidulans*. J. Am. Chem. Soc. *134*, 4709–4720.

Molitor, D., Liermann, J.C., Berkelmann-Löhnertz, B., Buckel, I., Opatz, T., and Thines, E. (2012). Phenguignardic acid and guignardic acid, phytotoxic secondary metabolites from *Guignardia bidwellii*. J. Nat. Prod. *75*, 1265–1269.

Piutti, C., and Quartieri, F. (2013). The Piancatelli rearrangement: new applications for an intriguing reaction. Molecules *18*, 12290–12312.

Rodrigues-Heerklotz, K., Drandarov, K., Heerklotz, J., Hesse, M., and Werner, C. (2001). Guignardic acid, a novel type of secondary metabolite produced by the endophytic fungus *Guignardia* sp.: isolation, structure elucidation, and asymmetric synthesis. Helv. Chim. Acta *84*, 3766–3772.

Schimmel, T.G., Coffman, A.D., and Parsons, S.J. (1998). Effect of butyrolactone I on the producing fungus, *Aspergillus terreus*. Appl. Environ. Microbiol. *64*, 3707–3712.

Schneider, P., Weber, M., Rosenberger, K., and Hoffmeister, D. (2007). A one-pot chemoenzymatic synthesis for the universal precursor of antidiabetes and antiviral bis-indolylquinones. Chem. Biol. *14*, 635–644.

Shah, F., Schwenk, D., Nicolás, C., Persson, P., Hoffmeister, D., and Tunlid, A. (2015). Involutin is an Fe^{3+} reductant secreted by the ectomycorrhizal fungus *Paxillus involutus* during Fenton-based decomposition of organic matter. Appl. Environ. Microbiol. *81*, 8427–8433.

Sievers, F., and Higgins, D.G. (2018). Clustal Omega for making accurate alignments of many protein sequences. Protein Sci. *27*, 135–145.

Sun, W., Guo, C., and Wang, C.C.C. (2016). Characterization of the product of a nonribosomal peptide synthetase-like (NRPS-like) gene using the doxycycline dependent Tet-on system in *Aspergillus terreus*. Fungal Genet. Biol. *89*, 84–88.

Verrier, C., Moebs-Sanchez, S., Queneau, Y., and Popowycz, F. (2018). The Piancatelli reaction and its variants: recent applications to high added-value chemicals and biomass valorization. Org. Biomol. Chem. *16*, 676–687.

Wackler, B., Schneider, P., Jacobs, J.M., Pauly, J., Allen, C., Nett, M., and Hoffmeister, D. (2011). Ralfuranone biosynthesis in *Ralstonia solanacearum* suggests functional divergence in the quinone synthetase family of enzymes. Chem. Biol. *18*, 354–360.

Yeh, H., Chiang, Y., Entwistle, R., Ahuja, M., Lee, K., Bruno, K.S., Wu, T., Oakley, B.R., and Wang, C.C.C. (2012). Molecular genetic analysis reveals that a nonribosomal peptide synthetase-like (NRPS-like) gene in *Aspergillus nidulans* is responsible for microperfuranone biosynthesis. Appl. Microbiol. Biotechnol. *96*, 739–748.

Zaehle, C., Gressler, M., Shelest, E., Geib, E., Hertweck, C., and Brock, M. (2014). Terrein biosynthesis in *Aspergillus terreus* and its impact on phytotoxicity. Chem. Biol. *21*, 719–731.

STAR★METHODS

KEY RESOURCES TABLE

REAGENT or RESOURCE	SOURCE	IDENTIFIER
Bacterial and Fungal Strains		
E. coli DH5α	Zymo Research	Zymo 5α
A. niger A1144 P2 (P*amyB*:*terR_ptrA*)	(Gressler et al., 2015)	N/A
A. niger P2 *melA* (P*terA*:*melA_ble*)	(Geib et al., 2016)	N/A
A. niger P2 $melA_{C\rightarrow S}$ (P*terA*:$melA_{C\rightarrow S}$ *_ble*)	This study	N/A
A. niger P2 $melA_{N\rightarrow D}$ (P*terA*:$melA_{N\rightarrow D}$ *_ble*)	This study	N/A
A. niger P2 $melA_A$:$invA5_{T\text{-}TE}$ (P*terA*:$melA_A$:$invA5_{T\text{-}TE}$*_ble*)	This study	N/A
A. niger ATNT16 (TetOn:*terR_ble*)	(Geib and Brock, 2017)	N/A
A. niger ATNT16Δ*pyrG*x24 (TetOn:*terR_ble*; Δ*pyrG*::*ptrA*)	This study	N/A
A. niger N402	American Type Culture Collection	N402
A. niger N402 NP4 (P*amyB*:*terR_ptrA*)	This study	N/A
A. niger NP4 *invA5* (P*terA*:*invA5_ble*)	This study	N/A
A. niger P2 *invA5* (P*terA*:*invA5_ble*)	This study	N/A
A. oryzae RIB40	American Type Culture Collection	RIB40
A. oryzae RIB40 OP12 (P*amyB*:*terR_ptrA*)	This study	N/A
A. oryzae RIB40 OP12_$pyrG^-$ (P*amyB*:*terR_ptrA*; $pyrG^-$)	This study	N/A
A. oryzae OP12 *melA* (P*terA*:*melA_ble*)	This study	N/A
A. oryzae OP12 *invA5* (P*terA*:*invA5_ble*)	This study	N/A
A. brasiliensis CBS101740	CBS-KNAW Collection	CBS101740
A. niger ATNT16 *abrA* (P*terA*:*abrA_hph*)	This study	N/A
A. oryzae OP12 $pyrG^-$ *abrA* (P*terA*:*abrA*_URA)	This study	N/A
A. brasiliensis OE *abrA* (P*gpdA*:*abrA_ptrA*)	This study	N/A
Chemicals, Peptides, and Recombinant Proteins		
VinoTaste Pro	Novozymes	Free sample
Lysing enzyme from *Trichoderma harzianum*	Sigma Aldrich	Cat#L1412
DMSO-d_6	Deutero	Cat#00905-10ml
4-Hydroxylphenylpyruvic acid	Sigma Aldrich	Cat#114286
Taq DNA Polymerase	New England BioLabs	Cat#M0273S
Phusion Green Hot Start II High-Fidelity DNA Polymerase	ThermoFisher Scientific	Cat#F537S
Phire Green Hot Start II DNA Polymerase	ThermoFisher Scientific	Cat#F124L
digoxigenin-11-dUTP	Sigma Aldrich	Cat#11093088910
anti-digoxigenin-alkaline phosphatase Fab fragments	Sigma Aldrich	Cat#11093274910
CDPstar	Sigma Aldrich	Cat#12041677001
Soluble Starch	Fisher Scientific	Cat#DF0178-17-7
Acetic anhydride puriss. p.a., ACS Reag.	Fluka	Cat#45830
Pyridin, EMSURE® ACS Reag.	Merck	Cat#1.09728.0500
Critical Commercial Assays		
In-Fusion® HD Cloning System	Takara/Clonetech	Cat#639647
MasterPure Yeast DNA kit	Epicenter	Cat#MPY80200
Mix & Go!	Zymo Research	Cat#T3001
Oligonucleotides		
	See Table S4	

(*Continued on next page*)

Continued

REAGENT or RESOURCE	SOURCE	IDENTIFIER
Recombinant DNA		
P*amyB*:*terR_ptrA*_pUC19	(Gressler et al., 2015)	N/A
SM-Xpress	(Gressler et al., 2015)	N/A
*his*_SM-Xpress	(Geib et al., 2016)	N/A
*his*_SM-Xpress_*hph*	This study	N/A
P*terA*:*his_melA_ble*_SM-Xpress	(Geib et al., 2016)	N/A
P*terA*:*his_melA*$_{C\rightarrow S}$ _*ble*_SM-Xpress	This study	N/A
P*terA*:*his_melA*$_{N\rightarrow D}$ _*ble*_SM-Xpress	This study	N/A
P*terA*:*his_melA*$_{A}$:*invA5*$_{T\text{-}TE}$_*ble*_SM-Xpress	This study	N/A
P*terA*:*his_invA5_ble*_SM-Xpress	This study	N/A
P*terA*:*abrA_his*_SM-Xpress_*hph*	This study	N/A
P*terA*:*abrA_his*_SM-Xpress_URA blaster	This study	N/A
pJET1.2/blunt (CloneJET)	ThermoFisher Scientific	Cat#K1232
*ptrA*_pJET1.2	(Fleck and Brock, 2010)	N/A
*ble*_pUC19	(Geib and Brock, 2017)	N/A
P*gpdA*:*abrA_ptrA*_pJET1.2	This study	N/A
Software and Algorithms		
ChemStation version Rev. B. 04. 03 [16]	Agilent	N/A
Chromeleon version 7.2	ThermoFisher Scientific	N/A
TopSpin version 3.5pl7	Bruker BipSpin	www.bruker.com/service/support-upgrades/software-downloads/nmr/free-topspin-processing/free-topspin-download.html
Other		
Dionex UltiMate3000	ThermoFisher Scientific	N/A
Eclipse XDB-C18 (4.6 × 150 mm, 5 μm)	Agilent	N/A
Agilent 1200 HPLC with autosampler, DAD and fraction collector	Agilent	N/A
EASYstrainer 40 μm	Greiner bio-one	Cat#542040
Amersham Nylon-Hybond^{+}	GE Healthcare	Cat#RPN303B
SpeedCycler^{2}	Analytik Jena	N/A
Miracloth	VWR	Cat#475855-1
Amicon 15-Ultra, 30 kDa cut-off	Merck	Cat#UFC803024
CHROMABOND C_{18}ec-column (0.5g)	MACHEREY-NAGEL	Cat#730014
Bruker Avance III spectrometer 500Mhz	Bruker	N/A
Bruker Avance III spectrometer 600Mhz	Bruker	N/A

CONTACT FOR REAGENT AND RESOURCE SHARING

Further information and reasonable requests for resources and reagents should be directed to and will be fulfilled by the Lead Contact, Matthias Brock (Matthias.brock@nottingham.ac.uk).

Requests for fungal strains and plasmids will need a material transfer agreement (MTA), if a use is intended.

EXPERIMENTAL MODEL AND SUBJECT DETAILS

The *A. niger* strain FGSC A1144 (Fungal Genetics Stock Center, Manhattan, Kansas, USA) served as parental wild-type strain for generation of the expression platform strains *A. niger* P2 (Gressler et al., 2015) and ATNT16 (Geib and Brock, 2017). *A. niger* strain N402 (also known as ATCC 64974; American Type Culture Collection, Manassas, Virginia, USA) was used as parental strain for generation of the expression platform strain NP4. *A. oryzae* RIB40 (also known as ATCC 42149, American Type Culture Collection) served as parental strain for generating the expression platform strain OP12. In addition, the A. *brasiliensis* strain CBS 101740 (CBS-KNAW

Collection, Utrecht, Netherlands) was used in this study. Genotypes of individual transformants and media compositions are listed in the Key Resources Table or Table S5. All *Aspergillus* strains were cultivated at 28°C. Liquid cultures were agitated on a rotary shaker at 150 rpm.

METHOD DETAILS

Preparation of Conidia Suspensions and Selection of Fungal Transformants

Conidia suspensions were prepared from agar slopes of AMM(-N)G50Gln10 solidified with 2% agar. Slopes were overlaid with 4 ml of phosphate buffered saline (PBS) containing 0.01% Tween 20 and conidia were collected by scrapping cultures with a cotton swab. For inoculation of media with a defined amount of conidia, suspensions were filtered through a 40 μm cell strainer (Greiner bio-one), washed once with PBS/Tween and counted by use of an improved Neubauer chamber. For selection of *A. niger* transformants either 140 μg/ml hygromycin B, 40 μg/ml phleomycin or 0.1 μg/ml pyrithiamine were used. For selection of *A. oryzae* transformants either 30 μg/ml phleomycin or 0.1 μg/ml pyrithiamine were added. Transformants from *A. brasiliensis* were selected by media supplementation with 0.1 μg/ml pyrithiamine. For transformation of expression platform strains ATNT16Δ*pyrG*x24 and OP12_*pyrG*$^{-}$ with deleted or disrupted *pyrG* gene the *pyrG* gene from *A. nidulans* FGSC A4 was used as a selection marker and protoplasts were regenerated on media without addition of 10 mM uridine.

Generation of Expression Platform Strains *A. niger* NP4, *A. oryzae* OP12 and *pyrG*$^{-}$ Strains

To generate alternative expression platform strains the wild-type strains *A. niger* N402 and *A. oryzae* RIB40 were selected as parental strains. Both strains were transformed with a P*amyB*:*terR_ptrA* plasmid (Gressler et al., 2015) that contains the *A. terreus* transcriptional regulator gene *terR* under control of the *A. oryzae* amylase promoter P*amyB* and the *ptrA* gene as pyrithiamine resistance marker for selection of transformants. Resulting transformants were checked by Southern blot analysis for single copy integration of the construct, resulting in the selection of *A. niger* NP4 and *A. oryzae* OP12 as alternative expression platform strains. For using the *pyrG* gene from *A. nidulans* as selectable marker in transformation of the expression platform strains *A. niger* ATNT16 and *A. oryzae* OP12, the intrinsic *pyrG* genes were either deleted or disrupted. For generating an OP12 *pyrG* negative strain 1×10^8 conidia were plated on 50 mM HEPES pH 7.0 buffered AMM(-N)G50Gln10 solid medium containing 20 mM uridine and 2 mg/ml fluoroorotic acid (Melford Biolaboratories). Plates were incubated at 28°C for 7 days and three individual colonies were recovered. Subsequent plating on media with or without 10 mM uridine confirmed uridine auxotrophy of the strains. Genomic DNA was isolated from one of the strains, the *pyrG* gene amplified and sequenced. Sequencing results with P1+P2 (see Table S4 for oligonucleotide sequences) confirmed a deletion of 8 bases at position 583-590bp in the *pyrG* coding region. The strain was termed OP12_*pyrG*$^{-}$. For ATNT16 a *pyrG* deletion cassette was generated by amplifying a 1 kb upstream region with oligonucleotides P3+P4 and a 1 kb downstream region with P5+P6. Oligonucleotides contained overlapping sequences to the *Kpn*I restriction site of pUC 19 and to the *Not*1 excised *ptrA* gene from plasmid *ptrA*_pJET1.2. The three fragments were assembled with the *Kpn*I restricted pUC19 vector by *in vitro* recombination. The deletion fragment was excised by *Kpn*I restriction and used for transformation of *A. niger* ATNT16 using pyrithiamine as selection marker. Resulting transformants were repeatedly streaked on pyrithiamine containing plates before tested for uridine auxotrophy. Southern blot analysis confirmed that strain ATNT16Δ*pyrG*x24 contained a *pyrG* deletion without ectopic integrations of the deletion construct and was used as *pyrG* negative ATNT16 strain in subsequent studies.

Generation of a URA-Blaster Cassette for Transformation of *pyrG*- Expression Platform Strains

For transformation of *pyrG* negative fungal expression platform strains a URA-blaster cassette was generated. The cassette consisted of a direct repeat of an 800 bp internal *E. coli prpB* fragment flanking the entire *A. nidulans pyrG* gene including its promoter and terminator region. The direct repeats enable excision of the *pyrG* gene by mitotic recombination allowing the marker to be re-used in subsequent transformation approaches. As recipient plasmid for the URA-blaster cassette the *ble*-gene was excised by *Not*I restriction from plasmid pUC-*ble* (Geib and Brock, 2017) leaving a *Not*I restriction site in the resulting pUC_*Not*I plasmid. The direct repeats of the *prpB* gene with overlaps to the *Not*I restriction site of pUC_*Not*I and the *A. nidulans pyrG* gene were amplified from plasmid pQE30_*prpB* (Brock et al., 2001) with oligonucleotides P7+P8 and P9+P10. A 1900 bp fragment enclosing the *A. nidulans pyrG* gene was amplified from genomic DNA of *A. nidulans* strain FGSC A4 with oligonucleotides P11+P12. The three PCR fragments were mixed with the *Not*I-restricted pUC_*Not*I plasmid and the URA-blaster cassette was assembled by *in vitro* recombination using the In-Fusion® HD Cloning System (Takara/Clonetech). The URA-blaster was excised by *Not*I restriction and used to replace alternative resistance markers in SM-Xpress plasmids.

Generation of Expression Constructs for Production of NRPS-like and Chimeric Proteins

All PCR amplifications for gene cloning procedures were carried out by using the Phusion Green Hot Start II High-Fidelity DNA Polymerase (ThermoFisher Scientific) in a SpeedCycler^{2} (Analytik Jena). PCR for generation of the mutated $melA_{C\rightarrow S}$ gene producing the amino acid exchange C733S was performed with oligonucleotide pair P13+P14 and P15+P16. Similarly, PCR for generation of the mutated $melA_{N\rightarrow D}$ producing the amino acid exchange N760D was performed with P13+P17 and P18+P19. The chimeric $melA_{A}$:$invA5_{T\text{-}TE}$ construct was assembled by amplifying the *melA* part with P13+P20 and the *invA5* part with P21+P22. The complete *invA5* gene was amplified with P23+P22. Assembly of the respective amplicons in SM-Xpress plasmids was performed by *in vitro*

recombination using the In-Fusion® HD Cloning System (Takara/Clonetech). For full-length expression of the *melA* gene in *A. oryzae* OP12, the previously generated plasmid his_*melA*-SM-Xpress (Geib et al., 2016) was used for fungal transformation.

For heterologous expression of the $atrA_{At}$ gene and gene fusions of *melA* and $atrA_{At}$ in *A. niger* ATNT16Δ*pyrG*x24 and *A. oryzae* OP12*pyrG*$^{-}$, PCR was performed on genomic DNA of *A. terreus* wild-type strains SBUG844 and A1156. The full-length $atrA_{At}$ gene was amplified with oligonucleotides P24+P25 and cloned by *in vitro* recombination into the *his*-SM-Xpress_URA plasmid. For the gene fusion construct $melA_{(A)}$:$atrA_{At(T\text{-}TE)}$ (C1) the *melA* sequence was amplified with oligonucleotides P26+P27 and the $atrA_{At}$ sequence with P28+P25. For the gene fusion construct $melA_{(A\text{-}T)}$:$atrA_{At(TE)}$ (C2) the *melA* sequence was amplified with oligonucleotides P26+P29 and the $atrA_{At}$ sequence with P30+P25. Finally, for the gene fusion construct $atrA_{At(A\text{-}T)}$:$melA_{(TE)}$ (C2) the $atrA_{At}$ sequence was amplified with oligonucleotides P24+P40 and the *melA* sequence with P41+P42.

For heterologous expression of the *abrA* gene in *A. niger* and *A. oryzae* expression platform strains the gene was amplified from genomic DNA of *A. brasiliensis* CBS101740 using oligonucleotides P31+P32. The resulting PCR fragment was fused by *in vitro* recombination with plasmid *his*_SM-Xpress_*hph* in which the original phleomycin resistance gene was replaced by the hygromycin B resistance cassette *hph*.

For homologous constitutive expression of the *A. brasiliensis abrA* gene in *A. brasiliensis* the gene was placed under control of the *gpdA* promoter from *A. nidulans*. The 992 bp promoter region of the *gpdA* gene was amplified with P33+P34 from genomic DNA of *A. nidulans* strain FGSC A4. The *abrA* gene was amplified from genomic DNA of *A. brasiliensis* CBS101740 with P35+P36. Both amplicons were fused by *in vitro* recombination into the *Hind*III (ThermoFisher Scientific) restricted *ptrA*_pJET1.2 plasmid (Fleck and Brock, 2010).

All assembled plasmids were transferred into and propagated in chemically competent *Escherichia coli* DH5α (Mix & Go!, Zymo Research). Plasmids were purified using the NucleoSpin Plasmid kit (Macherey and Nagel).

Fungal Transformation and Transformant Analysis

Mycelia for protoplast generation were generated by inoculating YEPD media with 2 - 3 × 10^6 conidia/ml of the strain to be transformed. After 22 h mycelium was harvested and incubated for 1 h at 28°C without agitation in citrate-phosphate buffer pH 7.3 containing 10 mM dithiotreitol. Protoplasts were generated in 20 ml potassium phosphate-buffered (pH 5.8) osmotic medium with 0.6 M potassium chloride as osmotic stabiliser and 1.3 g VinoTaste Pro (Novozymes) and 0.1g lysing enzyme (Sigma-Aldrich). Protoplasts were washed and mixed with the respective plasmids and PEG solution (25% PEG8000, 50 mM $CaCl_2$, 10 mM Tris/HCl pH 7.5) and incubated for 30 min on ice. After transformation protoplasts were regenerated on AMM(-N)G50Gln10 agar plates containing 1.2 M sorbitol as osmotic stabiliser and the respective selection marker (Geib and Brock, 2017).

Transformants were streaked twice onto AMM(-N)G50Gln10 agar containing the respective selectable marker. Genomic DNA from individual transformants was purified using the MasterPure Yeast DNA kit (Epicenter). Transformants carrying the P*amyB*:*terR* construct for generation of expression platform strains were checked by Southern Blot analysis for single copy integration. All other transformants carrying specific heterologous gene expression constructs were checked either by Southern Blot or diagnostic PCR using Phire Green Hot Start II DNA Polymerase (ThermoFisher Scientific) and oligonucleotides P37+P38 for NRPS-like enzyme genes and P33+P39 for homologous *abrA* overexpression.

Southern Blot Analysis

Southern Blots were performed by restriction of genomic DNA with suitable restriction enzymes, separation on a 0.8% agarose gel and transfer of fragments to a positively charged nylon membrane (Amersham Nylon-Hybond^{+}, GE Healthcare). Gene specific probes were amplified with Taq DNA Polymerase (NEB) and labelled by incorporation of digoxigenin-11-dUTP (Roche). Hybridisation was performed over night at 65°C and bands were visualised by subsequent hybridisation with anti-digoxigenin-alkaline phosphatase Fab fragments (Roche) and CDPstar (Roche) as substrate.

Heterologous Expression and Purification of Proteins

All NRPS-like enzymes were cloned with an *N*-terminal His-tag peptide. Protein purification followed a protocol as previously described (Geib et al., 2016). In brief, strains were grown in AMM(-N)Starch2%Gln20Talc for 32 - 40 h at 28°C under constant shaking at 150 rpm. Mycelium was harvested over Miracloth filter gauze (Merck), rinsed with tap water, pressed dry between paper tissues and frozen in liquid nitrogen. The mycelium was ground under liquid nitrogen to a fine powder, suspended in buffer A (50 mM Tris/HCl pH 7.5, 150 mM NaCl and 10% glycerol) and disrupted further by ultrasonication. The cell-free extract and cell debris were separated by centrifugation at 17 000 × g and filtered through a 0.45 μm filter (Sartorius). For purification a 3 ml Ni-Sepharose 6 Fast Flow (GE Healthcare) gravity flow column was used. After application of the cell-free extract, the column was washed with 4 volumes of buffer A supplemented with 20 mM imidazole and eluted with buffer A supplemented with 200 mM imidazole. Proteins were desalted by centrifugal concentration (Amicon 15-Ultra, 30 kDa cut-off, Millipore) and stored in 50% glycerol with 1 mM dithiothreitol at -20°C.

In Vitro Assays

In vitro product formation from NRPS-like enzymes followed a protocol as previously described (Geib et al., 2016) with some minor modifications. Purified proteins (0.5 – 1 mg) or cell-free extract (600 μl; 6 mg total protein) were mixed in a final volume of 5 ml with

PIPES buffer pH 7.5 (100 mM), ATP (10 mM), $MgCl_2$ (15 mM) and 7.5 mM *p*-hydroxyphenylpyruvate. Optionally, 3 mM DTT were added to enzymes containing a cysteine residue in the active site of the thioesterase domain. Assays were incubated for 18 h at 28°C in the dark with gentle agitation. For metabolite extraction assays were acidified to pH 3.5 with HCl and incubated for 10 min on ice. Precipitates were collected by centrifugation. Both, pellet and supernatant, were extracted separately with ethyl acetate. The organic solvent was evaporated under reduced pressure, the residue solved in methanol and analysed by HPLC as described.

Secondary Metabolite Analysis

For secondary metabolite analysis liquid cultures of AMM(-N)G50Gln10 (*A. niger*) or AMM(-N)Starch2%Gln20 (*A. oryzae*) were inoculated with 1×10^6 conidia/ml. For metabolite extraction from time dependent incubation AMM(-N)G100Gln20 was used. For induction of heterologous gene expression in *A. niger* ATNT16 strains the medium was additionally supplemented with 10 μg/ml doxycycline. After 36 - 48 h or at specifically indicated time points, cultures were harvested and separated into a cell-free culture filtrate and mycelium. Both fractions were extracted with ethyl acetate. The organic solvent layer was collected, dried over anhydrous sodium sulphate and evaporated under reduced pressure. Residual compounds were solved in methanol and subjected to HPLC analysis using a Dionex UltiMate3000 (ThermoFisher Scientific) and an Eclipse XDB-C18 column (4.6 × 150 mm, 5 μm; Agilent) following a gradient (COR_ESIA) of water + 0.1% formic acid (solvent A) and methanol (solvent B) with a flow rate of 1 ml/min: 0.5 min 10% B, 15 min 90% B, 17 min 90% B, 17.5 min 100% B, 22 min 100% B, 23 min 10% B, 25 min 10% B. For more detailed resolution of metabolites obtained from the time dependent extraction of *A. niger* P2 strains expressing the *invA5* gene a modified gradient (COR_ESIA_25-50) was applied at a flow rate of 1 ml/min: 0.5 min 10% B, 1.5 min 25% B, 12 min 50% B, 14 min 90% B, 15 min 100%B, 18 min 100% B, 20 min 10% B, 24 min 10% B.

High-resolution electrospray ionisation mass spectrometry (HR-ESI-MS) was carried out on an Accela UPLC-system combined with an Exactive mass spectrometer (Thermo Scientific). Separation of individual metabolites was achieved by using a Betasil C18 column (2.1 ×150 mm, 3 μm; Thermo Scientific) with water + 0.1% formic acid (solvent A) and acetonitrile + 0.1% formic acid (solvent B) as solvents. The following solvent gradient at a flow rate of 250 μl/min was applied: 1 min 5% B, 16 min 98% B, 19 min 98% B, 20 min 5% B.

Isolation and Structure Elucidation of Natural Products

Metabolites from P2 *invA5* or ATNT16 *abrA* culture filtrates were purified over a Zorbax RX-C18 column (9.5 × 250 mm, 5 μm) using an Agilent 1200 equipped with an auto-sampler, DAD and fraction collector. The following gradient of water + 0.1% TFA (A) and methanol (B) with a flowrate of 1.8 ml/min was applied: 0.5 min 25% B, 2 min 35% B, 20 min 40% B, 23 min 90% B, 25 min 100% B, 31 min 100% B, 34 min 25% B, 36 min 25% B. Peaks were automatically collected using slope and threshold parameters.

The 1D and 2D NMR spectra of **11**, **12**, **13** and **14** were recorded at 300 K on a Bruker Avance III spectrometer (Bruker BioSpin) at 500 and 600 MHz for proton and at 125 and 150 MHz for carbon spectra. DMSO-d_6 was used as solvent and internal standard. The solvent signals were referenced to δ_H 2.49 ppm and δ_C 39.5 ppm.

For final structure elucidation of atrofuranic acid (**13**) an acetylation was performed using the following method: pyridine (14 μl, 173.5 μmol) was added slowly to a suspension of **13** (9.1 mg, 26.8 μmol) in acetic anhydride (821 μl, 90.5 mmol) and stirred on ice for 30 min. The temperature was then raised to room temperature and stirred for another 18 h. After addition of 8 ml water, the mixture was transferred to a CHROMABOND® C_{18}ec-column (0.5 g), washed with 16 ml of water and eluted with 16 ml methanol. After evaporation of the solvent a complete triacetlyation of **13** was confirmed by HPLC-MS on an Agilent 1260 HPLC system equipped with a C_{18} column (Zorbax Eclipse XDB, 150 × 4.6 mm, 5 μm) and coupled to a 6130 Single Quadrupole mass detector by using the following gradient of CH_3CN in H_2O + 0.1% TFA: initial holding of 30% CH_3CN for 1 min, then increasing from 30 to 100% CH_3CN in 12 min and terminal holding of 100% CH_3CN for 8 minutes.

To obtain ^{13}C-labelled atrofuranic acid (**13**), two 50 ml AMM(-N)G100Gln20 cultures of *A. niger* ATNT16 cultures expressing an atromentin synthetase were supplemented with 2.2 mM 2-^{13}C-labelled L-tyrosine and incubated for 48 h at 28°C. Labelled atrofuranic acid (**13**) was extracted with ethyl acetate from *A. niger* mycelium. Extracts were dried under reduced pressure, solved in methanol, purified by HPLC as described above and subjected to NMR analyses.

Phylogenetic Tree Construction

To analyse the phylogenetic relationship of NRPS-like enzymes the thioesterase domain sequences were extracted by InterPro (Finn et al., 2017) using the alpha/beta hydrolase fold (SSF53474) as template. The following NRPS-like protein sequences were used: AtrA from *Tapinella panuoides* (accession no. Swiss-Prot: B7STY1); InvA from *P. involutus* (accession no. Swiss-Prot: A0A0S2E7W7); GreA from *Suillus grevillei* (accession no. Swiss-Prot: I6NXV7.1); MicA from *A. nidulans* (accession no. Swiss-Prot: Q5B7T4.1); TdiA from *A. nidulans* (accession no. GenBank: ABU51602.1); BtyA from *A. terreus* (accession no. GenBank: AUO29224.1) AtqA from *A. terreus* (accession NCBI Reference Sequence: XP_001210786.1); PgnA from *A. terreus* (accession NCBI Reference Sequence: XP_001217485.1); ApvA from *A. terreus* (accession NCBI Reference Sequence: XP_001211182.1); $AtrA_{At}$ from *A. terreus* (accession no. GenBank: MG384315); MelA from *A. terreus* (accession no. GenBank: AND66115); AbrA from *A. brasiliensis* (JGI protein ID Aspbr1 165333; GenBank: OJJ76880). The thioesterase domain of the polyketide synthase TerA from *A. terreus* (accession no. Swiss-Prot: Q0D1N9) was used as outgroup. The extracted protein domains were aligned using Clustal Omega (Sievers and Higgins, 2018) and assemblies were used for tree calculations with IQ-Tree by identifying the optimal tree

building algorithm resulting in a model with the highest likelihood (Kalyaanamoorthy et al., 2017). Bootstrap support was calculated by the ultrafast bootstrap approximation UFBoot2 implemented in IQ-Tree (Hoang et al., 2018). The results were plotted by using iTOL (Letunic and Bork, 2016).

QUANTIFICATION AND STATISTICAL ANALYSIS

Does not apply.

DATA AND SOFTWARE AVAILABILITY

No datasets or software was generated.

ADDITIONAL RESOURCES

No new website/forum was generated. This study did not include a clinical trial.

Cell Chemical Biology, Volume *26*

Supplemental Information

Cross-Chemistry Leads to Product Diversity from Atromentin Synthetases in Aspergilli from Section *Nigri*

Elena Geib, Florian Baldeweg, Maximilian Doerfer, Markus Nett, and Matthias Brock

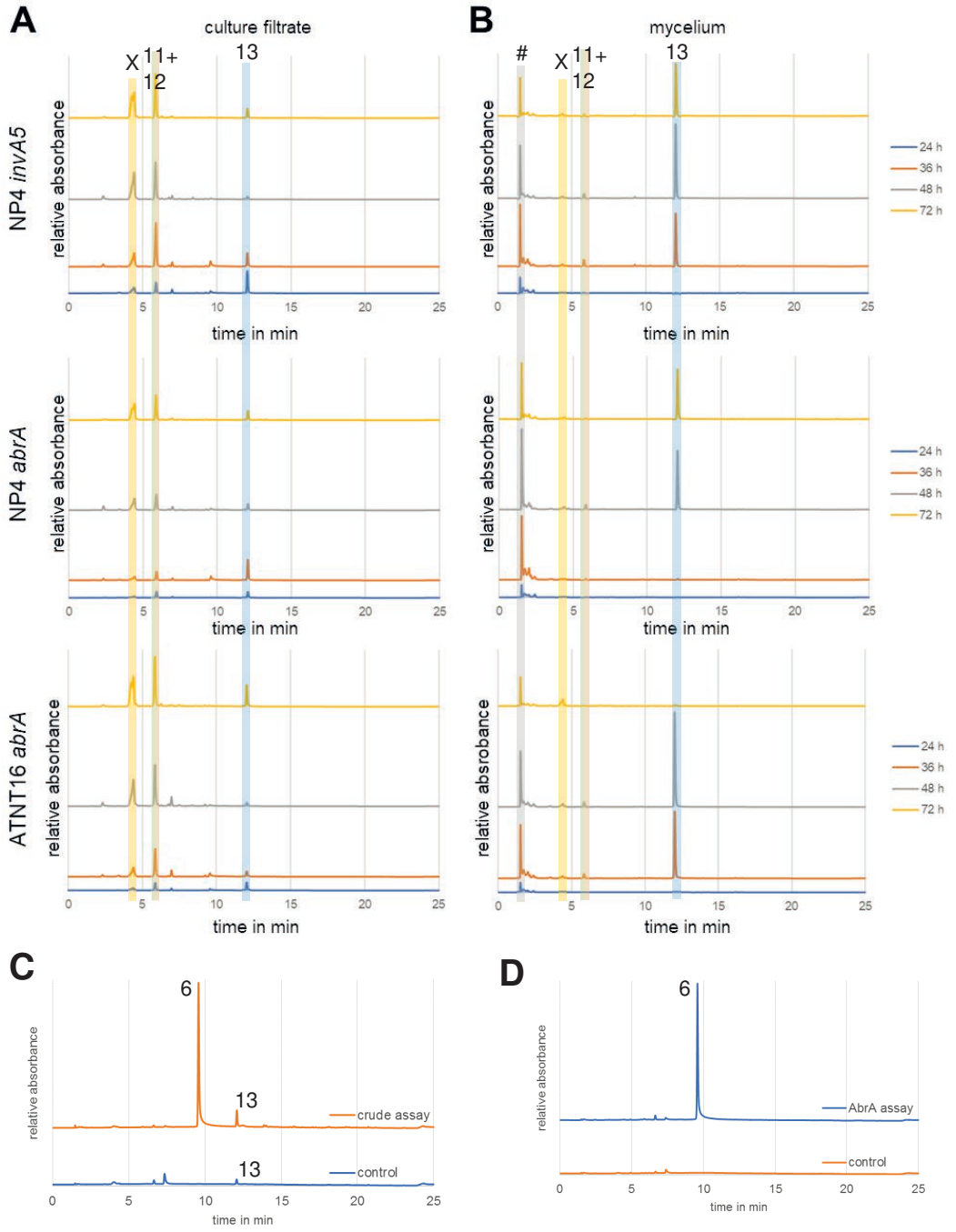

Figure S1 - Related to Figure 3: Time dependent extraction of (A) culture filtrates and (B) mycelium from heterologous *invA5* and *abrA* expression in the *A. niger* NP4 strain and *abrA* expression in *A. niger* ATNT16 strain. (C) *In vitro* assay with cell-free extract of an *invA5* expressing *A. niger* strain and 4-hydroxyphenylpyruvate as substrate. Minor amounts of atrofuranic acid (13) derive from the cell extract. Atromentin (6) is produced as the dominating metabolite. (D) *In vitro* assay with purified AbrA protein resulting in the production of atromentin (6). HPLC files were recorded with COR_ESIa method at 254 nm.

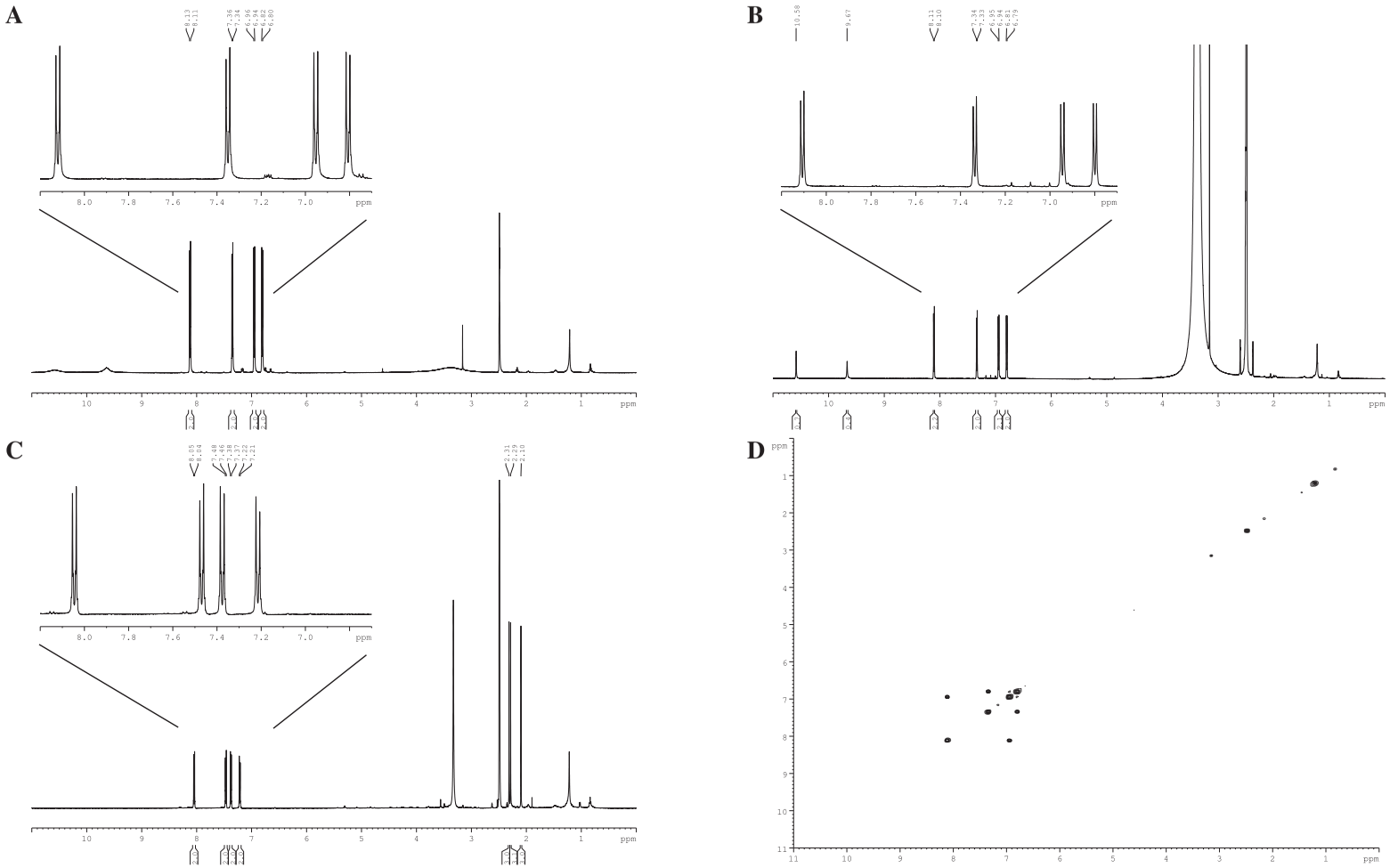

Figure S2 - Related to Figure 3: ^{1}H NMR spectrum of **13** (**A**), ^{13}C-labelled **13** (**B**) and **14** (**C**) in DMSO-d_6. **D:** ^{1}H, ^{1}H COSY NMR spectrum of **13** in DMSO-d_6

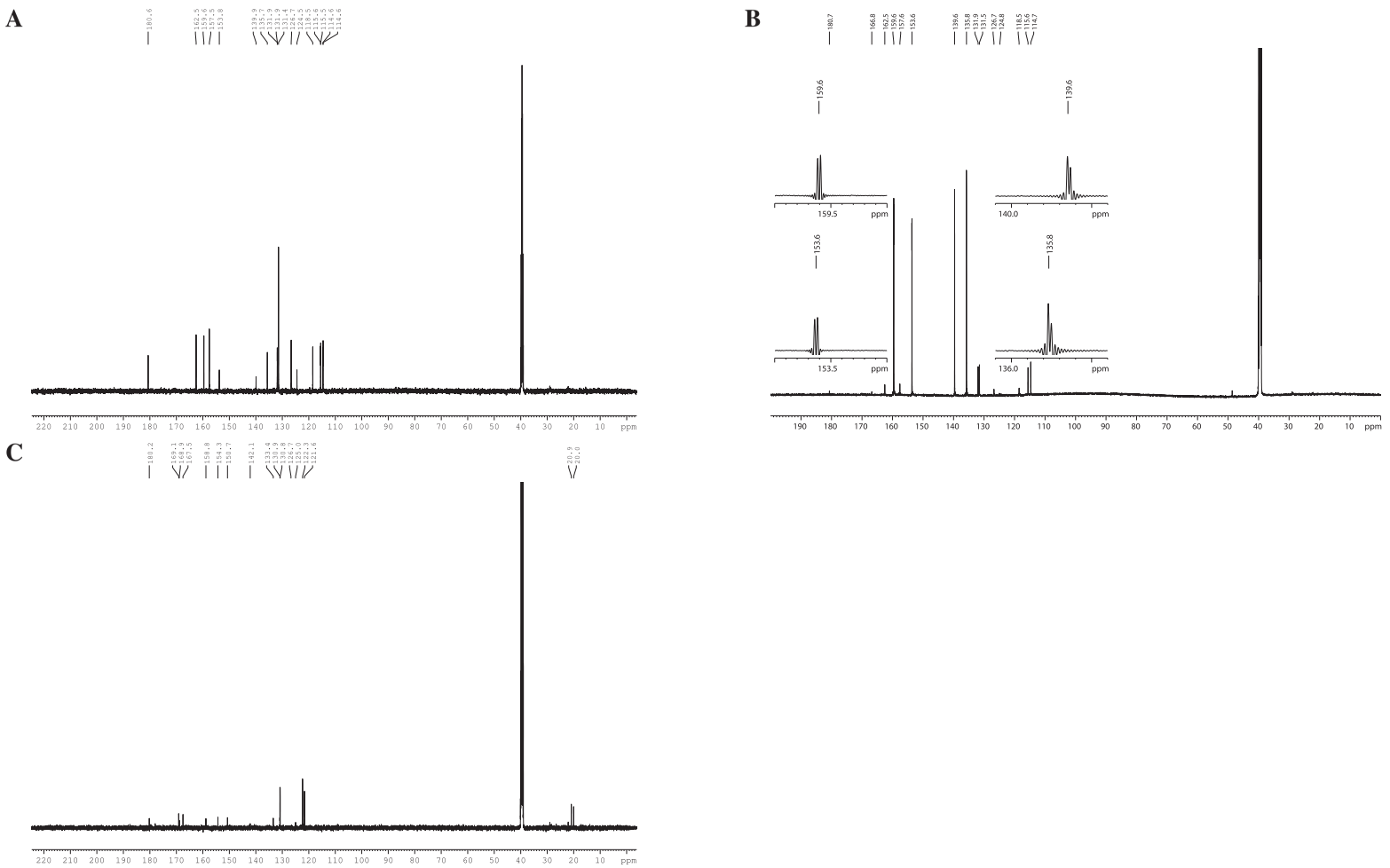

Figure S3 - Related to Figure 3: ^{1}H decoupled ^{13}C NMR spectrum of **13** (**A**), ^{13}C-labelled **13** (**B**) and **14** (**C**) in DMSO-d_6

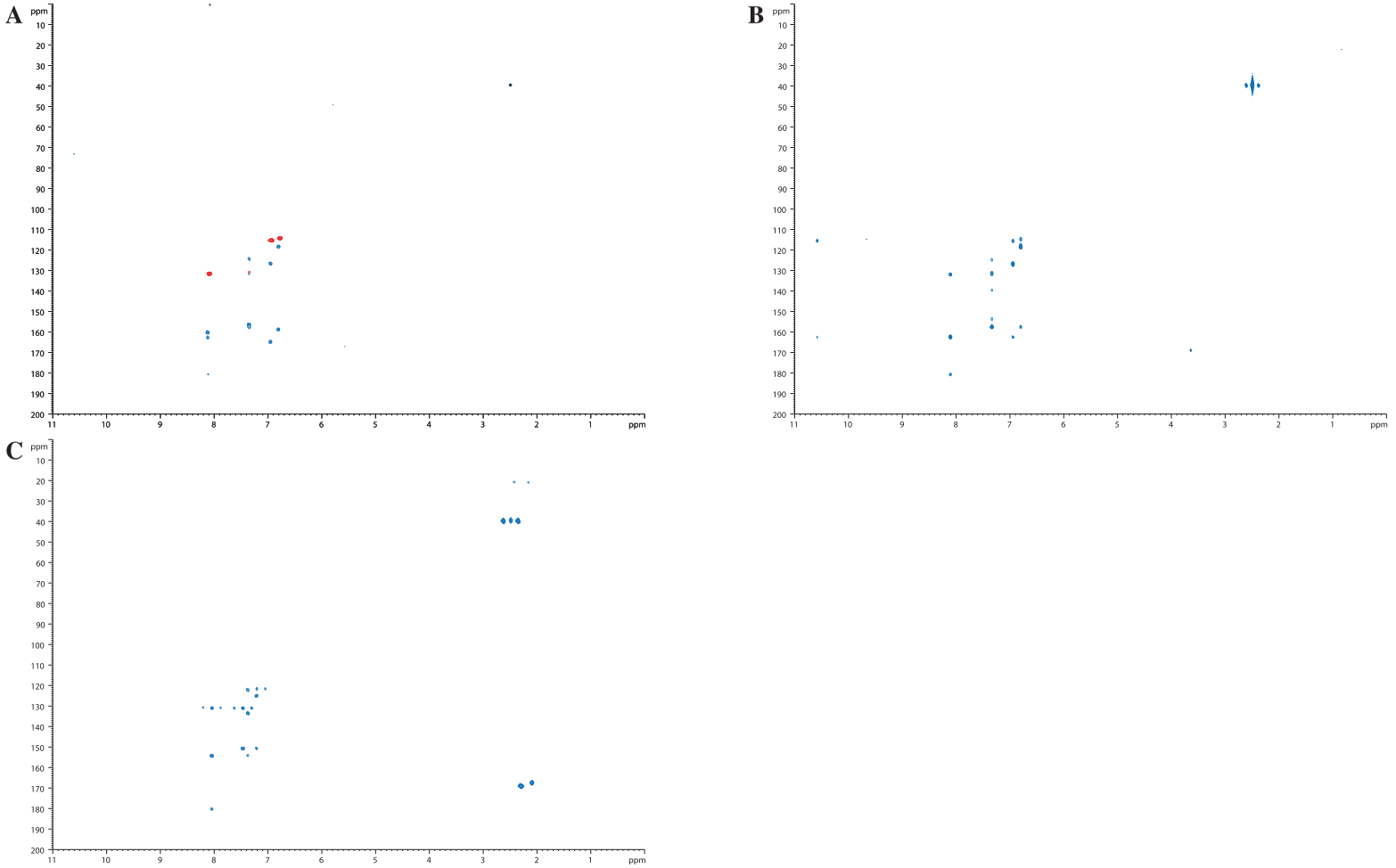

Figure S4 - Related to Figure 3: ^{1}H, ^{13}C HSQC (red) and HMBC (blue) NMR spectrum of **13** (**A**), ^{13}C-labelled **13** (**B**) and **14** (= acetylated 13) (**C**) in DMSO-d_6.

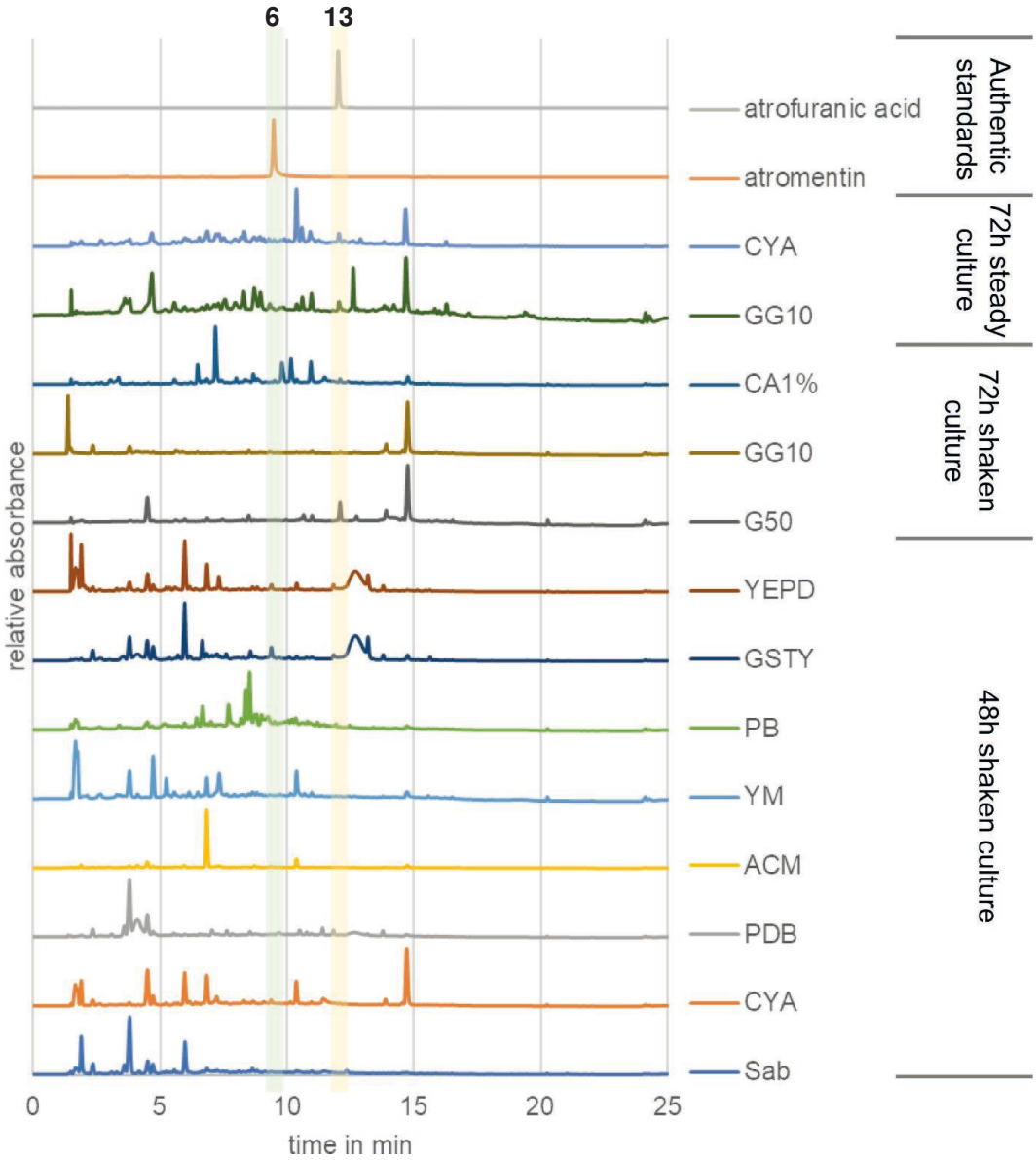

Figure S5 - Related to Figure 4: Culture filtrate extracts of *A. brasiliensis* in comparison to authentic atromentin (**6**) and atrofuranic acid (**13**) standards.

Table S1 - Related to Figure 3: NMR data for **12** in DMSO-d_6. COSY correlations are shown as bold bonds. HMBC correlations are shown as arrows.

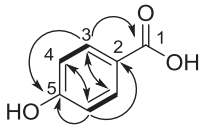

12

Position	δ_C, type	δ_H, M (J in Hz)	COSY[a]	HMBC[b]
1	167.2, C			
2	121.3, C			
3	131.5, CH	7.77, d (8.7)	4	1, 3, 5
4	115.1, CH	6.81, d (8.7)	3	2, 4, 5
5	161.6, C			

[a] COSY correlations are from proton(s) stated to the indicated proton. [b] HMBC correlations, optimized for 7.7 Hz, are from proton(s) stated to the indicated carbon.

Table S2 - Related to Figure 3: NMR data for **13** in DMSO-d_6. COSY correlations are shown as bold bonds. Key HMBC correlations are shown as arrows.

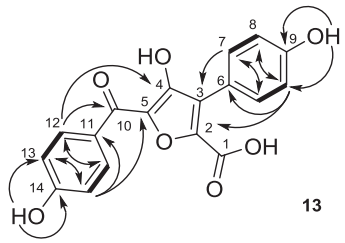

Position	δ_C, type	δ_H, M (*J* in Hz)	COSY[a]	HMBC[b]
1	166.8, C[c]			
2	153.8, C / 139.9, C[d]			
3	124.5, C			
4	180.6, C			
5	159.6, C / 135.7, C[d]			
6	118.5, C			
7	131.4, CH[e]	7.35, d (8.6)	8	2, 3, 7, 8, 9
8	114.6, CH[e]	6.81, d (8.6)	7	2, 6, 7, 8, 9
9	157.5, C			
9-OH	-	9.67, s[c]		8, 9
10	180.6, C			
11	126.7, C			
12	131.9, CH[e]	8.12, d (8.8)	13	10, 12, 13, 14
13	115.6, CH[e]	6.95, d (8.8)	12	5, 11, 12, 13, 14
14	162.5, C			
14-OH	-	10.58, s[c]		13, 14

[a] COSY correlations are from proton(s) stated to the indicated proton. [b] HMBC correlations, optimized for 7.7 Hz, are from proton(s) stated to the indicated carbon. [c] Chemical shifts were deduced from the NMR spectra of the labelled compound. [d] The different chemical shifts correspond to isomers of the compound. [e] Signal refers to two magnetically equivalent carbons.

Table S3 - Related to Figure 3: NMR data for **14** in DMSO-d_6. Key HMBC correlations are shown as arrows.

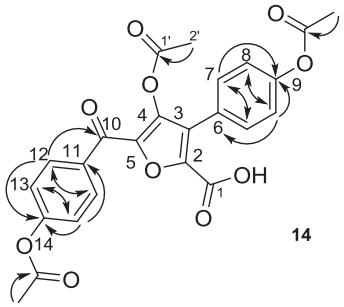

14

Position	δ_C, type	δ_H, M (*J* in Hz)	HMBC[a]
1	n.d.		
2	142.1, C		
3	126.7, C		
4	158.8, C		
5	n.d.		
6	125.0, C		
7	130.8, CH[b]	7.47, d (8.6)	7, 9
8	121.6, CH[b]	7.22, d (8.6)	6, 8, 9
9	150.7, C		
10	180.2, C		
11	133.4, C		
12	130.9, CH[b]	8.05, d (8.7)	10, 12, 14
13	122.3, CH[b]	7.38, d (8.7)	11, 13, 14
14	154.3, C		
1’	167.5, C		
2’	20.0, CH_3	2.10, s	1’
1’’	168.9, C		
2’’	20.9, CH_3	2.31, s	1’’
1’’’	169.1, C		
2’’’	20.9, CH_3	2.29, s	1’’’

[a] HMBC correlations, optimized for 7.7 Hz, are from proton(s) stated to the indicated carbon.
[b] Signal refers to two magnetically equivalent carbons.

Table S4 - Related to STAR methods: Oligonucleotides used in this study.

primer#	Sequence (5' – 3')	construct
1	CAGGCGGAGAAACGTGTGG	*A. ory pyrG*
2	GAGCACCAAATGGTGGCTAG	*A. ory pyrG*
3	GTGAATTCGAGCTCGGTACCCCTGCAGCTCTGTCATTGC	*A. nig ΔpyrG*
4	GTATAATACGCGGCCGCGTGTTGATGGAGGGGTTAATG	*A. nig ΔpyrG*
5	CGTAATCAAGCGGCCGCGGAGGATCGAAGTTCTGATGG	*A. nig ΔpyrG*
6	CTAGAGGATCCCCGGGTACCGCTGTCCCCTTTAAAGAGGC	*A. nig ΔpyrG*
7	CTCGGTACCCGCGGCCGCGCAGATTGTTGGCACCATC	*URA blaster*
8	CAGGTTGTCGAGCTTCTCTTC	*URA blaster*
9	GCAGATTGTTGGCACCATC	*URA blaster*
10	GAGGATCCCCGCGGCCGCCAGGTTGTCGAGCTTCTCTTC	*URA blaster*
11	GAAGCTCGACAACCTGCATGGTGTCCTCGTCGGC	*URA blaster*
12	GTGCCAACAATCTGCGGAACCTGACTACTACAATGTTG	*URA blaster*
13	CATCACAGCACCATGCATCACCATCACCATCACCAACCAAGCCTTATTCCCTC	*melA*$_{C\rightarrow S}$
14	CAAACGCCAACATCGACCCATAGGAATAGCC	*melA*$_{C\rightarrow S}$
15	ACGGACCATACGCTCTCGCCGGCTATTCCTATGGG	*melA*$_{C\rightarrow S}$
16	ATCACTGCTGCCATGGTTACATGCCCCTCTCAGCAAG	*melA*$_{C\rightarrow S}$
17	GAGGTAGATCGAAAGACCCGAC	*melA*$_{N\rightarrow D}$
18	GTCGGGTCTTTCGATCTACCTC	*melA*$_{N\rightarrow D}$
19	TGAAATCACTGCTGCTTACATGCCCCTCTCAGCAAG	*melA*$_{N\rightarrow D}$
20	GGAGAGCTTACCCAGGGTCG	*melA*:*invA5*
21	CTGGGTAAGCTCTCCAGGGCTCGTCTC	*melA*:*invA5*
22	ATCACTGCTGCCATGGTTACAGACCACGAGCTTCGAG	*invA5*
23	CATCACAGCACCATGGGCAGCAGCCATCATCATCATC	*invA5*
24	CATCACCATCACCATGGATCTTTCAAGAACCTCCAACAGC	*atrA*$_{At}$
25	CTGCTGTTATCCATGGCTAAATTCCCCGTGCTTCCAAC	*atrA*$_{At}$
26	CATCACCATCACCATGGACAACCAAGCCTTATTCCCTC	*melA*
27	CCGGGAGAGCTTACCCAG	*melA C1*
28	GGTAAGCTCTCCCGGTCTAGTATCAAGGCAAGCTACG	*atrA C1*
29	CTCGCGAACCGTGGTGTTTTC	*melA C2*
30	CACCACGGTTCGCGAGCTCAGCGCCGCGCTGCA	*atrA C2*
31	CATCACCATCACCATGGATCATTTGCCAATCTTACTGTATTC	*abrA*
32	AATCACTGCTGTTATCCATGGTCAAATTCCTCTTGCATCTAGTG	*abrA*
33	GAGGTTTAGAGCAAGCTTCCTTATTCGTTGACCTAGC	*An*P*gpdA*
34	AAATGACATTGTGATGTCTGCTCAAGC	*An*P*gpdA*
35	GACATCACAATGTCATTTGCCAATCTTACTG	*abrA*
36	CTCAGTTTCCTGAAGCTTCTCTACGGTATGCGAGGAAC	*abrA*
37	CCTCCAAGAGAGATCCAGAC	P*terA*
38	GAATTTTACCAGTGGCCTAGG	T*trpC*
39	CCTGGATAGAACTCTTCCTGC	*abrA*
40	TTCGCGGACCGTGGTGTTC	*atrA*$_{At}$ (A+T)
41	ACCACGGTCCGCGAACTTGCCGCTGCACTGGAC	*melA* (TE)
42	CTGCTGTTATCCATGGTTACATGCCCCTCTCAGCAAG	*melA* (TE)

Table S5 - Related to STAR methods: Media used in this study.

Minimal media	
AMM(-N)	0.52 g/l KCl, 0.52 g/l $MgSO_4 \times 7\ H_2O$, 1.52 g/l KH_2PO_4; 1 ml/l 1000× Hutner's trace elements; pH 6.5
G50Gln10	50 mM glucose and 10 mM glutamine
G50Gln10S1.2	50 mM glucose, 10 mM glutamine and 1.2 M sorbitol
G100Gln20	100 mM glucose and 20 mM glutamine
Starch2%Gln20	2% soluble starch and 20 mM glutamine
Starch2%Gln20Talc	2% soluble starch and 20 mM glutamine, 10 g/l talc
CA1%	1% casamino acids
AMM(-N)	6 g/l $NaNO_3$, 0.52 g/l KCl, 0.52 g/l $MgSO_4$ ´7 H2O, 1.52 g/l KH_2PO_4; 1 ml/l 1000× Hutner's trace elements; pH 6.5
G50	
Complex media	
YEPD	20 g/l peptone, 10 g/l yeast extract, 5 g/l glucose
YM	3 g/ l yeast extract, 3 g/l malt extract, 5 g/l meat peptone; pH 6.6
GSTY	30 g/l glucose, 2.5 g/l soytone, 0.5 g/l yeast extract, 1 g/l KH_2PO_4, 1 g/l $MgSO_4 \times 7\ H_2O$, 0.5 g/l NaCl, 0.5 g/l $CaCl_2 \times 2\ H_2O$, 2 mg /l $FeCl_3 \times 2\ H_2O$, 2 mg/l $ZnSO_4 \times 7\ H_2O$; pH 5.5
PB	20 g/l potato broth; pH 6.5
CYA	3 g/l $NaNO_3$, 5 g/l yeast extract, 30 g/l sucrose, 1.3 g/l K_2HPO_4 x 3 H_2O, 0.5 g/l $MgSO_4$ x 7 H_2O, 0.5 g/l KCl, 10 mg/l $FeSO_4$ x 7 H_2O, 5 mg/l $CuSO_4$ x 5 H_2O, 5 mg/l $ZnSO_4$ x 7 H_2O; pH 6.5
Sab	10 g/l peptone, 20 g/l glucose; pH 6.5
ACM	10 g/l glucose, 1 g/l yeast extract,2 g/l peptone, 1 g/l casamino acids, 0.075 g/l adenine, 10 ml/l vitamin solution (400 mg/l *p*-aminobenzoic acid, 50 mg/l thiamine HCl, 2 mg/l biotin, 100 mg/l nicotinic acid, 250 mg/l pyridoxine HCl, 1.4 g/l choline chloride, 100 mg/l riboflavin), 20 ml/l salt solution (26 g/l KCl, 26 g/l $MgSO_4 \times 7\ H_2O$, 76 g/l KH_2PO_4), 200 µl/l trace element solution (40 mg/l $Na_2B_4O_7 \times 10\ H_2O$, 800 mg/l $CuSO_4 \times 5\ H_2O$, 800 mg/l $FePO_4 \times H_2O$, 800 mg/l $MnSO_4 \times 4\ H_2O$, 800 mg/l $NaMoO_4 \times 2\ H_2O$, 8 g/l $ZnSO_4$); pH 6.5

3.5 Publikation 5

Biocatalytic Production of Psilocybin and Derivatives in Tryptophan Synthase-Enhanced Reactions

Blei, F.; Baldeweg, F.; Fricke, J.; Hoffmeister, D. *Chem. - Eur. J.* **2018**, *24*, 10028–10031.

Zusammenfassung:
Pilze der Gattung *Psilocybe* produzieren Psilocybin (4-Phosphoryloxy-N,N-dimethyltryptamin) als Hauptalkaloid. Zurzeit erlebt der Stoff eine Renaissance und wird als mögliches Medikament zur Behandlung von Depressionen und Angstzuständen in Erwägung gezogen. In dieser Arbeit wird eine verbesserte enzymatische Route zur biokatalytischen Produktion von Psilocybin durch Nutzung der Tryptophansynthase TrpB aus dem Pilz *Psilocybe cubensis* vorgestellt. Besonders hervorzuheben ist die kostengünstige Herstellung aus 4-Hydroxyindol und L-Serin. Die Substratflexibilität von TrpB erlaubt zudem die enzymatische Produktion von Isonorbaeocystin (7-Phosphoryloxytryptamine) – ein nicht natürliches Strukturisomer von Norbaeocystin (4-Phosphoryloxytryptamine) – sowie Serotonin (5-Hydroxytryptamine).

Angaben zum Eigenanteil von Florian Baldeweg (15%):
Verifizierung der Struktur von Isonorbaeocystin im Vergleich zu Psilocybin mittels NMR-Spektroskopie. Präparative und semipräparative Arbeiten zur Aufreinigung von Psilocybin, sowie chromatographische und chemische Hilfestellung bei der Aufreinigung von Isonorbaeocystin. Mitarbeit am Manuskript.

Jena, den

Prof. Dirk Hoffmeister

ChemPubSoc Europe

DOI: 10.1002/chem.201801047

CHEMISTRY A European Journal Communication

Biosynthesis

Biocatalytic Production of Psilocybin and Derivatives in Tryptophan Synthase-Enhanced Reactions

Felix Blei, Florian Baldeweg, Janis Fricke, and Dirk Hoffmeister*[a]

Abstract: Psilocybin (4-phosphoryloxy-*N*,*N*-dimethyltryptamine) is the main alkaloid of the fungal genus *Psilocybe*, the so-called "magic mushrooms." The pharmaceutical interest in this psychotropic natural product as a future medication to treat depression and anxiety is strongly re-emerging. Here, we present an enhanced enzymatic route of psilocybin production by adding TrpB, the tryptophan synthase of the mushroom *Psilocybe cubensis*, to the reaction. We capitalized on its substrate flexibility and show psilocybin formation from 4-hydroxyindole and L-serine, which are less cost-intensive substrates, compared to the previous method. Furthermore, we show enzymatic production of 7-phosphoryloxytryptamine (isonorbaeocystin), a non-natural congener of the *Psilocybe* alkaloid norbaeocystin (4-phosphoryloxytryptamine), and of serotonin (5-hydroxytryptamine) by means of the same in vitro approach.

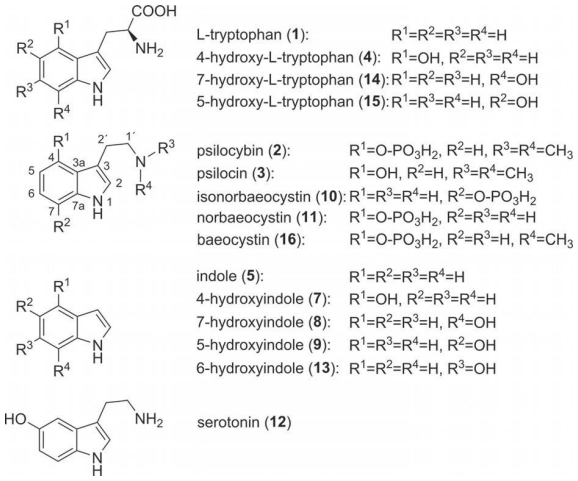

Scheme 1. Structures of *Psilocybe* tryptophan synthase substrates and products, and products of the in vitro reconstituted indole alkaloid synthesis pathway.

Among the most prominent natural products is the L-tryptophan (**1**)-derived alkaloid psilocybin (4-phosphoryloxy-*N*,*N*-dimethyltryptamine **2**, Scheme 1).[1] This major metabolite of *Psilocybe* carpophores—colloquially dubbed "magic mushrooms"—rapidly dephosphorylates upon ingestion to yield psilocin (**3**), which acts as the actual hallucinogen by agonistically binding primarily to the human $5HT_{2A}$-receptor.[2] Importantly, recent clinical studies plausibly underscore the potential pharmaceutical value of **2** in the treatment of nicotine addiction, anxiety with terminal-stage cancer patients, and depression.[3]

For access to **2** and **3**, various synthetic approaches have been established.[4] Recently, a biotechnological three-enzyme route beginning from 4-hydroxy-L-tryptophan **4** to **2** has been reported. This route utilizes the *Psilocybe cubensis* enzymes PsiD, PsiK, and PsiM, which provide decarboxylase, kinase, and methyltransferase activity, respectively.[5] We sought to enhance this enzymatic procedure by enzymatically producing **4** in situ via tryptophan synthase (E.C. 4.2.1.20), thus feeding lower-priced precursors to the process. The α-subunits of $\alpha_2\beta_2$-heterotetrameric bacterial tryptophan synthases catalyze the first half reaction (Figure 1), that is, the retro aldol-type cleavage of 1-(indole-3-yl)glycerol phosphate that releases D-glyceraldehyde 3-phosphate and provides indole **5** (Scheme 1) as substrate for the subsequent second half reaction. It is catalyzed by the β-subunit and includes a pyridoxal phosphate (PLP)-dependent condensation of **5** and L-serine **6** (Figure 1) into **1**.[6] Wild type or engineered prokaryotic tryptophan synthases of *Salmonella enterica* or *Pyrococcus furiosus* proved valuable in procuring β-methyl- or L-halotryptophans, respectively, via enzymatic conversion of substituted **5** and **6** (or L-threonine) by the β-subunit.[7] A recent study showed production of

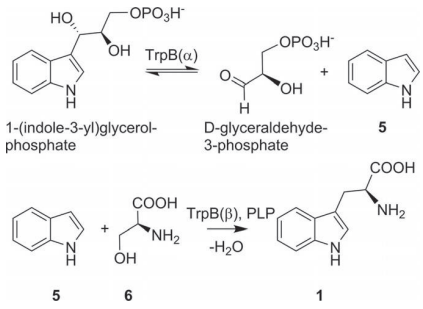

Figure 1. The tryptophan synthase reaction. Indole (**5**) formation is catalyzed by the α-subunit (TrpB(α)), L-tryptophan (**1**) production is catalyzed by the β-subunit (TrpB(β)).

[a] F. Blei, F. Baldeweg, J. Fricke, Prof. Dr. D. Hoffmeister
Department Pharmaceutical Microbiology at the Hans-Knöll-Institute
Friedrich-Schiller-Universität
Beutenbergstrasse 11a, 07745 Jena (Germany)
E-mail: dirk.hoffmeister@leibniz-hki.de

Supporting information and the ORCID identification number(s) for the author(s) of this article can be found under: https://doi.org/10.1002/chem.201801047.

4-halogenated or 4-nitro tryptophan by engineered TrpB variants.[8] Otherwise, tryptophan synthases generally showed low tolerance for 4-substituted indoles. Furthermore, hydroxy-substituted indoles, which are relevant for our purposes, had not been included in prior studies.

We recombinantly produced *P. cubensis* L-tryptophan synthase (TrpB). Here, we report on integrating it into a one-pot procedure to synthesize **2** from **6** and 4-hydroxyindole (**7**), that is, two inexpensive compounds, in four enzymatic steps, using enzymes of the same fungus. Choosing 7-hydroxyindole (**8**) and 5-hydroxyindole (**9**), we further describe an enzymatic synthesis for isonorbaeocystin (7-phosphoryloxytryptamine **10**), that is, a non-natural isomer of the psilocybin-family alkaloid norbaeocystin **11** (Scheme 1). We also show TrpB/PsiD-catalyzed synthesis of serotonin (**12**) in two enzymatic steps.

Typically, fungal tryptophan synthases are homodimers. Each monomer is bifunctional, includes an α- and a β-domain, and shows a mass of about 75 kDa.[9] Using known fungal TrpB sequences as a reference,[10] we identified a 2648 bp candidate gene in the genome of *P. cubensis*[5] that was disrupted by ten introns, according to an in silico analysis with Augustus software.[11]

The 2103 bp coding sequence encodes a 700 aa TrpB monomer (calculated molecular mass 75.5 kDa, calculated pI 5.9). The protein was most similar (85% identical aa) to predicted proteins of the mushrooms *Hebeloma cylindrosporum* (accession # KIM48772.1) and of *Galerina marginata* (KDR73575.1). The *trpB* cDNA was inserted into expression vector pET28a to create plasmid pFB14. It was used to transform *E. coli* KRX to produce TrpB as N-terminally tagged polyhistidine fusion protein (Figure S1 in the Supporting Information).

Optimum turnover took place at pH 8.0 and at 30 °C. TrpB followed Michaelis–Menten kinetics and showed K_m values of 40 μM and 16 μM for **5** and **7**, respectively, and 2.9 mM for **6** (Figure S2, Supporting Information). The values for **5** and **6** are comparable with prior data.[7e,9] Gel permeation chromatography confirmed the dimeric state of active TrpB (Figure S3). The TrpB substrate specificity was assessed using **7**, **8**, **9**, or 6-hydroxyindole **13** (Figure 2). Indoles **7**, **8**, and **9** were converted to 4-, 7-, and 5-hydroxy-L-tryptophan (compounds **4**, **14**, and **15**, respectively, at $t_R = 10.2$, 9.8, and 7.9 min), as determined by LC-MS (Figure 2, found masses *m/z* 221.0920, 221.0930, and 221.0927 $[M+H]^+$, respectively, calculated for $C_{11}H_{13}N_2O_3$: 221.0926). Product formation was not detected in the reaction with **13**, a signal with the expected mass and UV/Vis spectrum was not found.

Next, we extended the described PsiD/PsiK/PsiM-dependent **2** in vitro synthesis by adding TrpB and PLP to this multienzyme assay. Substrates **6** and **7** were initially present at 3 mM, and the reaction proceeded for 4 h. LC-MS analysis unequivocally proved **2** production, along with its immediate natural precursors baeocystin (**16**) and **11** (Figure 3, Figure 4).

The substrate tolerance of the Psi enzymes outside the **2** biosynthesis pathway has not been investigated in greater detail. Considering that **15** was a TrpB product, we re-ran the four-enzyme reaction, this time adding 3 mM **6** and **9** as respective substrates. LC-MS-analysis demonstrated that a product had formed ($t_R = 7.4$ min) whose mass suggested the loss of CO_2 (*m/z* 177.1022 $[M+H]^+$) hence implying **15** forma-

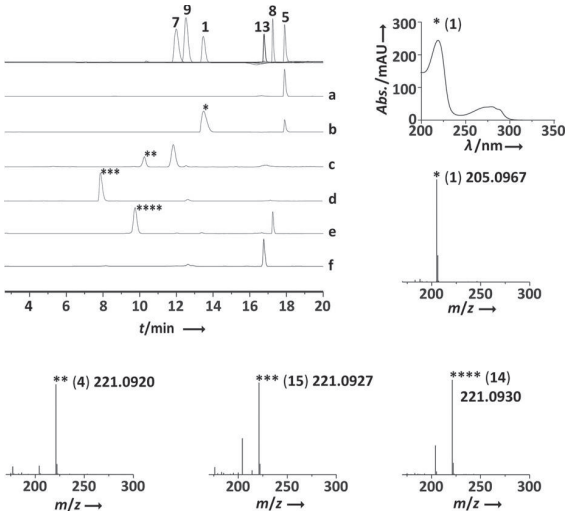

Figure 2. Product formation by *Psilocybe cubensis* TrpB. Chromatograms were extracted at $\lambda = 280$ nm, HR-ESIMS spectra of the compounds given in parentheses were recorded in positive mode, experimentally determined masses are indicated in the spectra. The calculated mass of **4**, **14**, and **15** is *m/z* 221.0926 ($[M+H]^+$), the calculated mass of **1** is *m/z* 205.0972. Top trace: overlayed separate chromatograms of authentic standards. Trace a: negative control with heat-treated TrpB and **5**. Trace b: reaction with **6** and **5**. Trace c: reaction with **6** and **7**. Trace d: reaction with **6** and **9**. Trace e: reaction with **6** and **8**. Trace f: reaction with **6** and **13**.

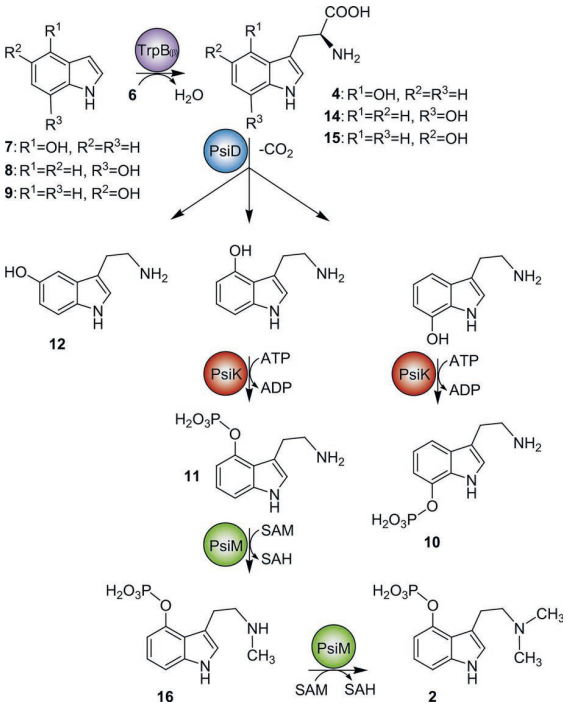

Figure 3. In vitro syntheses leading to serotonin (**12**), psilocybin (**2**), or isonorbaeocystin (**10**). The reactions included *Psilocybe cubensis* enzymes TrpB, PsiD, PsiK, and PsiM.

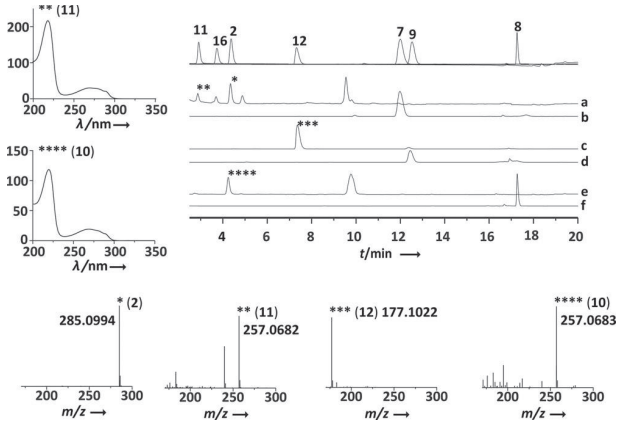

Figure 4. LC-MS analysis of product formation in multi-enzyme assays. Chromatograms were extracted at $\lambda = 280$ nm, HR-ESIMS spectra were recorded in positive mode, experimentally determined masses are indicated in the spectra. The calculated mass ($[M+H]^+$) of **2** is *m/z* 285.0999, of **10** and **11**: *m/z* 257.0686, of **12**: *m/z* 177.1022. Top trace: overlayed separate chromatograms of standards. Trace a: Reaction with TrpB, PsiD, PsiK, and PsiM and substrates **6** and **7**. The signal at $t_R = 4.8$ min is due to *S*-adenosyl-L-homocysteine. Trace b: negative control. Trace c: Reaction with TrpB and PsiD with substrates **6** and **9** (trace d: negative control). Trace e: Reaction with TrpB, PsiD, PsiK, and PsiM with substrates **6** and **8** (trace f: negative control). Signals at $t_R = 9.7$ and 9.6 min in traces a and e, respectively, represent intermediates 4- and 7-hydroxytryptamine, as identified by their UV/Vis spectra and by mass spectrometry (*m/z* 177.1 $[M+H]^+$).

tion and subsequent quantitative PsiD-catalyzed decarboxylation into **12**. This was confirmed by comparison with an authentic **12** standard. This finding further suggested that PsiD tolerates well the 5-hydroxy substitution, which confirmed a previous report.[12] The results also showed that 5-hydroxylated indoles do not serve as substrates for the kinase PsiK, as no second, that is, phosphorylated product was detectable. Assays run only with TrpB and PsiD resulted in identical chromatograms (Figure 4).

We repeated the four-enzyme reaction with **6** and **8**. LC-MS analysis indicated formation of a product whose UV/Vis spectrum and mass (*m/z* 257.0682 $[M+H]^+$) were equal to that of **11** (Figure 4, $t_R = 2.9$ min), but which differed in its retention time ($t_R = 4.2$ min), thus pointing to an isomeric product. Assuming that PsiD tolerates the 7-hydroxy group and that PsiK accepts it as phosphate acceptor substrate, we hypothesized that this product was identical to 7-phosphoryloxytryptamine **10** (Scheme 1). We chromatographically purified this compound from an upscaled assay, which yielded 2.36 mg of pure substance.

1D and 2D NMR spectra (Table 1, Figures S4–S9 in the Supporting Information) were recorded and compared to NMR data of **2** (Table 2, Figures S4 and S10–S14). In **10**, the bridgehead carbon C-3a was identified by HMBC correlations with H-1 and H-2, while C-7a was correlated to H-2. The HMBC correlation between carbons C-3a and C-7 with the H-5 triplet established the position of the phosphoryloxy group at C-7 (Figure S9). The signal at $\delta = 7.31$ ppm (H-4) showed HMBC correlations with C-3, C-6, and C-7a, thus providing final evidence for the structure of compound **10**, for which we propose the

Table 1. ^{1}H (600 MHz) and ^{13}C (150 MHz) NMR data for **10** in [D_6]DMSO.

Pos.	δ_H [ppm] (mult. *J* [Hz])	δ_C [ppm]	HMBC	COSY
1	10.97 (s, 1H)	–	3, 3a	2
2	7.20 (d, 2.0, 1H)	123.9	3, 3a, 7a	1
3	–	109.9	–	–
3a	–	129.5	–	–
4	7.31 (d, 7.86, 1H)	113.8	3, 6, 7a	5
5	6.95 (t, 7.77, 1H)	118.7	3a, 7	4, 6
6	7.02 (d, 7.68, 1H)	111.3	4, 7a, 7	5
7	–	137.8	–	–
7a	–	128.2	–	–
1′	3.07 (m, 2H)	39.3[a]	3	2′, NH_2
2′	2.97 (t, 7.62, 2H)	23.2	1′, 2, 3, 3a	1′
NH_2	7.75 (s, 2H)	–	–	1′

[a] value derived from 2D ^{1}H-^{13}C correlation spectrum (HMBC).

Table 2. ^{1}H (600 MHz) and ^{13}C (150 MHz) NMR data for **2** in [D_6]DMSO.

Pos.	δ_H [ppm] (mult. *J* [Hz])	δ_C [ppm]	HMBC	COSY
1	11.09 (s, 1H)	–	3, 3a	2
2	7.18 (d, 1.98, 1H)	123.7	3, 3a, 7a	1
3	–	108.2	–	–
3a	–	118.7	–	–
4	–	145.2	–	–
5	7.12 (d, 7.98, 1H)	107.6	3a, 7	6
6	6.99 (t, 7.74, 1H)	121.5	7a, 4	5, 7
7	6.93 (d, 7.89, 1H)	108.7	3a, 4, 5	6
7a	–	138.6	–	–
1′	3.32 (m, 2H)	58.1	2′, 3, $N(CH_3)_2$	2′
2′	3.18 (m, 2H)	21.2	1′, 2, 3, 3a	1′
$N(CH_3)_2$	2.82 (s, 6H)	42.3	1′, 2′	–

name isonorbaeocystin. Methylation of **10** by PsiM in detectable amounts was not observed.

Therefore, we conclude that PsiM, the methyltransferase of the **2** pathway, cannot tolerate a 7-phosphoryloxy-substituted compound as acceptor substrate. This finding underscores the previously noted specificity of PsiM, which prevents *N*,*N*-dimethyltryptamine and **3** formation as intermediates in the **2** pathway.[5]

Contrasting the use of the *trpB* gene in fungal genetics as a standard selection marker in **1**-auxotrophic hosts, very few fungal tryptophan synthases were investigated biochemically.[9a,13] *P. cubensis* TrpB is the first biochemically characterized tryptophan synthase of the basidiomycetes, which represent a phylum of more than 30000 species. The intrinsic tolerance of TrpB to substituted indoles allowed for its integration into a biocatalytic process that produces **2** congeners, including **10** and **12**, and that translates into a facile and more cost-effective enzymatic synthesis of **2**. The value of the substrate **4**, used in the previous procedure, is approximately US$ 180 $mmol^{-1}$, whereas the combined sales price for 1 mmol (each) of **6** and **7** as starting material in our refined process is about US$ 2.

Directed in vitro evolution and structure-based engineering of genes encoding biosynthesis enzymes proved instrumental to optimize catalytic activity, introduce new activities, and relax

specificities, to create libraries of natural product derivatives.[14] Thus, future work on enzyme engineering, in particular on the strictly specific methyltransferase PsiM, is warranted to access a larger structural diversity of **2** derivatives using only a small set of enzymes.

Experimental Section

Enzymatic reactions: All enzymatic in vitro reactions were carried out in triplicate. The enzyme concentration was 200 nM. In the case of multi-enzyme assays, each enzyme was present at this concentration. The reactions were stopped after the indicated incubation times by freezing and lyophilization. Subsequently, the residue was dissolved in methanol (MeOH), centrifuged for 10 min at 20000×g, and the supernatant was collected. The solvent was removed under reduced pressure, and the residue dissolved in H_2O:acetonitrile (9:1, v/v), filtered, and used for chromatography (see below). The in vitro characterization of TrpB was performed in a volume of 100 μL and 50 mM Tris-HCl buffer, pH 8.0 for 5 min at 30 °C (varied between 16–42 °C to determine the temperature optimum, and between pH 6.0 through 9.5 for the pH optimum). The substrates (**6**, and the respective indole substrate **5**, **7**, **8**, **9**, or **13**) were added at (each) 3 mM, the PLP concentration was 1 μM. Multi-enzyme reactions including TrpB, PsiD, PsiK, and PsiM were set up in a volume of 500 μL in 50 mM Tris-HCl buffer, pH 8.0, and proceeded for 4 h at 25 °C. The reactions yielding **2**, **10**, or **12** included **6** and indole substrates **7**, **8**, or **9** (3 mM final concentration each) as well as SAM, ATP, and $MgCl_2$ (6 mM each), the PLP concentration was 1 μM. Initially, all four enzymes were added. For subsequent assays yielding **12**, PsiK, PsiM, ATP, and SAM was omitted. The yield of **2** (20.7%) was determined by calculating the area under the curve of its chromatographic signal and compared to a standard curve, recorded with authentic compound.

Chemical analysis: LC-MS experiments were performed on an Agilent 1260 HPLC system equipped with a C_{18} column (Zorbax Eclipse XDB, 150×4.6 mm, 5 μm) and coupled to a 6130 Single Quadrupole mass detector, high-resolution mass spectrometry was performed on a Thermo Accela liquid chromatograph, following described parameters.[5] The 1D and 2D NMR spectra of **10** and **2** were recorded at 300 K on a Bruker Avance III spectrometer at 600 MHz for ^1H and at 150 MHz for ^{13}C spectra. [D_6]DMSO was used as solvent and internal standard. The solvent signals were referenced to $\delta_H = 2.50$ ppm and $\delta_C = 39.5$ ppm. Chemicals and solvents were purchased from Deutero, Key Organics, Sigma–Aldrich, Roth, TCI, and VWR. Alkaloids **2**, **11**, and **16** were purified from *P. cubensis* carpophores.

Detailed experimental procedures for microbiological and genetic methods, as well as for purification of enzymes and compound **10**, are described in the Supporting Information.

Acknowledgements

We thank A. Perner and H. Heinecke (Hans-Knöll-Institute Jena) for recording high-resolution mass and NMR spectra, respectively. F. Baldeweg acknowledges a doctoral fellowship by the Excellence Graduate School Jena School for Microbial Communication (JSMC). This work was supported by the Deutsche Forschungsgemeinschaft (grant HO2515/7-1). D.H.'s group is also supported by the DFG Collaborative Research Center ChemBioSys 1127.

Conflict of interest

The authors declare no conflict of interest.

Keywords: alkaloid · biosynthesis · enzymes · psilocybin · tryptophan synthase

[1] a) A. Hofmann, R. Heim, A. Brack, H. Kobel, A. Frey, H. Ott, T. Petrzilka, F. Troxler, *Helv. Chim. Acta* **1959**, *42*, 1557–1572; b) A. Y. Leung, A. H. Smith, A. G. Paul, *J. Pharm. Sci.* **1965**, *54*, 1576–1579.

[2] a) D. E. Nichols, *Pharmacol. Ther.* **2004**, *101*, 131–181; b) F. Hasler, U. Grimberg, M. A. Benz, T. Huber, F. X. Vollenweider, *Psychopharmacology* **2004**, *172*, 145–156.

[3] a) C. S. Grob, A. L. Danforth, G. S. Chopra, M. Hagerty, C. R. McKay, A. L. Halberstadt, G. R. Greer, *Arch. Gen. Psychiatry* **2011**, *68*, 71–78; b) M. W. Johnson, A. Garcia-Romeu, M. P. Cosimano, R. R. Griffiths, *J. Psychopharmacol.* **2014**, *28*, 983–992; c) A. Mahapatra, R. Gupta, *Ther. Adv. Psychopharmacol.* **2017**, *7*, 54–56.

[4] a) A. Hofmann, A. Frey, H. Ott, T. Petrzilka, F. Troxler, *Experientia* **1958**, *14*, 397–399; b) F. Troxler, F. Seemann, A. Hofmann, *Helv. Chim. Acta* **1959**, *42*, 2073–2103; c) S. Ametamey, F. X. Vollenweider, J. Patt, D. Bourquin, F. Hasler, H.-F. Beer, P. A. Schubiger, *J. Labelled Compd. Radiopharm.* **1998**, *41*, 585–594; d) F. Yamada, M. Tamura, M. Somei, *Heterocycles* **1998**, *49*, 451–457; e) H. Sakagami, K. Ogasawara, *Heterocycles* **1999**, *51*, 1131–1135; f) D. E. Nichols, S. Frescas, *Synthesis* **1999**, 935–938; g) O. Shirota, W. Hakamata, Y. Goda, *J. Nat. Prod.* **2003**, *66*, 885–887; h) N. Gathergood, P. J. Scammells, *Org. Lett.* **2003**, *5*, 921–923.

[5] J. Fricke, F. Blei, D. Hoffmeister, *Angew. Chem. Int. Ed.* **2017**, *56*, 12352–12355; *Angew. Chem.* **2017**, *129*, 12524–12527.

[6] a) E. W. Miles, H. Kawasaki, S. A. Ahmed, H. Morita, H. Morita, S. Nagata, *J. Biol. Chem.* **1989**, *264*, 6280–6287; b) M. F. Dunn, D. Niks, H. Ngo, T. R. Barends, I. Schlichting, *Trends Biochem. Sci.* **2008**, *33*, 254–264.

[7] a) R. J. Goss, P. L. Newill, *Chem. Commun.* **2006**, 4924–4925; b) D. R. Smith, T. Willemse, D. S. Gkotsi, W. Schepens, B. U. Maes, S. Ballet, R. J. Goss, *Org. Lett.* **2014**, *16*, 2622–2625; c) D. Francis, M. Winn, J. Latham, M. F. Greaney, J. Micklefield, *ChemBioChem* **2017**, *18*, 382–386; d) M. Herger, P. van Roye, D. K. Romney, S. Brinkmann-Chen, A. R. Buller, F. H. Arnold, *J. Am. Chem. Soc.* **2016**, *138*, 8388–8391; e) A. R. Buller, S. Brinkmann-Chen, D. K. Romney, M. Herger, J. Murciano-Calles, F. H. Arnold, *Proc. Natl. Acad. Sci. USA* **2015**, *112*, 14599–14604.

[8] D. K. Romney, J. Murciano-Calles, J. E. Wehrmüller, F. H. Arnold, *J. Am. Chem. Soc.* **2017**, *139*, 10769–10776.

[9] a) W. H. Matchett, J. A. DeMoss, *J. Biol. Chem.* **1975**, *250*, 2941–2946; b) C. J. Bailey, P. D. Turner, *Biochem. J.* **1983**, *209*, 151–157.

[10] a) C. Skrzynia, D. M. Binninger, J. A. Alspaugh, P. J. Pukkila, *Gene* **1989**, *81*, 73–82; b) S. E. Eckert, E. Kübler, B. Hoffmann, G. H. Braus, *Mol. Gen. Genet.* **2000**, *263*, 867–876.

[11] M. Stanke, R. Steinkamp, S. Waack, B. Morgenstern, *Nucleic Acids Res.* **2004**, *32*, W309–W312.

[12] H. T. Reynolds, V. Vijayakumar, E. Gluck-Thaler, H. B. Korotkin, P. B. Matheny, J. C. Slot, *Evol. Lett.* **2018**, *2*, 88–101.

[13] a) D. H. Wolf, M. Hoffmann, *Eur. J. Biochem.* **1974**, *45*, 269–276.

[14] a) C. A. Denard, H. Ren, H. Zhao, *Curr. Opin. Chem. Biol.* **2015**, *25*, 55–64; b) G. Williams, R. W. Gantt, J. S. Thorson, *Curr. Opin. Chem. Biol.* **2008**, *12*, 556–564.

Manuscript received: March 1, 2018
Revised manuscript received: April 27, 2018
Accepted manuscript online: May 11, 2018
Version of record online: June 19, 2018

CHEMISTRY
A European Journal

Supporting Information

Biocatalytic Production of Psilocybin and Derivatives in Tryptophan Synthase-Enhanced Reactions

Felix Blei, Florian Baldeweg, Janis Fricke, and Dirk Hoffmeister*[a]

chem_201801047_sm_miscellaneous_information.pdf

Table of Contents

Experimental Procedures

Microbiological methods and growth conditions. Undifferentiated mycelium of *Psilocybe cubensis* FSU12409 was grown at 25°C. For routine strain maintenance, solid malt extract peptone (MEP) medium was used (30 g L^{-1} malt extract, 3 g L^{-1} peptone, 18 g L^{-1} agar, pH = 5.6). Fruiting bodies were grown as described previously.[1] Media components were purchased from Roth and VWR.

Identification and cloning of the *trpB* gene. The *P. cubensis trpB* gene was identified by translating the genomic sequence *in silico* using the *Aspergillus nidulans* TrpB and *Coprinopsis cinereus* TRP1 sequences[2] as queries using tblastn.[3] TrpB gene models and intron/exon junctions were predicted using Augustus software.[4] The *trpB* sequence has been desposited with GenBank under accession # MG923680. Searches for similar proteins were performed using blastp.[3] Total *P. cubensis* RNA was isolated from carpophores using Promega's SV Total RNA Isolation System according to the manufacturer's instructions. First strand cDNA synthesis was primed with oligo-d(T)-primers. The first strand reaction served as template in a subsequent PCR to amplify *trpB* full-length cDNA. The reaction (50 µL) included 0.2 mM of each dNTP, 2 mM $MgSO_4$, and 0.2 µM of primers oFB48 (5´-TATATAAAGCTTCAATGGAGGCTATCAAAAAGGTT-3´) and oFB49 (5'-TATATACTCGAGTTAGAATTTTGTTGTGTGTCCAAC-3'), and 1 U of Phusion DNA polymerase (NEB) in HF buffer supplied with the enzyme. Thermal cycling was: initial hold at 98°C for 2 min, 35 cycles of 98°C for 15 s, 65°C for 20 s, and 72°C for 80 s, and a terminal hold at 72°C for 5 min. The PCR products of *trpB* were purified by gel electrophoresis, restricted with *Hin*dIII and *Xho*I, and ligated to the expression vector pET28a, restricted equally, to yield expression plasmid pFB14, which allows production of *N*-terminally hexahistidine-tagged TrpB protein. This plasmid was used to transform *E. coli* KRX (Promega).

Enzyme production and purification. PsiD, PsiK, and PsiM were produced as described.[5] To produce TrpB, *E. coli* transformants carrying pFB14 were grown overnight in 5 mL LB-medium, selecting for kanamycin resistance (50 µg mL^{-1}). For enzyme production, a published procedure was followed.[1] The four proteins were separately purified by metal affinity chromatography on Protino Ni^{2+}-NTA resin (Macherey-Nagel). Pure proteins were desalted on PD-10 columns (GE Healthcare), equilibrated and eluted with Tris-HCl (50 mM, pH = 8.0). The purification was verified by polyacrylamide gel electrophoresis (12% Laemmli gel, Figure S1). Protein concentrations were determined by Bradford's assay.[6] For size-exclusion chromatography, a GE Healthcare ÄktaPure 25 FPLC System was used that was equipped with a Superdex 200 increase 10/300 GL column (24 mL bed volume). Proteins were eluted in 10 mM phosphate buffer, pH = 7.4, with 140 mM NaCl at a flow of 0.5 mL min^{-1}. For calibration, the high molecular weight standard (GE Healthcare) was used. To determine kinetics, the L-serine concentration of was varied between 0.5 and 4 mM, the indole concentration was varied between 30 and 900 µM, 4-hydroxyindole was varied between 30 and 60 µM. The triplicated reactions were stopped after 20, 40, 60, 80, and 100 sec. by freezing the sample in liquid nitrogen. Other reaction conditions were as described in the experimental section of the main text.

Production and purification of isonorbaeocystin (10):

The scaled-up one pot **10** product formation assays were performed with *Psilocybe cubensis* enzymes TrpB, PsiD, and PsiK, buffered in 50 mM Tris-HCl, pH = 8.0, in a volume of 10 mL. L-serine and 7-hydroxyindole were added at 2 mM, ATP and $MgCl_2$ at 6 mM, and PLP at 1 µM final concentration. Incubation was for 4 h or overnight at 25°C. The water was evaporated under reduced pressure, the residue was dissolved in methanol, centrifuged, and the supernatant collected. The solvent was removed in a rotary evaporator, and the residue was brought up in acetonitrile (ACN):0.1% trifluoroacetic acid (TFA) in water (9:1, v/v).

Pure **10** was obtained by semipreparative HPLC on an Agilent 1260 instrument that was equipped with a Zorbax Eclipse XDB C-18 column (9.4 × 250 mm, 5 µm). A linear gradient (0.1% TFA in water/ACN) was run that increased from 10 to 23% acetonitrile within 10 min, at a flow of 2 ml min^{-1}. Remaining intermediate **14** was collected during the same chromatographic runs and converted into **10** in subsequent reactions with PsiD and PsiK under the above conditions. Final purification was accomplished by chromatography on the same instrument using a ThermoFisher Hypercarb column (4.6 × 150 mm, 5 µm) with a linear water/acetonitrile gradient (1 ml min^{-1}), increasing from 20 auf 27% ACN within 12 min. The fractions containing **10** were pooled, the solvent was removed under reduced pressure and the sample was lyophilized.

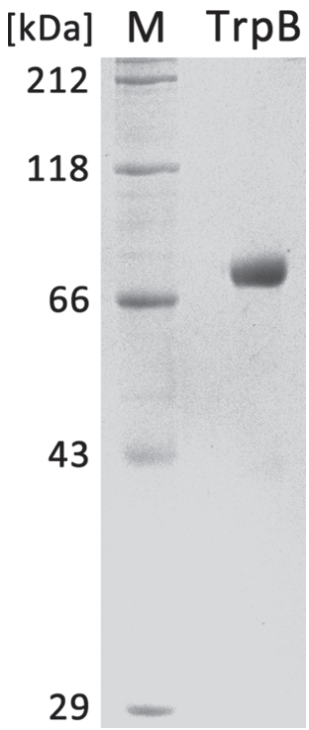

Figure S1. SDS-polyacrylamide gel electrophoresis with recombinantly produced *Psilocybe cubensis* tryptophan synthase TrpB. M: Molecular weight marker with indicated sizes.

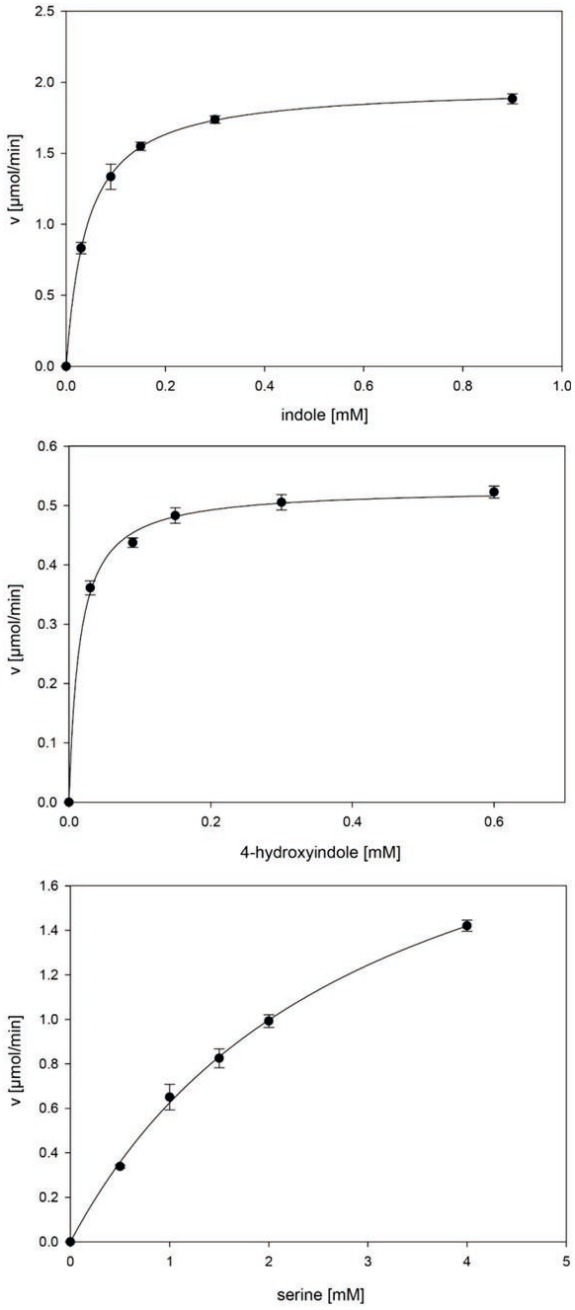

Figure S2. Plots of initial velocities of *Psilocybe cubensis* tryptophan synthase TrpB for indole, 4-hydroxyindole, and L-serine.

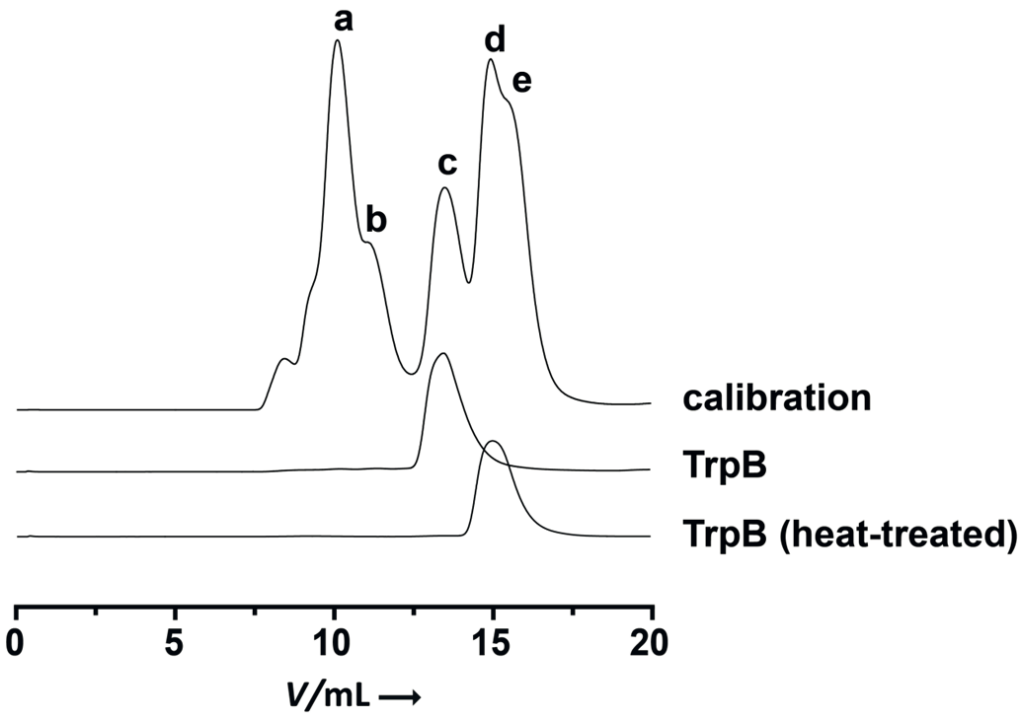

Figure S3. Size exclusion chromatography with native and heat-treated tryptophan synthase TrpB. Proteins were loaded onto a Superdex 200 column and eluted using 10 mM phosphate buffer with 140 mM NaCl. Heat-treated TrpB enzyme eluted at 14.7 mL (corresponding to ca. 77 kDa), whereas the untreated active enzyme already appeared at 13.4 mL, corresponding to ca. 155 kDa, i.e., the mass of dimeric TrpB. The calculated mass of monomeric *N*-terminally His-tagged TrpB is 77.6 kDa. The calibration track includes the following signals: a) 669 kDa (thyroglobulin), b) 440 kDa (ferritin), c) 158 kDa (aldolase), d) 75 kDa (conalbumin), e) 43 kDa (ovalbumin).

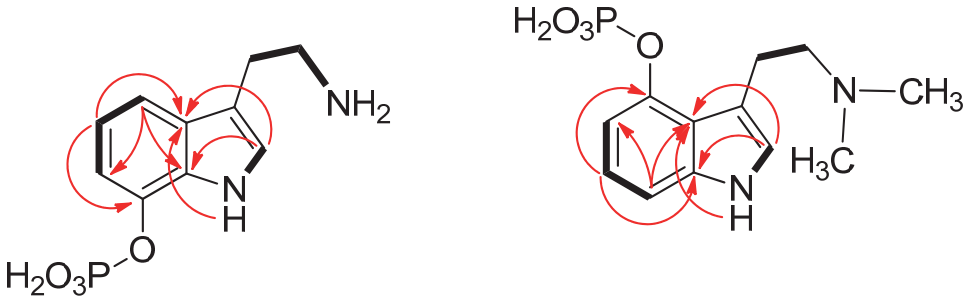

Figure S4. 2D NMR analyses that determine the position of the phosphoryloxy group in isonorbaeocystin (**10**). For comparison, correlations for psilocybin (**2**) are indicated. Key HMBC correlations (red arrows) and ^{1}H,^{1}H-COSY correlations (bold) are shown.

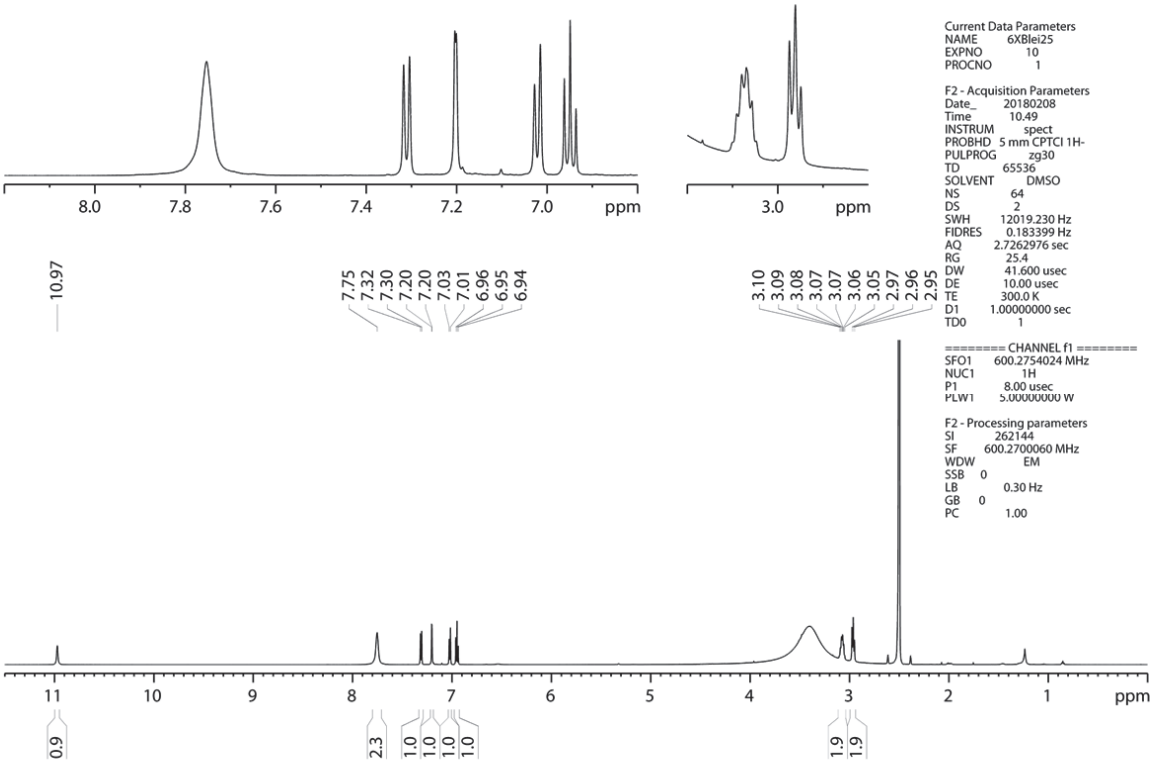

Figure S5. ^{1}H NMR spectrum of **10** in DMSO-d_6

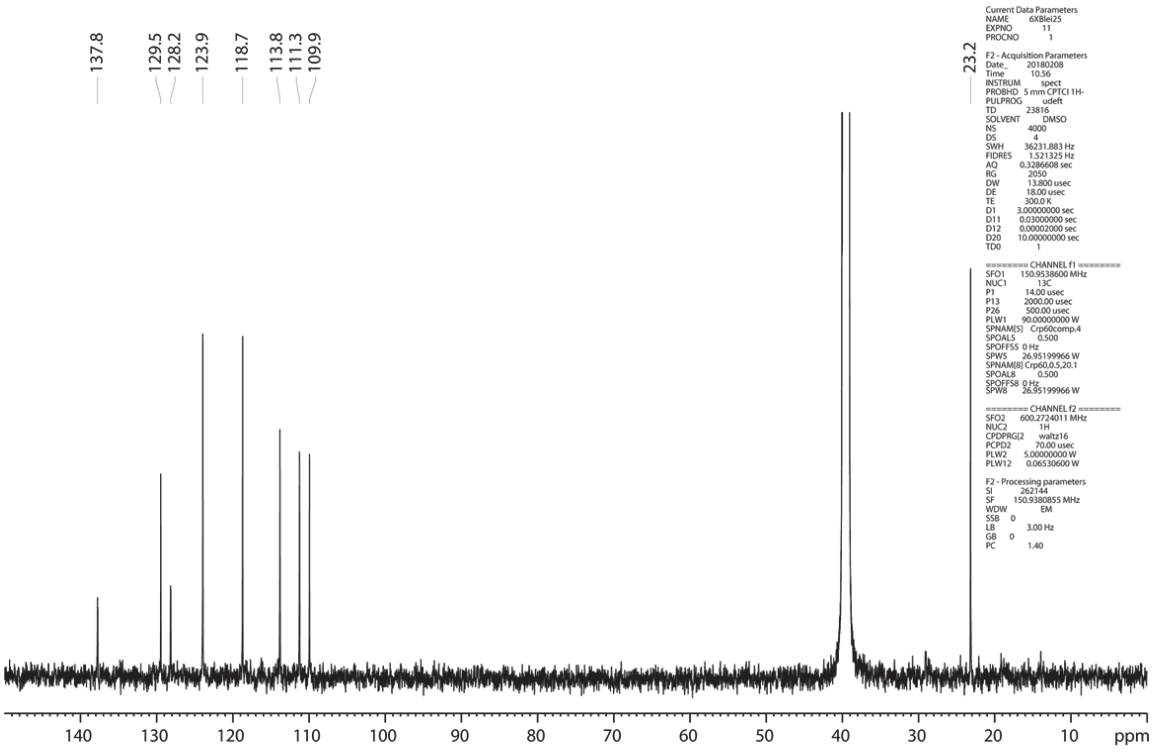

Figure S6. ^{1}H decoupled ^{13}C NMR spectrum of **10** in DMSO-d_6

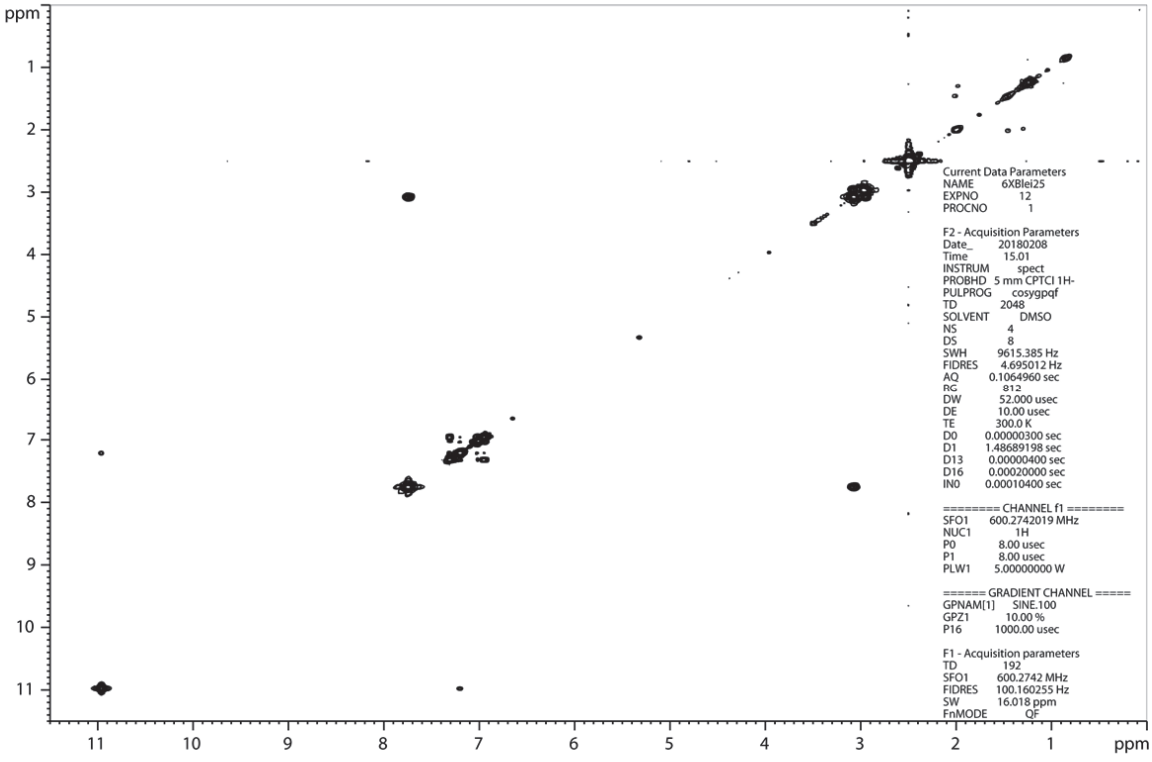

Figure S7. ^{1}H, ^{1}H COSY spectrum of **10** in DMSO-d_6

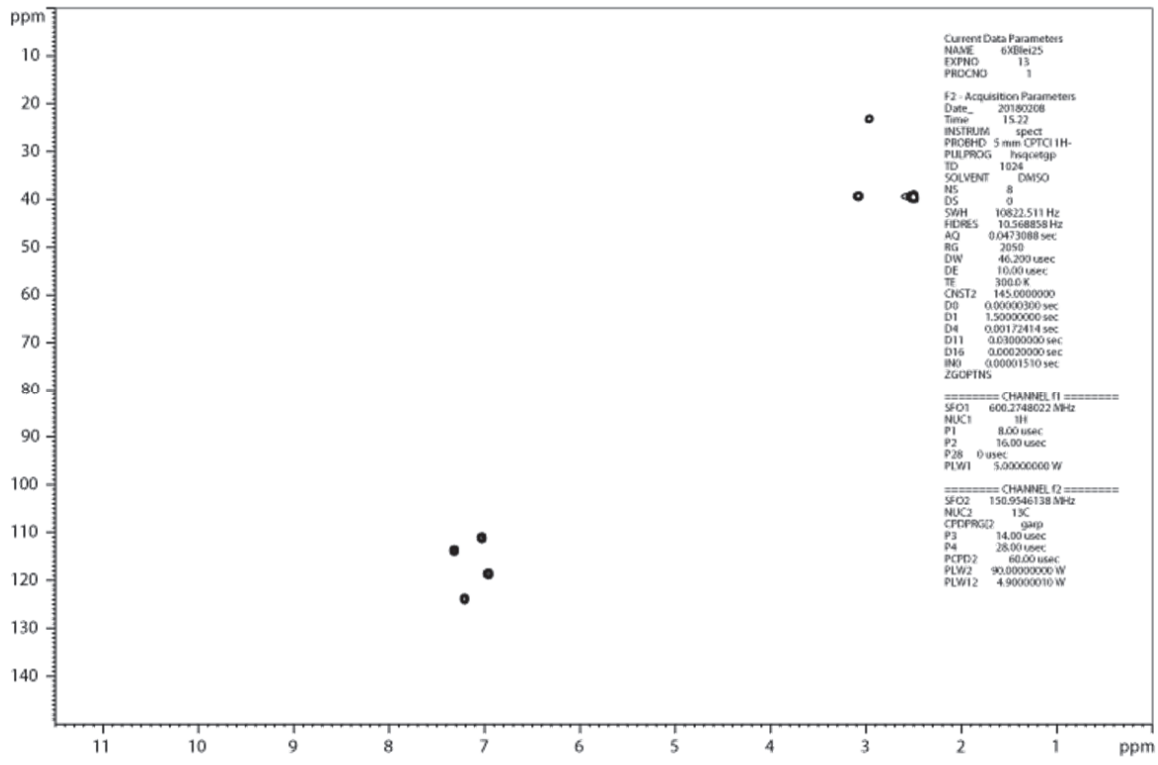

Figure S8. ^{1}H, ^{13}C HSQC spectrum of **10** in DMSO-d_6

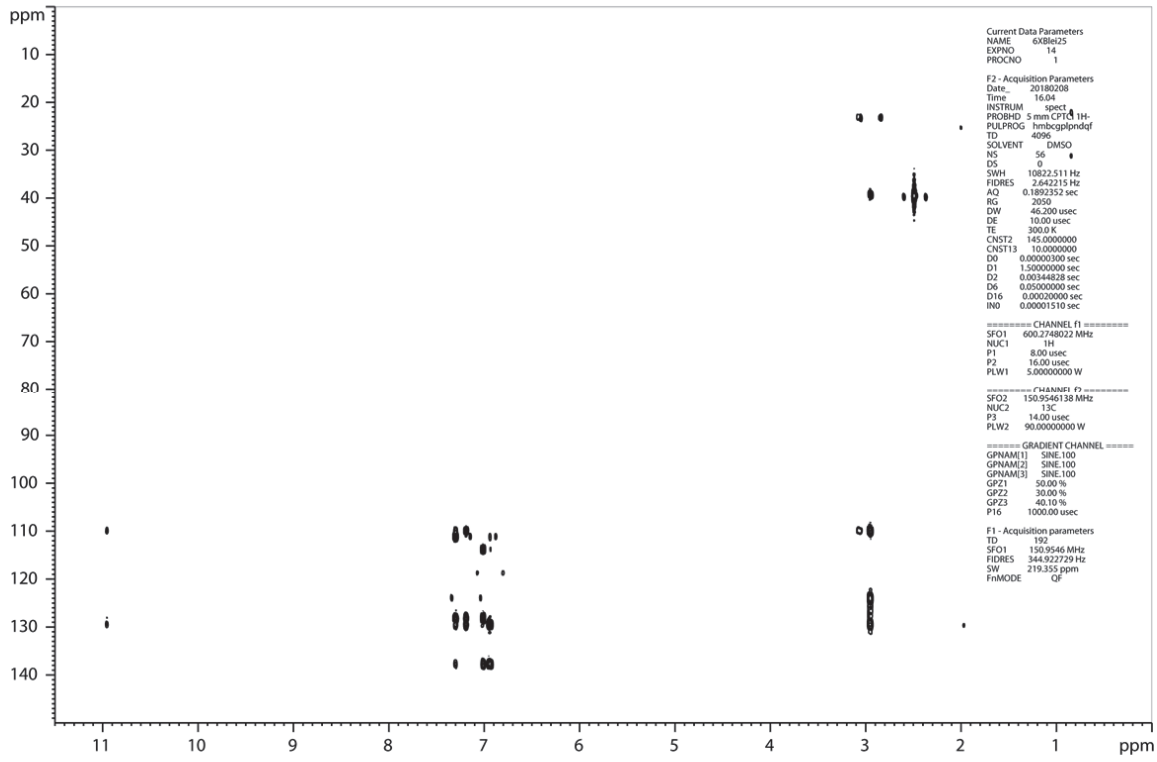

Figure S9. ^{1}H, ^{13}C HMBC spectrum of **10** in DMSO-d_6

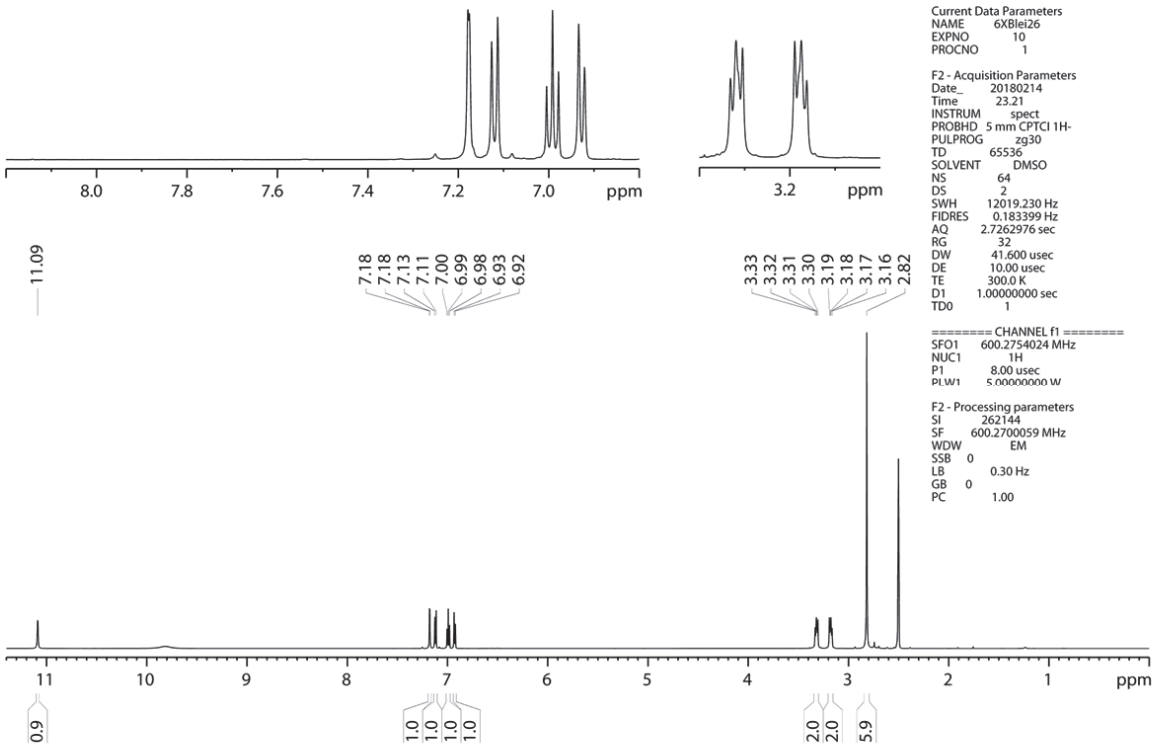

Figure S10. ^{1}H NMR spectrum of **2** in DMSO-d_6

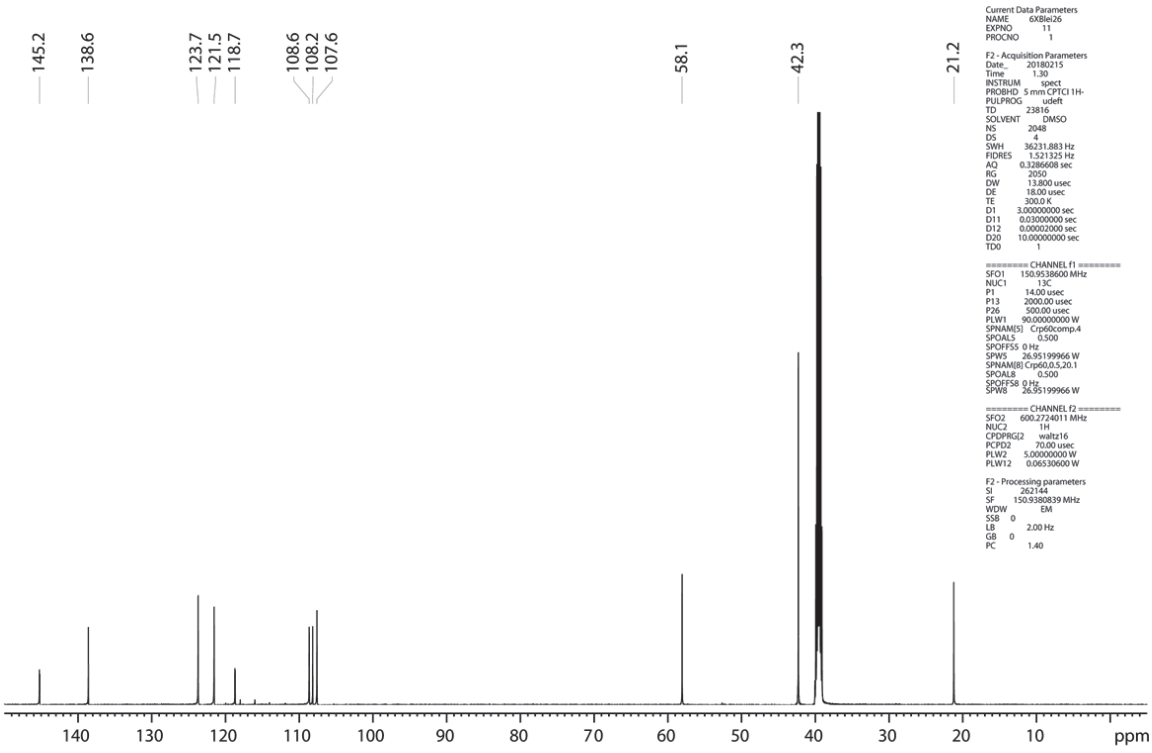

Figure S11. ^{1}H decoupled ^{13}C NMR spectrum of **2** in DMSO-d_6

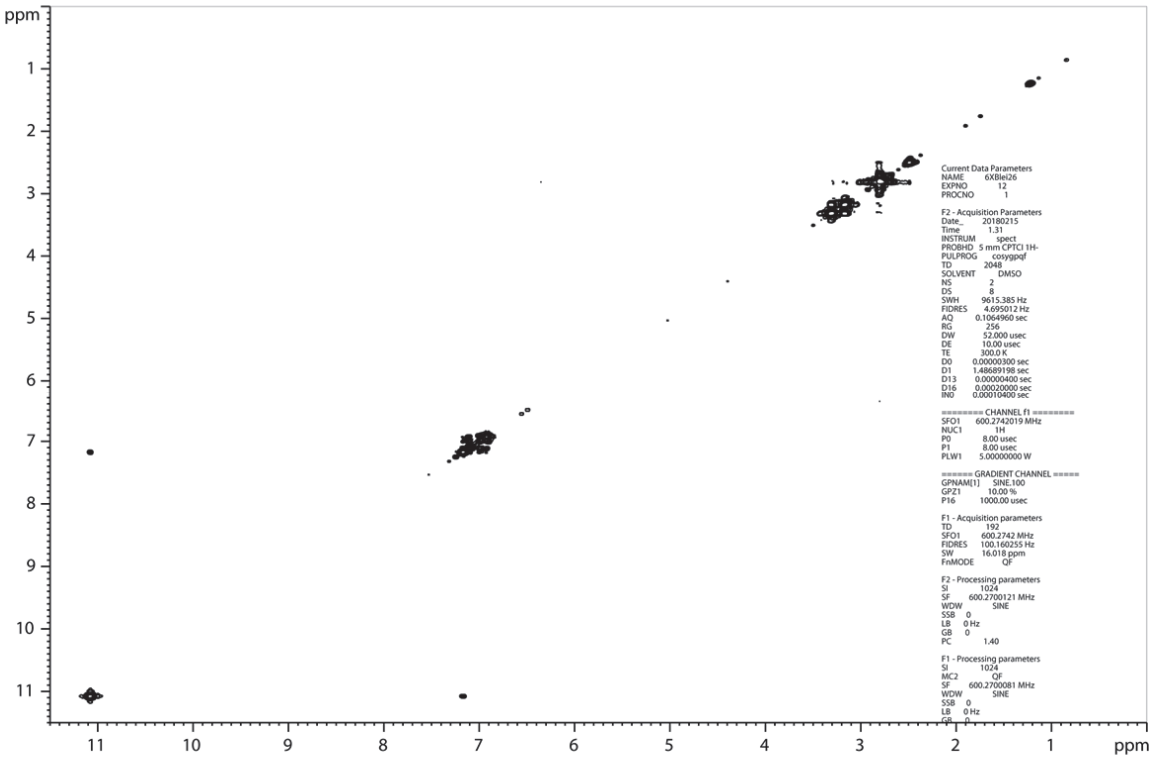

Figure S12. ^{1}H, ^{1}H COSY spectrum of **2** in DMSO-d_6

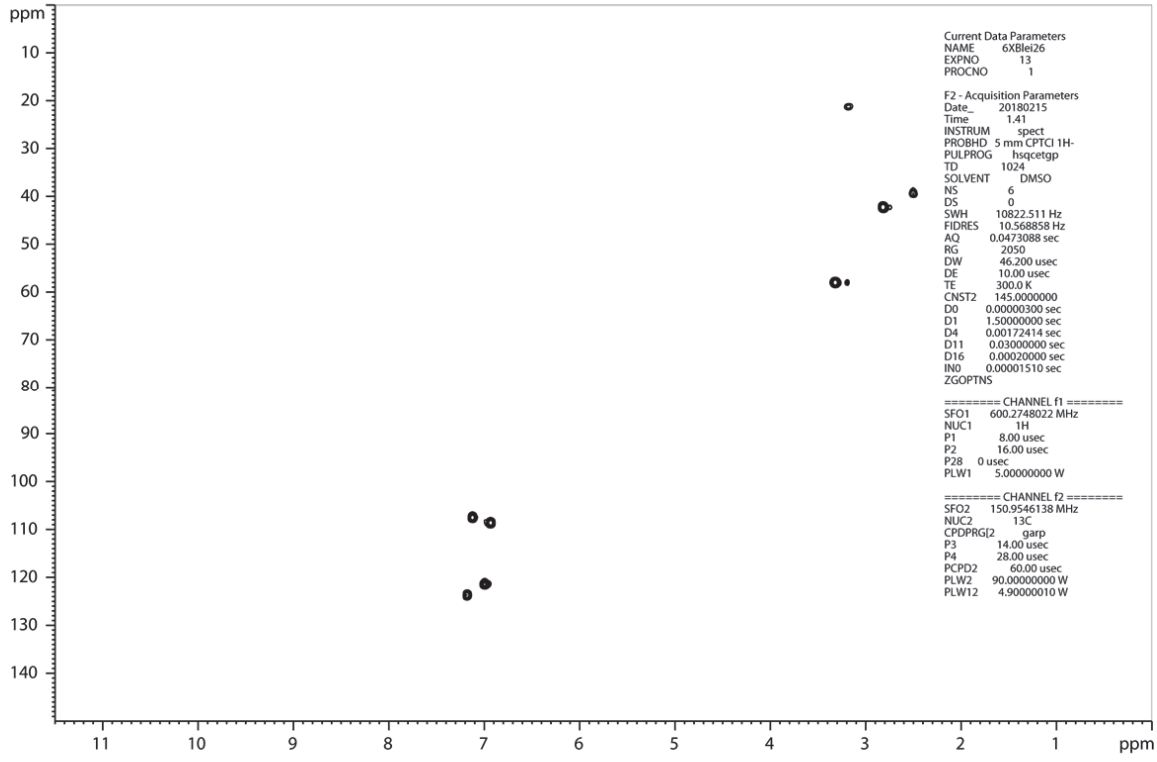

Figure S13. ^{1}H, ^{13}C HSQC spectrum of **2** in DMSO-d_6

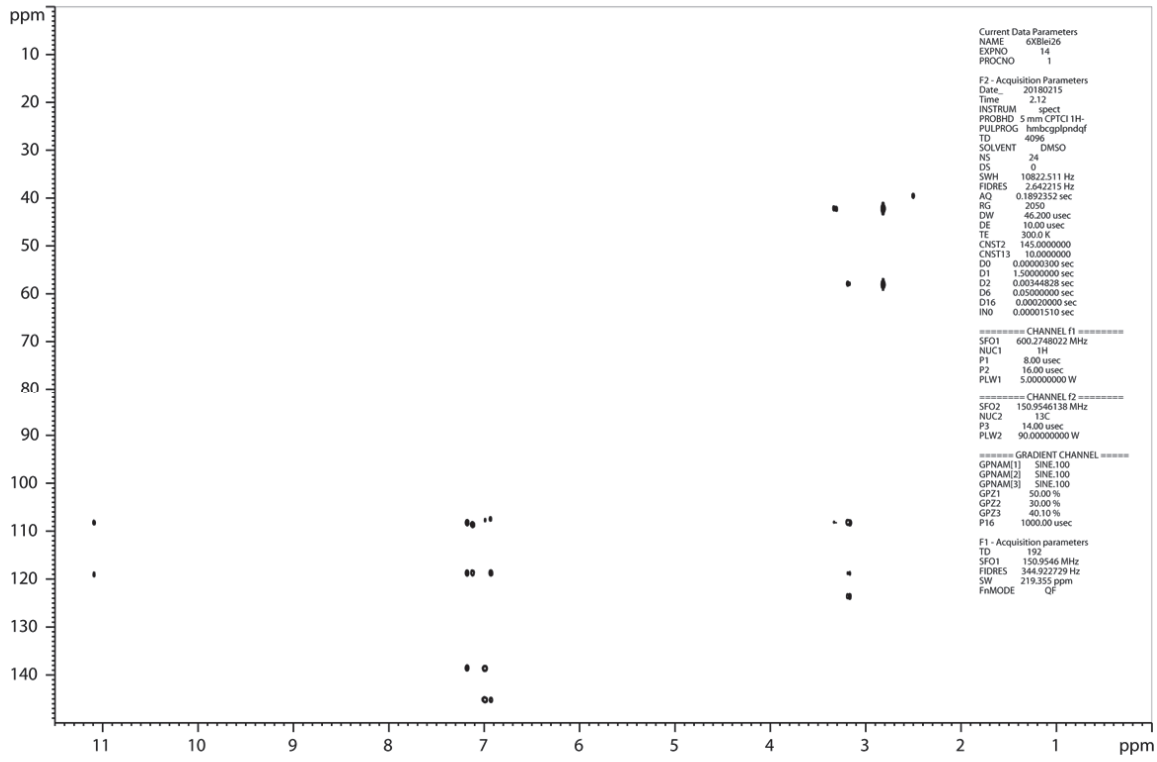

Figure S14. ^{1}H, ^{13}C HMBC spectrum of **2** in DMSO-d_6

References

[1] C. Lenz, J. Wick, D. Hoffmeister, *J. Nat. Prod*. **2017**, *80*, 2835-2838.

[2] (a) C. Skrzynia, D.M. Binninger, J.A. Alspaugh, P.J. Pukkila, *Gene* **1989**, *81*, 73-82; (b) S.E. Eckert, E. Kübler, B. Hoffmann, G.H. Braus, *Mol. Gen. Genet*. **2000**, *263*, 867-876.

[3] S.F. Altschul, T.L. Madden, A.A. Schäffer, J. Zhang, Z. Zhang, W. Miller, D.J. Lipman, *Nucleic Acids Res*. **1997**, *25*, 3389-3402.

[4] M. Stanke, R. Steinkamp, S. Waack, B. Morgenstern, *Nucleic Acids Res*. **2004**, *32*, W309-312.

[5] J. Fricke, F. Blei, D. Hoffmeister, *Angew. Chem. Intl. Ed*. **2017**, *56,* 12352-12355.

[6] M. Bradford, *Anal. Biochem*. **1976**, *72*, 248-254.

4 Unveröffentlichte Ergebnisse

4.1 Untersuchung des Einflusses von Antibiotika auf die Produktion von Malpinin durch *M. alpina* ATCC 32222

4.1.1 Einleitung

Um einen Hinweis darauf zu erhalten, ob ein Endosymbiont die gefundenen Naturstoffe produziert, wurden Kulturen von *M. alpina* ATCC 32222 unter eine starke antibiotische Behandlung gestellt. Eine ähnliche Methode führte schon bei *Rhizopus microsporus* und anderen *Mortierella* sp. zur Auslöschung des Endosymbionten.[93,94]

4.1.2 Methoden

Inkubation der Kulturen

Ein je 0,25 cm^2 großes Stück von *M. alpina*, ausgeschnitten vom Rand der Kultur, wurde zum einen auf eine einfache MEP-Platte (30 g Malzextrakt, 3 g Sojapeptone, 20 g Agar auf 1 L), zum anderen auf eine MEP-Platte, versetzt mit einer Mischung aus Antibiotika (100 µg mL^{-1} Ciprofloxacin, 50 µg mL^{-1} Chloramphenicol, 50 µg mL^{-1} Ampicillin und 50 µg mL^{-1} Kanamycin) transferiert. Die Kulturen wurden eine Woche bei 25 °C im Brutschrank inkubiert und anschließend im Kühlschrank aufbewahrt. In regelmäßigen Abständen wurden beide Kulturen auf frische Platten überführt. Nach vier Monaten wurden je 3 Kolben, welche 100 ml LB-Medium (5 g Hefeextrakt, 10 g Trypton, 10 g NaCl auf 1 L) enthielten, mit den beiden Kulturen inokuliert und bei 25 °C bei 120 RPM für eine Woche inkubiert.

Extraktion der Kulturen

Das Myzel wurde über Papierfilter in einem Büchnertrichter mittels Vakuum abgetrennt und in 50 mL-Probenröhrchen überführt. Die gefriergetrocknete und gewogene Biomasse wurde in 30 mL eines Lösemittelgemisches von Butanol, Methanol und Dimethylsulfoxid (12:12:1) aufgenommen, mit 10 Glasperlen und einem Löffel Seesand versetzt und im Homogenisator zerkleinert. Von der Flüssigkeit wurden je 1 mL abgenommen, zentrifugiert (20 817 x g, 600 s,

25 °C), über einen 0,22 µm PTFE-Filter filtriert und je 1 µL in die UPLC-MS injiziert. Unter Verwendung des in der Veröffentlichung 2 angegebenen Gradienten („Optimization of medium“) wurden die in den Proben enthaltenen Sekundärstoffe aufgetrennt und deren Massen erfasst.

4.1.3 Ergebnisse

Die Ionenchromatogramme wurden aus den Massenspuren extrahiert, die Fläche unter den Signalen bestimmt und mittels einer Kalibriergerade der Gehalt berechnet. Wie in Tabelle 1 und Abbildung 9 zu erkennen ist, hat die Behandlung nur einen leichten Einfluss auf die Produktion der Malpinine, verändert jedoch den Phänotyp.

Abbildung 9: Phänotypen der beiden unterschiedlich behandelten *M. alpina* Kulturen. Links: *M. alpina* ATCC 32222 nach antibiotischer Behandlung, Rechts: Kontrollstamm ohne antibiotische Behandlung.

Tabelle 1: Gehalt an Malpinin in den beiden unterschiedlich behandelten *M. alpina* Kulturen.

	Relativer Gehalt bezogen auf die getrocknete Biomasse Mittelwert ± Standardabweichung [µg ml^{-1}]	
Naturstoff	**Ohne Antibiotika**	**Mit Antibiotika**
Malpinin A	80.43 ± 26.04	65.81 ± 48.27
Malpinin B/C	4.47 ± 1.40	2.58 ± 2.11
Malpinin D	0.06 ± 0.03	0.06 ± 0.03

4.2 Bioaktivität von Ralsolamycin

4.2.1 Einleitung

Da Ralsolamycin, wie in Veröffentlichung 1 beschrieben, keinen Einfluss auf die Virulenz von *R. solanacearum* hatte, wurden weitere Untersuchungen zur Bioaktivität in Kooperation mit anderen Einrichtungen unternommen. Aufgrund der Lipopeptidstruktur lag die Vermutung nahe, dass Ralsolamycin zytotoxische oder antibiotische Eigenschaften aufweisen könnte.[95]

4.2.2 Ergebnisse

Zytotoxizität von Ralsolamycin

Die Zytotoxizität von Ralsolamycin (**29**) wurde an der TU Dortmund in der Arbeitsgruppe für Medizinische Chemie von Prof. Rauh untersucht. Die Messung erfolgte nach dem dort etablierten Protokoll.[96] **29** zeigte keine Zytotoxizität gegen die getesteten humanen Krebszelllinien.

Tabelle 2: Ergebnisse des Zell-Viabilitäts-Test (CellTiter-Glo®) von **29** gegen verschiedene Krebszelllinien. AN3-CA: Endometriumkarzinom, MCF-7: Brustkarzinom, ZR-75-1: Brustkarzinom, H1975: Nichtkleinzelliges Bronchialkarzinom.

	EC_{50} [nM]			
Zelllinie	AN3-CA	MCF-7	ZR-75-1	H1975
Doxorubicin	27 ±8	146 ±15	100 ±26	
Ralsolamycin	>30000 ±0	>30000 ±0	>30000 ±0	>30000 ±0

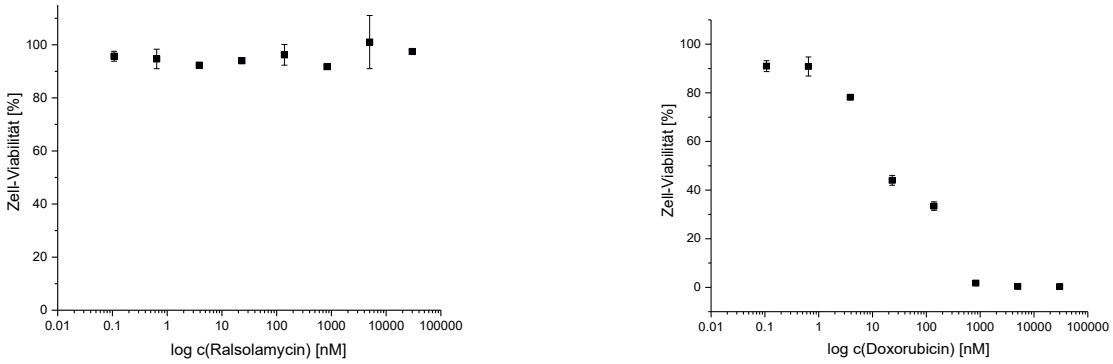

Abbildung 10: Dosis-Wirkungs-Kurve des Zell-Viabilitäts-Tests der AN3-CA-Zelllinie aus Tabelle 2. Links **29**, Rechts Doxorubicin

Antimikrobielle Aktivität von Ralsolamycin

Die antimikrobielle Aktivität wurde am Hans-Knöll-Institut in der Arbeitsgruppe von Dr. Voigt mittels Agar-Diffusions-Test nach dem dort etablierten Protokoll durchgeführt.[97] **29** zeigte eine schwache antimikrobielle Aktivität gegen alle getesteten Erreger.

Tabelle 3: Ergebnisse des Agar-Diffusions-Test auf antimikrobielle Aktivität von **29**. *Staph.*: *Staphylococcus*, *Pseud.*: *Pseudomonas*, MRSA: Methicillin-resistenter *Staphylococcus aureus*, VRE: Vancomycin-resistenter *Enterococcus faecalis*, *Myco.*:*Mycobacterium Sporo.*: *Sporobolomyces*, P: partieller Hemmhof mit einigen Kolonien, p: partieller Hemmhof mit wenigen Kolonien, F: Förderung des Wachstums.

Getesteter Stamm (JMRC-Stammnummer)	**Ralsolamycin 1000 µg ml^{-1} in MeOH**	**Ciprofloxacin 5 µg ml^{-1} in H2O**	**Amphotericin 10 µg ml^{-1} in DMSO**	**Kontrolle MeOH**
Bacillus subtillis STI:10880	14	31	-	0
Staph. aureus STI:10760	14	21	-	0
Escherichia coli ST:33699	12p	25/36p	-	0
Pseud. aeruginosa ST:33772	11P	28	-	0
Pseud. aeruginosa ST:337721	12P	28/37p	-	10
MRSA ST:33793	11P	0	-	0
VRE ST:33700	12F	18F	-	0
Myco. vaccae STI:10670	19	24p	-	0
Sporo. salmonicolor ST:35974	13	-	19p	10
Candida albicans STI:25000	10	-	21	0
Penicillium notatum STI:50164	10/15p	-	18p	10

5 Diskussion

5.1 Strukturvielfalt von Aminosäure-abgeleiteten Naturstoffen aus Mikroorganismen

Wie eingangs bereits dargestellt können Aminosäure-abgeleitete Naturstoffe aus Mikroorganismen neue Wirkstoffe darstellen oder unser Verständnis von Biosynthese-Vorgängen verbessern. In dieser Arbeit wurden die Isolation und Charakterisierung ebensolcher Stoffe aus Kulturen von *R. solanacearum*, *M. alpina* und *A. niger* oder aus *in vitro*-Reaktionen von Biosynthese-Enzymen aus *Psilocybe* gezeigt.

Obwohl diese alle aus Aminosäuren abgeleitet sind, wiesen sie eine erstaunliche strukturelle Diversität auf. Bis jetzt konnte nur den Malpininen eine biologische Funktion nachgewiesen werden. Warum so viele unterschiedliche Naturstoffe produziert werden, aber nur wenige überhaupt eine biologische Aktivität besitzen, versucht die *Screening*-Hypothese zu erklären. Die *Screening*-Hypothese geht von der Prämisse aus, dass biologische Aktivität von Sekundärmetaboliten eine selten vorkommende Eigenschaft ist. Biologisch potente Naturstoffe sind dann das Ergebnis einer unwillkürlichen Auslese (engl. *Screening*) von vielen Metaboliten gegen viele Ziele. Damit wäre die Wahrscheinlichkeit, einen Stoff zu produzieren, der mit einem Wirkziel interagieren kann und in der richtigen Konzentration am Wirkort vorliegt höher. Organismen, welche eine große Vielfalt an Naturstoffen herstellen, bei gleichzeitig niedrigen Kosten, hätten damit einen evolutionären Vorteil. Dabei sind Enzyme hilfreich, die aufgrund einer niedrigeren Substratspezifität eine höhere Diversität erzielen können.[98,99]

Dieser Mechanismus trifft auch auf die hier vorgestellten oligomeren Naturstoffe zu, da Derivate wie Ralsolamycin B, Malpinin B – E und Malpibaldin B – C als Nebenprodukte der jeweiligen NRPSs isoliert wurden. Das selbe Prinzip lässt sich auch auf die verbesserte *in vitro*-Biosynthese von Psilocybin übertragen. Die Substratflexibilität von PsiD und PsiK ermöglichte die Synthese des nicht natürlich vorkommenden Isonorbaeocystin. Dies zeigt eindrucksvoll, dass selbst Enzyme zur Biosynthese von Monomeren von der Natur darauf ausgelegt sind, ein breites Spektrum an Verbindungen synthetisieren zu können. Bei den in dieser Studie gezeigten aromatischen Dimeren wie Atromentin (**9**) oder Atrofuransäure (**30**) wird das Spektrum nicht durch Substratflexibilität, sondern durch unterschiedliche Verknüpfung der Monomeren und

sekundäre Modifikation erweitert (siehe Abschnitt 5.5). Die Befunde dieser Arbeit liegen also im Einklang mit der *Screening*-Hypothese.
Um strukturell neue Naturstoffe zu isolieren bietet es sich an, Mikroorganismen aus speziellen Nischen oder wenig beachtete Mikroorganismen als Naturstoffreservoir zu erschließen. Hier ist die Wahrscheinlichkeit niedriger bekannte Naturstoffe zu reisolieren, als zum Beispiel bei terrestrischen Actinomyceten. *R. solanacearum* als Pflanzenpathogen und *M. alpina* als „Zygomycet“ stellen eben solche ungewöhnlicheren Naturstoffproduzenten dar.

5.2 Ralsolamycin, ein neuer oligomerer Sekundärmetabolit aus *R. solanacearum* GMI1000

Untersuchungen zeigen, dass *R. solanacearum* nicht nur zur Naturstoffsynthese befähigt ist, sondern Biosynthesegene für Sekundärmetabolite, wie etwa von Staphyloferrin (**13**) und Hrp-dependent factor (**14**), auch unter dem Einfluss von Virulenz-assoziierten Regulatoren stehen.[54,55] Da Sekundärmetaboliten damit eine Rolle in der Pathogenese oder Anpassung an die Wirtspflanze zugeschrieben werden könnte, wurde das Genom von *R. solanacearum* GMI1000 nach weiteren Biosyntheseclustern untersucht und förderte beispielsweise bereits die Gencluster zur Biosynthese von Micacocidin (**11**) und den Ralfuranonen (**15**) zu Tage.[42,39] Letztere scheinen tatsächlich zur Virulenz in Tomatenpflanzen beizutragen.[100,101] Das Produkt des letzten noch nicht untersuchten Genclusters, namens Ralsolamycin (**29**), wurde in der vorliegenden Arbeit isoliert und charakterisiert. Die etablierte Struktur bestätigte die bioinformatischen Vorhersagen nur teilwiese und zeigt damit, wie wichtig chemische und biologische Methoden als Werkzeuge für das erfolgreiche *Genome Mining* sind.
Durch Vorversuche mit einer Geninaktivierungsmutante an Tomatenpflanzen (*Lycopersicon esculentum* Mill., cultivar Moneymaker) mittels Petiolen-Inokulations-Test, wurde ein möglicher Beitrag von **29** zur Virulenz von *Ralstonia* angenommen. Durch Wiederholung des Versuches mit einer größeren Pflanzenanzahl, Pflanzensamen aus anderer Bezugsquelle und Verwendung von frisch angezogenen Kulturen der Geninaktivierungsmutante konnte diese Hypothese zu einem späteren Zeitpunkt nicht bestätigt werden. Durch die Isolation von **29** in größeren Mengen konnte der Stoff auch direkt auf Blätter aufgetragen oder in die Petiolen eingebracht werden. Auch hier zeigte sich keine Wirkung auf die Tomatenpflanzen. Eine fast zeitgleich publizierte

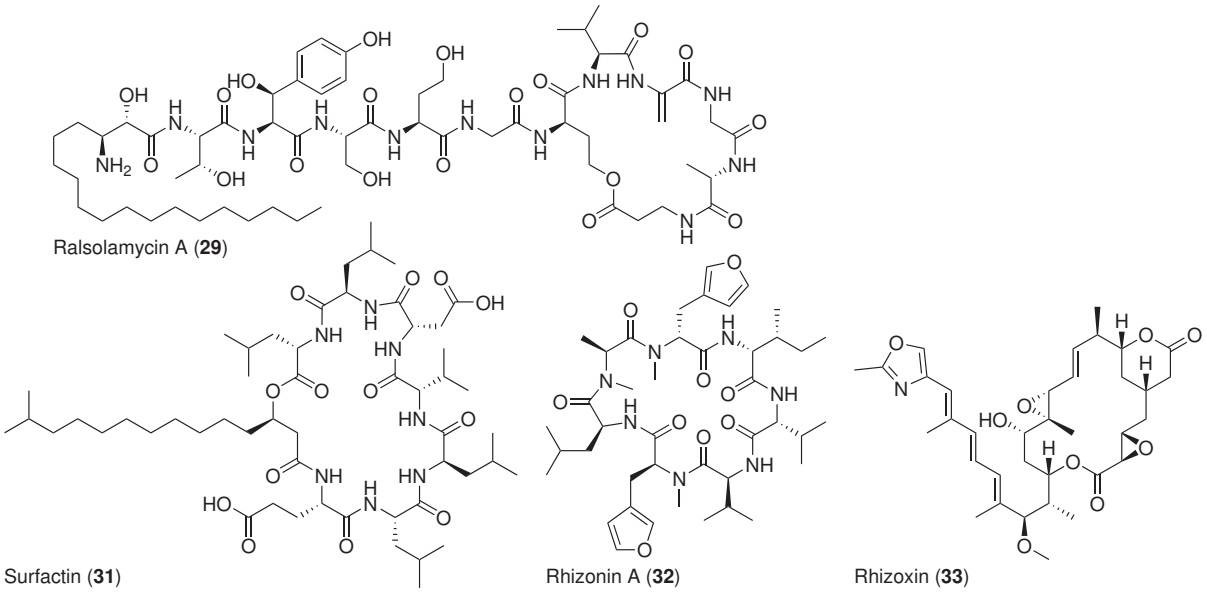

Abbildung 11: Strukturen der Zyklopeptide **29**, **31**, **32** sowie dem Phytotoxin **33**

Studie zu **29** zeigte jedoch eine Ralsolamycin induzierte Nekrose auf Blättern von Tabakpflanzen ab einer Konzentration von 100 µM. Dies bedeutet zum einen, dass die Wirkung von **29** wirtsabhängig zu sein scheint und zum anderen, dass eher eine Zytotoxizität als eine signalabhängige Wirkung besteht.[102] Eine durchgehend geringe antibiotische Aktivität gegen alle getesteten Bakterien und Pilze bestätigt diese Annahme (siehe Tabelle 3). Dagegen zeigt ein Zell-Viabilitäts-Test (CellTiter-Glo®) keine Zytotoxizität gegen humane Karzinomzelllinien (siehe Tabelle 2). Der zytotoxische Effekt auf Bakterien, Pilze und Pflanzen kann durch physiochemische Interaktionen mit der Zellmembran erklärt werden, deren Permeabilität erhöht und dadurch deren Funktion gestört wird. Ähnliches wurde bereits bei dem zyklischen Lipopeptid Surfactin (**31**) beobachtet. Auch hier steht eine schwächere Zytotoxizität gegen humane Krebszellen einer stärkeren gegen das Bakterium *Mycoplasma hyorhinis* gegenüber.[103]
Bei einigen Bakterien spielen Lipopeptide bei der Biofilmbildung, Motilität und Kolonieerweiterung eine Rolle. **31** trägt zum Beispiel zur Biofilmbildung und damit zur Funktion von *Bacillus* sp. als Biokontrollmittel gegen pflanzenpathogene Bakterien wie *Pseudomonas syringae* pv. *tomato* DC3000 bei.[104] Da **29** jedoch *in vivo* nur in geringen Mengen produziert wird, ist ein unmittelbarer Effekt als Biosurfaktant jedoch unwahrscheinlich. Zusätzlich zeigte die *rmyA*-Geninaktivierungsmutante keinen veränderten Phänotyp bezüglich der Biofilmbildung.
Weitere Veröffentlichungen schreiben **29** eine Rolle bei der mikrobiellen Kommunikation und Interaktion zu. So induziert **29** die Entwicklung von Chlamydosporen in Pilzen innerhalb der

Ascomyceten, Basidiomyceten und „Zygomyceten“.[105] Von den dickwandigen Chlamydosporen wird angenommen, dass sie das Überleben der Pilze unter widrigen Umwelteinflüssen sichern.[106] Einige, durch Co-Kultivierung erhaltene Chlamydosporen beinhalteten *R. solanacearum*. Dies zeigt, dass *R. solanacearum* zu einem endofungalen Lebensstil befähigt sein könnte.[105] Dieser Mechanismus könnte einen kleinen Beitrag zur ungewöhnlichen Persistenz von *R. solanacearum* leisten, da das Bakterium innerhalb der Chlamydosporen gut vor Umwelteinflüssen geschützt wäre. Bei verwandten gram-negativen Bakterien, insbesondere *Burkholderia* (*B.*) *rhizoxinica*, wurde bereits ein endofungaler Lebensstil in *Rhizopus microsporus* nachgewiesen.[107] *B. rhizoxinica* ist deshalb so besonders, weil es zum einen als endosymbiontisches Bakterium dem Pilz als Virulenzfaktor dient, zum anderen da es Sekundärmetabolite wie das Zyklopeptid Rhizonin (**32**) und das Makrolid Rhizoxin (**33**) produziert.[94,108] Einige Stämme der Gattung *R. solanacearum* besitzen über fast alle Phylotypen (z.B. CFBP2957, Phylotyp II; CFBP3059, Phylotyp III; PSI07, Phylotyp IV) verteilt ebenfalls das *rhi*-Gencluster zur Biosynthese für Rhizoxin. Während es in *Rhizopus microsporus* eine Rolle bei der Reiskeimlingsfäule spielt, wurde eine Beteiligung bei der Virulenz von *R. solanacearum* noch nicht nachgewiesen.[109] Bemerkenswerterweise besitzen Stämme, denen das *rhi*-Gencluster fehlt, das *rmy*-Gencluster und *vice versa*. Eine Ausnahme bildet der Stamm K60 (Phylotyp IIA), der bis auf **14** keine weiteren Sekundärmetabolite bildet. Damit steht er phylogenetisch außerhalb der restlichen Stämme und könnte eine Art Vorläuferstamm sein. Von diesem ausgehend könnten sich die anderen Stämme entwickelt haben.

Die Transkription der *rmy*-Gene unterliegt, ähnlich einiger der Virulenzgene (z.B. *hrpB*, *egl* und *fliC*), der Kontrolle des *PhcBSR quorum sensing*-Systems sowie PhcA. Es wurde gezeigt, dass die Genexpression von *rmyA* aufgrund dieses Systems mit der Dichte der Bakterienpopulation zunimmt.[110,111] Eine Mutation in diesem System (z.B. von *phcA* oder *phcB*) hat daher zum einen eine stark verminderte Virulenz und zum anderen eine Beendigung der Biosynthese von **29** zur Folge.

Interessanterweise reprimiert **29** das *imq*-Gencluster (NRPS für die Biosynthese von Imizoquinen) in *A. flavus*, welches eine Rolle bei der Verteidigung gegen oxidativen Stress und Germination des Pilzes spielt. Im Gegenzug reduzieren die Imizoquine das Wachstum von *R. solanacearum*, weswegen die Autoren einen Sekundärmetaboliten-vermittelten Antagonismus vorschlagen.[112] Ähnliches wurde auch für Bikaverin und Beauvericin aus *Fusarium fujikuroi*

und *Botrytis cinerea* beobachtet, welche die Sporen vor dem Einfall von *R. solanacearum* schützen könnten.[113] Zumindest einige Pilze erkennen **29** also als eine Art Warnsignal vor der Invasion durch *R. solanacearum*. In wie weit sich diese Ergebnisse auf die natürliche Umgebung übertragen lassen, wurde jedoch nicht untersucht.
Zusammenfassend ist **29** im Moment noch keine konkrete Rolle nachweisbar, was auf das sehr komplexe Geflecht aus Habitat, Wirtspflanze und konkurrierenden Mikroorganismen zurückzuführen ist.

5.3 Biosynthese von Naturstoffen durch pflanzenpathogene Bakterien aus genomischer Perspektive

Wie *R. solanacearum* sind auch andere pflanzenpathogene Bakterien mit der Etablierung der Genomsequenzierung vermehrt in den Fokus der Naturstoffforschung gelangt, da sich erst jetzt ihr volles Biosynthesepotential erahnen lässt. Programme wie AntiSMASH stellen dabei eine große Hilfe dar, sind aber längst nicht perfekt. So führte eine AntiSMASH-Analyse des Genoms von *Streptomyces scabiei* 87.22 (Zugangsnummer: NC_013929.1) zu insgesamt 32 Genclustern, eine manuelle Analyse zu 36 Genclustern. Außerdem sucht AntiSMASH nur nach den gängigsten Genclustern für die Biosynthese von Naturstoffen (z.B. Terpene, NRPs, PKs und RiPPs). So werden einzigartige Gencluster, wie das im Genom von *Erwinia amylovora* CFBP1430 (Zugangsnummer: NC_013961.1) vorkommende Gencluster zur Biosynthese von Thioguanin durch AntiSMASH übersehen. Auch Fehler bei der Sequenzierung und Annotation, wie bei den zwei fehlenden NRPS-Modulen im *rmyA*-Gen, dessen Sequenz in dieser Arbeit korrigiert wurde, oder die duplizierten Module des Terrechinon-Genclusters in der Genomsequenz von *A. nidulans*,[66] können sich negativ auf eine bioinformatische Vorhersage auswirken. Deshalb sollte diese auch nur als ein Werkzeug zur Aufklärung von Biosynthesewegen verstanden werden, welches im Zusammenspiel mit chemischen und biologischen Methoden verwendet werden sollte.
R. solanacearum fügt sich mit der Biosynthese von **11**, **15** und **29** nahtlos in eine Reihe von Naturstoff-produzierenden Pflanzenpathogenen ein, welche in der eingebundenen Übersichtsarbeit vorgestellt werden. Wie bereits oben erwähnt können Mikroorganismen aus Nischen neuartige Strukturen aufgrund ungewöhnlicher Biosynthesereaktionen produzieren. Ein passen-

des Beispiel ist die in der Übersicht aufgeführte Synthese von Albicidin durch eine NRPS in *Xanthomonas*. Unter anderem werden para-Aminobenzoesäuren als Substrate genutzt oder 3-Cyanoalanin *in trans* in das sich verlängernde Peptidrückgrat eingebaut. Ebenso ungewöhnlich ist die Biosynthese der antibiotisch wirksamen und phytotoxischen Zeamine durch *Dickeya* sp. Hier wird im letzten Schritt der Biosynthese der NRPS-Teil fast vollständig durch die Hydrolase ZmsN abgespalten. Das Studieren solcher ungewöhnlicher Biosynthesen und der dazugehörigen Gene zeigt, wie groß die Vielfalt an Naturstoffen ist.

5.4 Neue oligomere Sekundärmetabolite aus *M. alpina* ATCC 32222

5.4.1 Isolation und Strukturaufklärung von Malpinin, Malpikynin und Malpibaldin

Dass ein Blick aus der genomischen Perspektive Biosynthese-Kapazitäten für neue Naturstoffe aufdecken kann, zeigt *Mortierella*, ein Pilz aus der umgangssprachlichen Abteilung der „Zygomyceten". Denn nach wie vor hält sich das alte Dogma, dass „Zygomyceten" kaum zur Naturstoffbiosynthese befähigt sind. Bisher wurden „Zygomyceten" biotechnologisch zur Produktion von Ethanol, Carotinoiden, organischen Säuren (*Rhizopus* sp.) und Fettsäuren (*Mortierella* sp.) im größeren Umfang evaluiert. Publikationen über biologisch aktive Sekundärmetabolite wie die Derivate der Trisporsäure stellen eher eine Seltenheit dar.[114,115]
Die Genomsequenzierung von *M. alpina* ATCC 32222 (Zugangsnummer: ADAG00000000.1) zeigt aber entgegen dieser Prämisse außerordentlich viele Biosynthesegencluster für Naturstoffe.[58] Ebenfalls zeichnet die Menge an bisher aus *Mortierella* bekannten Sekundärmetaboliten, wie bereits in Abbildung 6 auf Seite 10 dargestellt, ein anderes Bild. In den isolierten Naturstoffen sind auch Stoffe von pharmazeutischem Interesse enthalten, wie etwa Calpinactam (**20**), welches antimykobakteriell wirkt oder „Ro 09-1679" (**21**), ein Thrombininhibitor.[63,116] *Mortierella* schien also zu einer weitreichenden Naturstoffbiosynthese befähigt und damit lohnenswert zur näheren Untersuchung. Daher wurde per *Genome Mining* versucht, diese unbekannten Substanzen zu isolieren. Mittels der Software AntiSMASH konnten 19 NRPS-Gencluster für die Produktion von oligomeren Naturstoffen ermittelt werden, von denen aber nur 13 einen funktionsfähigen Aufbau besaßen. Dies liegt wie gerade erwähnt an der unzureichenden Vorhersage aufgrund von fehlerhaften Sequenzen und Annotationen in publizierten Genomen.
Initial wurden verschiedene Extrakte von unterschiedlichen Kulturmedien und *M. alpina* Stäm-

men auf NRPS-Produkte untersucht (Molekulargewicht, UV-Absorption der Amidbindung bei 205 nm [π–π*] und 225 nm [n–π*]). Dieses Vorgehen führte zur erfolgreichen Isolation und Strukturaufklärung von drei Serien von NRPs, welche aus 13 Verbindungen bestehen. Die erste Serie sind die linearen Acetylpeptide Malpinin A – E (**34** – **38**). Deren oxidative Abbauprodukte Malpikynin A – E (**39** – **43**) bilden die zweite Serie an Substanzen und weisen die ungewöhnliche Aminosäure Kynurenin am C-terminalen Ende auf. Die dritte Serie beinhaltet die zyklischen Pentapeptide Malpibaldin A – C (**44** – **46**). Während **34** bereits unter dem Namen „MBJ-0173“ publiziert worden war, sind die restlichen Malpinine und Malpikynine neue Strukturen.[65] Eine Literatursuche zeigte, dass **44** die selbe Planarstruktur wie das Sansalvamide A-Peptid (**47**) besitzt, einem synthetischen Derivat von Sansalvamide A (**48**) aus der Gattung *Fusarium* (Abbildung 12 A). **47** fand aufgrund seiner Zytotoxizität Verwendung als Leitstruktur für die chemische Synthese von annähernd 100 Derivaten, darunter auch Diastereomere von **44** – **46**.[117,118,119] Die absolute Konfiguration von **44** und **45** wurde über Totalsynthese geklärt. Dabei stellte sich heraus, dass diese Isomere bisher weder synthetisiert wurden, noch hinsichtlich ihrer Bioaktivität charakterisiert wurden.

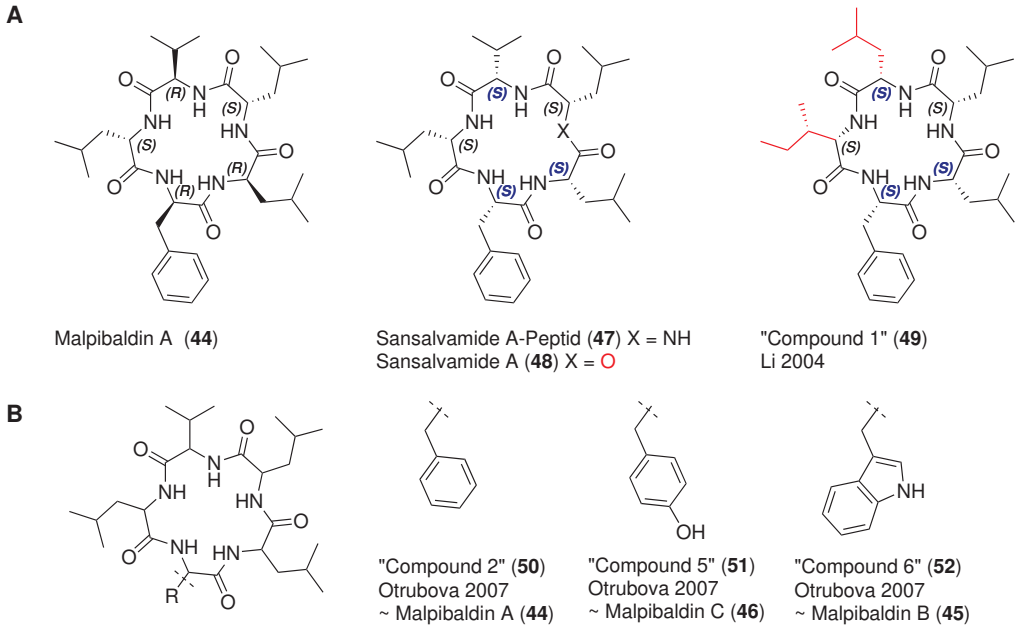

Abbildung 12: A. Strukturen von **44**, **47**, **48** und **49** mit Stereozentren. Blau: Abweichung in der Konfiguration im Vergleich zu **44**, Rot: Abweichung in der Struktur. B. Planarstrukturen von **50** – **52** und der entsprechenden Malpibaldine.

5.4.2 Bioaktivität von Zyklopentapeptiden

Für hydrophobe Zyklopentapeptide mit struktureller Ähnlichkeit zu **44** – **46** (Abbildung 12 A und Tabelle 4), wurden bereits vielversprechende Untersuchungen bezüglich der Bioaktivität durchgeführt. Beispielsweise hemmt ein hydrophobes Pentapeptid (**49**) aus *Cryptosporiopsis* sp. das Myzelwachstum verschiedener pflanzenpathogener Pilze und zeigt schwache zytotoxische Aktivität gegen humane Krebszelllinien.[120,121] Das bereits erwähnte Depsipeptid Sansalvamide A (**48**) aus *Fusarium* sp. zeigte hervorragende Aktivität gegen verschiedenste Krebszelllinien, wobei sich die Zyklisierung als erforderliches Merkmal für die Aktivität erwies.[122] Die Wirkung beruht auf der allosterischen Modulation von Hsp90, einem Chaperon. Dadurch kommt es zu einer Hemmung der Bindung von Proteinen wie IP6K2 (EC_{50} ca. 1 µM) am C-terminalen Ende von Hsp90 und damit zur Veränderung zellulärer Signaltransduktionswege.[123] Synthetische Sansalvamide-Derivate wie „Compound 2“ (**50**), „Compound 5“ (**51**) und „Compound 6“ (**52**) besitzen dieselbe Planarstruktur wie **44** – **46** und weisen ebenfalls antiproliferative Aktivität auf (Abbildung 12 B). Hierbei verringert sich die Wirkung gegen kolonale Krebszelllinien aufgrund der unterschiedlichen aromatischen Substituenten in der Reihenfolge **51**, **50** und **52**.

Tabelle 4: Vergleich der Strukturen von **44** – **46** mit bereits bekannten Verbindungen ähnlicher Struktur. Abweichungen zur Struktur der Malpibaldine fett markiert. *: Aktivität gegen Mikroorganismen oder gegen humane Krebszelllinien nachgewiesen. n.T.: nicht getestet.

Verbindung	Quelle	Strukturbausteine	Aktivität*
44	Diese Studie	D-Val-L-Leu-D-Phe-D-Leu-L-Leu	Nein
50	Otrubova 2007	**L**-Val-L-Leu-D-Phe-**L**-Leu-L-Leu	Ja
47	Carroll 2005	**L**-Val-L-Leu-**L**-Phe-**L**-Leu-L-Leu	Ja
49	Li 2004	**L-Leu-L-Ile-L**-Phe-**L**-Leu-L-Leu	Ja
53	Pan 2009	D-Val-L-Leu-**L**-Phe-D-Leu-L-Leu	Ja
54	Pan 2009	D-Val-L-Leu-D-Phe-**L**-Leu-L-Leu	Ja
45	Diese Studie	D-Val-L-Leu-D-Trp-D-Leu-L-Leu	Nein
52	Otrubova 2007	**L**-Val-L-Leu-D-Trp-**L**-Leu-L-Leu	Ja
46	Diese Studie	D-Val-L-Leu-D-Tyr-D-Leu-L-Leu	n.T.
51	Otrubova 2007	**L**-Val-L-Leu-D-Tyr-**L**-Leu-L-Leu	Ja

In der Wirkung gegen pankreatische Krebszelllinien setzt sich **50** gegenüber den anderen beiden ab.[119,117] Deswegen wurde Phenylalanin als Strukturelement in den meisten Derivaten beibehalten und die anderen vier Aminosäuren ausgetauscht. Eine lehrbuchmäßige Struktur-Wirkungsbeziehung konnten die Autoren zwar nicht etablieren, jedoch fassen sie zusammen, dass zwei aufeinander folgende D-Aminosäuren und eine N-Methylierung der Amidbindung neben den D-Aminosäuren die Wirkung verstärkt. Dieser Effekt scheint ein Resultat der veränderten Konformation des Pentazykluses zu sein.[119] Studien zur dreidimensionalen Struktur von Pentazyklen zeigen, dass diese jeweils eine Konformation bevorzugen.[124,125]
Gegensätzlich zu den publizierten Daten und trotzt ihrer Ähnlichkeit zu den in Tabelle 4 und Abbildung 12 vorgestellten Verbindungen, besitzen **44** und **45** weder zytotoxische noch antimikrobielle Aktivität. Da Moleküle, die bis auf die Konfiguration einer Aminosäure identisch sind (wie „Compound 57“ (**53**) und „Compound 33“ (**54**), Tabelle 4) Aktivität aufweisen, scheint dies besonders verwunderlich. Eine Erklärung ist, dass der Makrozyklus der Malpibaldine durch die vorliegende Konfiguration der Aminosäuren in einer sehr ungünstigen Konformation vorliegt und nicht als allosterischer Modulator von Hsp90 fungieren kann. Eine andere Möglichkeit könnte sein, dass die Pentapeptide nur gegen bestimmte Zelllinien oder unter bestimmten Versuchsbedingungen aktiv sind. Um die tatsächliche antiproliferative oder zytotoxische Wirkung der Malpibaldine zu ermitteln, erscheinen weitere Versuchsreihen sinnvoll.

5.4.3 Oberflächenaktivität von Malpininen

Wie bereits bei der Extraktion durch Schaumentwicklung zu sehen war und später durch Experimente bestätigt wurde, sind die Malpinine grenzflächenaktiv. Bisher bekannte oberflächenaktive Stoffe aus Pilzen wie Glycolipide oder Lipoproteine werden nicht durch NRPSs hergestellt.[126,127] Von bakterieller Seite sind bereits oberflächenaktive NRPS-Produkte wie das Lipopeptid Surfactin **31** bekannt. Im Vergleich zu **34** besitzt **31** aufgrund der größeren Anzahl an hydrophilen Gruppen und der Fettsäure jedoch eine stärkere Aktivität.[128] Die Malpinine könnten als Biotenside eine Funktion bei Transport und Sekretion der mehrfach ungesättigten Fettsäuren erfüllen. Mit dem Nachweis der Malpinine in den Öltröpfchen, welche sich auf dem Pilzmyzel bilden, verfestigt sich diese Annahme. Wie genau der zelluläre Transport und die Sekretion der Öltröpfchen stattfindet, ist noch nicht geklärt, jedoch gehören 4 %

der für *M. alpina* ATCC 32222 vorhergesagten Gene zu den Lipidtransportern.[58] Neben der oberflächenaktiven Eigenschaft wies Malpinin A auch schwache antimikrobielle, zytotoxische und antiproliferative Aktivitäten auf, die sich auf die tensidische Eigenschaft zurückführen lassen.

5.4.4 Biosynthese der NRPs aus *M. alpina*

Aufgrund der Struktur der isolierten Verbindungen handelt es sich wahrscheinlich um NRPs. Durch die Vorhersage der Substratspezifität der A-Domänen aller NRPS-Clustern mittels AntiSMASH konnte eine mögliche Biosynthese der Malpibaldine mittels einer fünfmoduligen NRPS postuliert werden (Zugangsnummer: ADAG01001033.1:69195-85922, Abbildung 13), während eine Zuordnung der Malpinine nicht möglich war. Die unvollständige C-Domäne vor dem ersten Modul ist aus der Gattung *Burkholderia* bekannt. Im Fall der Biosynthese von Heptarhizin wird angenommen, dass diese für die N-ständige Acetylierung verantwortlich ist.[129] Alle Versuche, eine heterolog produzierte, aktive A-Domäne für eine ATP-Austausch-Assay zu erhalten, um über die Bestimmung der Substratspezifität Malpibaldin mit dem Cluster zu verknüpfen, waren bislang nicht erfolgreich (per. Komm. Markus Gressler). Zum Beweis dieser Hypothese müsste in Zukunft der Gencluster entweder heterolog exprimiert oder eine Geninaktivierungsmutante erstellt werden. Eine Methode zur Geninaktivierung in *M. alpina* wurde bereits etabliert.[130]

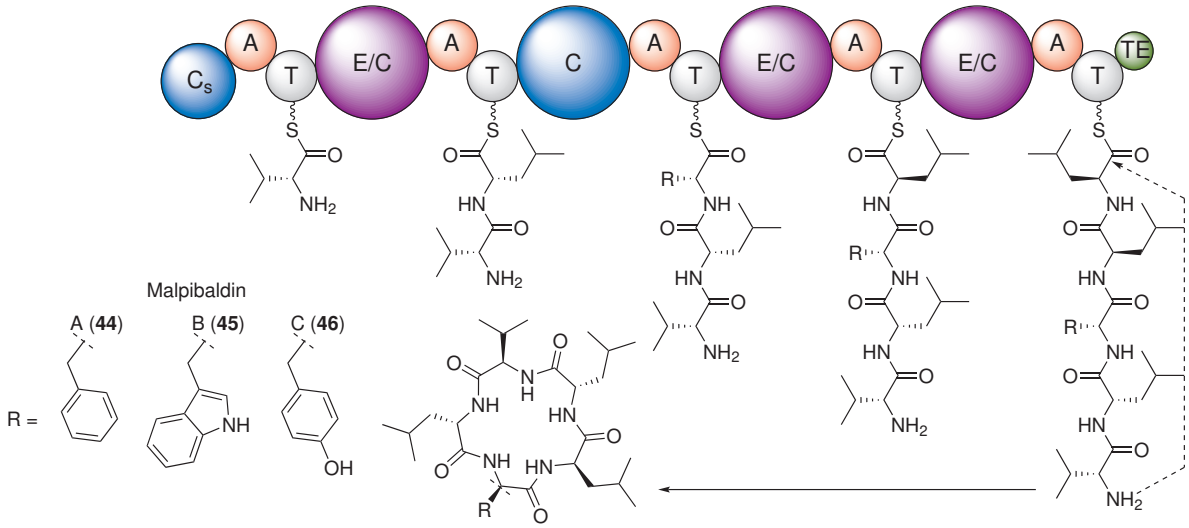

Abbildung 13: Hypothetische Biosynthese der Malpibaldine. C_S: Verkürzte C-Domäne, E/C: Duale E/C-Domäne.

Auffällig ist zudem der gehäufte Einbau von D-konfigurierten Aminosäuren in die Sekundärmetabolite (Malpinin: 5 von 7 Aminosäuren, Malpibaldin 3 von 5 Aminosäuren). Verbindungen, wie die in der Einleitung erwähnten Mortiamide (**17**) und Calpinactam (**20**) weisen ebenso einen erheblichen Anteil an D-Aminosäuren auf. Im Fallen der isolierten Verbindungen **34** – **46** erfolgt die Epimerisierung sehr wahrscheinlich *in situ* durch duale E/C Domänen innerhalb der NRPS. Einen Hinweis darauf gab die erhöhte Bildung von Malpinin D (**37**) durch Supplementation von L-Valin. Im Gegensatz dazu konnte durch die Supplementation von D-Valin keine Veränderung festgestellt werden. Außerdem weist das Gencluster, welches wahrscheinlich für die Malpibaldin-Synthese zuständig ist (Zugangsnummer: ADAG01001033.1:69195-85922, Abbildung 13) eben solche dualen E/C Domänen in der korrekten Reihenfolge auf. Der Einbau von D-Aminosäuren könnte die Funktion oder Wirkung durch Veränderung der dreidimensionalen Struktur verbessern. Auch ist der Abbau von D-Aminosäuren durch andere Mikroorganismen langsamer als der von L-Aminosäuren, was zur Stabilität des Produktes im Habitat des Pilzes beitragen könnte. Es ist nicht ungewöhnlich, dass in Antibiotika, Siderophoren oder oberflächenaktiven Stoffen (z.B. Surfactin) D-Aminosäuren als Bausteine genutzt werden.[131]

5.4.5 Endosymbiont als Naturstoffproduzent in *Mortierella*

Wie bereits in Abschnitt 5.2 erwähnt, können bakterielle Endosymbionten wie *B. rhizoxinica* für die eigentliche Biosynthese der isolierten Naturstoffe wie Rhizoxin (**33**) aus Pilzen wie *Rhizopus microsporus* verantwortlich sein. Ähnliches wurde auch von in Pflanzen lebenden Pilzen berichtet. Der Endosymbiont *Taxomyces andreanae*, ein aus *Taxus brevifolia* isolierter Ascomycet, soll für die Taxol Biosynthese verantwortlich sein.[132] Neuere Befunde sprechen jedoch gegen diese Theorie.[133,134] Hingegen konnte die Biosynthese der Maytansine durch den Ascomyceten *Hamigera avellanea* in den Wurzeln von *Putterlickia verrucosa* bewiesen werden.[135] Endosymbionten können auf vielfältige Weise Einfluss auf den Wirtsorganismus nehmen. So dient *B. rhizoxinica* als Virulenzfakor oder sorgt *Glomeribacter gigasporarum*, ein Endosymbiont des arbuskulären Mykorrhizapilzes *Gigaspora margarita*, für Nährstoffinteraktionen in einem komplexen Netzwerk aus Pflanze, Pilz und Bakterium.[136]

In letzter Zeit wurde vermehrt beobachtet, dass „Zygomyceten“ endosymbiontische Bakterien enthalten.[114] Aus Stämmen der Art *M. elongata* wurde der bakterielle Endosymbiont *Mycoa-*

vidus cysteinexigens isoliert, welcher phylogenetisch in die *Burkholderiaceae* eingeordnet wird. Damit gehören alle bisher gefundenen Endosymbionten aus „Zygomyceten“ zu den *Burkholderiaceae*.[137] Die Genomsequenzierung von *Mycoavidus cysteinexigens* zeigte, dass dessen Genom in Funktion und Größe gegenüber freilebenden *Burkholderiaceae* reduziert ist und keine NRPS-Gencluster besitzt.[93] Aufgrund dieser Funde wurde die Hypothese, dass ein Endosymbiont für die Naturstoffproduktion in *M. alpina* ATCC 32222 verantwortlich ist in dieser Arbeit zusätzlich untersucht. Die Versuche zeigen, dass *M. alpina* ATCC 32222 keinen Endosymbionten besitzt oder dieser zumindest nicht für die Produktion der isolierten Sekundärstoffe zuständig ist. Die Behandlung mit verschiedenen Antibiotika eines breiten Wirkspektrums über einen längeren Zeitraum beendete die Produktion der Sekundärmetaboliten nicht (siehe Unterabschnitt 4.1.3). Die äußerliche Veränderung, ähnlich dem Phänotypen eines Bakterien-freien *Mortierella* Stammes in einer Veröffentlichung, spricht gegen das Überleben des Endosymbionten.[93] Andererseits wurde das Gencluster zur Biosynthese der Malpinine nicht gefunden, was aber auf die lückenhafte Sequenzierung zurückgeführt werden kann. Diese zeigt sich vor allem in den oben erwähnten NRPS-Gencluster, welche keinen funktionsfähigen Aufbau besitzen. Ähnlich waren ja auch zwei NRPS-Module des *rmyA*-Gens im publizierten Genom von *R. solanacearum* GMI1000 bei der Sequenzierung und Annotation nicht erfasst worden, siehe Abschnitt 5.2. Weiterhin kann der Gencluster-Kandidat, welcher für die Produktion von Malpibaldin A-C zuständig sein könnte, aufgrund eines Introns dem Pilz zugeordnet werden. Weiterführend könnte die Endosymbiontenfreiheit zusätzlich durch fluoreszenz-mikroskopische Untersuchung des Myzels oder durch PCR-basierende 16S-Analysen von pilzlichen Homogenaten verifiziert werden.[137,138]

5.5 Wirtsabhängige Produktion von Atrofurnsäure und Atromentin durch Atromentin-Synthethasen

Homodimere, abgeleitet aus aromatischen Aminosäuren, genauer α-Keto-Säuren, sind relativ weit verbreitet in der Gattung *Aspergillus* und der Ordnung *Boletales*. Allein durch zwei 4-Hydroxyphenylpyruvat-Einheiten (aus Tyrosin) kann so durch unterschiedliche Verknüpfung, katalyisert durch NRPS-ähnliche Enzyme und eventuell anschließende Modifikationen, eine enorme Diversität entstehen (Abbildung 14 A).[139] Die neu entdeckte Atrofuransäure (**30**) besitzt ebenso eine 3-1, 2′-2-Verknüpfung wie Aspulvinon E (**24**). Jedoch wird **30** wirtsabhängig von

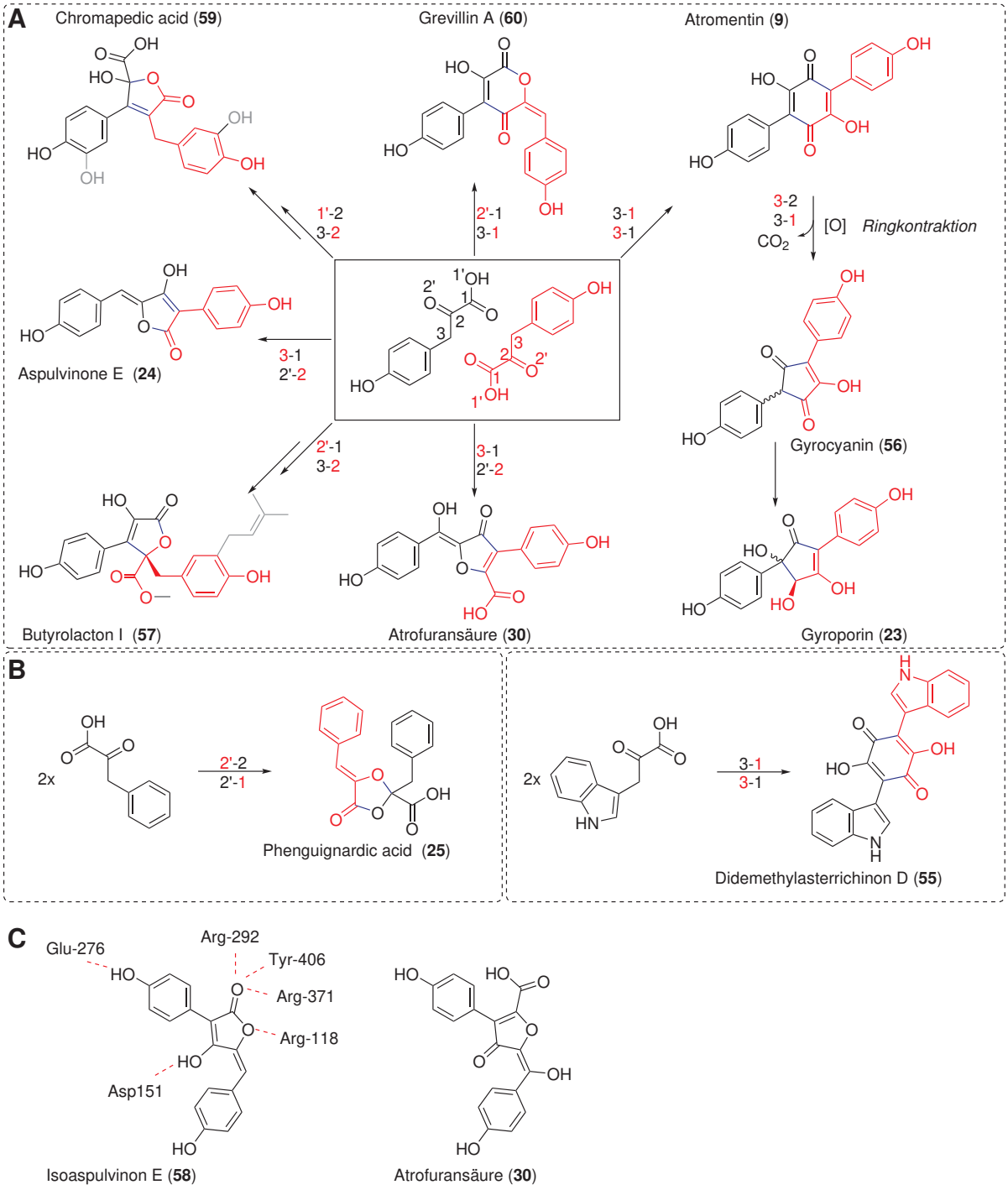

Abbildung 14: A. Beobachtete Verknüpfung von 4-Hydroxyphenylpyruvat-Einheiten von verschiedenen Atromentin-Synthetasen in *Aspergillus* und *Boletales*, vgl. Gruber et al 2014.[139] **B.** Verknüfung von Phenylpyruvat und Indolpyruvat. Verknüpfungen sind vom Elektronenpaardonor zum -akzeptor bezeichnet. **C.** Vergleich der Strukturen von **30** und **58**. Zusätzlich eingezeichnet sind die Interaktionen mit dem katalytischen Zentrum der Neuraminidase von Influenza-A-Virus H1N1.

Atromentin-Synthethasen wie AtrA oder InvA5 produziert, welche normalerweise die Bildung von Atromentin (**9**, 3-1, 3-1-Verknüpfung) katalysieren. Im Gegensatz dazu wird, nach aktuellem

Wissenstand, in jedem Wirt gleichermaßen **24** durch MelA oder ApvA hergestellt. Interessant ist, dass nach dem katalytischen Motiv von Braesel et al. (Aspargin und beendet von zwei Prolinen) alle vier genannten Enzyme einen Chinonring bilden müssten, weshalb dieses Motiv als unzureichend betrachtet werden kann.[38] Um ein verlässliches Vorhersagemodell für die Strukturbildung von Thioesterasen, wie den nichtribosomalen Code für die Substratspezifität von A-Domänen zu etablieren, müssen noch weitere NRPS-ähnliche Enzyme charakterisiert werden.[27] Interessanterweise scheinen sich die Atromentin-Synthetasen von Asco- und Basidomyceten unabhängig voneinander entwickelt zu haben, da sie in einem phylogenetischen Baum einzelne Gruppen bilden (Siehe Abbildung 5 in Veröffentlichung 4), was ein Vorhersagemodell zwischen den Abteilungen zusätzlich limitieren könnte. Der wohl bemerkenswerteste Aspekt an **30** ist jedoch die wirtsabhängige Biosynthese von **9** oder **30** in Aspergilli der Sektion *Nigri* durch die Atromentin-Synthetase. Durch Fütterungsexperimente von Atromentin wurde sichergestellt, dass **30** nicht durch sekundäre Modifikation aus Atromentin entsteht. Dies bedeutet, dass ein und dasselbe Ringbildungsmotiv wirtsabhängig einmal für einen Furanring und einmal für ein Chinonring stehen könnte. Für eine bioinformatische Vorhersage muss also auch das Wirtssystem als zusätzliche Variable beachtet werden.

Ebenso wirtsabhängig sind die bereits oben erwähnten sekundären Modifikationen. Die Produkte der NRPS-ähnlichen Enzyme scheinen als Grundkörper zur Produktion weiterer Sekundärstrukturen durch modifizierende Enzyme oder chemische Reaktion zu dienen. Beispiele hierfür sind Asp-melanin und Aspulvinon H aus **24**,[69,140] Involutin und Gyroporin aus **9**[38] oder Terrechinon A aus Didemethylasterrichinon D (**55**).[67,141] Während man in den Kulturen von *Paxillus involutus* und *A. niger* Gyroporin (**23**) finden kann, fehlt Gyrocyanin (**56**) als Zwischenprodukt in *A. niger* (Abbildung 14 A). Dies deutet auf eine unterschiedliche Biosynthese von **23** hin. In der Veröffentlichung 4 wird die Bildung von **23** durch eine Piancatelli-Umlagerung, Decarboxylierung und Oxidation über einen Metaboliten X vorgeschlagen. Ein Beweis für die Hypothese könnte eine zukünftige Strukturaufklärung von Metabolit X oder die Isolierung weiterer Metabolite bieten.

Dass es lohnenswert ist, weitere durch NPRS-ähnliche Enzyme gebildete Dimere zu isolieren, zeigen die sehr heterogenen pharmazeutischen Eigenschaften von einigen bereits isolierten Verbindungen. Allgemein stimulieren die γ-Butyrolactone die Sekundärstoffproduktion in bestimmten Pilzen, z.B. von Lovastatin (**4**), während Butyrolacton I (**57**) im speziellen als Inhibitor

der α-Glucosidase wirkt und damit gegen Typ-2-Diabetes eingesetzt werden könnte.[142,143] An anderer Stelle setzt Didemethylasterrichinon B1 an, welches als Antagonist des Insulin-Rezeptors wirkt.[144,145] Über *in silico/in vitro target fishing* wurde Atromentin als möglicher Inhibitor der 17-β-Hydroxysteroid-Dehydrogenase identifiziert, welche in Assoziation mit verschiedenen Krebsarten steht.[146] Auch direkte Zytotoxizität von Terrechinon A (**22**) und Asterrichinon-Derivaten wurde bereits nachgewiesen.[147,148] Antivirale Eigenschaften bieten beispielsweise Semicochliodinol A/B und Hinnulichinon als Inhibitor der Protease von HIV-1 sowie Isoaspulvinon E (**58**) als Inhibitor der Neuraminidase von Influenza-A-Virus H1N1.[149,150,151] Zumindest eine Grenzstruktur der in dieser Arbeit beschriebenen Atrofuransäure weist strukturelle Ähnlichkeit mit **58** auf (Abbildung 14 C). Es wurde gezeigt, dass die *E*-Konfiguration der Doppelbindung von **58** entscheidend für die korrekte Ausrichtung im katalytischen Zentrum der Neuraminidase ist. Allerdings könnte das fehlende Proton, das mit einem Asp-151 in Wechselwirkung tritt und die Carboxyl- anstatt der Ketogruppe, welche mit Arg-371, Tyr-406, Arg-292 wechselwirkt, eine veränderte Aktivität zur Folge haben.[151] Zusammenfassend könnte daher die zukünftige Untersuchung der biologischen Aktivität von **30** einen weiteren bioaktiven NRPS-ähnlichen Naturstoff hervorbringen.

5.6 Biokatalytische Erzeugung neuer Psilocybin-Derivate durch Substratflexibilität der Biosynthese-Enzyme

Auch wenn Naturstoffe nur aus einer Aminosäure aufgebaut werden, also Monomere sind, können dennoch zahlreiche unterschiedliche Verbindungen aus den korrespondierenden Biosynthesewegen hervorgehen. Bei den Psilocybin-Verwandten wird aus der aromatischen Aminosäure Tryptophan etwa Psilocin (**12**), Baeocystin (**26**), Norbaeocystin (**27**) und Norpsilocin (**28**), siehe Abbildung 8 auf Seite 11. Solche Derivate können enzymatisch durch unterschiedliche Biosynthese-Enzyme oder deren iterativer Reaktion entstehen. Ein besonderer Fall tritt ein, wenn ein Enzym flexibel in seiner Substratspezifität ist. Dann können nicht natürlich vorkommende Produkte durch eine Vorläufer-gesteuerte Biosynthese aus veränderten Substraten generiert werden. Häufig kommt diese Methode bei der Erzeugung von Antibiotika-Derivaten aus PKSs und NRPSs zum Einsatz.[152,153] In der vorliegenden Arbeit wurde unter anderem mit der Erzeugung von Isonorbaeocystin aus 4-Hydroxytryptophan die Flexibilität von PsiD und PsiK demonstriert.

Zieht man in Betracht, dass bereits Psilocybin-Verwandte wie Baeocystin als psychoaktiv beschrieben wurden, können durch die Derivatisierung des Tryptophans neue Wirkstoffe gestaltet werden.[154] Eine Veränderung der Selektivität und Affinität zu 5-HT_{2A} und 5-HT_{2C} Rezeptoren könnte zu einem günstigeren Wirkungs- und Nebenwirkunsprofil oder Pharmakokinetik führen. Aufgrund von in der Literatur beschriebenen Selbstversuchen ist ebenfalls bekannt, dass Psilocybin und Lysergsäurediethylamid (LSD) effizient gegen Cluster-Kopfschmerzen wirken, auch wenn klinische Studien noch ausstehen.[155] Das nicht-halluzinogene LSD-Derivat 2-Bromo-LSD war bereits Gegenstand einer kleinen Fallstudie. Allerdings wurde in der Vergangenheit ein Fall eines halluzinogenen Zustandes eines Laborarbeiters berichtet.[156,157] Es ist also durchaus vorstellbar, dass nicht-psychoaktive Psilocybin-Derivate aufgrund ihrer Tryptaminstruktur eine Aktivität gegen Cluster-Kopfschmerz besitzen könnten. Die Grundlage für die biotechnologische Herstellung dieser neuen Strukturderivate liegt in der kostengünstigen Bereitstellung der Substrate und Reaktionen mit hoher Ausbeute. Für die biotechnologische Herstellung von Tryptophan-Derivaten hat sich vor allem die Tryptophansynthase TrpB als nützlich erwiesen. Diese katalysiert die Bildung aus Serin und einem Indolgrundkörper. Somit lassen sich auch veränderte Aminosäuren wie halogenierte oder nitrierte Tryptophane biokatalytisch in hoher Ausbeute herstellen und als Substrate nutzen.[158]

5.7 Ausblick

Einerseits tragen die in dieser Arbeit neu isolierten und charakterisierten Aminosäure-abgeleiteten Naturstoffe zum Mosaik der Naturstoffforschung bei, andererseits eröffnen sie aber zeitgleich auch die Perspektiven auf weitere unbekannte Naturstoffe. Die wirtsabhängige Produktion von Atrofuransäure verdeutlicht, dass NRPS-ähnliche Enzyme noch nicht in Gänze verstanden sind. Die heterologe Produktion weiterer NRPS-ähnlicher Enzyme aus *Aspergillus* könnte, ähnlich wie es bei Atromentin und Atrofuransäure der Fall war, weitere neue Verbindungen liefern. Die gefundenen Acylpeptide und Zyklopeptide aus *M. alpina* zeigen, dass „Zygomyceten“ ein nicht genutztes Reservoir zur Isolation von Naturstoffen sind. Das Genom von *M. alpina* ATCC 32222 enthält noch weitere Gencluster, denen noch keine NRPs zugeordnet werden konnten. Die Kultivierung nach dem erwähnten OSMAC-Ansatz oder das Füttern mit Isotopen-markierten Substraten sollte noch weitere neue NRPs zu Tage fördern. Durch die in dieser Arbeit gezeigte

Substratflexibilität einer neu etablierten biokatalytischen Syntheseroute für Psilocybin können weitere Psilocybin-Derivate hergestellt und hinsichtlich ihrer Wirkung untersucht werden.
Die Notwendigkeit neuer Wirkstoffe, gerade von Antibiotika, und die eingangs dargestellte Relevanz von Naturstoffen unterstreicht den Stellenwert der Naturstoffforschung. Die Diversität der in dieser Arbeit gefundenen Strukturen und der Ausblick auf weitere Verbindungen, welche als Wirkstoffe dienen könnten, verdeutlichen die Unerschöpflichkeit der Natur. Daher kann man Goethe nur recht geben: "Denn die Natur ist aller Meister Meister!".

6 Summary

Amino acids represent universal building blocks in the biosynthesis of a variety of structurally diverse natural products. While mega-enzymes like non-ribosomal peptide synthetases (NRPS) produce oligomeric products, monomodular NRPS-like enzymes catalyze the homodimerization of two amino acid derivatives. Monomers like psilocybin are synthetized from amino acids by discrete enzymes. This work focused on the isolation and characterization of these compounds.
The bacterium *Ralstonia solanacearum* is one of the ecologically and economically most important plant pathogens. For the first time, the lipodepsipeptide ralsolamycin was isolated from cultures of the bacterium, the structure was elucidated and the contribution to the virulence was assessed. The identification of the oligomere closed one of the last gaps in the secondary metabolome of *R. solanacearum*.
In contrast, „zygomycetes“ eking out a niche existence and their secondary metabolome is insufficiently explored. In this work, three series (malpinins, malpikynins, malpibaldins) of nonribosomal peptides were isolated from *Mortierella alpina* and characterized. The heterogeneity of the structures of these 13 oligomers proves that „zygomycetes“ are capable of extensive secondary metabolite synthesis and represent worthwhile research objects.
While NRPSs are well studied, NRPS-like enzymes need further attention. The heterologous expression of atromentin synthetases (NRPS-like enzymes) in several Aspergilli led to the formation of a new dimeric product called atrofuranic acid in the place of atromentin. This demonstrates the major impact of host-systems in product-formation of the very same enzyme via cross-chemistry and helps to further understand NRPS-like enzymes.
Another approach to enhance the product diversity is given by the substrate flexibility of biosynthesis enzymes. Beside creating an enhanced biosynthetic route for psilocybin by utilization of the tryptophan synthase TrpB of *Psilocybe cubensis*, the formation of the unnatural product isonorbaeocystin from the substrate 7-hydroxyindole was shown.

7 Zusammenfassung

Aminosäuren stellen einen universellen Grundbaustein zur Biosynthese einer Vielzahl strukturell diverser Naturstoffe dar. Während Megaenzyme wie nichtribosomale Peptidsynthetasen (NRPS) oligomere Produkte erzeugen, wird durch monomodulare NRPS-ähnliche Enzyme in der Regel die Homodimerisierung zweier Aminosäureabkömmlinge katalysiert. Monomere wie das Psilocybin werden über eigenständige Enzyme aus Aminosäuren synthetisiert. Die Isolation und Charakterisierung dieser Verbindungen stand im Mittelpunkt dieser Arbeit.

Das Bakterium *Ralstonia solanacearum* ist eines der ökologisch und ökonomisch wichtigsten Pflanzenpathogene. Erstmalig wurde das Lipodepsipeptid Ralsolamycin aus den Kulturen des Bakterium isoliert, seine Struktur aufgeklärt und hinsichtlich seines Beitrags zur Virulenz charakterisiert. Die Identifikation dieses Oligomers schließt eine der letzten verbleibenden Lücken im Sekundärmetabolom von *R. solanacearum*.

Im Gegensatz dazu fristen „Zygomyceten“ bisher ein Nischendasein und ihre Sekundärmetabolome sind nur lückenhaft erforscht. In dieser Arbeit wurden drei Serien (Malpinine, Malpikynine, Malpibaldine) von größtenteils unbekannten nichtribosomalen Peptiden aus *Mortierella alpina* isoliert und charakterisiert. Die Heterogenität der Strukturen innerhalb dieser 13 Oligomere beweist, dass „Zygomyceten“ zu einer umfangreichen Sekundärstoff-Biosynthese befähigt sein können und lohnende Forschungsobjekte darstellen.

Während NRPSs zufriedenstellen untersucht wurden, besteht bei NRPS-ähnlichen Enzymen noch Nachholbedarf. Die heterologe Expression von Atromentin-Synthethasen in verschiedenen Aspergilli führte überraschenderweise zur Bildung eines neuen dimeren Produktes names Atrofuransäure anstelle von Atromentin. Dies belegt, dass das Wirtssystem über *Cross-chemistry* einen erheblichen Einfluss auf die Produktbildung durch ein und das selbe Enzym haben kann und hilft bei dem Verständnis der NRPS-ähnlichen Enzyme.

Ein weiterer Weg der Natur die Produktvielfalt zu erhöhen ist über die Substratflexibilität der Biosynthese-Enzyme. Neben der Etablierung einer effizienteren, biotechnologischen Syntheseroute für Psilocybin durch die Tryptophansynthase TrpB aus *Psilocybe cubensis* wurde auch erstmals die Synthese des nicht natürlich vorkommenden Isonorbaeocystin durch Verwendung von 7-Hydroxyindol als Substrat gezeigt.

Literaturverzeichnis

[1] Newman, D. J.; Cragg, G. M. *J. Nat. Prod.* **2016**, *79*, 629–661.

[2] Newton, G. G.; Abraham, E. P. *Nature* **1955**, *175*, 548.

[3] Staunton, J.; Wilkinson, B. *Chem. Rev.* **1997**, *97*, 2611–2630.

[4] Birch, A. J.; Holzapfel, C. W.; Rickards, R. W. *Tetrahedron* **1966**, *22*, 359–387.

[5] Alberts, A. W.; Chen, J.; Kuron, G.; Hunt, V.; Huff, J.; Hoffman, C.; Rothrock, J.; Lopez, M.; Joshua, H.; Harris, E.; Patchett, A.; Monaghan, R.; Currie, S.; Stapley, E.; Albers-Schonberg, G.; Hensens, O.; Hirshfield, J.; Hoogsteen, K.; Liesch, J.; Springer, J. *Proc. Natl. Acad. Sci. U. S. A.* **1980**, *77*, 3957–3961.

[6] Dreyfuss, M.; Härri, E.; Hofmann, H.; Kobel, H.; Pache, W.; Tscherter, H. *Eur. J. Appl. Microbiol.* **1976**, *3*, 125–133.

[7] Ikeda, H.; Omura, S. *Chem. Rev.* **1997**, *97*, 2591–2610.

[8] Arcamone, F.; Franceschi, G.; Penco, S.; Selva, A. *Tetrahedron Lett.* **1969**, *10*, 1007–1010.

[9] Corre, C.; Challis, G. L. *Chem. Biol.* **2007**, *14*, 7–9.

[10] Zani, C. L.; Carroll, A. R. *J. Nat. Prod.* **2017**, *80*, 1758–1766.

[11] Raaijmakers, J. M.; Mazzola, M. *Annu. Rev. Phytopathol.* **2012**, *50*, 403–424.

[12] Haefner, B. *Drug Discov. Today* **2003**, *8*, 536–544.

[13] Osbourn, A. E.; Field, B. *Cell. Mol. Life Sci.* **2009**, *66*, 3755–3775.

[14] Bachmann, B. O.; van Lanen, S. G.; Baltz, R. H. *J. Ind. Microbiol. Biotechnol.* **2014**, *41*, 175–184.

[15] Dewick, P. M. *Medicinal Natural Products: A Biosynthetic Approach*, 3rd ed.; Wiley: Chichester, 2009.

[16] Köksal, M.; Hu, H.; Coates, R. M.; Peters, R. J.; Christianson, D. W. *Nat. Chem. Biol.* **2011**, *7*, 431–433.

[17] Rawlings, B. J. *Nat. Prod. Rep.* **1998**, *15*, 275–308.

[18] Shen, B. *Curr. Opin. Chem. Biol.* **2003**, *7*, 285–295.

[19] Hertweck, C. *Angew. Chem., Int. Ed.* **2009**, *48*, 4688–4716.

[20] Fischbach, M. A.; Walsh, C. T. *Chem. Rev.* **2006**, *106*, 3468–3496.

[21] Ozcengiz, G.; Demain, A. L. *Biotechnol. Adv.* **2013**, *31*, 287–311.

[22] Arnison, P. G.; Bibb, M. J.; Bierbaum, G.; Bowers, A. A.; Bugni, T. S.; Bulaj, G.; Camarero, J. A.; Campopiano, D. J.; Challis, G. L.; Clardy, J.; Cotter, P. D.; Craik, D. J.; Dawson, M.; Dittmann, E.; Donadio, S.; Dorrestein, P. C.; Entian, K.-D.; Fischbach, M. A.; Garavelli, J. S.; Göransson, U.; Gruber, C. W.; Haft, D. H.; Hemscheidt, T. K.; Hertweck, C.; Hill, C.; Horswill, A. R.; Jaspars, M.; Kelly, W. L.; Klinman, J. P.; Kuipers, O. P.; Link, A. J.; Liu, W.; Marahiel, M. A.; Mitchell, D. A.; Moll, G. N.; Moore, B. S.; Müller, R.; Nair, S. K.; Nes, I. F.; Norris, G. E.; Olivera, B. M.; Onaka, H.; Patchett, M. L.; Piel, J.; Reaney, M. J. T.; Rebuffat, S.; Ross, R. P.; Sahl, H.-G.; Schmidt, E. W.; Selsted, M. E.; Severinov, K.; Shen, B.; Sivonen, K.; Smith, L.; Stein, T.; Süssmuth, R. D.; Tagg, J. R.; Tang, G.-L.; Truman, A. W.; Vederas, J. C.; Walsh, C. T.; Walton, J. D.; Wenzel, S. C.; Willey, J. M.; van der Donk, W. A. *Nat. Prod. Rep.* **2013**, *30*, 108–160.

[23] Lipmann, F.; Gevers, W.; Kleinkauf, H.; Roskoski, R. *Adv. Enzymol. Relat. Areas Mol. Biol.* **1971**, *35*, 1–34.

[24] Bode, H. B.; Brachmann, A. O.; Jadhav, K. B.; Seyfarth, L.; Dauth, C.; Fuchs, S. W.; Kaiser, M.; Waterfield, N. R.; Sack, H.; Heinemann, S. H.; Arndt, H.-D. *Angew. Chem., Int. Ed.* **2015**, *54*, 10352–10355.

[25] Schwarzer, D.; Finking, R.; Marahiel, M. A. *Nat. Prod. Rep.* **2003**, *20*, 275–287.

[26] Finking, R.; Marahiel, M. A. *Annu. Rev. Microbiol.* **2004**, *58*, 453–488.

[27] Stachelhaus, T.; Mootz, H. D.; Marahiel, M. A. *Chem. Biol.* **1999**, *6*, 493–505.

[28] Röttig, M.; Medema, M. H.; Blin, K.; Weber, T.; Rausch, C.; Kohlbacher, O. *Nucleic Acids Res.* **2011**, *39*, W362–W367.

[29] Bachmann, B. O.; Ravel, J. In *Chapter 8. Methods for in silico prediction of microbial polyketide and nonribosomal peptide biosynthetic pathways from DNA sequence data*; Hopwood, D. A., Ed.; Methods in Enzymology; Academic Press: Cambridge, 2009; Vol. 458; pp 181–217.

[30] Süssmuth, R. D.; Mainz, A. *Angew. Chem., Int. Ed.* **2017**, *56*, 3770–3821.

[31] Alonzo, D. A.; Magarvey, N. A.; Schmeing, T. M. *PLoS One* **2015**, *10*, e0128569.

[32] Lambalot, R. H.; Gehring, A. M.; Flugel, R. S.; Zuber, P.; LaCelle, M.; Marahiel, M. A.; Reid, R.; Khosla, C.; Walsh, C. T. *Chem. Biol.* **1996**, *3*, 923–936.

[33] Stachelhaus, T.; Hüser, A.; Marahiel, M. A. *Chem. Biol.* **1996**, *3*, 913–921.

[34] Belshaw, P. J.; Walsh, C. T.; Stachelhaus, T. *Science* **1999**, *284*, 486–489.

[35] Du, L.; Lou, L. *Nat. Prod. Rep.* **2010**, *27*, 255–278.

[36] Walsh, C. T.; Chen, H.; Keating, T. A.; Hubbard, B. K.; Losey, H. C.; Luo, L.; Marshall, C. G.; Miller, D. A.; Patel, H. M. *Curr. Opin. Chem. Biol.* **2001**, *5*, 525–534.

[37] Hühner, E.; Backhaus, K.; Kraut, R.; Li, S.-M. *Appl. Microbiol. Biotechnol.* **2018**, *102*, 1663–1672.

[38] Braesel, J.; Götze, S.; Shah, F.; Heine, D.; Tauber, J.; Hertweck, C.; Tunlid, A.; Stallforth, P.; Hoffmeister, D. *Chem. Biol.* **2015**, *22*, 1325–1334.

[39] Wackler, B.; Schneider, P.; Jacobs, J. M.; Pauly, J.; Allen, C.; Nett, M.; Hoffmeister, D. *Chem. Biol.* **2011**, *18*, 354–360.

[40] Sun, W.-W.; Guo, C.-J.; Wang, C. C. C. *Fungal Genet. Biol.* **2016**, *89*, 84–88.

[41] Forseth, R. R.; Amaike, S.; Schwenk, D.; Affeldt, K. J.; Hoffmeister, D.; Schroeder, F. C.; Keller, N. P. *Angew. Chem., Int. Ed.* **2013**, *52*, 1590–1594.

[42] Kreutzer, M. F.; Kage, H.; Gebhardt, P.; Wackler, B.; Saluz, H. P.; Hoffmeister, D.; Nett, M. *Appl. Environ. Microbiol.* **2011**, *77*, 6117–6124.

[43] Kage, H.; Kreutzer, M. F.; Wackler, B.; Hoffmeister, D.; Nett, M. *Chem. Biol.* **2013**, *20*, 764–771.

[44] Duitman, E. H.; Hamoen, L. W.; Rembold, M.; Venema, G.; Seitz, H.; Saenger, W.; Bernhard, F.; Reinhardt, R.; Schmidt, M.; Ullrich, C.; Stein, T.; Leenders, F.; Vater, J. *Proc. Natl. Acad. Sci. U. S. A.* **1999**, *96*, 13294–13299.

[45] Hansen, D. B.; Bumpus, S. B.; Aron, Z. D.; Kelleher, N. L.; Walsh, C. T. *J. Am. Chem. Soc.* **2007**, *129*, 6366–6367.

[46] Kang, H.-S.; Krunic, A.; Shen, Q.; Swanson, S. M.; Orjala, J. *J. Nat. Prod.* **2011**, *74*, 1597–1605.

[47] Hofmann, A.; Heim, R.; Brack, A.; Kobel, H.; Frey, A.; Ott, H.; Petrzilka, T.; Troxler, F. *Helv. Chim. Acta* **1959**, *42*, 1557–1572.

[48] Agurell, S.; Lars, J.; Nilsson, G. *Tetrahedron Lett.* **1968**, *9*, 1063–1064.

[49] Agurell, S.; Nilsson, J. L. G.; Liaaen-Jensen, S.; Schwieter, U.; Paasivirta, J. *Acta Chem. Scand.* **1968**, *22*, 1210–1218.

[50] Fricke, J.; Blei, F.; Hoffmeister, D. *Angew. Chem., Int. Ed.* **2017**, *56*, 12352–12355.

[51] Fricke, J.; Lenz, C.; Wick, J.; Blei, F.; Hoffmeister, D. *Chem. - Eur. J.* **2018**, im Druck.

[52] Genin, S.; Denny, T. P. *Annu. Rev. Phytopathol.* **2012**, *50*, 67–89.

[53] Salanoubat, M.; Genin, S.; Artiguenave, F.; Gouzy, J.; Mangenot, S.; Arlat, M.; Billault, A.; Brottier, P.; Camus, J. C.; Cattolico, L.; Chandler, M.; Choisne, N.; Claudel-Renard, C.; Cunnac, S.; Demange, N.; Gaspin, C.; Lavie, M.; Moisan, A.; Robert, C.; Saurin, W.; Schiex, T.; Siguier, P.; Thébault, P.; Whalen, M.; Wincker, P.; Levy, M.; Weissenbach, J.; Boucher, C. A. *Nature* **2002**, *415*, 497–502.

[54] Bhatt, G.; Denny, T. P. *J. Bacteriol.* **2004**, *186*, 7896–7904.

[55] Delaspre, F.; Nieto Peñalver, C. G.; Saurel, O.; Kiefer, P.; Gras, E.; Milon, A.; Boucher, C.; Genin, S.; Vorholt, J. A. *Proc. Natl. Acad. Sci. U. S. A.* **2007**, *104*, 15870–15875.

[56] Pauly, J.; Spiteller, D.; Linz, J.; Jacobs, J.; Allen, C.; Nett, M.; Hoffmeister, D. *ChemBioChem* **2013**, *14*, 2169–2178.

[57] Jang, H.-D.; Lin, Y.-Y.; Yang, S.-S. *Bioresour. Technol.* **2005**, *96*, 1633–1644.

[58] Wang, L.; Chen, W.; Feng, Y.; Ren, Y.; Gu, Z.; Chen, H.; Wang, H.; Thomas, M. J.; Zhang, B.; Berquin, I. M.; Li, Y.; Wu, J.; Zhang, H.; Song, Y.; Liu, X.; Norris, J. S.; Wang, S.; Du, P.; Shen, J.; Wang, N.; Yang, Y.; Wang, W.; Feng, L.; Ratledge, C.; Zhang, H.; Chen, Y. Q. *PLoS One* **2011**, *6*, e28319.

[59] Streekstra, H. *J. Biotechnol.* **1997**, *56*, 153–165.

[60] European Food Safety Authority, *EFSA J.* **2008**, *6*, 770.

[61] Dekker, K. A.; Aiello, R. J.; Hirai, H.; Inagaki, T.; Sakakibara, T.; Suzuki, Y.; Thompson, J. F.; Yamauchi, Y.; Kojima, N. *J. Antibiot.* **1998**, *51*, 14–20.

[62] Grunwald, A. L.; Berrue, F.; Robertson, A. W.; Overy, D. P.; Kerr, R. G. *J. Nat. Prod.* **2017**, *80*, 2677–2683.

[63] Kamiyama, T.; Umino, T.; Nakayama, N.; Itezono, Y.; Satoh, T.; Yamashita, Y.; Yamaguchi, A.; Yokose, K. *J. Antibiot.* **1992**, *45*, 424–427.

[64] Koyama, N.; Kojima, S.; Fukuda, T.; Nagamitsu, T.; Yasuhara, T.; Omura, S.; Tomoda, H. *Org. Lett.* **2010**, *12*, 432–435.

[65] Kawahara, T.; Itoh, M.; Izumikawa, M.; Sakata, N.; Tsuchida, T.; Shin-Ya, K. *J. Antibiot.* **2017**, *70*, 226–229.

[66] Bok, J. W.; Hoffmeister, D.; Maggio-Hall, L. A.; Murillo, R.; Glasner, J. D.; Keller, N. P. *Chem. Biol.* **2006**, *13*, 31–37.

[67] Balibar, C. J.; Howard-Jones, A. R.; Walsh, C. T. *Nat. Chem. Biol.* **2007**, *3*, 584–592.

[68] Gill, M.; Steglich, W. In *Pigments of Fungi (Macromycetes)*; Herz, W., Grisebach, H.,

Kirby, G. W., Tamm, C., Eds.; Progress in the Chemistry of Organic Natural Products; Springer Vienna: Vienna, 1987; Vol. 51; pp 1–297.

[69] Guo, C.-J.; Knox, B. P.; Sanchez, J. F.; Chiang, Y.-M.; Bruno, K. S.; Wang, C. C. C. *Org. Lett.* **2013**, *15*, 3562–3565.

[70] Leung, A. Y.; Smith, A. H.; Paul, A. G. *J. Pharm. Sci.* **1965**, *54*, 1576–1579.

[71] Nichols, D. E. *Pharmacol. Ther.* **2004**, *101*, 131–181.

[72] Hasler, F.; Grimberg, U.; Benz, M. A.; Huber, T.; Vollenweider, F. X. *Psychopharmacology* **2004**, *172*, 145–156.

[73] Mahapatra, A.; Gupta, R. *Ther. Adv. Psychopharmacol.* **2017**, *7*, 54–56.

[74] Grob, C. S.; Danforth, A. L.; Chopra, G. S.; Hagerty, M.; McKay, C. R.; Halberstadt, A. L.; Greer, G. R. *Arch. Gen. Psychiatry* **2011**, *68*, 71–78.

[75] Johnson, M. W.; Garcia-Romeu, A.; Cosimano, M. P.; Griffiths, R. R. *J. Psychopharmacol.* **2014**, *28*, 983–992.

[76] Leung, A. Y.; Paul, A. G. *J. Pharm. Sci.* **1968**, *57*, 1667–1671.

[77] Lenz, C.; Wick, J.; Hoffmeister, D. *J. Nat. Prod.* **2017**, *80*, 2835–2838.

[78] Challis, G. L. *J. Med. Chem.* **2008**, *51*, 2618–2628.

[79] Gross, H. *Appl. Microbiol. Biotechnol.* **2007**, *75*, 267–277.

[80] Nett, M. In *Genome Mining: Concept and Strategies for Natural Product Discovery*; Kinghorn, A. D., Falk, H., Kobayashi, J., Eds.; Progress in the Chemistry of Organic Natural Products; Springer International Publishing: Cham, 2014; Vol. 99; pp 199–245.

[81] Ziemert, N.; Alanjary, M.; Weber, T. *Nat. Prod. Rep.* **2016**, *33*, 988–1005.

[82] Challis, G. L.; Ravel, J. *FEMS Microbiol. Lett.* **2000**, *187*, 111–114.

[83] Blin, K.; Wolf, T.; Chevrette, M. G.; Lu, X.; Schwalen, C. J.; Kautsar, S. A.; Suarez Duran, H. G.; de Los Santos, E. L. C.; Kim, H. U.; Nave, M.; Dickschat, J. S.; Mitchell, D. A.; Shelest, E.; Breitling, R.; Takano, E.; Lee, S. Y.; Weber, T.; Medema, M. H. *Nucleic Acids Res.* **2017**, *45*, W36–W41.

[84] Kersten, R. D.; Yang, Y.-L.; Xu, Y.; Cimermancic, P.; Nam, S.-J.; Fenical, W.; Fischbach, M. A.; Moore, B. S.; Dorrestein, P. C. *Nat. Chem. Biol.* **2011**, *7*, 794–802.

[85] Gomez-Escribano, J. P.; Bibb, M. J. *J. Ind. Microbiol. Biotechnol.* **2014**, *41*, 425–431.

[86] Cociancich, S.; Pesic, A.; Petras, D.; Uhlmann, S.; Kretz, J.; Schubert, V.; Vieweg, L.; Duplan, S.; Marguerettaz, M.; Noëll, J.; Pieretti, I.; Hügelland, M.; Kemper, S.; Mainz, A.;

Rott, P.; Royer, M.; Süssmuth, R. D. *Nat. Chem. Biol.* **2015**, *11*, 195–197.

[87] Bode, H. B.; Bethe, B.; Höfs, R.; Zeeck, A. *ChemBioChem* **2002**, *3*, 619–627.

[88] Hewage, R. T.; Aree, T.; Mahidol, C.; Ruchirawat, S.; Kittakoop, P. *Phytochemistry* **2014**, *108*, 87–94.

[89] Marmann, A.; Aly, A. H.; Lin, W.; Wang, B.; Proksch, P. *Mar. Drugs* **2014**, *12*, 1043–1065.

[90] Cichewicz, R. H. *Nat. Prod. Rep.* **2010**, *27*, 11–22.

[91] Graupner, K.; Scherlach, K.; Bretschneider, T.; Lackner, G.; Roth, M.; Gross, H.; Hertweck, C. *Angew. Chem., Int. Ed.* **2012**, *51*, 13173–13177.

[92] Gross, H.; Stockwell, V. O.; Henkels, M. D.; Nowak-Thompson, B.; Loper, J. E.; Gerwick, W. H. *Chem. Biol.* **2007**, *14*, 53–63.

[93] Uehling, J.; Gryganskyi, A.; Hameed, K.; Tschaplinski, T.; Misztal, P. K.; Wu, S.; Desirò, A.; Vande Pol, N.; Du, Z.; Zienkiewicz, A.; Zienkiewicz, K.; Morin, E.; Tisserant, E.; Splivallo, R.; Hainaut, M.; Henrissat, B.; Ohm, R.; Kuo, A.; Yan, J.; Lipzen, A.; Nolan, M.; LaButti, K.; Barry, K.; Goldstein, A. H.; Labbé, J.; Schadt, C.; Tuskan, G.; Grigoriev, I.; Martin, F.; Vilgalys, R.; Bonito, G. *Environ. Microbiol.* **2017**, *19*, 2964–2983.

[94] Partida-Martinez, L. P.; de Looss, C. F.; Ishida, K.; Ishida, M.; Roth, M.; Buder, K.; Hertweck, C. *Appl. Environ. Microbiol.* **2007**, *73*, 793–797.

[95] Schneider, T.; Müller, A.; Miess, H.; Gross, H. *Int. J. Med. Microbiol.* **2014**, *304*, 37–43.

[96] Tomassi, S.; Lategahn, J.; Engel, J.; Keul, M.; Tumbrink, H. L.; Ketzer, J.; Mühlenberg, T.; Baumann, M.; Schultz-Fademrecht, C.; Bauer, S.; Rauh, D. *J. Med. Chem.* **2017**, *60*, 2361–2372.

[97] Krieg, R.; Jortzik, E.; Goetz, A.-A.; Blandin, S.; Wittlin, S.; Elhabiri, M.; Rahbari, M.; Nuryyeva, S.; Voigt, K.; Dahse, H.-M.; Brakhage, A.; Beckmann, S.; Quack, T.; Grevelding, C. G.; Pinkerton, A. B.; Schönecker, B.; Burrows, J.; Davioud-Charvet, E.; Rahlfs, S.; Becker, K. *Nat. Commun.* **2017**, *8*, 14478.

[98] Firn, R. D.; Jones, C. G. *Nat. Prod. Rep.* **2003**, *20*, 382–391.

[99] Firn, R. D.; Jones, C. G. *J. Exp. Bot.* **2009**, *60*, 719–726.

[100] Kai, K.; Ohnishi, H.; Mori, Y.; Kiba, A.; Ohnishi, K.; Hikichi, Y. *ChemBioChem* **2014**, *15*, 2590–2597.

[101] Mori, Y.; Ishikawa, S.; Ohnishi, H.; Shimatani, M.; Morikawa, Y.; Hayashi, K.; Ohnishi, K.;

Kiba, A.; Kai, K.; Hikichi, Y. *Mol. Plant Pathol.* **2018**, *19*, 454–463.

[102] Murai, Y.; Mori, S.; Konno, H.; Hikichi, Y.; Kai, K. *Org. Lett.* **2017**, *19*, 4175–4178.

[103] Vollenbroich, D.; Pauli, G.; Ozel, M.; Vater, J. *Appl. Microbiol. Biotechnol.* **1997**, *63*, 44–49.

[104] Bais, H. P.; Fall, R.; Vivanco, J. M. *Plant Physiol.* **2004**, *134*, 307–319.

[105] Spraker, J. E.; Sanchez, L. M.; Lowe, T. M.; Dorrestein, P. C.; Keller, N. P. *ISME J.* **2016**, *10*, 2317–2330.

[106] Couteaudier, Y.; Alabouvette, C. *Can. J. Microbiol.* **1990**, *36*, 551–556.

[107] Partida-Martinez, L. P.; Groth, I.; Schmitt, I.; Richter, W.; Roth, M.; Hertweck, C. *Int. J. Syst. Evol. Microbiol.* **2007**, *57*, 2583–2590.

[108] Partida-Martinez, L. P.; Hertweck, C. *ChemBioChem* **2007**, *8*, 41–45.

[109] Iwasaki, S.; Kobayashi, H.; Furukawa, J.; Namikoshi, M.; Okuda, S.; Sato, Z.; Matsuda, I.; Noda, T. *J. Antibiot.* **1984**, *37*, 354–362.

[110] Li, P.; Yin, W.; Yan, J.; Chen, Y.; Fu, S.; Song, S.; Zhou, J.; Lyu, M.; Deng, Y.; Zhang, L.-H. *Front. Microbiol.* **2017**, *8*, 1172.

[111] Perrier, A.; Barlet, X.; Peyraud, R.; Rengel, D.; Guidot, A.; Genin, S. *Microb. Pathog.* **2018**, *116*, 273–278.

[112] Khalid, S.; Baccile, J. A.; Spraker, J. E.; Tannous, J.; Imran, M.; Schroeder, F. C.; Keller, N. P. *ACS Chem. Biol.* **2018**, *13*, 171–179.

[113] Spraker, J. E.; Wiemann, P.; Baccile, J. A.; Venkatesh, N.; Schumacher, J.; Schroeder, F. C.; Sanchez, L. M.; Keller, N. P. *mBio* **2018**, *9*, e00820–18.

[114] Voigt, K.; Wolf, T.; Ochsenreiter, K.; Nagy, G.; Kaerger, K.; Shelest, E.; Papp, T. In *Genetic and Metabolic Aspects of Primary and Secondary Metabolism of the Zygomycetes*; Hoffmeister, D., Ed.; The Mycota; Springer International Publishing: Cham, 2016; pp 361–385.

[115] Schimek, C.; Wöstemeyer, J. *Phytochemistry* **2009**, *70*, 1867–1875.

[116] Koyama, N.; Kojima, S.; Nonaka, K.; Masuma, R.; Matsumoto, M.; Omura, S.; Tomoda, H. *J. Antibiot.* **2010**, *63*, 183–186.

[117] Otrubova, K.; McGuire, K. L.; McAlpine, S. R. *J. Med. Chem.* **2007**, *50*, 1999–2002.

[118] Rodriguez, R. A.; Pan, P.-S.; Pan, C.-M.; Ravula, S.; Lapera, S.; Singh, E. K.; Styers, T. J.; Brown, J. D.; Cajica, J.; Parry, E.; Otrubova, K.; McAlpine, S. R. *J. Org. Chem.* **2007**,

72, 1980–2002.

[119] Pan, P.-S.; Vasko, R. C.; Lapera, S. A.; Johnson, V. A.; Sellers, R. P.; Lin, C.-C.; Pan, C.-M.; Davis, M. R.; Ardi, V. C.; McAlpine, S. R. *Bioorg. Med. Chem.* **2009**, *17*, 5806–5825.

[120] Li, H.-J.; Lin, Y.-C.; Yao, J.-H.; Vrijmoed, L. L.; Jones, G. E. *J. Asian Nat. Prod. Res.* **2004**, *6*, 185–191.

[121] Talontsi, F. M.; Facey, P.; Tatong, M. D. K.; Tofazzal Islam, M.; Frauendorf, H.; Draeger, S.; Tiedemann, A. v.; Laatsch, H. *Phytochemistry* **2012**, *83*, 87–94.

[122] Belofsky, G. N.; Jensen, P. R.; Fenical, W. *Tetrahedron Lett.* **1999**, *40*, 2913–2916.

[123] Vasko, R. C.; Rodriguez, R. A.; Cunningham, C. N.; Ardi, V. C.; Agard, D. A.; McAlpine, S. R. *ACS Med. Chem. Lett.* **2010**, *1*, 4–8.

[124] Chatterjee, J.; Mierke, D.; Kessler, H. *J. Am. Chem. Soc.* **2006**, *128*, 15164–15172.

[125] Zhang, X.; Nikiforovich, G. V.; Marshall, G. R. *J. Med. Chem.* **2007**, *50*, 2921–2925.

[126] Rosenberg, E.; Ron, E. Z. *Appl. Microbiol. Biotechnol.* **1999**, *52*, 154–162.

[127] Vijayakuma, S.; Saravanan, V. *Res. J. Microbiol.* **2015**, *10*, 181–192.

[128] Arima, K.; Kakinuma, A.; Tamura, G. *Biochem. Biophys. Res. Commun.* **1968**, *31*, 488–494.

[129] Niehs, S. P.; Dose, B.; Scherlach, K.; Roth, M.; Hertweck, C. *ChemBioChem* **2018**, *19*, 2167–2172.

[130] Kikukawa, H.; Sakuradani, E.; Nakatani, M.; Ando, A.; Okuda, T.; Sakamoto, T.; Ochiai, M.; Shimizu, S.; Ogawa, J. *Curr. Genet.* **2015**, *61*, 579–589.

[131] Zhang, G.; Sun, H. J. *PLoS One* **2014**, *9*, e92101.

[132] Stierle, A.; Strobel, G.; Stierle, D. *Science* **1993**, *260*, 214–216.

[133] Staniek, A.; Woerdenbag, H. J.; Kayser, O. *Planta Med.* **2009**, *75*, 1561–1566.

[134] Heinig, U.; Scholz, S.; Jennewein, S. *Fungal Divers.* **2013**, *60*, 161–170.

[135] Kusari, S.; Lamshöft, M.; Kusari, P.; Gottfried, S.; Zühlke, S.; Louven, K.; Hentschel, U.; Kayser, O.; Spiteller, M. *J. Nat. Prod.* **2014**, *77*, 2577–2584.

[136] Ghignone, S.; Salvioli, A.; Anca, I.; Lumini, E.; Ortu, G.; Petiti, L.; Cruveiller, S.; Bianciotto, V.; Piffanelli, P.; Lanfranco, L.; Bonfante, P. *ISME J.* **2012**, *6*, 136–145.

[137] Sato, Y.; Narisawa, K.; Tsuruta, K.; Umezu, M.; Nishizawa, T.; Tanaka, K.; Yamaguchi, K.; Komatsuzaki, M.; Ohta, H. *Microbes Environ.* **2010**, *25*, 321–324.

[138] Ohshima, S.; Sato, Y.; Fujimura, R.; Takashima, Y.; Hamada, M.; Nishizawa, T.; Narisawa, K.; Ohta, H. *Int. J. Syst. Evol. Microbiol.* **2016**, *66*, 2052–2057.

[139] Gruber, G.; Kerschensteiner, L.; Steglich, W. *Z. Naturforsch., B: J. Chem. Sci.* **2014**, *69*, 432–438.

[140] Geib, E.; Gressler, M.; Viediernikova, I.; Hillmann, F.; Jacobsen, I. D.; Nietzsche, S.; Hertweck, C.; Brock, M. *Cell Chem. Biol.* **2016**, *23*, 587–597.

[141] Schneider, P.; Weber, M.; Rosenberger, K.; Hoffmeister, D. *Chem. Biol.* **2007**, *14*, 635–644.

[142] Schimmel, T. G.; Coffman, A. D.; Parsons, S. J. *Appl. Environ. Microbiol.* **1998**, *64*, 3707–3712.

[143] Dewi, R. T.; Tachibana, S.; Darmawan, A. *World Acad. Sci. Eng. Technol.* **2012**, *70*, 882–887.

[144] Zhang, B.; Salituro, G.; Szalkowski, D.; Li, Z.; Zhang, Y.; Royo, I.; Vilella, D.; Díez, M. T.; Pelaez, F.; Ruby, C.; Kendall, R. L.; Mao, X.; Griffin, P.; Calaycay, J.; Zierath, J. R.; Heck, J. V.; Smith, R. G.; Moller, D. E. *Science* **1999**, *284*, 974–977.

[145] Velliquette, R. A.; Friedman, J. E.; Shao, J.; Zhang, B. B.; Ernsberger, P. *J. Pharmacol. Exp. Ther.* **2005**, *314*, 422–430.

[146] Dellafiora, L.; Aichinger, G.; Geib, E.; Sánchez-Barrionuevo, L.; Brock, M.; Cánovas, D.; Dall'Asta, C.; Marko, D. *Food Chem.* **2019**, *270*, 61–69.

[147] He, J.; Wijeratne, E. M. K.; Bashyal, B. P.; Zhan, J.; Seliga, C. J.; Liu, M. X.; Pierson, E. E.; Pierson, L. S.; VanEtten, H. D.; Gunatilaka, A. A. L. *J. Nat. Prod.* **2004**, *67*, 1985–1991.

[148] Kaji, A.; Saito, R.; Nomura, M.; Miyamoto, K.; Kiriyama, N. *Biol. Pharm. Bull.* **1998**, *21*, 945–949.

[149] Fredenhagen, A.; Petersen, F.; Tintelnot-Blomley, M.; Rösel, J.; Mett, H.; Hug, P. *J. Antibiot.* **1997**, *50*, 395–401.

[150] Singh, S. B.; Ondeyka, J. G.; Tsipouras, N.; Ruby, C.; Sardana, V.; Schulman, M.; Sanchez, M.; Pelaez, F.; Stahlhut, M. W.; Munshi, S.; Olsen, D. B.; Lingham, R. B. *Biochem. Biophys. Res. Commun.* **2004**, *324*, 108–113.

[151] Gao, H.; Guo, W.; Wang, Q.; Zhang, L.; Zhu, M.; Zhu, T.; Gu, Q.; Wang, W.; Li, D. *Bioorg. Med. Chem. Lett.* **2013**, *23*, 1776–1778.

[152] Kreutzer, M. F.; Kage, H.; Herrmann, J.; Pauly, J.; Hermenau, R.; Müller, R.; Hoffmeister, D.; Nett, M. *Org. Biomol. Chem.* **2014**, *12*, 113–118.

[153] Grüschow, S.; Rackham, E. J.; Elkins, B.; Newill, P. L. A.; Hill, L. M.; Goss, R. J. M. *ChemBioChem* **2009**, *10*, 355–360.

[154] Gratz, J. *Ann. Mus. Civ. Rovereto* **1991**, *7*, 265–274.

[155] Sewell, R. A.; Halpern, J. H.; Pope, H. G. *Neurology* **2006**, *66*, 1920–1922.

[156] Karst, M.; Halpern, J. H.; Bernateck, M.; Passie, T. *Cephalalgia* **2010**, *30*, 1140–1144.

[157] Richards, N.; Chapman, L. F.; Goodell, H.; Wolff, H. G. *Ann. Intern. Med.* **1958**, *48*, 1078–1082.

[158] Romney, D. K.; Murciano-Calles, J.; Wehrmüller, J. E.; Arnold, F. H. *J. Am. Chem. Soc.* **2017**, *139*, 10769–10776.

Eigenständigkeitserklärung

Hiermit erkläre ich, dass ich die vorliegende Arbeit zum Thema

Biochemische Untersuchungen zu mono-, di- und oligomeren mikrobiellen Naturstoffen aus Aminosäuren

selbst verfasst und keine anderen als die angegebenen Quellen und Hilfsmittel verwendet habe. Die geltende Promotionsordnung der Fakultät für Biowissenschaften der Friedrich-Schiller-Universität Jena ist mir bekannt. Die Hilfe eines Promotionsberaters wurde nicht in Anspruch genommen, noch haben Dritte weder mittelbar noch unmittelbar geldwerte Leistungen für Arbeiten erhalten, die im Zusammenhang mit der vorgelegten Dissertation stehen. Diese Dissertation ist in gleicher oder ähnlicher Form noch bei keiner anderen Hochschule eingereicht oder als Prüfungsarbeit für eine staatliche oder andere wissenschaftliche Prüfung verwendet worden.

Jena, den

Florian Ewald Baldeweg

Anteilsverteilung der Co-Autoren an den Publikationen

Baldeweg, F.; Kage, H.; Schieferdecker, S.; Allen, C.; Hoffmeister, D.; Nett, M. Structure of Ralsolamycin, the Interkingdom Morphogen from the Crop Plant Pathogen *Ralstonia solanacearum*. *Org. Lett.* **2017**, *19*, 4868–4871. DOI:10.1021/acs.orglett.7b02329

Kage, H.:	Erstellung der gentechnisch veränderten Ralstonia-Stämme. Sequenzierung der fehlenden Genbereiche. Mitarbeit am Manuskript.
Schieferdecker, S.:	Chemische Synthese des Oxazolidins, Mitarbeit am Manuskript.
Allen, C.:	Zuarbeiten zur Ermittlung der Phytotoxizität von Ralsolamycin, Mitarbeit am Manuskript.
Hoffmeister, D.:	Mithilfe bei der Konzeption des Projektes, Mitarbeit am Manuskript.
Nett, M.:	Konzeption des Projektes, Erstellung des Manuskripts.

Baldeweg, F.; Hoffmeister, D.; Nett, M. A genomics perspective on natural product biosynthesis in plant pathogenic bacteria *Nat. Prod. Rep.* **2019**, *36*, 307–325. DOI:10.1039/c8np00025e

Hoffmeister, D.:	Mitarbeit am Manuskript.
Nett, M.:	Konzeption des Projektes, Erstellung des Manuskripts.

Baldeweg, F.; Warnke, P.; Fischer D.; Gressler, M. Fungal bio-surfactants from *Mortierella alpina*. *Org. Lett.* **2019**, *21*, 1444–1448. DOI:10.1021/acs.orglett.9b00193

Warnke, P.:	Versuche zur Oberflächenspannung und Hämolyse, Mitarbeit am Manuscript.
Fischer, D.:	Diskussion und Mitarbeit am Manuskript.
Gressler, M.:	Konzeption des Projektes, Initiales Medien-Screening, gentechnische Arbeiten, Proteinaufreinigung, MesG-Assay, Isolation der Malpinine, Erstellung des Manuskripts.

Geib, E.; **Baldeweg, F.**; Doerfer M.; Nett M.; Brock M. Cross-chemistry leads to product diversity from atromentin synthetases in Aspergilli from section *Nigri*. *Cell Chem. Biol.* **2019**, *26*, 223-234.e6. DOI:10.1016/j.chembiol.2018.10.021

Geib, E.: Anzucht der Kulturen, Isolation der Substanzen, chromatographische Analysen, gentechnische Arbeiten, Mitarbeit am Manuskript.

Doerfer M.: Isolation und NMR-Vorbereitung der ^{13}C-markierten Atrofuransäure, Mitarbeit am Manuskript.

Nett M.: Auswertung der NMR-Daten, Interpretation der Fütterungsstudien , Mitarbeit am Manuskript.

Brock M.: Konzeption des Projektes, Anzucht der Kulturen, Isolation der Substanzen, chromatographische Analysen, gentechnische Arbeiten, Erstellung des Manuskripts.

Blei, F.; **Baldeweg, F.**; Fricke, J.; Hoffmeister, D. Biocatalytic Production of Psilocybin and Derivatives in Tryptophan Synthase-Enhanced Reactions. *Chem. - Eur. J.* **2018**, *24*, 10028–10031. DOI:10.1002/chem.201801047

Blei, F.: Isolation der Reinsubstanzen, chromatographische Analysen, Durchführung der Enzymassays, gentechnische Arbeiten, Heterologe Produktion und Aufreinigung von TrpB. Mitarbeit am Manuskript.

Fricke, J.: Heterologe Produktion und Aufreinigung von TrpB (FPLC/ SDS-PAGE), Mitarbeit am Manuskript.

Hoffmeister, D.: Konzeption des Projektes, Erstellung des Manuskript.

Publikationen, Poster und Vorträge

Publikationen

2019 **Baldeweg, F.**; Warnke, P.; Fischer D.; Gressler, M. Fungal bio-surfactants from *Mortierella alpina*. *Org. Lett.* **2019**, *21*, 1444–1448. DOI:10.1021/acs.orglett.9b00193

2019 Geib, E.; **Baldeweg, F.**; Doerfer M.; Nett M.; Brock M. Cross-chemistry leads to product diversity from atromentin synthetases in Aspergilli from section *Nigri*. *Cell Chem. Biol.* **2019**, *26*, 223-234.e6. Im Druck. DOI:10.1016/j.chembiol.2018.10.021

2019 **Baldeweg, F.**; Hoffmeister, D.; Nett, M. A genomics perspective on natural product biosynthesis in plant pathogenic bacteria *Nat. Prod. Rep.* **2019**, *36*, 307–325. DOI:10.1039/c8np00025e

2018 Blei, F.; **Baldeweg, F.**; Fricke, J.; Hoffmeister, D. Biocatalytic Production of Psilocybin and Derivatives in Tryptophan Synthase-Enhanced Reactions. *Chem. - Eur. J.* **2018**, *24*, 10028–10031. DOI:10.1002/chem.201801047

2017 **Baldeweg, F.**; Kage, H.; Schieferdecker, S.; Allen, C.; Hoffmeister, D.; Nett, M. Structure of Ralsolamycin, the Interkingdom Morphogen from the Crop Plant Pathogen *Ralstonia solanacearum*. *Org. Lett.* **2017**, *19*, 4868–4871. DOI:10.1021/acs.orglett.7b02329

Poster

März 2018 **7th International Conference on Microbial Communication for Young Scientists**
Structure elucidation of ralsolamycin A

Vorträge

Oktober 2017 **JSMC Symposium 2017**
Structure elucidation of ralsolamycin and rhizochelin

September 2017 **VAAM Workshop: Biology of Bacteria Producing Natural Products**
Structure elucidation of ralsolamycin and its contribution to the virulence of the crop pathogen *Ralstonia solanacearum* GMI1000

Dezember 2016 **JSMC Symposium 2016**
Structure elucidation of ralsolamycin, a lipopeptide virulence mediator of *Ralstonia solanacearum*

Curriculum Vitae

Thesen zur Dissertation

„Biochemische Untersuchungen zu mono-, di- und oligomeren mikrobiellen Naturstoffen aus Aminosäuren“

von Florian Ewald Baldeweg

1. Im postgenomischen Zeitalter ist das *Genome Mining* ein Erfolg bringender Ansatz um neue Naturstoffe zu isolieren.

2. Ralsolamycin, ein nichtribosomales Peptid isoliert aus Kulturen des pflanzenpathogenen Bakteriums *Ralstonia solanacearum* GMI1000, trägt anders als erwartet, nicht zur Virulenz in Tomatenpflanzen (*Lycopersicon esculentum*) bei.

3. Die fehlerhafte Gensequenz von *rmyA* zeigt, dass in der Naturstoffforschung die Korrektur oder Verifizierung bioinformatischer Vorhersagen durch chemische und molekularbiologische Methoden unabdingbar ist.

4. Zygomyceten wie *Mortierella alpina* können entgegen einem alten Dogma sehr wohl zu einer ausgeprägten Sekundärstoff-Biosynthese befähigt sein und stellen eine damit ein Reservoir für neue Naturstoffe dar.

5. Ein Screening resultierte in 13 nichtribosomalen Peptiden (Malpinin A-E, Malpikynine A-E, Malpibaldin A-C) aus Kulturen von *Mortierella alpina* ATCC32222.

6. Die Malpinine sind Bioemulgatoren, die bei der Sekretion von Fettsäuren durch *Mortierella* eine Rolle spielen.

7. Anstelle von Atromentin wird Atrofuransäure durch Atromentin-Synthetasen in Kulturen von *Aspergillus niger* heterolog produziert.

8. Eine effizientere Route zur biotechnologischen Herstellung von Psilocybin mittels der Tryptophansynthase TrpB ermöglicht die Herstellung nicht natürlicher Produkte wie Isonorbaeocystin.

Danksagung

Mein besonderer Dank gilt Herrn Prof. Dr. Dirk Hoffmeister und Prof. Dr. Dirk Markus Nett, welche mich ermutigten wieder zurück nach Jena zu kommen, um das Promotionsvorhaben anzufangen. Beiden Betreuern möchte ich herzlich für die Aufnahme in ihre Arbeitsgruppen, für ihre offene Tür in Jena bzw. freie Telefonleitung nach Dortmund und für die wohl bestmögliche Betreuung danken.
Ebenfalls bedanke ich mich herzlich bei Herrn Dr. Pierre Stallforth und Herrn Prof. Dr. Harald Groß, die sich freundlicher Weise zur Begutachtung meiner Dissertation bereiterklärt haben, sowie bei allen Mitgliedern der Prüfungskommission.
Danken möchte ich auch Frau Andrea Perner und Frau Heike Heinecke für die MS- und NMR-Messdaten, welche das Fundament meiner Arbeit darstellen, sowie Frau Karin Martin für das bereitstellen von neuen Stämmen.
Auch allen Gruppenmitglieder der Nett und Hoffmeister Arbeitsgruppe spreche ich meinen Dank aus. Euere Vorarbeit, Mitarbeit, Zusammenarbeit und Diskussionen haben zum Erfolg dieser Promotion beigetragen. Die kollegialen Kaffeepausen mit Herrn Brandt und Dörfer oder zuletzt Herrn Wurlitzer steigerten nicht nur die Moral erheblich, sondern lieferten fruchtbare Lösungsansätze im Labor.